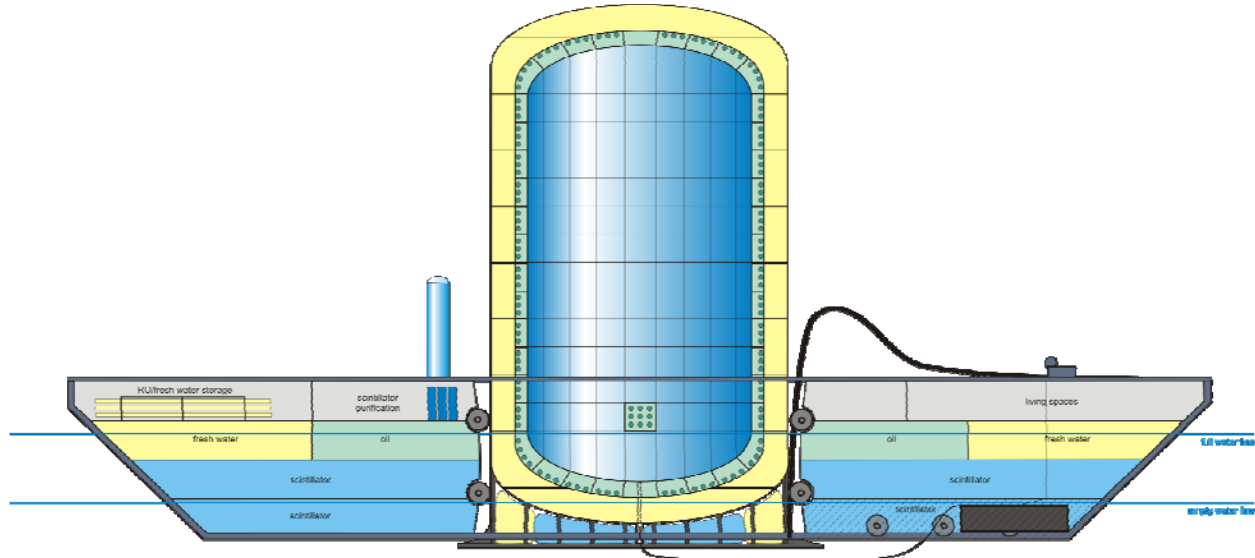


# A Deep Ocean Anti-Neutrino Detector near Hawaii - Hanohano

## Final Report



Prepared for:

**The National Defense Center of Excellence  
for Research in Ocean Sciences (CEROS)**  
73-4460 Queen Kaahumanu Highway, Suite 111  
Kailua-Kona, Hawaii 96740

Prepared by:

**MAKAI OCEAN ENGINEERING, INC.**  
Waimanalo, Hawaii 96734  
<http://www.makai.com>

and

**DEPARTMENT OF PHYSICS AND ASTRONOMY**  
University of Hawaii, Manoa

**Approved for Public Release, Distribution Unlimited**

## **DISCLAIMER**

The views, opinions, and/or findings contained in this article are those of the author and should not be interpreted as representing the official policies, either expressed or implied, of the Defense Advanced Research Projects Agency or the Department of Defense

**Approved for Public Release, Distribution Unlimited**

## TABLE OF CONTENTS

<b>DISCLAIMER .....</b>	<b>II</b>
<b>TABLE OF CONTENTS .....</b>	<b>III</b>
<b>LIST OF FIGURES .....</b>	<b>VI</b>
<b>LIST OF TABLES .....</b>	<b>VII</b>
<b>1. SUMMARY .....</b>	<b>1</b>
1.1 OVERALL RESULTS AND CONCLUSIONS:.....	1
1.2 CONCLUSIONS BY TASK .....	2
1.3 ORGANIZATION OF THIS REPORT.....	4
<b>2. 10-QUESTIONS.....</b>	<b>5</b>
2.1 THE PROBLEM.....	5
2.2 BARRIERS TO SOLVING THIS PROBLEM .....	5
2.3 OVERCOMING THESE BARRIERS .....	5
2.4 CAPABILITY BEING DEVELOPED - DOCUMENTATION .....	5
2.5 PRODUCT OF THIS EFFORT .....	5
2.6 QUANTITATIVE METRICS: .....	5
2.7 THE PAYOFF .....	6
2.8 TRANSITION MILESTONES.....	6
2.9 ENDORSEMENTS .....	6
2.10 OPM.....	6
<b>3. BACKGROUND .....</b>	<b>7</b>
3.1 TECHNICAL PROBLEM:.....	7
3.2 ANTI-NEUTRINO DETECTOR SYSTEMS .....	8
3.3 TECHNICAL ISSUES: .....	8
3.4 TECHNICAL OBJECTIVES: .....	9
3.5 CURRENT AND FOLLOW-ON DEVELOPMENT:.....	9
3.6 TECHNICAL RATIONALE:.....	11
3.6.1. Anti-neutrino detection:.....	11
3.6.2. Other Neutrino Programs:.....	11
3.6.3. Detecting Nuclear Activity:.....	12

3.6.4.	Detector Material:	13
3.6.5.	Background radiation:	14
3.6.6.	Geo-Neutrinos and Earth Composition:	15
3.6.7.	Georeactor:	16
3.7	TECHNICAL INNOVATION	17
<b>4.</b>	<b>WORK PERFORMED, TASK CONCLUSIONS</b>	<b>19</b>
4.1	PROJECT TEAM	19
4.2	TASKS	19
4.2.1.	TASK 1 - Determination of detector size, sensitivity, and location required to perform neutrino geophysics measurements.	19
4.2.1.1	Summary results and Conclusions	19
4.2.1.2	Detailed Report	20
4.2.2.	TASK 2 - Determination of detector size and sensitivity for nuclear deterrence	20
4.2.2.1	Summary results and Conclusions	20
4.2.3.	TASK 3 – Design of 20 m structure	21
4.2.3.1	Summary results and Conclusions	21
4.2.3.2	Detailed Report	22
4.2.4.	TASK 4 - Design of photo-detector and housing prototype	22
4.2.4.1	Summary results and Conclusions	22
4.2.4.2	Detailed Report	23
4.2.5.	TASK 5 – Study of means to prevent successive implosions and in situ testing	23
4.2.5.1	Summary results and Conclusions	24
4.2.5.2	Detailed Report	25
4.2.6.	TASK 6 - Electronics preliminary design for low power application	25
4.2.6.1	Summary results and Conclusions	25
4.2.6.2	Detailed Report	26
4.2.7.	TASK 7 – Simulation of deployment of vessel	26
4.2.7.1	Summary results and Conclusions	26
4.2.7.2	Detailed Report	27
4.2.8.	TASK 8 - Pressure testing of scintillation materials in the laboratory	27
4.2.8.1	Summary results and Conclusions	28
4.2.8.2	Detailed Report	28
4.2.9.	TASK 9 – Workshop	29
4.2.9.1	Summary results and Conclusions	29
4.2.9.2	Detailed Report	30
4.2.10.	TASK 10 - Design for communications networking inside vessel	30
4.2.10.1	Summary results and Conclusions	30
4.2.10.2	Detailed Report	31
4.2.11.	TASK 11 - Study of power and communication links to shore	31
4.2.11.1	Summary results and Conclusions	31
4.2.11.2	Detailed Report	31

4.2.12. TASK 12 – Conceptual Plans for Hanohano.....	31
4.2.12.1 Summary results and Conclusions.....	32
4.2.12.2 Detailed Report.....	34
4.2.13. TASK 13 - Engineering study for preparation of low radioactivity scintillation material .....	34
4.2.13.1 Summary results and Conclusions.....	34
4.2.13.2 Detailed Report.....	35
4.2.14. TASK 14 – Design and costing for ocean demonstration. ....	35
4.2.14.1 Summary results and Conclusions.....	35
4.2.14.2 Detailed Report.....	36
4.2.15. TASK 15 – Final report .....	36
4.3 OTHER PROGRESS .....	36
4.3.1. New Science .....	36
4.3.2. Other Geo-Neutrino Capable Detectors:.....	37
<b>5. CONCLUSIONS, ISSUES AND RECOMMENDATIONS.....</b>	<b>39</b>
5.1 OVERALL CONCLUSIONS.....	39
5.2 SUMMARY: ISSUES .....	40
5.3 RECOMMENDATIONS.....	40
<b>6. APPENDIX.....</b>	<b>42</b>
6.1 (A) TASK 1: HANOHANO NEUTRINO DETECTOR (SIZING ANALYSIS) .....	42
6.2 (C) TASK 3, 5, 7, 12, 13, 14: A DEEP OCEAN ANTI-NEUTRINO DETECTOR NEAR HAWAII – HANOHANO: OCEAN ENGINEERING ANALYSIS .....	42
6.3 (D) TASK 3, 5, 7: BASIS OF DESIGN SUMMARY DOCUMENT .....	42
6.4 (E) TASK 4: OPTICAL MODULE DESIGN .....	42
6.5 (F) TASK 6: ELECTRONIC DESIGN FOR RELIABILITY AND LOW POWER.....	42
6.6 (G) TASK 8: SCINTILLATOR TESTING .....	42
6.7 (J) TASK 10: INTERNAL COMMUNICATIONS NETWORKING .....	42
6.8 (K) TASK 11: POWER AND COMMUNICATION CABLE TO SHORE .....	42

## LIST OF FIGURES

Figure 1:	Conceptual Design of the 10,000 m <sup>3</sup> anti-neutrino detector .....	1
Figure 2:	Originally Envisioned 20m deep ocean anti-neutrino detector. ....	7
Figure 3:	Signal from an anti-neutrino and proton collision. ....	11
Figure 4:	Global geo-neutrino flux.....	14
Figure 5:	KamLAND observed rate at various predicted rate levels. ....	17
Figure 6:	Overall profile of the detector and barge. ....	32
Figure 7:	Plan view of the final Hanohano.....	32

## LIST OF TABLES

Table 1:	Calculated anti-neutrino fluxes [ $\times 10^6 \text{ cm}^{-2} \text{ s}^{-1}$ ] for sites around the world.(from Rothschild, et al, arXiv:nucl-ex/9710001). ....	15
Table 2:	Operating and planned Geo-neutrino projects worldwide.....	37

## 1. SUMMARY

The technical problem addressed in this work has been the challenge of manufacturing and installing deep ocean anti-neutrino detectors which can (1) detect in the long-range nuclear reactors and bomb tests around the world and (2) detect in the near-term geoneutrinos emitted from the earth for key scientific experiments and background measurements. These proposed detectors measure low energy anti-neutrinos from radioactive decays. Anti-neutrinos naturally arise from decays throughout the Earth, whether they originate from a hypothetical natural reactor at the Earth's core or from man-made nuclear reactors or nuclear weapon testing. No level of shielding can prevent this detection.

This CEROS-funded effort has been the first step in building a small (9 kilo-tonne fiducial volume) 24 kilo-tonne total mass detector in the deep ocean off Hawaii. This detector will initially be used for a clean measurement of the Earth's total radioactivity and a sensitive search for an Earth core reactor; it can also accomplish unique measurements of neutrino properties. At the same time, it will demonstrate the utility of multiple sensors in detecting man-made sources of radiation. Eventual funding for this project will be from the National Science Foundation.

There are specific engineering hurdles to be overcome before a detector of this size can be built and deployed in the deep ocean. Identifying and overcoming these challenges is the technical objective of this CEROS effort. The anticipated problems associated with the construction of the proposed detector are related to its (1) operation in the deep ocean and (2) very massive size.

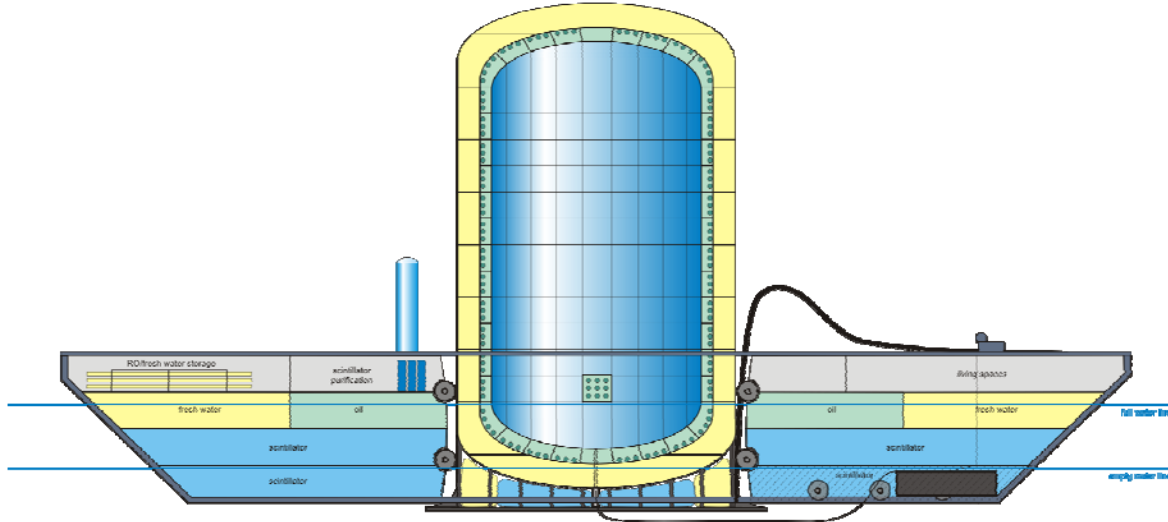


**Figure 1:** Conceptual Design of the 10,000 m<sup>3</sup> anti-neutrino detector

### 1.1 OVERALL RESULTS AND CONCLUSIONS:

**Hanohano feasibility:** Hanohano's critical components relative to operation in the deep ocean, massive construction, and deployment have been investigated and there are no show-stoppers. Key critical issues such as scintillator performance in the deep ocean, construction and deployment, low-power operations and control, failure survivability, and electronic design have been

investigated, prototyped and/or tested. At this time, this detector is a practical and technically feasible method of detecting anti-neutrinos.

**Hanohano as a Geoneutrino detector:** We have investigated the use of Hanohano for measurements of the uranium and thorium content of the Earth's mantle and core. Even modest resolution of the U/Th content is of great interest to geologists, as was highlighted by an international workshop held at UH in December 2005. U/Th are believed to dominate the internal heat of the earth, and be responsible for the geomagnetic field (outer core), the motion of the earth's landmasses, and volcanic activity (mantle). Yet, there are no direct measurements of the source and distribution of this heat source, which cannot be measured from the continents due to obscuration by the local high radioactivity of the continental crust. Measurements from the deep ocean over the thin oceanic crust can make the crucial observations. Into the bargain Hanohano can make a definitive search for the controversial claim of a natural reactor at the Earth's core. In studying the detector size needed to carry out these tasks we were driven to enlarge the initial plan to a detector mass in the ten kiloton range.

**Hanohano as a Neutrino Physics Instrument:** During the study of the design of Hanohano as required for the geoneutrino task it was learned that the application of this portable ten kiloton instrument to the study of neutrino physics was much more exciting than foreseen. This has evolved to the state of attracting worldwide attention in the elementary particle physics community. The basic plan involves stationing Hanohano 50-60 km offshore from a large nuclear power complex and using the reactor flux to make more precise measurements than otherwise possible, and even to be able to resolve the order of the neutrinos masses. It should be noted that, unlike some other plans for related (but more narrow) studies, the Hanohano plan is very broad band with multiple and interesting science outcomes.

**Hanohano relative to Nuclear Deterrence:** Hanohano in its initial form will provide important technology development and measurement of backgrounds needed for building a larger nuclear deterrence (ND) detector.

**Hanohano as a competitor:** Hanohano is unique among all proposed and pending neutrino detectors in the world: it can be larger, more cost effective than the competition and its portability makes it deployable to multiple locations of scientific interest. As a concept, it is the only one suitable for long range nuclear proliferation monitoring.

## 1.2 CONCLUSIONS BY TASK

- **Hanohano size conclusion:** Studies of detector counting rates and backgrounds have driven the size goal from 1.4 to 4 to 10 k-tonne. The basic requirement was to make useful measurements in one year, with the option of relocation on a roughly annual basis. Geologists have flagged important reasons for measurements at various locations in the world's oceans. The size increase also facilitates the ability to make unique and important measurements of neutrino properties. From the science standpoint, of course, larger is always better for more statistical power. It seems that the 9-10 kiloton range is adequate for the geological and elementary particle science.
- **Nuclear deterrence conclusion:** For the long range plan to use neutrinos in remote reactor monitoring and detecting nuclear testing, the present detector represents a large

step. At 10 kilotons (and up to about 100 kilotons) such an instrument is presently buildable with no technical showstoppers. Going beyond that scale, to the necessary sizes in the 1-100 megaton scale, will require technical development, particularly for ocean deployment. The presently proposed detector, while doing science justifiable on its own merits, will enable the next step through experience, understanding of backgrounds, and pushing the technology forwards.

- **Structure design conclusion:** A variety of anti-neutrino detector shapes and configurations were analyzed for deployability, stability, and structural integrity resulting in the elimination of most concepts and shapes and focusing on a cylindrical detector that is supported by a separate surface barge. This concept was optimal for a very wide range of detector sizes from 2 k-tonnes to 100 k-tonnes.
- **PMT design conclusion:** At this point the only viable photodetector for large scintillation detectors is the classic glass bulb photomultiplier tube (PMT). Due to the hundreds of atmospheres of deep ocean pressure, these PMTs must be protected by a glass instrument housing. There are four projects presently utilizing such detectors, and so viable well studied hardware is available for a starting point in the Hanohano design. At present a 10 inch diameter PMT in a 13 inch housing is favored, which is very similar to the (thousands of) units being installed in the deep ice at the South Pole in the ICECUBE detector.
- **Implosion conclusion:** We have analyzed and demonstrated a practical method of altering the pressure wave and preventing sympathetic implosions in the closely-spaced instrument housings needed in these detectors. This greatly reduces the perceived and real risk of operating this detector in the deep ocean.
- **Low Power operation conclusion:** We have examined the utilization of modern low power integrated electronics to the end of achieving sufficiently low power to enable one year operation on battery power alone. We have made an order of magnitude progress over older designs, and can foresee another order of magnitude gain in future design iterations. At present battery operation is marginally possible. However, for present operations with fiber optic cabling to shore there will be no problem in handling the <2kW we estimate for the 10 kiloton detector.
- **Deployment conclusion:** The Hanohano detector and support barge have been designed specifically for deployment simplicity and reliability. The detector can be built such that the scintillator and oil buoyancy supports the structure and makes deployment economically viable. Cable attachment and lays to shore are within cable laying state-of-the-art technology.
- **Scintillator test and selection conclusion:** We have examined various candidates for scintillation fluid and find that a commercially available liquid (LAB, a precursor to dish-soap), will meet our needs. Experimental studies of temperature and pressure dependence reveal no stoppers. Further work is needed for optical characterization and studies of the level of necessary filtration.
- **Internal communications conclusion:** A plan for a tree structure of internal connection has evolved which avoids dangers of single point failure. Cables will be used in the first level from PMT to digitizer, and fiber optics thereafter, with a

redundant path to shore. The design minimizes at-sea data processing and takes advantage of the ongoing advances in submarine fiber optic communications to send all data to shore.

- **Conceptual Plan conclusion:** A conceptual design of the 10,000 m<sup>3</sup> scintillator Hanohano detector and barge has been completed that will just fit through the Panama Canal. Weight, stability, structural needs, operational requirements, and physics needs have been checked and are reasonable; the conceptual vehicle is a feasible approach.
- **Scintillator processing conclusion:** We are fortunate that great progress has been made in recent years in the development of techniques for removing radioactive materials from liquid scintillators. These techniques can be used with Hanohano. The scintillator will be purified by four methods: water extraction, nitrogen stripping, vacuum distillation, and filtration.
- **Ocean Demo conclusion:** A small demonstration model has been conceptually designed for specific and critical next-step testing. This testing will include an ocean deployment of about a one ton module, large enough to demonstrate the radiopurity, protection from backgrounds, and the functionality of the optical modules. At present we lack funding to carry out this test.
- **Science Progress conclusion:** In the study of the detector and science applications we have reached the happy conclusion that the initial notion for a deep ocean scintillation detector, enlarged to a 9 kiloton scale, will be a detector of world importance for science on its own merits, and with a wide interdisciplinary program cutting across geology and physics.
- **Transition conclusion:** The team has focused on a transition to the National Science Foundation funding for Major Research Equipment and Facilities Construction (MREFC); proposals will be written in the current year with major contributions from this work.

### 1.3 ORGANIZATION OF THIS REPORT

- The overall program conclusions are provided above.
- Expanded details on each task and accomplishment are provided in the following chapter.
- For even more detail, the reader is referred to the full technical reports covering all tasks – these are attached to this report as appendices.
- Remaining issues and recommendations are at the end of this report.

## 2. 10-QUESTIONS

### 2.1 THE PROBLEM

- Big Picture: Deterrence: Inability to quantitatively monitor nuclear activity from uncooperative sources on a global scale. Science: Fundamental lack of understanding of the earth's composition, formation and origin of geomagnetic fields, and some neutrino properties.
- Our Problem: Building confidence that an anti-neutrino detector working in the deep ocean can provide valuable answers to these Big Picture Problems, developing stepping-stone technology, understanding backgrounds to future deterrence applications.

### 2.2 BARRIERS TO SOLVING THIS PROBLEM

- Finding credible solutions to operating the detector in the deep ocean: suitable scintillator fluid, optical detectors, low power requirements, communication, control, glass housing sympathetic implosions, contamination and deployment.

### 2.3 OVERCOMING THESE BARRIERS

- Developing preliminary designs for the overall detector and building and demonstrating key critical components.

### 2.4 CAPABILITY BEING DEVELOPED - DOCUMENTATION

- Ability to design critical electronics; fundamental understanding of the detector performance; ability to design, deploy and recover the detector structure; ability to test scintillators at depth and pressure.
- Reports, test results, technical papers, workshop proceedings

### 2.5 PRODUCT OF THIS EFFORT

- Conceptual design & sizing overall stepping-stone, science driven detector.
- Specific designs and prototypes of electronics; power and control.
- Define problem/opportunities with glass sphere sympathetic implosions.
- Demonstrate scintillator usability at depth and temperature

### 2.6 QUANTITATIVE METRICS:

- Sensitivity and cost/volume:
  - **Science**: First detector can measure science goals in ~ 1 year for each deployment/location. Measure backgrounds not measurable with small prototypes.

- **Nuclear Deterrence:** Long range cost reduction/megaton must go down by 100-1000, optical technology limited, some trades in sensitivity possible (need data from science results).
- First 10kT detector in \$40-\$44 million range; matches expectations.
- Acceptable scintillator: clarity at 6000m >10m; optical output > 5000 quanta/MeV
- Electronics power <1w/optical unit – good initial results; prefer lower for battery option.
- Engineering: 2 designs; stable, buildable, deployable, recoverable: 22 kT total, 10 k-m<sup>3</sup> scintillator.

## 2.7 THE PAYOFF

- Near Term: geophysical and elementary particle science & detector development; and,
- Long Term: a new arms control tool with a detection network providing incontrovertible evidence of nuclear weapons preparations/testing. Neutrino monitoring cannot be faked or shielded because it is unique in going to the energy source - the nuclear reactions.

## 2.8 TRANSITION MILESTONES

- Focus on NSF – team is on track to enter an NSF-MREFC program for the major funding. Emphasis on interdisciplinary science for first detector
- Transition in 2 years – pick up funding with NSF.
- This year: NSF proposals, collaboration for those proposals, solicit funds from other government agencies.

## 2.9 ENDORSEMENTS

- NSF – encouraging submittal of proposals
- Collaborators: U. Hawaii, HPU, U. Tohoku, UC Davis, other US, Europeans (Italy, Germany, France)
- Others....

## 2.10 OPM

- Workshops, people, ship time: UH this year: ~\$40k; UH/HPU support next year: \$77k

### 3. BACKGROUND

#### 3.1 TECHNICAL PROBLEM:

The long-range technical problem addressed in the proposed work is the challenge of manufacturing and installing deep ocean detectors which can monitor reactors and bomb tests around the world. These proposed detectors will measure low energy anti-neutrinos from radioactive decays. Anti- neutrinos naturally arise from decays throughout the Earth, perhaps from a hypothetical natural reactor at the Earth's core, and from man-made nuclear reactors or nuclear weapon testing. Anti-neutrinos pass freely through shielding materials, thus any reactor or bomb test could not be hidden from the proposed detector.

The construction of the proposed detector has two technical problems:

- 1. Located in the deep ocean:** Such detectors must be shielded from cosmic ray background radiation by being buried deep in mines, ice or in the deep ocean. There is an operating detector similar to the one being proposed, in Japan (KamLAND) in a mine cavity 1000 meters deep (2.5 km water equivalent), and not as deep as one would wish for proper shielding. Future detectors intended for the worldwide monitoring of nuclear activity must be better shielded (deeper) and located either in a widely distributed global grid or in close proximity (several hundred km) to the suspicious sources. *Only deep ocean detectors afford the flexibility of both placement (portability) and shielding to be practical for both nuclear deterrence and key geophysical science.*

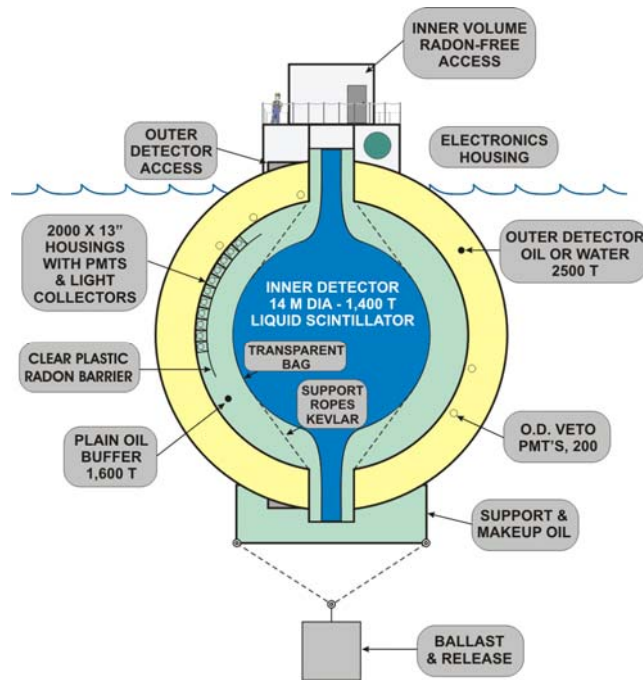


**Figure 2:** Originally Envisioned 20m deep ocean anti-neutrino detector.

2. **Large Size:** The proposed detector is a very large target mass of scintillating liquid surrounded by light sensors. The scintillator emits a unique light signature when struck by an anti-neutrino and this signal is detected by the surrounding light sensors (photomultiplier tubes). The frequency of neutrino detections is proportional to the target mass and the energy resolution to the number of light sensors. A 20m-diameter deep ocean detector containing 2000 photomultiplier tubes viewing an inner balloon of 1400 tons of scintillating material is shown schematically in the attached figure. There is an inner transparent balloon containing the high light output scintillating liquid, and a region outside the balloon containing only oil which has little sensitivity to radioactivity from the vessel walls, structure and photomultiplier glass. The detectors to be investigated in this program are of KamLAND size and larger. Detectors used for nuclear deterrence, a long-range goal, would be considerably larger than the one shown. *Therefore, the proposed detectors are both sizable and complex structures to be deployed in the very deep ocean.*

### 3.2 ANTI-NEUTRINO DETECTOR SYSTEMS

We will be discussing throughout this report three at-sea systems:

- *Component Demo:* This is a demonstration and test of key components to be used in the larger detectors that follow.
- *Geophysics/Particle Physics/Background Detector:* This detector, pictured above and similar to the KamLAND detector but operated in very deep water, would be used for measuring background radiation, refining the technology, and conducting fundamental earth and neutrino science.
- *Nuclear Deterrence Detector (NDD):* Many very large NDD units would comprise a network to monitor global man-made nuclear activity. This is a long range goal, well beyond the present study.

Throughout this document and the attached reports, we will refer to this first Geo/Particle/Background anti-neutrino detector as Hanohano. Hanohano stands for “excellence” in Hawaiian and the HANO stands for Hawaii Anti-Neutrino Observatory.

### 3.3 TECHNICAL ISSUES:

We have identified thirteen critical issues that need to be addressed to determine the feasibility of this large detector - issues that can be addressed in the proposed year of CEROS funding:

- What is the performance and design criteria of an initial Hanohano detector for measuring background noise and performing fundamental science? This will establish the Hanohano basis-of-design.
- What is the scope and size of a larger detector system capable of monitoring global man-made activity from human sources? This similarly determines the basis of design of a deterrence detector.
- For Hanohano, what is an optimal structure to be cost-effective and deployable?

- What is the design and arrangement of the deep water photo-detector units? This extends our knowledge of the overall design and electronic complexity.
- Can the photo-detector units be protected from chain-reaction implosions? One photo-detector implosion could severely damage the project – can we eliminate this risk?
- Can the electronics be designed for very low power consumption? Power is a costly factor in these large detectors – how can power be greatly lowered to eliminate power cables?
- Can the system be practically and economically deployed? These detectors are large and complex and deployment will be the largest risk.
- Will the scintillating materials function properly at the pressures and temperatures of the deep ocean? These materials have not been demonstrated under deep ocean conditions.
- Can a practical internal control communications system be built?
- Can power and data be transmitted to/from shore? Communication and power transfer to and from the detector need to be defined.
- What are the design details and costs for Hanohano? Cost is a major concern with these large detectors. A conceptual design will yield a more accurate cost estimate.
- How can the scintillation material be processed and delivered to the detector? This addresses the practical issue of deploying a detector with pure scintillation material.
- What needs to be tested and what is the cost for key component demonstration? This task defines the next step in component testing.

### 3.4 TECHNICAL OBJECTIVES:

The activities proposed for CEROS funding aimed to resolve the major outstanding technical issues that must be addressed before a national proposal can be successful. These include ocean engineering issues of vessel design, construction, handling, deployment and recovery, choice of scintillation materials for deep ocean use, design of optical detectors for use in close proximity under high pressure, electronics and communication, and selection of low radioactive background materials.

### 3.5 CURRENT AND FOLLOW-ON DEVELOPMENT:

This CEROS work is the first step in a much larger vision of anti-neutrino detector development. The CEROS funding constituted the high-risk funding used to scope out and address particularly challenging issues associated with this novel detector concept. Given the successful efforts, a strong technical argument can now be made to other funding agencies to continue the development. Table 1 illustrates the development stages and anticipated funding agencies. For each detector, the funding source is shown for the initial *Basis-of-Design* that defines the technical need and scope of the detector, the initial *Conceptual* design, the final detailed *design*, and the actual detector installation or *deployment*.

- *Base Technology*: This concept, at the beginning of this study, was in its infancy of development. The key technical issues are the core of this CEROS program, and are reported upon herein.
- *Component Demonstration*: At the end of year one, the team envisioned that there would be key components that will need follow-on in-situ testing and demonstration. These tests were designed in the first funding year. The team has request follow-on CEROS funding for conducting these tests.
- *Hanohano*: This detector's final design and construction is well beyond CEROS level of funding. It, however, has its basis-of-design and conceptual design developed within currently proposed and follow-on CEROS programs. With a clear resolution of major issues and a demonstration of key components, the team (lead at that time by UH) will pursue funding from both the National Science Foundation and the other government agencies.
- *Nuclear Deterrence Detector*: This detector system (a series of very large detectors) would require significant future funding.

### 3.6 TECHNICAL RATIONALE:

This section provides background technology discussion on anti-neutrino detection, other neutrino programs, detector materials, background radiation, geo-neutrinos, and a geo-reactor.

#### 3.6.1. Anti-neutrino detection:

The detection of electron anti-neutrinos (as opposed to electron neutrinos from the sun, which are abundant) uses the fortuitous fact that anti-neutrinos striking a proton can create a positron and a neutron. The positron immediately annihilates with an electron in the surrounding material and generates a light flash, whose light level is proportional to the initial anti-neutrino energy. The neutron wanders around for two hundred microseconds or so, and captures on another proton forming deuterium and emitting a characteristic flash of fixed energy (due to the 2.2 MeV binding energy of the deuteron). The signature of two pulses close in time and space, with the second of fixed energy, provides a wonderful discriminant for identifying electron anti-neutrinos uniquely, and is illustrated in Figure 2. This has been demonstrated by KamLAND, which measures electron anti-neutrinos averaging a distance of 180 km away. Therefore, due to the desirable sensitivity and clear signals, this detector will focus on anti-neutrinos.

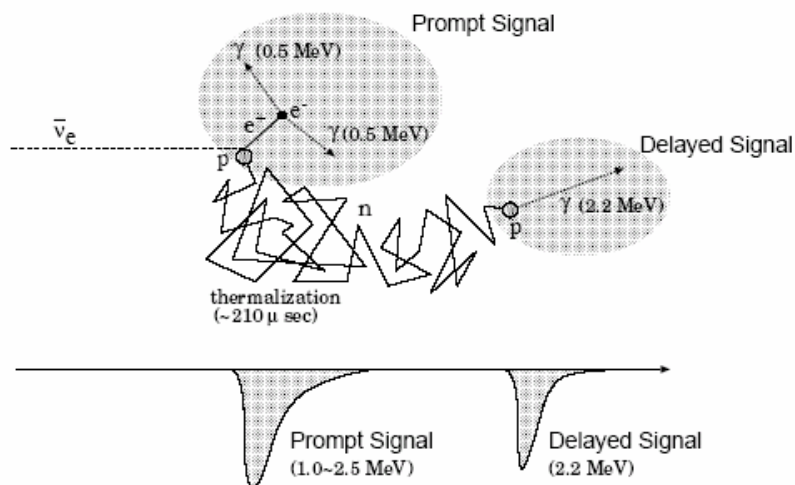


**Figure 3:** Signal from an anti-neutrino and proton collision.

#### 3.6.2. Other Neutrino Programs:

There are a number of other neutrino projects underway or planned around the world. Of these there are, for example, the ICECUBE Project at the South Pole, the ANTARES, NEMO and NESTOR projects in the Mediterranean, and the Lake Baikal Project. All of these are aimed at detection of very high energy cosmic ray neutrinos (with thresholds

more than a factor of 1000 higher than the presently discussed project, and thus totally insensitive to neutrinos from natural radioactivity or reactors). UH is the center of the (NASA funded) ANITA Project, which aims to find microwave pulses in the Antarctic Ice sheet, observed from a balloon, to detect super high energy cosmic neutrinos (a trillion times the energy of the present project sensitivity).

There are three operating projects which can detect solar neutrinos: KamLAND, Super-Kamiokande, and SNO. KamLAND has been mentioned as the prototype for the present project, though located in the Japanese Alps and overwhelmed with radioactivity from the local mountains and from the Japanese nuclear power reactors. Super-Kamiokande has the ability to detect some solar neutrinos above 6 MeV, but is insensitive to anti-neutrinos. The SNO Project in Sudbury, Canada detects solar neutrinos in heavy water. It does not have the sensitivity to detect the geo-neutrinos or reactor neutrinos, and it is scheduled to be shut down in two years. This project has considered conversion to detect anti-neutrinos, but again, it suffers from location on a continental plate and power reactors located within hundreds of kilometers.

Another low energy neutrino project, Borexino, is under construction in a mine tunnel (Gran Sasso laboratory) in the Appenine Mountains in Italy. It will have the sensitivity to measure geo-neutrinos and neutrinos from a geo-reactor, but suffers from the same location problem as does KamLAND and from the disadvantage of being 5 times smaller than KamLAND. It is in a crustal mountain range and not very far away from France, which has more nuclear power reactors than any other country.

There has been mention of possible competing projects from Russia (in the Caucasus, again in a mountain range and not very far from reactors), in Europe (talk of filling a tanker with scintillator and sinking it near Greece, but no evidence of realistic activity by the proposing Munich group). A little more developed plan by a Netherlands group for a project in Curacao calls for drilling from a land site with radial tunnels filled with detectors. It is our judgment that this project will prove to be very expensive compared to the present plan, and of course such a detector is not portable. This seems, however, to be the only serious competition for the science and long range goals we discuss herein. We are in communication with the Dutch group and hope they will choose to join us later, but for now they are pursuing their own rather different path. In sum, the present proposal has, for the moment, a free field to pursue two unique scientific goals, and by deploying in the ocean to be moving on a direct path towards long range goals for reactor and nuclear weapons monitoring.

### 3.6.3. Detecting Nuclear Activity:

The long-term aim of this effort is a network of huge underwater instruments which can keep track, literally, of the power output of all the world's power and research reactors. Most cooperating reactors provide monitoring agencies with day by day accounting of power output. Even without this, daily reactor operations change little, with fueling shutdowns only about every 18 months. An array with roughly 500 detectors around the world, roughly equal in number to the reactors, can back-calculate (tomography) based upon observed rates, to the power output of the individual reactors, most of whose powers

and locations are well known in any event. One can then solve for any new reactor powers and locations. There are alternative means of monitoring (eg. satellites, gas and dust emissions, and seismic and infrasound signatures for weapons testing), but these are indirect and susceptible to cloaking measures; there is no way to hide or fake the neutrino signal.

A first cut at employing an array of such detectors, located on approximately a 5 degree grid around the world's oceans (plus deployment in several lakes such as Baikal and Victoria to get better mid-continent coverage), with each cluster of 100 megatons effective mass, yielded sufficient sensitivity to detect operations at levels sufficient to make bomb material at the rate of several per year (<100 MWt level). Moreover this array would automatically give us the capability to detect clandestine nuclear weapons testing down to the sub-kiloton (TNT equivalent) level (the threshold desired by IAEA test ban monitors). This concept is relatively new, being initially proposed by the University of Hawaii in 2003, with only conceptual studies having been performed to date. Reference a conference on the concept at UH (<http://www.phys.hawaii.edu/~jgl/nacw.html>) and the Paris Neutrino 2004 Meeting (J.G. Learned at <http://neutrino2004.in2p3.fr/> at 1650 on 15 June 2004). We participated in a more recent meeting at Livermore National Laboratory which concentrated on near (10-100 m) reactor monitoring, but which also considered longer ranges, and at which Hanohano was discussed with interest (see conference webpage <http://www.llnl.gov/neutrinos/workshop/aap2006.html>).

The early studies were aimed at establishing an upper limit on what is possible, though not necessarily presently affordable. Further design refinements taking advantage of technical development and focusing upon those areas where most concern is centered (ocean engineering, optical detectors, and optimization of the grid of such detectors), can greatly reduce the cost of such a project.

#### 3.6.4. Detector Material:

The Liquid Scintillator (LS) used in the Japanese experiment is composed of 80.2% of dodecane ( $C_{12}H_{26}$ ), 19.8% of pseudocumene (1,2,4-trimethylbenzene,  $C_9H_{12}$ ), and 1.52 g/liter of PPO (2,5-diphenyloxazole,  $C_{15}H_{11}NO$ ), where PPO is the scintillating molecule, pseudocumene is for energy transfer, and dodecane is a dilutant. This composition was determined with examining light output, optical transparency, radioactive contamination, particle identification performance, alpha-particle quenching factor, Hydrogen/Carbon ratio, chemical stability, industrial supply capacity, and cost. Among several candidates, paraffin oil such as dodecane was found to be the best dilutant for the KamLAND LS. Since paraffin is an unsaturated compound, which contains neither unsaturated bond nor ring structure, it has good light transparency, high Hydrogen/Carbon ratio, and chemical stability. For the buffer oil, which is required to have the same density as that of the LS within 0.3% difference to protect the balloon, mixture of dodecane and isoparaffin with density adjustment was used. PPO is one of the most commonly used scintillation light emitters. The fraction of PPO, 1.52g/l, was determined by seeking balance of the light output and the cost. Addition of pseudocumene improved the light output and particle identification performance, but decreased the light transparency. The fraction of 20% was

chosen after considering the light output, light transparency, particle identification performance, chemical stability, flash point, and cost.

All of these issues need to be reinvestigated for the proposed ocean project. First we do not have the same concerns over flash point as does a mine based experiment. These are volatile (and non-toxic oils) and would evaporate from the surface after a spill, so we anticipate no environmental concerns (plus the Hanohano detector will be “double hulled”). However, we must contend with ocean pressure up to about 400 atmospheres and low temperatures ( $\sim 4^{\circ}\text{C}$ ), under which conditions some materials may suffer degraded transparency. A new liquid scintillator has been explored by an Italian research group. The scintillator consists of 1,2-dimethyl-4-(1-phenylethyl)-benzene (phenyl-o-xylylethane, PXE) as solvent and 1,4-diphenylbenzene (para-Terphenyl, p-Tp) as primary and 1,4-bis(2-methylstyryl)benzene (bis-MSB) as secondary solute. They achieved attenuation lengths of the scintillator mixture of 12 m at 430 nm after purification with an alumina column. A radio carbon isotopic ratio of  $^{14}\text{C}/^{12}\text{C} = 9.1 \times 10^{-18}$  has been measured in the scintillator. Initial trace impurities, e.g.  $^{238}\text{U}$  at  $3.2 \times 10^{-14}$  g/g could be purified to levels below  $10^{-17}$  g/g by silica gel solid column purification. Yet another material has come to our attention, LAB (linear alkybenzene, a precursor to dish soap production, and produced in large pure quantities. As will be discussed later this material has become our first choice for Hanohano.

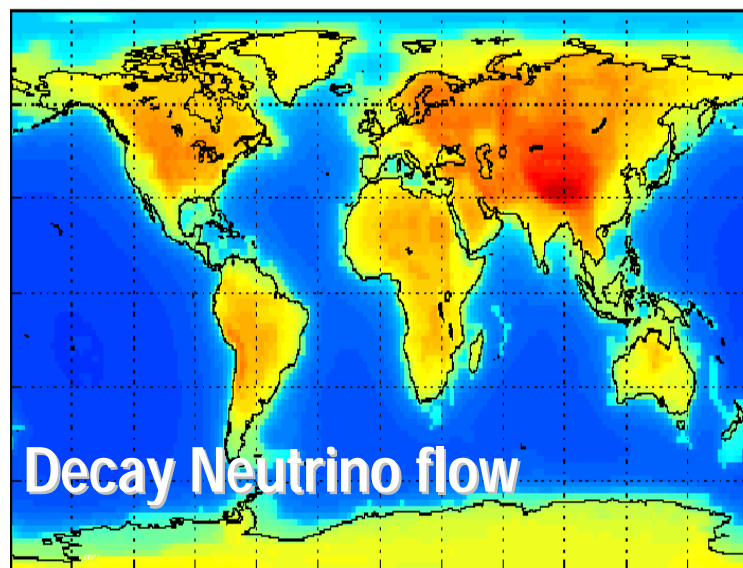


**Figure 4:** Global geo-neutrino flux.

### 3.6.5. Background radiation:

Figure 3 shows a color coded map of the expected flux of geo-neutrinos (electron anti-neutrinos from natural radioactivity), mostly due to naturally radioactive uranium and thorium decays and having energies as observed in the detector of between about 1.0 and 2.6 MeV.

While developing a detector for nuclear deterrence, and measuring background radiation, there are important science issues that can be resolved with the initial Hanohano. This detector will be used for a clean measurement of the Earth total radioactivity (yielding information about the composition of the earth's core) and a sensitive search for a core reactor. Development of this detector in the deep ocean will demonstrate its practical value in nuclear deterrence. Background geo-neutrino measurements demonstrate the technology, calibrate the background noise (some of which can only be measured in a large scale detector), and yield fundamental data important to science.

Site	Location		Uranium		Thorium		Total (U + Th)	Reactor bkgrnd
			crust	mantle	crust	mantle		
Gran Sasso Lab <i>(Italy)</i>	42N	14E	1.8	1.4	1.5	1.2	5.9	0.65
Kamioka Mine <i>(Japan)</i>	36N	137E	1.5	1.4	1.3	1.2	5.4	1.5
Sudbury <i>(Canada)</i>	47N	81W	2.3	1.4	1.9	1.2	6.8	1.3
Central Australia	25S	133E	1.9	1.4	1.6	1.2	6.1	0.016
Himalayas <i>(Tibet)</i>	33N	85E	2.5	1.4	2.1	1.2	7.2	0.054
Pacific Ocean <i>(Hawaii)</i>	20N	156W	0.22	1.4	0.16	1.2	3.0	0.027

**Table 1:** Calculated anti-neutrino fluxes [ $\times 10^6 \text{ cm}^{-2} \text{ s}^{-1}$ ] for sites around the world. (from Rothschild, et al, arXiv:nucl-ex/9710001).

### 3.6.6. Geo-Neutrinos and Earth Composition:

Geologists know a great deal about the near surface (few km) of the crust where the earth composition can be studied in the laboratory. About the lower crust, in the mantle and the core there is only speculation, and some intense debate about the earth composition. (In fact, we know more about the composition of the sun than we do about the bulk of the earth). In most places, the geo-neutrino rate is totally dominated by the crust and hence a measurement cannot reveal much about the deep earth composition. For example, the high flux of geo-neutrinos in Japan come predominantly from the earth's crust.

More quantitatively, in Figure 3 we see that Hawaii geo-neutrino rates are dominated by the flux from the mantle, and that the reactor background from the whole world is negligible. This is from a very simple earth model which assumes uniform distribution, and no U and Th at all in the core. More detailed estimates for Hawaii indicate that the lower mantle makes the largest contribution, 46.8%. The flux from the bulk mantle totals 73.0% of the total geo-neutrino flux, in great contrast to continental or near continental sites where the crust dominates. While seismic studies reveal sound velocities throughout the earth, one cannot determine the elemental mix, particularly of those trace elements that dominate the total heat flow from the earth (K, U, Th).

In summary, a measurement of the geo-neutrino flux from Hawaii will constitute the first probe for the deep earth concentrations of these transuranic elements, vital to understanding of earth heat budget, and hence to planet formation and many other areas such as plumes and continental motions.

### 3.6.7. Georeactor:

The hypothesis of a reactor at the core of the earth has been championed by J. Marvin Herndon over many years. The full story is too lengthy to repeat here (see <http://nuclearplanet.com/>), but the essence is that Herndon claims that the standard bulk silicate earth (BSE) model based upon Carbonaceous Chondrite (CI) meteorite samples is incorrect and that another meteorite category, called Enstatite Chondrites are more representative of the early earth accretion. The relative lack of oxygen in these compared to CI would mean that much of the heaviest elements had not floated like slag up into the earth's crust, but sunk to the bottom of the predominantly iron core. Earlier levels of  $^{235}\text{U}$  would have been sufficient to have permitted a natural reactor to ignite (as was observed to have taken place in the famous Oklo region in Africa, albeit from a different concentration mechanism). Herndon further hypothesizes that the energy produced, which he estimates at 3-10 TW (out of the measured earth total heat outflow of 31-44 TW), is sufficient to drive the deep earth circulation which in turn produces the earth's magnetic field. The natural poisoning of the reactor with decay material could then explain the fluctuations in the earth's geo-magnetic field. The supposition is that the geo-reactor shuts down while lighter substances diffuse from the inner core, whereupon the reactor reignites. Perhaps the most compelling piece of direct evidence for this scenario is that geologists have long known that the ratio of  $^3\text{He}/^4\text{He}$  in volcanic outflows (such as in Hawaii) is many times higher than can be explained by primordial abundance.  $^3\text{He}$  comes from Tritium decay, and in the earth's atmosphere since WWII it has been relatively higher than the past due to human activity. Yet the volcanic emission is greater yet, and no sensible geological model has been put forward to explain it. There are as well many other discrepancies with the BSE model, most prominently that of the potassium abundance of the earth which is lower than CI based expectations by a factor of about ten. Again geochemists have not done well in explaining how a not very volatile element such as potassium could have been depleted from the early liquid earth. This tends to impugn the entire BSE model.

Figure 4 shows the measured data from the KamLAND experiment plotted in five bins of expected rates (the Japanese power reactors turn on and off and so the neutrino rate changes). By extrapolating to zero in predicted rate one can look for a non-zero offset in observed rate, which could be due to a geo-reactor. One sees that the data perhaps hints at a positive intercept (dashed line is unconstrained fit, solid line fit forced through the background estimate), but unfortunately the statistical errors are far too great to draw any conclusions (as indicated by the shaded area). The rate due to the Herndon geo-reactor would amount to 0.03-0.10 events/day on this scale. One thus sees graphically why it is necessary to conduct a search for the putative geo-reactor from a location far from man-made power reactors. In Hawaii, with no power reactors within thousands of miles, the search for neutrinos from a geo-reactor becomes practical. Such electron anti-neutrinos have energy up to about 6 MeV and are thus distinguished from geo-neutrinos (Nuclear

reactor powered ships do not make enough anti-neutrino flux to be detectable with the presently discussed 20 m instrument).

We would expect to have lower backgrounds than in the present in the initial version of the KamLAND experiment due to both advances in techniques for radio-purification and by placing the detector in sufficiently deep ocean ( $>3$  km) to avoid cosmic ray generated backgrounds which are non-trivial at KamLAND. With a fiducial volume of approximately 1 kiloton we can expect a count rate from the geo-reactor of  $>27$  events per year, essentially background free and a five standard deviation observation even at the minimum power (3 TW) predicted by Herndon.

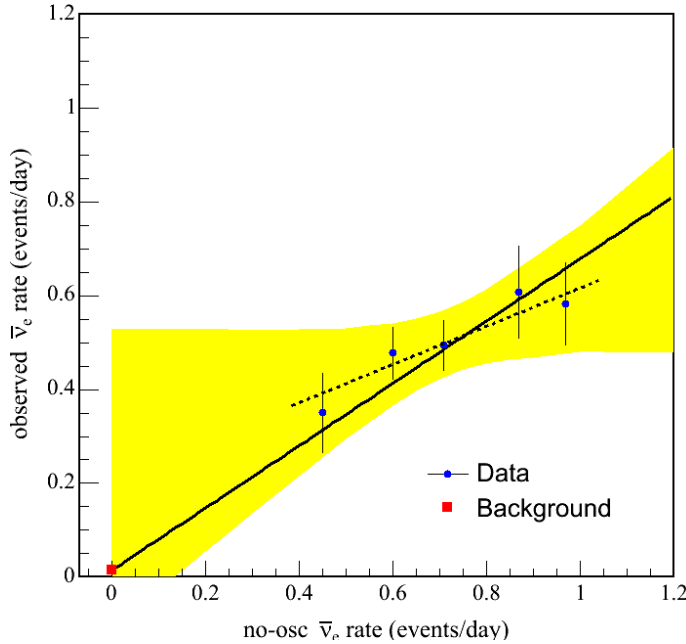


**Figure 5:** KamLAND observed rate at various predicted rate levels.

### 3.7 TECHNICAL INNOVATION

This work claims innovation in several areas:

- An innovative means of monitoring man-made nuclear activity throughout the world. Bomb tests and reactors could not be hidden from these detectors.
- *Breakthrough science from use of Hanohano:* This first detector will be extremely valuable for measuring the earth's total radioactivity from near Hawaii (the best region on earth for this), and resolving fundamental issues relative to (1) the composition of the earth and (2) the existence of a (hypothetical) natural reactor at the earth's core. The latter radical proposal has been gaining notice around the world, and if correct, would cause major revision of our understanding of the origins of the geo-magnetic field, the viability of life on this planet, and evolution of this and other planets. Our consideration of the use of Hanohano for measuring neutrino properties has revealed unique and exciting opportunities in elementary particle physics for the 10 kiloton detector.

- *Ocean engineering challenges:* The successful and cost-effective installation of these detectors in the deep ocean will require original structures, materials, and instrumentation components.

## 4. WORK PERFORMED, TASK CONCLUSIONS

### 4.1 PROJECT TEAM

This project was managed by Makai Ocean Engineering who focused the team on identifying issues and solutions to those issues relative to the specific Hanohano and NDD systems. The Physics and Astronomy Department of the University of Hawaii was a major subcontractor and responsible for all the science-related tasks of this work. Responsibility for tasks resided with Dr. Joe Van Ryzin (Principal Investigator) at Makai and Dr. John Learned at UH (Co-Principal Investigator). The project was coordinated through management and brainstorming meetings, and technical data exchange through a dedicated e-log website.

### 4.2 TASKS

The following sections describe each task requirement, what was accomplished, and the conclusions. For each task, the reader is referred to a specific formal report for the work. All detailed technical reports, as well as papers and conference descriptions and other background material are attached to this summary report.

#### 4.2.1. TASK 1 - Determination of detector size, sensitivity, and location required to perform neutrino geophysics measurements.

This task determines the size, sensitivity, and location of the detector needed to accurately identify and characterize the geophysical background signals. The required size of the detector depends on the duration of the observing period and the strength of the geophysical signals. The required sensitivity of the detector depends on the energy spectra of the geophysical signals. The location of the detector depends on the required overburden of matter for shielding cosmic radiation (depth of ocean water) and distance from significant local geophysical variations in uranium and thorium (e.g. island mass, ocean sediment).

##### 4.2.1.1 Summary results and Conclusions

A major component of this task was the generation of a computer program capable of detailed simulations of the various geophysical signals and other environmental backgrounds (e.g. K40). A second computer program was written and employed to study the neutrino physics capabilities of the Hanohano detector. Using information collected by a literature search, these programs facilitated initial optimization of first level detector design parameters: size, sensitivity, and location. The products of this task are recommendations for the detector size in tons, sensitivity in photoelectrons per MeV, and location in depth of ocean and distance from land masses.

- Required size for geo-reactor: with a goal of making a conclusive test of the georeactor hypothesis on a one year times scale it was necessary to move to a somewhat larger fiducial volume specification, several times that of KamLAND.
- For the useful study of the U/Th decay neutrinos from the mantle (and core) within a one year exposure it was necessary to increase the detector scale to the 9

kiloton range. It turned out later that this move had tremendous positive impact upon the neutrino physics capabilities as well.

#### 4.2.1.2 Detailed Report

The technical discussion and results of this task are reported in the report, “*Hanohano Neutrino Detector*” attached to this summary report.

#### 4.2.2. TASK 2 - Determination of detector size and sensitivity for nuclear deterrence.

The size and sensitivity of the detector capable of nuclear deterrence depends on the strength and spectra of the signals, proximity to the sources, and integrated detection time. The neutrino signals from possible sources require characterization. Of interest are neutrino emissions from nuclear explosions of various types and from nuclear reactors processing fuel for weapons grade fissile material. Luminosity and spectral information from these sources are needed for the generation of a computer program capable of detailed simulations. A thorough search of available literature recovers this information. Execution of the program established detection criteria as a function of source type, power, and proximity. These criteria lead to the specification of detector parameters including size, sensitivity, and number and distribution of modules.

##### 4.2.2.1 Summary results and Conclusions

- We have identified scale required for a network of ocean and lake bottom detectors (~500 to cover entire world, 3-5 to cover a specific region).
- The cost of 100 megaton scale detectors and engineering limits were studied. These are prohibitively expensive with present technology.
- A pacing technology is needed for 21st century photo detectors. There is the need to go from the present \$1/cm<sup>2</sup> to the order of \$10-100/m<sup>2</sup>. This was determined feasible and likely; component technology exists, product development needed.
- Engineering, water purification, and delivery systems all need studying. Study conclusions: no show stoppers, but much work to be done.
- A smaller scale Hanohano will demonstrate “small scale” (9 kiloton) detector, measure backgrounds, accumulate experience, yield excellent geology and provide important physics measurements.

#### 4.2.3. TASK 3 – Design of 20 m structure.

This task focused on determining the basic shape and configuration of a Hanohano structure taking into account the practical engineering issues of construction, testing, deployment, service in the deep ocean, recovery, and re-deployment. The primary issues are structural strength, weight for submergence, stability, and configuration to meet the needs of the science. Material constraints included structural loading (anchoring, deployment, and construction) as well as material limitations for the physics (transparency, low radioactive emissions, and fluid contamination), long term service (corrosion, serviceability), and cost.

##### 4.2.3.1 Summary results and Conclusions

As the work progressed, the scientific needs of the project varied. There was a overall physics need for a large detector and this was balanced against the practical feasibility for very large detectors and economic reality. This work evaluated a variety of concept shapes for the detector itself (cubes, spheres, cylinders) and for the ballast support structure (integrated or separate barge structure). The analysis considered five primary design constraints: weight and displacement for ease of deployment, stability during all phases of the operation, real-world size limits (canals and harbors), structural capability within the weight allowance, and cost. The engineering analysis considered detectors ranging from 2 to 120 k-tonnes.

- For the detector, cylindrical shapes were preferred for ease of construction and for lightweight construction of pressure hulls.
- The detector can be reliably submerged and recovered based on the buoyancy of the oil and scintillator as long as the steel mass is equal to or less than 15% of the scintillator plus oil mass. This is valid for all sized detectors.
- Two sizing constraints dictated the design: maintaining a 10m draft in harbors and keeping within 32.3m width for Panama Canal passage.
- Two configurations were evaluated:
  - An integrated system where the barge hull and detector are one structure.
  - A detachable system with a separate support barge and detector.
  - A single lowered detector (pictured in our proposal, Figure 2) was quickly abandoned as being unmanageable at a size larger than that illustrated.
- The detachable system was preferred:
  - The margin of safety on the weight goal is much larger for the detachable system. There is more future design flexibility.
  - There are fewer stability problems with the detachable system.
  - The detachable system concept could be used for very large detectors.

- Support barge can maintain multiple detectors, can be used to transport and store the scintillator, and can serve as the hotel for critical support equipment.
- Cost was not a factor in the decision; there were no clear cost advantages of one concept over the other.

#### 4.2.3.2 Detailed Report

The technical discussion and results of this task are reported in Chapter 2 of the report, “*A Deep Ocean Anti-Neutrino Detector near Hawaii – Hanohano: Ocean Engineering Analysis*” attached to this summary report.

#### 4.2.4. TASK 4 - Design of photo-detector and housing prototype.

This task determined the design modifications necessary for utilizing photomultiplier tubes (PMTs) in a deep ocean environment and produced a prototype module suitable for high pressure testing.

Historically, PMTs have been used in the deep ocean in optical modules for neutrino astronomy, which continues today. A standard method is to enclose the fragile photomultiplier tube inside two coupled hemispherical glass shells. The commercially available glass shells are thick enough to withstand the extreme hydrostatic pressure encountered on the ocean floor. The additional requirements of this application introduce many details, such as electronics, which must be addressed.

##### 4.2.4.1 Summary results and Conclusions

- Each PMT will be housed in a glass sphere to protect it from the large pressure at 4000 m. The remaining empty space in the sphere can be filled with syntactic foam to help absorb collapse energy in the event of catastrophic housing failure (see Task 5).
- A 10 inch PMT will nest with a Winston cone, a light collector which increases the optical capture of light emanating from the scintillator volume.
- Silicon gel (RTV) will be used to optically couple the PMT to the housing.
- There will be minimal electronics in the glass sphere: only the high voltage for the PMT dynode chain.
- Analog signals will be sent forward from the individual optical modules to neighborhood digitizers via either a coaxial cable or a twisted pair.
- The closest existing design is being employed in the ICECUBE experiment. Our version will have simpler electronics, a less expensive connection, and may have added syntactic foam.

- In the next iteration in the design we should evaluate the possibility of using the larger housing (accommodating 70% more photocathode collection area per unit). There are also several new types of PMT in pre-production, including a hybrid tube that appears to be a possibility.

Completed electronics prototypes:

- PMT voltage supply manufacturers were surveyed, sample devices are in hand, and several choices are available (used in South Pole and Mediterranean experiments).
- PMT signal electronics prototypes were constructed and tested at UH electronics facility; these are ready for second round ocean tests.
- Signal digitization electronics prototypes were constructed and tested at UH; they are ready for second round.
- There are no showstoppers: the power is as expected. The system needs further refinement with reliability testing, etc. The existing design is adequate for the proposal stage with predictable costing at this time. Another round of optimization is desirable.



#### 4.2.4.2 Detailed Report

The technical discussion and results of this task are reported in the report, “*Optical Module Design*” attached to this summary report.

#### 4.2.5. TASK 5 – Study of means to prevent successive implosions and in situ testing

The photo-detectors will be contained inside 13” glass spheres provided by Benthos. Glass spheres are highly reliable pressure housings for the deep ocean, but occasionally they do fail. We are not able to obtain statistics upon failure rates, though they are rare, and generally the oceanographic wisdom is that failures are associated with abuse of the housings on deck. Hence we must design for the potential of an implosion.

The sudden implosion of a glass sphere generates a sudden release of energy proportional to its volume times the pressure (>400 atmospheres). The pressure wave can significantly damage adjacent structures, and there are many reported, though not well documented, cases where adjacent glass spheres have successively imploded (typically a cluster of housings in a floatation package). Because Hanohano has many thousand spheres, each practically touching the other, the consequence of successive implosions could be catastrophic. This task analyzed this implosion process, performed analytical modeling of the implosion, did at-sea tests of the implosions, and investigated various methods of protecting adjacent spheres.

#### 4.2.5.1 Summary results and Conclusions

This task was a primary focus for the CEROS work and funding. The sympathetic implosion of spheres was considered a “show-stopper” for Hanohano. As a result of no second-year funding by CEROS (where we planned additional implosion tests) and the lack of conclusive results in our initial at-sea tests, the team decided to increase the level of testing in the current year to improve program confidence and chances of funding from other sources. Less critical tasks (14) were cut back to allow expansion of this more critical work.

- The level of energy released upon an implosion is significant. For a 13" diameter glass sphere at a depth of 4000 m, the theoretical energy stored is approximately 600 kJ. One quarter of this is converted into acoustic energy.
- We investigated methods of studying implosion mitigation with reduced-scale physical models (smaller, weaker spheres). This proved to be impractical because all key parameters of the implosion could not be effectively represented by a model.
- Analytical models (ALE3D) were run, which effectively and accurately modeled the implosion.
- Several methods of preventing successive implosions were investigated: oil inside sphere (reduce energy released), energy absorption material inside the spheres, barriers between the spheres, redirection of the shock wave, and alternate acrylic spheres.
- Two at-sea tests were performed with actual 13" spheres forced to implode at 4000m depth by weakening the glass.
- Glass spheres spaced at 0.8 m on center will have sympathetic implosion: one imploding sphere will cause the collapse of the adjacent sphere.
- Oil-filled (30%) spheres and concrete barriers did not prevent sympathetic implosions.
- High strength syntactic foam (30% volume) inserted in the imploding sphere absorbed enough energy to lower the peak pressure by 30% and widen the pressure wave sufficiently to prevent successive implosions of adjacent spheres in two out of two tests.

- We have a good indication that there is a solution, but lower cost solutions would be preferred and additional testing is required to demonstrate our safety factor on sympathetic implosion.



#### 4.2.5.2 Detailed Report

The technical discussion and results of this task are reported in Chapter 4 of the report, “*A Deep Ocean Anti-Neutrino Detector near Hawaii – Hanohano: Ocean Engineering Analysis*” attached to this summary report.

#### 4.2.6. TASK 6 - Electronics preliminary design for low power application.

This task produced a preliminary design for detector electronics minimizing power consumption.

Recent advancements in low power electronic components for particle detection applications open the possibility of deploying a detector with a self contained power source. In any case keeping the total detector power under a few kilowatts simplifies cable connection. This is an attractive prospect given the likely remote location of the detector and the simplification of deployment. A thorough literature search for components of potential use initiated this task. The preliminary design utilizes reliable, low power components which meet the operating criteria of the photo-detectors. Schematic drawings document the design. A report discusses the prototype design built at UH.

##### 4.2.6.1 Summary results and Conclusions

- Other projects in the ocean and ice (Nestor Nemo, and Antares, in the Mediterranean, and the ICECUBE project at the South Pole) have similar design requirements, and we have taken advantage of their studies.
- Power to 1w/PMT was achieved.
- Simple electronics were designed and tested, which will minimize cost and maximize reliability.
- A second round of design optimization is desirable. There are no show stoppers.

- PMTs under active development at present (hybrid) should be considered if available at the time of a second design iteration. No replacement for photomultiplier tubes is at present close to availability.

#### 4.2.6.2 Detailed Report

The technical discussion and results of this task are reported in the report, “*Electronic Design for Reliability and Low Power*” attached to this summary report.

#### 4.2.7. TASK 7 – Simulation of deployment of vessel.

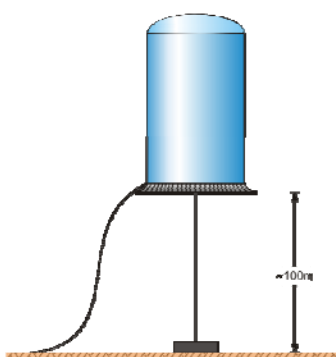
One of the major issues relative to Hanohano is whether it can be practically built, installed, maintained on the seabed and then retrieved. This task investigated issues relative to the movement of this vessel from the dock to a test location at 4000m and back again.

Hanohano is a unique underwater vehicle. When built, it may be the most massive structure ever deployed in the deep ocean. Typically, the engineering mission of Hanohano is to reliably place on the seabed at 4000 m a vehicle with a mass of 25 kilo tonnes and retrieve it after a year of service. Nuclear submarines, in contrast, are smaller. A Titanium Soviet Alfa class submarine is capable of 800 m depth and has a displacement of 3 k-tonne; a US Virginia Class submarine is roughly 13 k-tonne with a shallower depth capability and with a cost exceeding 2 billion dollars. These submarine costs are in the range of billions of dollars. The Hanohano mission is to move twice that mass to much greater depths at roughly 1% the budget.

#### 4.2.7.1 Summary results and Conclusions

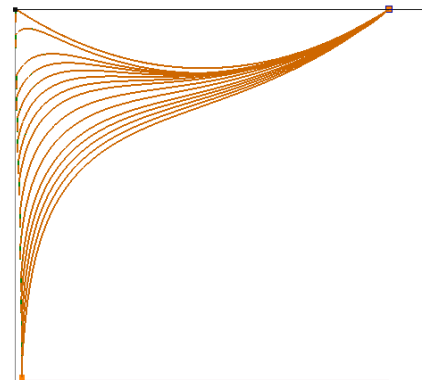
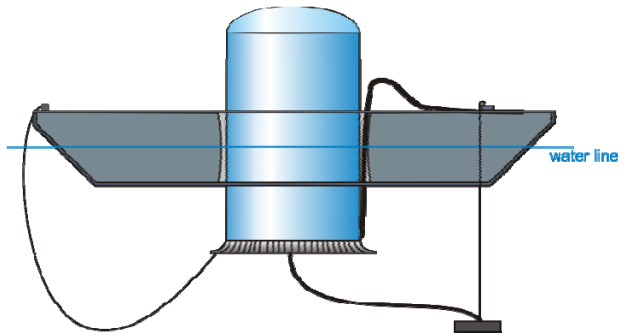
The team evaluated deployment issues relative to detector weight and displacement, cost for buoyancy, reliability of recovery, ascent and descent speeds, bottom impact oscillations, marine stability during flooding and deballasting, and deployment of the cable to shore during sinking.

- Because of the low density of the scintillator and oil, Hanohano can practically and economically descend to the seabed at 4000 m and ascend again by dropping a bottom anchor. The operation could be very safe, similar to a very large scale bathyscaphe (deepest manned dive to 11,000 m in 1957).



- Hanohano would descend 4000 m and ascend rather rapidly, approximately 30 minutes each way.
- Hanohano will have to be suspended off the seafloor by a minimum of 100 m on a pendant attached to a concrete anchor. This clearance allows for safe touchdown and the resulting oscillations upon impact.

- The detector would be controllably flooded prior to sinking. The filling sequence is important for proper stability.
- The final configuration of Hanohano allows for high stability and rapid towing during transit, similar to a standard barge.
- Hanohano can be easily recovered by releasing the concrete anchor on the seabed. This can be done once the mission is accomplished, or if the detector needs to be recovered for maintenance. The bottom anchor is abandoned.
- The power and communication cable can be attached prior to submergence. It is monitored during descent and then laid to shore in a conventional deep water cable lay. Two methods of cable lay have been developed.



The deployment of the vessel is critical to all the engineering analysis performed. In particular, Chapter 2 discusses the deployment considerations that drive the overall design and Chapter 3 discusses the deployment of the 10 k-m<sup>3</sup> detector.

#### 4.2.7.2 Detailed Report

The deployment of the vessel is critical to all the engineering analysis performed. The technical discussion and results of this task are reported in “*A Deep Ocean Anti-Neutrino Detector near Hawaii – Hanohano: Ocean Engineering Analysis*” attached to this summary report. In particular, Chapter 2 discusses the deployment considerations that drive the overall design and Chapter 3 discusses the deployment of the 10 k-m<sup>3</sup> detector.

#### 4.2.8. TASK 8 - Pressure testing of scintillation materials in the laboratory.

This task explored the suitability of standard scintillation oils for use in the deep ocean environment. Although scintillation oil is commonly used in the experimental laboratory, its optical and mechanical properties at high pressure and low temperature need to be measured. It is known that oil at very low temperatures can become cloudy as the paraffin (longer hydrocarbon chains) in the oil precipitates out of solution. The temperature at which this occurs is known as the pour point, which can be depressed with certain additives. The possibility of using different mixtures or additives to achieve the desired characteristics is investigated. Properties of interest include: volume changes (bulk modulus and thermal expansion coefficient), fluid flow characteristics (viscosity), verifying that all components of the scintillation oil remain mixed (miscibility), and optical properties including attenuation over an appropriate wavelength range. The light

production capability (photons per MeV of ionizing energy) is not considered at this point, as expert opinion indicates no expectation of variation.

#### 4.2.8.1 Summary results and Conclusions

We have confirmed that we have a working scintillator material:

- LAB – linear alkylbenzene is an excellent material.
- Clarity: >10 m attenuation
- Proton density = 0.122
- Optical output >5000 photons/MeV
- Cost ~\$10M
- Specific gravity is 0.85 at surface temperature and pressure, and 0.9 under high pressure low temperature bottom conditions.
- Compressibility = 3.4% (vs 1.5% seawater)
- Thermal contraction = 2% (vs 0.5% seawater)
- LAB is compatible with acrylics and has low toxicity.
- LAB is manufactured in industrial quantities (soap) and has multiple suppliers, so it is widely available.
- Similar material has been employed in the 1 kilo-ton KamLAND experiment in Japan (in which UH is a collaborator).
- Radio purification has been demonstrated for similar liquids, under development (Canada) for LAB, lab studies UH.
- Alternatives materials were studied and multiple suppliers were contacted. Several options are available if problems occur in the future (none foreseen).
- Specific gravity and compressibility are acceptable for providing buoyancy to the detector structure.
- The oil must retain its ability to flow at depth to allow for calibration procedures. Our initial data shows some indication of this effect in the small and not well protected samples used in initial tests. It is expected that ultra-filtering will remove this problem (as indicated from some measurements made on LAB at Brookhaven National lab).



#### 4.2.8.2 Detailed Report

The technical discussion and results of this task are reported in a UH Master's dissertation, attached to this summary report. Graduate student Peter Grach used this task for his graduate research work.

#### 4.2.9. TASK 9 – Workshop

This task was removed from the CEROS-funded project during cost negotiations and therefore is not a deliverable. This task was extremely critical, perhaps one of the most critical of all the tasks, and it was performed with UH funds. Building collaborative support and cross-education within the scientific community was critical in terms of subsequent funding.



The conference, *Neutrino Sciences 2005: Neutrino Geophysics*, was an international workshop organized and hosted by the University of Hawaii in December 2005. The workshop was an unqualified success (see [www.phys.hawaii.edu/~sdye/hnsc.html](http://www.phys.hawaii.edu/~sdye/hnsc.html) for the scientific agenda and links to presentations) in bringing together world leaders in geology and neutrino detection to share information on geology, neutrino geophysics, detector technology, and nuclear monitoring. This meeting has led to formation of a working group to initiate a Major Research Equipment funding request from the National Science Foundation. A special session of the Spring American Geophysical Union meeting, which is titled *Geo-neutrinos, a new tool for the study of the solid Earth*, was scheduled by geologists attending the Hawaii workshop to facilitate this effort.

We are submitting this workshop as our contribution to the Educational Outreach Program. The 3-day seminar was attended by numerous UH students.

##### 4.2.9.1 Summary results and Conclusions

This world's first workshop on neutrino geophysics was conducted at the University of Hawaii inviting leaders in neutrino physics and the geosciences. Scientists with widely varying backgrounds in geology and physics exchanged "science" and collaborated on how to use a new tool in physics to solve critical problems in the Geosciences.

- This effort contributes to establishing Hawaii as a recognized center of expertise in the design, construction, deployment, and maintenance of deep ocean neutrino detectors, and in the long run for nuclear deterrence and science.
- A number of leading geologists have endorsed the project and wish to be involved.
- The team received critical design feedback from the neutrino physics community on scintillators and the operation of neutrino detectors.

- The needs of geologists were further refined, which impacted the design criteria for Hanohano. Overall, the community encouraged larger detectors located at several globally dispersed sites.

#### **4.2.9.2 Detailed Report**

The UH will publish the proceedings from this 3-day conference (roughly 300 pages) to be printed in December, 2006, in a refereed publication. A brief description of the conference is attached to this report with a list of papers presented. The paper presented by the UH Hanohano team at this conference is also attached.

#### **4.2.10. TASK 10 - Design for communications networking inside vessel.**

This task designs the communication network inside the detector vessel. On the order of 4000 photo-detectors require command and control signals from the central computer. These signals turn high voltage on and off, monitor noise rates, and run calibration procedures. Networking to provide reliable communication is required for a successful project. A literature search commenced this task.

##### **4.2.10.1 Summary results and Conclusions**

- The simplest possible data handling will be used: send everything to shore. Past projects have faced a similar challenge, and generally have resorted to significant signal processing at the remote location. The swiftly advancing fiber optics communication technology makes it easily possible to send every photomultiplier pulse to shore for processing, including trigger finding.
- A two layer tree structure of data connections, with minimal electrons at the PMTs is recommended.
- A tree structure will be used (as opposed to a local area network) whereby individual modules are connected to neighborhood digitizers and these units connected to the main controller/multiplexer to communicate to shore.
- A redundant high level controller/multiplexer and communications path to shore is recommended.
- The PMTs will be as simple as possible, and employ one cost and power effective intermediate layer of digitizers (roughly the square root of the total number of channels, about 64 units). Failure of one or two such units would be tolerable. Above this the system will be redundant, with two parallel main controller/multiplexers and channels to shore.
- The physical connections will be via cable from the optical modules (PMTs in housings) to the digitizers, and fiber optics for signals there above.
- All connectors and cables internal to the detector can be in oil, a well known technique for ultra-reliable deep ocean connection (as used in manned submersibles).
- The pre-assembly (and testing) of the entire system can be accomplished entirely at pier side.

#### 4.2.10.2 Detailed Report

The technical discussion and results of this task are reported in the report, “*Internal Communications Networking*” attached to this summary report.

#### 4.2.11. TASK 11 - Study of power and communication links to shore.

The decisions reported above are part of this task as well. Namely we recognize that with 4000 optical modules with a data rate of 10,000 pulses per second (mostly noise) leads to a data rate of order 1 gigabit per second. Fiber optic communications links have gone more than an order of magnitude beyond this (two orders in demonstration links), so we will not even push available capacity. Also typical ocean cables have a few fibers, which we can utilize for redundancy.

Power for the array is estimated in the range of 2 kW. If we accomplish another round of design this could be reduced even further, but the present loading is again well within the capability of existing ocean telecom cables. A matter for further exploration and engineering is the use of higher voltages. In the past DC-DC supplies have been limited to input voltages of 500V, whereas ocean telecom cables are typically designed for several kilovolts. Higher voltages are desirable due to lower currents and less voltage drop across the cable. Also AC power would be very nice to employ because transformers are passive and extremely reliable devices (operable at pressure and under oil). While existing practices will suffice, utilizing higher voltage levels and AC power would make for more reliable and simpler operation of the detector.

##### 4.2.11.1 Summary results and Conclusions

- The data communications needs of Hanohano (about 1 Gb/s) are well within standard submarine telecom practice and pose no problems.
- Based on deployment modeling, the cable can be attached to Hanohano prior to submergence and effectively monitored while Hanohano submerges without excessive tensions in the cables; two methods have been modeled. Once successfully operating on the seabed, the cable can be laid to shore with conventional methods.
- Power at the level of several kilowatts provides no great challenge and is well within current technology and practice.
- New DC to DC converters developed with the Neptune project are ideal for this project.

#### 4.2.11.2 Detailed Report

The technical discussion and results of this task are reported in the report, “*Power and Communication Cable to Shore*” attached to this summary report.

#### 4.2.12. TASK 12 – Conceptual Plans for Hanohano.

This task integrated the results from the above tasks and prepared a conceptual design for a single detector. This task focused on details for the larger detector once the optimization

had been performed in the earlier tasks. Details such as final weights and stability, structural checks, deck and equipment arrangements, deployment details, general operations, plumbing and wiring, compensation, and PMT placement details and were considered in this task.

#### 4.2.12.1 Summary results and Conclusions

As our work progressed, the originally envisioned spherical detector, Figure 2, containing 1.4 k-tonnes of scintillator grew into a 9 k-tonne detector system with a dramatically different shape and operational scenario – driven by the engineering and mission needs. The final detector and barge are shown in the figure below.

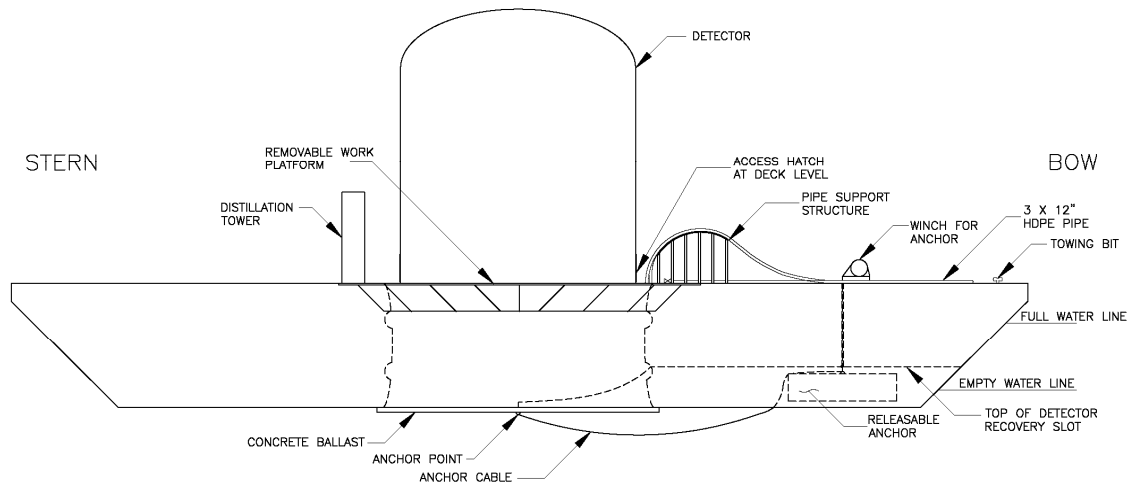


**Figure 6:** Overall profile of the detector and barge.

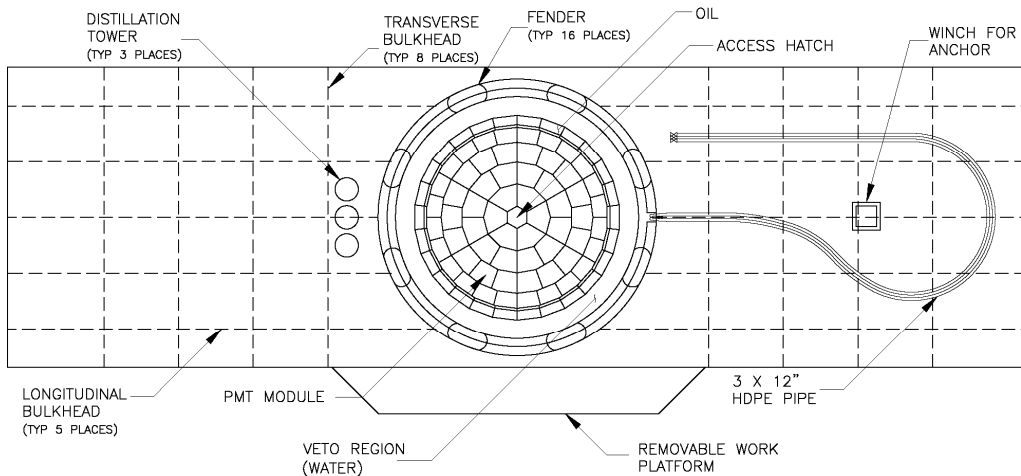


**Figure 7:** Plan view of the final Hanohano

- The final design focused on the detachable configuration with a separate support barge and detector.

**Barge:**

- The support barge has a overall length of 112 m, a beam of 32.3 m (just fitting the Panama Canal), and an overall height of 13.8 m. Fully loaded draft is less than 10 m.
- The support barge has a conventional barge-shaped bow and stern. With a nominal draft, the detector can be towed safely and reliably to any location on the world's oceans.
- The barge contains tanks for storing all the scintillator and all the oil used in the detector. Multiple stainless tanks are used to maintain the liquid purity, to facilitate transfer during purity distillation, and to maintain barge stability when tanks are partly filled; nitrogen is used in unfilled voids to maintain purity.
- The barge serves as the hotel for detector support. Crew quarters, lab space, generators, water production equipment, nitrogen storage, and scintillator cleaning equipment are located in or on the barge.
- The detector uses a nominal  $7000 \text{ m}^3$  of fresh water to eventually flood the veto region during submergence. This fresh water is generated with a built-in RO plant. Producing the fresh water needed is more economical than transporting it.
- The estimated cost of the support barge is 8.9 million dollars.

**Detector:**

- The detector is cylindrical with an outer diameter of 26 m, and an overall height of 44.7 m. The fiducial volume has a diameter of 20 m and an overall height of 35 m. There is a buffer layer 1 m thick surrounding the scintillator and a 2 m layer of fresh water veto region surrounding that layer.
- There are approximately 4300 phototubes spaced at a nominal 0.8 m in the buffer region surrounding the fiducial volume. Clear Lexan plates separate the scintillator region from the surrounding oil.
- The 2 m wide veto region is built in layers with horizontal grated decks spaced at a nominal 4.8 m. Decks are accessible within the detector through stairwells in the veto region. The veto region is the main manned access into the detector, with all wiring and plumbing going through this area.
- Some decks within the veto region are water tight, to provide stable and minimal free-surface flooding stages during deployment.
- Large polypropylene compensator bags are located at the bottom of the detector to compensate for volume changed due to compression and cooling at 4000 m depth. The compensator bags compensate for the fresh water and scintillator only. The oil buffer region is compressed by a flexing of the Lexan cover plate; therefore, the oil volume change is compensated by larger scintillator fluid

compensation bags. Compensation is about 5% of the total volume of the detector – half of that is due to cooling, half due to compression.

- Pre-cooling the scintillator and oil were considered, but this did not prove to be economically viable.
- The detector has a nominal concrete ballast of 744 tonnes (wet). This will vary as the structural requirements are refined.
- The detector has an anchor weight of 607 tonnes (wet). When the detector is launched, it weights 86 tonnes (wet), including the anchor. When it drops its anchor and leaves the bottom after a lengthy deployment, it is 87 tonnes buoyant. Transit times up and down are 38 and 39 minutes respectively.
- Each PMT compartment contains 9 PMTs in a 3x3 array. These compartments are kept isolated from each other in order to (1) avoid differential pressures across the Lexan plate due to density variations between the oil and the scintillator and (2) to isolate damage to a single compartment in case there is a PMT sphere implosion. (If there is an implosion, and the Lexan plate leaks, only the oil from one compartment will mix into the scintillator – a contamination level that is not desirable but acceptable to the physics.)
- All plumbing for flooding and draining the interior of the detector is contained within the veto region.
- The estimated cost of the Detector is 29.1 million dollars. Deployment would be an additional 2 million.

#### 4.2.12.2 Detailed Report

The technical discussion and results of this task are reported in Chapter 3 of the report, “*A Deep Ocean Anti-Neutrino Detector near Hawaii – Hanohano: Ocean Engineering Analysis*” attached to this summary report.

#### 4.2.13. TASK 13 - Engineering study for preparation of low radioactivity scintillation material.

This task considers the handling of the scintillator during the lifecycle of Hanohano. It investigates means of constructing the detector and storage tanks, cleaning them, and filling them such that a minimum amount of radioactive material is introduced to the scintillator. In addition, this task determines means of purifying the scintillator of the small amount of contamination that will inevitably occur. The UH physics department has gained experience from the KamLAND and Borexino projects in achieving the needed levels of radiopurity.

##### 4.2.13.1 Summary results and Conclusions

- Scintillator is sensitive to all radioactive particles, including: oxygen, radon, krypton, uranium, thorium, potassium, as well as other noble gasses and chemical contaminants.

- To prevent radioactive contamination of the detector and storage tanks, they must be constructed of stainless steel and welded using electrodes free of thorium. The welds must be inspected and a leak test performed. All surfaces must be electropolished and have a surface roughness less than 0.6  $\mu\text{m}$ .
- After construction is completed, the inner cylinder and storage tanks will adhere to clean room regulations. Anything entering the detector or storage tanks must first be cleaned. People entering the clean room must pass through an air lock with an air shower and wear a clean suit, mask, and boots.
- All inner surfaces of the detector will be cleaned at least four times by lowering a large collapsible scaffolding through the access hatch. The storage tanks must also be cleaned.
- The tanks will be dried with nitrogen and stored full of nitrogen so they have no further contact with air.
- The scintillator will undergo four purification processes to remove any trace radioactive elements: water extraction, nitrogen stripping, vacuum distillation, and filtration.
- When transporting scintillator from the tanks to the detector, the scintillator will be pumped into the detector and the nitrogen is pumped out and into the storage tanks. In this way, the detector can be completely filled without ever exposing the scintillator or detector to air.

#### 4.2.13.2 Detailed Report

The technical discussion and results of this task are reported in Chapter 5 of the report, “*A Deep Ocean Anti-Neutrino Detector near Hawaii – Hanohano: Ocean Engineering Analysis*” attached to this summary report.

#### 4.2.14. TASK 14 – Design and costing for ocean demonstration

It was desired to deploy a reduced scale detector in the ocean at the end of the second year of CEROS funding. There is a need to test and demonstrate a reduced scale detector with reduced instrumentation and power. The goal is to test key components and materials such as the scintillating fluids, several photo-detectors, communications, deployment methods, and fabrication procedures. The demonstration of these basic instrumentation functions in the deep ocean was viewed as necessary in order to build confidence in funding agencies such as NSF that such a detector could be built and operated in the deep ocean.

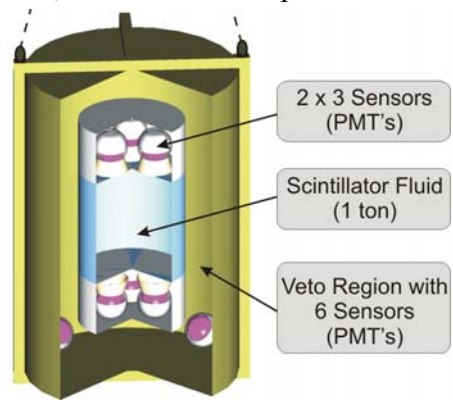
##### 4.2.14.1 Summary results and Conclusions

The anticipated second year of funding from CEROS has not materialized so this planned demonstration will not be done. Realizing that the Hanohano program needed to find other sources of funding, greater emphasis was placed on other tasks and efforts. For instance, additional at-sea implosion tests were conducted in order to achieve some immediate results (and not have to wait for the 2<sup>nd</sup> year component test). Additional efforts were made, with CEROS assistance, at contacting other funding agencies. The ocean

demonstration module has been conceptually designed, but it is not a complete design ready for fabrication and deployment.

- A small anti-neutrino demo structure was designed to test and demonstrate detector electronics, the scintillator, and some critical aspects of deployment.
- Six active PMT's and three veto-region PMTs are installed in a cylindrical package (xxx tonnes) that would be lowered by a UH oceanographic ship.
- Tests were planned for testing the PMT electronics, communications with the detector, clarity and performance of the scintillator, and critical displacement variations (compression and cooling) at 4000 m.
- A separate structure was designed for further testing of the impact of implosions. This test would evaluate the damage to a PMT chamber of 9 PMT spheres and the Lexan cover in the event of an implosion. The resistance to sympathetic implosions in a final system configuration would be demonstrated.

#### 4.2.14.2 Detailed Report



The technical discussion and results of this task are reported in Chapter 6 of the report, “*A Deep Ocean Anti-Neutrino Detector near Hawaii – Hanohano: Ocean Engineering Analysis*” attached to this summary report.

#### 4.2.15. TASK 15 – Final report

This report is the final report for this work. It constitutes this document plus numerous attached detailed reports covering each task.

### 4.3 OTHER PROGRESS

#### 4.3.1. New Science

- Geological goals defined for first round
  - Hanohano can measure U/Th within 12% in 1 year, increased HH size.
  - Successive location at several ocean sites can help understand important issues of mantle homogeneity and turbulent motion.
- New physics possibilities identified
  - Precisely measure mixing angles, Theta\_13, Theta\_12 and determination of the neutrino mass hierarchy – fundamental characteristics of neutrinos that need to be understood.
  - Place Hanohano 50-60 km offshore from San Onofre Reactor in California will proved interesting new physics opportunities, and the ability to tie in with on-shore monitoring.

#### 4.3.2. Other Geo-Neutrino Capable Detectors:

Hanohano is a detector capable of detecting anti-neutrinos from the Earth – geo-neutrinos. Numerous projects capable of detecting geo-neutrinos are emerging from the physics community. Among these Hanohano is unique in both location and portability. Its location on an oceanic plate is far from continental crust and nuclear reactors, which are the major sources of background to the signals from Earth's mantle and core. Hanohano is movable due to its inherent ocean-going design. This allows the project to measure signals at various locations providing important geophysical data and demonstrating capability for nuclear monitoring deployment. All other projects are sited in deep mines on continental plates with nuclear reactors in the vicinity. These projects, which are primarily motivated by solar neutrinos and neutrino oscillations, can provide important geophysical measurements complimentary to Hanohano. They have good sensitivity to radioactivity in the continental crust yet are insensitive to radioactivity in the mantle and the possible geo-reactor in the core. Moreover, these projects cannot be moved without incurring enormous expense, time, and effort.

A comparison of operating and planned geo-neutrino projects worldwide is provided in Table 2. It is evident from the estimated signal to background ratios that Hanohano is at least a factor of ten times more sensitive to radioactivity in the mantle and to the possible fission reactor in the core than any of the other projects. This sensitivity makes Hanohano an extremely important new tool for the study of solid Earth composition and dynamics and for measuring critical background signals for long-range nuclear monitoring.

<u>Project</u>	<u>Size (kT)</u>	<u>Mantle (ev/y)</u>	<u>Crust (ev/y)</u>	<u>Reactor (ev/y)</u>	<u>Mantle Signal/Bkg</u>	<u>Geo-reactor Signal/Bkg</u>	<u>Start date</u>
<u>Baksan</u>	<u>5.0</u>	<u>45</u>	<u>180</u>	<u>351</u>	<u>0.15</u>	<u>0.08</u>	<u>???</u>
<u>Borexino</u>	<u>0.1</u>	<u>1</u>	<u>5</u>	<u>19</u>	<u>0.06</u>	<u>0.03</u>	<u>2006-2007</u>
<u>EARTH</u>	<u>4.0</u>	<u>36</u>	<u>108</u>	<u>281</u>	<u>0.18</u>	<u>0.08</u>	<u>???</u>
<u>HSD</u>	<u>100</u>	<u>900</u>	<u>3600</u>	<u>14,000</u>	<u>0.11</u>	<u>0.04</u>	<u>???</u>
<u>KamLAND</u>	<u>0.8</u>	<u>7</u>	<u>22</u>	<u>240</u>	<u>0.07</u>	<u>0.02</u>	<u>Operating</u>
<u>LENA</u>	<u>50</u>	<u>450</u>	<u>1800</u>	<u>7000</u>	<u>0.11</u>	<u>0.04</u>	<u>???</u>
<u>SNO+</u>	<u>1.0</u>	<u>9</u>	<u>36</u>	<u>87</u>	<u>0.14</u>	<u>0.07</u>	<u>2007-2008</u>
<b><u>Hanohano</u></b>	<b><u>4.0</u></b>	<b><u>36</u></b>	<b><u>12</u></b>	<b><u>18</u></b>	<b><u>2.00</u></b>	<b><u>1.27</u></b>	<b><u>2010</u></b>

**Table 2:** *Operating and planned Geo-neutrino projects worldwide*

The detectors for the projects listed in Table 2 are very large. Borexino, the smallest of the lot, has a diameter of 18m. With the exception of Hanohano, all are built to stay in one place at the bottom of a mine in some remote location. This tends to increase construction costs over a project like Hanohano, which can be built in a shipyard where large structures are routinely constructed.

In comparison to other planned projects, Hanohano has five major advantages:

- Hanohano can be large, detecting more events, and is less constrained in size than other detectors.
- Hanohano can be efficiently constructed in a shipyard, where large structures can be economically built. This is an economic edge on the competition.
- Hanohano initial deployment location makes it more sensitive to meaningful geo-neutrino measurements.
- Hanohano is the only portable detector – capable of providing measurements at several key locations.
- Hanohano's portability and ocean use makes it the only configuration suitable for far-field nuclear deterrence work.

## 5. CONCLUSIONS, ISSUES AND RECOMMENDATIONS

### 5.1 OVERALL CONCLUSIONS

**Hanohano feasibility:** Hanohano's critical components relative to operation in the deep ocean, massive construction, and deployment have been investigated and there are no show-stoppers. Key critical issues such as scintillator performance in the deep ocean, construction and deployment, low-power operations and control, failure survivability, and electronic design have been investigated, prototyped and/or tested. At this time, this detector is a practical and technically feasible method of detecting anti-neutrinos.

**Hanohano as a Geoneutrino detector:** We have investigated the use of Hanohano for measurements of the uranium and thorium content of the Earth's mantle and core. Even modest resolution of the U/Th content is of great interest to geologists, as was highlighted by an international workshop held at UH in December 2005. U/Th are believed to dominate the internal heat of the earth, and be responsible for the geomagnetic field (outer core), the motion of the earth's landmasses, and volcanic activity (mantle). Yet, there are no direct measurements of the source and distribution of this heat source, which cannot be measured from the continents due to obscuration by the local high radioactivity of the continental crust. Measurements from the deep ocean over the thin oceanic crust can make the crucial observations. Into the bargain Hanohano can make a definitive search for the controversial claim of a natural reactor at the Earth's core. In studying the detector size needed to carry out these tasks we were driven to enlarge the initial plan to a detector mass in the ten kiloton range.

**Hanohano as a Neutrino Physics Instrument:** During the study of the design of Hanohano as required for the geoneutrino task it was learned that the application of this portable ten kiloton instrument to the study of neutrino physics was much more exciting than foreseen. This has evolved to the state of attracting worldwide attention in the elementary particle physics community. The basic plan involves stationing Hanohano 50-60 km offshore from a large nuclear power complex and using the reactor flux to make more precise measurements than otherwise possible, and even to be able to resolve the order of the neutrinos masses. It should be noted that, unlike some other plans for related (but more narrow) studies, the Hanohano plan is very broad band with multiple and interesting science outcomes.

**Hanohano relative to Nuclear Deterrence:** Hanohano in its initial form will provide important technology development and measurement of backgrounds needed for building a larger nuclear deterrence (ND) detector.

**Hanohano as a competitor:** Hanohano is unique among all proposed and pending neutrino detectors in the world: it can be larger, more cost effective than the competition and its portability makes it deployable to multiple locations of scientific interest. As a concept, it is the only one suitable for long range nuclear proliferation monitoring.

More detailed conclusions are provided in Chapter 4 for each task.

## 5.2 SUMMARY: ISSUES

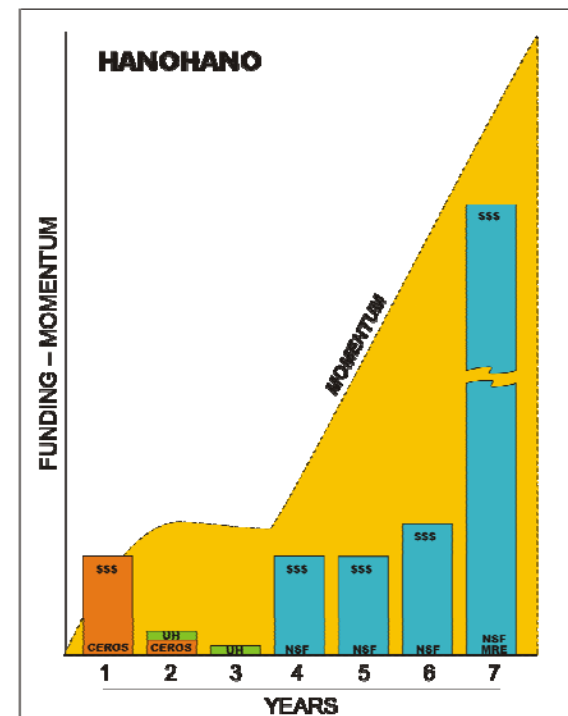
While we have made great progress, the design is not complete and all issues have not been resolved. The more significant issues are:

- Funding: we do not have a solid source of funding for follow-on work. This is the focus of the next year of reduced-effort work.
- We have demonstrated a possible solution to the implosion issue – more tests will be required to validate this solution and to determine if other low-cost solutions are equally effective. At the same time, we need to demonstrate the implosion resistance in a simulated Hanohano PMT chamber.
- There remains a great deal of refinement and optimization in the overall design. This analysis has shown one possible and practical solution to the deep water detector opportunity; a final design will undoubtedly lead to an even more practical and cost effective design.
- Further studies are required to identify the best opportunities for initial geological results.
- More work is needed with simulation studies for the physics measurements possible off-shore from a reactor complex.

## 5.3 RECOMMENDATIONS

Based on scientific interest, need and enthusiasm, and based on no significant technical show-stoppers for Hanohano, the team should proceed with the following:

- Submit formal proposals in 2007 to the National Science Foundation for the MREFC program and supporting science and instrumentation programs.
- Move toward formal collaborative agreements with national and international geoscientists and physicists (targeted for late March '07).
- Build further the scientific justification of the detector by developing multi-discipline use of the detector; provide justification for use in particle physics.
- Encourage and support the geoscience community in formally investigating the relationship between anticipated Hanohano measurements and key geoscience theory.



- Conduct a minimal-cost demonstration of the detectors and scintillator in the deep water by piggy-backing onto a UH Northwest Islands cruise. This test further builds confidence and momentum in the NSF proposal process.
- Conduct a second workshop at UH that will focus on both ND and science.

## **6. APPENDIX**

The following documents are attached as additional submitted reports:

- 6.1 (A) TASK 1: HANOHANO NEUTRINO DETECTOR (SIZING ANALYSIS)
- 6.2 (C) TASK 3, 5, 7, 12, 13, 14: A DEEP OCEAN ANTI-NEUTRINO DETECTOR  
NEAR HAWAII – HANOHANO: OCEAN ENGINEERING ANALYSIS
- 6.3 (D) TASK 3, 5, 7: BASIS OF DESIGN SUMMARY DOCUMENT
- 6.4 (E) TASK 4: OPTICAL MODULE DESIGN
- 6.5 (F) TASK 6: ELECTRONIC DESIGN FOR RELIABILITY AND LOW POWER
- 6.6 (G) TASK 8: SCINTILLATOR TESTING
- 6.7 (J) TASK 10: INTERNAL COMMUNICATIONS NETWORKING
- 6.8 (K) TASK 11: POWER AND COMMUNICATION CABLE TO SHORE

## Appendix

**Task 1: Hanohano Neutrino Detector (sizing analysis)**

Appendix

# DETECTOR SIZE AND SENSITIVITY

*A report submitted to Makai Ocean Engineering*

S.T. Dye, G. Guillian, and J.G. Learned  
*University of Hawaii, Manoa*

## Abstract

We consider the detector size, location, depth, backgrounds, and radio-purity required of a mid-Pacific deep-ocean instrument to accomplish the twin goals of making a definitive measurement of the electron anti-neutrino flux due to Uranium and Thorium decays from the earth's mantle and core, and of observing or eliminating the hypothetical natural reactor at the core of the earth. We take the experience with the KamLAND detector in Japan as our baseline for sensitivity and background estimates. We conclude that such an instrument adequate to accomplish these tasks in several years should have an effective mass of 4 kilotons, be placed at least at 4 km depth, may be located close to the Hawaiian Islands (no significant background from them), and should aim for KamLAND radio-purity levels, except for radon contamination, where it should exceed those in KamLAND caused by the high radon levels in the mine.

## **1.0 Introduction and Assumptions**

This report furnishes recommendations for the size and sensitivity needed by a deep ocean anti-neutrino detector near Hawaii (Hanohano) to perform geophysics measurements. This project is the first step in a long-range plan leading to remote monitoring of nuclear reactors and clandestine nuclear weapons testing. While the present project is tiny in comparison with the instruments necessary for nuclear deterrence, it enables accumulation of expertise, development of technology, and the first measurement of backgrounds to be encountered by a global monitoring system. Knowledge of these “backgrounds” is in fact needed for future detector design. Moreover, these first explorations present wonderful scientific opportunities, which justify the project on its own merit.

The reader is assumed to be somewhat familiar with the general goals of the project, the work accomplished by the KamLAND experiment (the present half-kiloton project in a mine in Japan), and some relevant elementary particle, nuclear, and neutrino physics. In short, the design of and experience with KamLAND provides an excellent guide to detector size and location needed to approach two geophysics goals.

### **1.1 First Goal: Measurement of Geo-neutrinos**

The first is measurement, not merely detection, of the electron anti-neutrino flux from the mantle and core (mantle/core) of Earth due to Uranium and Thorium (U/Th) decays. Because the concentrations of U/Th are much higher in the continental crust than in the oceanic crust and mantle (the core is usually assumed by geologists to be free of U/Th), only locations far

from the continental crust, like Hawaii, are well suited to this measurement.

Whereas the concentrations of U/Th in the outermost Earth’s crust can be sampled directly, measurement of the “geo-neutrino” flux provides the only viable method for determining these concentrations in the mantle. These values are only known very poorly at present and speculated upon by geologists (concentrations typically inferred from the U/Th concentrations in meteorites plus assumptions about Earth accretion and differentiation). Note that geologists generally quote such numbers without error ranges, simply because there are too many unknowns: U/Th concentrations and distributions are generally acknowledged to be informed guesses. Hence the geological community welcomes information carried by neutrinos from the otherwise inaccessible inner Earth. This was made evident by the reception of the first KamLAND results on the measurement of geo-neutrinos (mostly from the local crust in Japan), published as a cover article in the 28 July 2005 issue of *Nature*<sup>1</sup>. This paper heralding the first positive detection of Earth’s total radioactivity, marks a beginning for neutrino geophysics, long a tantalizing goal<sup>2,3,4</sup>. The article reported  $28 \pm 13$  total antineutrino events from an exposure of about 1 kiloton-year (kt-y), of which only 7 can be attributed to the mantle. While a start, the report does not add much new information about Earth’s composition.

Several groups of physicists have made calculations of these neutrino fluxes<sup>5,6,7,8</sup>, and there are two PhD dissertations from KamLAND which contain significant modeling<sup>9,10</sup>.

## **1.2 Second Goal: Detection of Hypothetical Geo-reactor**

The second motivation for Hanohano is to search for a hypothetical nuclear reactor at Earth's core. This theory, long propounded by J. Marvin Herndon<sup>11</sup>, has not met acceptance by the geological community, who have generally preferred the idea that much of the U/Th rose from the molten, early inner Earth as slag, rather than sank to the core as elemental metal. Yet, many geologists say that there really is no evidence against Herndon's hypothesis since the conditions at Earth's formation are little known. Moreover, there are peculiarities in the isotopic content of Earth, and most particularly the observed high ratio of He<sup>3</sup>/He<sup>4</sup> coming out of oceanic volcanic hot spots (such as Hawaii and Iceland), which a natural reactor could explain (He<sup>3</sup> comes from Tritium decay, made abundantly in reactors).

As discussed elsewhere<sup>11</sup>, this hypothetical energy source in the range of 1 to 10 terawatts of thermal (TW<sub>t</sub>) power could be the enigmatic power source driving the deep Earth plumes, and hence ultimately responsible for the motion of landmasses (plate tectonics) as well as Earth's magnetic field (geo-dynamo). The neutrino flux from this putative geo-reactor is very hard to measure in a location anywhere near electrical power reactors, especially in places such as Japan, Europe and North America<sup>12,13</sup>.

At KamLAND the geo-reactor would present a flux of only a few percent that due to power reactors around Japan. This is very hard to distinguish from the reactor flux because the energy spectrum at the source of natural or man-made reactors is essentially indistinguishable. However, since reactors at distances of a few

hundred kilometers are not so far as to have all neutrino oscillations effects (see next section) washed out, a study has been made seeking an unchanging geo-reactor signal added to the somewhat variable (roughly by a factor of two) power reactor flux<sup>14</sup>. In fact the initial results of this study are marginally positive at the one standard deviation level. This is sufficient for claiming an upper limit of such a power source (<20TW<sub>t</sub>). Although tantalizing, the study lacks the sensitivity required to detect and measure the power of the geo-reactor if it exists.

For nuclear reactor monitoring the background due to geo-reactor neutrinos is probably more serious, due to similar energy spectra, than that due to geo-neutrinos. Detection of a clandestine nuclear reactor requires knowledge of the existence and power of all other reactors. This is especially true of a possible geo-reactor which could have a power greater than all current man-made reactors combined.

## **1.3 Neutrino Oscillations**

In the following discussion, all processes that involve neutrino production and subsequent detection assume that neutrino oscillations occur, as is now accepted. The oscillation parameters employed are the best-fit values from global fits to all solar and reactor neutrino experiments as of this time<sup>15</sup>. Since the baseline of neutrino propagation considered in this context (thousands of kilometers) is much larger than the oscillation lengths (<100 km) for the energy scale under consideration, the neutrinos can be considered to a good approximation to be fully mixed. The effect of oscillations can be accounted for by reducing the event rate by 0.60 compared to the rate without oscillations.

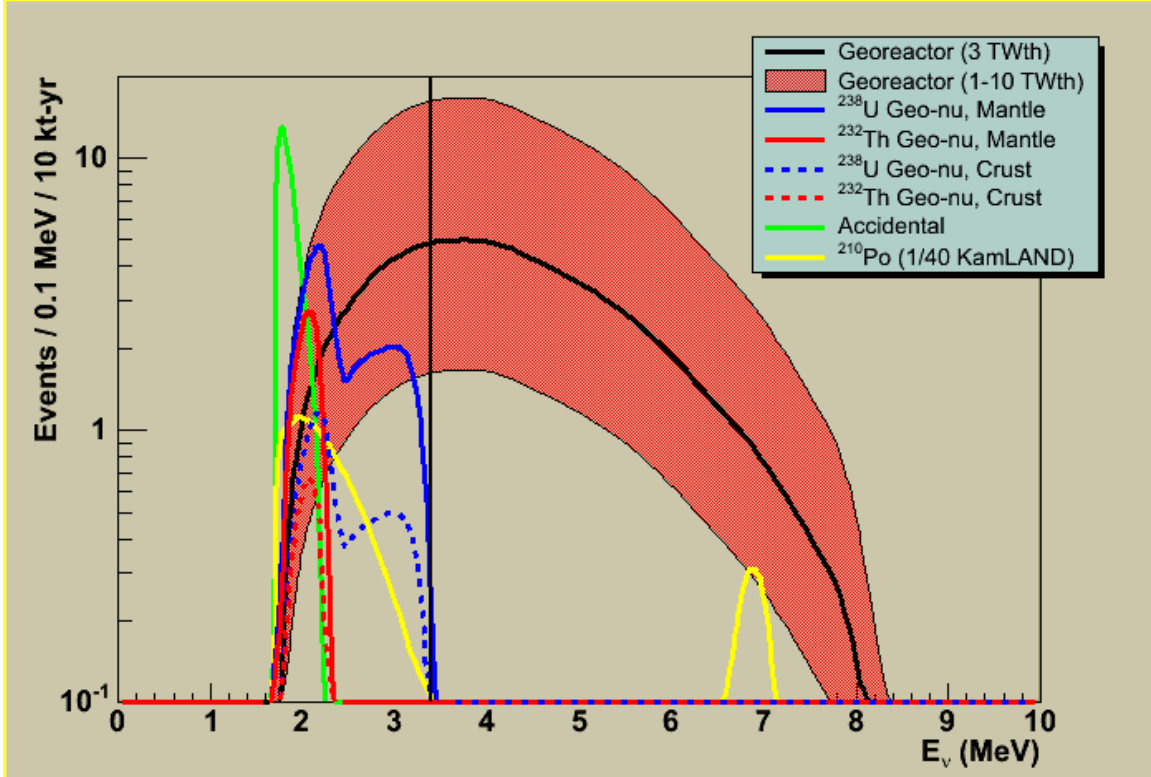


**Figure 1:** The neutrino event energy spectrum of the hypothetical, Earth-centered, natural nuclear reactor as detected by a mid-Pacific, deep ocean detector (orange band)<sup>14</sup>. These events dominate the detected inverse beta decay events above 3.4 MeV of neutrino energy. The yellow curve illustrates background for Radon exposures equivalent to KamLAND, but not in a mine. This might be better in practice, but is adequate. Below 3.4 MeV of neutrino energy one sees the U/Th decay neutrinos as expected in the BSE model: Earth's mantle and core (blue/red), oceanic and continental crusts (dashed blue/red). Accidents at the same level as in KamLAND (scaled by volume), which appear at the low end of the region (green) are probably over estimated.

The energy window for the geo-neutrino analysis is 1.7 to 3.4 MeV, while that for the geo-reactor analysis is 3.4 MeV to 9.3 MeV. The visible energy of the positron annihilation, prompt signal, in the detector is 0.9 MeV less than the neutrino energy. The second tag for neutron capture is at 2.2 MeV of visible energy. The spectra of the contributions to the signal are as illustrated in Figure 1, where all spectra are fully mixed.

## 2.0 Geo-neutrino Detection Sensitivity

Hanohano's location in the middle of the Pacific Ocean makes it sensitive primarily to geo-neutrinos originating from Earth's mantle. The nominally expected event rate of geo-neutrinos of mantle (and core, normally assumed by geologists to be zero) origin based upon the Bulk Silicate Earth (BSE) model<sup>7</sup> is 45 events per 10 kt-yr. This is a factor of four larger than the 11 events per 10 kt-yr for geo-neutrinos from the oceanic and continental crusts.

Because of the uncertainty of the modeling we cannot assign a meaningful error estimate to the event rate from the mantle. We know based upon meteorites that it should be not much less, but could be as much as a factor of two greater.

This is illustrated in Figure 2 (a), which shows the integrated neutrino flux out to various distances from a detector located near Hawaii. The situation is reversed at a continental location with the same mantle/core flux but about ten times the crust flux (see Figure 2 (b)). In this analysis the “signal” is the mantle geo-neutrino event rate. The crust geo-neutrinos are considered part of the background. Figure 3, which shows a map of the geo-neutrino interaction rate at different positions on Earth’s surface, demonstrates the clear difference between Hanohano and similar land-based detectors<sup>16</sup>.

The conclusion is that the mantle/core flux is extremely difficult to measure at continental locations, which yield mainly crust fluxes. Measurements in several locations around the world permit disentanglement of crust and mantle/core fluxes, and ultimately would allow for Earth neutrino tomography, but in further generations of experiments.

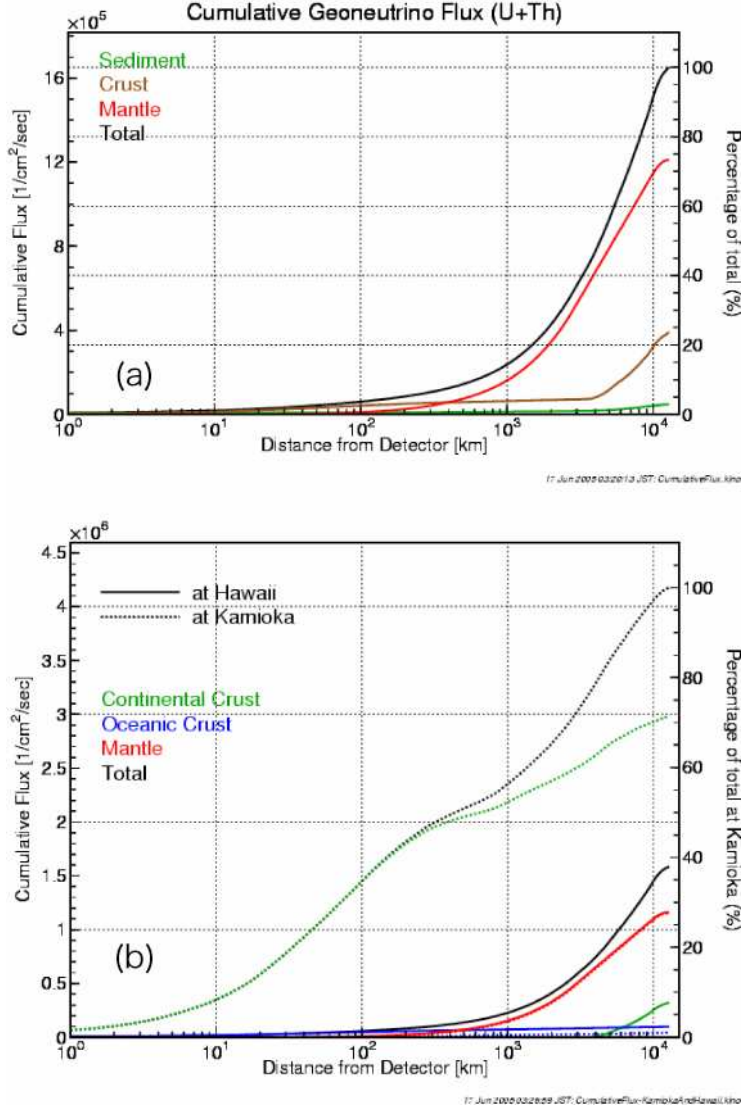


**Figure 2:** (a) The cumulative geo-neutrino flux from different geological structures as a function of distance from the detector at Hawaii. (b) Comparison of the cumulative flux versus distance at Hawaii and Kamioka (site of KamLAND). The mantle contribution dominates the crust at Hawaii; the reverse is true at Kamioka. The graphs were adopted from S. Enomoto’s Ph. D. thesis<sup>10</sup> (some cosmetic changes made by the authors).

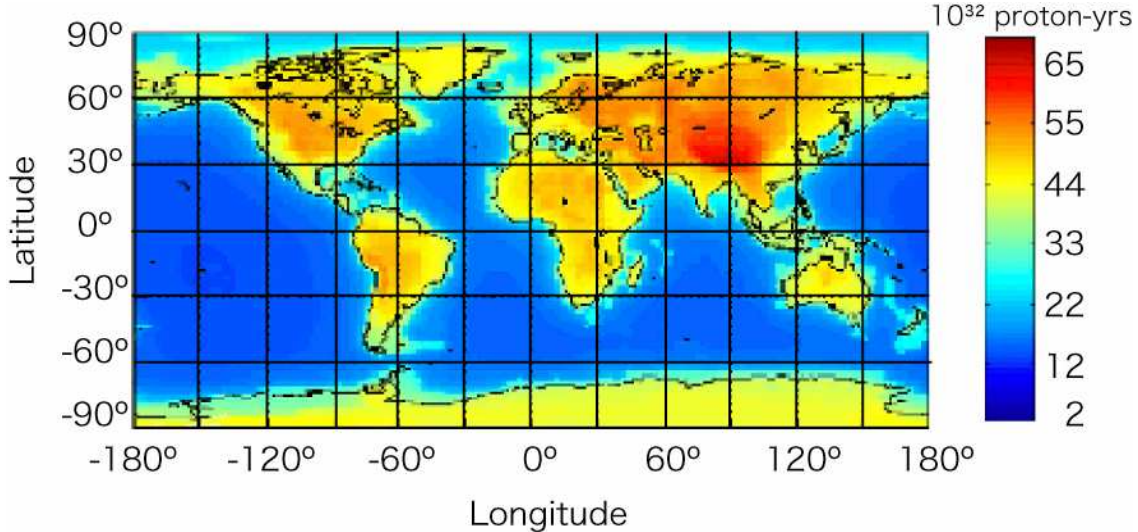


**Figure 3:** The predicted geo-neutrino yield (events per  $10^{32}$  free protons per year) on Earth’s surface. Figure adopted from Mantovani *et al.* **Error! Bookmark not defined.** (some cosmetic changes made by authors). One sees that the yield is dominantly due to crust radioactivity near all major landmasses (red - light blue) and dominantly due to the mantle radioactivity in mid-ocean locations (deep blue).

## 2.1 Geo-neutrino Backgrounds

Likely backgrounds for geo-neutrinos (based upon KamLAND experience) are:

- ${}^9\text{Li}$  produced by cosmic rays traversing the detector
- Fast neutrons from cosmic rays passing near the detector
- $\alpha$  decay of  ${}^{210}\text{Po}$  followed by  ${}^{13}\text{C}(\alpha, n){}^{16}\text{O}$  in the scintillating oil
- Accidental coincidence events
- Antineutrinos from commercial nuclear reactors
- Antineutrinos from a geo-reactor

Background contribution due to fast neutrons can be ignored since they occur at the edge of the fiducial (inner, software-defined) volume; they are efficiently removed in the data analysis. The estimated event rate (based upon KamLAND data) from each process is shown in Table 1.

The lithium background is due to cosmic ray muons traversing the detector, and is minimized with increasing depth. At the depth of KamLAND, equivalent to 2.15 km of water, it is a major nuisance. By 4 km depth the Li background is almost negligible. However, this background level in KamLAND is achieved at the cost of applying tight cuts to the data, which results in the removal of significant amount of good data. These cuts, moreover, introduce systematic errors that obscure the signal. For these reasons, the most favorable strategy is to go as deep as possible so that the cosmic ray background rate is so low that the application of cuts to remove  ${}^9\text{Li}$  events becomes unnecessary. Greater depth alleviates a multiplicity of background problems, including entering fast neutrons and significant dead time around muon transits. Our judgment is that 2 km depth is not tolerable, 3 km might be acceptable, but 4 km depth is adequate. Fortunately the abyssal plane of the ocean is 4-5 km in depth.

<b>Background Source</b>	<b>Rate (1/10 kt-y)</b>
$^9\text{Li}$ (2.15 km depth)	$40 \pm 7$
$^9\text{Li}$ (3 km depth)	$10 \pm 2$
$^9\text{Li}$ (4 km depth)	$3 \pm 1$
$^{210}\text{Po}$	$12 \pm 2$
Accidentals	$(<)30 \pm 3$
Commercial Reactors	$5.0 \pm 0.1$
Geo-reactor	19 per $\text{TW}_t$
Crustal Geo-vs	$11 \pm 3$
<b>Total, Non-Mantle</b>	<b><math>61 \pm 5</math></b>

**Table 1:** Background sources and rates expected for the mantle geo-neutrino analysis for energies between 1.7 and 3.4 MeV. The  $^{210}\text{Po}$  background assumed to be 40 times purer than the level for KamLAND's scintillating oil.

The Polonium background, due to alphas which interact with  $^{13}\text{C}$ , stems mostly from Radon contamination at KamLAND. The mine levels of radon are 40 times those in the free air outside, and in the course of experimental preparation the KamLAND scintillating oil was exposed to mine air. While the Radon itself decays in a matter of months, further decay products lead to the initially unrecognized Polonium background, which can simulate inverse beta decay. The levels shown are conservatively high.

The "accidentals" are a bit more complicated being due to uncorrelated coincidences between real radioactive decay events, some of which in this estimate may be associated with long lived excitations by cosmic ray muons. Moreover, some of the radioactivity comes from the periphery of the detector, the balloon and supporting ropes in KamLAND. Thus this scales with detector outer surface area not volume. For present purposes we take the conservative assumption that the rate per

unit volume will be the same as in KamLAND, but we can doubtless do better than indicated.

The calculation of the contribution from distant commercial power reactors can be carried out to about 2% precision, and should be well known. Nuclear powered ships and submarines will make a negligible contribution. Submarine power plants are in the range of 100  $\text{MW}_t$ , as compared to 2  $\text{GW}_t$  for power reactors. Ships cruise at a small fraction of maximal power generally, and are shut down in port at Pearl Harbor. With cooperation of the military these can be accounted for in any event (since we only need to know flux at the detector and not power or range of the ships).

In arriving at detector parameters for geo-neutrino measurement, we shall assume that the geo-reactor power is zero, or at least that we know it perfectly from the measurements above 3.4 MeV of neutrino energy.

The final "background" we take to be the less interesting contribution to the U/Th neutrino flux from the oceanic (and distant continental) crust. Again, error estimates for these geological models are hard to come by, but based upon the detailed studies for Kamioka (the site of KamLAND), we can assume the crust contribution is good to about 25%.

We have also made a preliminary estimate of the additional flux of neutrinos due to the proximity of the Hawaiian Islands. When we assume that the Big Island can be modeled as a cone of height 10 km and radius 100 km, and that our detector is located a mere 10 km from the effective source center of Mid Oceanic Ridge Basalt, the contribution would amount to

only 5% of the mantle/core flux. When a site is finally chosen we will have to do a more careful calculation, but for now we can safely conclude that proximity to the Hawaiian Islands will not affect the experimental goal of measuring the mantle/core flux.

The total geo-neutrino “background” rate at 4 km depth (without geo-reactor but including crust neutrinos) is  $61 \pm 5$  per 10 kt-y, compared to a (mantle/core) signal rate of 45 per 10 kt-y. The signal significance for a 10 kt-y exposure is thus  $S/\sqrt{S+B} = 4.4$  sigma dominated by counting statistics. Thus detection of mantle neutrinos above background would be extremely significant (>99.999%). Yet if the exposure were only 1 kt-y, it would be marginal at only 1.4 sigma (>90%). If we have estimated the background perfectly, then the background subtracted mantle geo-neutrino signal would be  $45 \pm 7$ , a 15% measurement (statistical uncertainty only).

In order to confirm the above conclusion, we performed simulations where the combined energy spectrum of the signal and background are varied randomly and a multi-component fit is done for the number of signal events. The results improve, particularly depending upon how well we are able to constrain the background components. If the geo-reactor exists, one can see from Figure 1 that the fit above 3.4 MeV will be clean and will permit precise prediction in the lower energy geo-neutrino regime, allowing accurate subtraction.

### 3.0 Geo-reactor Neutrino Detection Sensitivity

The energy spectrum of antineutrinos produced in a nuclear fission reactor spans the range of ~0 to about 10 MeV, much

Geo-reactor Background	Rate (1/10 kt-y)
$^9\text{Li}$ (2.15 km)	$63 \pm 12$
$^9\text{Li}$ (3 km)	$16 \pm 3$
$^9\text{Li}$ (4 km)	$4 \pm 1$
$^{210}\text{Po}$	$3 \pm 2$
Accidentals	$35.1 \pm 0.3$
Commercial Reactors	$10.0 \pm 0.2$
<b>Geo-reactor Bkgd Total</b>	<b><math>52 \pm 2</math></b>

**Table 2:** Background sources and corresponding rates expected for mid-ocean geo-reactor neutrino detection. The  $^{210}\text{Po}$  background assumed to be 40 times purer than the level for KamLAND’s scintillating oil.

wider than the 0 to 3.4 MeV for geo-neutrinos. In the energy region 1.8 MeV (threshold energy for anti-neutrino interaction with target) to 3.4 MeV, geo-neutrinos are a background to the geo-reactor. A lower energy threshold of 3.4 MeV is applied to completely remove this background. We set an upper bound of 9.3 MeV for convenience (the probability that a geo-reactor neutrino has greater energy is negligible). In this energy range (3.4 – 9.3 MeV) the geo-reactor neutrino event rate is 38 events /  $\text{TW}_t$  / 10 kt-y.

The background sources for geo-reactor neutrino detection are from the same sources as for geo-neutrino detection, but less at higher energies. The event rates differ because of the different energy window and analysis cuts. We summarize them in Table 2. At a depth of 4 km the total background rate is 52 per 10 kt-y, compared to the signal for a 1  $\text{TW}_t$  geo-reactor of 38 per 10 kt-y. The signal detection significance for a 1  $\text{TW}_t$  geo-reactor per 10 kt-y exposure is  $S/\sqrt{S+B} = 4.0$  sigma. If the geo-reactor exists at the high power end of Herndon’s range, 10  $\text{TW}_t$ , we would detect it at 18 sigma. Assuming we have pinned down the backgrounds (via fitting the spectrum and

other means), the geo-reactor power can be resolved to 5-16% going from the upper to lower expected power levels ( $10-1 \text{ TW}_t$ ), limited by statistical fluctuations, not systematic uncertainty.

As with geo-neutrino detection, we performed simulation studies of Hanohano's sensitivity to the geo-reactor assuming various signal and background levels and an initial 10 kt-y exposure. Using the knowledge of expected spectrum for both signal and background will add to our confidence in detecting any geo-reactor signal, as well as improving background estimate precision. We confirm that the error on a positive power measurement will remain dominated by statistical fluctuations, not systematic uncertainty.

We have not herein considered the further confirmation of the location of any positive geo-neutrino signal by neutrino direction measurement. This was accomplished by the Chooz experiment team<sup>17</sup> (operating nearby a power reactor) by using the difference between the location of the initial (positron annihilation) and second (neutron capture) effective vertices, and is due to the slight neutron momentum in the direction of the incoming neutrino. The prospects for confirmation that the putative geo-reactor signal is coming from generally the direction of the center of Earth depends upon detector design (electronics and photomultiplier time resolution and scintillating oil decay lifetime). Our first estimates are not very encouraging unless the geo-reactor is at the higher end of the possible power levels.

We conclude that the geo-reactor measurement is easier than the mantle/core geo-neutrino measurement. If

the geo-reactor exists at level suggested (and important for driving plumes), we should be able to convincingly detect it and make useful measurements of the power.

#### **4.0 Recommended Detector Specifications**

Based on the foregoing results, we recommend that:

- A detector fiducial volume of 4 kt (about 8 times KamLAND).
- The planned total live time should be at least 2.5 years, yielding a 10 kt-y exposure.
- A depth of 4 km is sufficiently deep to comfortably accomplish geophysics goals; 2 km is not acceptable, and 3 km would be marginal. Depths greater than about 4 km do not make significant improvements in backgrounds.
- The scintillating oil must be as free of  $^{210}\text{Po}$  as possible, with a goal of forty times less than the initial KamLAND contamination. This goal should be attainable since the level observed in KamLAND is almost certainly due to high radon levels in the mine environment in which the scintillating oil was placed for many months. Minimization of radon pollution at all stages of scintillating oil handling is a high-priority engineering goal.
- A deep ocean (or mid-ocean island) location, far from continents, is required to resolve the mantle/core flux of U/Th decay neutrinos from backgrounds and neutrinos from local crust sources.

- A location near the Hawaiian Island land mass does not add significantly to the crust background to measurement of mantle/core U/Th geo-neutrinos.
- With the stated goal of 10 kt·y exposure and 4 km depth and expected backgrounds we can achieve a 15% measurement of the mantle/core total of U/Th neutrinos, and hence this level of global concentration.
- Again, with stated assumptions on exposure and backgrounds, we can measure a geo-reactor power to 5-16% precision for source powers in the expected range of 10-1TW<sub>t</sub>. If the geo-reactor is not present, we can set upper limits to the power of <0.5TW<sub>t</sub> at >95% confidence level.

In sum we find that a 4 kiloton, deep ocean detector can achieve the geophysics goals of this proposed experiment. In doing so, we measure the low energy neutrino backgrounds important for nuclear deterrence to levels between one and two orders of magnitude better than past attempts.

*Acknowledgement:* Peter Grach, Jelena Maricic, Sandip Pakvasa, Gary Varner, Mavourneen Wilcox, and our KamLAND colleagues, all made significant contributions to the work reported herein.

---

<sup>1</sup> T. Araki *et al.*, *Experimental investigation of geologically produced antineutrinos with KamLAND*, Nature (London) **436**, 499 (2005).

<sup>2</sup> G. Eder, *Terrestrial Neutrinos*, Nucl. Phys. **78**, 657 (1966).

---

<sup>3</sup> C. Avilez, G. Marx, and B. Fuentes, *Earth as a source of antineutrinos*, Phys. Rev. D **23**, 1116 (1981).

<sup>4</sup> L.M. Krauss, S.L. Glashow, and D.N. Shramm, *Antineutrino astronomy and geophysics*, Nature (London) **310**, 191 (1984).

<sup>5</sup> S. Enomoto, E. Ohtani, K. Inoue, and A. Suzuki, hep-ph 0508049 (2005).

<sup>6</sup> G. Fiorentini, M. Lissia, F. Mantovani, and R. Vannucci, hep-ph/0401085 (2004).

<sup>7</sup>R.S. Raghavan *et al.*, *Measuring the Global Radioactivity in the Earth by Multidetector Antineutrino Spectroscopy*, Phys. Rev. Lett. **80**, 635 (1998).

<sup>8</sup> C.G. Rothschild, M.C. Chen, and F.P. Calaprice, *Antineutrino geophysics with liquid scintillator detectors*, Geophys. Res. Lett. **25**, 103 (1998).

<sup>9</sup> Nikolai Tolich, Ph.D. Thesis, Stanford University (2005).

<sup>10</sup> Sanshiro Enomoto, Ph.D. Thesis, Tohoku University (2005).

<sup>11</sup> J.M. Herndon, Proc. Nat. Acad. Sci., **93**, 646 (1999); D.F. Hollenbach and J.M. Herndon, Proc. Nat. Acad. Sci., **98**, 11085 (2001).

<sup>12</sup> R.S. Raghavan, *Detecting a Nuclear Fission Reactor at the Center of the Earth*, hep-ex/0208038 (2002).

<sup>13</sup> G. Domogatski *et al.*, *Neutrino Geophysics at Baksan I: Possible Detection of Georeactor Antineutrinos*, hep-ph/040122 (2004).

---

<sup>14</sup> Jelena Maricic, Ph.D. Thesis, University of Hawaii (2005).

<sup>15</sup> KamLAND Collaboration, T. Arakaki *et al.*, Phys. Rev. Lett. **94**, 081801 (2005).

<sup>16</sup> F. Mantovani et al., Phys. Rev. D **69**, 013001 (2004).

<sup>17</sup> M. Appolonio et al., Phys. Rev. D **61**, 012001 (2000).

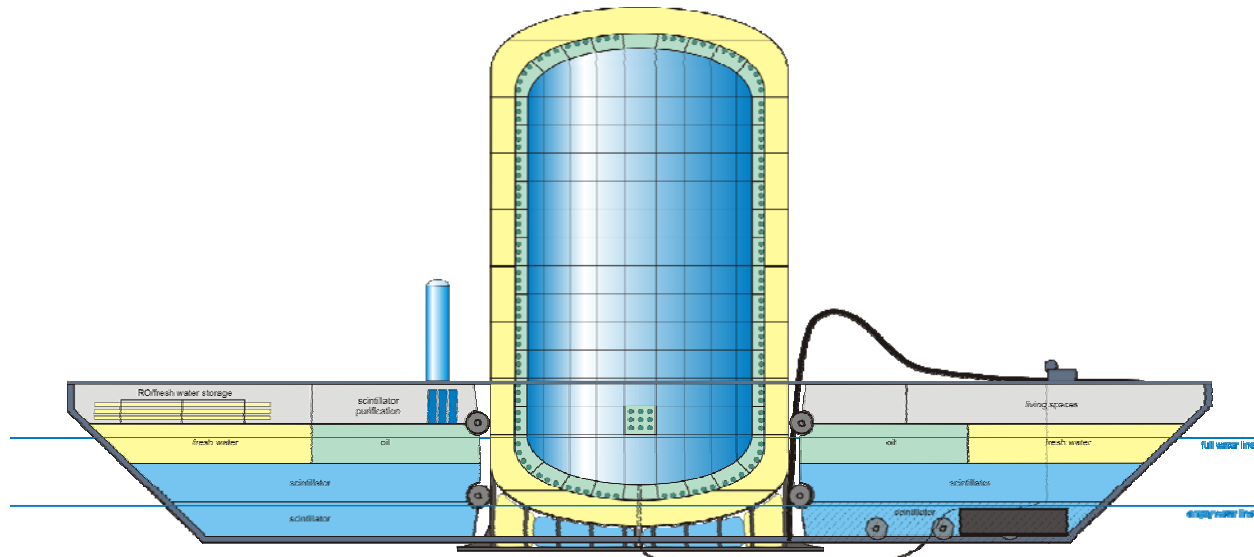
## **Appendix**

**Task 3, 5, 7, 12, 13, 14: A Deep Ocean Anti-Neutrino Detector near Hawaii –  
Hanohano: Ocean Engineering Analysis**

Appendix

# A Deep Ocean Anti-Neutrino Detector near Hawaii - Hanohano

## Ocean Engineering Analysis



Prepared for:

**The National Defense Center of Excellence  
for Research in Ocean Sciences (CEROS)**  
73-4460 Queen Kaahumanu Highway, Suite 111  
Kailua-Kona, Hawaii 96740

Prepared by:

**MAKAI OCEAN ENGINEERING, INC.**  
Waimanalo, Hawaii 96734  
<http://www.makai.com>

November, 2006

## TABLE OF CONTENTS

<b>TABLE OF CONTENTS .....</b>	<b>II</b>
<b>LIST OF FIGURES .....</b>	<b>IX</b>
<b>LIST OF TABLES .....</b>	<b>XIV</b>
<b>1. INTRODUCTION .....</b>	<b>16</b>
1.1 PURPOSE OF THIS DOCUMENT .....	16
1.2 CONCEPT OVERVIEW AND BASIS OF DESIGN .....	16
1.2.1. Concept Overview .....	16
1.2.2. Hanohano concept.....	18
1.3 THE OCEAN ENGINEERING CHALLENGE.....	18
1.3.1. Primary Engineering Questions .....	18
1.3.2. Feasibility analysis/Conceptual Design.....	18
1.4 TASKS REPORTED IN THIS REPORT.....	18
1.4.1. TASK 3 – Design of 20 m structure.....	18
1.4.1.1 Summary results and Conclusions.....	19
1.4.2. TASK 5 – Study of means to prevent successive implosions and in situ testing.....	20
1.4.2.1 Summary results and Conclusions.....	20
1.4.3. TASK 7 – Simulation of deployment of vessel.....	21
1.4.3.1 Summary results and Conclusions.....	22
1.4.4. TASK 12 – Conceptual Plans for Hanohano.....	23
1.4.4.1 Summary results and Conclusions.....	23
1.4.5. TASK 13 - Engineering study for preparation of low radioactivity scintillation material .....	25
Summary results and Conclusions .....	25
1.4.5.1 Summary results and Conclusions.....	26
1.4.6. TASK 14 – Design and costing for ocean demonstration. ....	26
1.4.6.1 Summary results and Conclusions .....	26
1.5 BASIS OF DESIGN DOCUMENT .....	27
1.6 ENGINEERING APPROACH:.....	27
<b>2. CONFIGURATION ANALYSIS AND SELECTION:.....</b>	<b>29</b>
2.1 INTRODUCTION .....	29
2.1.1. What is in this chapter .....	29
2.1.2. The basic candidates: .....	30
2.1.2.1 Shape.....	30

2.1.2.2	Configuration .....	30
2.2	<b>BUOYANCY, WEIGHT AND SIZE LIMITATIONS .....</b>	32
2.2.1.	Weight limitations.....	32
2.2.2.	Size Limitations .....	33
2.2.3.	Weight Balance.....	33
2.2.4.	Material densities as a function of pressure and temperature .....	33
2.2.5.	Impact of Scintillator Shape .....	35
2.2.6.	Example Analysis: Integrated Structure .....	36
2.2.7.	Pre-Cooling of the Detector.....	39
2.2.8.	Detachable Detector.....	41
2.2.9.	Weight, Size Limits .....	43
2.3	<b>SIZE, STABILITY, AND PERIOD OF ROLL.....</b>	44
2.3.1.	Introduction to Stability .....	44
2.3.2.	Integrated Design.....	46
2.3.2.1	Detector Shape .....	47
2.3.2.2	Vessel Size.....	47
2.3.2.3	Empty Detector .....	51
2.3.2.4	Filling the Integrated Detector.....	52
2.3.2.5	Detector Completely Full of Oil, Scintillator, and Water.....	57
2.3.2.6	Other Stability Considerations.....	58
2.3.2.7	Submerging.....	60
2.3.3.	Validation of Stability Curves .....	61
2.3.3.1	Construction.....	61
2.3.3.2	Testing .....	62
2.3.3.3	Results.....	63
2.3.4.	Detachable Design .....	64
2.3.4.1	Size.....	64
2.3.4.2	Surface Stability.....	64
2.3.4.3	Submerged Stability.....	71
2.3.5.	Results.....	71
2.4	<b>STRUCTURAL ANALYSIS .....</b>	72
2.4.1.	Overview.....	72
2.4.1.1	Goals of analysis.....	72
2.4.1.2	Detector scaling .....	72
2.4.1.3	Pressure containment.....	72
2.4.2.	Stages of structural analysis.....	73
2.4.2.1	Loading conditions .....	74
2.4.2.2	Materials .....	74
2.4.3.	Weight and Strength of an Integrated Vessel with Cube Detector .....	74
2.4.3.1	Detector concept .....	74
2.4.3.2	Detector analysis Inputs.....	77
2.4.3.3	Detector analysis Details .....	79

2.4.3.4	Hull bending moment .....	81
2.4.3.5	Hull structural model .....	84
2.4.3.6	Hull analysis .....	86
2.4.3.7	Intermediate conclusion.....	93
2.4.4.	Weight and strength of an integrated vessel with cylinder detector .....	94
2.4.4.1	Design concept.....	94
2.4.4.2	Detector analysis inputs .....	94
2.4.4.3	Detector analysis details .....	94
2.4.4.4	Hull structural model and Analysis .....	95
2.4.4.5	Intermediate Conclusion.....	97
2.4.5.	Weight and Strength of a Detachable Cylindrical Detector .....	98
2.4.5.1	Design concept.....	98
2.4.5.2	Detector analysis inputs .....	98
2.4.5.3	Detector analysis details .....	98
2.4.5.4	Hull structural model and analysis.....	99
2.4.5.5	Intermediate Conclusion.....	100
2.4.6.	Structural steel vs. dead weight .....	101
2.4.6.1	Comparison.....	102
2.4.7.	Summary.....	103
2.5	COST .....	104
2.5.1.	Total Projected Cost.....	104
2.5.2.	Detailed Parameters .....	105
2.6	DESIGN CONCEPT SELECTION .....	105
2.6.1.	Size selection: .....	105
2.6.1.1	Experimental Needs.....	106
2.6.1.2	The Panama Canal .....	106
2.6.1.3	Practicality .....	106
2.6.1.4	Cost .....	106
2.6.1.5	Size Selected.....	107
2.6.2.	Concept selection.....	107
2.6.2.1	Integrated Concept.....	107
2.6.2.2	Detachable Concept .....	108
2.6.2.3	Concept Selected.....	109
2.6.2.4	Cost implications .....	109
<b>3.</b>	<b>10,000 M<sup>3</sup> DETECTOR CONCEPTUAL DESIGN.....</b>	<b>110</b>
3.1	PURPOSE OF THIS SECTION .....	110
3.2	ILLUSTRATION OF OVERALL CONCEPT. ....	110
3.2.1.	Size, Weight, and Shape .....	110
3.2.2.	Major Design Output .....	111
3.2.2.1	Scintillator.....	111
3.2.2.2	Detector.....	111

3.2.2.3	Barge.....	111
3.3	DEPLOYMENT .....	111
3.3.1.	Deployment scenario – step by step .....	112
3.3.1.1	Initial Transit and Loading .....	112
3.3.1.2	Initial outfitting and access .....	112
3.3.1.3	Initial testing, shallow flooding .....	112
3.3.1.4	Towing .....	113
3.3.1.5	Transfer liquids on site .....	113
3.3.1.6	Production of fresh water.....	115
3.3.1.7	Lowering anchor .....	116
3.3.1.8	Cable Connection to Detector.....	116
3.3.1.9	Release of detector.....	117
3.3.1.10	Descent times .....	118
3.3.1.11	Cable connection to shore.....	118
3.3.1.12	Seabed contact, oscillations .....	122
3.3.1.13	Liftoff, oscillations.....	124
3.3.1.14	Recovery .....	124
3.3.1.15	Removal of fluids. ....	125
3.3.1.16	Return to Port.....	125
3.4	DETECTOR DESIGN DISCUSSION .....	125
3.4.1.	Overall illustration .....	125
3.4.2.	Weight and buoyancy .....	127
3.4.3.	Compensator Bags .....	130
3.4.4.	PMT module design.....	132
3.4.4.1	Lexan window.....	132
3.4.4.2	Fluid transfer.....	133
3.4.4.3	Mounting detectors .....	136
3.4.4.4	Service access .....	136
3.4.4.5	Implosion discussion .....	136
3.4.5.	Internal Cables and Plumbing.....	136
3.4.5.1	Cable routes and access .....	136
3.4.5.2	Plumbing .....	136
3.4.6.	Structural steel .....	137
3.4.6.1	Pressure loading requirements .....	137
3.4.6.2	Wall thickness .....	137
3.4.6.3	Hard points for docking .....	137
3.4.6.4	Reason for detector shape .....	137
3.4.6.5	Internal steel requirements.....	138
3.4.6.6	Access throughout the detector.....	139
3.4.6.7	Probable weight .....	140
3.4.6.8	Anchor attachment point, compensator bag support .....	140
3.4.7.	Stability.....	141
3.4.7.1	Size .....	141

3.4.7.2	Empty.....	141
3.4.7.3	Filling the Detector .....	141
3.4.7.4	Submerging.....	145
3.4.7.5	Conclusion .....	145
3.5	BARGE DESIGN DISCUSSION.....	145
3.5.1.	Primary design restraints .....	145
3.5.1.1	Moon pool and Panamax .....	145
3.5.1.2	Storage of high purity liquids .....	146
3.5.2.	Layout.....	146
3.5.3.	Moon Pool Structure.....	146
3.5.4.	Detector Restrain System .....	147
3.5.4.1	Requirements .....	147
3.5.4.2	Mechanism.....	147
3.5.5.	Scintillator and oil storage .....	147
3.5.5.1	Location .....	148
3.5.5.2	Hardware.....	148
3.5.6.	Pre-cooling Fluids.....	148
3.5.6.1	System Description.....	148
3.5.6.2	Heat Analysis.....	148
3.5.6.3	Capital Costs.....	150
3.5.6.4	Operating Costs.....	150
3.5.6.5	Neglected Costs .....	150
3.5.6.6	Savings.....	150
3.5.6.7	Conclusions and Recommendations .....	151
3.5.7.	Freshwater production – reverse osmosis.....	151
3.5.7.1	System Description.....	151
3.5.7.2	Capital Costs .....	152
3.5.7.3	Operating Costs.....	152
3.5.7.4	Neglected Costs .....	152
3.5.7.5	Savings.....	152
3.5.7.6	Conclusion and Recommendations.....	153
3.6	COST ESTIMATE .....	153
3.6.1.	Construction Costs.....	153
3.6.1.1	Detector costs.....	153
3.6.1.2	Barge costs .....	154
3.6.2.	Deployment costs.....	155
3.6.3.	Summary .....	156
4.	GLASS SPHERE IMPLOSION ANALYSIS AND TESTING .....	157
4.1	DESCRIPTION OF THE PROBLEM.....	157
4.1.1.	PMT pressure housing .....	157
4.1.2.	Glass sphere implosion failure.....	157
4.1.3.	Sympathetic implosion .....	158

4.2	IMPLOSION STUDIES .....	158
4.2.1.	Background.....	158
4.2.2.	Implosion mechanism overview .....	159
4.2.3.	Acoustic shockwave .....	160
4.3	MITIGATION OPTIONS .....	161
4.3.1.	Modular arrangement.....	162
4.3.2.	Alternate materials for sphere – acrylic vs glass .....	162
4.3.3.	Hardhats around sphere .....	163
4.3.4.	Fill voids in sphere.....	163
4.3.5.	Shock absorbent barriers between spheres .....	164
4.4	ANALYTICAL MODELING .....	164
4.4.1.	Objective.....	164
4.4.2.	Computer programs for blast and shock effects .....	164
4.4.2.1	Applications.....	164
4.4.2.2	Availability .....	164
4.4.2.3	ALE3D.....	165
4.4.3.	Description of the model.....	165
4.4.3.1	Arbitrary Lagrangian-Eularian (ALE) 3D code.....	165
4.4.3.2	Computational cycle .....	166
4.4.3.3	Distribution .....	166
4.4.4.	Sphere Implosion .....	166
4.4.4.1	Previous studies .....	166
4.4.4.2	Base case.....	167
4.4.4.3	Routine.....	167
4.4.5.	Fill the void.....	170
4.4.6.	Barriers.....	173
4.4.6.1	Setup .....	173
4.4.6.2	Over-pressure attenuation.....	174
4.4.6.3	Conclusions.....	175
4.5	PHYSICAL MODELING.....	175
4.5.1.	Location .....	176
4.5.2.	Vessel.....	176
4.5.3.	Objectives .....	177
4.5.4.	First at-sea tests.....	177
4.5.4.1	Filler study .....	178
4.5.4.2	Stand-off distance study.....	179
4.5.4.3	Estimated Ascent/Descent times of packages.....	179
4.5.4.4	Weakening strategy.....	182
4.5.4.5	Filling spheres.....	182
4.5.4.6	Hydrophones.....	183
4.5.4.7	Day 1 summary .....	185
4.5.5.	Second at sea tests.....	189

4.5.5.1	Day 2 summary.....	191
4.6	CONCLUSIONS .....	195
<b>5.</b>	<b>PREPARATION OF LOW RADIOACTIVITY SCINTILLATION MATERIAL .....</b>	<b>198</b>
5.1	SCINTILLATOR PURITY .....	198
5.1.1.	Requirements during construction.....	198
5.1.2.	Cleaning the detector .....	198
5.1.3.	Purifying the scintillator .....	200
5.1.4.	Storage .....	201
5.1.5.	Transporting the scintillator.....	201
<b>6.</b>	<b>OCEAN DEMONSTRATION.....</b>	<b>203</b>
6.1	OBJECTIVE: .....	203
6.1.1.	PMT – Scintillator demonstration.....	203
6.1.2.	PMT implosion demonstration .....	203
6.2	LIMITED DESIGN: .....	203
6.3	PMT-SCINTILLATOR DESIGN.....	204
6.3.1.	Requirements .....	204
6.3.2.	Design Approach .....	204
6.3.3.	Cost Estimate .....	206
6.4	PMT-IMPLOSION DESIGN – PHASE II .....	206
6.4.1.	Requirements .....	206
6.4.2.	Design Approach .....	207
6.4.3.	Cost Estimate .....	208
<b>7.</b>	<b>CONCLUSIONS .....</b>	<b>209</b>
7.1	ENGINEERING CONCLUSIONS .....	209
7.1.1.	Shape, Size.....	209
7.1.2.	Configuration .....	209
7.1.3.	Design .....	209
7.1.4.	Deployment.....	209
7.1.5.	Overall feasibility .....	209
<b>8.</b>	<b>APPENDIX – BASIS OF DESIGN .....</b>	<b>210</b>

## LIST OF FIGURES

Figure 1-1:	Initially envisioned 20m deep ocean anti-neutrino detector.....	17
Figure 1-2:	Overview of the final Hanohano.....	24
Figure 2-1:	Candidate scintillator shapes .....	30
Figure 2-2:	The initial Hanohano concept, lowered sphere.....	31
Figure 2-3:	The integrated concept - providing a means of surface transport and bathyscaphe-like deployment .....	31
Figure 2-4:	Detachable detector: separating the transport structure from the underwater detector.....	32
Figure 2-5:	Illustration of metacentric height.....	45
Figure 2-6:	Example Stability Curve.....	46
Figure 2-7:	Effect of GM on Stability Curve.....	48
Figure 2-8:	Effect of Hull Height on Stability Curve .....	49
Figure 2-9:	Hull Dimensions .....	51
Figure 2-10:	Stability Curve for an Empty Detector .....	52
Figure 2-11:	Stability Curves for a 10,000 m <sup>3</sup> Panamax Detector Partially Full of Scintillating Fluid and Oil .....	53
Figure 2-12:	Stability Curves for a 10,000 m <sup>3</sup> Square Hull Detector Partially Full of Scintillating Fluid and Oil .....	54
Figure 2-13:	Stability Curves for a 25,000 m <sup>3</sup> Detector Partially Full of Scintillating Fluid and Oil .....	55
Figure 2-14:	Stability Curves for a 10,000 m <sup>3</sup> Detector Partially Full of Fresh Water – Without Seawater Ballast.....	56
Figure 2-15:	Stability Curves for a 10,000 m <sup>3</sup> Detector Partially Full of Fresh Water – With Seawater Ballast.....	57
Figure 2-16:	Stability Curve for a Detector Completely Full of Scintillating Fluid and Oil...58	58
Figure 2-17:	Angle at which the Vessel becomes Unstable .....	59
Figure 2-18:	Acceleration Limit .....	60
Figure 2-19:	Drawing and pictures of scale model.....	62
Figure 2-20:	Testing the scale model.....	63
Figure 2-21:	Filling the Inner Cylinder of a 4000 Cubic Meter Detector .....	65
Figure 2-22:	Filling the Outer Cylinder of a 4000 Cubic Meter Detector.....	66
Figure 2-23:	Filling the Bottom Two Meters of the Outer Cylinder of a 4000 Cubic Meter Detector.....	67
Figure 2-24:	Filling the Inner Cylinder of a 10,000 Cubic Meter Detector .....	68
Figure 2-25:	Filling the Outer Cylinder of a 10,000 Cubic Meter Detector.....	68
Figure 2-26:	Filling a 10,000 Cubic Meter Detector with Bulkheads .....	69
Figure 2-27:	Filling the Inner Cylinder of a 25,000 Cubic Meter Detector .....	70
Figure 2-28:	Filling the Inner Cylinder of a 25,000 Cubic Meter Detector .....	70
Figure 2-29:	Hydrostatic Pressure in a Water Storage Tank .....	73
Figure 2-30:	Stiffened Panel.....	75

Figure 2-31:	Double Hull Design in Cube Detector Concept.....	76
Figure 2-32:	Individual Stiffening Bar and Associated Plate for Use in the Euler-Bernoulli Beam Equation.....	76
Figure 2-33:	Pressure Gradient in Detector on Surface.....	78
Figure 2-34:	Design Pressure Distribution in Detector .....	79
Figure 2-35:	Bending Moments Due to Uneven Loading .....	82
Figure 2-36:	Vessel in Short Period Ocean Waves .....	82
Figure 2-37:	Vessel in a Wave Where Wavelength Equals Vessel Length.....	82
Figure 2-38:	Vessel Sagging in Waves.....	83
Figure 2-39:	Vessel Hogging in Waves.....	83
Figure 2-40:	Generic Design Plot Showing Weight and, Buoyancy Curves.....	85
Figure 2-41:	Shear, Bending Moment, and Load Curves Based on Above Weight and Buoyancy Curves.....	86
Figure 2-42:	Weight Curve for an Integrated Cube Detector Hull.....	87
Figure 2-43:	Load Curve for 4096 m <sup>3</sup> Integrated Cube Detector in Flat Water.....	87
Figure 2-44:	Shear and Bending Moment Curves for 4096 m <sup>3</sup> Integrated Cube Detector in Flat Water .....	88
Figure 2-45:	Buoyancy Curve of a 4096 m <sup>3</sup> Detector in Waves .....	89
Figure 2-46:	Load Curve of a 4096 m <sup>3</sup> Integrated Cube Detector in Waves.....	90
Figure 2-47:	Shear and Bending Moment Curves for a 4096 m <sup>3</sup> Integrated Cube Detector in Waves .....	90
Figure 2-48:	Added Mass of Steel Needed to Withstand Bending Moments in Integrated Cube Detector Hulls.....	91
Figure 2-49:	Suitability Plot for Rectangular Based Integrated Cube Detector .....	92
Figure 2-50:	Suitability Plot for Square Based Integrated Cube Detector .....	93
Figure 2-51:	Suitability Plot for a Rectangular Integrated Cylinder Detector.....	96
Figure 2-52:	Suitability Plot for a Square Hull Integrated Cylinder Detector.....	97
Figure 2-53:	Bending Moment Comparison between Detachable Detector Concept and Integrated Concept.....	100
Figure 2-54:	Suitability Plot for Detachable Cylindrical Detector .....	101
Figure 2-55:	DWT vs. Lightship Weight of Existing Vessels.....	102
Figure 2-56:	Cost per Dead Weight Tonne of Typical Double Hull Oil Tankers .....	104
Figure 3-1:	Overview of Barge and Detector Assembly .....	110
Figure 3-2:	Lowering and testing Hanohano in shallow water.....	113
Figure 3-3:	fully loaded Hanohano being towed, the detector is empty.....	113
Figure 3-4:	Hanohano compartments that are sequentially flooded.....	114
Figure 3-5:	Scintillator, Oil and Water are transferred into the Detector which submerges through the moon pool.....	115
Figure 3-6:	The anchor is lowered and excess cable pays out from the detector until the anchor is at the correct depth .....	116
Figure 3-7:	The power and communications cable is passed off to a cable-lay ship .....	117
Figure 3-8:	The anchor cable and filler pipes are released from the detector .....	118
Figure 3-9:	Site location and profile, West Hawaii at Keahole, Point. Cable distance from shore laboratory to Hanohano is 18.7 km .....	119

Figure 3-10:	A safe deployment of the Hanohano shore cable during detector descent .....	122
Figure 3-11:	The detector oscillates after impact with the bottom (horizontal movement exaggerated).....	123
Figure 3-12:	Oscillations of the detector upon touchdown .....	123
Figure 3-13:	Oscillations of the Detector upon surfacing .....	124
Figure 3-14:	The barge moves over the detector during recovery.....	125
Figure 3-15:	Diagram of Detector Elements .....	126
Figure 3-16:	Pillow Tank.....	131
Figure 3-17:	Pillow Tank Layout .....	132
Figure 3-18:	Schematic of an Individual PMT Module Showing Fluid Ports.....	134
Figure 3-19:	Schematic of Bottom Three Rows of PMT Module Quadrant. Curvature of the Detector is Not Shown for Clarity .....	135
Figure 3-20:	Layout of Support Columns between Detector and Concrete Ballast .....	139
Figure 3-21:	Temporary Scaffolding System .....	140
Figure 3-22:	Diagram and Stability Curve of Empty Detector.....	141
Figure 3-23:	Diagram and Stability Curve of Detector with 2 meters of Fresh Water .....	142
Figure 3-24:	Diagram and Stability Curve of Detector with Two meters of Fresh Water and Oil and Scintillating Fluid 1.5 m from Full. ....	142
Figure 3-25:	Diagram and Stability Curve of Detector with 2 meters of Fresh Water and Half Full of Scintillating Fluid and Oil.....	143
Figure 3-26:	Diagram and Stability Curve of Half Full Detector.....	143
Figure 3-27:	Diagram and Stability Curve of Detector Half Full of Fresh Water and Scintillating Fluid and Oil 2 meters from Full.....	144
Figure 3-28:	Diagram and Stability Curve of a Full Detector .....	144
Figure 3-29:	Side View of Barge Showing Layout of Components in the Hull.....	146
Figure 3-30:	Cooling Costs and Capacities .....	149
Figure 4-1:	A PMT housed inside a Benthos 13" outside diameter spherical glass pressure housing. ....	157
Figure 4-2:	Once the sphere implodes, the in-falling surface of cavity rapidly accelerates towards the center. The huge momentum collision at the center forms a shockwave with a large peak overpressure. By spreading alone, the pressure attenuates as $1/r$ .....	160
Figure 4-3:	The peak under-pressure and peak over-pressure appear at opposing extremes of the target sphere; resulting in a large delta P. The implosion wave shown is for a 17" sphere in ~4400m depth, referenced to 1m standoff and is derived from experimental data [Orr and Schoenberg 1976].....	161
Figure 4-4:	The software as supplied from LLNL consists of three significant components. GEN3D – grid and “restart” file generator, ALE3D – The main solver, VisIt – a post processor that can be used to visualize output.....	166
Figure 4-5:	A view of the eighth sphere domain boundary, radius = 15 cm. ....	168
Figure 4-6:	A radial view of the implosion simulation domain.....	168
Figure 4-7:	A comparison between an experimentally derived implosion pressure wave (experienced at 1m from the center of the imploding sphere) and the prediction made by ALE3D. Note: for the purposes of comparison, the	

experimental data has been shifted through time such that the peak pressure is aligned with that shown by the ALE3D prediction.....	169
Figure 4-8: It was possible to have the model output pressure as a function of time anywhere in the domain. This figure compares the progress of the spherical pressure wave as it moved past 1m, 2m and 8m radius monitoring positions. The 1/r attenuation of pressure can be seen.....	170
Figure 4-9: Comparison of the effect of filling 30% of the void with steel or foam.....	171
Figure 4-10: The basic characteristics of actual commercially available syntactic foams were used in the model. Three foams were considered, the crush properties of two are shown above.....	172
Figure 4-11: Simulations were run with various foams occupying 30% of the spherical bubble void. The foams each had unique crush strength characteristics. All pressures are measured at 1m from the implosion source center. ....	173
Figure 4-12: This figure shows conceptually the arrangement of a barrier at a stand off distance of 0.5 m from the implosion source.....	174
Figure 4-13: The attenuation effects of a thick steel barrier and an acrylic barrier. Pressure is measured at 1m from the imploding sphere center.....	175
Figure 4-14: Implosion test site, approximately 32 nautical miles South West of Honolulu harbor.....	176
Figure 4-15: The M/V Huki Pono .....	177
Figure 4-16: Non-recoverable single weakened spheres – filler study.....	178
Figure 4-17: From left to right: Steel weights, surface flags, hydrophone cables, sphere string wire rope, netted spheres (resting in concrete filled buckets – also weights) and buoyancy modules (yellow). .....	180
Figure 4-18: Recoverable string layout – stand-off distance study.....	181
Figure 4-19: A weakened sphere, netted up awaiting deployment.....	182
Figure 4-20: A 13" sphere contained inside the 17" vacuum chamber. Foam has been placed inside the previously disassembled 13" sphere. A balloon is used to verify that a vacuum has been achieved and maintained.....	183
Figure 4-21: One of the hydrophones used in the at-sea tests. This hydrophone was mounted on a 6' steel rod with lead weights to maintain downward looking. ....	184
Figure 4-22: Two complete laptop/hydrophone systems were installed for recording acoustic events.....	184
Figure 4-23: Weighted light bulbs were used to assist with hydrophone system setup. ....	185
Figure 4-24: Example of hydrophone ringing – the upper pane is an implosion event recorded with the suspected faulty hydrophone, the lower pane is the same implosion event recorded with an alternative hydrophone. ....	187
Figure 4-25: Acoustic signals as recorded by hydrophone.....	188
Figure 4-26: Deployment of 30% volume foam filled weakened sphere.....	189
Figure 4-27: Simple double sphere sympathetic implosion assembly.....	190
Figure 4-28: Two sets of weights and target spheres awaiting the addition of weakened implosion spheres at a stand off distance of 0.8m OC.....	191
Figure 4-29: The arrangement of a source sphere, target sphere and concrete barrier between them. ....	191

Figure 4-30:	An example of an as-recorded implosion event and it's corresponding bottom reflection. The elapsed time between the primary acoustic signal and the reflected signal is approximately 2.2 seconds. This equates to a round trip distance of 3300m, indicated the implosion occurred in 3250m water depth.....	193
Figure 4-31:	A spectral view of the as-recorded signals shown in Figure 4-30. Note the high intensity, broad spectrum implosion event.....	193
Figure 4-32:	This as-recorded acoustic profile demonstrates two peaks, indicative of a double implosion event. The time difference between the two peaks corresponds to the expected signal delay due to the separation distance of the two spheres.....	194
Figure 4-33:	This as-recorded acoustic profile demonstrates a double implosion event where the weakened sphere was 30% volume filled with oil. The profile of the implosion slightly differs from an empty sphere. The over-pressure wave is slightly spread in time and the lead-in negative part of the signal is of longer duration, with high frequency components. This may be attributable to a slower glass failure mechanism or the presence of the partial fill.....	194
Figure 4-34:	This as-recorded event shows the implosion of a sphere 30% filled with precision strength syntactic foam. The lead-in under-pressure portion of the signal is similar to the oil filled sphere. The over-pressure portion of the signal is significantly spread and of lower amplitude when compared with the empty sphere implosion.....	195
Figure 5-1:	Four-step Purification System (cite source).....	201
Figure 6-1:	Arrangement for the Scintillator-PMT test module.....	205
Figure 6-2:	Arrangement for the PMT sphere implosion test module.....	208

## LIST OF TABLES

Table 2-1:	Table of fluid densities for surface and at-depth conditions.....	34
Table 2-2:	Material densities used for Hanohano operational scenarios.....	35
Table 2-3:	Shape parameters for a 4.5 k-m <sup>3</sup> scintillator (4 kT) detector.....	36
Table 2-4:	Shape parameters for a 10 k-m <sup>3</sup> scintillator (9 kT) detector.....	36
Table 2-5:	Weight, displacement, dimensions of Integrated Detector, 5.4 k-T .....	39
Table 2-6:	Weight and Displacement of Pre-cooled detector (same size detector as in preceding table).....	40
Table 2-7:	Detachable Detector weight and mass.....	42
Table 2-8:	Barge portion of a 6 k-m <sup>3</sup> detachable system .....	43
Table 2-9:	Dimensions of a Cylindrical Integrated Detector .....	50
Table 2-10:	Submerged Centers of Buoyancy and Gravity .....	61
Table 2-11:	Scale Model Test Results.....	63
Table 2-12:	Dimensions of the Detachable Detector and Barge .....	64
Table 2-13:	Detector Cube Support Structure Dimensions.....	81
Table 2-14:	Detector Cylinder Structural Dimensions.....	95
Table 2-15:	Detachable Cylinder Structural Dimensions.....	99
Table 2-16:	DWT vs. Lightship Weight for Hanohano Detector Designs .....	102
Table 2-17:	Unit Costs Used in Projected Cost Estimation .....	105
Table 3-1:	Typical mechanical characteristics of fiber optic cable suitable for supporting Hanohano .....	120
Table 3-2:	Deployment and Recovery depths for fiber optic cables and joint characteristics – From Alcatel Submarine Networks .....	121
Table 3-3:	Material densities used for the detector submergence and recovery .....	127
Table 3-4:	Mass and displacement for the 10,000 m <sup>3</sup> detachable detector .....	129
Table 3-5:	Rough barge dimensions and weights for the 10,000 m <sup>3</sup> detector .....	130
Table 3-6:	Chilling Capacity Required to Account for Environmental Heat Gain .....	149
Table 3-7:	Cooling Loads to Chill Oil and Scintillating Fluid with Over 10 Days .....	150
Table 3-8:	Unit Costs for Cooling Process.....	150
Table 3-9:	Capital Costs of Pure Aqua 180,000 GPD Reverse Osmosis System .....	152
Table 3-10:	Electronics Costs .....	153
Table 3-11:	Detector Construction Costs .....	154
Table 3-12:	Scintillator and Oil Costs .....	154
Table 3-13:	Barge Construction Costs .....	154
Table 3-14:	Reverse Osmosis Equipment Costs .....	154
Table 3-15:	Machinery Costs .....	155
Table 3-16:	Plumbing Costs .....	155
Table 3-17:	Transportation Costs .....	155
Table 3-18:	Personnel Costs.....	156
Table 3-19:	Disposable Materials Cost .....	156
Table 3-20:	Hanohano Cost Summary .....	156

Table 4-1:	Representative computer programs used to simulate blast effects and structural response.....	165
Table 4-2:	Estimated Ascent/Descent times for the two test series. ....	179
Table 4-3:	Summary of tests deployed and depths of implosion day1. ....	188
Table 4-4:	Summary of Day 2 testing .....	192
Table 5-1:	US FED STD 209E cleanroom standards.....	199
Table 6-1:	Cost estimate for the PMT-scintillator demonstration module.....	206
Table 6-2:	Cost estimate for the PMT-sphere implosion test module.....	208

# 1. INTRODUCTION

## 1.1 PURPOSE OF THIS DOCUMENT

This document is our final engineering report on the work performed in 2005 and 2006 for The National Defense Center of Excellence for Research in Ocean Sciences (CEROS), 73-4460 Queen Kaahumanu Highway, Suite 111, Kailua-Kona, Hawaii 96740.

This project, “A Deep Ocean Anti-Neutrino Detector near Hawaii” was lead by Makai Ocean Engineering with the University of Hawaii Astronomy and Physics department as a major subcontractor. A number of tasks have been completed on this project and have resulted in separate reports. This report is the final report for the ocean engineering portion of this work.

The report is written with the following purposes:

- Report to CEROS our engineering progress
- Document our work for future development
- Provide an engineering background for future NSF proposals

A separate main report on this project serves to link all the individual reports and provides the background and rationale for this effort. The main report is entitled “A Deep Ocean Anti-Neutrino Detector near Hawaii – Hanohano: Final Report” dated November, 2006, and this engineering report is presented as an appendix to this main report.

## 1.2 CONCEPT OVERVIEW AND BASIS OF DESIGN

### 1.2.1. Concept Overview

The long-range technical problem addressed in this work is the challenge of manufacturing and installing deep ocean detectors which can monitor reactors and bomb tests around the world. These proposed detectors will measure low energy anti-neutrinos from radioactive decays. These neutrinos naturally arise from decays throughout the Earth, perhaps from a hypothetical natural reactor at the Earth's core, and from man-made nuclear reactors or nuclear weapon testing. Anti-neutrinos pass freely through shielding materials, thus any reactor or bomb test could not be hidden from the proposed detector.

The construction of the proposed detector has two technical problems:

- 1) *Located in the deep ocean:* Such detectors must be shielded from cosmic ray background radiation by being buried deep in mines, ice or in the deep ocean. There is an operating detector similar to the one being proposed in Japan (KamLAND) in a mine cavity 1000 meters deep (2.5 km water equivalent), and not as deep as one would wish for proper shielding. Future detectors intended for the worldwide monitoring of nuclear activity must be better shielded (deeper) and located either in a widely distributed global grid or in close proximity (several hundred km) to the suspicious sources. *Only deep ocean*

detectors afford the flexibility of both placement (portability) and shielding to be practical for both nuclear deterrence and key geophysical science.

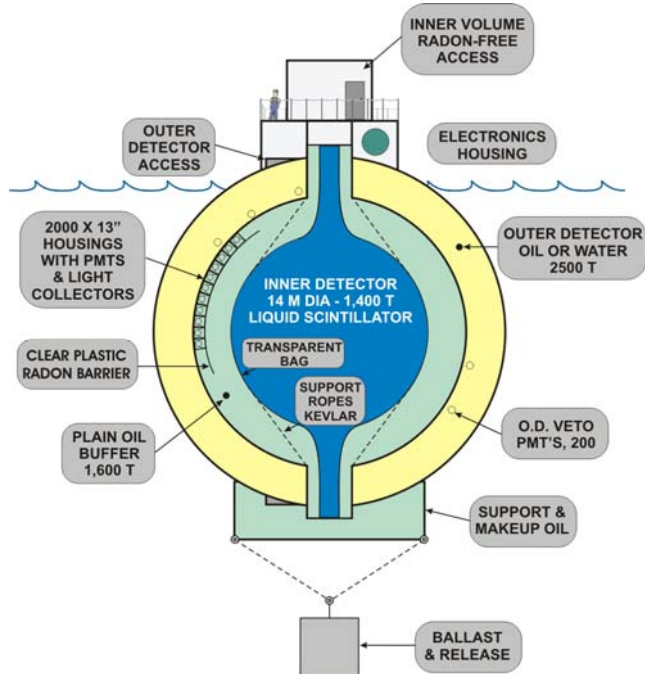


**Figure 1-1:** Initially envisioned 20m deep ocean anti-neutrino detector.

- 2) *Large Size*: The proposed detector is a very large target mass of scintillating liquid surrounded by light sensors. The scintillator emits a unique light signature when struck by an anti-neutrino and this signal is detected by the surrounding light sensors (photomultiplier tubes). The frequency of neutrino detections is proportional to the target mass and the energy resolution to the number of light sensors. A 20m-diameter deep ocean detector containing 2000 photomultiplier tubes viewing an inner balloon of 1400 tons of scintillating material is shown schematically in the attached figure. There is an inner transparent balloon containing the high light output scintillating liquid, and a region outside the balloon containing only oil which has little sensitivity to radioactivity from the vessel walls, structure and photomultiplier glass. The detectors to be investigated in this program are of KamLAND size and larger. Detectors used for nuclear deterrence, a long-range goal, would be considerably larger than the one shown. *Therefore, the proposed detectors are both sizable and complex structures to be deployed in the very deep ocean.*

This CEROS-funded effort is intended to be the first step toward building a large detector in the deep ocean off Hawaii. This detector will initially be used for a clean measurement of the Earth's total radioactivity and a sensitive search for an earth core reactor. At the same time, it will demonstrate the utility of multiple sensors used in detecting man-made sources of radiation.

### **1.2.2. Hanohano concept**

Throughout this document, we will refer to this first overall anti-neutrino detector as Hanohano. Hanohano stands for “excellence” in Hawaiian and the HANO stands for Hawaii Anti-Neutrino Observatory.

## **1.3 THE OCEAN ENGINEERING CHALLENGE**

There are specific engineering hurdles to be overcome before a detector of this size can be built and deployed in the deep ocean. Overcoming these challenges is the technical objective of this effort.

### **1.3.1. Primary Engineering Questions**

- For Hanohano, what is an optimal structure to be cost-effective and deployable?
- What is the design and arrangement of the deep water photo-detector units? This extends our knowledge of the overall design and electronic complexity.
- Can the photo-detector units be protected from chain-reaction implosions? One photo-detector implosion could severely damage the project – can we eliminate this risk?
- Can the system be practically and economically deployed? These detectors are large and complex and deployment will be the largest risk.
- What are the design details and costs for Hanohano? Cost is a major concern with these large detectors. A conceptual design will yield a more accurate cost estimate.
- How can the scintillation material be processed and delivered to the detector? This addresses the practical issue of deploying a detector with pure scintillation material.

### **1.3.2. Feasibility analysis/Conceptual Design**

The primary engineering effort has been in the “invention” of a deep water detector configuration that best meets the unique needs of the experiment and can be economically built, transported, submerged and recovered from the deep ocean. The CEROS tasks that are reported in this volume are as follows:

## **1.4 TASKS REPORTED IN THIS REPORT**

The following sections summarize each engineering task requirement, what was accomplished, and the conclusions. The details of each task is reported in a separate chapter, with the exception of the deployment task which is discussed throughout the report and most specifically in Chapters 2 and 3.

### **1.4.1. TASK 3 – Design of 20 m structure.**

This task focused on determining the basic shape and configuration of a Hanohano structure taking into account the practical engineering issues of construction, testing, deployment, service in the deep ocean, recovery, and re-deployment. The primary issues are structural strength, weight for submergence, stability, and configuration to meet the

needs of the science. Material constraints included structural loading (anchoring, deployment, and construction) as well as material limitations for the physics (transparency, low radioactive emissions, and fluid contamination), long term service (corrosion, serviceability), and cost.

#### 1.4.1.1 Summary results and Conclusions

As the work progressed, the scientific needs of the project varied. There was a overall physics need for a large detector and this was balanced against the practical feasibility for very large detectors and economic reality. This work evaluated a variety of concept shapes for the detector itself (cubes, spheres, cylinders) and for the ballast support structure (integrated or separate barge structure). The analysis considered five primary design constraints: weight and displacement for ease of deployment, stability during all phases of the operation, real-world size limits (canals and harbors), structural capability within the weight allowance, and cost. The engineering analysis considered detectors ranging from 2 to 120 k-tonnes.

- For the detector, cylindrical shapes were preferred for ease of construction and for lightweight construction of pressure hulls.
- The detector can be reliably submerged and recovered based on the buoyancy of the oil and scintillator as long as the steel mass is equal to or less than 15% of the scintillator plus oil mass. This is valid for all sized detectors.
- Two sizing constraints dictated the design: maintaining a 10m draft in harbors and keeping within 32.3m width for Panama Canal passage.
- Two configurations were evaluated:
  - An integrated system where the barge hull and detector are one structure.
  - A detachable system with a separate support barge and detector.A single lowered detector (pictured in our proposal,
  - ) was quickly abandoned as being unmanageable at a size larger than that illustrated.
- The detachable system was preferred:
  - The margin of safety on the weight goal is much larger for the detachable system. There is more future design flexibility.
  - There are fewer stability problems with the detachable system.
  - The detachable system concept could be used for very large detectors.
  - Support barge can maintain multiple detectors, can be used to transport and store the scintillator, and can serve as the hotel for critical support equipment.
  - Cost was not a factor in the decision; there were no clear cost advantages of once concept over the other.

The technical discussion and results of this task are reported in Chapter 2.

#### 1.4.2. TASK 5 – Study of means to prevent successive implosions and in situ testing.

The photo-detectors will be contained inside 13" glass spheres provided by Benthos. Glass spheres are highly reliable pressure housings for the deep ocean, but occasionally they fail. We are not able to obtain statistics upon failure rates, though they are rare, and generally the oceanographic wisdom is that failures are associated with abuse of the housings on deck. Hence we must design for the potential on an implosion.

The sudden implosion of a glass sphere generates a sudden release of energy proportional to its volume times the pressure (>400 atmospheres). The pressure wave can significantly damage adjacent structures, and there are many reported, though not well documented, cases where adjacent glass spheres have successively imploded (typically a cluster of housings in a floatation package). Because Hanohano has many thousand spheres, each practically touching the other, the consequence of successive implosions could be catastrophic. This task analyzed this implosion process, performed analytical modeling of the implosion, did at-sea tests of the implosions, and investigated various methods of protecting adjacent spheres.

##### 1.4.2.1 Summary results and Conclusions

This task was a primary focus for the CEROS work and funding. The sympathetic implosion of spheres was considered a “show-stopper” for Hanohano. As a result of no second-year funding by CEROS (where we planned additional implosion tests) and the lack of conclusive results in our initial at-sea tests, the team decided to increase the level of testing in the current year to improve program confidence and chances of funding from other sources. Less critical tasks (14) were cut back to allow expansion of this more critical work.

- The level of energy released upon an implosion is significant. For a 13" diameter glass sphere at a depth of 4000 m, the theoretical energy stored is approximately 600 kJ. One quarter of this is converted into acoustic energy.
- We investigated methods of studying implosion mitigation with reduced-scale physical models (smaller, weaker spheres). This proved to be impractical because all key parameters of the implosion could not be effectively represented by a model.
- Analytical models (ALE3D) were run that effectively and accurately modeled the implosion.
- Several methods of preventing successive implosions were investigated: oil inside sphere (reduce energy released), energy absorption material inside the spheres, barriers between the spheres, redirection of the shock wave, and alternate acrylic spheres.
- Two at-sea tests were performed with actual 13" spheres forced to implode at 4000m depth by weakening the glass.

- Glass spheres spaced at 0.8m on center will have sympathetic implosion: one imploding sphere will cause the collapse of the adjacent sphere.
- Oil-filled (30%) spheres and concrete barriers did not prevent sympathetic implosions.
- High strength syntactic foam (30% volume) inserted in the imploding sphere absorbed enough energy to lower the peak pressure by 30% and widen the pressure wave sufficiently to prevent successive implosions of adjacent spheres in two out of two tests.
- We have a good indication that there is a solution, but lower cost solutions would be preferred and additional testing is required to demonstrate our safety factor on sympathetic implosion.



The technical discussion and results of this task are reported in Chapter 4.

#### 1.4.3. TASK 7 – Simulation of deployment of vessel.

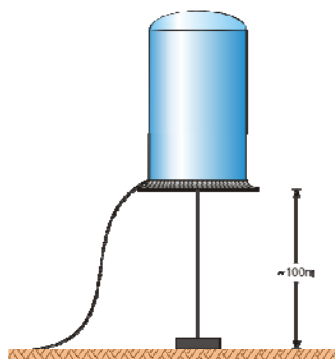
One of the major issues relative to Hanohano is whether it can be practically built, installed, maintained on the seabed and then retrieved. This task investigated issues relative to the movement of this vessel from the dock to a test location at 4000m and back again.

Hanohano is a unique underwater vehicle. When built, it may be the most massive structure ever deployed in the deep ocean. Typically, the engineering mission of Hanohano is to reliably place on the seabed at 4000 m a vehicle with a mass of 25 kilo tonnes and retrieve it after a year of service. Nuclear submarines, in contrast, are smaller. A Titanium Soviet Alfa class submarine is capable of 800 m depth and has a displacement of 3 k-tonne; a US Virginia Class submarine is roughly 13 k-tonne with a shallower depth capability and with a cost exceeding 2 billion dollars. These submarine costs are in the range of billions of dollars. The Hanohano mission is to move twice that mass to much greater depths at roughly 1% the budget.

#### 1.4.3.1 Summary results and Conclusions

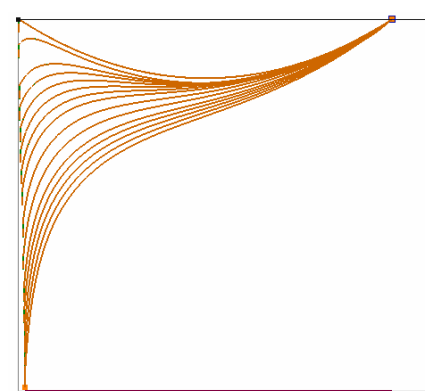
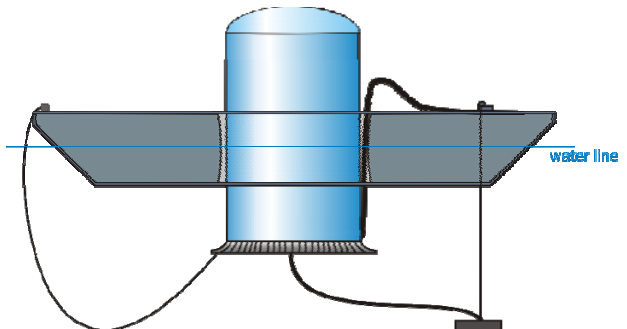
The team evaluated deployment issues relative to detector weight and displacement, cost for buoyancy, reliability of recovery, ascent and descent speeds, bottom impact oscillations, marine stability during flooding and deballasting, and deployment of the cable to shore during sinking.

- Because of the low density of the scintillator and oil, Hanohano can practically and economically descend to the seabed at 4000 m and ascend again by dropping a bottom anchor. The operation could be very safe, similar to a very large scale bathyscaphe (deepest manned dive to 11,000 m in 1957).



- Hanohano would descend 4000 m and ascend rather rapidly, approximately 30 minutes each way.
- Hanohano will have to be suspended off the seafloor by a minimum of 100 m on a pendant attached to a concrete anchor. This clearance allows for safe touchdown and the resulting oscillations upon impact.

- The detector would be controllably flooded prior to sinking. The filling sequence is important for proper stability.
- The final configuration of Hanohano allows for high stability and rapid towing during transit, similar to a standard barge.
- Hanohano can be easily recovered by releasing the concrete anchor on the seabed. This can be done once the mission is accomplished, or if the detector needs to be recovered for maintenance. The bottom anchor is abandoned.
- The power and communication cable can be attached prior to submergence. It is monitored during descent and then laid to shore in a conventional deep water cable lay. Two methods of cable lay have been developed.



The deployment of the vessel is critical to all the engineering analysis performed. In particular, Chapter 2 discusses the deployment considerations that drive the overall design and Chapter 3 discusses the deployment of the 10 k-m<sup>3</sup> detector.

#### 1.4.4. TASK 12 – Conceptual Plans for Hanohano.

This task integrated the results from the above tasks and prepared a conceptual design for a single detector. This task focused on details for the larger detector once the optimization had been performed in the earlier tasks. Details such as final weights and stability, structural checks, deck and equipment arrangements, deployment details, general operations, plumbing and wiring, compensation, and PMT placement details and were considered in this task.

##### 1.4.4.1 Summary results and Conclusions

As our work progressed, the originally envisioned spherical detector, Figure 1-2, containing 1.4 tonnes of scintillator grew into a 9 k-tonne detector system with a dramatically different shape and operational scenario – driven by the engineering and mission needs. The final detector and barge are shown in the figure below.

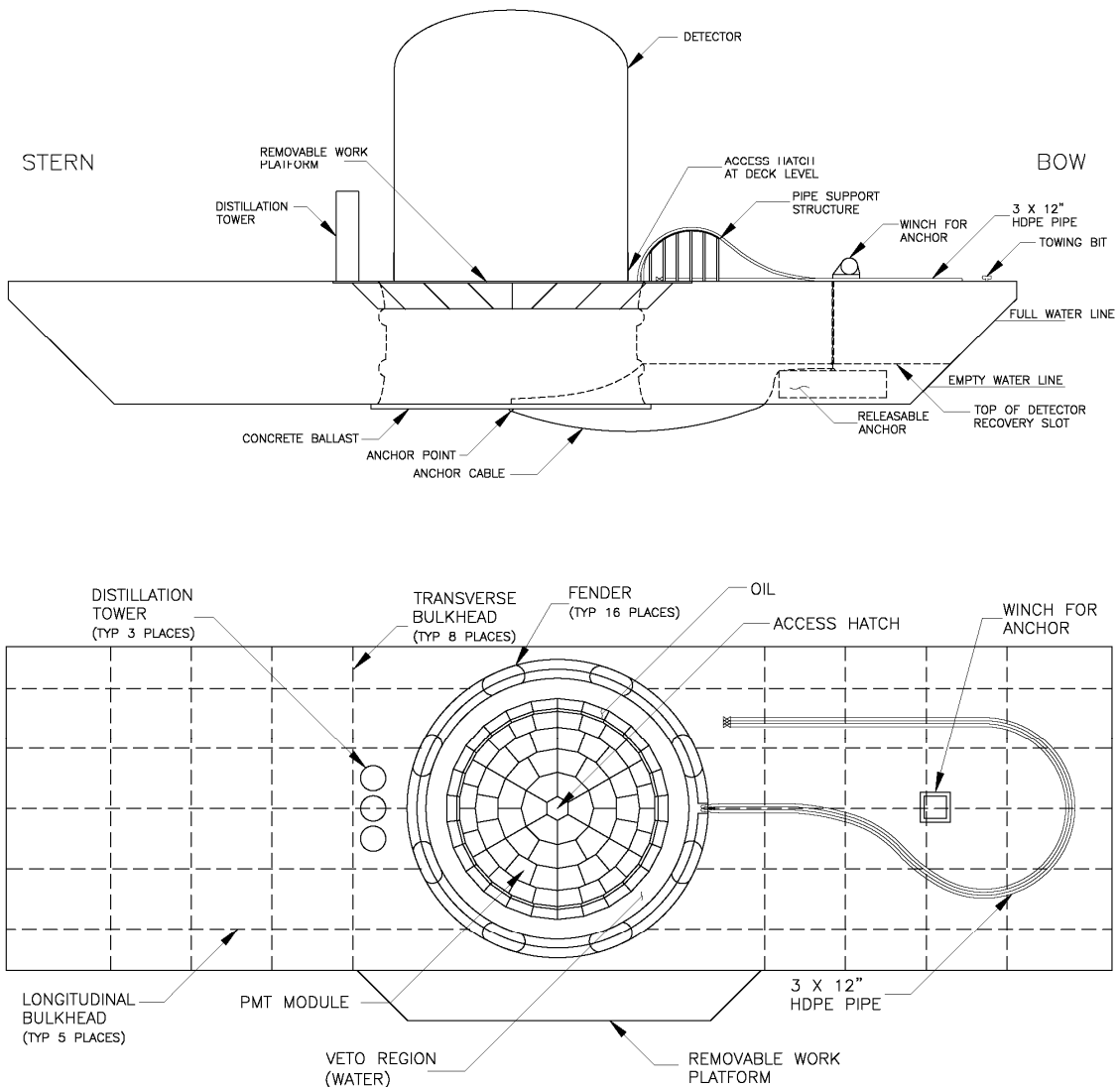


**Figure 1-2:** Overview of the final Hanohano

- The final design focused on the detachable configuration with a separate support barge and detector.

**Barge:**

- The support barge has a overall length of 112 m, a beam of 32.3 m (just fitting the Panama Canal), and an overall height of 13.8 m. Fully loaded draft is less than 10 m.
- The support barge has a conventional barge-shaped bow and stern. With a nominal draft, the detector can be towed safely and reliably to any location on the world's oceans.
- The barge contains tanks for storing all the scintillator and all the oil used in the detector. Multiple stainless tanks are used to maintain the liquid purity, to facilitate transfer during purity distillation, and to maintain barge stability when tanks are partly filled; Nitrogen is used in unfilled voids to maintain purity..
- The barge serves as the hotel for detector support. Crew quarters, lab space, generators, water production equipment, nitrogen storage, and scintillator cleaning equipment are located in or on the barge.
- The detector uses a nominal  $7000 \text{ m}^3$  of fresh water to eventually flood the veto region during submergence. This fresh water is generated with a built-in RO plant. Producing the fresh water needed is more economical than transporting it.
- The estimated cost of the support barge is 6.4 million dollars.

**Detector:**

- The Detector is cylindrical with an outer diameter of 26 m, and an overall height of 44.7 m. The fiducial volume has a diameter of 20 m and an overall height of 35 m. There is a buffer layer 1 m thick surrounding the scintillator and a 2 m layer of fresh water veto region surrounding that layer.
- There are approximately 4300 phototubes spaced at a nominal 0.8 m in the buffer region surrounding the fiducial volume. Clear Lexan plates separate the scintillator region from the surrounding oil.
- The 2 m wide veto region is built in layers with horizontal grated decks spaced at a nominal 4.8 m. Decks are accessible within the detector through stairwells in the veto region. The veto region is the main manned access into the detector, with all wiring and plumbing going through this area.
- Some decks within the veto region are water tight, to provide stable and minimal free-surface flooding stages during deployment.
- Large polypropylene compensator bags are located at the bottom of the detector to compensate for volume changed due to compression and cooling at 4000 m depth. The compensators compensate for the fresh water and scintillator only. The Oil buffer region is compressed by a flexing of the Lexan cover plate, therefore the oil volume change is compensated by larger scintillator fluid

compensation bags. Compensation is about 5% of the total volume of the detector – half of that is due to cooling, half due to compression.

- Pre-cooling the scintillator and oil were considered but this did not prove to be economically viable.
- The detector has a nominal concrete ballast of 744 tonnes (wet). This will vary as the structural requirements are refined.
- The detector has an anchor weight of 607 tonnes (wet). When it is launched, it weights 86 tonnes. When it leaves the bottom after a lengthy deployment, it is 87 tonnes buoyant, once it drops its anchor weight. Transit times up and down are 38 and 39 minutes respectively.
- Each PMT compartment contains 9 PMTs in a 3x3 array. These compartments are kept isolated from each other in order to (1) avoid differential pressures across the lexan plate due to density variations between the oil and the scintilarot and (2) to isolate damage to a single compartment in case there is a PMT sphere implosion. (If there is an implosion, and the Lexan plate leaks, only the oil from one compartment will mix into the scintillator – a contamination level that is not desirable but acceptable to the physics.)
- All plumbing for flooding and draining the interior of the detector is contained within the veto region.
- The estimated cost of the Detector is 30.1 million dollars.

The technical discussion and results of this task are reported in Chapter 3.

#### 1.4.5. TASK 13 - Engineering study for preparation of low radioactivity scintillation material.

This task considers the handling of the scintillator during the lifecycle of Hanohano. It investigates means of constructing the detector and storage tanks, cleaning them, and filling them such that a minimum amount of radio active material is introduced to the scintillator. In addition, this task determines means of purifying the scintillator of the small amount of contamination that will inevitably occur. The UH physics department has gained experience from the KamLAND and Borexino projects in achieving the needed levels of radiopurity. A written report describes the methods and procedures for meeting the purity specifications.

##### Summary results and Conclusions

- Scintillator is sensitive to all radioactive particles, including: oxygen, radon, krypton, uranium, thorium, potassium, as well as other noble gasses and chemical contaminants.
- To prevent radioactive contamination of the detector and storage tanks, they must be constructed of stainless steel and welded with electrodes free of thorium. The welds must be inspected and a leak test performed. All surfaces must be electropolished and have a surface roughness less than  $0.6 \mu\text{m}$ .
- After construction is completed, the inner cylinder and storage tanks will adhere to clean room regulations. Anything entering the detector or storage tanks must

first be cleaned. People entering the clean room must pass through an air lock with an air shower and wear a suit, mask, and boots.

- All inner surfaces of the detector will be cleaned at least four times by lowering a large collapsible scaffold through the access hatch. The storage tanks must also be cleaned.
- The tanks will be dried with nitrogen and stored full of nitrogen so they have no further contact with air.
- The scintillator will undergo four purification processes to remove any trace radioactive elements.
  - Water extraction
  - Nitrogen stripping
  - Vacuum distillation
  - Filtration
- When transporting scintillator from the tanks to the detector, the scintillator will be pumped into the detector as the nitrogen is pumped out and into the storage tanks to prevent contact with air.

#### 1.4.5.1 Summary results and Conclusions

The technical discussion and results of this task are reported in Chapter 5.

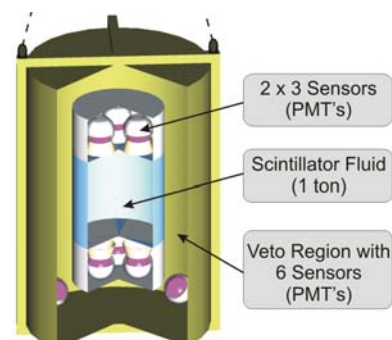
#### 1.4.6. TASK 14 – Design and costing for ocean demonstration.

It was desired to deploy a reduced scale detector in the ocean at the end of the second year of CEROS funding. The need is to test and demonstrate a reduced scale detector with reduced instrumentation and power. The goal is to test key components and materials such as the scintillating fluids, several photo-detectors, communications, deployment methods, and fabrication procedures. The demonstration of these basic instrumentation functions in the deep ocean was viewed as necessary in order to build confidence in funding agencies such as NSF that such a detector could be built and operated in the deep ocean.

#### 1.4.6.1 Summary results and Conclusions

It was desired to deploy a reduced scale detector in the ocean at the end of the second year of CEROS funding. The need is to test and demonstrate a reduced scale detector with reduced instrumentation and power. The goal is to test key components and materials such as the scintillating fluids, several photo-detectors, communications, deployment methods, and fabrication procedures. The demonstration of these basic instrumentation functions in the deep ocean was viewed as necessary in order to build confidence in funding agencies such as NSF that such a detector could be built and operated in the deep ocean.

- A small anti-neutrino demo structure was



designed to test and demonstrate detector electronics, the scintillator, and some critical aspects of deployment.

- Six active PMT's and three veto-region PMTs are installed in a cylindrical package that would be lowered by a UH oceanographic ship.
- Tests were planned for testing the PMT electronics, communications with the detector, clarity and performance of the scintillator, and critical displacement variations (compression and cooling) at 4000 m.
- A separate structure was designed for further testing of the impact of implosions. This test would evaluate the damage to a PMT chamber of 9 PMT spheres and the Lexan cover in the event of an implosion. The resistance to sympathetic implosions in a final system configuration would be demonstrated.

The technical discussion and results of this task are reported in Chapter 6.

## 1.5 BASIS OF DESIGN DOCUMENT

The project team has worked on this program for nearly 16 months. A primary document coordinating this effort has been a Basis of Design (BOD) document that defined the ocean engineering requirements of the structure and evolved as the design changed. For example, the original concept was for a detector configured as shown in Figure 1-1. The concept at the end of the project is considerably different both in size, shape, deployment and operation.

The Basis of Design Document is attached as Appendix A.

## 1.6 ENGINEERING APPROACH:

This engineering effort was conducted by Makai Ocean Engineering in collaborative effort with the Department of Physics and Astronomy at the University of Hawaii. UH provided science criteria for the detector, and UH assisted with innovative suggestions and solutions throughout the effort.

The engineering effort started with the Basis of Design – an evolving document that defines the basic engineering criteria for this detector based on the physics involved, the mission envisioned, and practical operations and economics.

The essence of the detector is as follows: A massive quantity of scintillating fluid in a relatively compact and undivided shape encased in an optically clear container and surrounded by a layer of oil 1 m thick and a second layer of fresh water 2 m thick. The scintillating and oil layers are to be extremely clean and contamination free. This whole system is to be placed on the seafloor at 4000 m deep and operate unattended for a nominal year, being attached to shore through a power and fiber optic cable.

The engineering team evaluated a variety of concepts and detector shapes in order to determine the engineering limitations and opportunities of Hanohano. This design process, evaluating Hanohano from the big picture point of view, is discussed in Chapter 2. Once a size, shape and configuration were selected, a more focused conceptual design of a 10,000 m<sup>3</sup> scintillator detector was prepared.

Since the overall goals of the program were to identify problems and opportunities, and to determine the feasibility of construction, deployment, and operation of this detector in the deep ocean, the engineering team searched for one or more solutions to the engineering problems envisioned. The concepts presented are not intended to be the only feasible solution or even the optimal solution. By finding one or more practical solutions or concepts, we had accomplished our goal: the detector can be built and operated.

## **2. CONFIGURATION ANALYSIS AND SELECTION:**

### **2.1 INTRODUCTION**

#### **2.1.1. What is in this chapter**

The engineering challenge has been determining the best structure to contain the anti-neutrino detector in order to satisfy the unique and complex needs of the physics – the most stringent requirement being the deep seafloor placement and retrieval of a very massive structure. The Basis of Design (BOD) attached to this document defines the engineering requirements of this detector.

From the beginning, there were basic questions such as:

- What is the shape of the detector?
- How large is the detector fiducial volume? How large can it be?
- What is the best configuration such that it can be practically built and operated?

This chapter answers the above questions.

The design process was initiated by brainstorming the basic problem in order to derive a variety of attractive candidates. Makai then analyzed these detector candidates looking for possible showstoppers or fundamental constraints. The fundamental design limits with Hanohano have been analyzed in terms of:

- Weight and Displacement: can it be lowered and retrieved? This analysis defines the total weight and displacement of candidates and sets limits on structure size.
- Stability: is it stable at all points of its life cycle? This analysis defines the gross dimensions of the structure and determines which configurations are stable at several critical stages of the lifecycle.
- Structure: Can it be practically built? With the size, weight and shape constraints driven by in-water submergence and stability, this analysis determines the likelihood that a cost-effective structure could be built.
- Operations: Can it be practically operated throughout its lifecycle including transportation, deployment, outfitting, testing, etc? These considerations, sometimes quite complex, have been included throughout the evaluation.
- Cost: Are there identifiable cost restraints? There is a science need to be large and that needed to be matched with financial reality – cost was a factor in selecting a final size.
- Size: Are there identifiable size restraints? Most of the analysis was done as a function of overall size in order to determine if there is a fundamental scale factor in the selection process.

This chapter primarily discusses weight, stability and structure for several candidates as a function of overall size. A logic is presented that finally focuses the design to a particular size and

configuration. That specific selection is then further refined in Chapter 3, the conceptual design of Hanohano.

### 2.1.2. The basic candidates:

#### 2.1.2.1 Shape

The heart of the Hanohano detector is a very large unobstructed volume of scintillator fluid contained in a transparent shell. The container holding this fluid will be subjected to a range of varying forces throughout the life cycle. What is the ideal shape of this volume? This analysis considers spheres, cubes, cylinders with flat ends, cylinders with rounded ends, and elevated cylinders. These are illustrated in Figure 2-1.

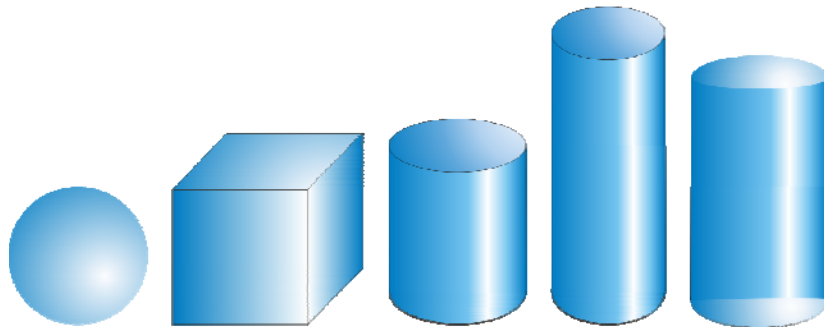


**Figure 2-1:** Candidate scintillator shapes

#### 2.1.2.2 Configuration

Three basic configurations were considered in this analysis:

- **Small lowered system:** The initial proposed configuration is illustrated in Figure 2-2. This concept envisioned a relatively small spherical scintillator volume that was lowered to the seabed by a deployment vessel. This design is similar to existing neutrino detectors operated in deep mines. The realized disadvantages were handling, transport and severe size limitations. Detailed analysis of this structure was terminated early as it became readily apparent that handling would greatly limit the size of the detector.

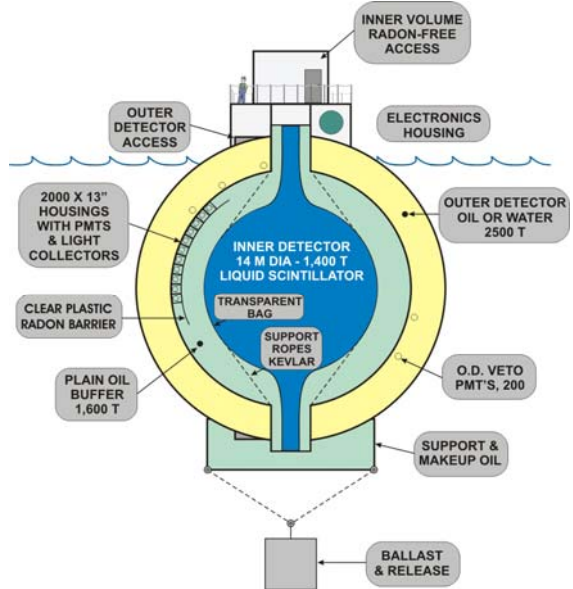


**Figure 2-2:** The initial Hanohano concept, lowered sphere.

- **Integrated System:** In an attempt to accommodate much larger scintillator volumes, a barge-like hull was added to the detector as shown in Figure 2-3. This barge could support the detector filled with scintillator, dock at a main port, transport to the test site, and controllably flood the barge and submerge to the bottom without lowering lines. The buoyancy control is based on a balance between the steel structure and the lift from a low-density scintillator.

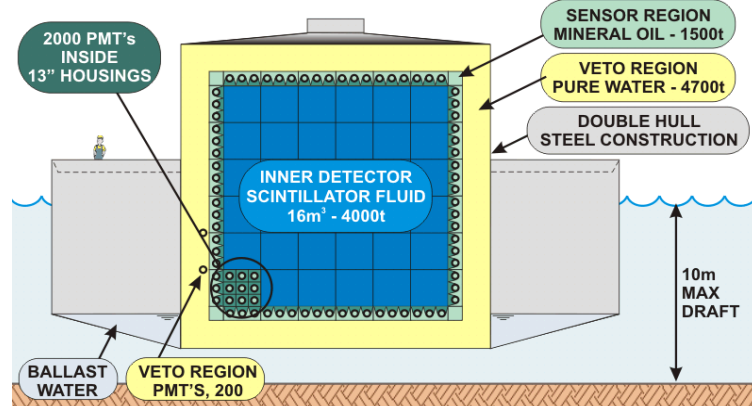


**Figure 2-3:** The integrated concept - providing a means of surface transport and bathyscaphe-like deployment

- **Detachable System:** In response to stability and weight restraints that made the structural design of the integrated system questionable, the detachable system was envisioned as shown in Figure 2-4. This system separates the barge functions from the detector functions and thus improves stability and weight issues. Only the structure (weight) absolutely needed on the seabed submerges. Furthermore, to keep high stability, the detector fluids are stored in the barge for transport and transferred to the detector as part of the submerging process; this concept never has the massive detector supported high above the sea surface.

The barge remains dry and is thus a practical location for fluids storage, fluids transport, support equipment, lab space and hotel.

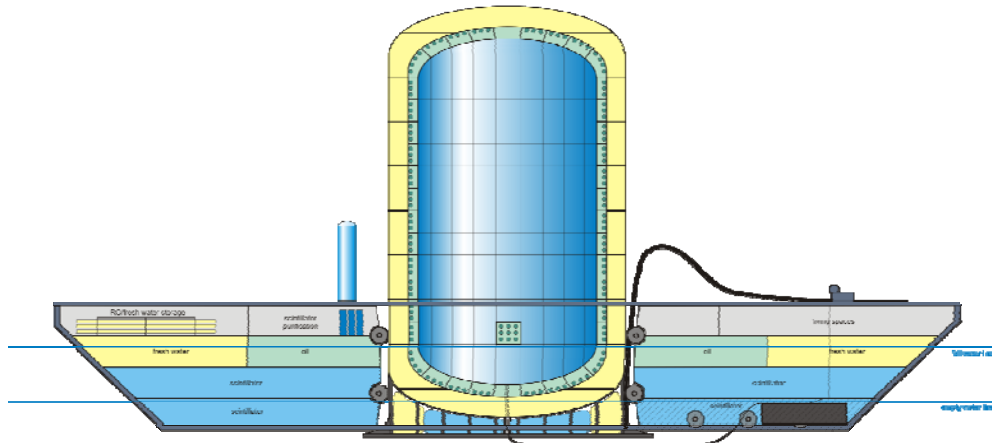


**Figure 2-4:** *Detachable detector: separating the transport structure from the underwater detector*

## 2.2 BUOYANCY, WEIGHT AND SIZE LIMITATIONS

This section evaluates the submerged and surfaced detector in terms of weight, displacement, and draft and determines whether the detector can reliably accomplish a 4000 m deep roundtrip mission. The evaluation determines the weight limits for the structure, the submergence and resurfacing times, and the volumes, weights and displacements of all components throughout the mission cycle. In addition, this broad evaluation looks at the practical size limitations of the overall detector.

### 2.2.1. Weight limitations

Hanohano is a unique underwater vehicle. When built, it may be the most massive structure ever deployed in the deep ocean. The engineering mission of Hanohano is to reliably place on the seabed at 4000 m a vehicle with a mass of 25 kilo tonnes and retrieve it after a year of service. Nuclear submarines, in contrast, are smaller. A Titanium Soviet Alfa class submarine is capable of 800 m depth and has a displacement of 3 kT; a US Virginia Class submarine is roughly 13 kT with a shallower depth capability. These submarine costs are in the range of billions of dollars. The Hanohano mission is to go to 4000 m at 1% the budget.

Hanohano can not be economically lowered to the seabed with a winch and line. At 4000 m operating depth, a winch with any significant payload capability (relative to the 25 kT mass), would exceed any practical limits for winch size, drum size, and cable costs. Steel cable struggles under its own weight at these lengths; and synthetic line is costly. 4000 m of 1 kT synthetic line (supporting 4% of the vehicle mass) would cost in the order of \$20 million (\$5/m/tonne-breaking-strength) at a 5:1 safety factor. Use of this type of gear would require extraordinary equipment at sea and add considerably to the overall project costs. It was therefore determined that to be economically viable, Hanohano must submerge and resurface based on its own weight and buoyancy.

## 2.2.2. Size Limitations

There are basically two size limitations driving the overall structural dimensions of Hanohano:

- Panama Canal: It is desirable that Hanohano be able to fit through the Panama Canal. With future experimental sites being global, being able to fit through the canal is desirable. Alternate passage is possible through the Suez Canal or through the Straights of Magellan if this Panama size is not achievable. The Panama Canal limitations are:
  - width - 32.3m
  - length - 294.1m
  - draft - 12m in fresh water
  - height - 57.9m
- Draft: 10 m max draft in-harbor was selected as desirable for outfitting and testing the detector prior to deployment. This would allow the detector to operate both in Honolulu harbor and in Kawaihae on the Big Island. This depth is typical of many large harbors, so this draft is suitable for global operation.

## 2.2.3. Weight Balance

Hanohano is economically feasible only because its primary payload, the scintillator, can be buoyant. A preferred scintillator will have a low specific gravity, providing sufficient buoyancy to support the entire Hanohano structure. Two of the early deep diving manned submersibles, the Trieste and the FNRS-2, were patterned after dirigibles and employed gasoline as the buoyancy material. The Trieste descended successfully to 10,000 m depth, carrying two men in a small steel sphere.

This section evaluates the total weight balance of Hanohano taking into account the density and displacement of all components at all working pressures and temperatures. The net result is the maximum allowable structure weight as a function of Hanohano size.

## 2.2.4. Material densities as a function of pressure and temperature

The primary materials envisioned for Hanohano are:

- Scintillator: Several candidate fluids have been considered for Hanohano. Linear Alkylbenzene, or LAB, has been the front-runner in terms of performance, availability and cost (See UH report on Scintillator testing); it has been selected for this engineering analysis. Note that the density of Dodecane is lower, but this material has less desirable compatibility with acrylics. Using LAB 501 is a more conservative approach for this engineering feasibility.
- Oil: Makai has assumed the oil properties are the same as LAB 501. This is easily achievable in a mineral oil - some oils have a density of 0.84.

- Fresh Water: Fresh water is loaded into the outermost layer of the detector. Oil is an alternative, but fresh water is the more convenient. This region provides human access to the electronics and an oil-free region would be preferable.
- Steel: both carbon and stainless steels will be used in Hanohano as the most common structural material. Aluminum is an alternate possibility if the submerged weight becomes critical, but steel is preferred as it is a more economical material to use.
- Concrete: Some ballast weight will be needed to provide stability and some weight will have to be left on the seabed to recover the detector. Concrete is the most economical weight to use for ballast and anchors.

The densities of the various fluids are shown in Table 2-1 below. The conditions considered are 28° C at 1 atm on the surface, and 1.5° C at 4000 atm on the seabed.

**Density of Hanohano fluids:**

	Temp C	Depth, m m	Ambient Seawater Salinity ppt	Ambient Seawater Density kg/m³	Flooding Seawater Salinity ppt	Flooding Seawater Density kg/m³	Fresh Water Density kg/m³	LAB Density kg/m³	DD Dodecane Density kg/m³	LAB 501 linear alkylbenzene kg/m³	LAB 540 linear alkylbenzene kg/m³
Surface: Pressure only	28	0	35	1022.397	35	1022.397	996.237	852.339	746.000	852.339	852.292
	28	4000	35	1039.137	35	1039.137	1013.695	881.474	771.500	-	-
Temperature only	1.5	0	35	1028.010	35	1028.010	999.924	870.159	765.396	870.159	869.782
Temp and Pressure	1.5	4000	35	1046.391	35	1046.391	1019.476	899.903	790.896	2.09%	2.05%
Temp and Press and Salinity	1.5	4000	34.6	1046.082 2.32%		2.35%	2.33%	5.58%	6.02%	-	-100.00%

**Table 2-1: Table of fluid densities for surface and at-depth conditions**

To evaluate the net buoyancy and weight of the Hanohano detector, the densities of the above materials are needed under the following conditions:

- Launch: The detector is on the surface at a nominal ambient temperature of 28° deg C. At this point, when released, the detector must be negatively buoyant in order to submerge.
- Touchdown: As the detector submerges, the pressure increases to 4000 m of seawater and the fluids in the detector compress. The detector, because of its mass, remains at the starting temperature of 28° C.
- Lift-Off: Once Hanohano is ready for recovery, it has cooled to ambient temperature (1.5° C). The temperature drop further contracts the fluids.
- Surfaced: As Hanohano quickly ascends, it remains cool but the pressure returns to one atmosphere. The decrease in pressure allows the fluids to expand, but they are still denser than they were at launch because of their low temperature. (Due to adiabatic expansion, the temperature cools slightly, approximately 0.3° C, but this is not included in this analysis).

Since the fluids contract and expand during the deployment, additional fluid must be available to move into the detector. This additional fluid is provided by a system of flexible compensation bags. See section 3.4.3 for details on the compensation system.

The following table provides the material densities that have been used for each of the liquids and primary solids in this analysis. One option that is considered in this analysis is pre-cooling the scintillator, oil and fresh water to minimize the density variations during descent and thereby minimizing the size of the disposable anchor any fluid volume compensation required during the deployment.

Materials Properties		Launch	Touchdown	Lift off	Surfaced
density scintillator	tonnes/m3	0.852	0.882	0.900	0.870
pre cooled	tonnes/m3	0.870	0.900	xxxx	xxxx
density oil	tonnes/m3	0.852	0.882	0.900	0.870
pre cooled	tonnes/m3	0.870	0.900	xxxx	xxxx
density of fresh water	tonnes/m3	0.996	1.014	1.019	1.000
pre cooled	tonnes/m3	1.000	1.019	xxxx	xxxx
density steel	tonnes/m3	7.840	7.842	7.842	7.840
density concrete	tonnes/m3	2.404	2.410	2.410	2.404
density ambient seawater	tonnes/m3	1.022	1.046	1.046	1.022

**Table 2-2:** Material densities used for Hanohano operational scenarios

### 2.2.5. Impact of Scintillator Shape

A variety of scintillator volume shapes were considered. The primary factors driving scintillator shape were:

- The Scintillator container's width is the primary factor in determining the overall width of the total structure. The width of the scintillator plus 6 m (1 m each side for the oil layer and 2 m each side for the veto region) determines the minimum width of the total structure. In addition, there needs to be some added width for structure and stability. To fit a vessel in the Panama Canal, total widths need to be less than 32.3m.
- As the scintillator shape changes, the volumes and mass of the surrounding oil and fresh water change as well. Depending upon the overall size of the detector, these volumes can be actually greater than the scintillator volume. These additional masses drive up the cost of the detector because additional steel is needed to contain and support these added fluids.
- To adequately cover the scintillator volume with PMT sensors, the number of PMTs required varies with scintillator shape. For this analysis, we assumed that PMT spacing is 0.8 m (or 1 PMT per  $0.64 \text{ m}^2$ ). This is an engineering estimate; it is not a rigorous physics requirement.
- As will be discussed later, some shapes are easier and lighter to fabricate than others.

Table 2-3 and Table 2-4 below show the primary dimensions and volumes for two different sized scintillator volumes ( $4.5 \text{ k-m}^3$  and  $9 \text{ k-m}^3$ ).

- The sphere is the most efficient in terms of minimal volumes and surface area, however it is the least efficient in terms of width and, as will be discussed later, rather difficult to build.

- A cube is fairly compact, but a cylinder (#3) with the same width as the equivalent cube is more efficient in terms of oil and water volumes and in surface area (PMT's).
- If width needs to be further reduced, the cylinder can be raised as in case #4. This narrower width comes at a cost of higher volumes and surface areas.

		1 cube	2 cylinder	3 Sp Cylinder	4 High Cylinder	5 sphere
Shape:						
Scintillator:						
Width	m	16.51	17.89	16.51	14.54	20.48
Length	m	16.51	17.89	16.51	14.54	20.48
Height	m	16.51	17.89	21.03	29.09	20.48
Volume	$\text{m}^3$	4,500	4,500	4,500	4,500	4,500
Oil volume	$\text{m}^3$	1,842	1,684	1,695	2,182	1,451
Water Volume	$\text{m}^3$	5,064	4,530	4,559	4,948	3,775
Bottom Area	$\text{m}^2$	507	448	398	331	551
Scint'r Surface	$\text{m}^2$	1,635	1,509	1,518	1,661	1,318
Phototubes:	#	2555	2358	2373	2596	2060

**Table 2-3:** Shape parameters for a  $4.5 \text{ k-m}^3$  scintillator (4 kT) detector.

		1 cube	2 cylinder	3 Sp Cylinder	4 High Cylinder	5 sphere
Shape:						
Scintillator:						
Width	m	21.54	23.35	21.54	18.98	26.73
Length	m	21.54	23.35	21.54	18.98	26.73
Height	m	21.54	23.35	27.44	37.96	26.73
Volume	$\text{m}^3$	10,000	10,000	10,000	10,000	10,000
Oil volume	$\text{m}^3$	3,051	2,796	2,814	3,811	2,417
Water Volume	$\text{m}^3$	7,846	7,063	7,107	7,729	5,942
Bottom Area	$\text{m}^2$	759	677	596	490	841
Scint'r Surface	$\text{m}^2$	2,785	2,569	2,586	2,829	2,245
Phototubes:	#	4351	4015	4040	4420	3507

**Table 2-4:** Shape parameters for a  $10 \text{ k-m}^3$  scintillator (9 kT) detector.

All five of the above shapes were used in the preliminary vessel analysis.

### 2.2.6. Example Analysis: Integrated Structure

The following Table 2-5 shows a weight and displacement balance sheet for a typical Hanohano scenario in the Integrated Structure configuration (Reference Sections 2.3.2 and 2.4.4). The following discussion is on the major features of this tabular presentation.

- The effective scintillator volume of this detector is  $6,000 \text{ m}^3$ , 5.4 k-tonnes. This is the usable volume of scintillator on the seafloor and once the scintillator has cooled. Note that the beginning volume (on the surface), is  $6,335 \text{ m}^3$ .
- The shape of the scintillator is an elevated cylinder where the diameter is equal to that of a similar volume cube. The diameter is 18.2 m and the height is 23.2 m.

- There is a 1 m thickness layer of oil surrounding the scintillator. This is followed by a 2 m layer of fresh water.
- None of the liquids are pre-cooled prior to launch.
- The assumed steel is equivalent to 17% of the total mass of the scintillator plus the oil. Makai used this as a standard ratio (steel to scintillator + oil mass) since we were comparing this structure to small and medium sized tankers. Tankers are sized based on their deadweight – DWT – which is predominately the weight of their oil cargo. In our case, this is closely equivalent to the scintillator plus oil mass (the Hanohano DWT). The space between the outer and inner hull, filled with fresh water, was considered as the space in a double hull tanker. Therefore, this ratio was useful when looking at construction costs and weights of standard tankers.
- The minimum weight to sink is 0.7% of the DWT. Knowing the initial and final weight of Hanohano during deployment will be a problem, because it will be very difficult to “weigh.” Therefore, there will have to be conservative values used for both the submergence and lift-off buoyancies.
- The minimum buoyancy to lift off is 0.7% of DWT. This needs to be safely larger than the maximum error in the bottom weight and displacement calculations.
- The minimum weight on the seabed is 0.2% of DWT. With the above numbers, this is easily achieved.
- The primary table shows the mass, displacement, and size of the scintillator, oil, water, concrete and steel during the four phases of the deployment: launch, touchdown, lift-off and surfacing.
- Note that the scintillator volume is 6,000 m<sup>3</sup> on the bottom just before lift-off. This is when the scintillator is at maximum pressure and minimum temperature. The scintillator is 36% of the total mass of the detector; its volume change is 335 m<sup>3</sup>.
- The oil mass is 12% of the total mass of the detector and requires changes volume by 114 m<sup>3</sup>.
- The fresh water volume is nearly equal to that of the scintillator and its mass is 37% of the total mass of the detector making it the heaviest component. The fresh water will require a volume compensation system with a capacity of 125 m<sup>3</sup>. Fresh water is considerably less compressible than scintillator.
- The spreadsheet computes the minimum concrete required to:
  - Provide the minimum launch weight,
  - Provide the minimum on-bottom anchoring weight,
  - And allow for the minimum lift-off buoyancy once an anchor is dropped.

- In this configuration, 907 tonnes of concrete are added to the structure of which 633 tonnes (358 tonnes wet) are dropped on the seabed during retrieval.
- The mass distribution between components is shown in the column to the right. 36% is in scintillator, 12% in oil, 37% in fresh water, 8% in steel, 4% in a droppable anchor, and 2% in ballast.
- The column to the far right shows the change in volume for the scintillator, oil and fresh water. The compensator bags will be needed slightly larger than these volumes; the total of the three compensator volumes is  $573 \text{ m}^3$  which is 3.9% of the total displacement volume of the detector.
- The detector will leave the surface negatively weighted at nearly 51 tonnes. Once it reaches the seabed, after compression, the system will have a net weight of 100 tonnes. After it has cooled, and a 358 wet tonnes anchor is dripped, the detector is buoyant by 51 tonnes. Once it reaches the surface, it is 108 tonnes buoyant.
- The total size of the barge portion of the detector is computed at the bottom of the table. The hull beam is 27.9 m allowing it to fit through the Panama Canal; effective length is 52m. Draft fully loaded is 10 m; draft fully empty is 1 m. The actual length will be greater than 52 m once a proper bow and stern is built into the hull (this analysis assumes a rectangular solid).
- Descent speeds and times are computed at the bottom. Upon submergence, the detector initially sinks at 0.67 m/s and reaches a velocity of 0.93 m/s just before touchdown; the total drop takes 84 minutes. The recovery time is a little less at 81 minutes.
- Anchoring on the seabed is easily accomplished. The required weight on the seabed for this detector in a strong deep water current of 0.15 m/s is only 1.5 tonnes. The actual net weight on the bottom will be 100 tonnes at touchdown and over 300 tonnes after cooling. These weights are driven by the margins of error on the recovery and the density change of the detector due to cooling on the bottom.

Overall, the above detector appears reasonable, as long as the structure can be built within the weight budget assumed above and the structure is stable. The structural and stability analyses are discussed in sections that follow.

The beauty of Hanohano, from the engineering point of view, is that this very large mass can be submerged and recovered fairly easily using the buoyancy of the scintillator and oil fluids. If these fluids were not so buoyant, this structure would be prohibitively expensive. Buoyancy, in general, is very expensive for the deep ocean – costing between \$15 and \$35 per buoyant pound. Therefore, it is particularly fortunate that these component weights and displacements balance out so nicely without requiring auxiliary buoyancy.

<b>Hanohano Integrated Detector</b>		shape:				% mass	dVol
		<u>6</u> width	<u>3</u> length	Sp Cylinder height			
Volume Effective Scintillator	k-m^3						
Hanohano shape: Sp Cylinder							
Scintillator dimensions	m	18.17	18.17	23.15			
Bottom Area	m^2	459					
Layer thickness:	m	xxxx	1.00	2.00			
Volumes payload liquids:	m^3	6,000	2,033	5,337			
Pre-cooled? 1=yes, 0=no		0	0	0			
Steel to DWT ratio for module		0.170	fraction of scintillator + oil mass				
Min weight to sink		0.007	fraction of scintillator + oil mass				
Min Lift off Buoyancy		0.007	fraction of scintillator + oil mass				
Min On-bottom weight		0.002	fraction of scintillator + oil mass				
Scintillator, size (width)	m	18.2	Launch	Touchdown	Lift off	Surfaced	
Volume	m^3	6,335		6,125	6,000	6,205	335m^3 (5.3%)
Mass	tonnes	5,399		5,399	5,399	5,399	36%
Oil, size (width)	m	20.2					
Volume	m^3	2,146		2,075	2,033	2,102	114m^3 (5.3%)
Mass	tonnes	1,829		1,829	1,829	1,829	12%
Fresh water, size (width)	m	24.2					
Volume	m^3	5,462		5,368	5,337	5,442	125m^3 (2.3%)
Mass	tonnes	5,441		5,441	5,441	5,441	37%
Steel Used:	tonnes	1,229		1,229	1,229	1,229	8%
Volume	m^3	156.7		156.7	156.7	156.7	
Concrete, min required:	tonnes	987.5		835.8			
Used:	tonnes	987.5		987.5			
	m^3	410.8		409.8			
Anchor, min lift off:	tonnes	632.9		632.9	-	-	4%
	m^3	263.3		262.6	-	-	
	wet tonnes	363.7		358.2	-	-	
Ballast:	tonnes	354.6		354.6	354.6	354.6	2%
	m^3	147.5		147.5	147.5	147.5	
	wet tonnes	203.8		203.8	-	-	
Total Module Displacement:	tonnes	14,836		14,786	14,304	14,362	100%
Volume	m^3	14,511		14,135	13,674	14,053	573m^3 (3.9%)
Total Module Weight, full	tonnes	14,886		14,886	14,253	14,253	
Net weight:	tonnes	50.6		99.9	-51.0	-108.7	
goals:		50.6		14.5	-50.6		

#### Integrated Barge

Added width:	m	<u>3.70</u>		
beam	m	27.87	Panamax OK	
Draft	m	<u>10.00</u>		
Length	m	52.25		
Drag Area:	m^2	1456		
Gr Anchor Req'd, 0.15m/s, f=0.5	tonnes		1.51	
Empty draft	meters	1.06		
Freeboard, surfaced:	meters			0.23
Submerge - Surface time:	minutes		<u>84</u>	<u>81</u>
Submerge - Surface max velocity:	m/s		0.93	0.98
Submerge - Surface min velocity:	m/s	0.67		0.66

**Table 2-5:** Weight, displacement, dimensions of Integrated Detector, 5.4 k-T

#### 2.2.7. Pre-Cooling of the Detector

The above detector volume can be pre-cooled to avoid the large displacement change due to cooling of the fluids. The advantages of this would be:

- The size of the compensator bags would be reduced. Table 2-6 illustrates the configuration with pre-cooled scintillator and oil. Water was not pre-cooled

because of difficulty in maintaining its temperature on the outside of the detector and the smaller benefits. In this illustration, the required size of the compensator bags is reduced by about 40%.

- Since the detector density at launch is closer to the final bottom density, the droppable anchor can be reduced. This weight changes from 358 wet tonnes to 182 wet tonnes.

#### Hanohano Integrated Detector

	k-m^3	shape:				
		6 width	3 length	Sp Cylinder height		
Volume Effective Scintillator	m	18.17	18.17	23.15		
Hanohano shape: Sp Cylinder						
Scintillator dimensions	m	459				
Bottom Area	m^2					
Layer thickness:	m	<u>Scintillator</u>	<u>Oil</u>	<u>Water</u>		
Volumes payload liquids:	m^3	xxxx	1.00	2.00		
Pre-cooled? 1=yes, 0=no		6,000	2,033	5,337		
Steel to DWT ratio for module		<u>1</u>	<u>1</u>	<u>0</u>		
Min weight to sink		0.170	fraction of scintillator + oil mass			
Min Lift off Buoyancy		0.007	fraction of scintillator + oil mass			
Min On-bottom weight		0.007	fraction of scintillator + oil mass			
		0.002	fraction of scintillator + oil mass			
Scintillator, size (width)	m	18.2	Launch	Touchdown	Lift off	Surfaced
Volume	m^3	6,205		6,000	6,000	6,205
Mass	tonnes	5,399		5,399	5,399	5,399
Oil, size (width)	m	20.2				
Volume	m^3	2,102		2,033	2,033	2,102
Mass	tonnes	1,829		1,829	1,829	1,829
Fresh water, size (width)	m	24.2				
Volume	m^3	5,462		5,368	5,337	5,442
Mass	tonnes	5,441		5,441	5,441	5,441
Steel Used:	tonnes	1,229		1,229	1,229	1,229
Volume	m^3	156.7		156.7	156.7	156.7
Concrete, min required:	tonnes	677.1		525.9		
Used:	tonnes	677.1		677.1		
	m^3	281.7		281.0		
Anchor, min lift off:	tonnes	322.5		322.5	-	-
	m^3	134.2		133.8	-	-
	wet tonnes	185.3		<b>182.5</b>	-	-
Ballast:	tonnes	354.6		354.6	354.6	354.6
	m^3	147.5		147.5	147.5	147.5
	wet tonnes	203.8		<b>203.8</b>	-	-
Total Module Displacement:	tonnes	14,525		14,476	14,304	14,362
Volume	m^3	14,207		13,838	13,674	14,053
Total Module Weight, full	tonnes	14,576		14,576	14,253	14,253
Net weight:	tonnes	50.6		99.7	-51.0	-108.7

**Table 2-6:** Weight and Displacement of Pre-cooled detector (same size detector as in preceding table)

Compensator bag reduction and anchor weight reduction are the primary advantages of pre-cooling; all other aspects of the detector remain unchanged. The question of whether there is economic benefit to pre-cooling is analyzed in the following chapter, section 3.5.6, using the final detector size and configuration.

### 2.2.8. Detachable Detector

Makai also analyzed the detachable detector, discussed in sections 2.3.4 and 2.4.5. The rationale for this arrangement is to minimize unnecessary weight on the seabed. The hull of the integrated detector is needed in port and for towing to site, but is not needed on the seabed. Therefore, if the hull could be left on the surface, there would be more steel and concrete available for the detector construction. This weight safety factor is important at this point in the design – further design issues need to be solved without being severely restricted in weight.

A weight and displacement analysis for the detachable system is illustrated in Table 2-7 and Table 2-8. Note the following:

- We have reduced the required steel for the detector only. Since the volumes of buoyant fluids have remained unchanged, the total weight of the steel plus ballast has not changed.
- The detector, with its smaller ascent and descent profile, sinks and rises more quickly. This detector would travel the 4 km distance in about 45 minutes.
- The barge primary dimensions, weight and displacements are provided in Table 2-8. The barge is a nominal 58 m long (rectangular solid), 32.3 m beam (fits in Panama Canal) and has a fully loaded draft of 9.6 m. Empty, the draft is 1.9 m.
- The barge has a capacity to carry all the scintillator and oil in separate compartments within the hull. Total capacity of these compartments is  $8481 \text{ m}^3$ . This represents 56% of the total inner volume of the barge. In addition, there is space for detector support and machinery.
- There is a recovery slot in the barge that provides a minimum of 1m clearance between the barge and the detector on all sides and 2 m clearance vertically. This side clearance volume would be filled with fenders.

**Hanohano Barge - detachable concept**

Barge freeboard, fully loaded	m	3.3	
Horiz clearance: detector to barge	m	1	
Barge beam / moonpool width PanamaMax?	m/m	1.5 1	ratio barge beam to Hanohano detector hole 1=yes, 0=ignore (use above for width)
Steel to DWT ratio for barge		0.2	fraction of scintillator + oil mass
Barge Hotel, Machinery mass		0.15	Fraction of primary steel structure
Vert Recov Clearance, barge/detector	m	1.90	
Barge maximum draft	m	10	
Min excess volume inside barge		0.2	unused by scintillator or oil

Geometry:

Guess effective Length:	m	<b>58.0</b>	
Beam, overall	m	32.30	
Deck ea.side of detector:	m	3.1	19% of beam
Moonpool, width	m	26.2	
Moonpool, area	m^2	537.8	
Position Moonpool, from bow	% length	50%	
Water plane area, above slot	m^2	1335.6	
Water plane area, at slot	m^2	845.6	
Total Height:	m	12.9	

Empty Barge, Ready for Recovery:

Weight, vol payload:		tonnes	
Barge Steel Structure:	tonnes	1,446	
Hotel, Machinery, Misc:	tonnes	217	
Total:	tonnes	1,663	
Displacement, empty:	m^3	1626.2	
Draft, empty:	m	1.9	
Height of the recovery slot:	m	4.1	from bottom

Fully Loaded Barge:

	tonnes	m^3
Scintillator Load:	5,399	6,335
Oil Load:	1,829	2,146
Empty detector, pre launch	tonnes	2,216
Barge Steel Structure:	tonnes	1,446
Hotel, Machinery, Misc:	tonnes	217
Total:	tonnes	11,108      8,481
Displacement, Fully Loaded:	m^3	10,864
Draft, Fully Loaded:	m	9.62

OK draft

Volume Barge:

Required Volume:	m^3	15,272	
% Used	%	8,481	
		56%	OK volume

Area outside surface:	m^3	5,540	assumes moonpool is circle
Average thickness of steel, surface:	mm	33	

**Table 2-7:** Detachable Detector weight and mass.

### Hanohano Barge (detachable configuration)

Barge freeboard, fully loaded	m	3.3	
Horiz clearance: detector to barge	m	1	
Barge beam / moonpool width PanamaMax?	m/m	1.5 1	ratio barge beam to Hanohano detector hole 1=yes, 0=ignore (use above for width)
Steel to DWT ratio for barge		0.2	fraction of scintillator + oil mass
Barge Hotel, Machinery mass		0.15	Fraction of primary steel structure
Vert Recov Clearance, barge/detector	m	1.90	
Barge maximum draft	m	10	
Min excess volume inside barge		0.2	unused by scintillator or oil

#### Geometry:

Guess effective Length:	m	87.0	
Beam, overall	m	32.30	
Deck ea.side of detector:	m	3.1	19% of beam
Moonpool, width	m	26.2	
Moonpool, area	m^2	537.8	
Position Moonpool, from bow	% length	50%	
Water plane area, above slot	m^2	2272.3	
Water plane area, at slot	m^2	1402.9	
Total Height:	m	9.4	

#### Empty Barge, Ready for Recovery:

Weight, vol payload:		tonnes	
Barge Steel Structure:	tonnes	1,446	
Hotel, Machinery, Misc:	tonnes	217	
Total:	tonnes	1,663	
Displacement, empty:	m^3	1626.2	
Draft, empty:	m	1.2	
Height of the recovery slot:	m	3.3	from bottom

#### Fully Loaded Barge:

	tonnes	m^3
Scintillator Load:	5,399	6,335
Oil Load:	1,829	2,146
Empty detector, pre launch	tonnes	2,291
Barge Steel Structure:	tonnes	1,446
Hotel, Machinery, Misc:	tonnes	217
Total:	tonnes	11,182      8,481
Displacement, Fully Loaded:	m^3	10,937
Draft, Fully Loaded:	m	6.07

OK draft

#### Volume Barge:

Required Volume:	m^3	18,435	
% Used	%	46%	OK volume

Area outside surface:	m^3	6,746	assumes moonpool is circle
Average thickness of steel, surface:	mm	27	compare to other barges?

**Table 2-8:** Barge portion of a 6 k-m<sup>3</sup> detachable system

### 2.2.9. Weight, Size Limits

Based on the above analysis, we can establish a maximum steel allowance for the detector system. Since the primary buoyancy and payload of the detector is the scintillator and oil, the steel allowance is computed as a percent of the total mass of the scintillator plus oil. This number is therefore fairly independent of the final size of the detector.

- For the Integrated Detector, a maximum dry steel weight of 15% of the weight of the scintillator plus oil is desirable. Values could be slightly higher, but there would be little weight available for stability ballast. Therefore an upper goal of 15% was established.

- Similarly, the detachable detector has a maximum dry steel weight of 15% of the scintillator plus oil. The maximum steel allowable for the barge is not a critical number. A value of 20% was used for the barge in the above computations; however this number could be larger or smaller with the primary penalty/benefit being the fabricated cost of steel.
- The above values are relatively independent of overall size. A value of 15.1% for a 4 k-tonne corresponds to a value of 14.9% for a 100 k-tonne detector. Therefore the steel limits are relatively independent of size.

## 2.3 SIZE, STABILITY, AND PERIOD OF ROLL

This section evaluates the stability of the Hanohano structure throughout the various phases of its operational life: filling, testing, transport, sinking, and recovery. Concepts that are unstable are eliminated as candidates for further consideration. This section examines a variety of detector sizes to see if stability dictates a maximum detector size. It establishes design limitations for the Hanohano structure.

Hanohano has a particularly difficult stability challenge due to the high elevation of the detector during transit and the narrow hull required to fit through the Panama Canal. In addition, there are large volumes of fluid that, during filling, slosh around in the tanks and add to the instability.

### 2.3.1. Introduction to Stability

A general background of ship stability is presented here. The effect of a free surface, which is very significant in this situation, is explained in this section.

Stability of a vessel is a concern because surface vessels have a center of gravity, CG, above their center of buoyancy, CB, so they are not inherently stable. The center of buoyancy occurs at the centroid of the displaced water and acts upwards. When the vessel begins to tip, the center of buoyancy should move to the side farther than the center of gravity so a righting moment will be created and the vessel will be returned upright. Note how the relative movement of CG and CB in Figure 2-5 create a righting moment. The geometry of a ship's hull is designed to shift the center of buoyancy to create positive righting moments, even at large angles.

An important concept to stability is metacentric height, GM. The metacenter, M, is the point at which vertical lines through the original and new centers of buoyancy intersect. The metacentric height is the vertical distance between the metacenter and the center of gravity. For small angles of roll, the metacentric height can be used to predict the stability of a vessel. If the metacenter is above the center of gravity, the metacentric height is positive, and the vessel will likely be stable. However, if the metacenter is below the center of gravity, the metacentric height is negative and vessel may capsize. Figure 2-5 illustrates the concept of metacentric height.

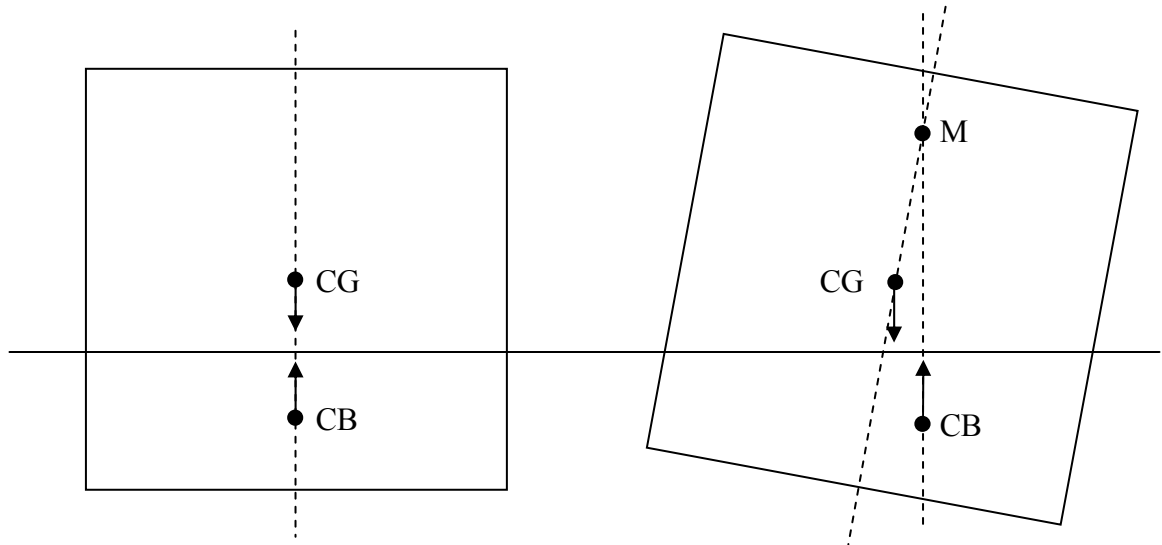


**Figure 2-5:** Illustration of metacentric height

An approximation of metacentric height is determined by draft, d, beam of the vessel, B, and the height of the center of gravity above the keel, KG, as shown in Equation 2-1.

$$GM = \frac{d}{2} + \frac{B^2}{12 \cdot d} - KG$$

**Equation 2-1:** Metacentric height

Since metacentric height is only an indication of initial stability at small angles, the righting moment for several angles must be determined to ensure the vessel is sufficiently stable. The static moment is often plotted versus angle, resulting in a plot known as a stability curve. Figure 2-6 is an example of such a curve. For a positive angle, if the moment is also positive it is a righting moment and returns the vessel upright. At any point where the moment is negative, the vessel is unstable and would capsize.

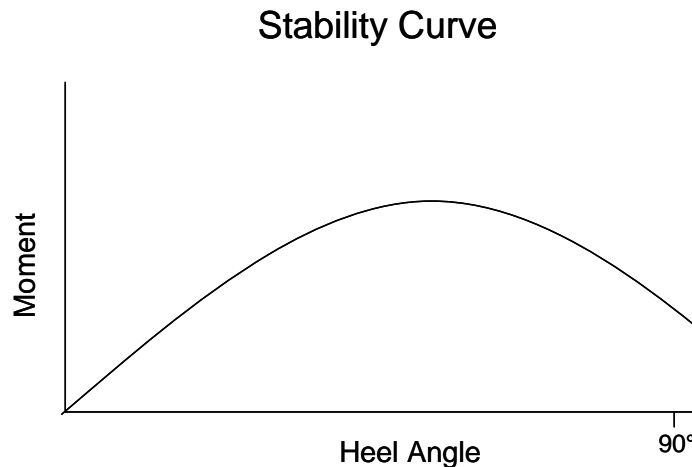


**Figure 2-6:** Example Stability Curve

Metacentric height is not only an indication of stability, but also period of roll. Period of roll represent the amount of time it takes a vessel to roll to one side and back again when it is hit by a wave. This value is important in two ways. First, if it is too short, the vessel will swing violently upright in a very short time. Second, resonance with wave period can occur. If the wave period is the same as the period of roll, the waves will reinforce the ship's movement each cycle and induce large roll angles. Typical waves have a period of less than 12 seconds. Therefore, a vessel should have a period greater than 12 seconds in order to avoid the excessive motion caused by resonance. The relationship between period, metacentric height, beam, B, and a constant C is given by Equation 2-2. The value of C for a typical ship is 0.44.

$$T = \frac{C \cdot B}{\sqrt{GM}}$$

**Equation 2-2: Period of Roll**

A free surface in the vessel can decrease stability. Usually, when a vessel is at some angle the center of buoyancy moves toward the side of the vessel deeper in the water, but the center of gravity remains along the centerline of the vessel. However, if a fluid with a free surface exists, the fluid will flow until the free surface is parallel with the sea water level, thus shifting the center of gravity in the same direction as the center of buoyancy. If the center of gravity moves farther than the center of buoyancy, the righting moment will be negative and act to push the vessel over. This free surface effect will be a major concern when filling the detector.

As the draft increases, the center of buoyancy moves up relative to the keel of the vessel. At some draft, the centers of gravity and buoyancy will be at the same point. Further increasing the draft will raise the center of buoyancy above the center of gravity and the vessel will be innately stable. However, when they occur at the same point, it is important to ensure that when the vessel is at an angle, the center of buoyancy still moves to create a righting moment.

Since this vessel will sink to the ocean floor and resurface, it must also be stable when completely submerged. This will only occur if the center of buoyancy is above the center of gravity when the vessel is submerged. Therefore, when designing this vessel to be stable on the surface, it is important to ensure the submerged stability is not adversely affected.

### 2.3.2. Integrated Design

This section addresses the stability of the integrated design concept, where the detector and the barge are permanently connected.

### 2.3.2.1 Detector Shape

Both a cubic and a cylindrical detector were considered. This section compares the stability of the two different shapes with and without a free surface.

When the effect of the free surface is not considered, the center of gravity is the major difference between the two shapes. For the same amount of scintillating fluid, the cylinder will be taller than the cube. Therefore, the cylinder would have a higher center of gravity and will be less stable.

A free surface reduces the righting arm as shown in Equation 2-3, where  $R$  is reduction in righting arm,  $i$  is the area moment of inertia of the detector volume,  $\rho$  is the density of the fluid,  $\Phi$  is the heel angle, and  $\nabla$  is the displacement of the ship.

$$R = i \cdot \rho \cdot \frac{\sin \phi}{\nabla}$$

#### ***Equation 2-3: Reduction in Righting Arm due to the Free Surface***

The only difference between a cube and cylinder in Equation 2-3 is the area moment of inertia. The equations for the area moment of inertia are shown in Equation 2-4 and Equation 2-5 for a cube and a cylinder, respectively.

$$i = \frac{D^4}{12}$$

#### ***Equation 2-4: Area Moment of Inertia of a Cube***

$$i = \frac{\pi \cdot r^4}{4}$$

#### ***Equation 2-5: Area Moment of Inertia of a Cylinder***

For a 10,000 cubic meter detector, the area moment of inertia of a cube is 18,000, whereas that of a cylinder is 14,600. This means the righting arm of the cube will be reduced more, and therefore the free surface has a greater effect on the stability of a cube.

The higher center of gravity of the cylinder is detrimental to its stability. However, the free surface negatively impacts the stability of the cube more than that of the cylinder. Thus, there are potential problems with both shapes and the decision will be left up to structural considerations. A cylindrical detector is analyzed below.

### 2.3.2.2 Vessel Size

The effect of vessel size on stability is presented here. Stability imposes constraints on the beam and height of the hull, while the length is determined by draft. These stability constraints will be used to choose a vessel size for a given detector size.

## Beam

The beam is determined by stability requirements for a detector filled with scintillating fluid and oil. The fresh water is not included since it can more easily be filled at sea. A wider hull creates a larger metacentric height and therefore a more stable vessel. First, it is important that the vessel is stable during all stages of its lifecycle. However, if the vessel becomes very stable, two problems can occur. The shorter period could resonate with wave period, or the strong righting moment can push the vessel upright quickly causing it to become uncomfortable for workers. Thus, choosing the width of the hull is a compromise between stability and period of roll.

The effect of the width of the hull, and therefore GM, on stability can also be seen graphically in Figure 2-7. Increasing GM increases the moment at all angles, while keeping the same general shape of stability curve. Therefore, increasing GM will improve stability.

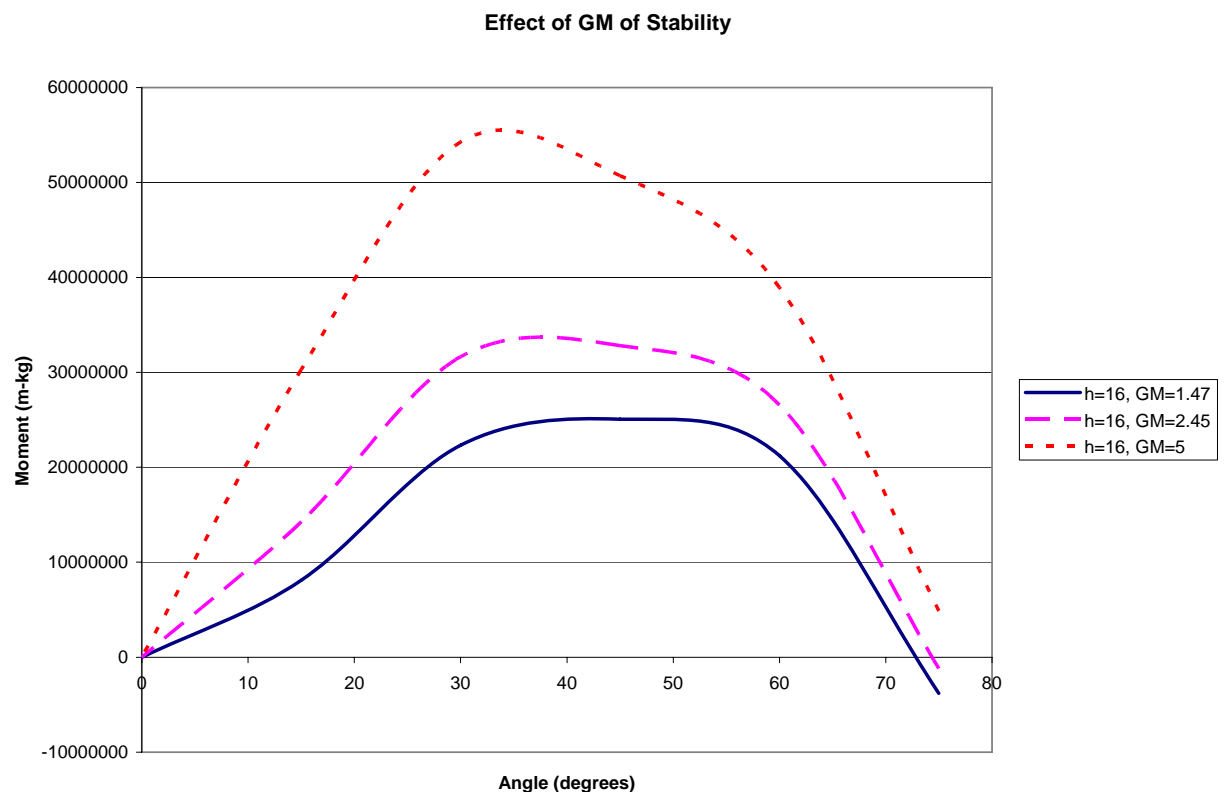


**Figure 2-7:** Effect of GM on Stability Curve

## Length

A typical deep harbor has a depth of approximately 10 meters, so the length of the vessel is chosen such that the draft is 10 meters when the detector is full of scintillating fluid and oil. The draft requirement causes the length to increase rapidly with size. This increases the amount of steel necessary for two reasons. First, the sheer size requires more steel.

Second, as the length increases, so does the bending moment caused by the detector load, and the hull must become proportionally stronger in addition to being larger. Therefore, there will be a point where the amount of steel necessary is greater than the amount of buoyancy available, which results in a maximum detector size, assuming a 10 meter draft limit.

### Height

Stability is affected by the height of the hull. If the hull is too low, water will wash over the deck at small angles and decrease the righting moment. However, increasing the height of the hull raises the center of gravity. If it is too high, the center of gravity will remain above the center of buoyancy when the vessel is later submerged, which would result in instability. Therefore, the height of the hull was determined such that the vessel would be stable both on the surface and when submerged. The effect of height of the hull on the righting moment can be seen in Figure 2-8, where  $h$  is the height of the hull. The height of the hull changes the overall shape of the stability curve, with higher hulls resulting in larger moments in the middle of the curve. This graph shows there is a minimum hull height for the vessel to be stable.

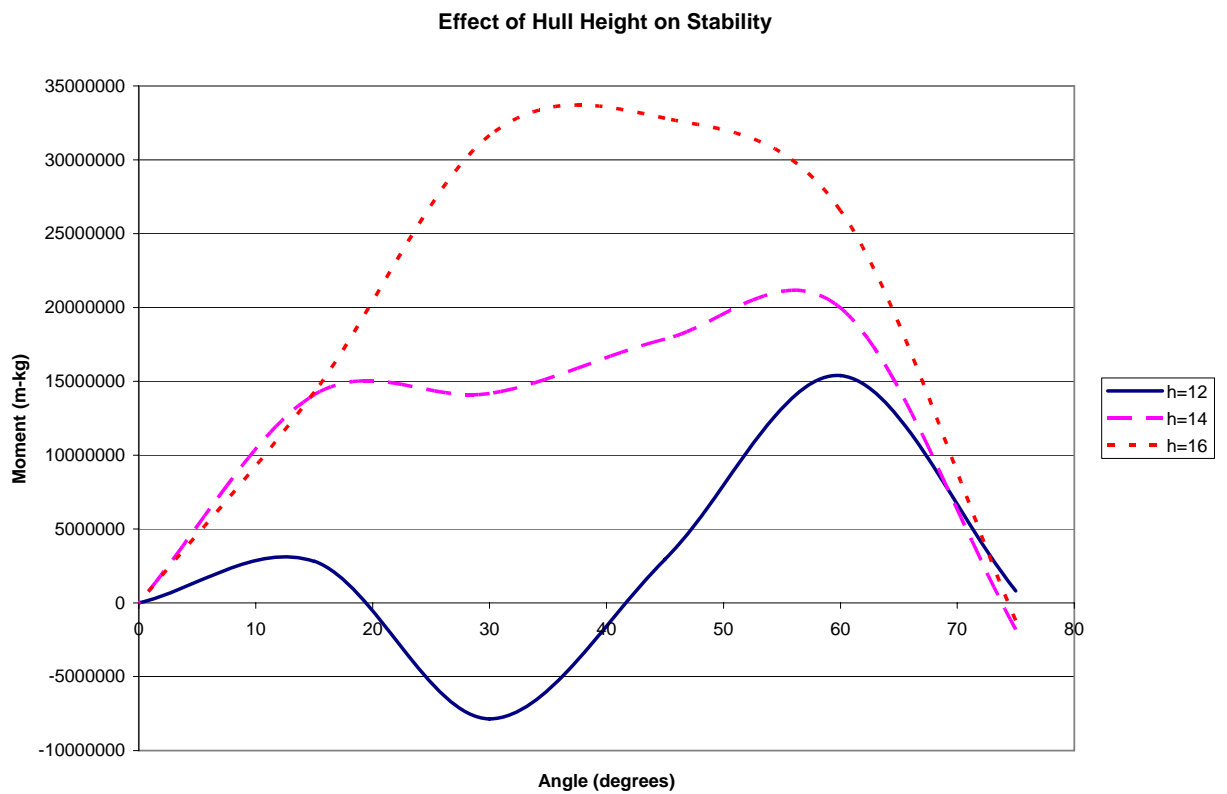


**Figure 2-8:** Effect of Hull Height on Stability Curve

The large dip in the  $h=12$  line represents the effect of water washing over the deck of the vessel.

## Results

The length of the vessel is calculated directly. The hull height and width are adjusted iteratively to achieve the desired stability. For a set of hull dimensions, the stability curves are plotted. If the curves show the vessel to be stable up to at least 45 degrees at all points in the lifecycle, then those dimensions are acceptable. If not, the width or height was adjusted and the stability curves are examined again. This iterative process results in hull dimensions that meet the stability criteria. The dimensions used in the following stability analysis are shown in Table 2-9. It is evident that the vessel is square (beam equals length) for sizes below 14,000 cubic meters of scintillator. In addition, the period of roll, T, becomes shorter as the size increases.

Diameter (m)	V scin (m <sup>3</sup> )	V oil (m <sup>3</sup> )	V H <sub>2</sub> O (m <sup>3</sup> )	Height (m)	Beam (m)	Length (m)	GM (m)	T (s)
15.87	4000	1710	4756	14	26.69	26.69	0.3	15.58
17.1	5000	1968	5358	14	27.96	27.96	0.3	16.33
19.13	7000	2433	6436	15	32.3	32.3	0.35	16.29
21.54	10000	3051	7846	15	37	37	0.4	16.4
24.1	14000	3782	9492	16	43.1	43.1	1	11.42
26.68	19000	4600	11314	16	48	51.32	2	8.88
29.24	25000	5489	13275	16	50	63.59	3.6	7.31
31.75	32000	6437	15351	16	51	78.54	4.6	6.91
34.2	40000	7436	17526	17	52	95.02	5.8	6.55
36.59	49000	8481	19790	17	54	110.83	8	6.02
38.93	59000	9568	22132	17	56.15	127.09	9.5	5.83
41.21	70000	10694	24546	18	59.9	140.15	12	5.53
43.44	82000	11854	27028	18	63.86	152.87	15	5.27
45.63	95000	13048	29572	18	70	160.5	19	5.02
47.77	109000	14272	32176	18	74.35	172.35	25	4.76
49.87	124000	15526	34835	18	80.56	180.01	32	4.56
51.92	140000	16808	37547	18	87	187.29	40	4.4

**Table 2-9:** Dimensions of a Cylindrical Integrated Detector

The above beam and length dimensions are presented graphically in Figure 2-9. This graph also depicts the maximum beam allowed through the Panama Canal, which shows that only vessels under 7000 cubic meters have a beam below the limit.

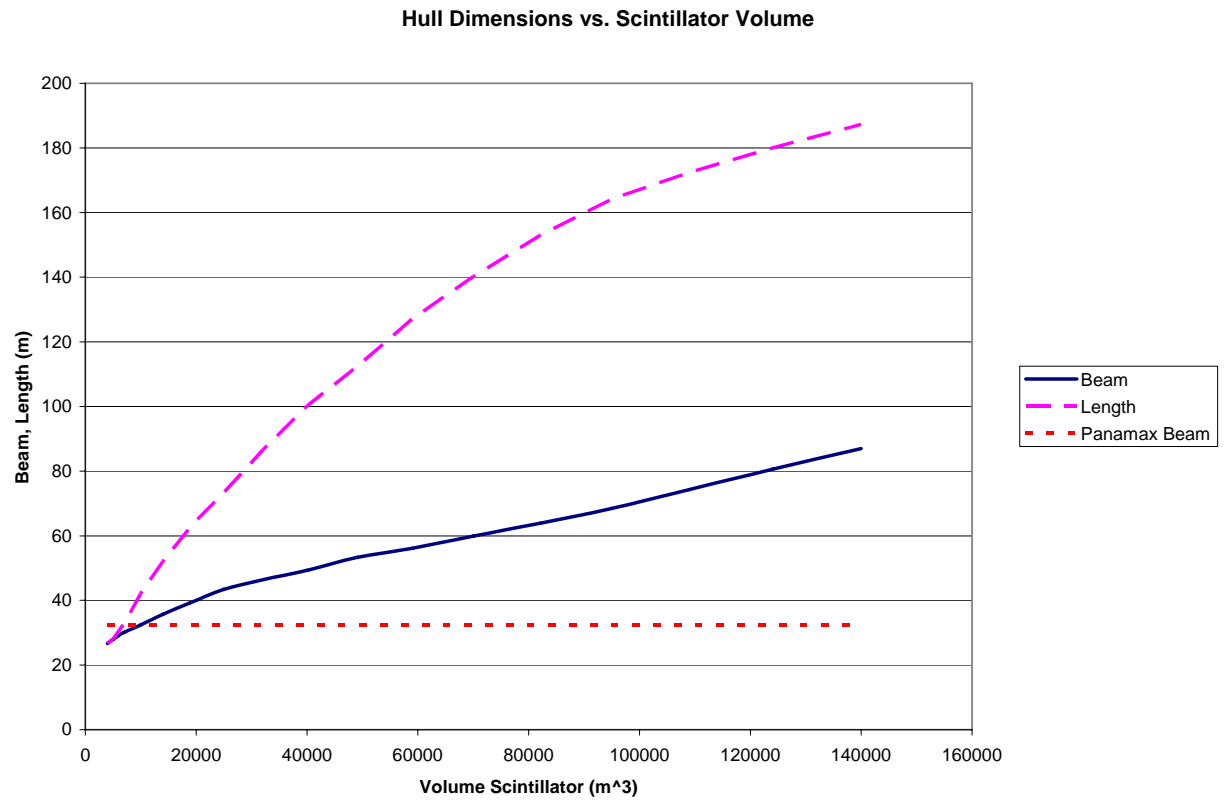


**Figure 2-9:** Hull Dimensions

#### 2.3.2.3 Empty Detector

When the integrated detector is empty, it is very stable due to its low center of gravity. The stability curves for an empty vessel are presented in Figure 2-10, where  $V$  is the volume of scintillator the detector holds. The righting moment is large and positive to approximately 70 degrees. This means the vessel could tip 70 degrees and still return upright. Any angle greater than this would cause the vessel to capsize.

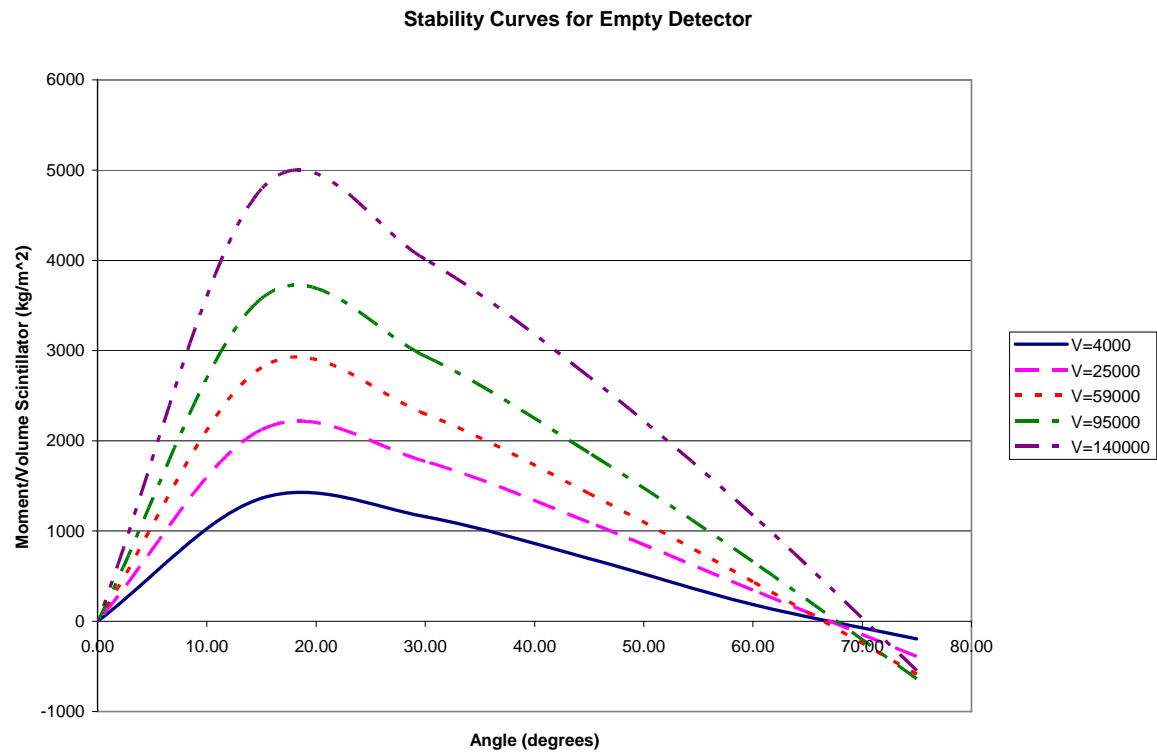


**Figure 2-10:** Stability Curve for an Empty Detector

#### 2.3.2.4 Filling the Integrated Detector

This section analyzes the stability of the integrated vessel when the cylindrical detector is being filled. During filling, the large free surface of the scintillating fluid and oil could result in instability. When the vessel tips, large amounts of fluid will move to the lower side. If too much fluid moves, it could shift the center of gravity so far that the vessel tips over. Tankers typically use bulkheads to divide large spaces into smaller watertight ones and therefore limit this sloshing effect. However, the physics requirements prohibit bulkheads in the inner cylinder. They can be used in the outer cylinder to limit the movement of the fresh water if necessary.

It was found that for low levels of fluid the shallow draft causes the center of buoyancy to move significantly farther to the side than when the vessel is full. Therefore, even though the center of gravity has shifted, the center of buoyancy shifts far enough that the vessel remains stable for the majority of the time. However, as the fluid level approaches the top of the cylinder, the higher center of gravity combined with the free surface effect can cause stability problems.

Smaller detectors, less than 14,000 cubic meters, will need a hull that is completely square in order to maintain stability. For a 10,000 cubic meter detector, a hull with a Panamax beam of 32.3 m will be unstable as the scintillating fluid and oil nears the top of the cylinder, whereas a beam of 37 m, which results in a square hull, is stable. The stability curves of a 10,000 m<sup>3</sup> detector partially full of scintillating fluid and oil are

shown in Figure 2-11 and Figure 2-12 for a square hull. “H” is the height of the oil and scintillator in the detector measured from the bottom of the oil. These graphs show that a 10,000 cubic meter detector cannot be made stable and able to fit through the Panama Canal. It will only be stable if it is too wide to pass though the Panama Canal.

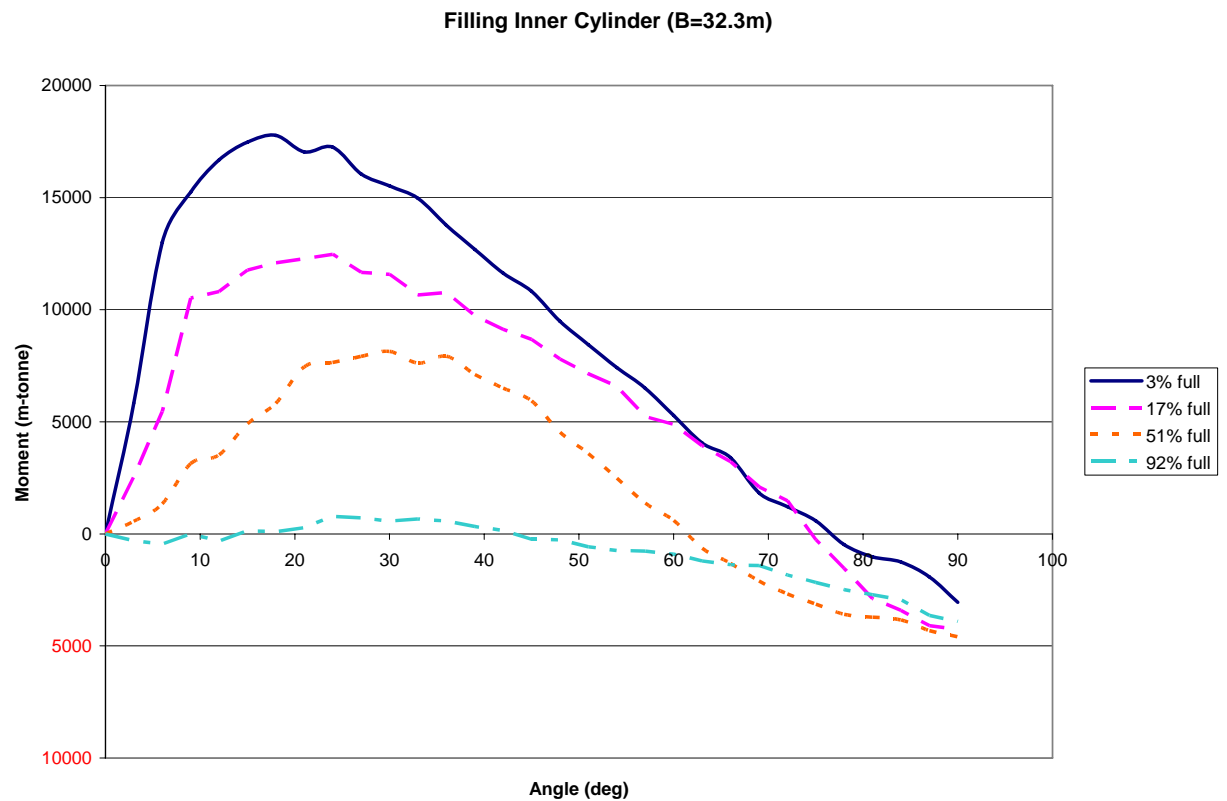


**Figure 2-11:** Stability Curves for a  $10,000 \text{ m}^3$  Panamax Detector Partially Full of Scintillating Fluid and Oil

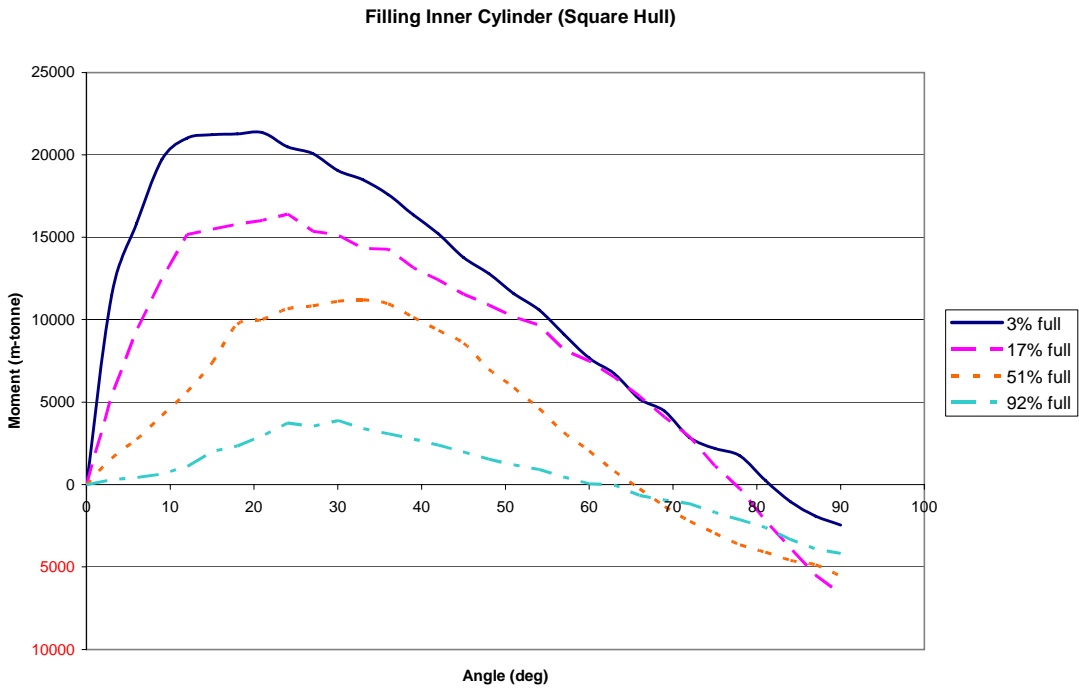


**Figure 2-12:** Stability Curves for a 10,000 m<sup>3</sup> Square Hull Detector Partially Full of Scintillating Fluid and Oil

For detectors greater than 14,000 cubic meters, the hull will be rectangular, though still much more square than a typical vessel. The partially full stability curves for a 25,000 cubic meter detector are shown in Figure 2-13, where ‘h’ is once again the height of the oil and scintillator measured from the bottom of the oil. This graph shows the 25,000 cubic meter detector with hull dimensions from Table 2-9 is stable while filling the inner detector, though it will take very little force to cause it to list when nearly full.

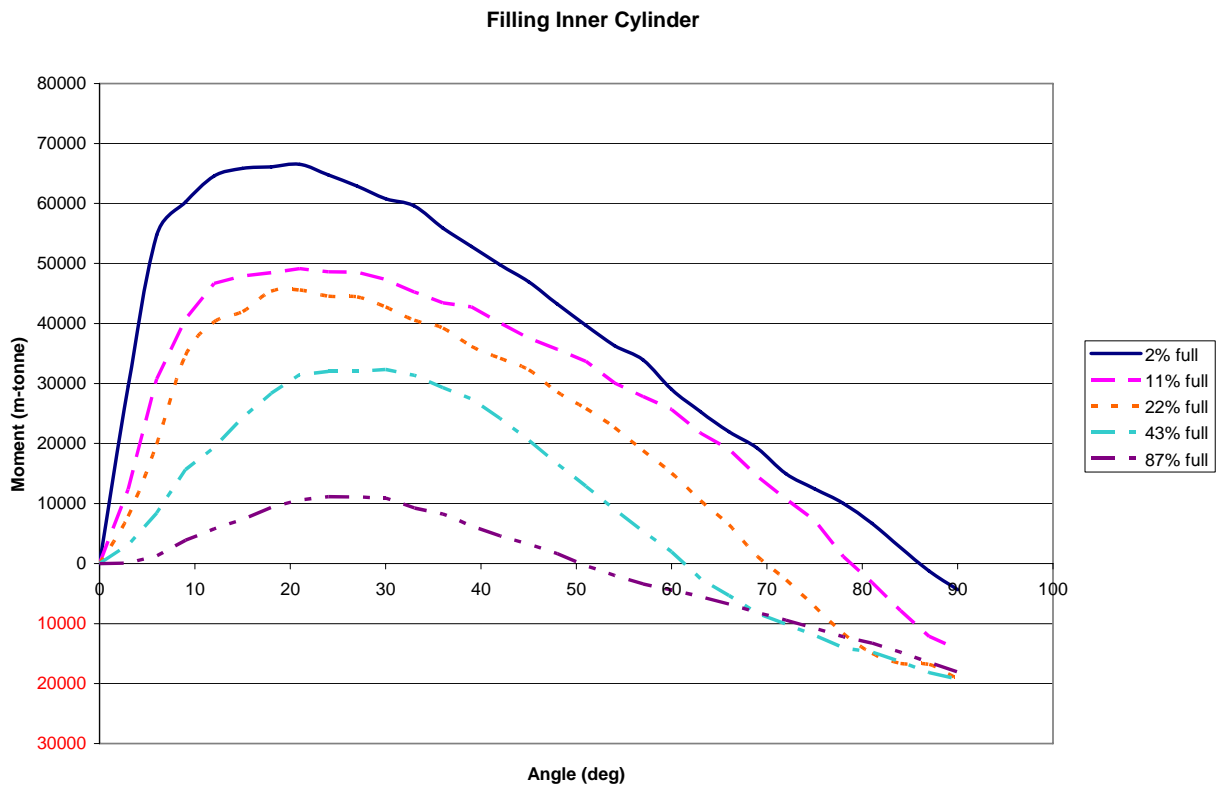


**Figure 2-13:** Stability Curves for a 25,000 m<sup>3</sup> Detector Partially Full of Scintillating Fluid and Oil

While adjusting the beam can create a vessel that is stable during filling of the scintillating fluid and oil, it cannot ensure stability when filling the fresh water, as seen in Figure 2-14. As the outer cylinder becomes nearly full, the integrated vessel is very unstable.

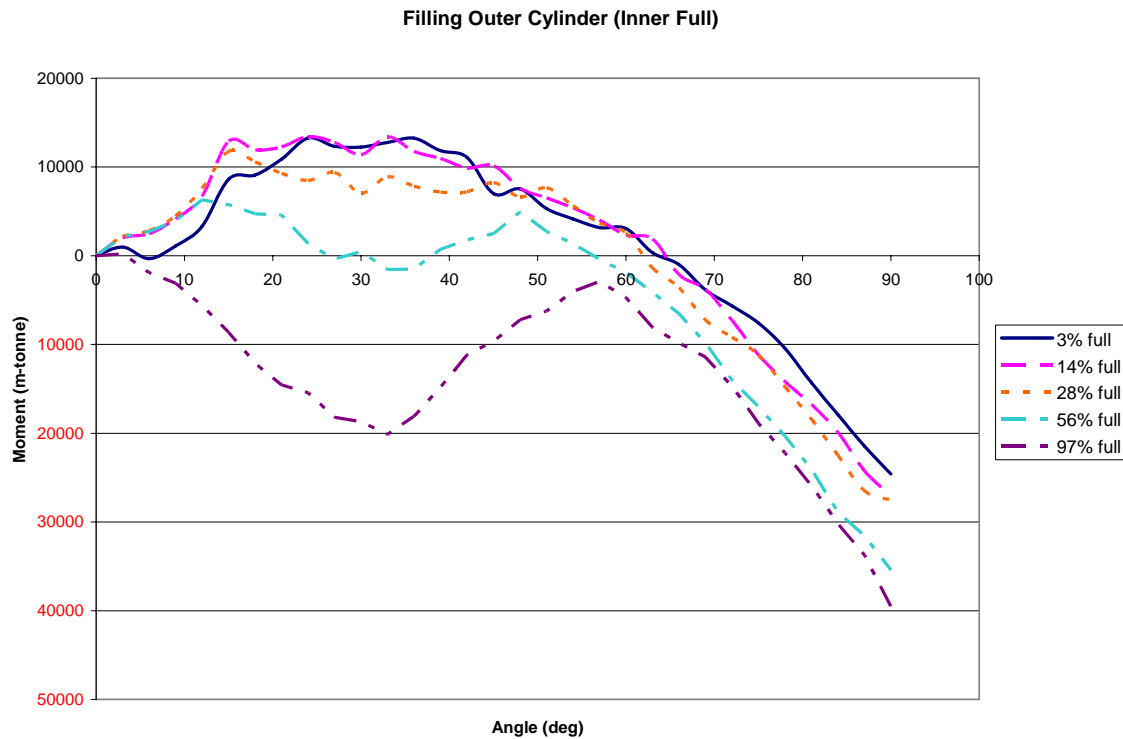


**Figure 2-14:** Stability Curves for a 10,000 m<sup>3</sup> Detector Partially Full of Fresh Water – Without Seawater Ballast

The above effect is due to the fact that the fresh water sits on the outside of the scintillating fluid and oil, and therefore has a higher area moment of inertia. As indicated in Equation 2-3 above, a higher moment of inertial causes greater free surface effects. Simply widening the hull to compensate for the greater effect would produce impractically wide vessels.

The solution to this stability problem is to first fill the hull with salt water. Flooding the hull with salt water increases the draft of the vessel and lowers its center of gravity. Once the salt water has ballasted the vessel and increased its draft, the fresh water can be safely added, as Figure 2-15 shows. To prevent the free surface of the salt water from creating problems, the hull will have numerous bulkheads like typical tankers use. Comparison of Figure 2-14 and Figure 2-15 shows the salt water ballast has a great effect on stability and with it the vessel is stable while filling the fresh water.

**Filling Outer Cylinder (Inner and Hull Full)**

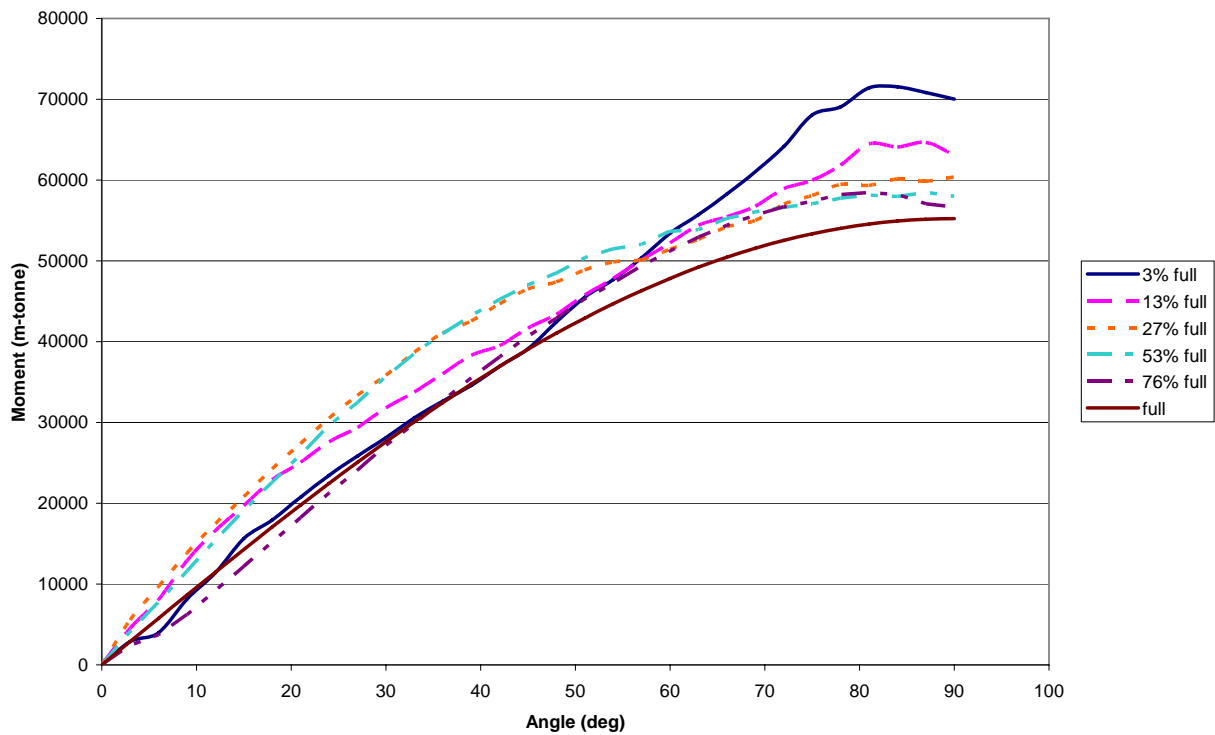


**Figure 2-15:** Stability Curves for a 10,000 m<sup>3</sup> Detector Partially Full of Fresh Water – With Seawater Ballast

The integrated vessel with a cylindrical detector can be made stable at all times during filling. Filling must occur in a specific order:

1. Inner cylinder with scintillator and oil
2. Hull with sea water
3. Outer cylinder with fresh water

In addition, numerous bulkheads in the hull are required to divide the free surface into small sections that will have less effect on stability. The integrated vessel can be stable, but it will be very wide, and only detectors with less than 7000 cubic meter of scintillator will fit through the Panama Canal.

#### 2.3.2.5 Detector Completely Full of Oil, Scintillator, and Water

When the cylindrical detector is completely full, the integrated vessel is stable for all sizes, using the hull dimensions presented in Table 2-9. The stability curves, presented in Figure 2-16, show that the vessels are all stable to at least the 45° minimum.

**Stability Curves with Scintillator and Oil**

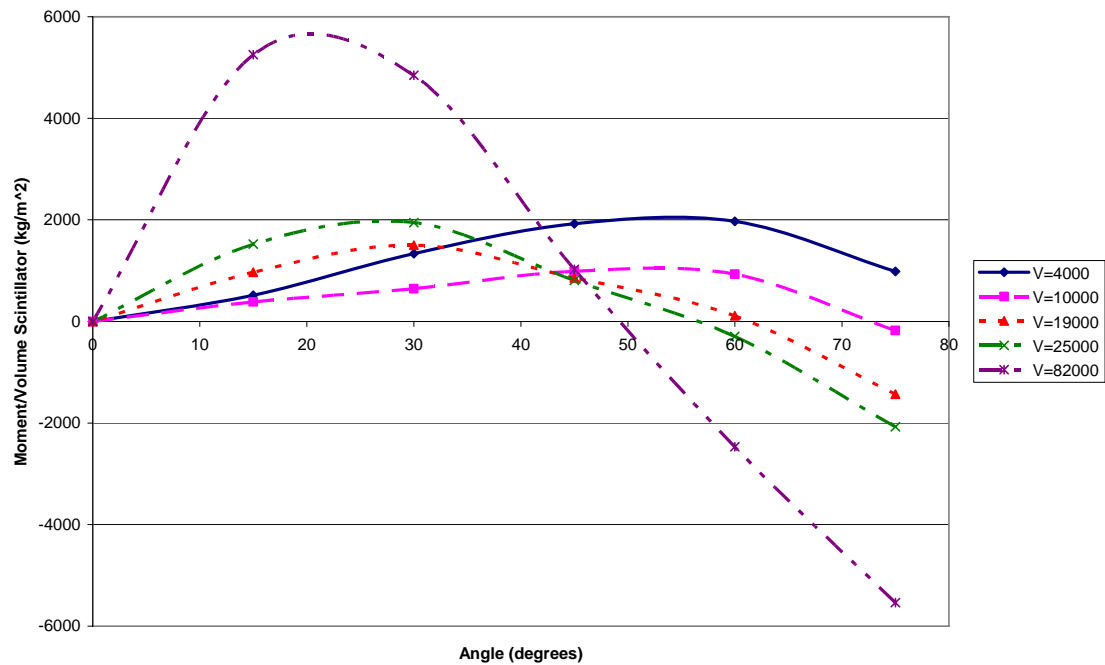


**Figure 2-16:** Stability Curve for a Detector Completely Full of Scintillating Fluid and Oil

#### 2.3.2.6 Other Stability Considerations

There are two angles which are pertinent to stability: the angle at which water washes over the deck, and the angle at which the vessel becomes unstable. These two angles for both the empty and full cases are compared in Figure 2-17. When full, the deck washes over at approximately 20 degrees. The vessel is stable up to at least 45 degrees for all detector sizes, as dictated by the stability requirements.

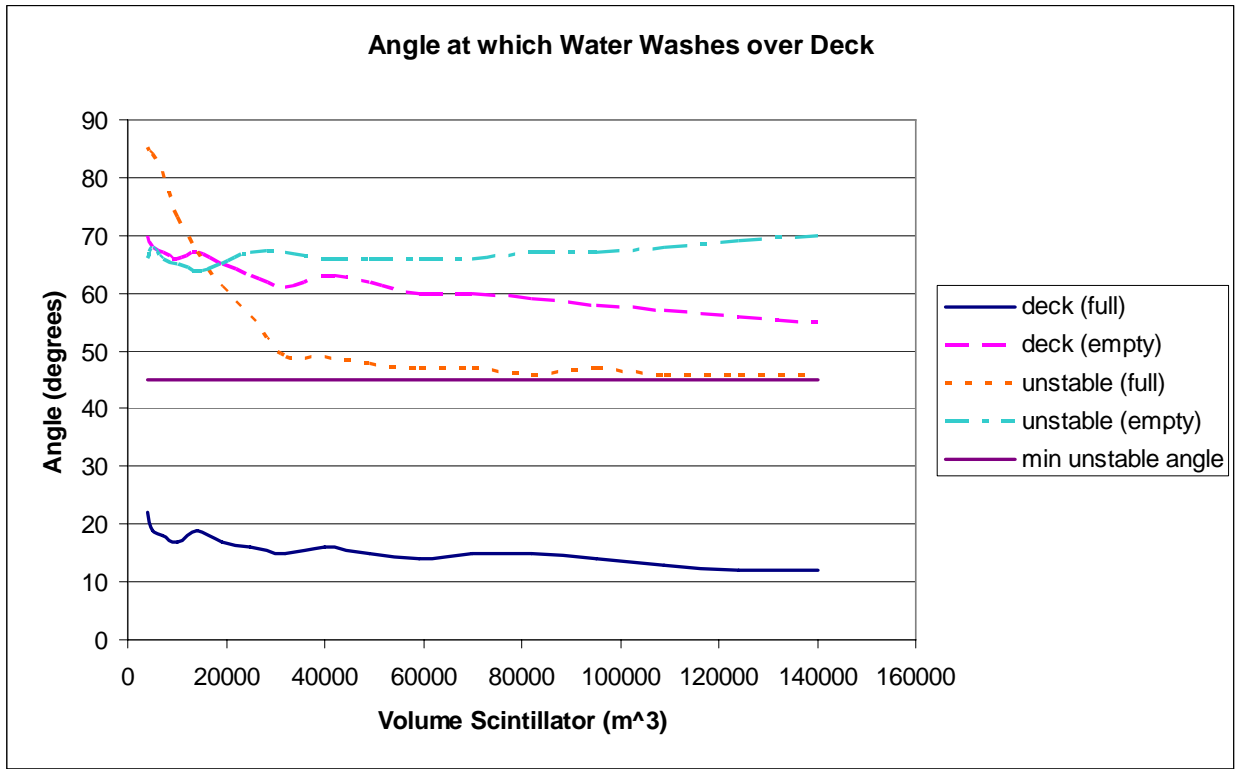


**Figure 2-17:** Angle at which the Vessel becomes Unstable

Standard acceleration limits are based on the type of work being performed aboard the vessel. Heavy manual work acceleration limits were investigated, and the results presented below show the vessel is below the limits for all sizes. As seen in Figure 2-18, the accelerations fall far below the limit.

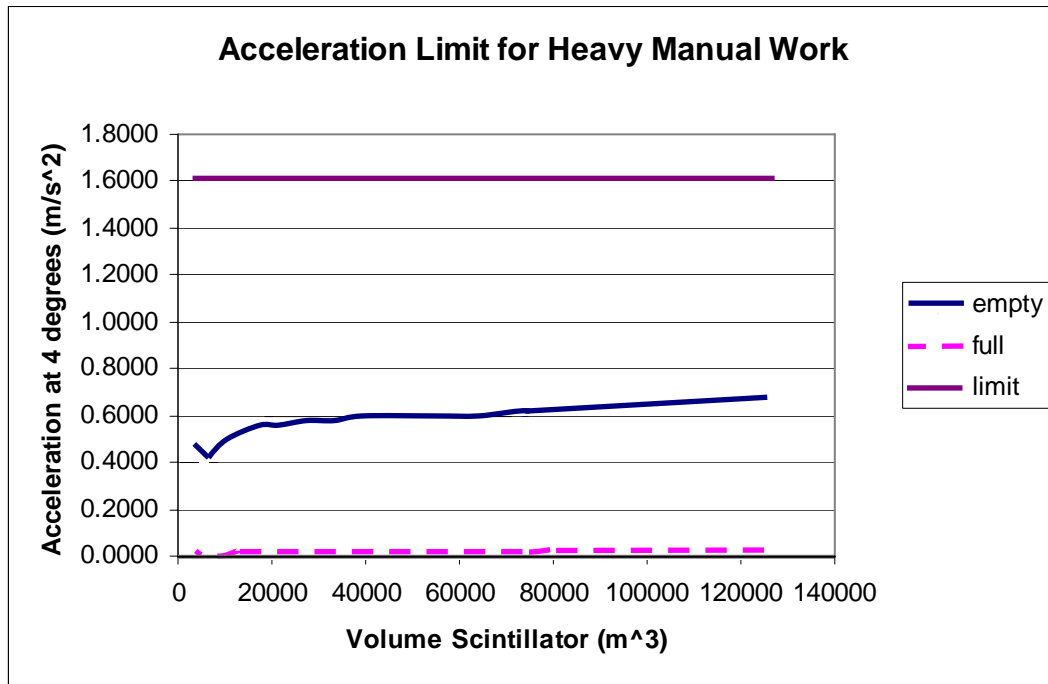


**Figure 2-18:** Acceleration Limit

#### 2.3.2.7 Submerging

When it is time to sink the integrated vessel, the detector will be full of scintillating fluid, oil, and fresh water, the hull will be full of salt water, and a large concrete weight will be attached to the bottom. In addition to sinking the vessel, the concrete weight will also keep it upright during its journey to the bottom. To resurface, the concrete will be dropped, and the vessel will float back to the surface. On the way up, the vessel must stay upright without any additional weight on its bottom. To accomplish this, the center of buoyancy must be higher than the center of gravity such that there is a righting moment when the vessel heels. The above analysis has taken this requirement into consideration, and Table 2-10 shows the center of buoyancy, center of gravity, and the distance between them when the vessel is submerged without concrete. The center of buoyancy is above the center of gravity (GB is positive) for all size detectors, which means they are all stable when completely submerged.

V scin (m^3)	KG (m)	KB (m)	GB (m)
4000	5.17	5.78	0.6
5000	5.11	5.88	0.77
7000	5.4	6.52	1.12
10000	5.45	6.79	1.34
14000	5.82	7.43	1.6
19000	5.86	7.57	1.71
25000	5.89	7.66	1.77
32000	5.92	7.73	1.82
40000	6.29	8.26	1.98
49000	6.31	8.31	2
59000	6.33	8.34	2.01
70000	6.71	8.85	2.14
82000	6.72	8.87	2.15
95000	6.73	8.89	2.15
109000	6.75	8.9	2.16
124000	6.76	8.91	2.16
140000	6.76	8.92	2.16

**Table 2-10:** Submerged Centers of Buoyancy and Gravity

At some point during both sinking and resurfacing, the centers of gravity and buoyancy will be located at the same height. When sinking, this occurs after the final weight is added and the detector begins its descent to the ocean floor. Soon after the weight is added, the vessel will pass through the point where KG and KB are equal. However, the concrete will add extra stability and the vessel will be stable. When the vessel is finished collecting data on the ocean floor and resurfaces, it will once again go through the point where KG and KB are equal, but this time without the concrete. Since it will move through the point quickly, it should only be unstable for a very brief period, and then a righting moment would occur again and prevent capsizing. Submarines also avoid problems at this point by passing through it quickly.

### 2.3.3. Validation of Stability Curves

This section discusses the process of validating the above stability curves. Since the process of creating a stability curve is involved and complicated, a scale model of the integrated vessel with a cylindrical detector was constructed to test and compare to the analytic results.

#### 2.3.3.1 Construction

A 1:50 scale model of the integrated vessel was constructed. The hull was made of wood, and the detector of aluminum flashing. Both cylinders were reinforced with aluminum tubing. The hull and both cylinders were completely sealed using marine caulking. Weight limitations were a major limiting factor during the construction process and greatly limited the strength of the finished model.

Since filling the cylinder with water is preferable to oil for environmental and cleaning purposes, closed-cell Styrofoam was added to the inner cylinder such that the density and moment of inertia of the inner cylinder filled with Styrofoam and water is equal to the

density of scintillator. In this way, the inner cylinder can simply be filled with water, but the resulting free surface effect will be the same as if it were scintillator.

A drawing and pictures of the scale model are shown in Figure 2-19.

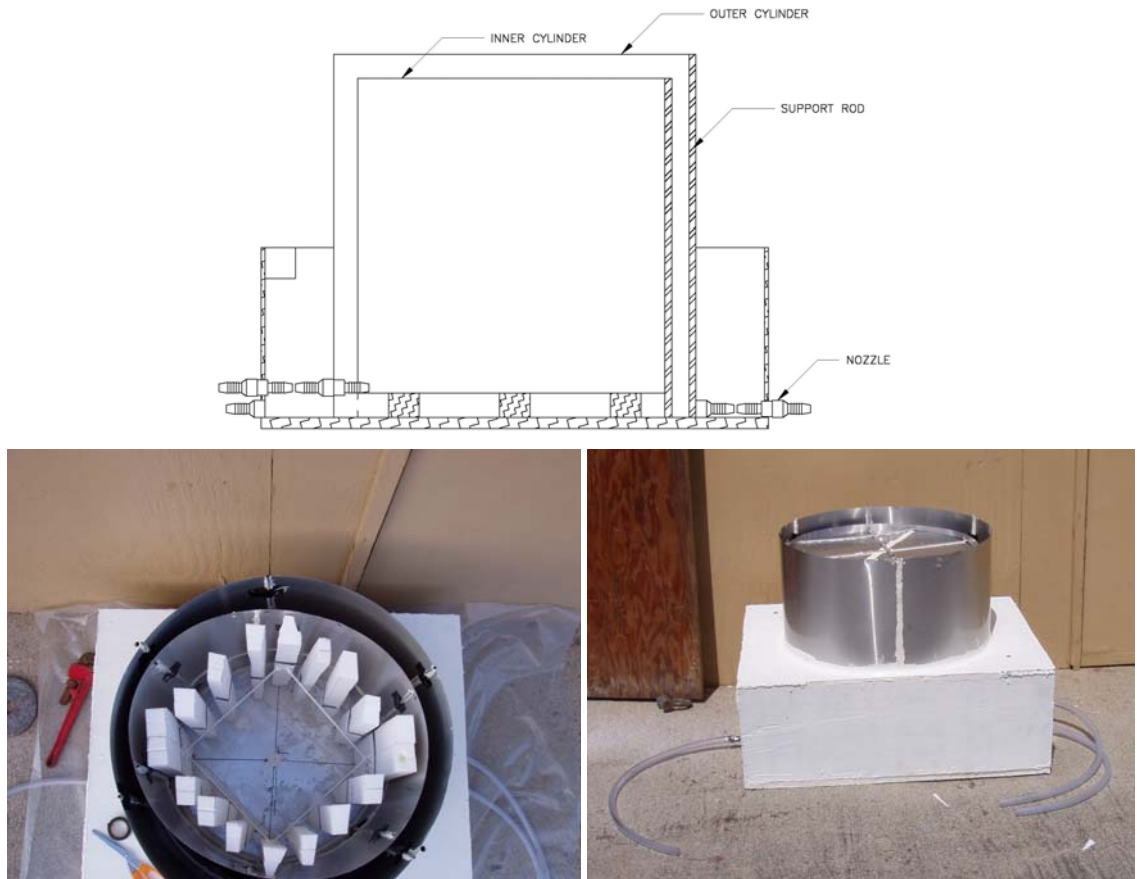


**Figure 2-19:** Drawing and pictures of scale model

#### 2.3.3.2 Testing

The test was performed in a pool in order to limit uncertainty due to wave motion in open water. The cylinders were filled with fresh water using a garden hose. The experimental setup is shown in **Error! Reference source not found.**.

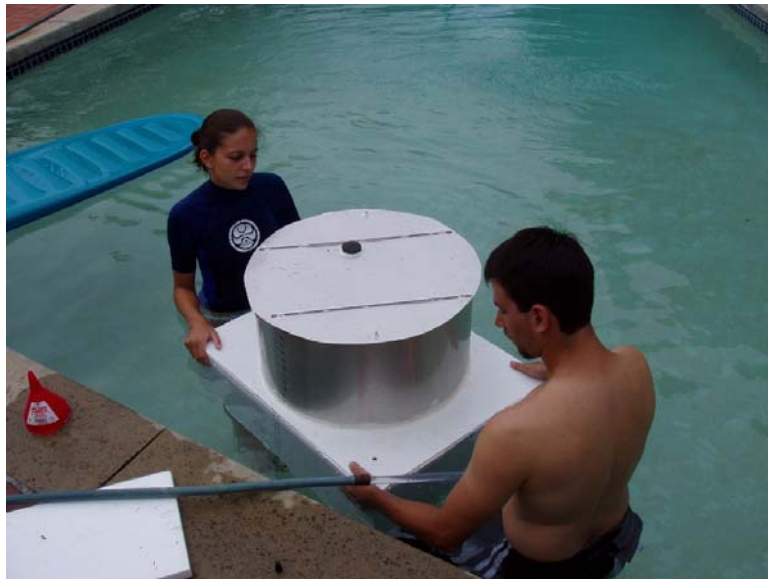


**Figure 2-20:** Testing the scale model

First the inner cylinder was filled with fresh water. Periodically during the filling process, the water level and draft were recorded. Then the model was tipped until it became unstable. When the model was borderline stable/unstable the height of the water line on the side of the cylinder was recorded. This data allows the maximum stable angle to be estimated.

When tipping the inner cylinder, the weight of the fluid caused the seal along the bottom of the inner cylinder to break. This resulted in leakage between the two cylinders, thus invalidating this test from this point on.

Since one cylinder could no longer be filled at a time, in the next test both cylinders were filled simultaneously. Once again, the fluid level, draft, and water line when tilted were recorded.

### 2.3.3.3 Results

The results of filling both cylinders simultaneously show the same trend as the analytical method. However, the maximum stable angle varies significantly. The analytical results agree with the fluid volume at which the vessel becomes completely unstable. The results the maximum stable angle test in which both cylinders are filled simultaneously are shown in Table 2-11.

Water Height (in)	Experimental Angle (deg)	Calculated Angle (deg)
12	47	75
16	27	18
20	0	3

**Table 2-11:** Scale Model Test Results

There was a large amount of uncertainty in the measurements due to the instability of the model when data was collected. The model was invariably not exactly at the borderline between stability and instability when the data was taken. In addition, the experimental angle is an estimation. The analytical approach agrees very closely with the experiment about the fluid volume at which the vessel becomes completely unstable, which is the most important part of the calculations. Therefore, it was concluded that the analytical stability curves are a reasonable approximation and are valid.

#### 2.3.4. Detachable Design

This section addresses the stability of the detachable design concept. The detector and barge will separate, and only the detector will sink to the ocean floor to perform the experiment. A cylindrical detector is also used in the following analysis.

##### 2.3.4.1 Size

For a detachable detector and barge, the width of the barge will be determined by stability, period of roll, and the largest beam allowed through the Panama Canal. The length will be such that the draft is less than 10 meters when fully loaded. The height of the hull is determined by stability and the desired minimum freeboard. In addition, the height to width ratio of the cylinder will be adjusted to allow a reasonable width of barge on either side of the moon pool. These conditions result in the dimensions presented in Table 2-12.

V Scintillator (m <sup>3</sup> )	Cylinder Diameter (m)	Cylinder Height (m)	Beam (m)	Length (m)	Hull Height (m)
4000	14.6	25.6	28	50	13.8
10000	19.8	34.7	32.3	95	13.8
25000	26.9	47.1	42	155	13.8

**Table 2-12:** Dimensions of the Detachable Detector and Barge

##### 2.3.4.2 Surface Stability

This section examines the stability of the detachable detector on the surface for several size detectors. Analysis of the integrated vessel shows stability problems are most likely to occur during the filling process. Therefore, the stability of the partially full detachable detector is analyzed in this section. The stability of the barge is also discussed.

The barge under consideration in this chapter is not fundamentally different than existing barges. The stability of a barge is well documented and understood and does not present any difficult engineering challenges. The moon pool in this particular barge will present structural challenges, but does not significantly affect stability. Therefore, the stability of the barge will not be analyzed here.

Ideally, the detector and barge will both be stable individually. As discussed above, the barge can easily be designed to be stable. Since there are no weight limitations on the barge, ballast can also be added as necessary. The stability of the detector will be analyzed in depth below.

The available buoyancy in the detector allows it to resurface with more weight than is structurally required in the cylinder. Therefore, ballast can be added to the bottom of the cylinder to promote stability. Concrete ballast on the bottom of the detector will greatly improve its stability both on the surface and when submerged. In addition, if filling the detector becomes a problem, bulkheads could be added to the outer cylinder such that the fresh water can be filled in stages and used as additional ballast.

It would be beneficial to have the detector stable independent of the barge. However, it is not necessary. Therefore, if stability of the detector becomes a problem during filling, the barge could be used to support it. This arrangement would still be more stable than the integrated vessel because all the liquids and weight would be stored low and both the detector and barge can be ballasted.

The detector will be the least stable during the filling process due to the free surface effect, which allows fluid to move and negatively affect the center of gravity as explained in section 2.3.1. Therefore, stability during filling is examined for detectors of several sizes.

For the 4000 cubic meter detector, filling the inner cylinder is completely stable. Figure 2-21 shows the stability curves for this process.

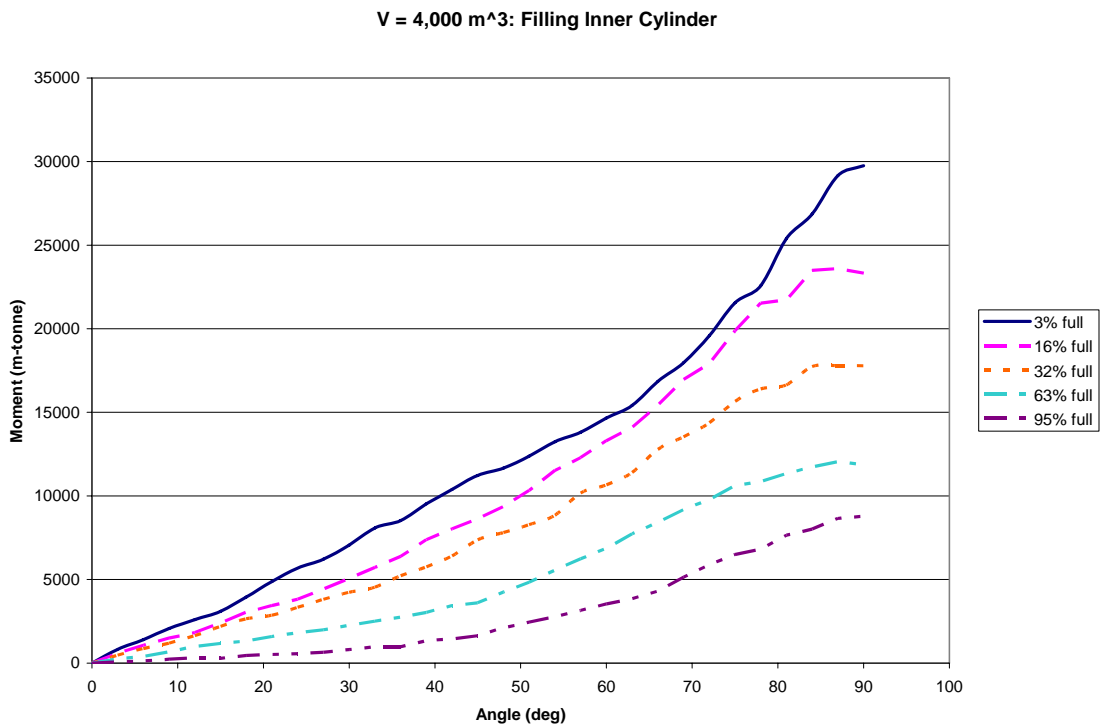


**Figure 2-21:** Filling the Inner Cylinder of a 4000 Cubic Meter Detector

Note that all lines remain above the x-axis, which indicates a positive righting moment at all times. However, filling the first two meters of the outer cylinder is unstable when there is only a small amount of fluid. Figure 2-22 shows the stability curves for filling the veto region.

$V = 4,000 \text{ m}^3$ : Filling Outer Cylinder (Inner Full)

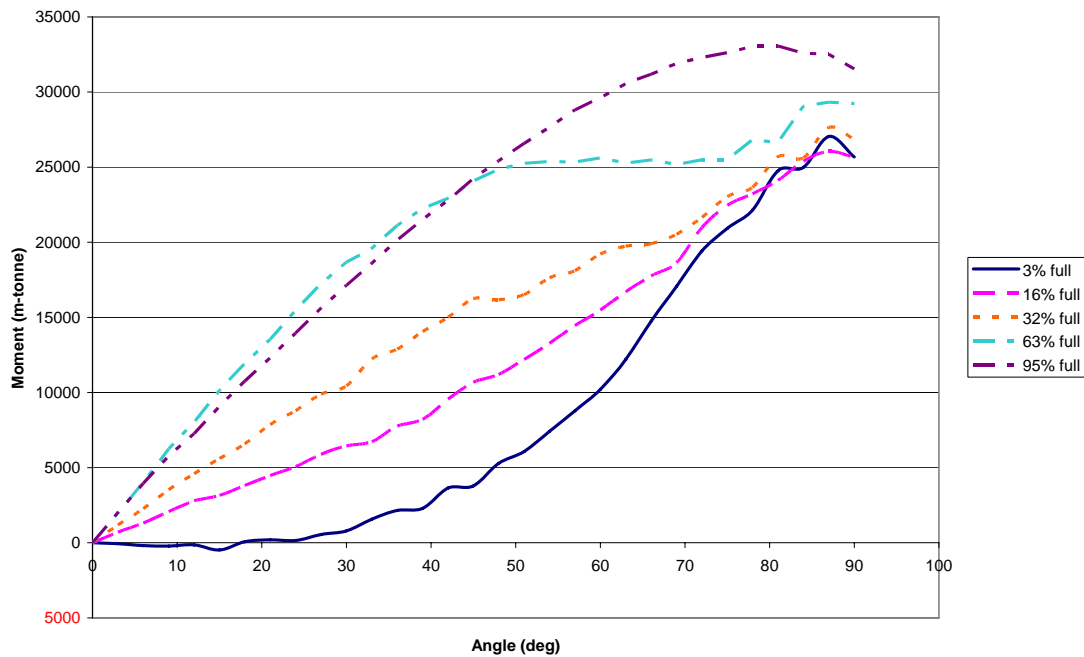


**Figure 2-22:** Filling the Outer Cylinder of a 4000 Cubic Meter Detector

The 3% full line dips below the x-axis between 10 and 20 degrees. This indicates the righting moment is negative and the vessel will be unstable.

Adding bulkheads in the outer cylinder will reduce the free surface and therefore increase stability. In this case, putting a bulkhead two meters from the bottom of the outer cylinder will make the filling process stable, as seen in Figure 2-23.

**V = 4,000 m<sup>3</sup>: Outer Cylinder 3% Full**

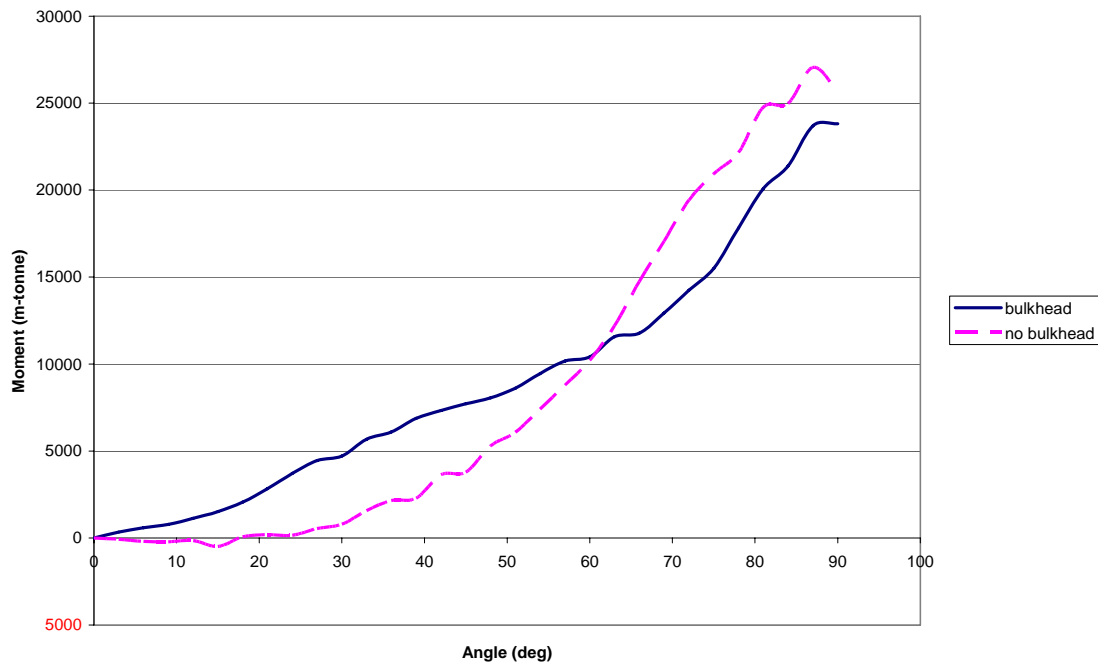


**Figure 2-23:** Filling the Bottom Two Meters of the Outer Cylinder of a 4000 Cubic Meter Detector

Next, a 10,000 cubic meter cylinder is analyzed. The resulting stability curves are presented in Figure 2-24 and Figure 2-25.

**V = 10,000 m<sup>3</sup>: Filling Inner Cylinder**

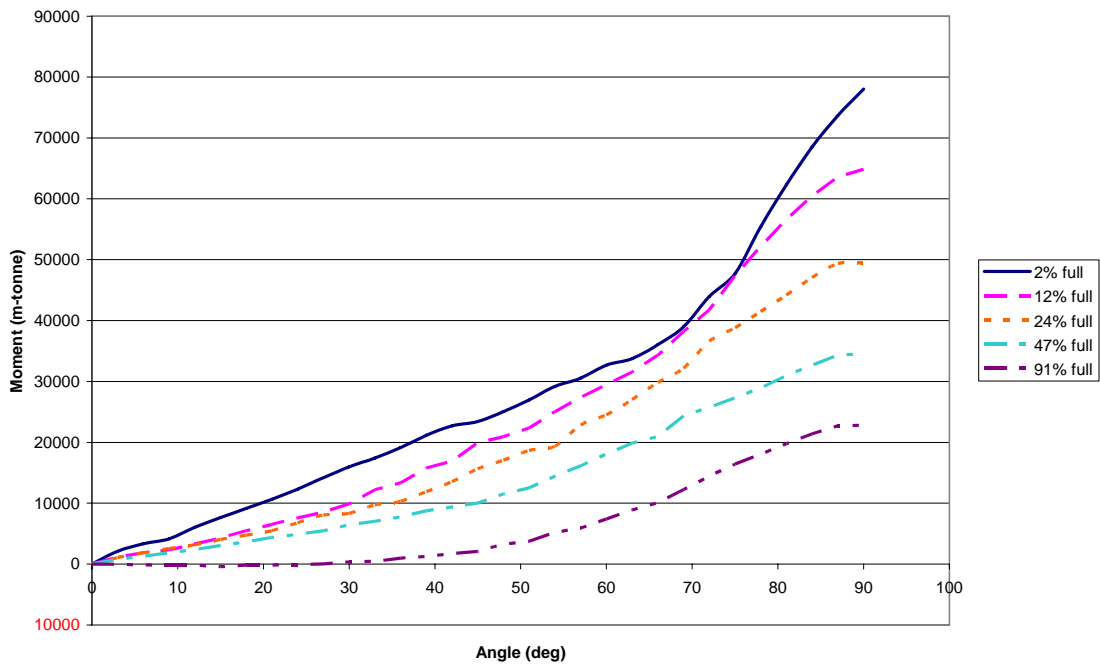


**Figure 2-24:** Filling the Inner Cylinder of a 10,000 Cubic Meter Detector

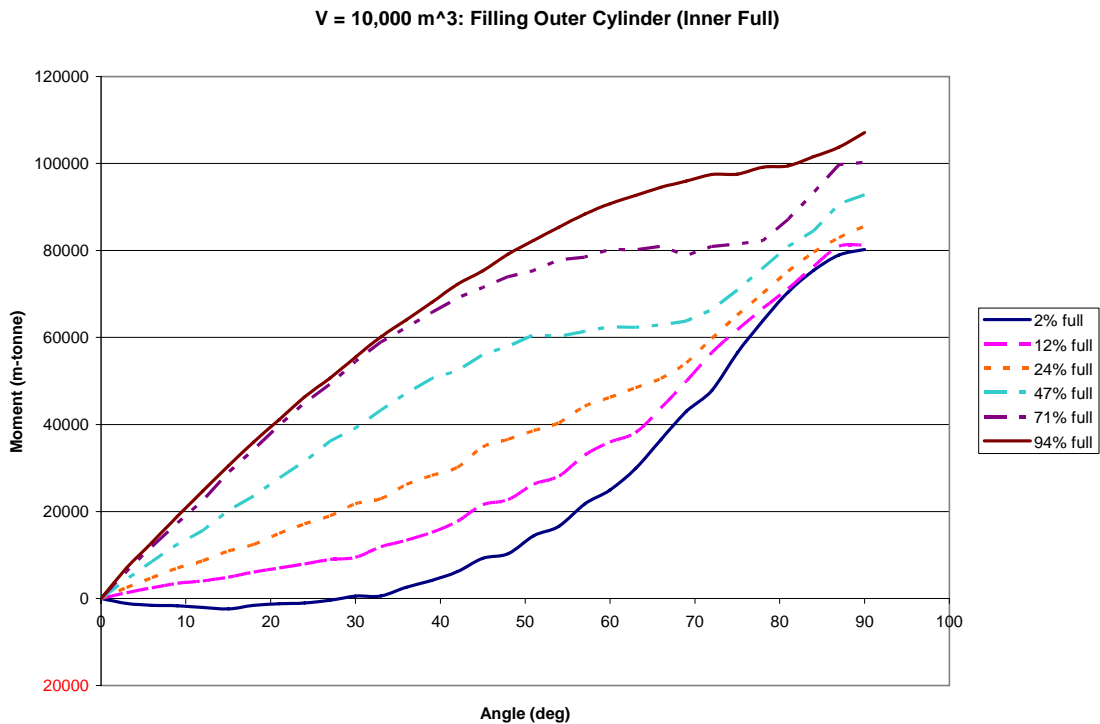


**Figure 2-25:** Filling the Outer Cylinder of a 10,000 Cubic Meter Detector

Similar to the 4,000 cubic meter detector, the 10,000 cubic meter detector also has stability problems when the veto region is filled with a small amount of liquid. In addition, it is also unstable when the inner cylinder is nearly full. These problems can be solved by adding bulkheads in the veto region. First, a bulkhead two meters above the bottom of the veto region solves the stability problems while filling that area. To address the instability while filling the scintillator, another bulkhead will be located in the veto region half way up the cylinder. After the inner cylinder is filled half way, then the veto region will be filled to the second bulkhead. The bulkhead restricts this fluid to the lower half of the detector, where it can act as ballast. The added stability from this ballast overcomes the inner cylinder's instability. The stability curves for all steps are shown in Figure 2-26.

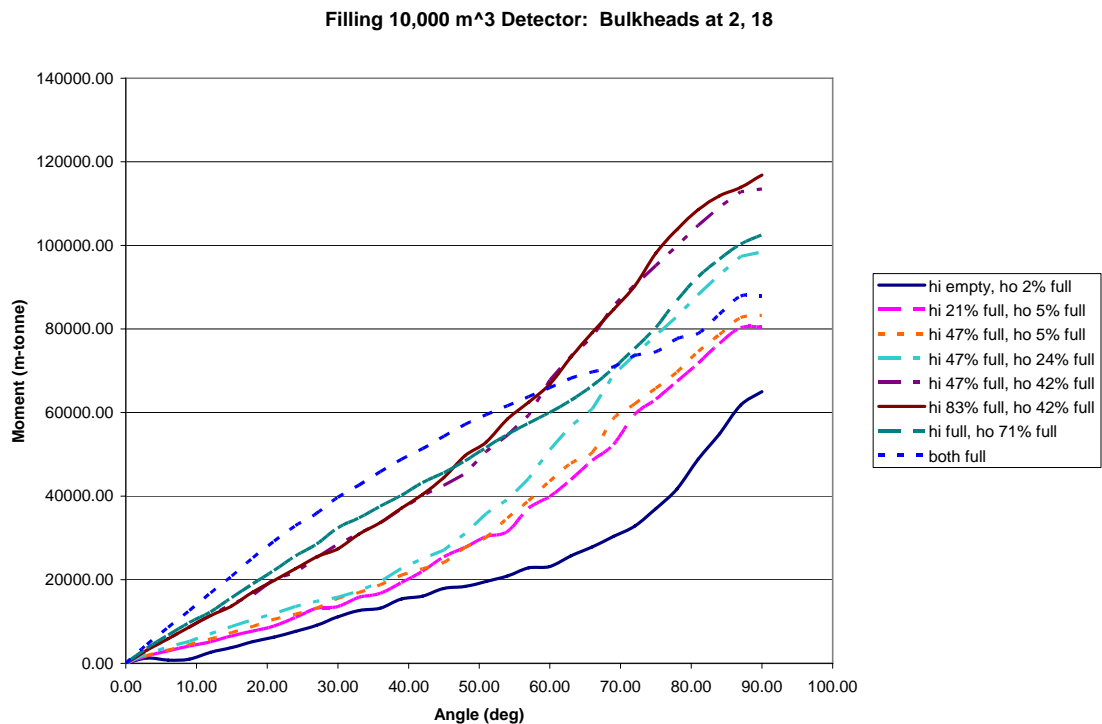


**Figure 2-26:** Filling a 10,000 Cubic Meter Detector with Bulkheads

Since all the lines are above the x-axis, the recommended filling procedure ensures stability at all times.

The stability curves for a 25,000 cubic meter detector are shown in Figure 2-27 and Figure 2-28. They show that a detector of this size is stable at all times during the filling process.

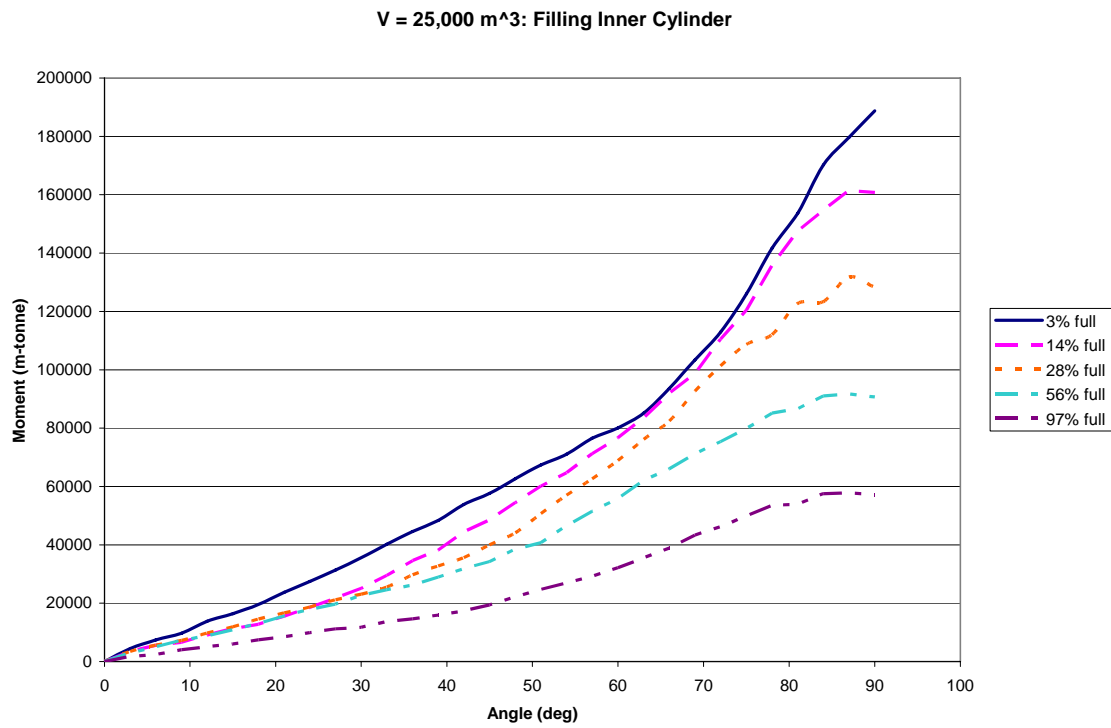


**Figure 2-27:** Filling the Inner Cylinder of a 25,000 Cubic Meter Detector

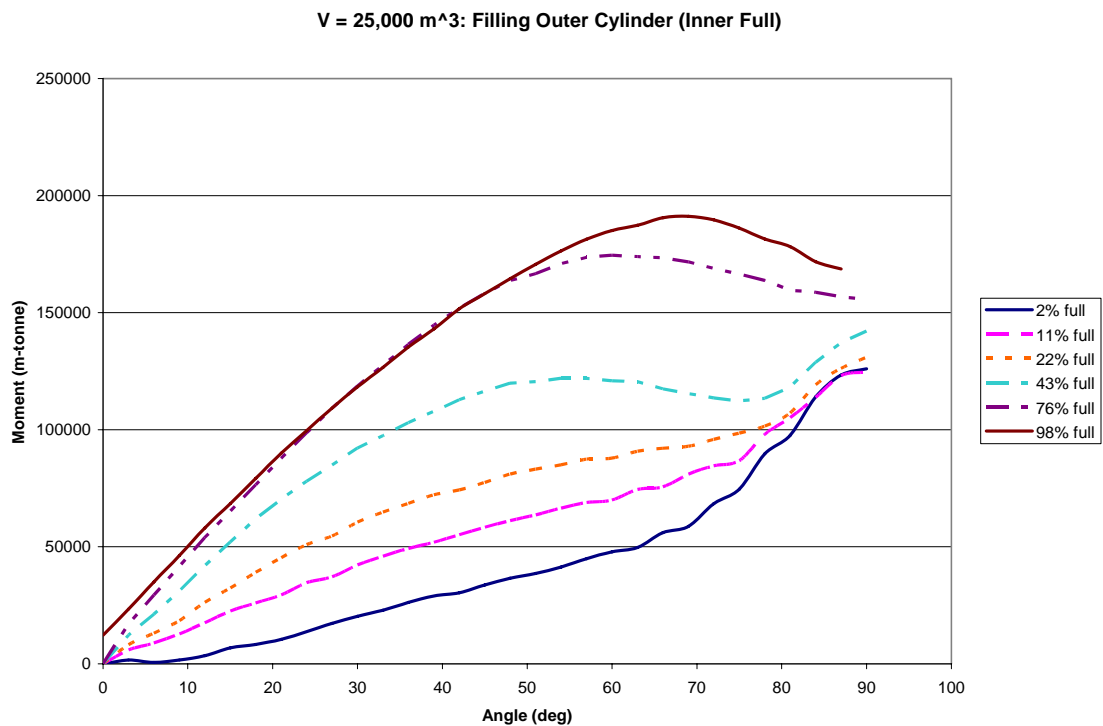


**Figure 2-28:** Filling the Inner Cylinder of a 25,000 Cubic Meter Detector

The flexibility of the two part vessels allows for methods of improving stability that cannot be applied to the integrated vessel, such as adding ballast and bulkheads. Therefore, stability of the detachable vessel is better than that of the integrated vessel.

#### 2.3.4.3 Submerged Stability

Submerged stability requires that the center of buoyancy be above the center of gravity. Since the geometry is uniform, the center of buoyancy of the detector will be located half way up the detector. Since the bottom of the detector is heavier than the top and also has extra ballast weight, the center of gravity will be located significantly below the half way mark and the detector will therefore be stable when submerged.

#### 2.3.5. Results

The stability of the integrated vessel is harmed by the weight limits imposed by the finite amount of buoyancy available. Due to the weight limit, there is little or no allowable weight left for ballast. In addition, since the scintillating fluid and oil must be filled in the harbor, the draft when filled with these two liquids is limited to 10 m, whereas a deeper draft could improve stability. If the water must also be filled in the harbor as well, additional stability problems would result.

Also, as the detector becomes larger, and therefore taller, the large amount of fluid raises the center of gravity, causing instability. Instability of the integrated vessel must be overcome at several points during the filling process by changing the fill order and adding a large number of bulkheads in the space between the hull and detector.

When the integrated vessel is completely submerged, the large volume of the hull lowers the center of buoyancy significantly, which results in a smaller righting moment. The surface stability and submerged stability of the integrated vessel are both marginal, though they do meet the stability criteria of stable to at least 45 degrees.

In addition to the stability concerns, the integrated vessel is wider than a detachable vessel. Therefore, a smaller detector would have to be used if the integrated vessel were to fit through the Panama Canal. Specifically, a 10,000 tonne detector with a detachable vessel could fit through the canal, whereas an integrated vessel would be limited to a 7000 tonne detector.

Stability problems of the detachable vessel can be minimized by adding ballast to both the barge and detector. In addition, adding bulkheads to the outer cylinder and filling the detector in a specific order limits the free surface effect. The barge is not fundamentally different from a typical barge, the stability of which is well understood and is not a concern. Therefore, both the barge and the detector can be made stable for all stages in the detector's life cycle.

The integrated vessel has both a larger beam and is less stable. However, the two part vessel is entirely stable and can support a larger detector for the same beam, which would

allow a larger detector to pass through the Panama Canal. Therefore, based on size and stability, a detachable vessel is preferred to an integrated vessel.

## 2.4 STRUCTURAL ANALYSIS

### 2.4.1. Overview

#### 2.4.1.1 Goals of analysis

The goals of the structural analysis are two-fold: to identify impractical concepts and get rough sizes on structural members. The valuable output of structural analysis from the perspective of practicality is weight. The analysis tells how much steel is required to make the Hanohano components strong enough to carry out their functions. Weight can invalidate a configuration by determining that the components are too heavy to float back to the surface once the experiment is complete, or by determining that the components are so large and heavy as to be impractical to construct.

By roughly sizing structural components, Makai has progressed into a conceptual design of a suitable configuration. The details of this design are given in chapter 3, but the analysis methods are the same as those presented here.

#### 2.4.1.2 Detector scaling

The two detector shapes considered in this analysis (cubes and cylinders) are treated differently in terms of comparing varying fiducial volumes:

- Analysis of the cube detector is highly dependent on detector size. The flat walls of a cube must withstand the hydrostatic pressure inside the detector primarily through bending. The geometry of bracing members within the veto region of the detector has a large effect on the weight of the walls required. Design of an efficient geometry is a time consuming process that must be repeated for each size to be evaluated. To solve this problem, Makai has designed geometry for a  $4096 \text{ m}^3$  (16 m cube) detector only. The weight of all other sizes of cube detectors was determined by assuming that detector weight scaled linearly with detector volume. Makai feels this is a conservative approach that will not have an adverse effect on the conclusions of the analysis.
- The cylindrical detector supports hydrostatic pressure through tension in the walls. ASME has provided standard methods of analysis for cylindrical pressure vessels. These methods scale easily to varying sizes of detectors, so all cylindrical detector sizes were analyzed individually.

#### 2.4.1.3 Pressure containment

The detector portion of the Hanohano project can be modeled as a large pressure vessel analogous to a water storage tank on land. The pressure in such a tank is proportional to the height of the liquid in the tank. Figure 2-29 shows how the pressure varies in a 20m tall water tank.

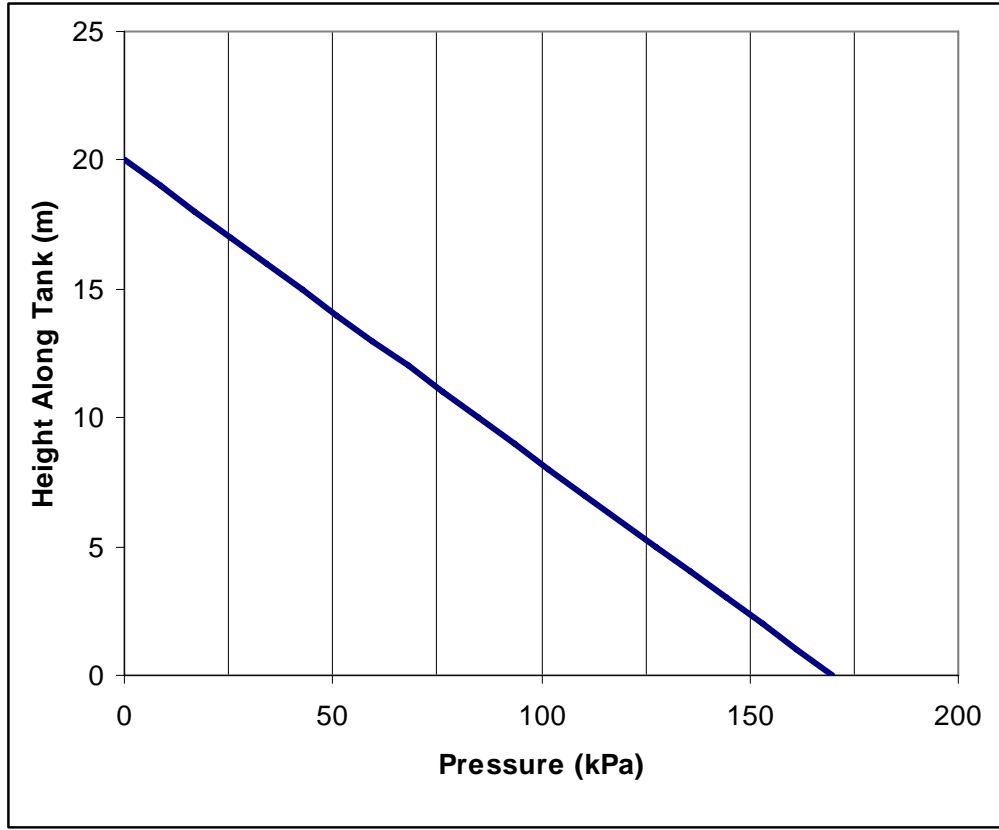


**Figure 2-29:** Hydrostatic Pressure in a Water Storage Tank

The detector must be able to withstand a similar pressure gradient. This is a critical point of analysis since the amount of pressure the detector must withstand is proportional to the amount of steel required to build it. The buoyancy limitations described in section 2.2.9 set a maximum amount of steel available for the detector, and therefore give criteria upon which invalid configurations can be eliminated.

#### 2.4.2. Stages of structural analysis

The Hanohano project requires a unique vessel with capabilities that no existing ship can supply. In an effort to efficiently brainstorm, analyze and accept or discard ideas, Makai used the following method:

- Brainstorm a variety of overall concepts
- Select the most likely candidate based on general preliminary analysis
- Do more detailed analysis on candidate at a variety of fiducial volumes until a show-stopping problem is encountered or until analysis is complete
- If no show-stopping problems are encountered, select the candidate for conceptual design

The following is an overview of the structural analysis performed in the third step outlined above.

#### 2.4.2.1 Loading conditions

The primary design point of any configuration is the weight and displacement of the detector itself. One characteristic that is common to all configurations is that the detector must have enough buoyancy to return to the surface at the end of the experiment. Therefore, detector weight was the first aspect of a configuration that was analyzed.

Once it was concluded that the detector itself was not so heavy as to invalidate the configuration, the transport vehicle was analyzed. Both integrated and detachable configurations have a hull component that stabilizes the detector during deployment and transport. The hull was first analyzed neglecting the effects of waves. Once it was determined that the flatwater loading conditions alone did not invalidate the configuration, waves were introduced to the analysis and the load analysis was complete. This staged analysis method prevented Makai from spending excessive time on analyzing a configuration that had a fundamental flaw.

#### 2.4.2.2 Materials

Once the loading conditions above were determined, the amount of material required to support those loads could be calculated. Makai considered both steel and aluminum as possible construction materials. Aluminum's lower density allows it to provide more strength per pound of submerged weight than steel. The submerged weight of an aluminum structure is one-half to one-third that of a steel structure. Therefore, an aluminum vessel can function similarly as a steel vessel and be more likely to meet the submerged weight criteria. However, this lighter submerged weight comes at a high economic cost. An aluminum vessel is estimated to cost twice that of a comparable steel vessel.

Each configuration/size combination was analyzed with both steel and aluminum as construction materials. This allowed Makai to balance the fiducial volume, wet weight, and size of the hull/detector assembly.

### 2.4.3. Weight and Strength of an Integrated Vessel with Cube Detector

#### 2.4.3.1 Detector concept

The detector concept for this configuration is a cube. Selection of this shape was based on the fact that oil tankers typically have square shaped compartments to hold the oil. A cube was selected because it minimizes the dimensions of all faces. Larger faces feel larger bending moments for any given pressure, so it is beneficial to keep faces as small as possible. Since simple flat plates are inefficient pressure walls, the concept of the stiffened panel is used to increase the strength of the cube detector.

A stiffened panel consists of a flat plate with parallel stiffening bars attached to one side. Figure 2-30 shows a typical stiffened panel.

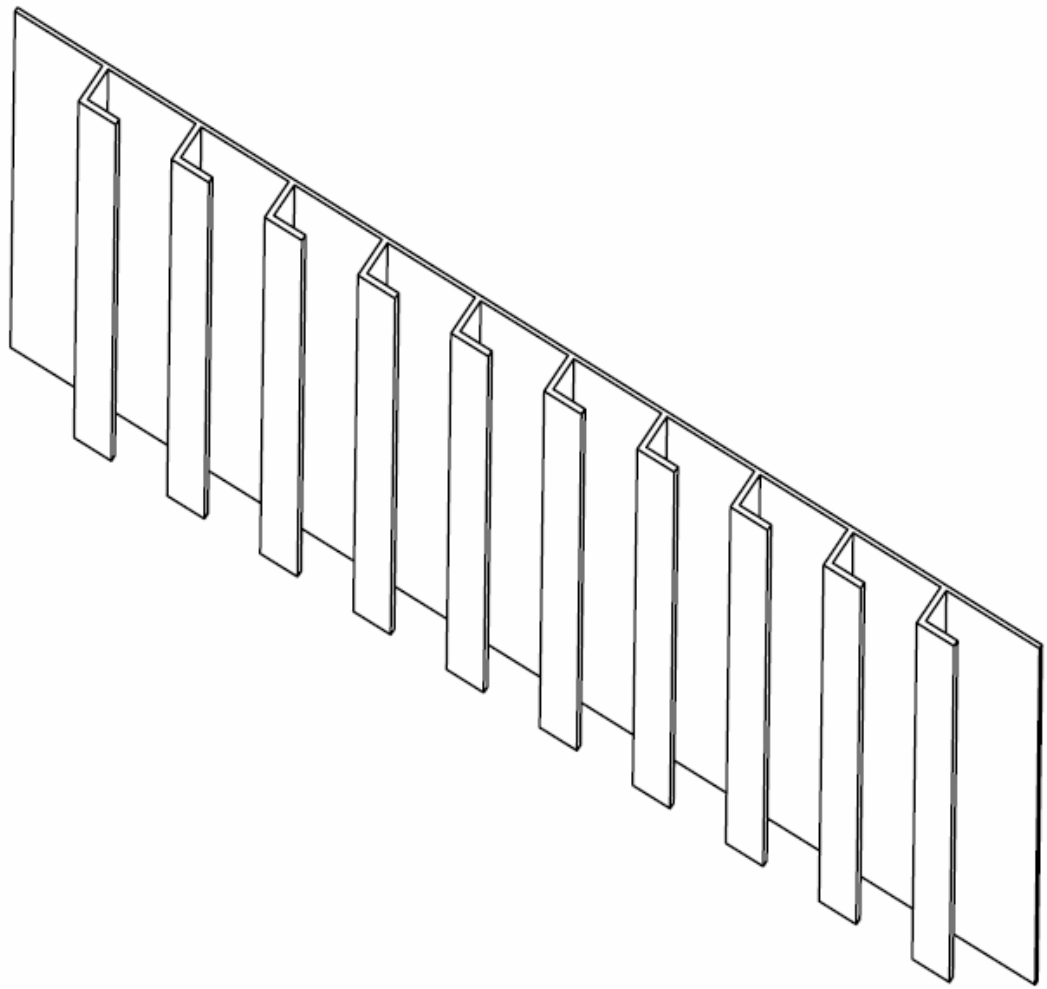


**Figure 2-30:** *Stiffened Panel*

The stiffening bars serve to strengthen the panel by preventing it from bending out of shape. Panels such as this are commonly used to support pressure loads. For example, the plating on a ship's outer hull is often constructed of stiffened panels.

The detector is too large to use a stiffened panel for each side of the cube. Instead, each wall is broken into two sub-panels. Between the two panels, an extremely strong cross-member connects the outer cube wall across the veto region to the inner wall that houses the PMTs. This cross-member allows the inner and outer walls to transfer force between each other, and therefore reinforce each other. Figure 2-31 shows a schematic of the inner and outer walls tied together through a heavy cross-member. This design is an example of double hull construction.

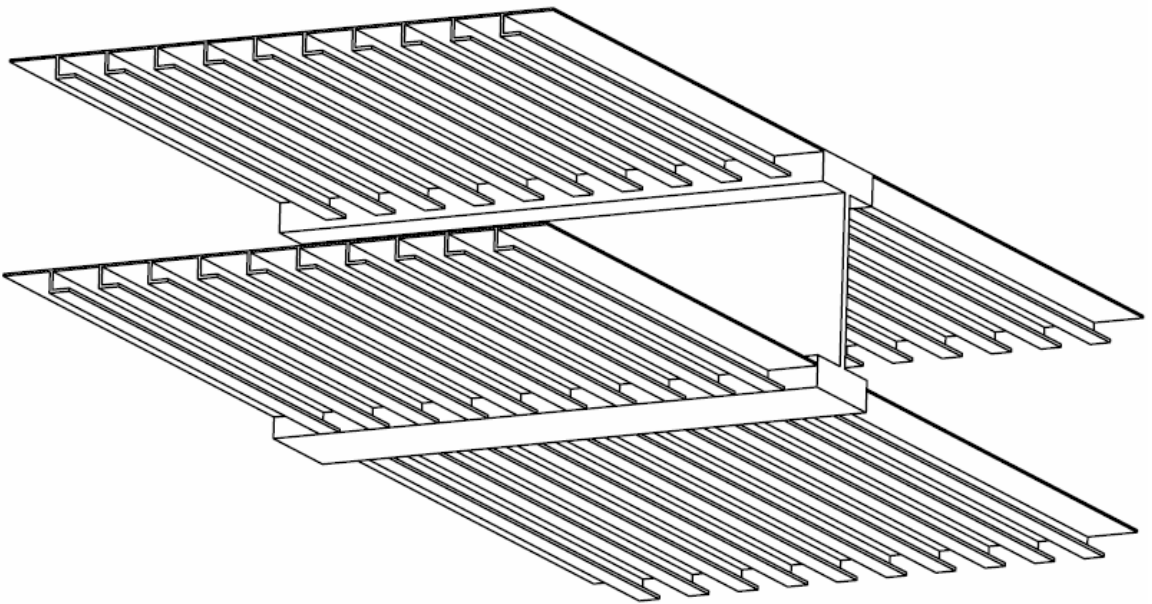


**Figure 2-31:** Double Hull Design in Cube Detector Concept

In order to determine the maximum size of each panel and the amount of stiffening each panel requires, Makai employed an analysis method utilizing the Euler-Bernoulli beam equation. In simplified form, the Euler-Bernoulli beam equation is  $\sigma = \frac{Mc}{I}$ , where  $\sigma$  = bending stress,  $M$  = bending moment,  $c$  = half the height of the vessel, and  $I$  = the moment of inertia of structural members. Moment of inertia and vessel height are aspects of the geometry of the vessel. Makai's analysis determines the bending moment so that the moment of inertia and vessel height can be optimized to keep the bending stress within allowable limits. The limits on bending stress are inherent to the material in question. In order to use this method, each stiffening bar and the portion of plate next to it was considered as if it had been cut off from the rest of the plate. Figure 2-32 shows the portion of the plate considered.

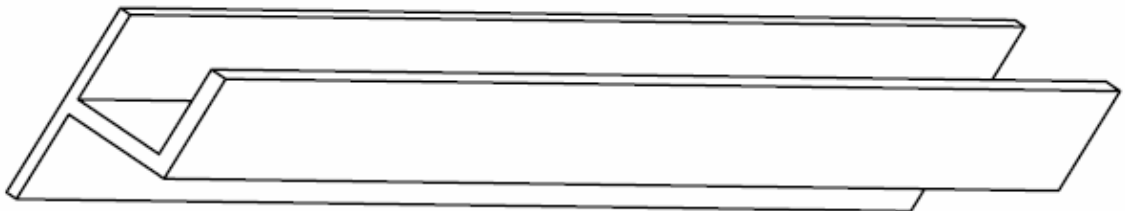


**Figure 2-32:** Individual Stiffening Bar and Associated Plate for Use in the Euler-Bernoulli Beam Equation

The Euler-Bernoulli equation predicts how thick the plate and stiffening bar need to be in order to support a particular load. In the case of the detector, the load is the pressure exerted on the walls by the scintillating fluid, oil, and freshwater inside. Makai developed a software package that calculated the thickness of plate and stiffener spacing required to support the pressure loads. It also calculated the overall thickness of the cross-members required to reinforce the panels.

The next section details the inputs required by the software package and summarizes the results of the analysis.

#### 2.4.3.2 Detector analysis Inputs

The primary inputs to the software package are the cube size and the pressure gradient. The cube size is defined by the fiducial scintillator volume of  $4096 \text{ m}^3$  (the volume of a 16 m cube). The pressure gradient is related to the size in that the height of the cube defines the maximum pressure. However, there is a subtlety present in the calculation of the hydrostatic load in that it varies through the lifetime of the cube. When the detector is on the surface, it has been designed to withstand the full hydrostatic pressure resulting from a full load of all fluids. In this case, the pressure gradient is similar to that of a water tank on land.

However, once the detector is submerged, the loading conditions change. Since the scintillating fluid, oil, and freshwater are all less dense than seawater, these fluids exert pressure against the top of the detector as they try to float back up to the surface. In order to eliminate the risks associated with a pressure vessel that must withstand pressure outside greater than that inside, Makai has decided to ensure the pressure inside the detector at the bottom is equal to that outside the detector. Figure 2-33 shows the pressure gradient on the inner wall under these conditions.

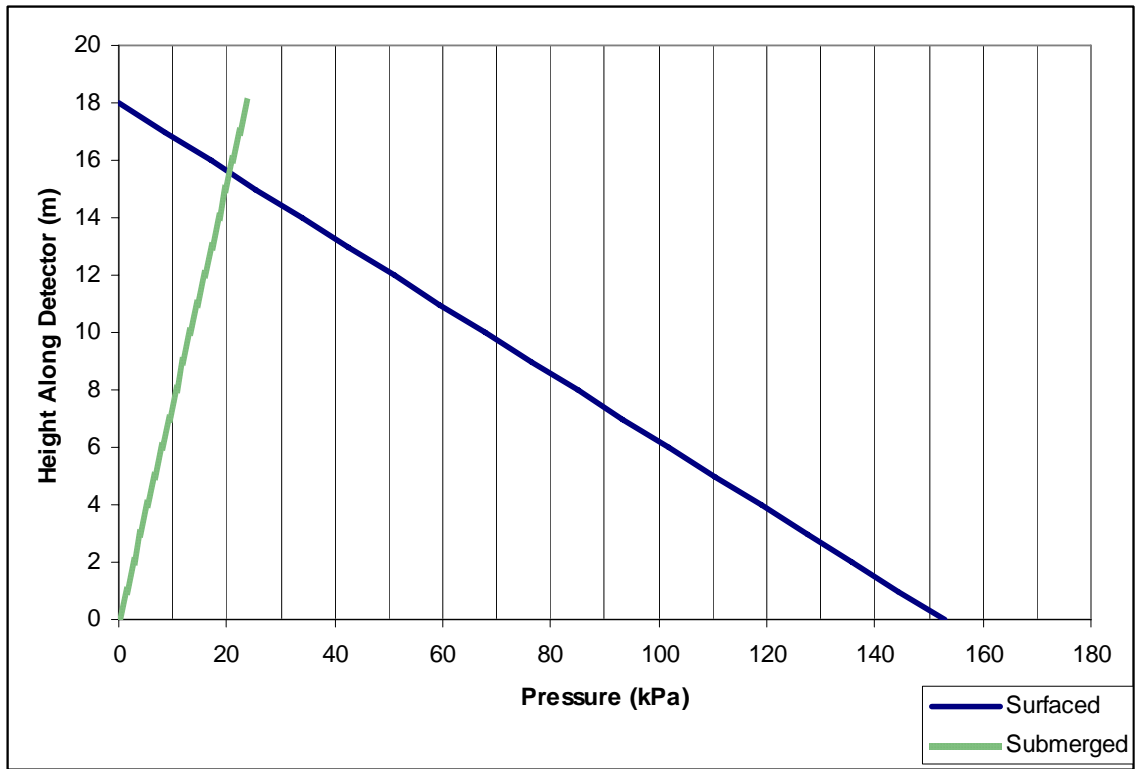


**Figure 2-33:** Pressure Gradient in Detector on Surface

Here, the buoyant fluids exert more pressure on the top of the detector than on the bottom. In order to design for the worst case conditions, Makai used a pressure distribution as shown in Figure 2-34.

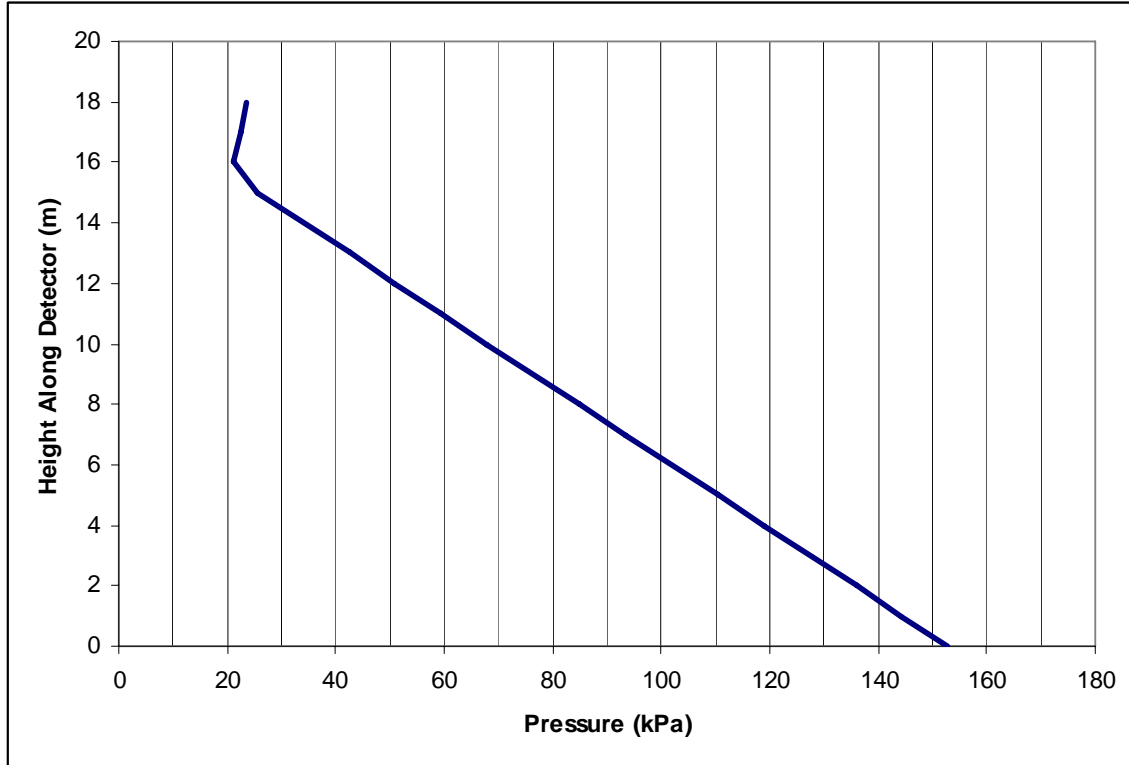


**Figure 2-34:** Design Pressure Distribution in Detector

While this pressure distribution does not correspond to any particular moment in the lifetime of the detector, it does represent the maximum pressures at any given point on the inside of the detector wall.

#### 2.4.3.3 Detector analysis Details

Section 2.4.3.1 above gave a general overview of how the software utility calculated the size of plates and stiffeners required to withstand the hydrostatic pressures. The following paragraphs will give more detail as to how the utility determines the values.

The stiffened panel “beams” shown in Figure 2-32 are used to model the panel as a whole. Each stiffening bar is treated as a beam, and the sum of all the beams is the model for the entire panel. The software utility calculates the forces on each segment, and then determines how thick the plate and stiffener need to be. Two criteria are used to calculate the thickness: maximum bending stress and buckling.

Maximum bending stress refers to the beam’s ability to withstand bending moments. The fact that the beam has a pressure load across its entire surface but is only supported at the ends (by the other walls of the cube or the cross-members) means the beam will bend. If bent too far, the metal will deform and the structural integrity of the detector will be compromised. The Euler-Bernoulli equation is used to find the dimensions of the plate and stiffening bar that will keep bending stresses down to safe levels. The calculations to size the beams have been carried out with a safety factor of 2.

Buckling refers to a mode of failure not addressed by the Euler-Bernoulli equation. The bending stress analysis detailed above assumes the beams are perfectly shaped. However, real beams have small imperfections in their shape. These imperfections can allow forces to concentrate in a single area and deform the beam earlier than perfectly formed beam would be. Fortunately, buckling is typically only a problem for structures built from thin materials. As a check, Makai calculated the critical stress at which buckling would occur in the beams. The critical stress was greater than the design stress under all conditions. The safety factor of 2 applied to buckling stresses as well as bending stresses. The top two sections of Table 2-13 below summarize the results of Makai's analysis. The stiffener sizes are given in imperial units because they have been selected from standard angle iron sizes.

Reinforcing the panels are heavy cross-members tied into the corners of the detector. The largest stresses occur at the center of a stiffened panel. In order to keep the panels as light as possible, they must be as small as possible. The heavy cross-members cut the large sides of the detector into three smaller panels, and therefore reduce the stress in each panel.

Analysis of the cross-members was limited to bending stress. The objective of the analysis was not the design of an extraordinarily large beam, but instead to determine how heavy such a beam might be. Therefore, Makai modeled each beam as a pair of 15.2 cm thick metal slabs. Each of the pair of slabs was placed in the veto region; one was on the inside of the outer wall and the other on the outside of the inner wall as shown in Figure 2-31. In this arrangement, the slabs acted as a pair of beam flanges separated by a gap of about 2m.

The forces on the panels above and below the slabs are carried by the slabs in bending. Makai calculated the moment of inertia required to support the loads and met the requirements by varying the width of the 15.2 cm thick slabs. The third section of Table 2-13 shows the dimensions and weights required for the two cross-members in each wall.

Inner Wall	
Dimensions	
Plating Thickness	6 to 9 mm
Stiffener Size	8 x 354 x 0.5 in
Stiffener Spacing	25 cm
Weight	
Plating Weight	14 tonne
Stiffener Weight	12 tonne
<b>Inner Wall Weight</b>	<b>25 tonne</b>
Outer Wall	
Dimensions	
Plating Thickness	14 to 21 mm
Lower Stiffener Size	8 x 433 x 0.875 in
Upper Stiffener Size	8 x 433 x 1.125 in
Stiffener Spacing	25 cm
Weight	
Plating Weight	47 tonne
Stiffener Weight	37 tonne
<b>Outer Wall Weight</b>	<b>84 tonne</b>
Cross-members	
Dimensions	
Lower Cross-member Size	70 x 1800 x 15 cm
Middle Cross-member Size	80 x 1800 x 15 cm
Weight	
Lower Cross-member Weight	30 tonne
Middle Cross-Member Weight	34 tonne
<b>Total Detector Weight</b>	<b>1173 tonne</b>

**Table 2-13:** *Detector Cube Support Structure Dimensions*

The final line of the table above gives the total estimated structural weight of the detector. This value was compared to the maximum allowable weight calculated using the methods of section 2.2.9, 1050 tonnes. Since the detector itself is over weight, a steel integrated cube detector cannot satisfy the weight requirements. However, since aluminum is being considered as an alternate material, Makai proceeded with hull structural analysis.

#### 2.4.3.4 Hull bending moment

Two fundamental structural problems within the scope of Makai's hull analysis are bending due to uneven loading and bending due to the presence of waves. Most vessels experience conditions of uneven loading. The shape of the hull, restricted locations for machinery and crew accommodations and the logistics of efficient loading and unloading of the vessel all contribute to the inability to load a ship perfectly evenly across its entire length. Since the ship cannot be loaded evenly, bending moments are induced in the vessel. Figure 2-35 depicts a vessel that has been loaded unevenly and the bending moments associated with such a loading condition.



**Figure 2-35:** Bending Moments Due to Uneven Loading

The vessel has been more heavily loaded in the center than at the ends, and the center therefore tends to sink lower as the vessel bends somewhat. The figure has been greatly exaggerated to more clearly show the effect. The condition in which the center of the vessel tends to drop is known as sagging. The opposite condition, that in which the vessel has been more heavily loaded on the ends and the center tends to rise, is known as hogging. The tendency of a vessel to sag or hog under its own loading condition helps determine the conditions under which wave-induced bending loads are analyzed.

The second structural problem considered is the effect of waves on the bending moments in a vessel. If one were to look at a vessel in waves, as shown in Figure 2-36, one can see that there are areas where the water comes higher on the hull at wave crests, and areas where the water is lower on the hull at wave troughs.

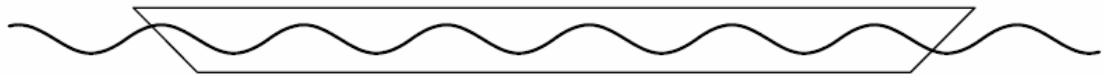


**Figure 2-36:** Vessel in Short Period Ocean Waves

This variation in water level creates variation in the forces that buoy the vessel up in the water. The effect is more easily seen under the worst case scenario: when the length of the waves is exactly equal to the length of the vessel. Figure 2-37 shows a ship under these conditions.



**Figure 2-37:** Vessel in a Wave Where Wavelength Equals Vessel Length

There is a much higher water level at the ends of the ship than in the center. Therefore, the buoyancy forces are much greater at the ends than in the middle. Like the variation in loading, this variation in buoyancy force creates bending moments in the ship, causing it to sag or hog. Figure 2-38 shows the same conditions as Figure 2-37, but with the sag exaggerated to show the effect.

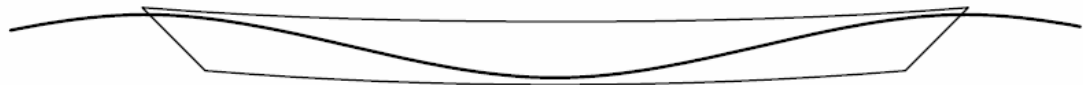


**Figure 2-38:** Vessel Sagging in Waves

In order to determine the worst-case conditions the vessel will see in service, the vessel's tendency to hog or sag is first determined. This is accomplished by analyzing its typical loading condition. Then, if the vessel tends to sag under its own weight, the effect of waves is analyzed as shown in Figure 2-38. If instead the vessel hogs under its own weight, the effect of waves is analyzed under conditions shown in Figure 2-39.



**Figure 2-39:** Vessel Hogging in Waves

The combined effect of load-induced and wave-induced bending determines how strong a ship has to be. The Hanohano project is particularly sensitive to bending loads. Under the conditions shown above, the greatest bending moments are found in the center of the ship. All of the design concepts Makai deemed potentially suitable involve placing the detector in the center of a hull. Since the detector must be hollow, this arrangement limits the amount of space available for structural support at the point of greatest bending moment. A reasonable estimate of maximum bending moments is required to make a reasonable assessment as to the suitability of a particular design concept.

There are other forces that must be considered when designing a ship. Racking forces are created when waves hit the side of a ship and try to flatten it. Also, slamming forces arise from the bow of the vessel crashing up and down in the waves while underway. However, these forces are not determined as easily as bending forces, and are typically secondary considerations. Therefore, they lie outside the scope of this analysis.

#### 2.4.3.5 Hull structural model

Again, the analysis was simple when compared to traditional naval architecture design. Characteristics such as bow and stern shape, framing details, machinery details, and crew accommodations do not have a large effect on the overall weight of the structure, and therefore have been neglected in Makai's analysis. Instead, the analysis focuses on bending moments in the hull as described in above

Makai modeled the hull in a manner analogous to the cross-members in the detector cube. The top and bottom decks were considered slabs that acted as flanges in a beam. The walls of the ship are considered as the web between the flanges, and have been included in the flexural stiffness analysis. However, shear stress through the walls has not been considered because transfer of shear forces is a task taken up by the framing within the ship, and design of the ship's frame is beyond the scope of this analysis. Similarly, the ship's framing serves to stiffen the deck and keel plating against buckling, so no buckling analysis has been conducted on the hull.

The model's stiffness is initially based solely on the minimum plating thickness recommended by Det Norske Veritas (DNV) standards. DNV is a Norwegian vessel classification organization that provides vessel design standards. In the case of the 4096 m<sup>3</sup> detector, the top deck and keel plating were 8.3 mm thick and the side plating was 4.5 mm thick. The analysis assumes that the plating removed from the top deck to make room for the detector is placed over the remaining deck so as not to lose the stiffness it provides. The top deck plating at the center of the hull is 46 mm thick. Once the bending loads have been determined, the top and bottom plates are thickened until the bending stresses are within allowable limits.

The overall hull shape considered is a simple rectangular prism, or box. This basic shape allows for quick structural analysis while maintaining a reasonable approximation to a real vessel. Two versions of the rectangular prism are considered: one with a rectangular base and one with a square base.

The rectangular base hull follows the traditional logic of naval architecture. One of the primary driving forces behind vessel design is efficient movement through the water. Efficient movement through the water is accomplished by a long, sleek shape. However, Makai observed that efficient movement through the water may not be the primary driving force behind the Hanohano design, and therefore considered a square-based hull as well.

A square base minimizes the bending loads in the hull. Bending loads are proportional to the length of a beam, so a shorter vessel is subjected to smaller bending loads. The downside of a square-based hull is that it must be wider than an elongated hull. The maximum draft limitation defined in section 2.2.2 means that the vessel displacement is constant at that draft. Another way to look at this limitation is that the area of the base of hull is fixed. Therefore, in order to shorten the hull and reduce bending loads, one must widen it. A wider hull is awkward to tow and may be limited for Panama Canal transit. Within Panamax capabilities and at a similar draft, the maximum sized detector possible with a square hull is smaller than the maximum detector possible with a rectangular hull.

The analysis below will assume a rectangular hull. The analysis of a square hull is similar in nature, and the results will be presented at the end of the section.

Hull bending analysis is typically performed using a series of force curves to determine the loading on the vessel. The first curve generated is the weight curve. This curve represents the amount of weight the hull must support at along its length. Figure 2-40 includes an example of a weight curve. The second curve is a buoyancy curve. A buoyancy curve represents how much buoyant force the water is exerting along the length of the hull. In flat water, the buoyancy along the hull is constant, and the buoyancy curve is the dashed line in Figure 2-40. A more detailed discussion of interesting buoyancy curves will be presented together with hull bending moments in waves later in this chapter. The difference between the buoyancy curve and the weight curve is known as the load curve, and it is this curve that defines the bending moments present in a vessel.

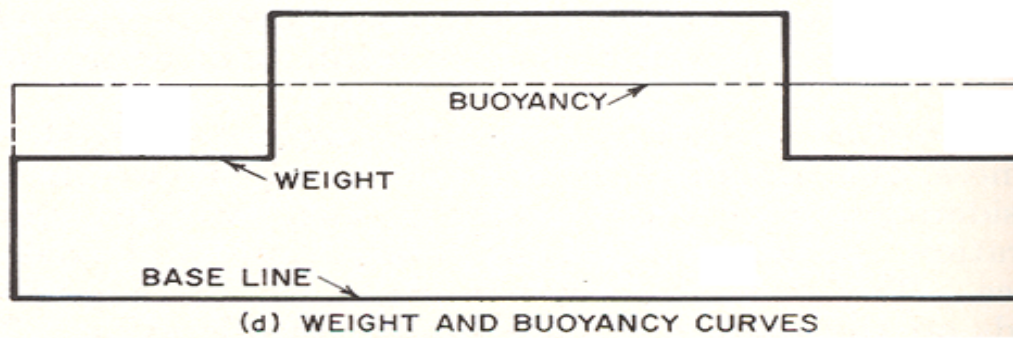


**Figure 2-40:** Generic Design Plot Showing Weight and, Buoyancy Curves

The load curve shows the resultant of all vertical forces acting on the vessel along its length. Therefore, it can be either above the x-axis (buoyant forces are greater than weight forces) or below the x-axis (weight forces are greater than buoyant forces). However, no matter what the shape of the load curve, the sum of the area under the curve must be zero. This represents the reality that the vessel has a nominally stable condition where the sum of all vertical forces is zero.

However, the fact that the sum of all forces is zero does not mean that the vessel does not need to resist internal forces. If the weight and buoyancy forces are not uniform (i.e. – the load curve is not flat), there will be bending moments on the hull. The hull is designed such that it can withstand these bending forces, and the final two curves are used to do so.

The final two curves used in preliminary vessel design are the shear curve and bending moment curve. These curves determine the magnitude of the internal forces within the ship. The shear curve represents how strongly the various parts of the ship want to move vertically relative to one another. The bending moment curve shows how strongly the ship wants to hog or sag. Figure 2-35 shows typical shear, bending moment, and load curves

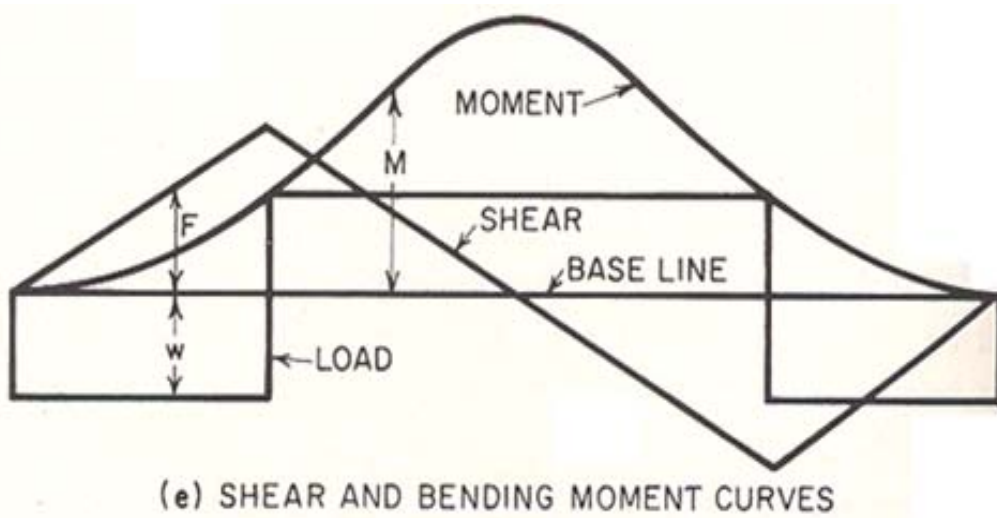


**Figure 2-41:** Shear, Bending Moment, and Load Curves Based on Above Weight and Buoyancy Curves

Since shear analysis is not considered in this analysis, Makai is primarily concerned with the bending moment curve. Again, since the detector takes up a large portion of the center of the hull, Makai's analysis focuses only on the bending moments in that area. The assumption is that if the hull is practical at the point where maximum load meets minimum space, then the hull as a whole is practical.

#### 2.4.3.6 Hull analysis

The general hull size and shape is driven by stability and draft constraints. The calculations of hull size based on these constraints are explained in section 2.3.2.2, and only the results will be presented here. For the  $4096 \text{ m}^3$  detector, the dimensions of a rectangular supporting hull are 28 m long by 22 m wide by 14 m high. The dimensions of a square hull are 25 m long by 25 m wide by 14 m high. These dimensions drive the following analyses.

The first condition under which the hull is analyzed is bending in still water. This neglects the effects of waves, and looks at the bending induced by the loading conditions of the barge. It is particularly important to look at loading conditions in this analysis because Hanohano utilizes unique hull/payload arrangements. Most vessels carry their payload within their hulls and spread the load across as much length as possible. The hull carrying the detector however, carries a significant portion of its load above the deck, and has it concentrated at the center of the hull. Figure 2-42 shows the weight curve for the integrated cube detector concept.

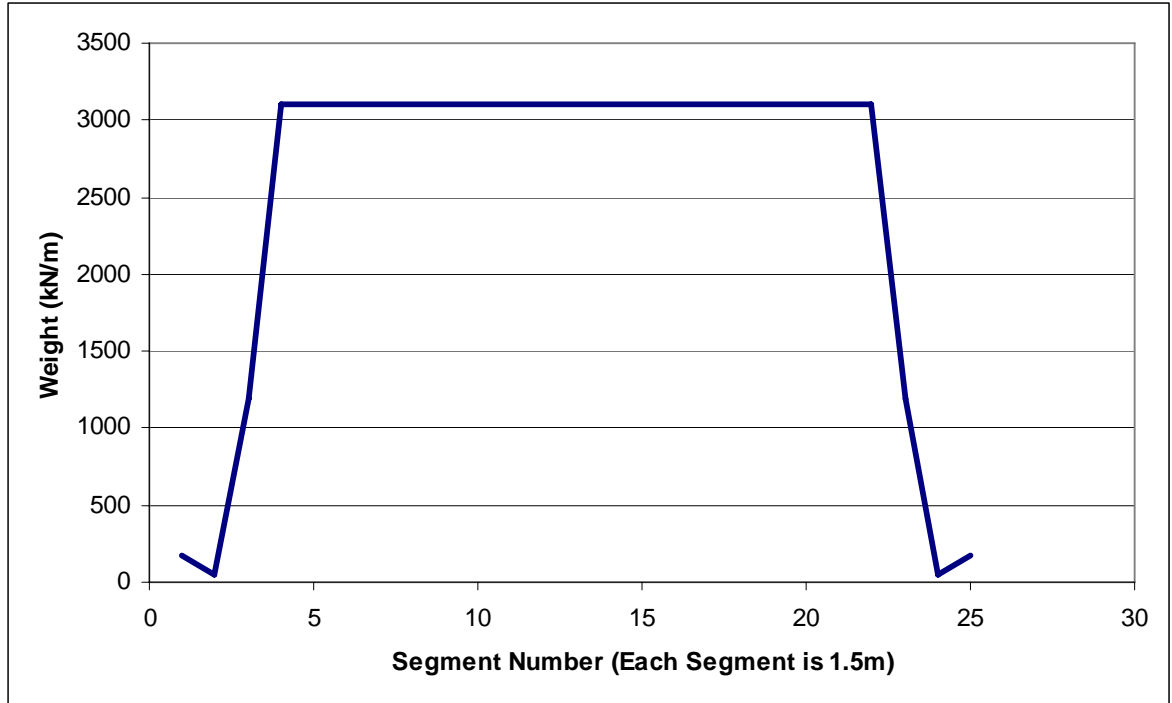


**Figure 2-42:** Weight Curve for an Integrated Cube Detector Hull

Since this analysis is considered in the absence of waves, the buoyancy curve is flat, and the load curve appears as shown in Figure 2-43.

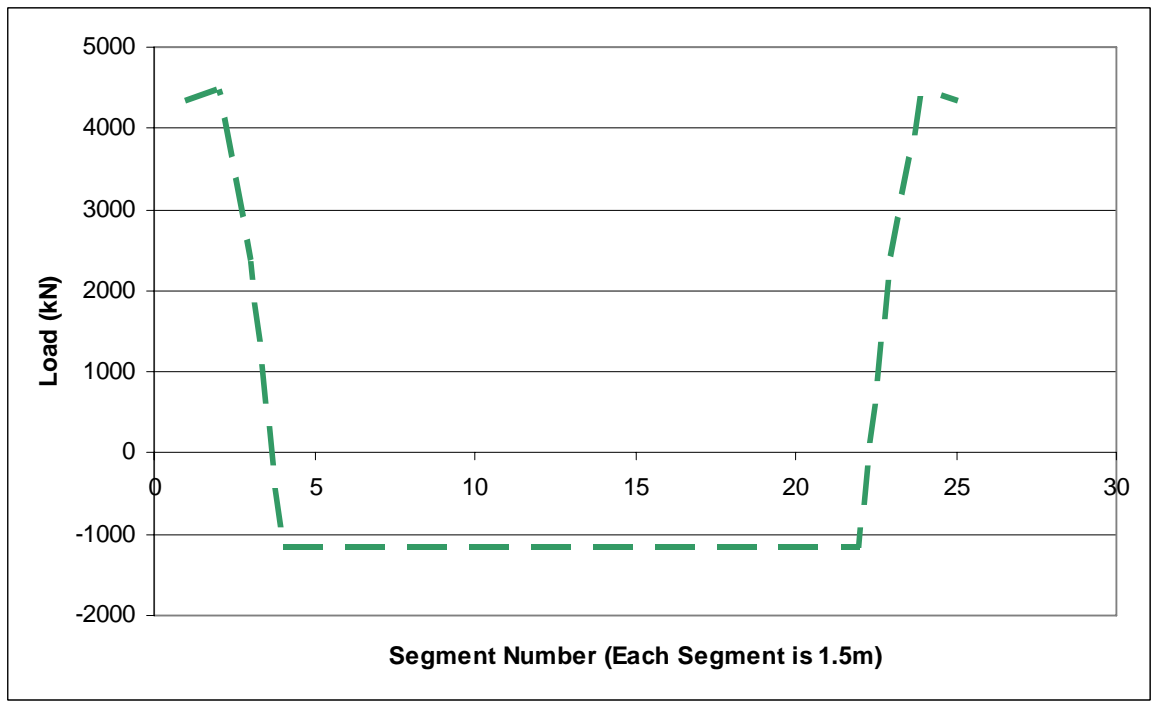


**Figure 2-43:** Load Curve for 4096 m<sup>3</sup> Integrated Cube Detector in Flat Water

The negative section in the center of the load curve represents the zone over which the weight of the detector exceeds its buoyancy. This indicates the vessel will sag when fully loaded. The maximum bending moments can be found from Figure 2-44.

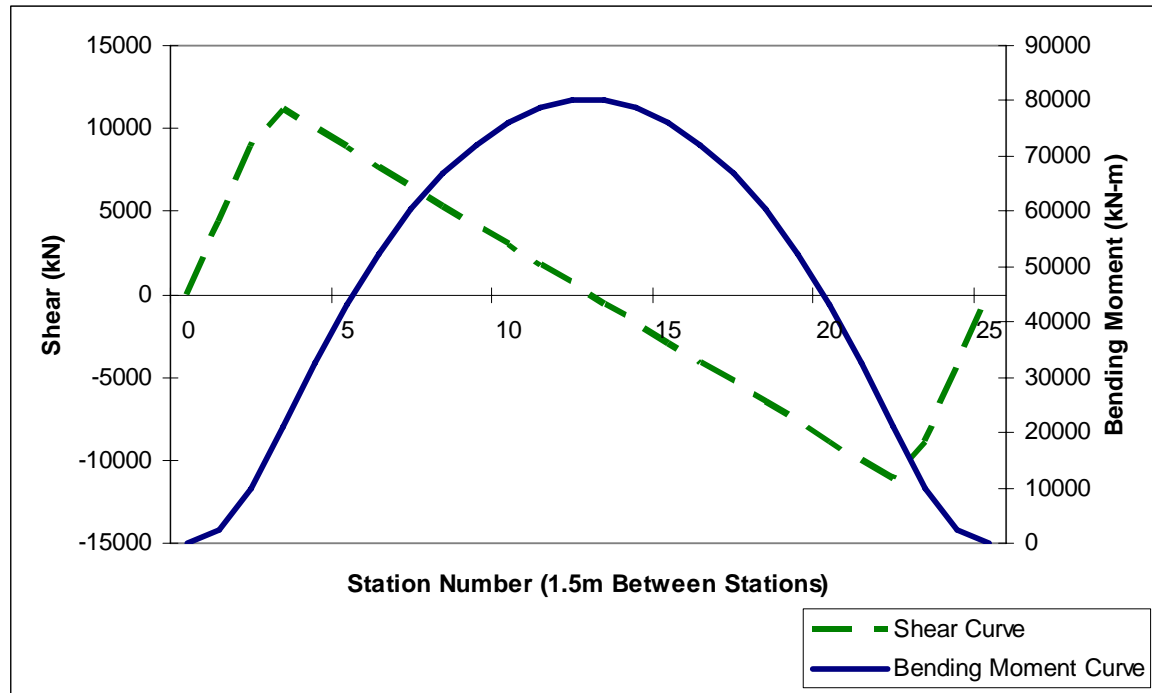


**Figure 2-44:** Shear and Bending Moment Curves for 4096 m<sup>3</sup> Integrated Cube Detector in Flat Water

The maximum bending moment is 80,000 kN-m, and it is this value that is used to determine how thick the plating on the top deck and keel needs to be. The vessel height is typically fixed by stability constraints, not structural. Therefore, the vessel height used in the structural analysis is that which is required for stability. With this assumption, the allowable bending stress ( $\sigma$ ), bending moment (M), and vessel height ( $2*c$ ) are known. Makai then proceeded to determine the moment of inertia required to satisfy the Euler-Bernoulli beam equation. This moment of inertia required was compared to the moment of inertia provided by the plating defined by the DNV standards. The results of the analysis were that the stiffness provided by the plating was sufficient to support the bending loads.

Once it was determined that the vessel was practical in flat water, the bending moment of the vessel in waves was considered. Introduction of waves changes the buoyancy curve from a flat line to a curve that matches the waveform. Since the vessel tends to sag in flat water, the worst case scenario is that in which a wave of wavelength equal to ship length has its trough right in the middle of the vessel. The height of the wave to be used cannot be calculated from first principles. It would be well beyond the scope of this analysis to attempt to completely define the structural strength of the vessel and model the stresses it may feel in a storm. However, vessels are often completely designed without such in-depth modeling. Wave height equations have been derived in the naval architecture industry from empirical data. The equations were written such that the wave-induced

bending moments match the maximum allowable moments in existing successful vessels. This wave height is called effective wave height because it does not necessarily correspond to a real wave the vessel could encounter, but instead to the height of the wave that will predict the bending moments the vessel will have to withstand. The equation used for this analysis is  $H_{eff} = 0.6 * L^{0.6}$ , where  $H_{eff}$  is the effective wave height and L is the vessel's length overall. This arrangement produces the buoyancy curve shown in Figure 2-45.

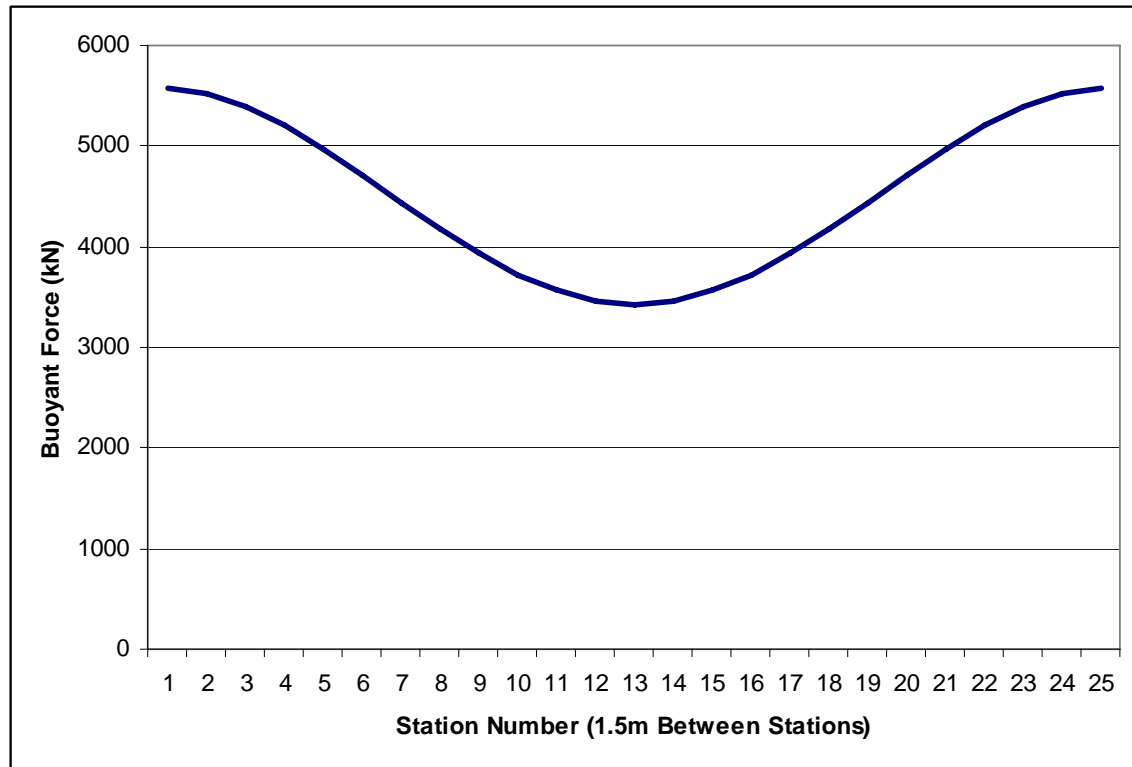


**Figure 2-45:** Buoyancy Curve of a 4096 m<sup>3</sup> Detector in Waves

The variation in buoyancy also changes the load curve, shear curve, and bending moment curve. The wave affected version of the curves can be seen in Figure 2-46 and Figure 2-35.

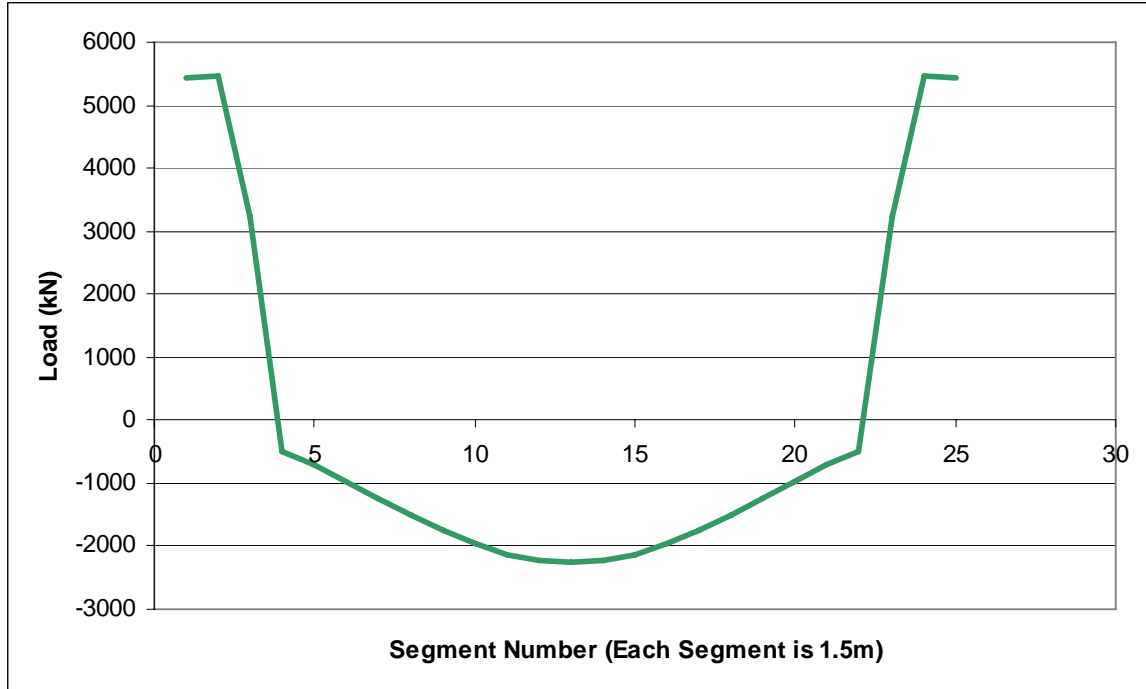


**Figure 2-46:** Load Curve of a 4096 m<sup>3</sup> Integrated Cube Detector in Waves

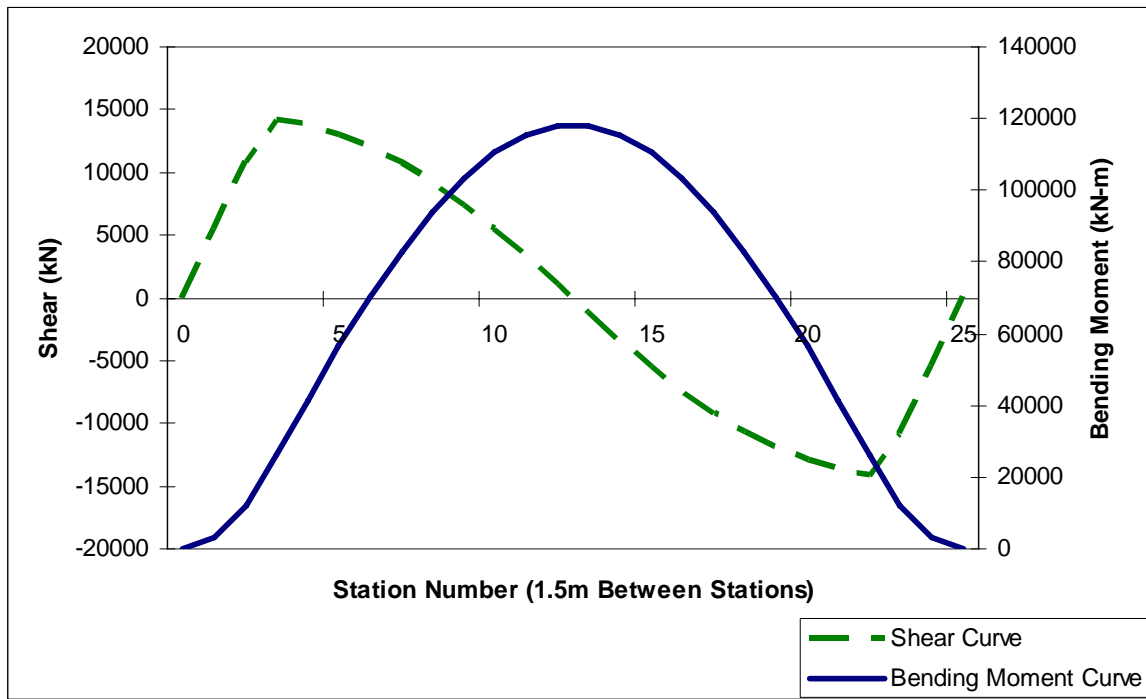


**Figure 2-47:** Shear and Bending Moment Curves for a 4096 m<sup>3</sup> Integrated Cube Detector in Waves

The bending moment was increased about 50% to 12,000 kN-m. However, the plating on the top deck and keel was still sufficient to withstand the bending moments, so no additional material was needed.

Since no additional material was needed, the estimated total lightship weight of the vessel was 1275 tonnes. This value includes the weight of the detector and the steel plating that makes up the hull. It does not include any structural reinforcement that would be required to withstand any forces beyond the bending moments.

In order to explore the optimum size detector, Makai repeated the above analysis for a variety of detector sizes up to 125,000 m<sup>3</sup> (a 50 m cube). The weight of the detector was scaled as described in section 2.4.1.2. The size of the hull was scaled in such a way as to continue to satisfy stability and draft requirements. Also, Makai performed the analysis for a variety of detector sizes with a square based hull. Figure 2-48 shows the results of the analysis in the case of a steel vessel.

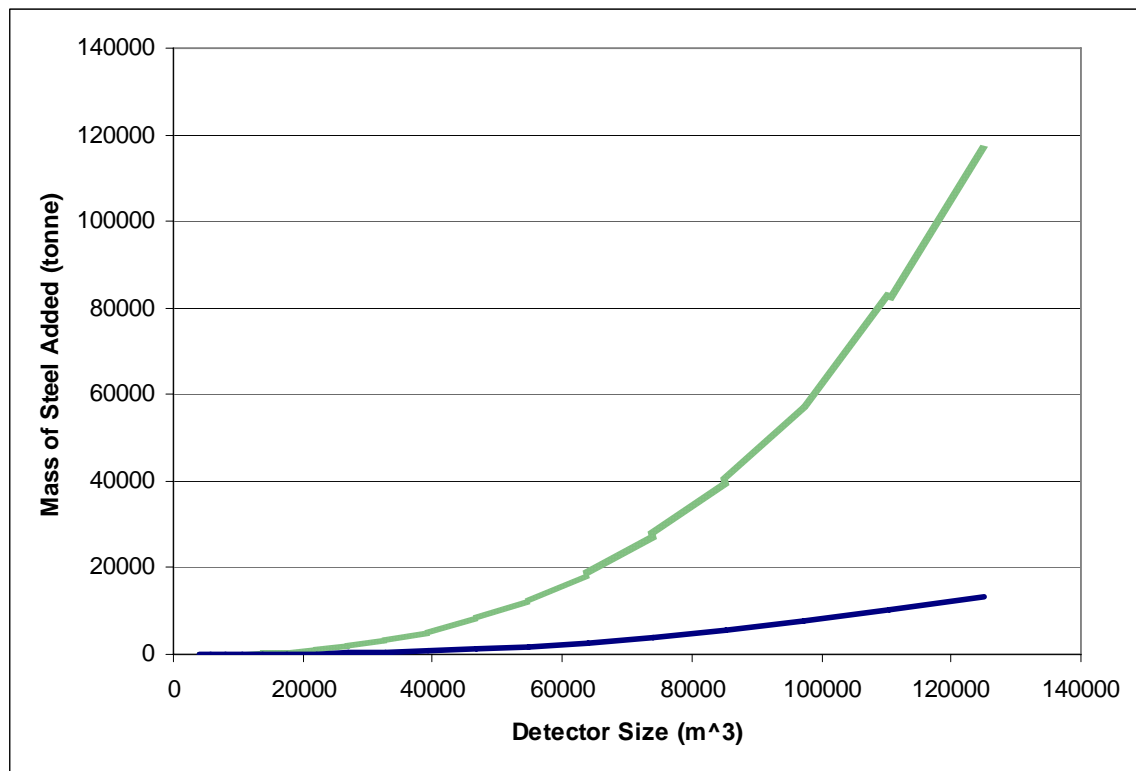


**Figure 2-48:** Added Mass of Steel Needed to Withstand Bending Moments in Integrated Cube Detector Hulls

As detector size increases, the amount of steel required to maintain structural integrity for a rectangular based hull increases dramatically. This is a preliminary indicator that the rectangular integrated cube detector may be a difficult concept to realize. The fact that weight is extremely sensitive to size limits diversity. In comparison, the mass that must be added to the square barge increases more slowly. This indicates that the square barge may be a more practical concept. The lightship weight of the 4096 m<sup>3</sup> square based hull was

1249 tonnes. The 26 tonne decrease over the rectangular hull is not enough to justify the increased width of the vessel. The square based hull only becomes desirable at larger detector volumes.

Ultimately, the goal of Makai's analysis is to determine the sizes at which a particular concept can be constructed. A convenient manner to present the results of the above analysis is a graph showing the lightship weight of the vessel at various sizes and the maximum weight. Instead of plotting lightship weight directly, Makai plots lightship weight divided by detector volume. This enhances the plot because it reveals not only whether a particular size is practical, but also the sensitivity of the concept to variation in size. Makai has also included the results of an aluminum vessel in order to determine if aluminum is a desirable construction material. Figure 2-49 shows the plot for a rectangular based cube detector.

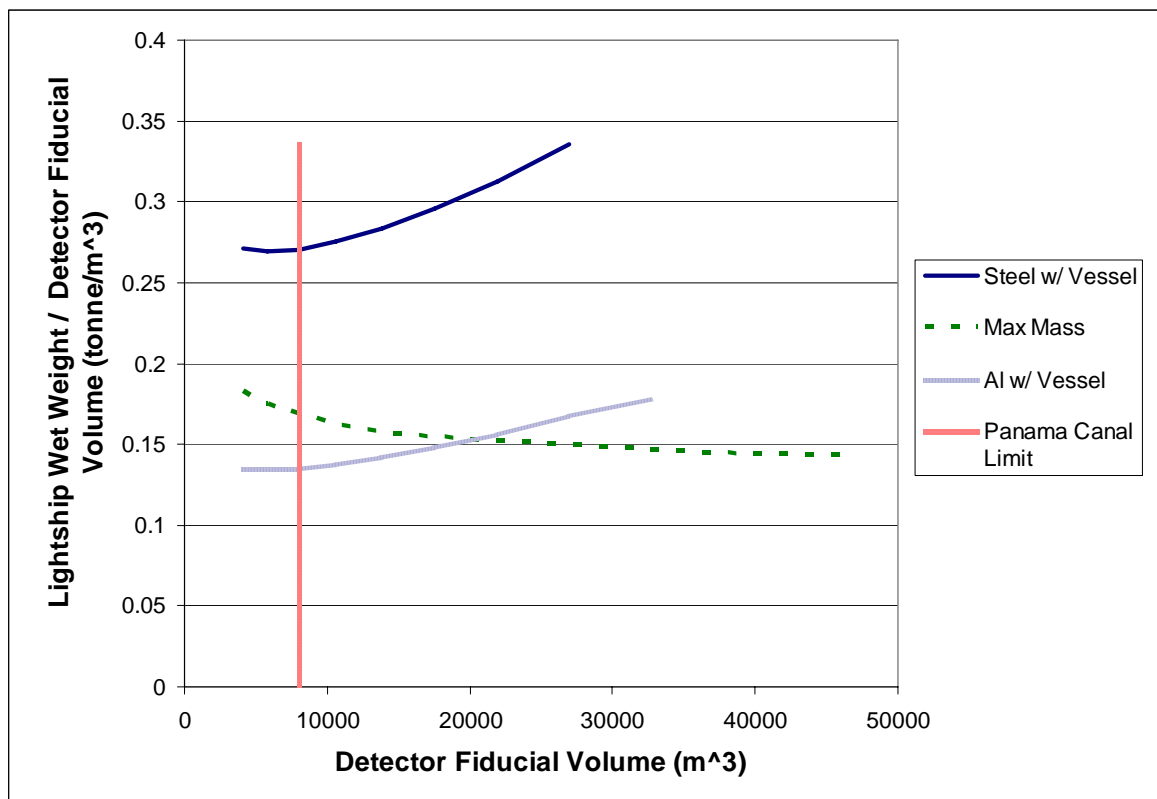


**Figure 2-49:** Suitability Plot for Rectangular Based Integrated Cube Detector

Steel is not a feasible construction material for this concept. A steel vessel is overweight for all detector sizes considered. Even when using aluminum, only detectors up to 17,500  $m^3$  of scintillator are at all workable for this concept. All larger sizes weight too much and would not come back to the surface after the experiment. The line representing the Panama Canal Limit on the plot shows the maximum size detector that could fit through the Canal. The maximum size for this concept is 8000  $m^3$  of scintillator. Since Makai's analysis was not conservative in terms of overall vessel weight, the rectangular integrated

cube detector concept was abandoned at this point. The next concept to receive attention was the square based integrated cube detector. Its plot is shown in Figure 2-50.

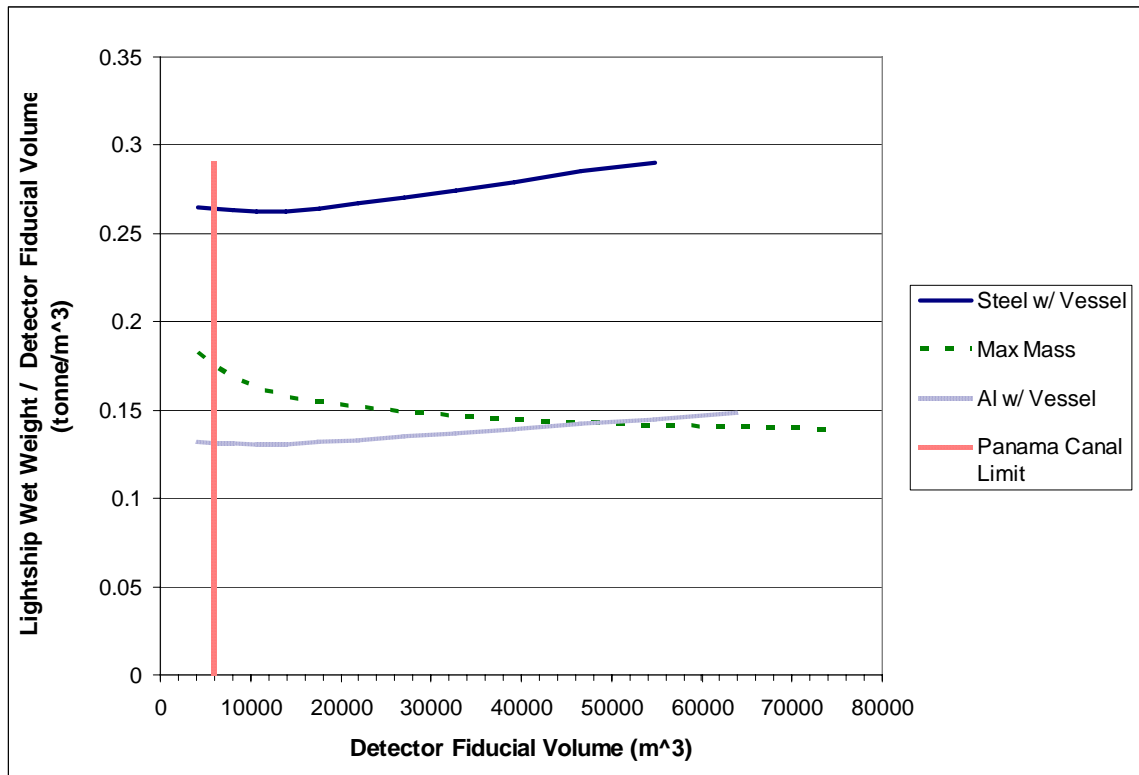


**Figure 2-50:** Suitability Plot for Square Based Integrated Cube Detector

Again, only an aluminum detector has a chance of being underweight. Detectors up to 46,000 m<sup>3</sup> are feasible in the above plot. The sensitivity to size has decreased, but not enough to indicate the square based hull improves the chances of an integrated cube concept to successfully return from the seafloor. Note that the Panama Canal Limit line has shifted to the left. A square hull is wider than the stability calculations require for a given detector size, so only a 6000 m<sup>3</sup> detector can fit through the Canal with a square hull.

#### 2.4.3.7 Intermediate conclusion

The results of the above analysis indicate that the integrated cube detector will be too heavy to meet the requirements of the Hanohano project. While final concept selection was reserved until each concept under consideration had been analyzed, Makai decided it would be more beneficial to explore an alternative concept than to further develop the integrated cube detector.

The primary factor driving the weight of the vessel is the weight of the detector itself. This stems from the fact that large cubes make for inefficient pressure vessels. This is because internal pressure puts the flat walls into bending, and bending is a less efficient mode of carrying load than pure compression or tension. To address this problem, Makai next

looked at an integrated cylindrical detector. A cylinder resists internal pressure through tension rather than bending, and this should allow for a lighter detector

#### 2.4.4. Weight and strength of an integrated vessel with cylinder detector

##### 2.4.4.1 Design concept

The concept of the integrated cylindrical detector is similar to the integrated cube detector. The detector and hull still form a single unit, and both rectangular and square hulls are considered. The primary difference is in the shape of the detector.

A cylindrical pressure vessel is more common than a cube-shaped one. Water towers, gas storage tanks and grain silos all take use a cylindrical shape. This is because the cylinder withstands pressure solely through tension in the walls. The amount of stress in the walls of a cylinder is proportional to the amount of pressure on the wall, and follows the hoop stress equation,  $\sigma = \frac{pr}{t}$ , where  $\sigma$  is tensile stress in the wall, p is pressure on the wall, r is the radius of the cylinder, and t is the thickness of the wall. The ends of a cylindrical pressure vessel are usually not flat. They have rounded ends that take the shape of half of an oblate spheroid (a hemisphere that has been flattened so it is half as tall as it is wide). This rounded shape helps ensure that all forces are resisted in tension instead of bending. In the case of the integrated detector concept, only the top of the cylinder has a spheroid end.

A second benefit of the cylindrical detector is that no special reinforcement structures are required. Tensile forces distribute themselves naturally throughout the wall of the cylinder, so there is no need for stress concentrators like the heavy cross-members in the cube concept.

##### 2.4.4.2 Detector analysis inputs

Again, the primary inputs for the analysis are detector size and pressure gradient. However, the cylinder allows for the introduction of a new variable that affects the inputs: the ratio of the detector's height to its diameter (H/D ratio). With the cube, a perfectly symmetrical detector was desirable because there was a high structural cost for any side to be larger than necessary. With the cylinder, that cost is reduced because wall thickness is linearly related to detector height rather than exponentially. Therefore, a variety of cylinder heights can be explored. For the analysis below, H/D ratio is assumed to be one.

##### 2.4.4.3 Detector analysis details

The hoop stress equation given above allows calculation of the wall thickness t based on the radius and thickness of the cylinder. Since the cube concept has been abandoned, it no longer makes sense to determine detector size based on convenient cube sizes. For example, 4096 m<sup>3</sup> is no longer convenient because a 16m cube does not have the same volume as a 16m cylinder. Instead, a base detector volume of 4000 m<sup>3</sup> was used for this analysis.

A 4000 m<sup>3</sup> detector has an inner diameter of 19.7m, and an outer diameter of 23.7m. With an H/D ratio of 1, the detector has an inner height of 19.7m and an outer height of 23.7m. The height gives a pressure gradient nearly identical to that shown in Figure 2-33.

With the pressure distribution, allowable tensile stress, and cylinder radius known, Makai calculated the required thickness of the detector wall. Since the maximum pressure varies along the height of the detector, the thickness of the wall was varied. A minimum thickness of 6 mm was selected to ensure overall ruggedness and a degree of conservatism. The results of Makai's analysis are shown in Table 2-14.

Inner Cylinder Minimum Thickness Maximum Thickness Weight	6.0 mm 8.5 mm 133 tonne
Outer Cylinder Minimum Thickness Maximum Thickness Weight	6.0 mm 20.7 mm 349 tonne
<b>Total Detector Weight</b>	<b>482 tonne</b>

**Table 2-14:** *Detector Cylinder Structural Dimensions*

A savings of 754 tonnes has been realized over the cube detector.

#### 2.4.4.4 Hull structural model and Analysis

The hull structural model was identical to that used for the cube detector. The vessel outer dimensions were the same and steel plating thicknesses were obtained from DNV standards. The analysis also followed the same pattern. The vessel was first analyzed in still water, and then in worst case waves. Since the detector itself is not a significant portion of the fully loaded weight of the vessel, the load, shear, and bending moment curves are extremely similar to those from the cube detector, and will not be repeated here.

However, the detector is a significant portion of the vessel's structural weight, and the fact that it is 754 tonnes lighter than the cube detector makes it a more likely candidate for Hanohano. Figure 2-51 shows the suitability plot for the cylindrical detector concept.

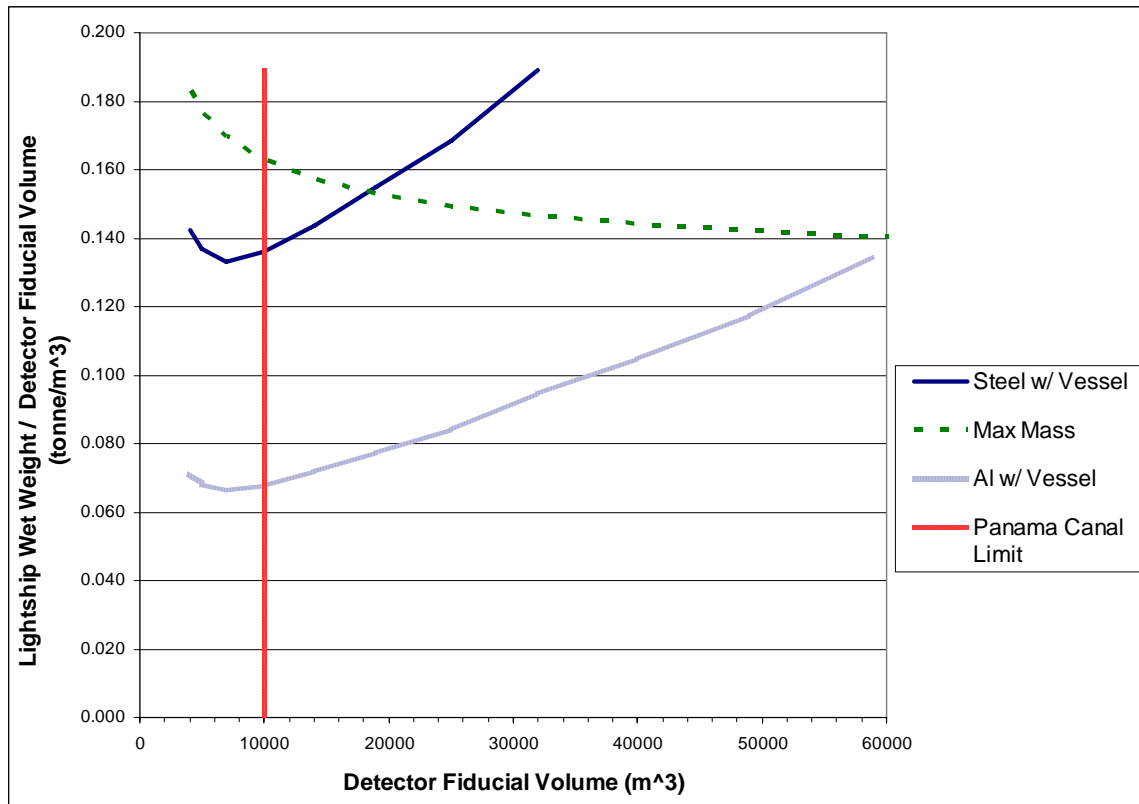


**Figure 2-51:** Suitability Plot for a Rectangular Integrated Cylinder Detector

In contrast to Figure 2-49, the steel cylindrical concept is shown to be possible up to  $16,000 \text{ m}^3$  fiducial volume. The aluminum concept is possible up to  $59,000 \text{ m}^3$ . Also, the rectangular base allows the vessel to fit through the Panama Canal up to  $10,000 \text{ m}^3$ . Figure 2-52 shows the plot for a square based hull.

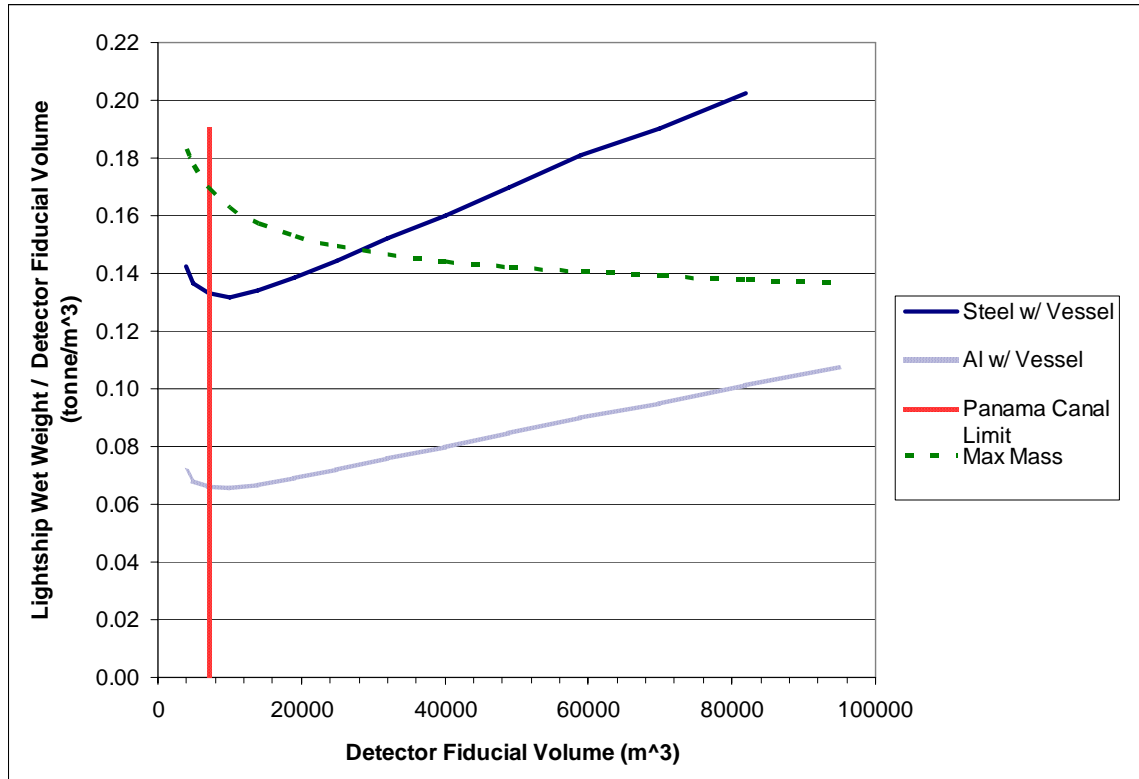


**Figure 2-52:** Suitability Plot for a Square Hull Integrated Cylinder Detector

The square based hull concept increases the range over which the vessel is below the maximum allowable weight. The steel vessel could contain up to 25,000 m<sup>3</sup> of scintillating fluid. The aluminum vessel is light enough to be built over the entire range of sizes considered for the study. The downfall of the square hull is again that the Panama Canal limitations become more stringent and the vessel will be more difficult to tow. The detector could only be 7,000 m<sup>3</sup> and still make it through the canal.

#### 2.4.4.5 Intermediate Conclusion

The integrated cylindrical detector concept shows more promise than the cube concept. However, Makai retained several reservations at this point in the design process:

- The detector has only been sized to withstand hydrostatic pressure and longitudinal bending, yet at least 75% of the allowable steel for the submersible components had already been allocated. More structural support would be needed to withstand other forces.
- No consideration has yet been given to onboard machinery or hardware for fluid pumping, purification, transport, etc.
- Preliminary stability analysis had indicated that stability could be difficult to obtain with the integrated design. Additional weight may be needed as ballast to keep the vessel upright.

- Although an aluminum vessel had the potential to alleviate the above problems; it was an expensive option that Makai preferred to leave as a last resort.

Therefore, Makai did not discount the integrated cylindrical concept at this point, but decided to explore a third design.

#### 2.4.5. Weight and Strength of a Detachable Cylindrical Detector

##### 2.4.5.1 Design concept

The detachable detector concept builds on the knowledge gained from the previous integrated designs. It is clear that the cylindrical detector is superior to the cube in strength to weight ratio, so it is used as the detector shape. Also, concerns arose that stability and weight could be an issue for an integrated design. Makai sought to surmount this obstacle by separating the tasks of transporting equipment and conducting the experiment.

In this concept, transport functions are carried out by a custom designed barge. The barge is capable of storing and pumping scintillating fluid and oil, releasing and docking the detector module and generally performing all functions not specifically required to be performed by the detector. The detector, in turn, need only sink to the bottom, collect data, and return to the surface. With this arrangement, no weight needs to be allocated on the detector for stability while underway, pumps, purifiers, or transport.

The only significant variation in design of the detachable cylinder from the integrated cylinder is the detachable cylinder has spheroids on both ends. This change makes the detector larger to account for the reduced volume of a spheroid end vs. a flat end.

##### 2.4.5.2 Detector analysis inputs

The detector analysis was conducted in a similar way as was done for the integrated cylinder concept. Again, the H/D ratio could be modified to optimize the design, but a ratio of one is used for this initial analysis. Therefore, the pressure distribution is again the same as that shown in Figure 2-33.

##### 2.4.5.3 Detector analysis details

The detector sizing calculations are similar to those in section 2.4.4.3. They use very similarly sized detectors, but do not consider the hull in the weight calculations. Therefore, the detector weight comprises the entire submersible module weight. The slightly larger cylinder has a diameter of 26 m, as opposed to the 23.7 m in the integrated design. The increased diameter requires thicker walls. Table 2-15 shows the increased dimensions and weights for the detachable cylinder.

Inner Cylinder	
Minimum Thickness	6.0 mm
Maximum Thickness	9.0 mm
Weight	146 tonne
Outer Cylinder	
Minimum Thickness	6.0 mm
Maximum Thickness	21.7 mm
Weight	379 tonne
<b>Total Detector Weight</b>	<b>525 tonne</b>

**Table 2-15:** *Detachable Cylinder Structural Dimensions*

The detachable detector is 43 tonnes heavier than the detector integrated with a hull.

#### 2.4.5.4 Hull structural model and analysis

The basic hull model used for the detachable concept was the same as that used for the integrated concept. The difference is in the overall size of the vessel, as explained below, not in the engineering principles driving the analysis.

The hull for the detachable concept is much larger than that for the integrated concept. Not only must it be large enough to contain the detector, it must also have enough space to store the scintillating fluid and oil. Other factors increasing the size of the vessel are the need for storage or production of fresh water, anchor handling equipment, detector docking equipment, and transport. The overall estimated size of the vessel to accomplish these tasks is 44 m long by 31.51 m wide by 13.8 m high.

Since the vessel stores the scintillating fluid and oil in its own hull instead of in the detector, the loading conditions are quite different than those in the integrated vessel. In the integrated vessel, the weight of the fluids was concentrated in the center of the vessel. In the case of the detachable vessel, the fluids are distributed about the ends of the vessel and in the center is a low-density area occupied by the empty detector. This means that where the integrated vessel sags in still water, the detachable vessel hogs. Therefore, the detachable hull is analyzed in waves with the crest of the wave in the center of the vessel, and the troughs at the bow and stern.

Also, the greater length of the vessel creates higher bending moments in the vessel. To demonstrate these effects, Figure 2-53 shows bending moment curves for both the rectangular integrated hull and the detachable hull.

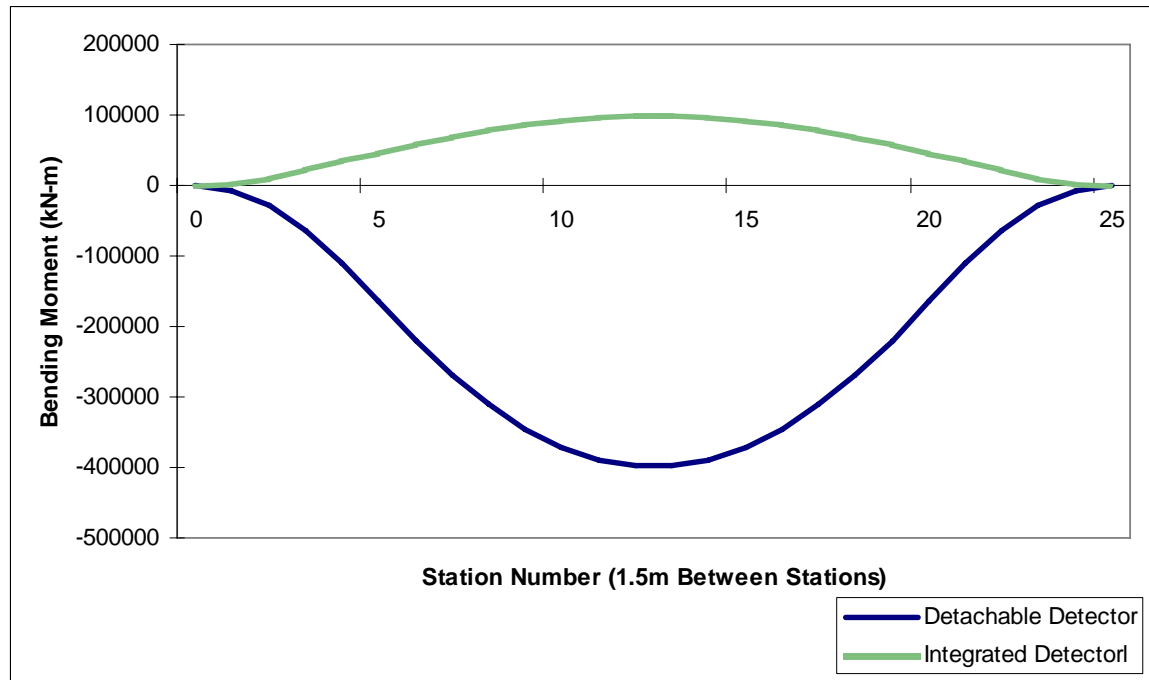


**Figure 2-53:** Bending Moment Comparison between Detachable Detector Concept and Integrated Concept

Note that the bending moments are negative for the detachable hull and positive for the integrated hull. This is due to the fact that the vessels are bending in opposite directions. Also, the detachable hull experiences bending moments four times greater than the integrated hull. This effect is a function of the greater length of the vessel and the increased effective wave height used in the worst case bending analysis.

Since the hull is not required to submerge and resurface, there is no show-stopping excessive weight problem associated with high bending moments. The increased amount of steel required to stiffen the vessel has no inherent cost beyond increasing the cost of the barge. However, space becomes a concern. Since the hull has a moon pool in the center to accommodate the detector, there is less space available for structural support. Since evaluation of this problem requires selection of a specific detector size and geometry, it was deferred to a more detailed design stage (see chapter 3).

#### 2.4.5.5 Intermediate Conclusion

Ultimately, the primary concern of this analysis is whether or not the detector can successfully accomplish its mission. Therefore, the hull has been disregarded when considering intermediate conclusions. Figure 2-54 shows the suitability plot for the detachable cylindrical detector.

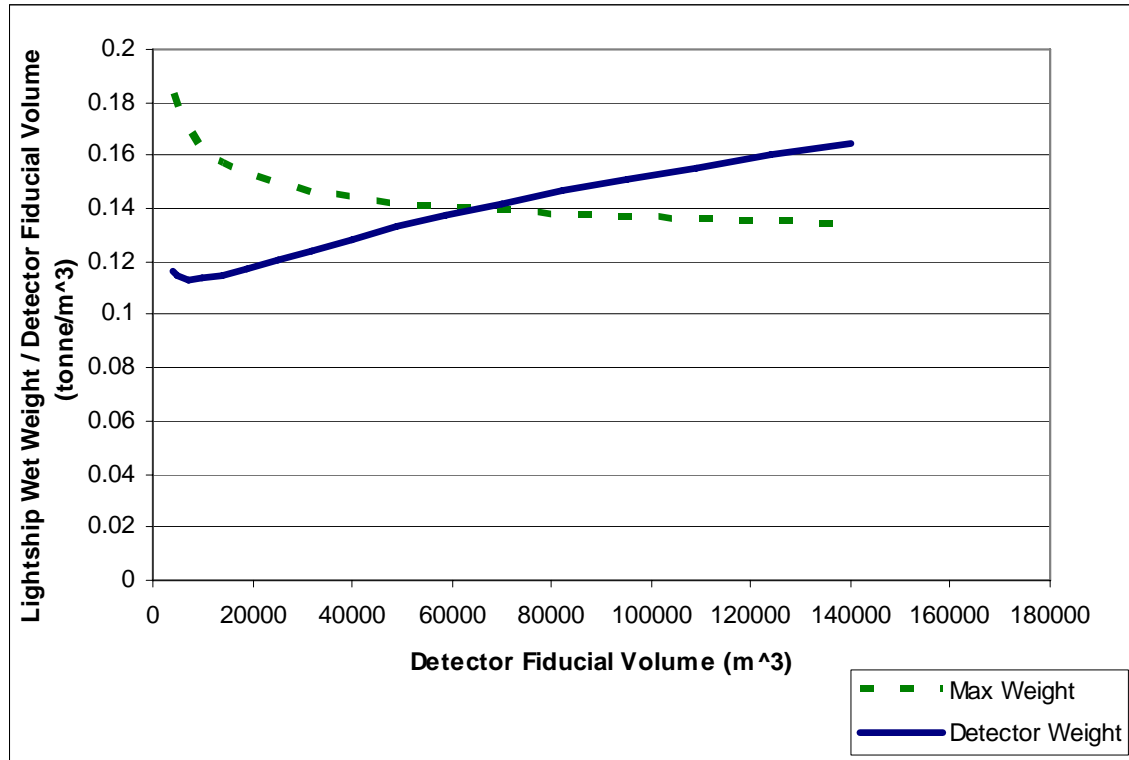


**Figure 2-54:** Suitability Plot for Detachable Cylindrical Detector

There is no Panamax line on the above plot because the hull has been disregarded. Since the H/D ratio of the detector can be varied in this concept, the volume of the detector itself is not definitively tied to the width of the hull. A steel detector is possible up to 59,000 m<sup>3</sup>. This is a distinct improvement over the 25,000 m<sup>3</sup> for the square integrated cylindrical detector. Also, the plot indicates the suitability of the detector is not as sensitive to detector volume as other concepts have been. Unlike the integrated detectors, which required at least 75% of the total weight allocated to structure, the detachable detector requires 65%. Also, the detachable detector does not need as much additional structural support beyond that which has been calculated. The hull is intended to take the brunt of the environmental loads, so the detector itself can be less rugged than in an integrated design.

With two viable concepts to explore, the integrated cylindrical detector and the detachable cylindrical detector, Makai chose to select one for further analysis. First, Makai compared the two designs to existing vessels, as described below in the next section. Then, Makai began the analysis process described in section 2.6.

#### 2.4.6. Structural steel vs. dead weight

Modern vessels are often categorized by the ratio of their weight to their cargo capacity. To keep the units consistent, their cargo capacity is calculated as the weight of fresh water they could carry if all cargo compartments were filled. This weight is known as a vessel's dead weight tonnage (DWT). Well designed and efficient ships have a very low lightship

weight (no cargo) to DWT ratio. Comparing the detectors weight to its DWT allows Makai to place our design in the context of modern vessel construction

#### 2.4.6.1 Comparison

Makai collected data on existing cargo vessels from the web. The DWT was plotted against lightship weight for each vessel. Figure 2-55 below shows the results of the research.

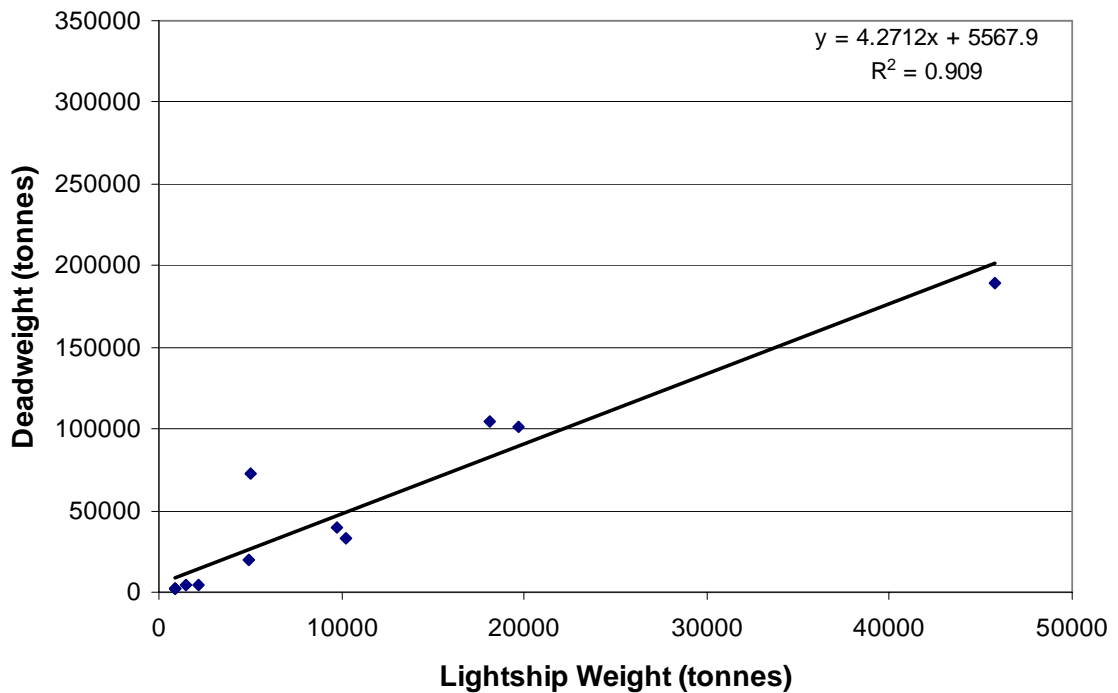


**Figure 2-55:** DWT vs. Lightship Weight of Existing Vessels

The plot includes a linear regression averaging the data points. The regression is shown in the upper right corner of the plot. Neglecting the 5568 tonne offset, the regression indicates that vessels can carry 4.27 tonnes in DWT for each tonne of structure. This means vessels tend to weigh about 23% of their DWT.

The detectors as designed all represent extremely efficient designs. Table 2-16 shows the DWT vs. lightship weight for the detector designs considered above.

	DWT [tonne]	Lightship Weight [tonne]	Ratio
Integrated Cube	5832	1173	20.1%
Integrated Cylinder	5138	655	12.8%
Detachable Cylinder	5138	525	10.2%

**Table 2-16:** DWT vs. Lightship Weight for Hanohano Detector Designs

The integrated cube detector is in the ballpark of existing vessels. However, it is still more efficient than a typical cargo carrier. Even more extreme are the cylindrical detectors, at 12.8% for the integrated detector and 10.2% for the detachable detector.

The results presented above indicate that designing the detector is an ambitious undertaking. Not only will it be the largest vessel to submerge to 4000 m and return, it will do so as one of the most efficient vessels ever constructed. However, Makai feels such a design is within the realm of possibility because there are significant differences between typical oil tankers and the detector. First of all, the oil tanker requires machinery for propulsion and energy. The detector will be towed or transported by another vessel, and therefore does not need this equipment. The tanker also has accommodations for crew, but the detector does not. The final and most significant difference between a tanker and the detector is shape.

Tankers are built with a length to beam ratio of about eight. This ratio balances the costs for structural strength to support a long ship and the costs for energy to push a broad ship through the water. In other words, it is cheaper to put money into structure than into fuel when a tanker's length to beam ratio is less than eight. The detector however, need only make one trip every year or two. Therefore, conventional logic on vessel shape does not apply. The integrated detectors have a length to beam ratio of 1.3. This lower ratio means the detectors feel much lower bending forces than a tanker does, and therefore require much less structural steel to support themselves. Counteracting this effect in the integrated cube detector is the large tank. Oil tankers utilize many smaller compartments because doing so limits the strength required of any one tank. The sheer size of the cube detector requires enough steel to make its weight comparable to tanker weights. The detachable detector does not have to withstand bending moments at all since it is transported by the separate vessel.

The differences between an oil tanker and the detector justify the differences in their lightship weight to DWT ratio. The detector will be an efficient vessel, but only because it has been freed from some of the limitations that drive typical vessel design.

In terms of selecting detector shape and configuration, it is desirable to keep in mind the high steel usage in working tankers and the limited design performed so far on Hanohano. A concept that has the highest safety factor in terms of total weight would be preferable; as the design proceeds, the steel requirement will invariably go up.

#### 2.4.7. Summary

Analysis has been presented on an integrated cube detector, an integrated cylindrical detector, and a detachable detector. The integrated detectors were analyzed in with both rectangular and square hulls. Cube detectors with both square and rectangular hulls can not be built out of steel. Up to a 46,000 m<sup>3</sup> detector can be built out of aluminum with a square hull. Cylindrical hulls fared better, where 16,000 m<sup>3</sup> and 25,000 m<sup>3</sup> could be built out of steel with rectangular and square hulls respectively. The lightest concept is the detachable detector. A detachable detector can be built out of steel up to 59,000 m<sup>3</sup>.

## 2.5 COST

### 2.5.1. Total Projected Cost

The total projected cost of a given concept was related to the amount of various components that were required to complete construction. The mass of steel, mass of concrete, volume of scintillator, and number of PMT's were the parameters used to obtain a projected cost.

The mass of steel was based on the structural calculations for the concepts considered. However, in order to carry out both structural and cost analyses simultaneously, the preliminary results of the structural analysis were converted into a ratio of steel to cargo weight. In the case of HanoHano, the “cargo” is the mass of the scintillating fluid and oil. Use of this ratio allows the costs of different size detectors to be compared without recalculation of structural loads. The cost for steel was developed by comparing the cost and weights of existing vessels found on the web. Since vessels are classified by their dead weight tonnage rather than their lightship weight, costs are more readily available based on dead weight tonnage than on lightship weight. Figure 2-56 summarizes the data collected.

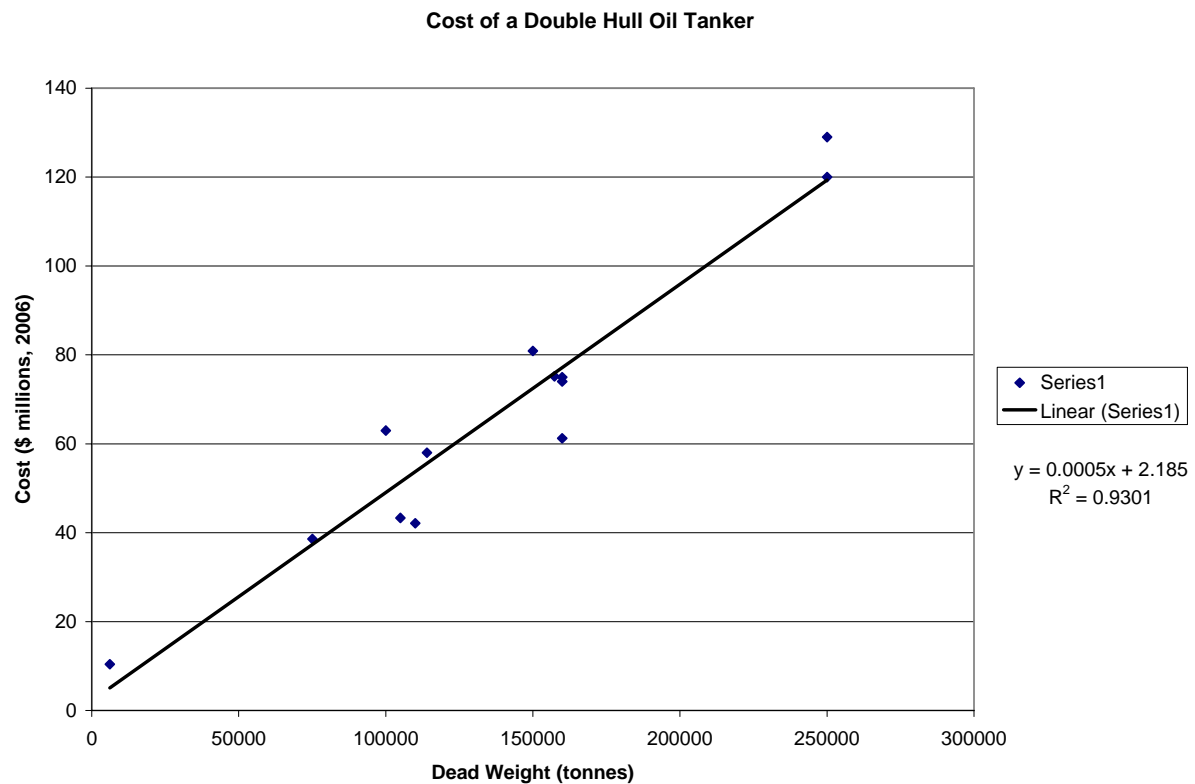


**Figure 2-56:** Cost per Dead Weight Tonne of Typical Double Hull Oil Tankers

The regression on the right side of the plot shows that double hull oil tankers cost roughly \$.0005 million per dead weight ton, or \$500 per dead weight ton. Given that typical

tankers lightship weight is 20% of their dead weight tonnage, this translates into \$2500 per lightship tonne. In order to reflect the added complexity of the detector over a more traditional vessel, a factor of 1.4 was applied to the costs of existing vessels. This gives a total cost of \$3500 per tonne for the detector.

The mass of concrete was determined by the amount of ballast required according to preliminary stability analysis. Also, the overall size of the detector determined how large of a weight would have to be releasable in order to recover the detector.

The volume of scintillating fluid and number of PMT's were directly tied to the size and shape of detector under consideration. However, the two parameters do not necessarily vary as a pair because the number of PMT's is a surface area effect rather than a volumetric effect.

The cost for each of the above parameters is summarized below in Table 2-17.

Cost of Detector Steel	3500 \$/MT
Cost of Barge Steel	2500 \$/MT
Cost of Concrete	500 \$/m <sup>3</sup>
Phototubes	4500 ea
Scintilator & oil	100 \$/m <sup>3</sup>

**Table 2-17:** Unit Costs Used in Projected Cost Estimation

### 2.5.2. Detailed Parameters

Whenever possible, Makai obtained specific costs on components not included in the total projected cost. Costs for reverse osmosis equipment, chilling equipment, compensation bags, and diesel fuel were obtained. The costs for RO, chilling, and compensation are discussed below in their respective sections.

Fuel is required on the barge for generation of electricity. Regardless of whether the generation equipment is onboard the barge or on a support vessel, fuel is required to produce electricity. Review of Caterpillar marine generators indicated that approximately 81.4 gallons of diesel is required to generate 1 MW-hr of electricity. Combining this value with an estimated cost of diesel at \$2.86 per gallon yields an electrical rate of \$232.80 per MW-hr, or \$0.23 per kW-hr. This value was used whenever electrical operating costs were a parameter in a cost analysis.

## 2.6 DESIGN CONCEPT SELECTION

### 2.6.1. Size selection:

There are several competing pressures that determine the size of the detector. The first is the requirement of the experiment. The quantity of data collected is proportional to fiducial mass and time. The larger the mass of scintillating fluid in the detector, the greater the quantity of data that can be collected in the detector's lifetime. Therefore, science dictates that the detector should be as large as possible. Opposing this pressure are transport logistics, practicality and cost. Transport logistics refers to how hard it is to

move the detector around the globe. For example, if the detector is too large to fit through the Panama Canal, then more challenging or longer circumnavigation routes must be selected. Practicality refers to the need for the detector to be built confidently with existing technology. Finally, the cost of the detector must be low enough to attract funding.

#### 2.6.1.1 Experimental Needs

While it is true that the largest possible detector would be ideal, such a requirement does little to help select a size for the conceptual design. Communication with the physicists at UH initially placed the detector volume around 4000 m<sup>3</sup>. However, as analysis progressed, and collaboration with other scientific groups grew, the desire for a larger detector formed. It was concluded that a 10,000 tonne (about 11,000 m<sup>3</sup>) detector would be desirable, and could meet the physicists' experimental needs. Such a fiducial volume is not too large for the PMT sensors to detect events toward the middle of the volume.

#### 2.6.1.2 The Panama Canal

It was decided that at this point in the design process that it would be best if the conceptual design could make use of the Panama Canal. Growing scientific interest in the detector and the availability of scintillator on the East Coast indicated that a transit from the Atlantic to the Pacific may be a requirement multiple times within the life of this detector. Routes other than the Panama Canal are extremely long or dangerous for delicate equipment. The option has been left open for future design to remove this requirement.

The requirement to be able to fit through the Panama Canal means that larger detectors must be taller than they are wide (i.e. – have an H/D ratio of greater than one). Makai's analysis found that at H/D ratios greater than three, the detector begins to get heavy and the number of PMT's required gets excessive. In order to fit a detector with an H/D of three or less through the Panama Canal, 18,000 m<sup>3</sup> is the ultimate limit on fiducial volume. In order to maintain stability throughout and have sufficient beam for structural requirements, a fiducial volume of 10,000 m<sup>3</sup> is the practical limit.

#### 2.6.1.3 Practicality

In order to be practical, the detector must have a design that is reasonably comparable to existing installations. This is a somewhat nebulous requirement that has been addressed by comparing the proposed detector to existing vessels.

All sizes of detector considered for this study are smaller than the large oil tankers that have been constructed. Therefore, the detector will not stretch the capabilities of existing facilities. Section 2.4.6.1 addresses the ambitious design of the detector, and concludes that while it is light compared to tankers of similar size, there are justified reasons for the discrepancy.

#### 2.6.1.4 Cost

The lower the cost of a concept, the more likely it is to be constructed. However, a detector that is so small as to have minimal scientific value is not likely to be constructed. Therefore, a balance is required between cost and scientific value, and this is a subjective judgment. Based on the \$2500/tonne for construction given earlier, the steel structures for

Hanohano would cost between \$8 and \$10 million, depending upon the concept used (integrated vs. detachable – see section 2.6.2.4). Upon consulting with UH, such a cost was considered reasonable considering other Major Research Facilities funded by NSF. Costs were therefore not a limiting factor in the size selection.

#### 2.6.1.5 Size Selected

A detector with a fiducial volume of 10,000 m<sup>3</sup> (9,000 tonnes) has been selected for the conceptual design. This size is acceptable to meet the physicists' needs without imposing unnecessary difficulties in terms of transportation. It is also small enough from a practical standpoint that it can be designed using standard shipbuilding procedures.

### 2.6.2. Concept selection

#### 2.6.2.1 Integrated Concept

Since the vessel will be required to pass through the Panama Canal with a fiducial volume of 10,000 m<sup>3</sup>, the square hull detector cannot be used. The following comments are restricted to the rectangular hull concept.

The primary advantages of the integrated are:

- The entire unit is self-contained because the detector and barge are integrated. It is simple.
- The detector can be prepared, outfitted, and tested dockside. All that has to be accomplished on-site is final testing and deployment.
- It should be the lightest configuration available.

The primary disadvantages of the integrated concept are:

- A vessel will be required to tow the detector and provide quarters for the crew.
- Its inherent instability: the high elevation of the scintillator and oil create stability problems. High usage of all available weight in the structure drives a minimal ballast weight.
- Weight limitations: since the hull is integrated with the detector, its weight counts against the total allowable weight of the system. This detector takes a lot of weight to the seabed that is not needed.
- Small weight safety factor: weight, buoyancy and displacement are critical for Hanohano. If later design issues or refinements force added structure, there may not be any additional weight available. The very high cost of auxiliary buoyancy at 4000 m is a financial project breaker.
- All onboard components must submerge. Winches, pumps, and other onboard components would have to be removed before submergence or built to withstand submergence to 4000 m depth. The support equipment for this detector will be extensive – a dedicated support vessel will be required to house all this equipment.

- There are no alternate storage facilities for the scintillator and oil. If the detector is to be vacated, an onshore storage vessel of equivalent volume will be required to store these liquids without contamination.

It was the increasing list of disadvantages for this concept that drove the team into considering the detachable concept.

#### 2.6.2.2 Detachable Concept

The main concept of the detachable concept was to separate the underwater tasks from the surface support tasks: to avoid taking anything underwater that was not necessary and to provide space for functions that are to be done on the surface.

The primary advantages of the detachable concept are:

- Nothing is taken to the bottom except those components directly relating to the experiment. Therefore the maximum amount of weight is available for detector structure and ballast. Only 65% of the detector's allowable weight is required for structural members. This provides a reasonable safety margin for stability during deployment and for future design to add components as needed without redesigning to fit a strict weight budget.
- The primary seagoing vessel is similar to a standard barge. This means that standard naval architecture procedures can be used for its design and construction. Also, stability is not a concern since the barge has no real limitations beyond the draft limitation and beam limit of the Panama Canal. Therefore, it can be designed to withstand a wide variety of operational conditions.
- The detachable system can be stable at all times. During transit and surface operations, the scintillator and oil are evenly distributed in the barge. During filling of the detector, it lowers in the water and there is never a huge mass supported high above the sea surface.
- The barge can carry all equipment required for the detector deployment and support with minimal additional cost. The tow boat can be limited to towing only and be a boat of opportunity.
- The barge is an alternate storage vessel for the scintillator and oil. Therefore it can be used for pick-up and original transit of these large volumes and these containers can be used for transfer and cleaning of the scintillator.
- A single barge could support multiple detectors.

The disadvantages of the detachable concept are:

- There are two components that must be parted and mated at sea. This will involve a more complex dynamic design and limit sea states for operation.
- At first glance, there are more components to be constructed: a detector plus a separate support barge, and potentially more steel. However this system actually provides more features than the integrated system (alternate storage for the

fluids, accommodations for the support staff) and those structures would need to be provided elsewhere with the integrated system at likely comparable costs.

#### **2.6.2.3 Concept Selected**

Based on the above analysis, the detachable concept is more practical and a safer approach for the 10,000 m<sup>3</sup> detector. The primary reasons are:

- The detachable system is more stable.
- The detachable system has a greater safety factor on allowable weight.
- The detachable system could be scaled upward considerably.
- The detachable system solves the issues relative to hotel loads and taking unnecessary equipment to 4000 m depth.
- The detachable system provides storage for the scintillator, for pickup, cleaning, and maintenance on the detector.
- The detachable detector is more easily transported with a standard barge shape.

#### **2.6.2.4 Cost implications**

The cost differences between the integrated and detachable concepts were negligible and did not play a role in the selection. While the integrated detector, under a strict weight budget, could conceivably be built with less steel, this savings is unlikely to be realized. Unresolved issues and risks with the integrated detector would most likely make the costs very comparable; these include onshore storage facilities for the scintillator and oil, protection and hotel room for onboard support equipment, high cost of minimum-weight designs, and outfitting a support ship specifically to support Hanohano.

### 3. 10,000 M<sup>3</sup> DETECTOR CONCEPTUAL DESIGN.

#### 3.1 PURPOSE OF THIS SECTION

With a detachable detector selected, work can focus on the conceptual design of the barge/detector system. The goals of conceptual design are to show a higher level of detail than the preliminary analysis, determine if any show stopping challenges arise from more detailed analysis, and identify major costly or technically challenging components. This section will first give an overall view of the design selected, then move into the detailed design and analysis sections. Detailed design and analysis will be presented on deployment, detector design, barge design, and cost.

#### 3.2 ILLUSTRATION OF OVERALL CONCEPT.

##### 3.2.1. Size, Weight, and Shape

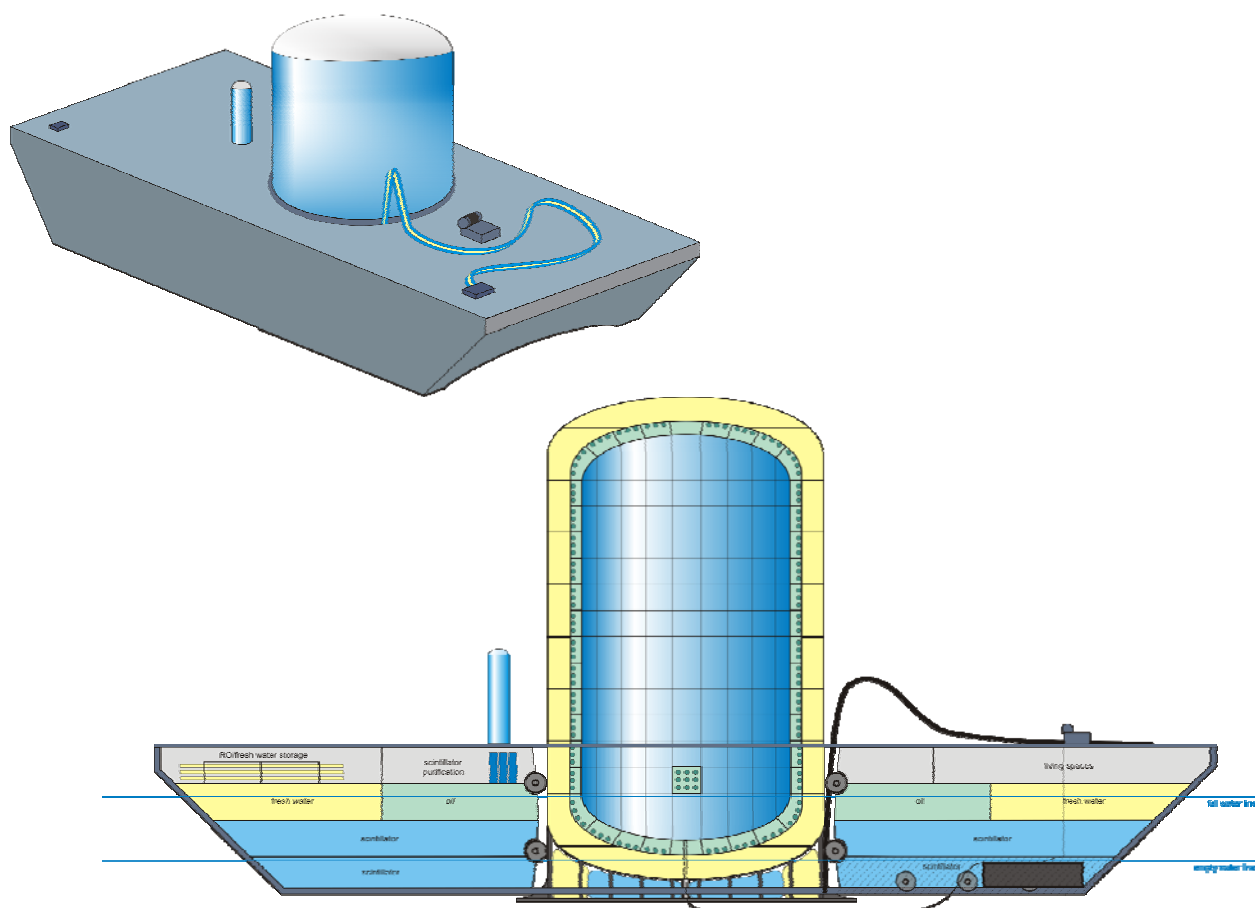


**Figure 3-1:** Overview of Barge and Detector Assembly

Figure 3-1 shows an overview of the detachable detector and barge. The detector is 44.7 m tall from the top of the dome to the bottom of the ballast concrete. The outer diameter of the cylinder is 26.01 m. The barge is 112 m long and 32.3 m wide. It has an overall depth of 13.8 m. The detector weighs 1600 tonnes, and the barge weighs 2850 tonnes.

### 3.2.2. Major Design Output

The gross output of the conceptual design process is the sizing of the major aspects of Hanohano. These components are the scintillator, the detector, and the barge

#### 3.2.2.1 Scintillator

As explained in section 2.6.1.5, the selected fiducial volume of the scintillating fluid is 10,000 m<sup>3</sup>. The scintillating fluid to fill this volume weighs 8523 tonnes. However, since the scintillating fluid changes volume both with temperature and with pressure, the volume of a given mass of scintillator will change from deployment to recovery. Therefore, the detector has compensator bags installed between the bottom of the veto region and the ballast concrete. An additional 770 m<sup>3</sup> (656 tonnes) of scintillator is stored in these bags. This scintillator will be forced through pipes into the detector as the fluid inside shrinks. Compensation in this manner ensures the detector walls do not have to withstand the pressure at 4000 m deep.

#### 3.2.2.2 Detector

The detector is 44.7 m tall overall and has a diameter of 26.01 m. The concrete ballast has a larger diameter (31.2 m) that allows it to rest against the keel of the barge when the detector is empty. There is a 3 m space between the bottom of the detector and the top of the ballast to store the compensator bags. There is a valve in the wall of the detector in this region that allows the compensator bags to be either exposed to or isolated from the environment. There is a 2 m veto region between the outer wall of the detector and the stainless steel PMT module compartments. This region is filled with 7777 m<sup>3</sup> of fresh water. The PMT modules have a total of 3970 m<sup>3</sup> of oil. The detector weighs a total of 1600 tonnes, including a 23% safety factor that reserves weight for future needs.

#### 3.2.2.3 Barge

The barge is 112 m long by 32.3 m wide. The beam of the barge has been set such that it can fit through the Panama Canal. The length of the vessel is set such that its draft is 10 m when fully loaded. This allows the barge to be outfitted in most commercial harbors. It is capable of carrying all of the scintillator and oil necessary to fill the detector. It also has a reverse osmosis plant onboard for fresh water production to fill the veto region. There is a moon pool in the center of the barge with a nominal diameter of 29 m. This space is where the detector sits when it is docked with the barge. There is also a 4.5 m high slot in the bow of the barge. When the detector is empty (i.e. – it is not carrying the detector or any scintillator), this slot is above the waterline, and provides the space needed for the detector to move into the moon pool during recovery. The barge weighs a total of 2850 tonnes.

## 3.3 DEPLOYMENT

The round trip cycle of the detector, from the dock to the seafloor at 4000 m and back to the dock is the deployment cycle. This operational requirement imposed a major constraint on the design. Deployment considerations have driven all structural, stability, weight, displacement, and general arrangement decisions that have been presented throughout this report. This section summarized the deployment cycle for the 10,000 m<sup>3</sup> detector. To some extent, this section presents detector components and concepts that are only first introduced later in this chapter. However, it is

important that the reader understand this process for it is critical to the design development. Hanohano design details follow this section.

### 3.3.1. Deployment scenario – step by step

The following sequence describes the operation and deployment of the Hanohano detector – from the ocean engineering standpoint (not the physics).

#### 3.3.1.1 Initial Transit and Loading

It is assumed that the detector and the barge are mated and locked, while empty, in the shipyard. When both the barge and the detector are empty, the detector restraint system is used to lock the detector and barge together (see section 3.5.4).

The barge can be used to pick up the scintillator and oil. Known LAB scintillator sources are in Baltimore and in Toronto, both on the East Coast. If the detector and barge are fabricated on the East Coast, they can be towed empty to the scintillator manufacturer and the appropriate quantities of scintillator and veto region oil are loaded onto the barge. This will take the draft of the barge to about 10 m. The detector at this point is buoyant and pressing firmly up on the base of the barge.

Hanohano is then towed to Hawaii. The barge, fully loaded, and detector will fit through the Panama Canal. The barge is a conventional shape and can be reliably and safely towed. The configuration is rugged and stable, even though the detector is high above the barge. The detector at this point is empty, and the elevated mass is small compared to the loaded barge.

#### 3.3.1.2 Initial outfitting and access

Hanohano is then brought into Honolulu harbor. Researchers have access to the interior of the detector via the veto region which has multiple stories – 10 total. All plumbing and electrical cables are routed through the veto region and there is access to each PMT compartment. Stairwells inside the veto region allow technicians to climb to any level. Access is at the barge deck level.

For interior access, Hanohano can be outfitted with a temporary interior work level that is accessed from the top; the level is powered vertically within the scintillator volume. This feature is described in the task report “Preparation of Low Radioactivity Scintillation Material” as a part of chapter 5.

#### 3.3.1.3 Initial testing, shallow flooding

Hanohano can be tested in shallow water just outside of Honolulu harbor. Once fully outfitted and operational, the barge is towed outside the harbor and moored in 100m water depth. The flooding process described below is followed and tested. Instead of using fresh water in the veto region, seawater can be used for a quick cycle. The detector becomes low in the water but is just floating within the moon pool. The anchor is not lowered, so the detector is not in danger of sinking. The detector could be lowered in 12 hours and then recovered in a similar time.

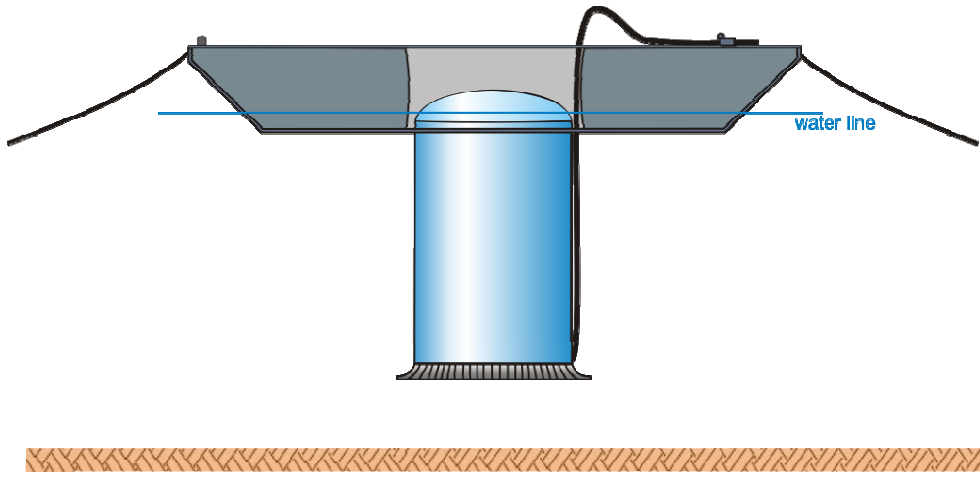


**Figure 3-2:** Lowering and testing Hanohano in shallow water

By this process, the electronics and deployment cycle are fully tested in safe waters. If there are problems, the tests are repeated as many times as necessary.

#### 3.3.1.4 Towing

Hanohano is towed to the final test site with the barge fully loaded and the detector empty. In this condition, the system is very stable. The system will tow similar to any other large barge. In this case, the tow is 250 km to Kawaihae, Hawaii. Transit time would be approximately 24 hours.

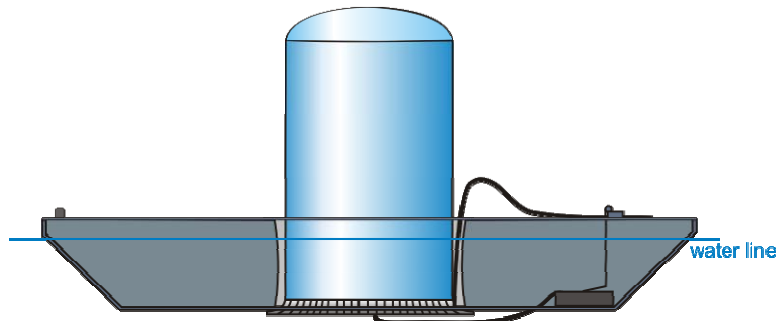


**Figure 3-3:** fully loaded Hanohano being towed, the detector is empty.

#### 3.3.1.5 Transfer liquids on site

Once the detector reaches the deployment site, the detector is ready to begin filling. The space below the lowest bulkhead (see Figure 3-23) has already been filled, so the detector is ready for scintillator and oil. To avoid excessive pressure across the Lexan panels in the detector, both fluids are filled simultaneously. First, all the valves isolating the PMT compartments in the bottom spheroidal end of the detector are opened. The valves to all other compartments are closed. The 1850 gpm oil pump on the barge turns on and begins to fill the oil through 3" pipes. The nitrogen that is in the compartments evacuates the compartments through ½" lines. Once the oil has fill the lowest compartment, the 4200 gpm scintilllator pump on the barge turns on and the fiducial volume begins to fill. Like the PMT compartments, the internal volume has a nitrogen line that allows gas to escape

as the detector is filled. After the compartments in the lower spheroid are filled, they are pressurized to bow the Lexan panels towards the center of the detector. This bow plays a role in volume compensation, as explained in section 3.4.4.1. All compartments are pressurized in this way.

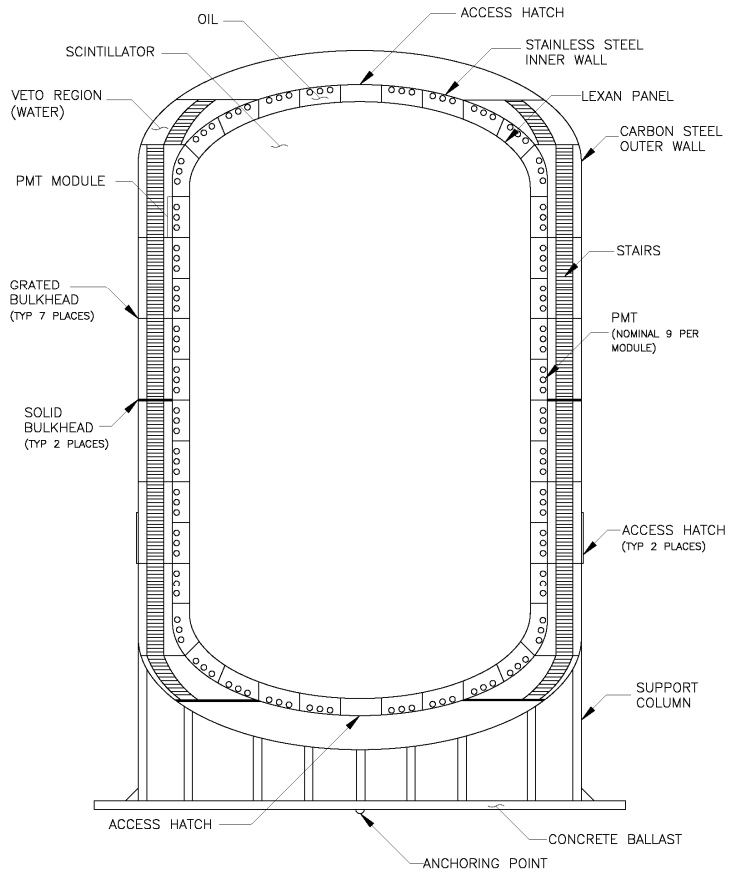


**Figure 3-4:** Hanohano compartments that are sequentially flooded

Then, the valves to the first row of PMT compartments in the vertical body of the detector open. Both the scintillating fluid and oil continue to flow as the first row of compartments is filled. It is during this stage of deployment that the detector would not be stable on its own. However, the detector does not have enough fluid in it yet to sink in the moon pool. Therefore, the concrete ballast is still pressed against the keel and provides stability support. Also, the detector restraint system described in section 3.5.4 provides backup support.

Once the first row has been filled, its valves close and the valves to the second row open. This process is repeated until all compartments in the lower half of the detector have been filled. During the filling of its lower half, the detector will begin to sink in the moon pool. In order to provide stability support and avoid impact between the barge and detector, the detector restraint system is left active. Instead of supporting the fill weight of the detector, the system keeps the detector locked to the barge by pulling it slightly upwards. The pulling force acts as a preload on the connection between the barge and the detector; it must be overcome before the two will move relative to one another. Since the preload

need not increase as the detector fills, the restraint system should always pull the detector out of the water by the same amount. Therefore, the system allows the detector to sink as it fills.

Once the scintillator and oil have reached the halfway point, the pumps shut off. The fresh water is then pumped into the veto region between the two solid bulkheads. Filling this second part of the veto region ensures the detector is stable as the rest of the oil and scintillator are filled.

After the second section of the veto region is filled, the oil and scintillator are pumped in as before. As each row fills, the valves are closed and those to the next row are opened. Once all the compartments in the vertical portion of the detector are full, the valves to the upper spheroid are opened. All compartments in the spheroid are open to oil, and they fill from lowest to highest. During this process, the scintillator will reach the top of the detector, and the scintillator pump is turned off. Similarly, once the highest PMT compartment is filled, the oil pump is turned off. The fresh water again turns on and fills the remainder of the veto region and completes the fluid transfer process.

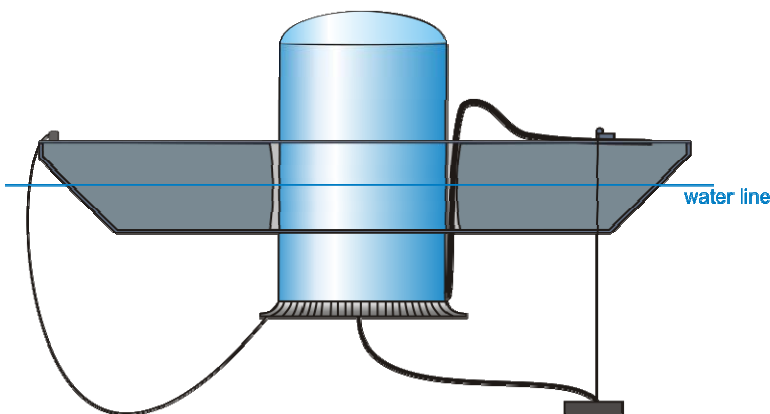


**Figure 3-5:** Scintillator, Oil and Water are transferred into the Detector which submerges through the moon pool.

### 3.3.1.6 Production of fresh water

In the conceptual design, it was determined to be more economical to produce the fresh water for Hanohano with an RO plant onboard than to carry the fresh water. Water production would commence in advance of deployment and about 20% of that needed would be stored on the barge and about 20% loaded into the detector (which will still be buoyant and not sink below the barge). On site, another 60% of the total volume would be produced. This production paces the flooding – the time dependent upon the size of the RO system purchased. The conceptual RO plant would produce the remaining 60% water in 7 days. Doubling the size would cut the flooding to 3.5 days. Increasing storage on board could also be used to reduce this time.

### 3.3.1.7 Lowering anchor

The onboard winch lowers the anchor attached to the underside of the barge. The anchor is held below the bottom of the Detector to avoid contact. As the separation increases, the pendant cable stored on top of the anchor pays out.

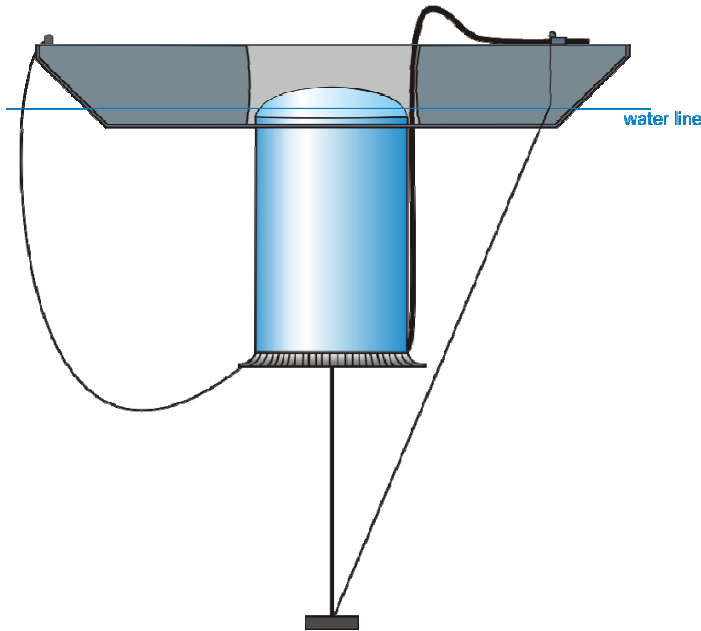


**Figure 3-6:** The anchor is lowered and excess cable pays out from the detector until the anchor is at the correct depth

### 3.3.1.8 Cable Connection to Detector

A cable ship moves alongside the barge and the cable connected to the Detector is handed over to the ship. The ship backs off several hundred meters and splices the onboard cable to the Detector length. The cable ship backs off several km prior to the submergence, paying out cable.

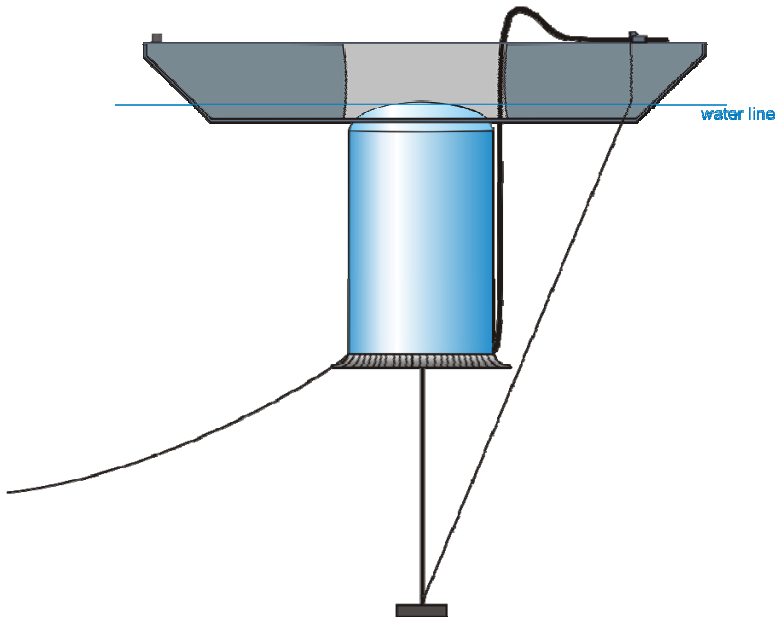


**Figure 3-7:** The power and communications cable is passed off to a cable-lay ship

### 3.3.1.9 Release of detector

Once the detector structure is fully flooded, it will be over 520 tonnes buoyant and float with several meters of freeboard. The winch has lowered the 607 tonne (wet) anchor and the anchor load is transferred to the detector as the 100 m tether becomes tight. The filler pipes are released from the detector, and the detector restraint system is disengaged. The lowering winch can release the anchor by cutting the cable or, if more sophistication is desired, with a release at the anchor. If the cable is cut (the more economical approach), the cable will harmlessly fall to one side (it should be on the opposite side of the shore cable).

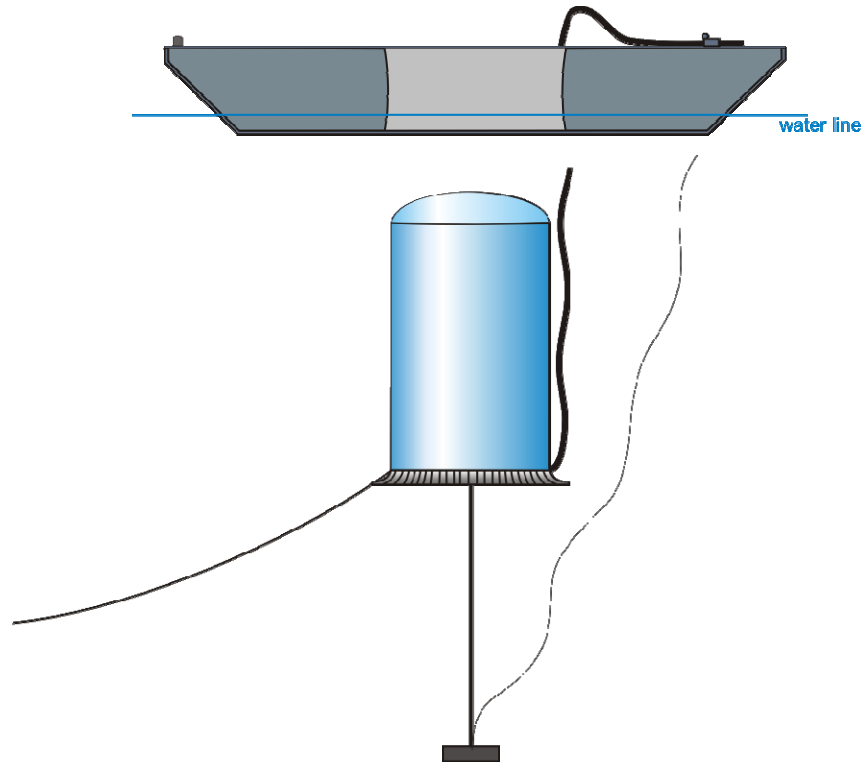


**Figure 3-8:** The anchor cable and filler pipes are released from the detector

### 3.3.1.10 Descent times

Once the anchor is released by the winch, the detector plus anchor have a wet weight of 87 tonnes. Once it reaches the seabed, after compression, the system will have a net weight of 174 tonnes. The descent speed will vary from 1.4 m/s to a maximum velocity of 2 m/s. By integrating over the full depth, the descent time would be 39 minutes.

This descent time is fast, but is actually convenient. The impact on the seabed is acceptable (see section 3.3.1.12) and the faster descent places the detector more accurately on the seabed. If we have an average horizontal current of 0.1 m/s (conservative for deep water which is most of the descent), we would have a maximum horizontal offset of 250 m. Longer descent times would result in larger offsets.

### 3.3.1.11 Cable connection to shore.

Figure Figure 3-9 shows the bathymetric profile and possible cable route to the closest site at 4,200 m depth to shore. The shore location is the Natural Energy Laboratory of Hawaii Authority. NELHA has laboratory space close to shore and can (and has) supported similar offshore experiments and operations. NELHA has a drilled tunnel from the laboratory to an offshore location at 30m depth, thus providing a conduit for easily landing and protecting the cable to shore.

The distance offshore is 17.988 km; the cable length along the bottom (including required slack) is about 19 km. For practical considerations, about 22 km of cable would be needed.

The cable supplying power and communications to Hanohano will be a standard fiber optic cable used in cross ocean communications. These cables typically have 4 or more pairs of fiber optic strands plus a power conductor that supplies typically 10 kW of power at high voltage (several thousand volts). The mechanical properties of these cables are shown in Table 3-1. Cables types that would be used in this installation would be Lightweight (LW) or Lightweight Protected (LWP) in deep water and Single Armor (SA) approaching shore and going through the shoreline crossing.

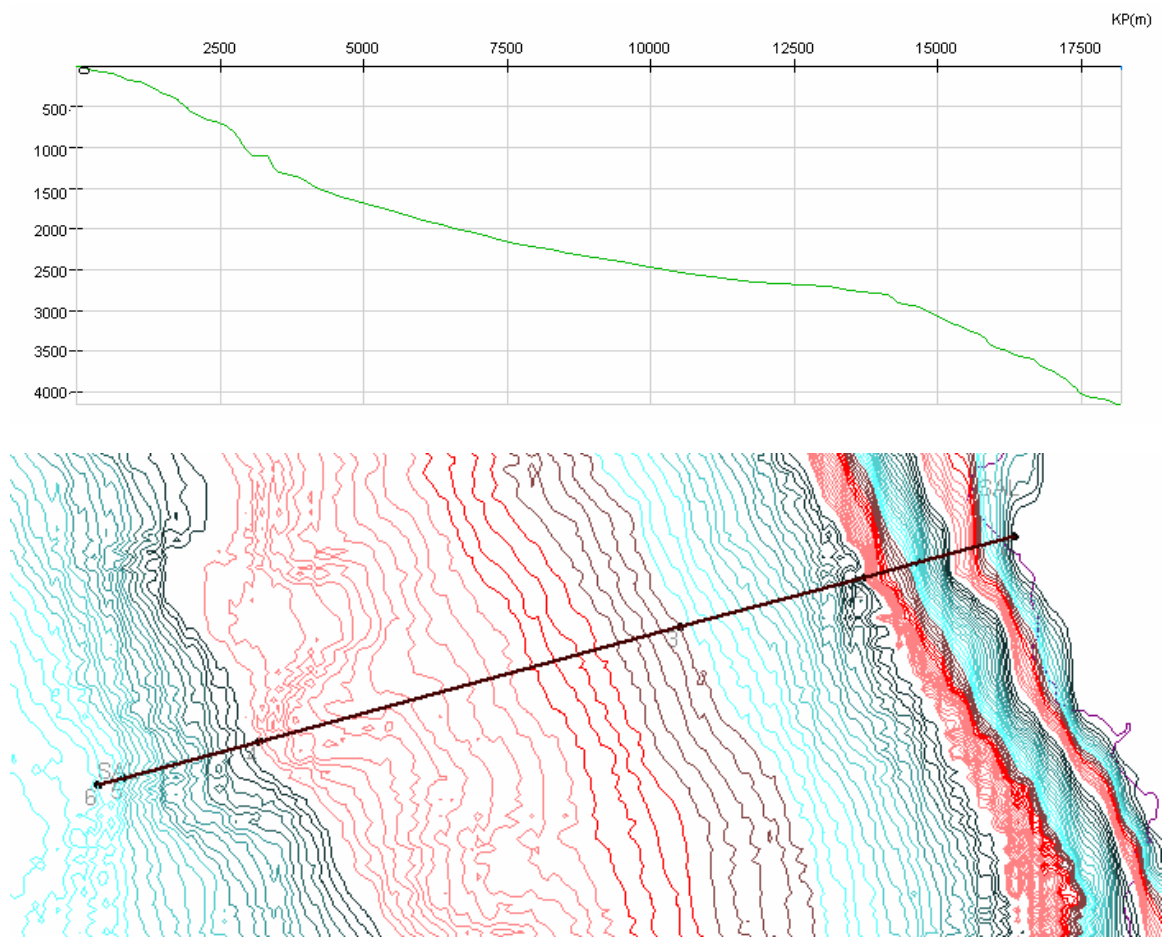


**Figure 3-9:** Site location and profile, West Hawaii at Keahole, Point. Cable distance from shore laboratory to Hanohano is 18.7 km.

**OALC-5 (14mm) CABLE AND ASSOCIATED UNDERWATER PLANT**

CABLE TYPE	STOWAGE FACTOR Cubic metres / km	OUTSIDE DIAMETER (mm)
Light Weight LW	0.18	14 (PE sheath)
Light Weight Screened LWP	0.34	19.6 (PE sheath)
Single Armour SA	0.6	26 (PP rovings)
Double Armour DA	1.2	35 (PP rovings)

**Weights (Nominal)**

CABLE TYPE	WEIGHT IN AIR Tonnes / km	WEIGHT IN WATER Tonnes / km
LW	0.44	0.28
LWP	0.63	0.32
SA	1.6	1.0
DA	3.5	2.4

**A.4 Tensile Strength of Cable Types**

CABLE TYPE	NPTS (kN)	NOTS (kN)	NTTS (kN)	Min Cable Breaking Load (kN)
LW	20	30	50	60
LWP	20	30	50	60
SA	50	130	160	190
DA	50	150	200	270

These figures are for 1.8% fibre proof tests.

**A.5 Hydrodynamic Constants**

CABLE TYPE	(Rad.m/Sec) Lay / Recovery	(Degree.knots) Lay / Recovery
LW	0.416 / 0.488	46 / 54
LWP	0.376 / 0.441	42 / 49
SA	0.577 / 0.577	64 / 64
DA	0.770 / 0.770	86 / 86

**Table 3-1:** Typical mechanical characteristics of fiber optic cable suitable for supporting Hanohano

**Typical / Maximum Deployment Depth for Cable Types**

Cable Type	Typical Depth		Maximum Depth	
	Surface Lay	Burial	Surface	Burial
LW	7000 m	-	8000 m	-
LWP	3500 m	-	7000 m	-
SA	1500 m	1500 m	2000 m*	2000 m*
DA	200 m	200 m	500 m	500 m

**Recovery Depths for cable with R3/4 6fp Repeater with 5kN margins from NTTs.**

Cable Type	Adverse Conditions (1knot,75degree,4m)	Standard Conditions (0.7 knot,80 degree,4m)
LW	5700	7100
LWP	4400	5800
SA	2000	2000
DA	500	500

**14 mm / 84 mm Joint Data**

14 mm / 84 mm Joint ID	LW/LWP	SA	DA
Length over bend limiters (m)	<b>1.480</b>	<b>1.710</b>	<b>1.710</b>
Rigid length (m)	<b>0.370</b>	<b>0.590</b>	<b>0.590</b>
Maximum diameter (m)	<b>0.170</b>	<b>0.140</b>	<b>0.140</b>
Diameter at mid point of joint (m)	<b>0.130</b>	<b>0.123</b>	<b>0.123</b>
Weight of joint in air (kg)*	<b>27</b>	<b>47</b>	<b>50</b>
Weight of joint in water (kg)*	<b>9</b>	<b>25</b>	<b>28</b>
Minimum bend radius of joint under tension (m)	<b>1.5</b>	<b>1.5</b>	<b>1.5</b>
Minimum bend radius of joint under no tension (m)	<b>1.5</b>	<b>1.5</b>	<b>1.5</b>

**Table 3-2:** Deployment and Recovery depths for fiber optic cables and joint characteristics – From Alcatel Submarine Networks

Laying the cable to shore can be accomplished at the same time as the deployment of the detector.

- The cable is loaded onto a separate cable lay ship (either a stand-by cable ship or a modified University vessel); the total cable length for this run is short and cable could be laid on deck if the ship is not a specialty cable ship.
- Just prior to the Detector being fully flooded and ready to submerge, the cable ship comes alongside and makes the connection to the Detector. A short length of cable can be passed to the cable shop from the support barge, and a splice is put into the cable (see Figure 3-7).
- The cable ship can either stay close or back off several km from the Detector. During submergence, the cable ship will be in tension control mode and will keep the surface cable tension a constant. This will pay out cable as needed. Makai simulated several possible cable deployments with our cable control software, MakaiLay. The results of one analysis are shown in Figure 3-10. The cable lay is based on a highly controlled constant bottom tension deployment –

an active cable control system would be required, this is now standard in much of the cable installation industry.

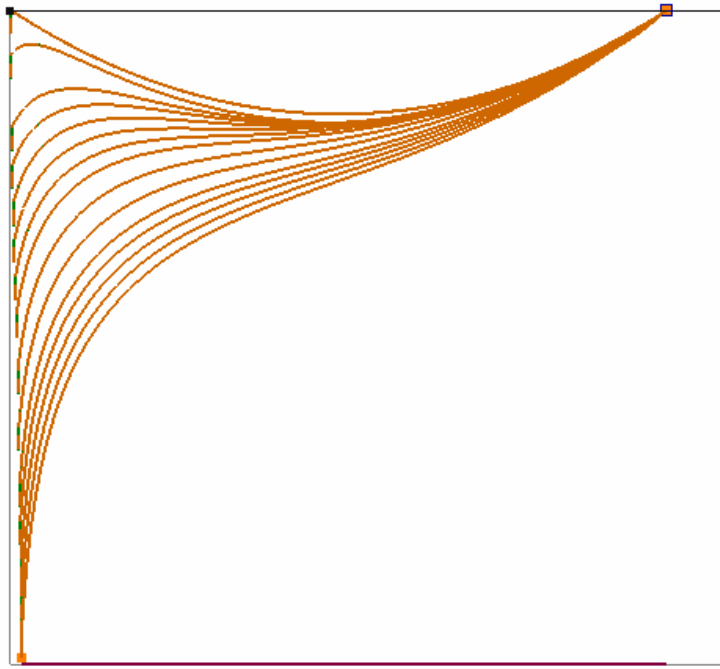


**Figure 3-10:** A safe deployment of the Hanohano shore cable during detector descent.

### 3.3.1.12 Seabed contact, oscillations

The Detector contacts the seabed at a velocity approaching 2 m/s due to the compression of fluids and the drop in displacement. Upon contacting the seabed, the anchor will stop but the detector will “overshoot”. The Detector will then oscillate on the bottom, slowly disbursing its kinetic energy through water drag, and hop up as much as 50 m above and 10 m below its final equilibrium position. Figure 3-11 shows the detector bouncing off the bottom.

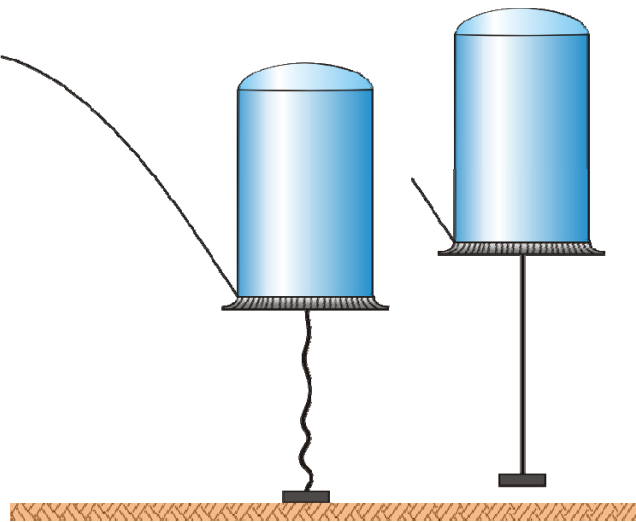


**Figure 3-11:** The detector oscillates after impact with the bottom (horizontal movement exaggerated)

This oscillation will go on for roughly 15 minutes or more with the anchor being lifted off the bottom for about five hops over the first 6 minutes (after that, the rise is taken up by the elasticity in the tether rope). With a nominal bottom current, the detector would not hop horizontally more than a few meters. Since the detector is still well above the seabed (on a nominal 100 m detector), there is no danger to the detector or to the attached cable. Figure 3-12 shows the significant duration of oscillations.

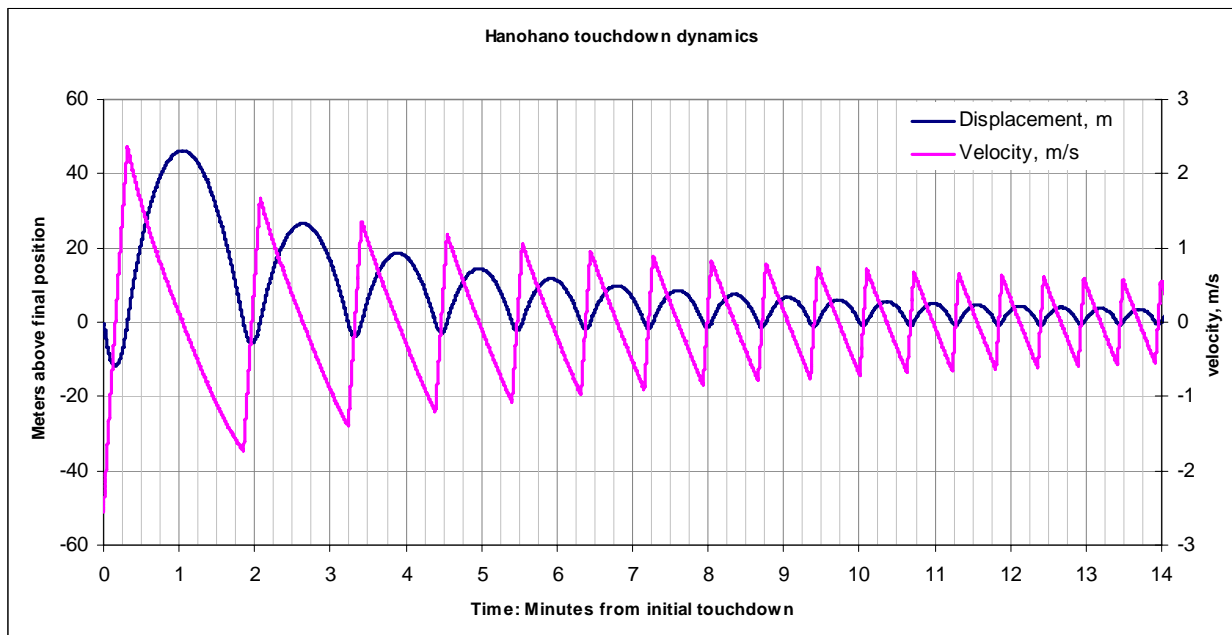


**Figure 3-12:** Oscillations of the detector upon touchdown

### 3.3.1.13 Liftoff, oscillations

For recovery, the anchor weight is released and the Detector rises rapidly. A command is sent via the communications cable or acoustically to remotely cut both the communications cable and the anchor pendant line (synthetic line). After it has cooled, and a 608 wet tonnes anchor is dropped, the detector is buoyant by 88 tonnes. Once it reaches the surface, it is 187 tonnes buoyant. This transit takes 38 minutes. If the detector is released before it has cooled, it will be even more buoyant and ascent times will be faster. The surface boats will need to be at least 1 km away from the Detector location.

The detector will rise above the surface and oscillate similar to the oscillations on the seabed, but the amplitude of the oscillations will be smaller. Figure 3-13 shows the maximum oscillations upon surfacing; it will rise 18 m above the surface and then fall 40 m below. These oscillations will continue for many minutes. .

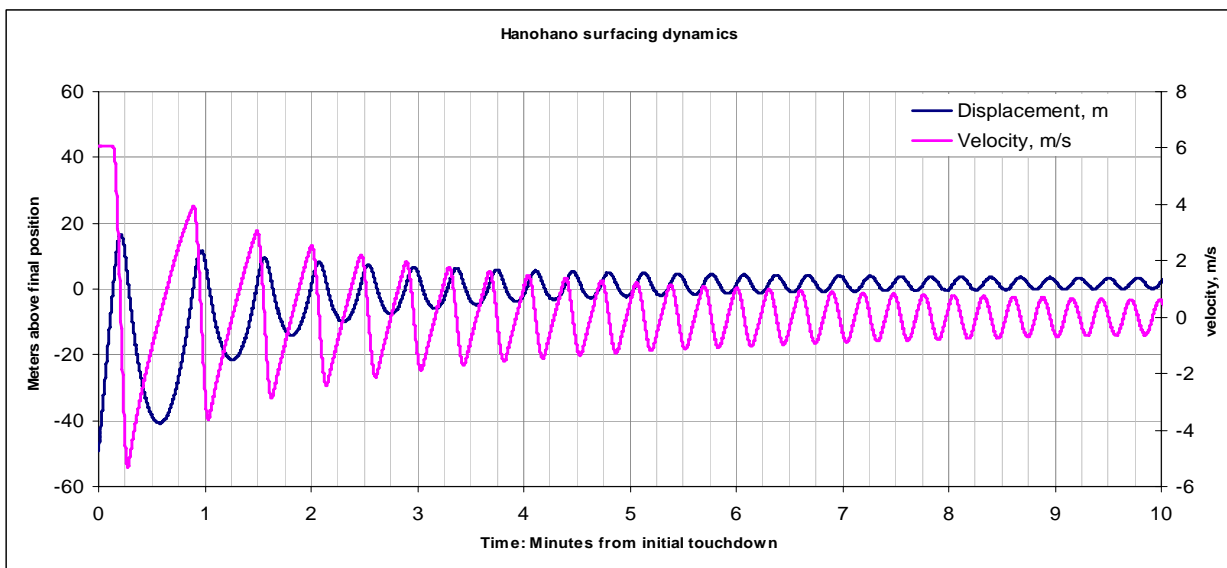


**Figure 3-13:** Oscillations of the Detector upon surfacing

### 3.3.1.14 Recovery

Recovery occurs by moving the barge over the detector. The barge hull aft of the moon pool has a catamaran shape. The barge, empty of fluids, floats high with a 4 m gap between the top of the cutout and sea level. The gap between the bottom of the barge and the top of the detector is fendered well and the normal floating positions of these two structures is such that there is an interference fit – the barge is lifted somewhat and the detector is pushed under – this makes a solid and continuous contact between the two structures and avoids slamming at all points. The lead contact point is more heavily fendered than the mid section of the barge.

The detector in this conceptual design is shown in the middle of the barge. In the final design, it may be advantageous to move the detector slightly aft – perhaps at the 30% position – to keep the barge level during recovery. There will need to be a careful balance of equipment fore and aft for proper balance in all phases of detector loading.

The detector is pushed into the moon pool. Roller tire fenders (the detector restrain system) center the detector and winches rotate the detector to align the transfer hoses. Figure 3-14 shows the barge docking with the detector.

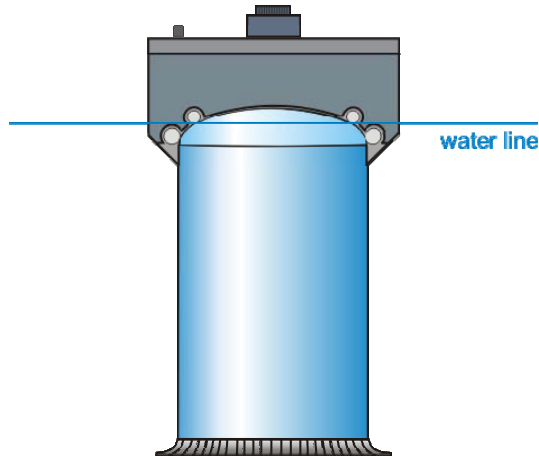


**Figure 3-14:** The barge moves over the detector during recovery

### **3.3.1.15 Removal of fluids.**

The transfer hoses are connected to the hoses on the barge and the pumps transfer the oil and scintillator into the barge. This is a reverse procedure from the loading – total time is 12 to 24 hours. When fully raised, the latching dogs are engaged between the detector and the barge.

### **3.3.1.16 Return to Port**

The tow back to Honolulu (or other close port) is the same as the tow out.

## **3.4 DETECTOR DESIGN DISCUSSION**

This section details the conceptual design of the detector itself. After an overall view of the detector and its features, design work will be presented on weight and buoyancy, volume compensation, PMT module design, internal cables and plumbing, structural steel, and stability.

### **3.4.1. Overall illustration**

Much of the design work on the detector went into the structure itself. Items such as compensation bags, PMT modules, and plumbing were routed around the decisions that were made for structural and stability reasons. Figure 3-15 shows a general view of the detector structure.

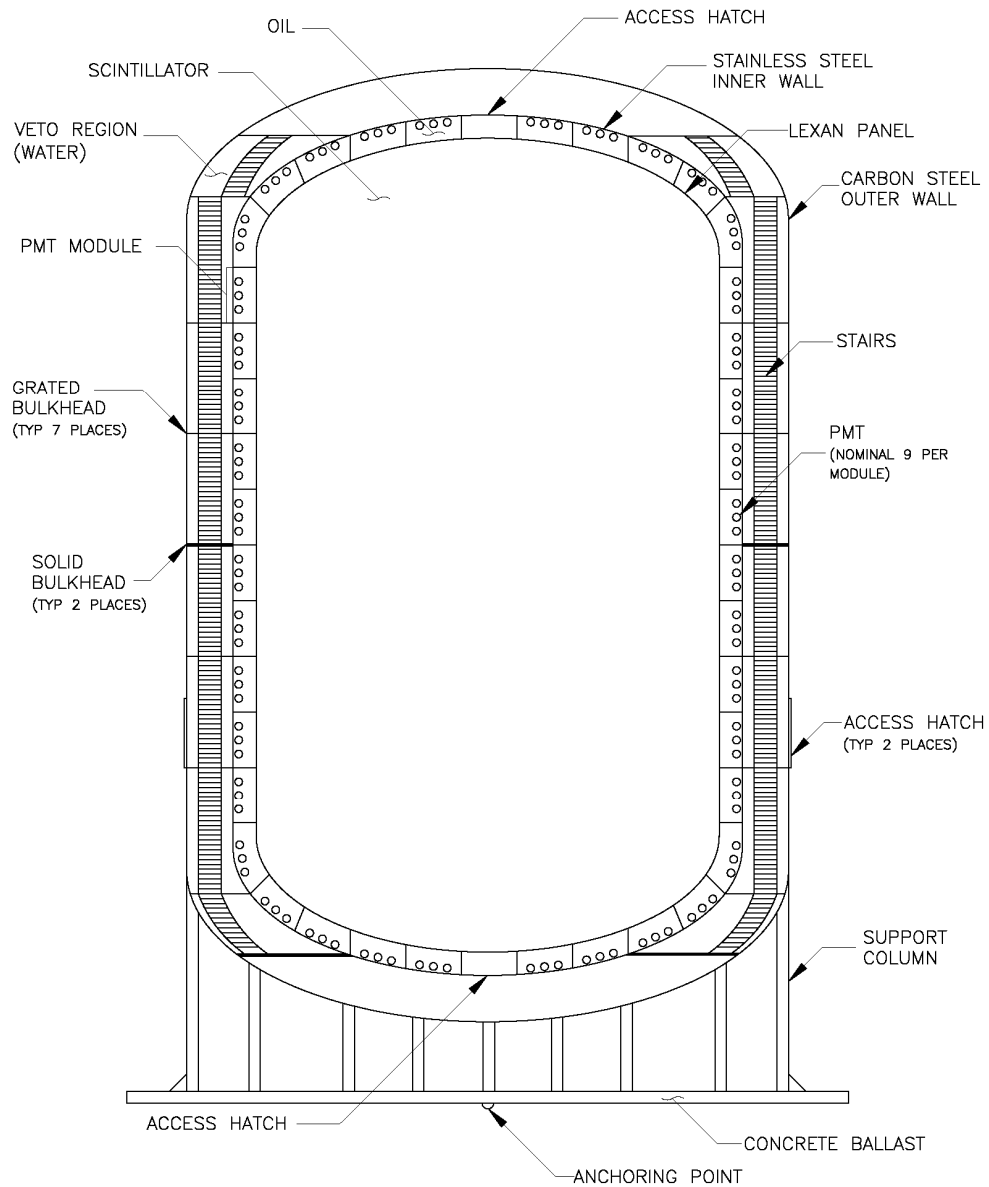


**Figure 3-15: Diagram of Detector Elements**

The key design characteristics of the detector are:

- Carbon steel outer skin with 2 access hatches. The hatches are designed to sit at deck level when the detector is docked.
- 2m veto region that fills with freshwater during deployment. This zone accommodates all plumbing and cabling. There are 10 levels separated by grated and solid bulkheads. Stairways and hatches provide access from one level to another.
- Stainless steel inner skin. This encloses the 3x3 PMT modules. Each module has a bolted hatch in the skin that allows access to the module from the veto region.

- Lexan module covers. Clear Lexan plates cover the inner side of each module. These covers separate the oil-filled module from the scintillator-filled interior volume.
- Interior volume access hatches. The uppermost and lowermost segments of the detector are not occupied by PMT modules. Instead, access hatches allow people and equipment into the interior volume and compensation space.
- Compensation space. A 3 m tall space between the bottom of the outer skin and the top of the ballast concrete. This space is filled with volume compensation bags and support columns. The columns tie the detector to the ballast concrete. This space is surrounded with a watertight wall that has a single valve to control hydraulic access.
- Ballast concrete. A  $\frac{1}{2}$  m thick layer of concrete serves is hung below the detector to enhance stability. The concrete lowers the center of gravity of the detector. It also provides the attachment point for the releasable anchor and seals the compensation space.

### 3.4.2. Weight and buoyancy

Table 3-3 shows the densities of the primary materials that make up the detector. During launch, the pressure is one atmosphere and the temperature is assumed to be 26 deg C. At touchdown, the temperature of the fluids is assumed to be unchanged, but the pressure elevated to 4000 m. At liftoff, the detector is at the same pressure, but has now cooled to 1.5 deg C. Once it has resurfaced, the detector pressure has returned to one atmosphere, but the temperature is still cold (in fact, due to expansion, it is slightly colder).

Materials Properties		Launch	Touchdown	Lift off	Surfaced
density scintillator	tonnes/m3	0.852	0.882	0.900	0.870
density oil	tonnes/m3	0.852	0.882	0.900	0.870
density of fresh water	tonnes/m3	0.996	1.014	1.019	1.000
density steel	tonnes/m3	7.840	7.842	7.842	7.840
density concrete	tonnes/m3	2.404	2.410	2.410	2.404
density ambient seawater	tonnes/m3	1.022	1.046	1.046	1.022

**Table 3-3:** Material densities used for the detector submergence and recovery

Table 3-4 illustrates the volumes, weights, and displacements of these materials for a 10,000 m<sup>3</sup> detector. These weights are critical for the successful deployment of this instrument. The scintillator, oil and fresh water are the buoyant members of this detector, while the steel, concrete, and instruments are weight. These must balance such that it sinks and ascends as desired.

- The shape of the scintillator is an elevated cylinder, the height is 33 m and the diameter is 20.44 m. This analysis assumes flat ends to the cylinder – the final design will round these ends. The overall detector is roughly 26.5 m diameter and 39 m high plus room for compensator bags and ballast at the base.
- None of the liquids are pre-cooled prior to launch. This is not cost effective (see section 3.5.6).

- The assumed steel is equivalent to 13% of the total mass of the scintillator plus the oil. This was an achievable number as determined in the structural analysis. The actual value may be more or less, the weight variation being adjusted with an equal adjustment in the concrete ballast. In other words, this number is conservative and flexible.
- The minimum weight on the seabed is much more than needed for effective anchoring. Anchoring weight is not a design criterion; the weights used are driven by minimum safety factors for ascent and descent.
- The primary table shows the mass, displacement, and size of the scintillator, oil, water, concrete and steel during the four phases of the deployment: launch, touchdown, lift-off and surfacing.
- The effective scintillator volume of this detector is 10,000 m<sup>3</sup>, 9 k-tonnes. This is the usable volume of scintillator on the seafloor and once the scintillator has cooled. Note that the beginning volume (on the surface and including the compensation volume), is 10,558 m<sup>3</sup>. The scintillating fluid represents 37% of the total mass of the detector.
- The oil mass is 14% of the total mass of the detector and requires compensation of 208 m<sup>3</sup>. However, for this detector, we use flexible Lexan panels to compensate for the oil and provide larger compensation on the scintillator fluid – see section 3.4.4.1)
- The fresh water volume is large - nearly equal to that of the scintillator and its mass is 32% of the total mass of the detector. It is the second heaviest component. The fresh water will require a volume compensation system with a capacity of 176 m<sup>3</sup>. Fresh water is considerably less compressible than scintillator.
- The detector has a total concrete load of 1353 tonnes (wet). Of this, 608 tonnes are used for an anchor and 745 tonnes are used for ballast. These values:
  - Provide the minimum launch weight,
  - Exceed the minimum on-bottom anchoring weight,
  - And allow for the minimum lift-off buoyancy once an anchor is dropped.
- The minimum weight to sink the detector on the surface is 86.5 tonnes (0.7% of the scintillator plus oil mass).
- The minimum buoyancy for lift off after the experiment is completed is a similar 87 metric tonnes.
- The mass distribution between components is shown in the column to the right. 37% is in scintillator, 14% in oil, 32% in fresh water, 7% in steel, 4% in a droppable anchor, and 5% in ballast.
- The column to the far right shows the change in volume for the scintillator, oil and fresh water. Two compensator bags will be needed slightly larger than these volumes; the total of the compensator volumes is 766 m<sup>3</sup> for the combined oil

and scintillator and 176 m<sup>3</sup> for the fresh water. Overall, this is 4.0% of the total displacement volume of the detector.

- The detector will leave the surface weighted at 87 tonnes. Once it reaches the seabed, after compression, the system will have a net weight of 174 tonnes. The descent will have a maximum velocity of 2 m/s and a total time of 39 minutes.
- After it has cooled, and a 608 wet tonnes anchor is dropped, the detector is buoyant by 88 tonnes. Once it reaches the surface, it is 187 tonnes buoyant. This transit takes 38 minutes.

Hanohano Detachable Detector		k-m <sup>3</sup>	shape:		
			10 width	4 length	High Cylinder height
Volume Effective Scintillator		m	20.44	20.44	32.71
Hanohano shape: High Cylinder		m <sup>2</sup>	549		
Scintillator dimensions					
Bottom Area					
Layer thickness:		m			
Volumes payload liquids:		m <sup>3</sup>	Scintillator	Oil	Water
Pre-cooled? 1=yes, 0=no			xxxx	1.00	2.00
Steel to DWT ratio for module			10,000	3,732	7,528
Min weight to sink			0	0	0
Min Lift off Buoyancy			0.130	fraction of scintillator + oil mass	
Min On-bottom weight			0.007	fraction of scintillator + oil mass	
			0.007	fraction of scintillator + oil mass	
			0.002	fraction of scintillator + oil mass	
Scintillator, size (width)	m		Launch	Touchdown	Lift off
Volume	m <sup>3</sup>	10,558	10,209	10,000	10,341
Mass	tonnes	8,999	8,999	8,999	8,999
Oil, size (width)	m	22.4			
Volume	m <sup>3</sup>	3,941	3,810	3,732	3,860
Mass	tonnes	3,359	3,359	3,359	3,359
Fresh water, size (width)	m	26.4			
Volume	m <sup>3</sup>	7,703	7,571	7,528	7,675
Mass	tonnes	7,674	7,674	7,674	7,674
Steel Used:	tonnes	1,602	1,602	1,602	1,602
Volume	m <sup>3</sup>	204	204.2	204.2	204.3
Concrete, min required:	tonnes	2,369	2101.5		
Used:	tonnes	2,369	2369.3		
	m <sup>3</sup>	986	983.2		
Anchor, min lift off:	tonnes	1,074	1073.6	-	-
	m <sup>3</sup>	447	445.5	-	-
	wet tonnes	617	607.6	-	-
Ballast:	tonnes	1,296	1295.7	1295.7	1295.7
	m <sup>3</sup>	539	539.0	539.0	539.0
	wet tonnes	744.6	744.6	-	-
Total Module Displacement:	tonnes	23,916	23,828	23,017	23,117
Volume	m <sup>3</sup>	23,393	22,778	22,003	22,619
Total Module Weight, full	tonnes	24,003	24,003	22,929	22,929
Net weight:	tonnes	86.5	174.9	-87.9	-187.7
goals:		86.5	24.7	-86.5	
Gr Anchor Req'd, 0.15m/s, f=0.5	tonnes		2.41		
Empty draft	meters	5.16			
Freeboard, surfaced:	meters				0.33
Submerge - Surface time:	minutes		39	38	
Submerge - Surface max velocity:	m/s		1.99	2.09	
Submerge - Surface min velocity:	m/s	1.42		1.41	

**Table 3-4:** Mass and displacement for the 10,000 m<sup>3</sup> detachable detector

Table 3-5 shows the first-cut approximation for the size of the supporting barge. The barge is sized to fit through the Panama Canal, carry the whole load of oil and scintillator, and have a draft less than 10 m when in port. A rectangular barge with an length overall (LOA) of 95 m, a beam of 32.3 m, and a draft of 9.5 m satisfies these requirements. The actual dimensions of the barge are modified further in this chapter.

<b>Hanohano Barge (detachable configuration)</b>			
Barge freeboard, fully loaded	m	3.8	
Horiz clearance: detector to barge	m	1	
Barge beam / moonpool width	m/m	1.5	ratio barge beam to moonpool dia
PanamaMax?		1	1=yes, 0=ignore (use above for width)
Steel to DWT ratio for barge		0.2	fraction of scintillator + oil mass
Barge Hotel, Machinery mass		0.15	Fraction of primary steel structure
Vert Recov Clearance, barge/detector	m	1.90	
Barge maximum draft	m	10	
Min excess volume inside barge		0.2	unused by scintillator or oil
<b>Geometry:</b>			
Guess effective Length:	m	<b>95.0</b>	
Beam, overall	m	32.30	
Deck ea.side of detector:	m	1.9	12%     OK Panama of beam
Moonpool, width	m	28.4	
Moonpool, area	m^2	635.4	
Position Moonpool, from bow	% length	50%	
Water plane area, above slot	m^2	2433.1	
Water plane area, at slot	m^2	1399.7	
Total Height:	m	13.3	
<b>Empty Barge, Ready for Recovery:</b>			
Weight, vol payload:		<b>tonnes</b>	
Barge Steel Structure:	tonnes	2,472	
Hotel, Machinery, Misc:	tonnes	371	
Total:	tonnes	2,842	
Displacement, empty:	m^3	2780.0	
Draft, empty:	m	2.0	
Height of the recovery slot:	m	4.2	from bottom
<b>Fully Loaded Barge:</b>			
Scintillator Load:		<b>tonnes</b>	<b>m^3</b>
Oil Load:	tonnes	8,999	10,558
Empty detector, pre launch	tonnes	3,359	3,941
Barge Steel Structure:	tonnes	3,971	
Hotel, Machinery, Misc:	tonnes	2,472	
Total:	tonnes	371	
Displacement, Fully Loaded:	m^3	19,171	14,499
Draft, Fully Loaded:	m	18,751	OK draft
<b>Volume Barge:</b>			
Required Volume:	m^3	27,997	
% Used	%	14,499	
		52%	OK volume

**Table 3-5:** Rough barge dimensions and weights for the 10,000 m<sup>3</sup> detector

### 3.4.3. Compensator Bags

When the detector sinks to the ocean floor, the pressure increases and the temperature decreases. These factors both cause the fluids in the detector to compress. Additional fluids must be added to compensate for the space left by the compression. Otherwise, external pressure would build up. The extra compensation fluids will be in large flexible bags called pillow tanks, which are shown in Figure 3-16.



**Figure 3-16:** Pillow Tank

Several pillow tanks will be need for the scintillator and fresh water. The tanks will be exposed to the ocean and hoses will connect them to the detector. As the fluids inside the detector compress, the pressure inside the detector and pillow tanks will decrease. Since the bag is exposed to the ocean, the external pressure will compress the bag, forcing fluid into the detector until the pressures are once again in equilibrium. This will prevent any pressure on the structure of the detector. A schematic of the pillow tank layout is shown in Figure 3-17.

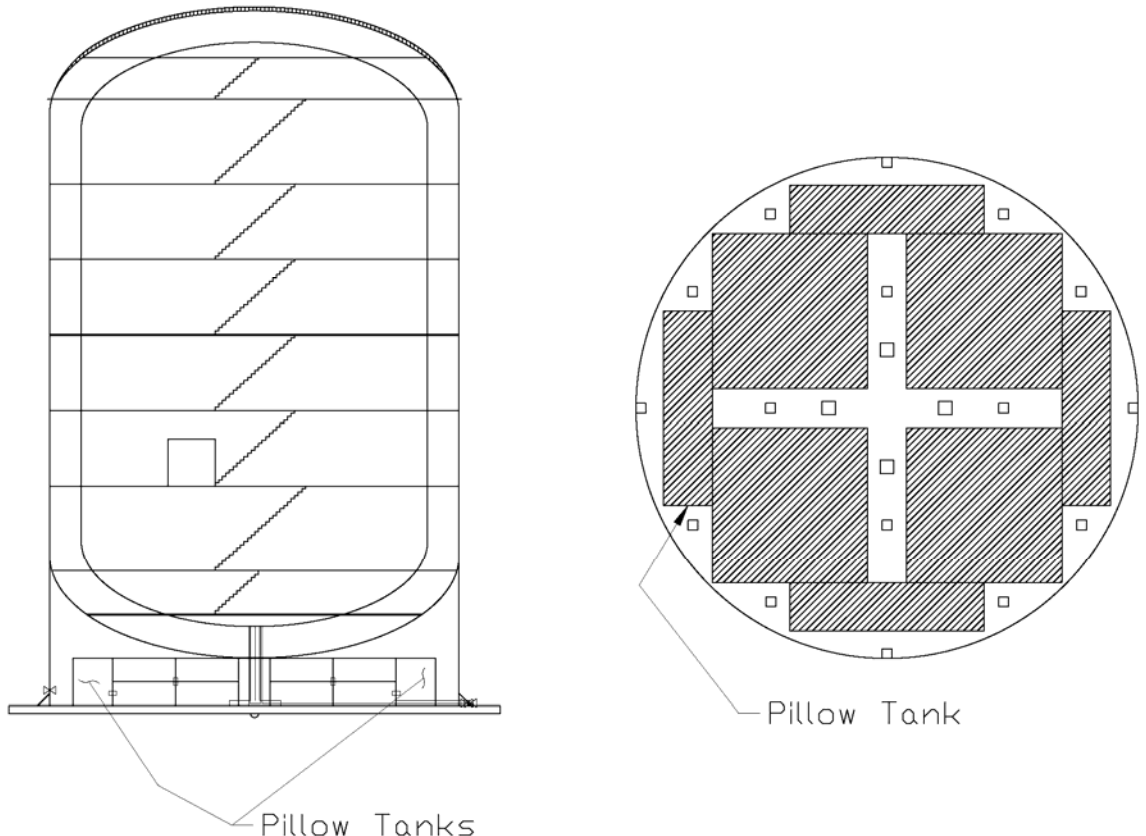


**Figure 3-17:** *Pillow Tank Layout*

#### 3.4.4. PMT module design

The photomultiplier tubes will be grouped into 3x3 grids. Organization into compartments of 9 PMTs limits the stress placed on the Lexan windows, allows for variable pressure compensation to balance density difference between oil and scintillator, and minimizes the threat of oil contaminating the scintillating fluid. The following sections detail the design elements of the PMT modules and how they relate to the above benefits.

##### 3.4.4.1 Lexan window

Separating the scintillating fluid volume from the oil buffer region surrounding the PMTs is a Lexan panel. The panels serve not only to keep the oil and scintillating fluid separate, they also provide volume compensation to the oil buffer.

As detailed in section 3.3.1.5, part of the deployment procedure is to pressurize each PMT module. Pressurizing a module causes the Lexan panel to bow outwards. As the detector sinks and cools, the volume of oil in the module decreases, and the panel progressively flattens out and eventually bows inwards. This change from convex to concave allows the panel to provide volume compensation to the module without actually introducing new fluid to the space. By logic similar to that presented in section 2.4.3.1 on a cube shaped detector, a large panel has to withstand more force than a small panel. Using many

modules allows each one to have its own panel which is much smaller than a single large panel would be, and therefore much thinner.

A second pressure consideration arises from a difference in the densities of the scintillating fluid and the oil. If the fluids are of different densities, there will be a difference in pressure in the two fluids at any given depth. This pressure difference will cause the panel to deflect the same way intentional pressurization does. Unless there is some compensation for the pressure difference, the forces on the panels could become too large to feasibly support. Separation of the oil buffer layer into modules allows the pressure in individual modules to be adjusted to compensate for the density driven effects.

#### 3.4.4.2 Fluid transfer

The interior environment of each module must be controlled with the same care as that in the scintillating volume. The only two fluids that should enter the module once it has been cleaned are oil and nitrogen. Also, each module must be isolated from all other modules. These two goals are accomplished through the use of a sealed system that has two valves per module.

Sealing the system means that once the modules and oil have been decontaminated, no interior part of the modules, oil storage tanks, nitrogen storage tanks, or plumbing are exposed to the atmosphere. This ensures that only nitrogen and oil can get into a module.

The need for two valves per module is imposed by the logistics of filling and emptying the modules. Since the system is sealed, the entry of oil into a compartment must be balanced by the exit of nitrogen. The inverse is true during the emptying process. Both entry and exit processes must happen simultaneously, so there needs to be two ports into the module. Figure 3-18 shows a schematic of a PMT module.

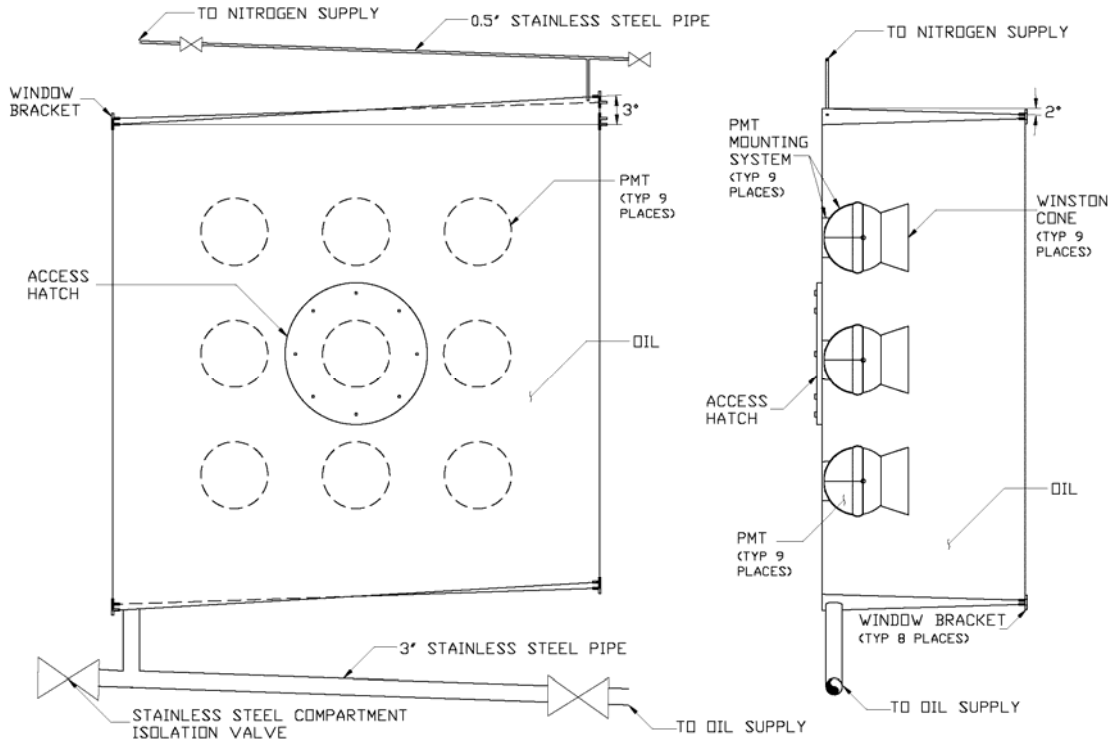


**Figure 3-18:** Schematic of an Individual PMT Module Showing Fluid Ports

Note that the top and bottom of the module are not square. The bottom of the module is slanted and twisted to give a low spot in the module. When draining, the oil will be sure to drain into the drain line connected to the port rather than pooling on the floor of the detector. Similarly, the top of the module creates a high point. As the module is filled, air will be driven up into the nitrogen line. There will be no room for air pockets to be trapped.

For draining and filling purposes, the modules around the detector are grouped circumferentially into quadrants. Each quadrant is served by a separate set of lines. Figure 3-19 shows the bottom three rows of one of the quadrants.

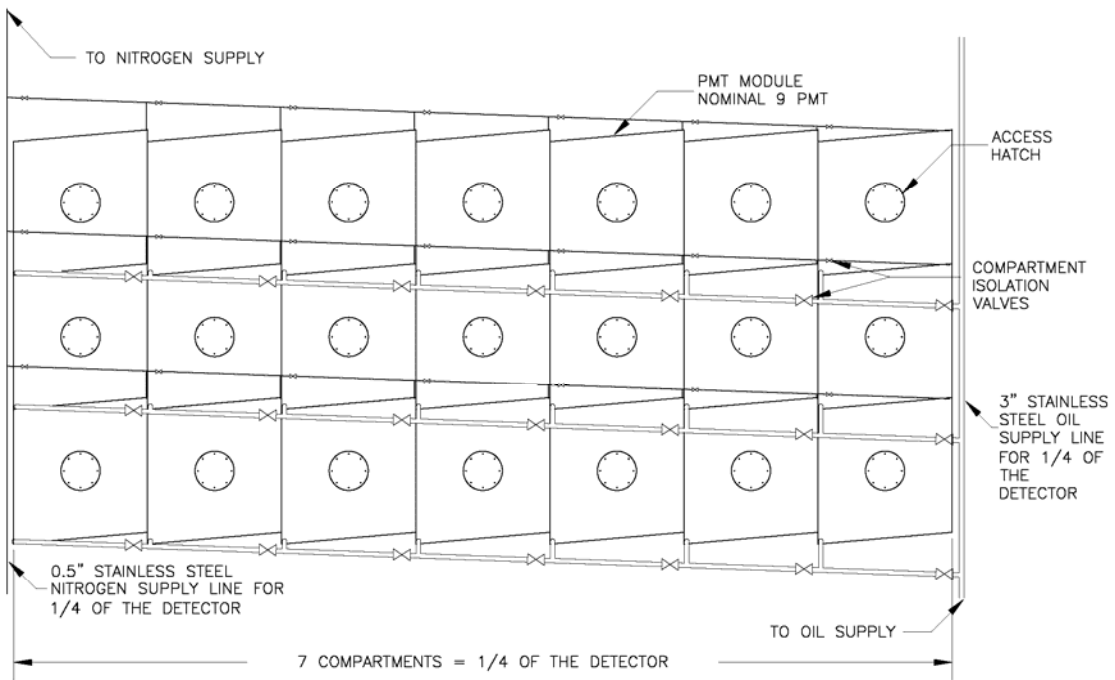


**Figure 3-19:** Schematic of Bottom Three Rows of PMT Module Quadrant.  
Curvature of the Detector is Not Shown for Clarity

The vertical pipes on the left and right of the quadrant are the nitrogen and oil drain/fill lines respectively. These lines serve all modules in the quadrant. The slanted horizontal lines leading from the vertical lines carry oil and/or nitrogen to each module. Each module has a valve on each line. These valves allow for isolation and pressurization of the modules. For example, once the bottom row has been completely filled, the valves on the nitrogen drain/fill line can be closed. Then, more oil is pumped into the modules, and the modules become pressurized. After the correct pressure is obtained, the valves on the oil drain/fill line are closed. Each module then has a closed valve on its top and bottom, and is hydraulically separated from its neighbors. Then the filling process can continue as the same process is repeated for the next row.

Once all the modules are filled and all the valves are closed, each module is independent of the others. The benefit of this is evident in the case where one of the Lexan panels fails. If a panel leaks (i.e. – because it was damaged by the implosion of a PMT), the oil in the module will mix with the scintillating fluid inside the detector. If the modules could hydraulically communicate with each other, extensive mixing could occur and hinder the experiment. Instead, with the modules hydraulically separate, the failure of a panel only mixes the volume of oil in that one module. The small amount of oil in a single module could be tolerated when diluted into the much larger volume of scintillating fluid inside the detector. Thus, independent modules help mitigate the effects of the failure of any one module.

#### 3.4.4.3 Mounting detectors

The detectors are mounted using a ring of slightly smaller diameter than the glass sphere. This ring fits over the sphere and is bolted to the back of the PMT compartment. To help stabilize the sphere, a rounded bracket is used to support its base. Further design is required because the effects of temperature and pressure may cause the mounting system to loosen. If the sphere shrinks more than the ring and bolts do, it could rotate or shift in the mounting system and hinder the experiment.

#### 3.4.4.4 Service access

All access to PMT modules is granted through a single hatch in each PMT compartment. This hatch is shown in Figure 3-18. Once the hatch is removed, the center PMT module is removed. Other modules can then be unbolted and removed for service.

#### 3.4.4.5 Implosion discussion

Implosion of glass spheres presents a significant risk to the success of the experiments Hanohano will undertake. Isolation of the PMT modules into compartments helps limit the liability by ensuring no more than 9 PMTs can be affected at a time. However, it would be ideal if even the PMTs within a compartment could withstand the implosion of a neighbor. Testing has begun on use of concrete barriers or foam filled PMT modules to determine if they can help mitigate the forces of an implosion. However, the results are not definitive enough to allow confident design of anti-implosion measures. See chapter 4 for a more complete description of the work done on imploding spheres.

### 3.4.5 Internal Cables and Plumbing

#### 3.4.5.1 Cable routes and access

Each PMT must have a data and power cable connected to it. These cables run through sealed connections across the back of the PMT modules. The cables from any given compartment will be gathered in a conduit and routed through the veto region to a digitizer. Although this limits access to any individual cable, it is easier to handle a compartment's cables all at once than it is to route and protect all cables individually.

#### 3.4.5.2 Plumbing

Most of the piping in the detector is needed to fill or drain the PMT compartments. Fill pipes are 3" in diameter and run through the veto region along the bottom of the detectors they service. Each pipe serves  $\frac{1}{4}$  of a row of PMT compartments. There are also  $\frac{1}{2}$ " nitrogen lines that allow gas into or out of the compartment as it is drained or filled. These lines will be filled with oil during the filling process to ensure there is no gas in the system at deployment. There are 4 vertical fill pipes that each serve a quadrant of the detector. Similarly, there are 4 vertical nitrogen lines. See Figure 3-18 and Figure 3-19.

### 3.4.6. Structural steel

#### 3.4.6.1 Pressure loading requirements

Since the exact operational requirements of the vessel have not yet been defined, Makai took a conservative approach to the selection of pressure loading requirements. The vessel has been structurally designed such that the veto region can be filled independently of the oil and scintillator volumes. Stability analysis indicates that such a scenario would be difficult to obtain, but it is conceivable that future work would require the capability. In addition, future work could require the detector to be filled without sinking. Sinking exposes the detector to external water pressure that helps counteract the internal pressure in the veto region and therefore allows the detector walls to be thinner. This counteracting pressure has not been considered in the structural analysis of the detector.

The oil and scintillator must be added simultaneously. The Lexan panels between the two fluids have been optimized for fluid compensation and light transmission, not structural strength. In short, the panels cannot withstand the pressure gradient induced by independent filling and would fail. However, the stainless steel wall outside the oil layer has been designed to allow the oil and scintillator volumes to be full while the veto region remains empty. Again, such a condition is not stable throughout the filling process, but it is possible that the capability would be desirable in future design.

#### 3.4.6.2 Wall thickness

The inner and outer structural walls of the detector are the stainless steel wall separating the oil from the veto region and the outer carbon steel wall, respectively. Since the oil is of a lower density and depth than the fresh water intended for the veto region, the inner wall is thinner. The inner wall has a maximum thickness of 17.8 mm at the bottom where the pressures are greatest, and a minimum thickness of 6 mm at the top where the pressures are smallest. The spheroidal top and bottom segments are the same thickness as the top and bottom of the walls. The outer wall has a maximum thickness of 39.4 mm at the bottom and a minimum of 6 mm at the top.

#### 3.4.6.3 Hard points for docking

The variety of pipes needed to fill and drain the detector requires it to have a fixed orientation relative to the barge. Therefore, stiffened tracks can be used under the wheels of the detector restraint system. This is accomplished simply by placing a beam on the inside of the outer wall (i.e. – in the veto region) of the detector wherever the wheels will run. The top of the detector will be stiffened overall to withstand the impacts that may occur while it travels through the slot in the bottom of the barge.

#### 3.4.6.4 Reason for detector shape

The selection of an appropriate H/D ratio for the detector was driven by the barge size limitations imposed by the maximum size allowed in the Panama Canal. A short and squat detector will require a wider barge than a tall and thin detector. The ratio was selected to be the lowest possible and still leave enough room for structural steel without exceeding the limits of the canal.

Beyond the barge limitations, there is a cost to having a tall and thin detector. The taller the detector is, the greater the pressure it must contain, and the heavier it becomes. Also, a tall and thin detector requires more PMT's since it has more surface area. However, as long as H/D is between 1 and 3, these costs are weak functions of H/D, and the penalty is small. Therefore, the selection of an H/D ratio of 1.75 does not constitute a problem.

It is important to note that the selection of H/D, and indeed hull geometry in general, have been driven by the need to fit through the Panama Canal. Should the canal be widened, or an alternative route selected, the detector and barge could change shape to a more cost-efficient configuration.

#### 3.4.6.5 Internal steel requirements

The structural design of the detector itself is relatively simple. The thickness of the walls and ends of the detector are calculated based on the pressure they must resist (see section 2.4.2.1). The detector is given overall rigidity by connecting the steel walls across the veto region to establish a double hull. This connection is made via the grates and bulkheads used to access the PMT modules.

The only other structural component of the detector is the support system between the ballast concrete and the detector bottom. The structure must be open to make room for the compensation bags. It also must be able to withstand both compression and tension forces. When the detector is empty and docked with the barge, the concrete ballast is pressed against the keel of the barge, and the detector's weight rests on top of it. The support system transfers the weight of the detector to the concrete ballast. When the detector is deployed, a valve is opened so that the space between the ballast and detector is exposed to the environment. This forces the buoyancy force to act not on the bottom of the ballast, but directly on the bottom of the detector. Since the buoyancy force is no longer acting on the ballast, it now "hangs" from the support system.

The support system is comprised of steel columns that are welded to the outer wall of the detector on one end, and embedded in the concrete ballast on the other. They are distributed as shown in Figure 3-20 to spread the load across the concrete and avoid cracking it.

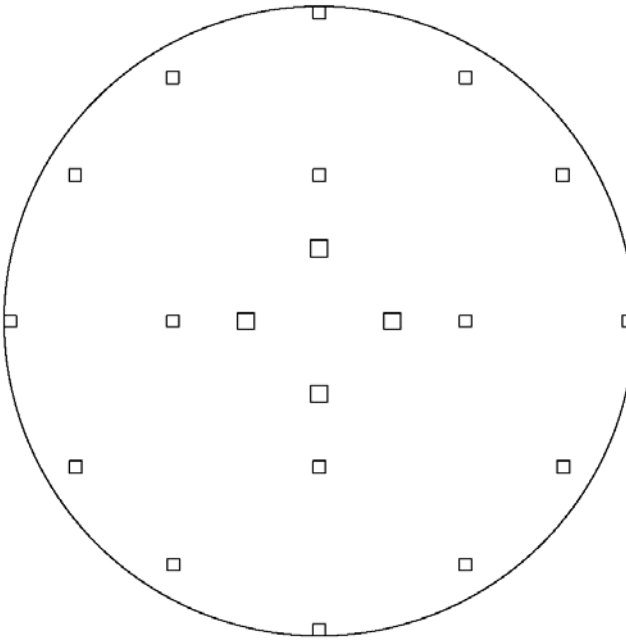


**Figure 3-20:** Layout of Support Columns between Detector and Concrete Ballast

The four columns closest to the center are large to help tie the detector into the attachment point for the releasable anchor.

#### 3.4.6.6 Access throughout the detector

Access to the detector is provided through four hatches. The first is on top of the detector. A hatch is placed there in the outer wall, and the PMT module at the very top of the detector has been omitted in favor of a hatch. These hatches provide access to the interior volume of the detector for installation and cleaning of Lexan panels. Since any permanent scaffolding would be detrimental to the experiment, a temporary scaffold can be lowered through the hatches into the interior volume. This scaffold hangs from a winch that can be mounted on top of the detector. The scaffolding system is shown in Figure 3-21

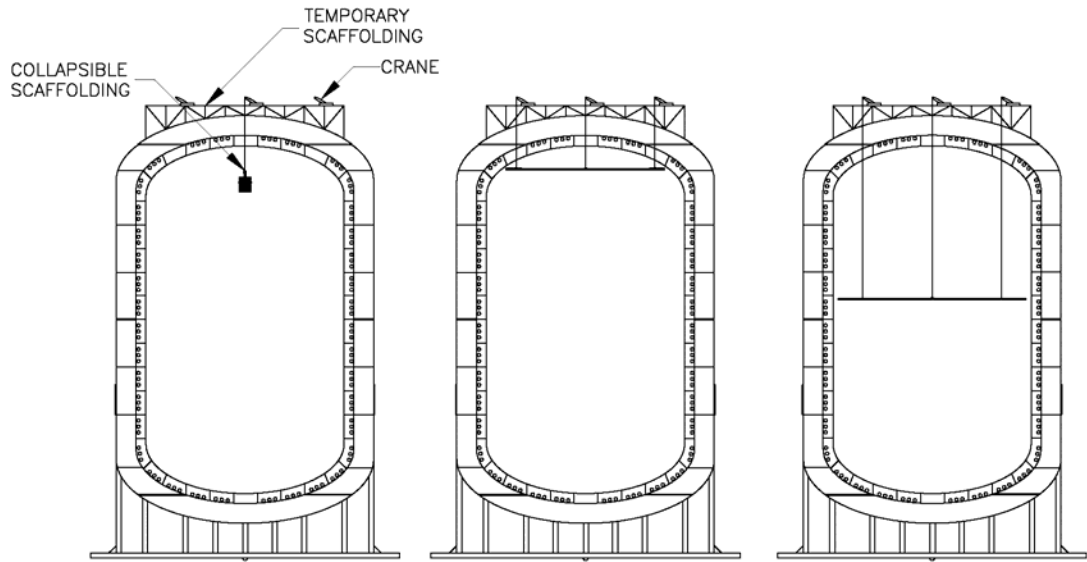


**Figure 3-21:** *Temporary Scaffolding System*

There is a similar pair of hatches in the bottom of the detector. These allow access to the compensation space between the detector and the concrete ballast.

There are two more hatches in the sides of the detector. These are placed to be at the level of the top deck when the detector is empty and docked with the barge. The hatches lead to one of the grated bulkheads that serve as walking surfaces inside the detector. The bulkheads are connected by stairways that allow workers to move from one level to another. Each level allows access to two rows of PMT modules. The two solid bulkheads in the detector have sealable hatches that allow workers to use the stairways to access them.

#### 3.4.6.7 Probable weight

The structural analysis of the detector as described in section 2.4.5.3 predicts a 1300 tonne detector with a fiducial volume of 10,000 m<sup>3</sup>. At this early stage of design, there is uncertainty in any analysis. To account for this, Makai has applied a safety factor of 1.23 on the weight calculations, and used a detector weight of 1600 tonnes. This weight represents the weight of structural steel only, and does not include weights for compensation bags or ballast.

#### 3.4.6.8 Anchor attachment point, compensator bag support

The releasable anchor is tied to a heavily reinforced point at the center of the ballast concrete. The connection point is structurally tied to the 4 nearest support columns so the concrete does not take the primary load.

The compensator bags rest on top of the ballast concrete. They are tied to the support columns to prevent shifting, but the concrete itself provides most of the support.

### 3.4.7. Stability

An in-depth stability analysis of the detachable design with a cylindrical 10,000 cubic meters detector is presented here.

#### 3.4.7.1 Size

The width of the barge will be 32.3 m, the largest beam allowed through the Panama Canal. The length is determined such that the draft is no more than 10 m when fully loaded, which results in a length of 100 m. The height is determined by the desired minimum freeboard, and is 13.3 m high. The cylinder's height to width ratio is 1.75 in order to allow 2.2 m on either side of the moon pool.

#### 3.4.7.2 Empty

While the barge is underway, the detector will be empty of all fluids. The scintillator and oil will be stored in tanks on the barge, and a reverse osmosis plant will be on board to produce water when it is time to fill the outer layer of the detector. The empty detector with ballast would have a draft less than the 10 m draft of the barge. Therefore, the flanges at the bottom of the detector will be pushing up against the bottom of the barge and will help hold it in place. In addition, the detector restraint system will keep the cylinder and barge locked together. These two systems will account for the differences in motion and period the detector and barge would otherwise experience. Figure 3-22 shows a diagram and stability curve for the empty detector.

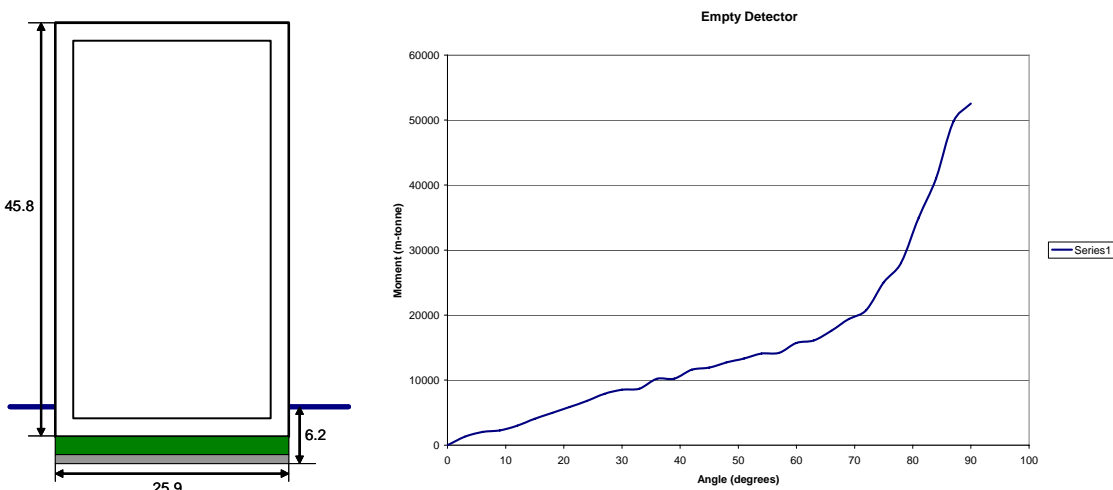


**Figure 3-22:** Diagram and Stability Curve of Empty Detector

#### 3.4.7.3 Filling the Detector

As in the case of the integrated vessel, the free surface effect could cause instability during the filling process and must be considered. The first filling process investigated is filling the scintillating fluid and oil simultaneously and completely, and then filling the fresh water. During filling, the draft of the detector will be allowed to increase in order to improve stability.

Filling the scintillating fluid and oil creates a period of instability when the fluids are nearly full. Since this filling process is not entirely stable, the next attempted plan filled the two meter gap between the bottoms of the inner and outer cylinder first, and then proceeded with filling the inner cylinders. This method improved the stability when filling the scintillating fluid and oil, but when the inner cylinder was nearly full it was still unstable. In addition, filling the bottom two meters of the outer cylinder was unstable, as seen in Figure 3-23 and Figure 3-24.

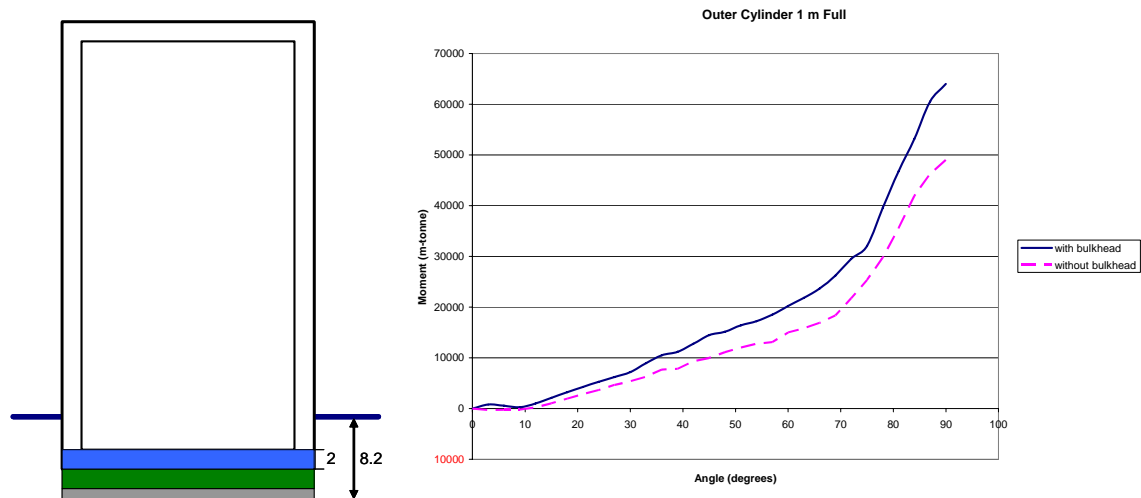


**Figure 3-23:** Diagram and Stability Curve of Detector with 2 meters of Fresh Water

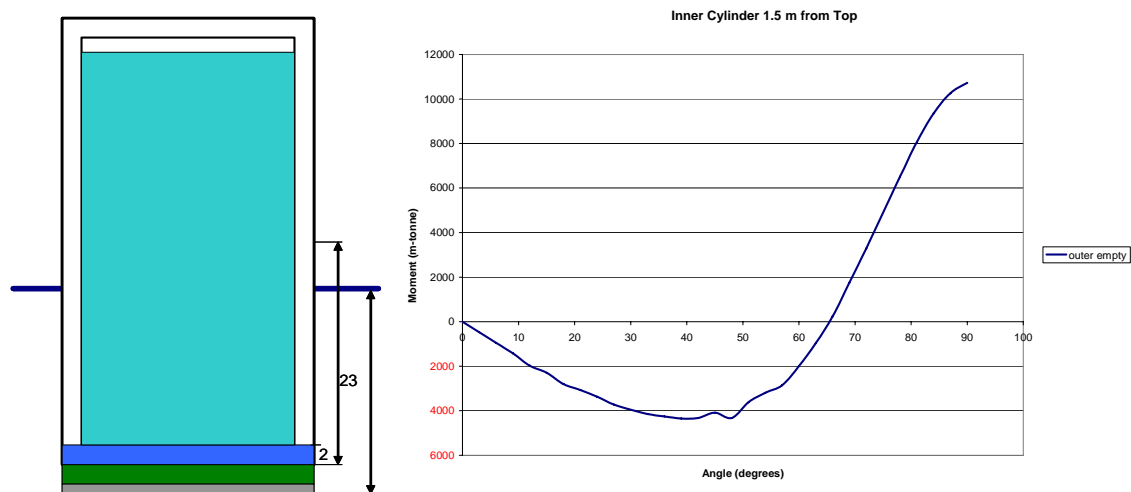


**Figure 3-24:** Diagram and Stability Curve of Detector with Two meters of Fresh Water and Oil and Scintillating Fluid 1.5 m from Full.

A specific filling sequence was developed to solve the stability problems. The outer cylinder will have bulkheads so it can be filled in stages to limit the free surface effect. The first bulkhead will be located even with the bottom of the inner cylinder at 2 m, and the second will be halfway up the detector.

First, the bottom two meters of the outer cylinder is filled with freshwater. The bulkhead prevents water from sloshing when completely full, and also limits it while it is filling, resulting in a stable process, as seen in the stability curve above in Figure 3-23. The detector with bulkheads is stable, whereas a detector without would be unstable. These first two meters of fluid will ballast the detector while the inner cylinder is partially filled.

Next, the inner cylinder is filled with oil and scintillating fluid simultaneously until it is half full, as seen in Figure 3-25. Continuing to fill the inner cylinder at this point would raise the center of gravity of the detector enough that it would become unstable. Therefore, more water is added to the outer cylinder until the second bulkhead at half full is reached. Adding the water decreases the center of gravity and increases the draft, both of which promote stability, which is shown in Figure 3-26.

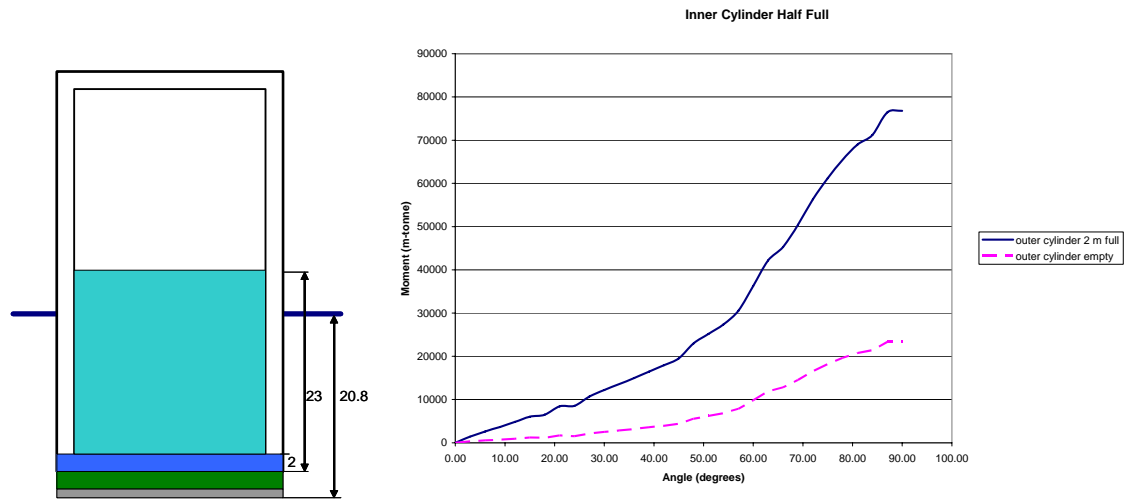


**Figure 3-25:** Diagram and Stability Curve of Detector with 2 meters of Fresh Water and Half Full of Scintillating Fluid and Oil

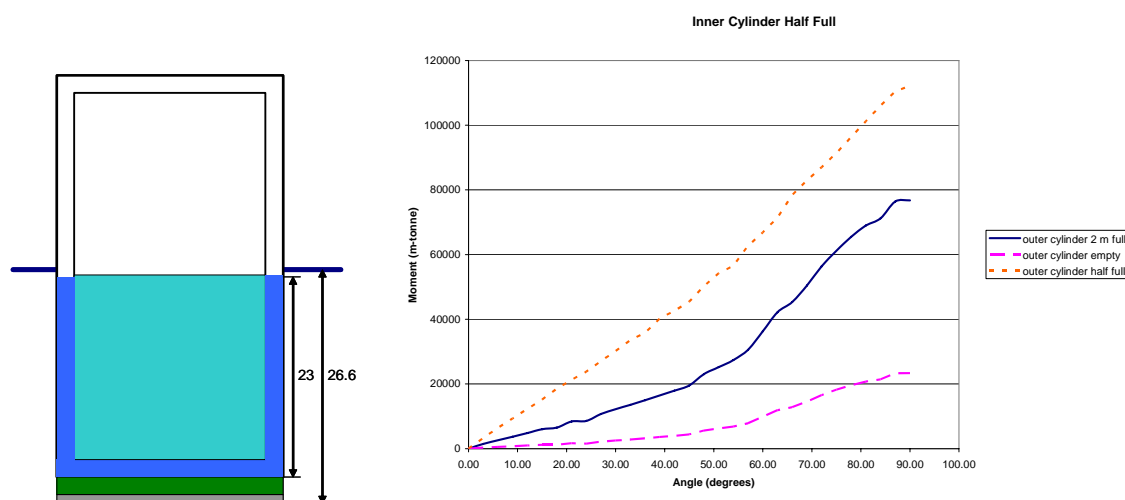


**Figure 3-26:** Diagram and Stability Curve of Half Full Detector

Once the outer cylinder is half full and the bulkhead is preventing a free surface, the inner cylinder is completely filled with oil and scintillating fluid. The entire process of filling the inner cylinder is now stable, which Figure 3-27 demonstrates. Lastly, the outer cylinder is filled completely, which is also stable.

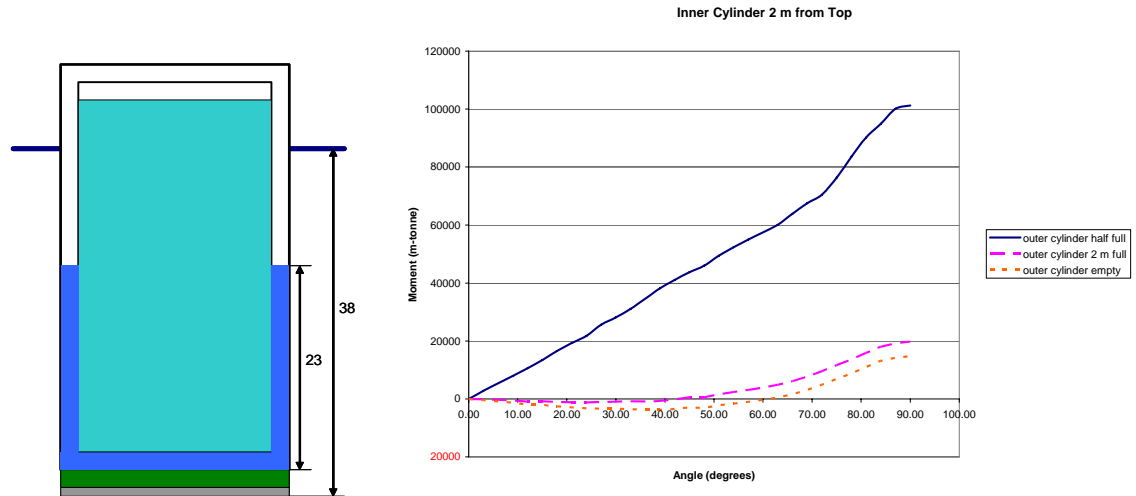


**Figure 3-27:** Diagram and Stability Curve of Detector Half Full of Fresh Water and Scintillating Fluid and Oil 2 meters from Full.

When the detector is completely filled, it will have very little freeboard, which is shown in Figure 3-28. At this point, the detector and barge will be separate, the concrete anchor will detach from the barge and the detector will sink to the ocean floor.

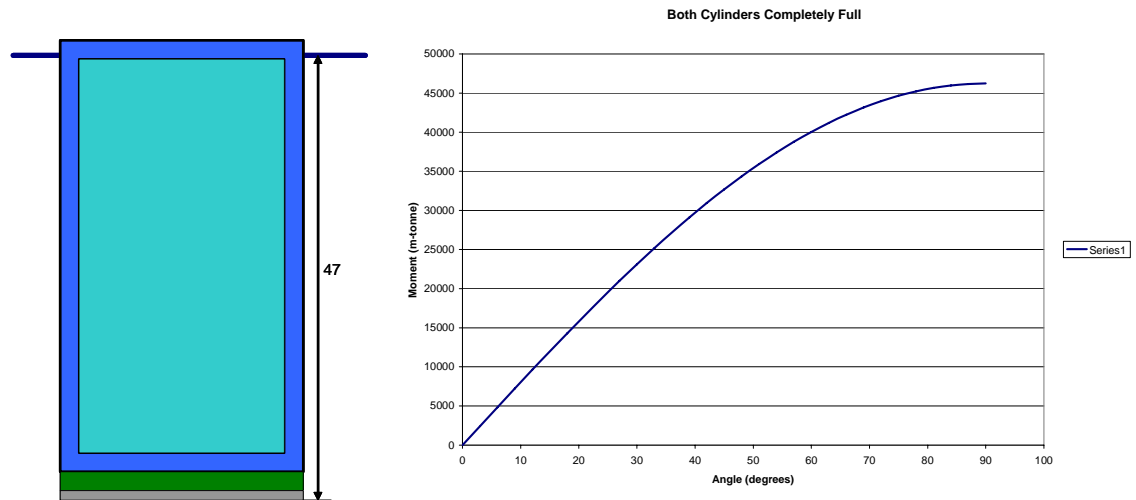


**Figure 3-28:** Diagram and Stability Curve of a Full Detector

If the filling process outlined above is used, the detector will be stable during the entire process.

#### 3.4.7.4 Submerging

For the detachable vessel, KG and KB are at the same point during filling. At all times during the filling process, the center of buoyancy moves to create a positive righting moment. This includes when KG and KB are at the same point.

Unlike the integrated vessel, the detachable vessel will have ballast on the bottom of the detector. This weight will ensure the detector's stability when completely submerged.

#### 3.4.7.5 Conclusion

The detector will be stable during the entire filling process if it is filled in the following order:

1. Bottom two meters (bulkhead) of outer cylinder with water
2. Inner cylinder half way with oil and scintillator
3. Outer cylinder half way (bulkhead) with water
4. Inner cylinder completely full
5. Outer cylinder completely full

The detector is also stable when it is completely empty, completely full, and when completely submerged. Therefore, it is stable at all times during its lifecycle.

### 3.5 BARGE DESIGN DISCUSSION.

#### 3.5.1. Primary design restraints

The barge has been designed to resemble a typical cargo barge as much as possible. While this barge is required to perform operations beyond that which a typical barge can perform, those operations do not require extensive changes to the overall structure of the vessel. The design factors that cause the vessel to deviate from a typical barge are the need to accommodate both the moon pool and Panamax limitation, and the storage of high purity liquids

##### 3.5.1.1 Moon pool and Panamax

The large moon pool in the center of the vessel is a significant deviation from typical barge design. The pool restricts the placement of structural steel and gives the vessel a minimum width. It is the minimum width that creates the balance moon pool size and the Panamax limitation. The minimum width also has an effect on the length of the vessel. Since the required displacement of the hull is set (such that the draft is 10 m), a wide vessel means a short vessel. This is why the barge has a length to beam ratio of about 3.5 instead of the more typical 6-8.

### 3.5.1.2 Storage of high purity liquids

While barges exist to carry liquids that require special care, oil and scintillating fluid are particularly onerous. The fluids must be protected from solid, liquid, gaseous, and radioactive contamination. They must be stored in stainless steel tanks, and be pumped through electropolished stainless steel pipes. Also, the pumps used cannot contribute any contaminants to the fluids.

### 3.5.2 Layout

The layout of the barge is shown in Figure 3-29.

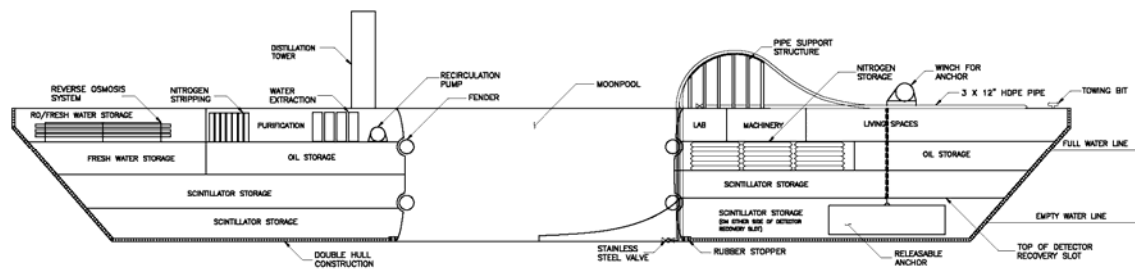


**Figure 3-29:** Side View of Barge Showing Layout of Components in the Hull

The major features of note are:

- Double hull construction
- Storage tanks for scintillator, oil, and freshwater
- Reverse osmosis plant for freshwater production
- Scintillator and oil purification equipment
- Nitrogen storage tanks
- Fluid fill pipes and support structure
- Releasable anchor and winch
- Detector recovery slot and fenders
- Moon pool

### 3.5.3. Moon Pool Structure

The presence of the moon pool introduces a challenge to the design of the barge. The middle section of a ship typically experiences larger forces than the rest. Therefore, the middle sections of ships usually have more structural steel to help counter these forces. Often this extra steel is distributed across the top deck and keel. However, the moon pool takes up much of the space that would normally be reserved for structure. Therefore, all the structure must be concentrated in the thin sections of hull next to the moon pool. A

total of 1.67 m<sup>2</sup> of steel is required at the top deck and keel next to the moon pool to stiffen the vessel.

A second structural effect of the moon pool is that structural members must pass around it. Longitudinal structural members in ships typically run all the way from the bow to the stern. In order to accomplish this with the Hanohano barge, the members must be routed from towards the outer edges of the barge as they approach the moon pool.

### 3.5.4. Detector Restrain System

The detector restraint system locks the barge and detector together when they are docked and during some stages of deployment. It allows the detector to take advantage of the extra stability provided by the barge and protect both structures from damage due to impact with each other.

#### 3.5.4.1 Requirements

The detector restraint system must be able to stop the detector from moving about inside the moon pool. At the same time, it must allow the detector to sink or rise as it is filled or emptied. Finally, it must be able to pull the detector up slightly to provide stability to the connection.

#### 3.5.4.2 Mechanism

The detector restraint system uses wheels that can be driven to rotate about their own axis, and to move into or out of the moon pool. These wheels are simply hubs with tires on them. When the detector is in the moon pool, the wheels are hydraulically moved inwards and press against the detector. This pressure creates friction between the tire and the detector. The inward force stabilizes the detector laterally, and the friction stops the detector from moving up and down independently of the wheels.

The fact that the wheels can be driven and that the detector cannot move vertically without the wheels turning means that they can have some influence on the detector's movement. It would take an extraordinary amount of force to hold the detector out of the water while it was being filled; more than the friction between the wheels and detector could supply. However, the wheels can move the detector slightly upwards. By moving the detector upwards, a constant force is imposed between the detector and barge. This constant force acts as a buffer against the environmental forces trying to move the detector and barge separately. With both relative lateral and relative vertical movements restrained, the detector and barge are locked together.

### 3.5.5. Scintillator and oil storage

Storage and transport of the scintillating fluid and oil are primary tasks of the barge. Since the fluids are so sensitive, it would be difficult to find an independent vessel outfitted to properly transport them. Using the barge to transport the fluids makes it possible to pick them up directly from the source and eliminate any third party contamination risks.

### 3.5.5.1 Location

The fluids are stored as far towards the bow as possible. During deployment, fluids are pumped out of the barge and into the detector. This causes the detector to sink, and the barge to rise. Eventually, the barge will rise enough that the recovery slot will come above the waterline. This causes a sharp reduction in waterplane area and buoyancy at the bow. A sharp reduction in buoyancy can cause the barge to change trim and tip forwards. One effect that can counteract the tipping is an uneven reduction in weight. If more weight is removed from the bow than the stern during deployment, then the stern will sink relative to the bow and help flatten the barge. Storing as much fluid as possible in the bow maximizes this effect.

### 3.5.5.2 Hardware

The fluids will be contained in stainless steel tanks throughout the hull. Stainless steel meets the contaminant-free requirements set forth by the UH physics department. The tanks will be subdivided to minimize the free surface effects during as the tanks are filled or emptied.

Transport of fluids into and out of the tanks will take place through stainless steel pipes. In order to ensure the pipes do not harbor any contaminants, they will be electropolished. Electropolishing removes any nooks or crannies that can capture contaminant and protect it from cleaning processes.

## 3.5.6 Pre-cooling Fluids

Pre-cooling the scintillating fluid and oil is proposed as a method of reducing the size of the releasable gravity anchor used to submerge and resurface the detector. It will also reduce the change in volume of the scintillating fluid by eliminating or reducing the temperature-dependent factor.

### 3.5.6.1 System Description

Trane Centra-Vac chillers were analyzed as suitable high capacity cooling systems. The chillers typically produce chilled water which could be run through a heat exchanger that will cool the scintillating fluid and oil. The fresh water has very little temperature-dependent density variability, so it will not be chilled. It also serves to act as an insulator to buffer the cooling oil from heat gain from the environment.

### 3.5.6.2 Heat Analysis

The amount of chilling capacity required depends on the amount of time available for cooling and the rate the fluids take on heat from the environment. The rate of heat gain from the environment is a constant value that is composed of solar radiation and conduction/convection from the air and ocean. Table 3-9 shows the environmental heat gain values Makai has used in this analysis.

Component	Capacity Required
Solar Heat Gain	57 ton AC
Conductive/Convective Heat Gain	307 ton AC

**Table 3-6:** Chilling Capacity Required to Account for Environmental Heat Gain

The variable portion of the chilling capacity needed is tied to the rate at which the oil is to be cooled. There is a fixed amount of energy that must be removed from the oil in order to bring it to the desired temperature. It takes more cooling capacity to remove that energy quickly than to do so slowly. Figure 3-30 shows the required installed cooling capacity and its associated cost as a function of the allowable time to conduct the operation.

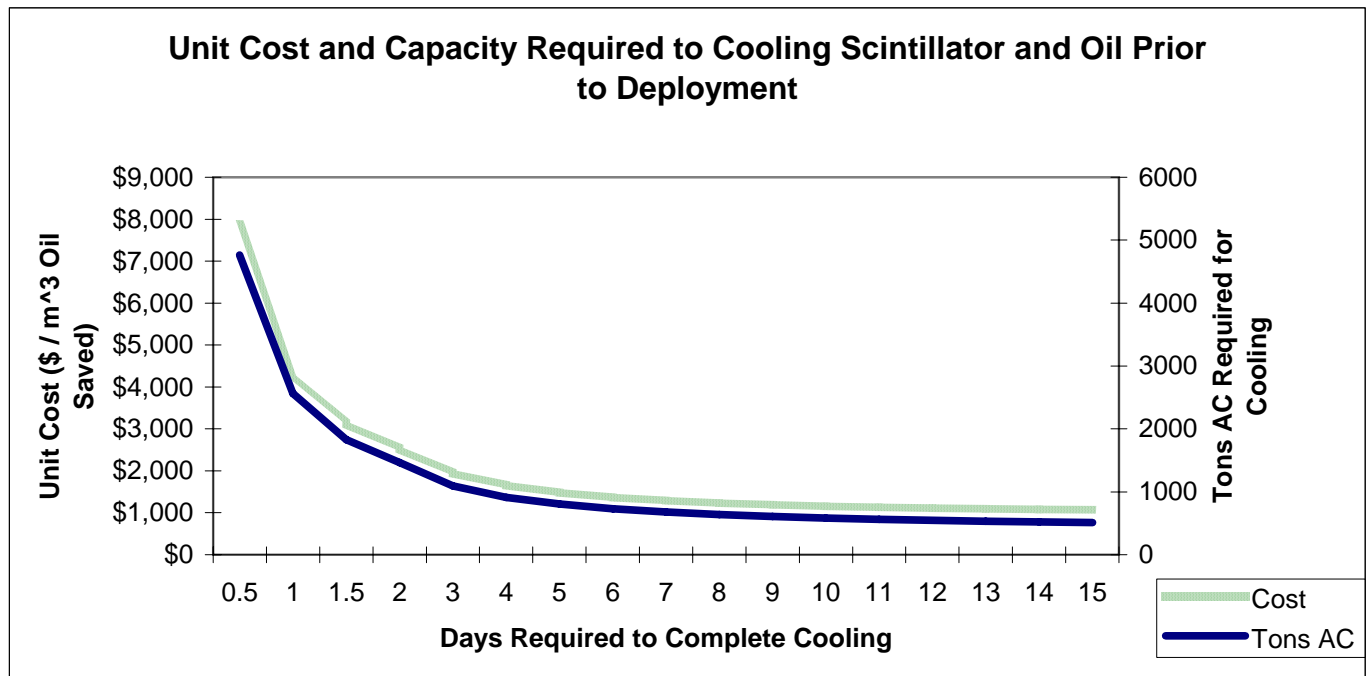


**Figure 3-30:** Cooling Costs and Capacities

The figure shows the trend towards smaller chillers as the allotted time increases. The graph does not tend towards zero because the minimum cooling capacity must be greater than that required to meet the daily environmental heat gain. At extremely long allowable times, the cost will begin to rise again because the amount of fuel required to power the chillers is directly proportional to the amount of time they are required to run.

In light of the trend indicated by Figure 3-30, it is prudent to allow as much time as possible for the cooling process to run. Assuming reverse osmosis is selected as the method of providing fresh water, a long period of time must already be set aside. By allowing the cooling process a comparable time period, there will be no further impact on the vessel's operations. Therefore, Makai has assumed a 10 day cooling period in the following cost analysis. Table 3-7 shows the cooling loads associated with this time period.

Component	Capacity Required
Cooling Oil	47 ton AC
Cooling Scintillator	173 ton AC
Solar Heat Gain	57 ton AC
Conductive/Convective Heat Gain	307 ton AC
<b>Total</b>	<b>583 ton AC</b>

**Table 3-7:** Cooling Loads to Chill Oil and Scintillating Fluid with Over 10 Days

### 3.5.6.3 Capital Costs

The only capital costs considered were the purchase, shipping and installation of the Centra-Vac chillers. Table 3-8 shows pricing guidelines provided by Trane.

Chiller Cost	\$350.00 \$/ton
Installation	\$150.00 \$/ton
Freight	\$30,000.00

**Table 3-8:** Unit Costs for Cooling Process

The total probable capital cost for cooling system is \$324,000.

### 3.5.6.4 Operating Costs

Since the cooling process will be running at the same time as the reverse osmosis process, the only operating cost is the cost of fuel to power the chillers. Trane's product literature indicates the Centra-Vac system requires 0.65 kW of power per ton of air conditioning supplied. This number is combined with the cost of power derived in section 2.5.2, the capacity of the system as shown in Table 3-7, and the 10 day running time to give a total operating cost of \$33,000 per deployment.

### 3.5.6.5 Neglected Costs

The primary neglected costs in this analysis are associated with transferring heat from the oil to the working fluid of the chillers. This could be accomplished by running oil directly through the chillers instead of chilled water, or by using an intermediate heat exchanger. The costs associated with these options depend on a more detailed design than can be done within the scope of this report. Therefore, the costs have been delegated to later phases of analysis.

### 3.5.6.6 Savings

Decreasing the volume change in the detector during deployment has two effects. First, it decreases the size of the releasable gravity anchor that is used to submerge and resurface the detector. The anchor must be big enough to sink the detector in its least dense state just prior to deployment. By cooling the detector, the density of the detector just prior to deployment is increased, and therefore the amount of weight required to sink it is decreased. The amount of concrete required is decreased by 106 m<sup>3</sup>, which amounts to \$106,000 at \$1000 per cubic meter.

The second effect of decreasing the volume change is that less oil and scintillator needs to be reserved as compensation. Compensation bags cost approximately \$106 per m<sup>3</sup> of capacity. Precooling reduces the compensation volume by 299 m<sup>3</sup>. This reduction in volume translates to a savings of \$31,400. In addition to conserving compensator bags, the volume of scintillating fluid and oil required is reduced. At an estimated cost of \$100 per m<sup>3</sup>, the savings in fluids is \$29,900.

### **3.5.6.7 Conclusions and Recommendations**

The capital cost of cooling the oil and scintillator is \$324,000. The savings in capital cost for oil, scintillator, and compensator bags is \$61,300. This leaves a difference of \$262,700. The operating cost of precooling the fluids is \$33,000 per deployment in fuel. The benefit per deployment is a \$106,000 savings in anchor concrete. This results in a net savings of \$73,000 per deployment. Using a simple payback analysis, the precooling system would pay itself off in four deployments.

At this stage in the design, with only a single detector being serviced by the barge, a payback of four deployments is not sufficient to justify installing the precooling system. If, however, future designs account for multiple detectors served by the same barge or an extremely long lifetime, the precooling system will need to be re-evaluated.

## **3.5.7. Freshwater production – reverse osmosis**

### **3.5.7.1 System Description**

The reverse osmosis system required to produce enough fresh water for the Hanohano project stretches the state of the art in system size. Pure Aqua has a 182,000 gallon per day system that meets the project needs, and it is this system that the following description is based on. The system includes pre-filtration equipment and up to two phases of reverse osmosis.

The pre-filtration step is required to protect the reverse osmosis membrane from both dissolved and suspended solids in the working liquid. Seawater can be particularly harsh on membranes due to the fact that it contains high concentrations of dissolved solids and variable concentrations of suspended biological material. Pure Aqua recommends a 10 micron sand filtration tank, a 5 micron filtration bag, and finally a 1 micron filter cartridge as a complete pre-filtration system. The system will occupy 5 tanks measuring 8 feet in diameter by 9 feet tall. The space required for such a system has been included in the probable cost analysis.

The first phase of reverse osmosis will produce 182,000 gallons of drinking water (200-500 PPM dissolved solids) from 455,000 gallons of seawater (42,000 PPM dissolved solids) each day. The discrepancy between seawater intake and freshwater output is due to the need to avoid precipitation of dissolved solids in the brine solution that is a byproduct of the reverse osmosis process.

The second phase of reverse osmosis is optional. It is capable of taking the 182,000 gallons of drinking water from the first phase, and producing 146,000 gallons of high-

purity water (2-5 PPM dissolved solids). The need for the second phase has not yet been established, but it has been assumed present in the analysis.

### 3.5.7.2 Capital Costs

The primary cost of a reverse osmosis system that sees intermittent use is the capital cost for the equipment. Table 3-9 below itemizes the costs of each component of the system.

1st Phase	\$250,000.00
2nd Phase	\$80,000.00
Prefilter	\$50,000.00
Feed Pump	\$20,000.00
Space and Installation	\$200,000.00
<b>Total</b>	<b>\$600,000.00</b>

**Table 3-9:** Capital Costs of Pure Aqua 180,000 GPD Reverse Osmosis System

### 3.5.7.3 Operating Costs

One part of the cost of operating the reverse osmosis system is the cost of the diesel fuel required to run a generator that supplies the needed electricity. Product literature from Pure Aqua indicates the system consumes about 100 kJ of energy per gallon of water produced. Based on the cost of power derived in section 2.5.2, the operating cost of the reverse osmosis system is \$21,000.

The second part of the operating cost is the cost of the time required to complete the operation. Even with the 182,000 GPD system, it will take 14 days to fill the detector with high-quality water. At an estimated cost of \$30,000 per day, the operation would cost \$424,000.

### 3.5.7.4 Neglected Costs

Some of the true cost of reverse osmosis overlaps with general vessel construction costs. For example, the ship's power grid must be capable of supplying the needed power to the reverse osmosis pumps. However, it is unknown at this time if additional capacity beyond that which is required for standard ship operations will be needed. Therefore, the costs for generating equipment have been neglected in this analysis. By similar logic, the costs for plumbing the system into the detector and seawater inlet pipe have not been considered.

### 3.5.7.5 Savings

The benefit of utilizing reverse osmosis technology is that the vessel does not have to store fresh water while underway. The vessel cost analysis presented in section 2.4.6 gave an approximate cost of \$500 per dead weight ton. The 2 million gallons of water required by Hanohano would cost about \$3.9 million in vessel capital cost. The cost of transporting the extra volume has not been considered.

### 3.5.7.6 Conclusion and Recommendations

Overall, the probable cost of a single deployment using reverse osmosis to provide the fresh water would be a little over \$1 million. The unit cost would be \$0.51 per gallon of fresh water.

The cost for carrying fresh water on a single deployment would be \$3.9 million. The unit cost would be \$1.89 per gallon. With a probable savings of \$1.38 per gallon, the analysis indicates that reverse osmosis is strongly favored as a cost effective method of providing fresh water to the detector. At this stage, Makai recommends pursuing reverse osmosis as the sole source of fresh water for the project.

## 3.6 COST ESTIMATE

The total cost for the Hanohano project consists of construction costs and deployment costs. The construction costs encompass all costs to build the detector and the costs of scintillating fluid and oil. The deployment costs encompass the costs to clean and calibrate the detector, towing to and from the site, deployment, recovery, the cost of producing freshwater, and the cost of the releasable anchor. Note that many of the costs are dependent upon more detailed design, and have been roughly approximated in this analysis.

### 3.6.1. Construction Costs

The construction costs have been separated into the detector construction costs and the barge construction costs. This separation will facilitate future work in analyzing the benefits of supporting multiple detectors from a single barge.

#### 3.6.1.1 Detector costs

The bulk of the detector costs consist of electronics to collect and transmit data. The electronics system includes the PMT modules, connections to 64 bit digitizers, the digitizers themselves, a multiplexer control module, a power control and conditioning unit, and equipment to calibrate the detector. A variety of cables and connectors are assumed in the prices for the above components. The costs are based on past experience with anti-neutrino detectors. A total of \$21.8 million is required for these components. Table 3-10 shows the electronics cost breakdown.

Component Costs	Number	Units	Unit Cost	Item Cost	Category Cost
<b>Electronics</b>					<b>\$21,755,000</b>
Photomultiplier Tube Modules - similar to ICECUBE	4350	ea	\$4,500.00	\$19,575,000	
64 Channel Digitizers and Connections	64	ea	\$20,000.00	\$1,280,000	
Multiplexer Control Module	2	ea	\$100,000.00	\$200,000	
Power Controller and Conditioner	1	ea	\$200,000.00	\$200,000	
Calibration Gear	1	ea	\$500,000.00	\$500,000	

**Table 3-10:** *Electronics Costs*

The second largest cost for the detector is its materials and construction. This includes the steel for the inner and outer walls, PMT compartments, compensation bags, and concrete ballast, but not the releasable anchor. The costs are based on construction costs typical of modern vessels, budgetary quotes from pillow tank suppliers, and previous experience

with precast concrete anchors. The components cost a total of \$5.9 million. Table 3-11 shows the detector construction cost breakdown.

Component Costs	Number	Units	Unit Cost	Item Cost	Category Cost
<b>Construction</b>	<b>\$5,870,500</b>				
Detector Structural Steel	1600	tonne	\$3,500.00	\$5,600,000	
Concrete Ballast	541	m <sup>3</sup>	\$500.00	\$270,500	
<b>Compensation</b>	<b>\$91,949</b>				
Compensator Bags	945	m <sup>3</sup> stored	\$97.30	\$91,949	

**Table 3-11:** Detector Construction Costs

The final aspect of the detector cost is the cost of scintillating fluid and oil. These fluids cost a total of \$1.5 million. The costs are based on past experience with scintillating fluids in other anti-neutrino detectors. Table 3-12 shows the scintillator and oil cost breakdown.

Component Costs	Number	Units	Unit Cost	Item Cost	Category Cost
<b>Fluids</b>	<b>\$1,452,800</b>				
Scintillating Fluid Delivered to Barge	10558	m <sup>3</sup>	\$100.00	\$1,055,800	
Oil Delivered to Barge	3970	m <sup>3</sup>	\$100.00	\$397,000	

**Table 3-12:** Scintillator and Oil Costs

Overall, the detector will cost \$29.1 million.

### 3.6.1.2 Barge costs

The largest portion of the detector cost is for the materials and construction of the vessel itself. These costs have been estimated based on typical costs for modern vessels. The barge's construction will cost \$6.2 million. Table 3-13 shows the construction cost breakdown.

Component Costs	Number	Units	Unit Cost	Item Cost	Category Cost
<b>Construction</b>	<b>\$6,192,500</b>				
Barge Structural Steel	2477	tonne	\$2,500.00	\$6,192,500	

**Table 3-13:** Barge Construction Costs

The next portion of the barge's cost is the reverse osmosis equipment needed to produce fresh water. The cost is based on a budgetary quote by Pure Aqua. The equipment costs \$520,000. Table 3-14 shows the reverse osmosis equipment cost breakdown.

Component Costs	Number	Units	Unit Cost	Item Cost	Category Cost
<b>Reverse Osmosis Equipment - 182,000 gallons per day</b>	<b>\$520,000</b>				
Equipment FOB Factory	1	ea	\$320,000.00	\$320,000	
Delivery and Installation	1	ea	\$200,000.00	\$200,000	

**Table 3-14:** Reverse Osmosis Equipment Costs

The third portion of the barge's cost is the machinery needed to move and purify the scintillator. This includes pumps, motors, and purification equipment. It was beyond the scope of the this study to select specific purification equipment, therefore the line item for

this equipment has been estimated based on other anti-neutrino detector projects. The total machinery cost for the barge is \$2 million. Table 3-15 shows the machinery cost breakdown.

Component Costs	Number	Units	Unit Cost	Item Cost	Category Cost
<b>Machinery</b>					<b>\$2,090,417</b>
Scintillator Pump - 4200 GPM	1	ea	\$46,866.00	\$46,866	
Motor	1	ea	\$5,400.00	\$5,400	
Oil Pump - 1850 GPM	1	ea	\$35,750.50	\$35,751	
Motor	1	ea	\$2,400.00	\$2,400	
Scintillator Purifying Equipment	1	ea	\$2,000,000.00	\$2,000,000	

**Table 3-15:** *Machinery Costs*

The final cost for the barge is the plumbing required to transfer scintillator and oil to and from the detector. These costs have been based on standard piping costs in Makai's experience. The total plumbing cost is \$168,000. Table 3-16 shows the plumbing cost breakdown.

Component Costs	Number	Units	Unit Cost	Item Cost	Category Cost
<b>Plumbing</b>					<b>\$167,804</b>
Scintillator Fill Pipes - 12" HDPE Pipe	200	m	\$29.50	\$5,900	
Oil Fill Pipe - 8" HDPE Pipe	100	m	\$13.49	\$1,349	
N2 Drain and Fill Lines - 1/2" Stainless Steel Pipe	1020	m	\$11.29	\$11,516	
Installation	850	joints	\$3.74	\$3,179	
Oil Drain and Fill Lines - 3" Stainless Steel Pipe	1020	m	\$100.00	\$102,000	
Installation	850	joints	\$51.60	\$43,860	

**Table 3-16:** *Plumbing Costs*

The total cost for the barge is \$9.0 million.

### 3.6.2. Deployment costs

The most expensive deployment cost is transporting the vessel. A nominal 30 days of transport has been allotted. This includes cost for both a tug, and operating the barge itself. It does not include costs for the time required to produce fresh water. Those costs are included separately under the fresh water production table. The costs are based on typical rates for a large tug in Hawaii. A total of \$900,000 has been allotted for transportation costs. Table 3-17 shows the transportation cost breakdown.

Component Costs	Number	Units	Unit Cost	Item Cost	Category Cost
<b>Transportation</b>					<b>\$900,000</b>
Tug - 3400hp in Honolulu	30	day	\$20,000.00	\$600,000	
Barge Operation	30	day	\$10,000.00	\$300,000	

**Table 3-17:** *Transportation Costs*

The next deployment cost is the cost of manpower required to prepare and man the detector. This analysis assumes that each deployment will require the replacement of some PMTs, Lexan panels, electrical connectors, and re-cleaning the surfaces in contact with the scintillator and oil. It also includes the cost of the manpower beyond standard crew

required on deployment and recovery operations. The costs are based on costs to employ technicians, graduate students, and professors. The total personnel cost per deployment is \$544,000. Table 3-18 shows the personnel cost breakdown.

Component Costs	Number	Units	Unit Cost	Item Cost	Category Cost
<b>Personnel</b>	<b>\$544,000</b>				
PMT Installation, Cleaning, a Deployment Team	120	man-month	\$3,200.00	\$384,000	
	20	man-month	\$8,000.00	\$160,000	

**Table 3-18:** Personnel Costs

The final deployment cost is that for disposable materials. These include the fresh water produced by reverse osmosis and the releasable anchor. The freshwater production cost is detailed in section 3.5.7.3, and the concrete cost is based on past experience with precast concrete anchors. The total cost for disposable materials is \$584,400.

Component Costs	Number	Units	Unit Cost	Item Cost	Category Cost
<b>Disposable Materials</b>	<b>\$584,409</b>				
Concrete Releasable Anchor	448	m^3	\$500.00	\$224,000	
Fresh Water Made Via Reverse Osmosis	7796	m^3	46.23	\$360,409	

**Table 3-19:** Disposable Materials Cost

Overall, the each deployment costs \$2 million.

### 3.6.3. Summary

To address the possibility of a single barge serving multiple detectors, the cost estimate has been broken into capital costs and deployment costs. The capital costs for the Hanohano project include \$29.1 million for the detector, and \$9.0 million for the barge, for a total of \$38.1 million. The deployment costs total \$2.0 million. The total cost for the project and a single deployment is \$40.2 million. Table 3-20 shows the overall cost summary.

<b>Total Cost</b>	<b>\$40,169,378</b>
<b>Barge Cost</b>	<b>\$8,970,720</b>
<b>Detector Cost</b>	<b>\$29,170,249</b>
<b>Deployment Cost</b>	<b>\$2,028,409</b>

**Table 3-20:** Hanohano Cost Summary

A detailed summary of project costs, including the entire cost estimate table, has been included in the Basis of Design document in the appendix.

## 4. GLASS SPHERE IMPLOSION ANALYSIS AND TESTING

### 4.1 DESCRIPTION OF THE PROBLEM

#### 4.1.1. PMT pressure housing

The proposed Hanohano anti-neutrino detector will use numerous photomultiplier tubes (PMTs) deployed in the deep ocean. To protect the PMTs from the intense hydrostatic pressures at 4000 m depth, they must be housed in individual pressure vessels. In addition, to efficiently containing the geometry of the PMT and electronics, the housing must also be optically clear and radio-pure.

These requirements have steered selection towards using spherical glass instrument housings. These types of housings have been successfully used by oceanographers for some time and, more recently, in other neutrino detector projects, e.g. ICECUBE. The structural symmetry of a sphere gives it phenomenal strength when resisting evenly distributed pressure forces. This high compressive strength is necessary because at 4000 m, the pressure is equivalent to several tons per square inch. Glass is an obvious material selection because of its optical clarity and incredible strength when loaded in compression.

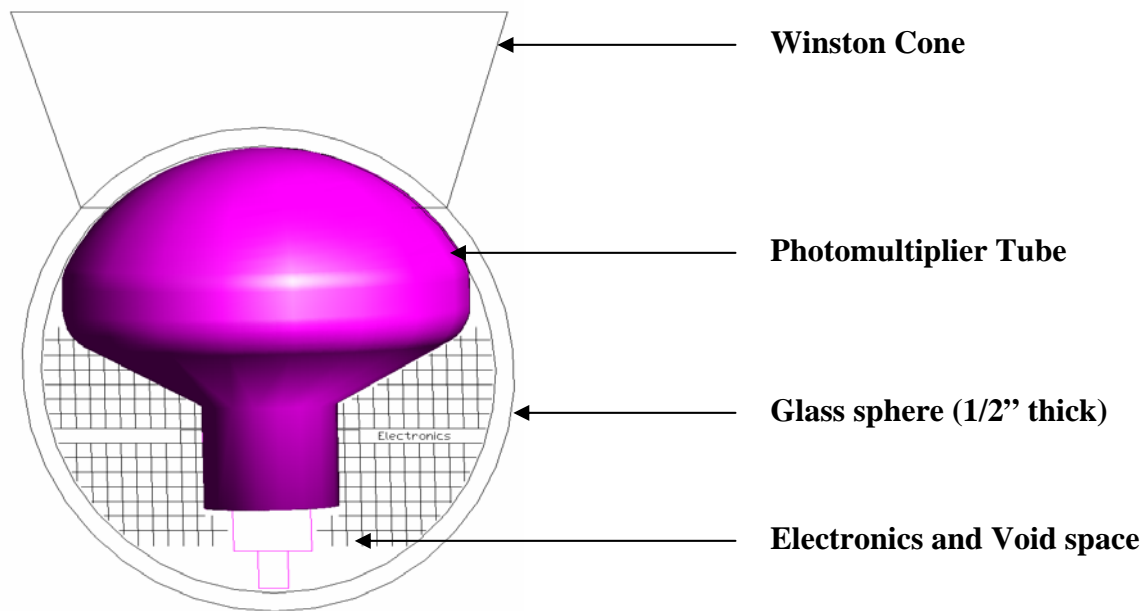


**Figure 4-1:** A PMT housed inside a Benthos 13" outside diameter spherical glass pressure housing.

#### 4.1.2. Glass sphere implosion failure

While hollow glass spheres are very strong in compression, they are not particularly resilient to shockwaves and uneven loading. Lab testing and extensive application in the field show that, in general, spherical glass pressure housings are very reliable, but failures do occur. Failure will invariably be attributable to an uneven loading situation that might

result from imperfection in the glass, incorrect assembly or some unconventional shock loading.

If a sphere happens to fail at depth, the resulting implosion releases a considerable amount of energy. More specifically, the potential energy stored by the sphere is equal to the void volume multiplied by the imposed hydrostatic pressure. The implosion of a 13" diameter spherical void at a depth of 4000 m will release (at a comparable rate) an amount of energy equivalent to that which is stored in approximately 150 g of high explosive. Following an implosion failure, some of this stored energy is released as acoustic energy; emanating as a shockwave.

#### 4.1.3. Sympathetic implosion

The chances of a sphere failing are small, and a single failure or even several independent failures throughout the detector would have virtually no effect on operability. However, the Hanohano detector will use several thousand spheres in close proximity and a major concern is the shockwave resulting from a single implosion failure could set off a catastrophic chain reaction of implosions among the surrounding spheres. This domino-effect failure mechanism is termed “sympathetic implosion” and has been experienced in a variety of physical contexts or systems.

The most pertinent example of a catastrophic sympathetic implosion event occurred at the flagship neutrino detector “Super-K”. During a routine filling operation on November 12<sup>th</sup> 2001, approximately 7,000 of the 11,146 photomultiplier tubes (22" diameter, roughly spherical in shape) were destroyed. The sound of PMTs successively imploding could clearly be heard by scientists in the nearby control room. This event highlighted the risk of having so many frail PMT's close together in a pressurized fluid. (Picture to right – Courtesy: Kamioka Observatory, ICRR(Institute for Cosmic Ray Research), The University of Tokyo).



## 4.2 IMPLOSION STUDIES

### 4.2.1. Background

Previous work on imploding spheres has concentrated on gaining a better understanding of the formation of shock waves by physically imploding 17" diameter glass spheres [Ore & Schoenberg, 1976]. There are also some examples of intentional glass sphere implosion being used as an acoustic source for calibration of hydrophone listening arrays in the deep ocean. To our knowledge, no studies have specifically focused on sympathetic implosion of glass spheres in the deep ocean. Anecdotal information from glass sphere manufacturer

Benthos suggests that the implosion of one glass sphere in close proximity to another could cause the second sphere to fail. Both destruction and survival situations have been experienced in the pressure testing tank at the Benthos labs.

In the 1990's, the University of Hawaii performed some studies to evaluate the effect of these shock waves on cabling and mooring components for the DUMAND project [Gorham, Rosen, Bolesta, Learned, Reise, 1999]. This study showed that the deep water implosion of a glass sphere releases a significant amount of energy; enough to damage steel and titanium structural elements in close proximity to the implosion.

Other efforts include numerical simulations to evaluate the relative vulnerability of the MiniBoone detector compared with the geometry in the Super K [Brookhaven National Laboratory]. Unfortunately, the physical situation and parameters of these detectors is quite different from the proposed deep ocean Hanohano. The implosion experience at Super K was with PMT's directly exposed in a much lower pressure environment.

#### 4.2.2. Implosion mechanism overview

A deep ocean implosion of a spherical void results in a large release of energy. Some of this energy is transferred to acoustic energy and hence a given implosion has a characteristic acoustic signal. The significant features of the acoustic signal are an initial negative pressure wave as the sphere collapses, followed by a large spike after the momentum collision at the center of collapse. To help explain the mechanism of implosion, the idealized case of a perfect sphere collapsing is given stepwise consideration:

- Collapse Begins
- Initial pressure drop propagates radially out as acoustic wave
- Entire water mass begins accelerating radially inward
- In-falling surface of cavity decreases in area as  $1/r^2$
- Velocity therefore increases at same rate
- Water mass meets at center
- Acoustic pressure wave formed from momentum of collision
- Wave propagates radially out

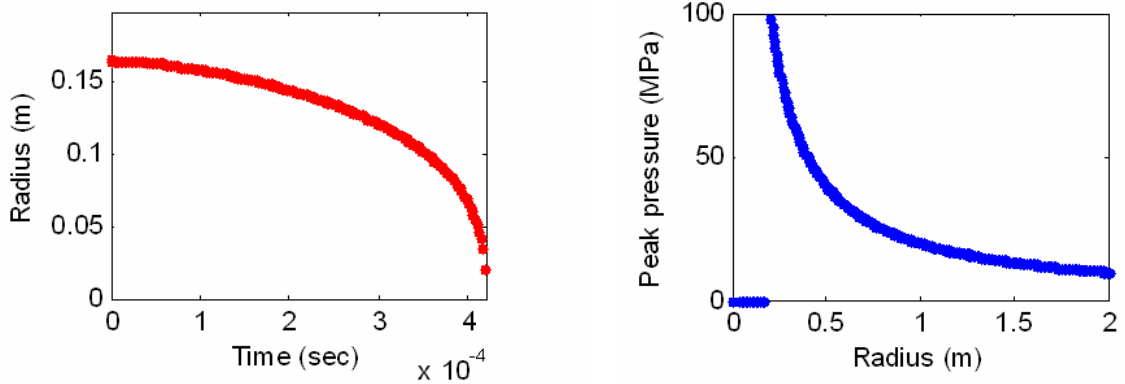


**Figure 4-2:** Once the sphere implodes, the in-falling surface of cavity rapidly accelerates towards the center. The huge momentum collision at the center forms a shockwave with a large peak overpressure. By spreading alone, the pressure attenuates as  $1/r$ .

#### 4.2.3. Acoustic shockwave

As the shockwave emanates out, the pressure attenuates by  $1/r$ , where  $r$  is the distance from the center of the implosion. Any object in close vicinity of the implosion will experience an implied stress due to the overpressure of the shockwave. The maximum implied stress as described by Gorham et al. (1992) is:

$$P_{\max}(r) = \frac{1}{r} P_{\max}(1m) 10^{D\alpha(f)/20}$$

where :

$P_{\max}(1m)$  = peak pressure referenced to 1m

$D$  = depth in km

$\alpha(f)$  = spectral attenuation coefficient in dB/km

$f$  = frequency in Hertz

Since the imploding sphere and a prospective target sphere are the same diameter, the characteristic length of the implosion shockwave presents the worst case for the target sphere; the greatest possible differential pressure over the sphere (see Figure 4-3).

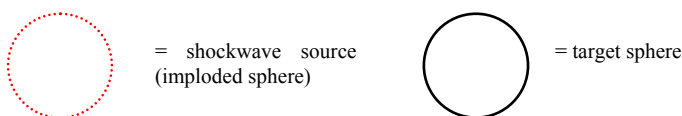
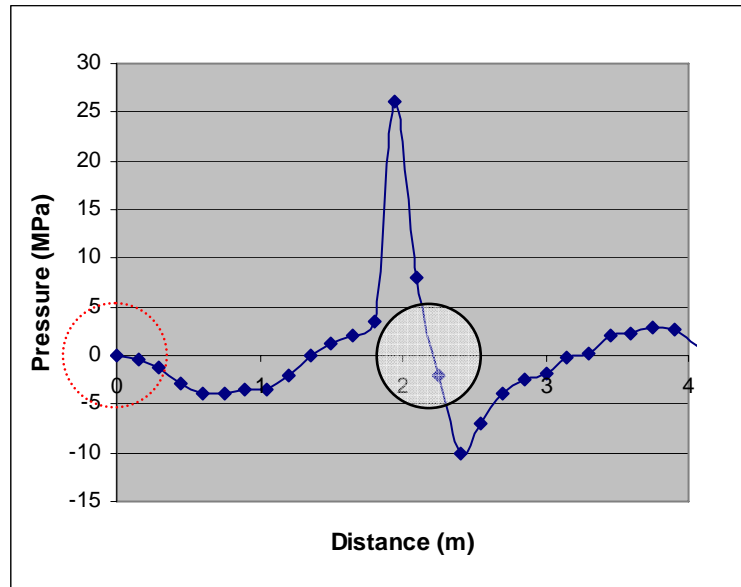


**Figure 4-3:** The peak under-pressure and peak over-pressure appear at opposing extremes of the target sphere; resulting in a large delta  $P$ . The implosion wave shown is for a 17" sphere in ~4400m depth, referenced to 1m standoff and is derived from experimental data [Orr and Schoenberg 1976]

### 4.3 MITIGATION OPTIONS

The ultimate goal is to have a reliable strategy for preventing successive implosions of spheres.

We propose to investigate three methods of preventing successive implosions of glass spheres. One method, or some combination of the three, may prove to be effective in eliminating implosion risk.

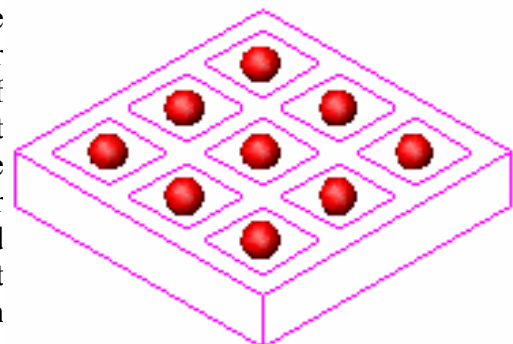
- Reduce the shock wave intensity by incorporating energy absorption materials inside all available free space within the sphere. For instance, deformable and crushable materials will slow the sudden collapse and absorb energy. This reduces the total energy released and widens the release period, thereby reducing the intensity.
- Insert structural elements inside the sphere to force the implosion and the resulting shock wave to be non-symmetrical. Thus, the primary energy could be directed along a radial line either directly into the detector or directly outward (ie, away from adjacent detectors).

- Provide shielding/protecting materials for the adjacent spheres. The oceanographic community believes based on practical experience that plastic and elastomeric “hardhats” help prevent successive implosions. Protection concepts would include: glass sphere coatings, elastomeric shields, rigid shields, soft absorption pockets and sacrificial devices.

We propose several tools for solving this problem. The first will be an analytical modeling of the shock wave and numerical efforts to reduce, reshape and absorb the energy released. This numerical approach will not be able to precisely predict the results of this implosion and whether the adjacent sphere implodes or not. The analytical approach will result in a variety of techniques that should be tested. In order to sort through a variety of concepts at a relatively low cost, we propose a scaled-down "proof of concept" test that will compare various methods (combinations of the above three). The scaled-down test will involve smaller and weaker spheres in shallower water. The most promising concepts will be evaluated during a full scale at-sea test at the appropriate water depth for Hanohano. Pairs of spheres will be mounted to a frame, and one of the spheres will be pre-weakened by grinding a flat on one side to serve as the imploding sphere. The frame will be lowered until the pre-weakened sphere implodes. The objective will be to confirm survivability of the adjacent sphere due to the shock waves generated by the imploding sphere.

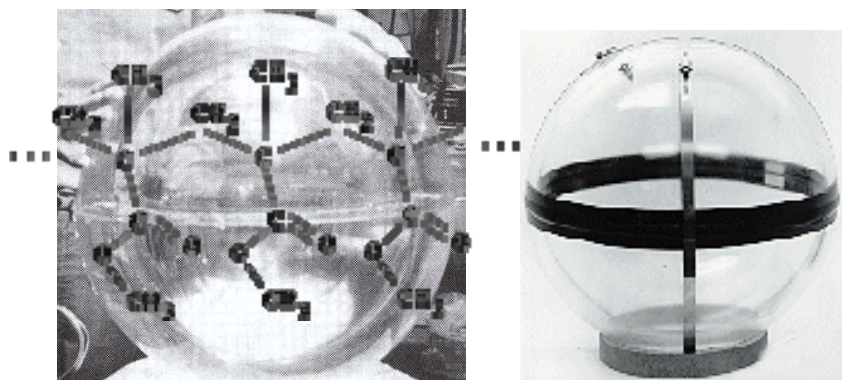
#### 4.3.1. Modular arrangement

The full size Hanohano detector will have 2000 photo detectors housed in spheres. These will be mounted around the periphery of the scintillator arranged in modules. By separating the array of PMTs-in-spheres into modules of 9 it is hoped that a catastrophic failure of one sphere will cause the failure (or partial damage) to, at most, 8 other photo-detectors and ancillaries. This is considered to be a prudent damage limitation strategy, since it is anticipated that the detector will retain functionality even in the event a modest number of PMTs become inoperable.



#### 4.3.2. Alternate materials for sphere – acrylic vs glass

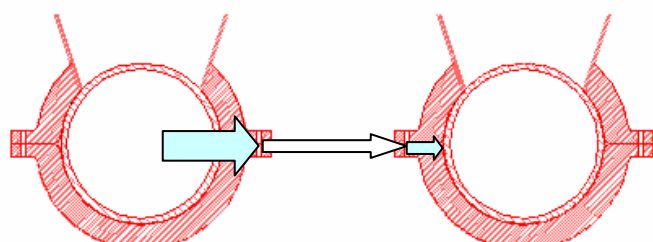
Glass spheres assembled from two hemi-spheres are commonly used for flotation applications and housing underwater instrumentation. This is a standard, commercially available product; the overall diameter typically 12-18 inches and the wall thickness 0.5-2 inches. Glass is used because of its optical clarity, ease of manufacture, low cost and incredible compressive strength. The downside to glass is its poor tensile strength and poor toughness. These latter properties mean the glass spheres are susceptible to brittle fracture and readily implode if hit with a shockwave of sufficient magnitude.



It has been proposed the spherical pressure vessels be fabricated from acrylic. Acrylic has greater fracture toughness and is more malleable than glass. For decades acrylic has been used with success in the construction of Pressure Vessels for Human Occupancy (PVHO). Acrylic is not as strong in compression as glass. Consequently, a larger wall thickness is needed to sufficiently resist the hydrostatic pressure; typically 3-4 inches. Potential challenges faced in using acrylic are: limited historic use for this application, not a standard product, chemical incompatibility, inelastic behavior (creep).

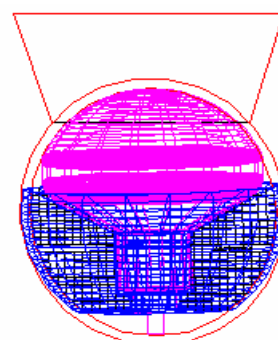
#### 4.3.3. Hardhats around sphere

It is common practice to encapsulate glass spheres (used for deep ocean applications) within plastic “hardhats”. The hardhats are a standard product sold by the suppliers of the glass spheres. There are several variations in design, typically they are fabricated from polyethylene and are assembled in two halves fastened at the centerline flange. For our application, custom made hardhats could be used with a provision for the Winston cone. The hardhats will provide protection during storage, handling, deployment, installation and in service. It is anticipated that the hardhats will provide modest attenuation of a shockwave in the event of a sphere implosion. They may help to absorb some of the outward radiated energy from an imploding sphere as well as shield an intact sphere from the oncoming shockwave.



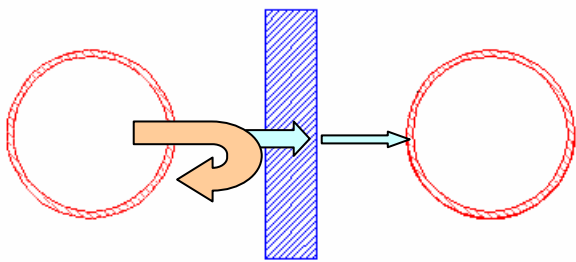
#### 4.3.4. Fill voids in sphere

Since the energy released from an implosion is proportional to the volume of the void, it is prudent to fill all possible void space within the sphere. This may be conveniently achieved by fabricating syntactic foam inserts for the void space or pouring a resin/coarse filler matrix into the sphere during assembly. The filler will serve a secondary purpose in supporting the PMT and electronics within the sphere.



#### 4.3.5. Shock absorbent barriers between spheres

In the event of a single sphere implosion, the resulting shockwave will quickly propagate to intact neighboring spheres. By placing a physical barrier between each sphere any shockwave can be attenuated in order to reduce the risk of a sympathetic implosion. The barrier will primarily be designed to absorb the shockwave energy through a mechanism of gross inelastic deformation. Research has found that non-homogenous, non-isotropic syntactic foams can be effective at absorbing shock wave energy. That is, foams with various size fillers and a multitude of discontinuities. In addition to absorption, the mismatch of acoustic impedance between the seawater and the barrier will result in some reflection of acoustic energy.



### 4.4 ANALYTICAL MODELING

#### 4.4.1. Objective

To computationally model the implosion shock wave and concepts intended to reduce, reshape and absorb the energy released. At this stage, the modeling approach is not expected to precisely predict the results of this implosion and whether an adjacent sphere implodes or not. It is intended that the analytical approach will result in the identification of appropriate scenarios to be tested.

#### 4.4.2. Computer programs for blast and shock effects

##### 4.4.2.1 Applications

Computational methods are proven techniques that are used extensively in commercial engineering design and evaluation. For example, in the automotive industry, crashworthiness design is based on computer simulations which can predict passenger acceleration levels, and hence whether a crash can be survived without serious injury. Use of computer programs can reduce the need for prototype testing, thus providing a potential for reducing overall project costs.

Since there are a limited number of commercial applications for modeling deep water implosions, no computer program is known to have been specifically developed. Instead, we looked to another common application of computational modeling for an adaptable model: blast and shock effects.

##### 4.4.2.2 Availability

The table below summarizes a partial listing of computer programs that have been used to model blast-effects on structures. It has been found that software availability to the private

sector varies, with some codes available for sale, others classified as “export controlled” and some having limited availability due to national security classification.

Some codes were found to have been discontinued, not suitable for the implosion application or simply will not run on a personal computer. In the latter case, these codes are of sufficient complexity to require parallel workstations or serious mainframe hardware.

Several of the codes identified in the table below were found to be suitable and available, and one vendor offered their professional services and would work as a subcontractor to complete the modeling themselves. Unfortunately, it was found that all of the commercial options came at too high of a price for this study.

#### 4.4.2.3 ALE3D

Success was found in one non-commercial model – ALE3D from Lawrence Livermore National Labs (LLNL). Under a collaboration agreement, a version of the ALE3D software was supplied to Makai Ocean Engineering.

**Table 4-1:** *Representative computer programs used to simulate blast effects and structural response.*

Summary of Computational Codes

Name	Purpose	Type	Corporate Author	Reference
BLASTX	Blast prediction	Semi-empirical	SAIC	Britt and Lumsden, 1994
CTH	Blast prediction	First-principle	Sandia National Laboratories	McGlaun et al., 1990
FEFLO	Blast prediction	First-principle	SAIC	Baum et al., 1994
FOIL	Blast prediction	First-principle	Applied Research Associates, Waterways Experiment Station*	Windham et al., 1993
HULL	Blast prediction	First-principle	Orlando Technology, Inc.	Guner, 1992
SHARC	Blast prediction	First-principle	Applied Research Associates, Inc.	Hikida et al., 1988
DYNA3D	Structural response	First-principle	Lawrence Livermore National Laboratory	Whirley and Engelmann, 1993
EPSA-II	Structural response	First-principle	Weidlinger Associates	Atkash et al., 1994
FLEX	Structural response	First-principle	Weidlinger Associates	U.S. Department of Energy, 1992
ALEGRA	Coupled analysis	First-principle	Sandia National Laboratories	Budge and Peery, 1993
ALE3D	Coupled analysis	First-principle	Lawrence Livermore National Laboratory	American Society of Mechanical Engineers, 1993
DYNA3D/ FEFLO	Coupled analysis	First-principle	Lawrence Livermore National Laboratory/SAIC	Löhner et al., 1995
FUSE	Coupled analysis	First-principle	Weidlinger Associates	Sandler and Rubin, 1990
MAZe	Coupled analysis	First-principle	TRT Corporation	Schlamp et al., 1995

#### 4.4.3. Description of the model

##### 4.4.3.1 Arbitrary Lagrangian-Eularian (ALE) 3D code

ALE3D is a three-dimensional, multi-physics finite-element code that is designed to be parallelized. It can also be run on a single workstation and is compatible with a multitude of platforms. It can account for thermal transport, chemistry, advanced materials and incompressible flow. ALE3D utilizes arbitrary Lagrangian-Eularian techniques to simulate fluid dynamics (explicit and implicit) and elastic-plastic response on an unstructured mesh. The grid may consist of arbitrarily connected hexahedra, beam, and

shell elements. The mesh can be constructed from disjoint blocks of elements which interact at the boundaries via slide surfaces.

#### 4.4.3.2 Computational cycle

The basic computational cycle consists of a Lagrangian step followed by an advection step. In the advection step, nodes in selected materials can be relaxed either to relieve distortion or improve accuracy and efficiency. ALE3D thus has the option of treating structural members in a Lagrangian mode and treating materials which undergo large distortions in an ALE mode, all within the same mesh/problem configuration. The code has a range of equation-of-state and constitutive descriptions that are appropriate for modeling hydrodynamic shock phenomena. Several options are available for describing explosive detonations. ALE3D is currently being applied to a number of studies involving the effects of explosive events.

#### 4.4.3.3 Distribution

ALE3D has been distributed under a collaborative licensing agreement by Lawrence Livermore National Laboratory. At the request of the Department of Defense, it is being treated as an export controlled code. The code runs on a variety of workstations. A graphics post-processor, VisIt 1.5, is provided with the code. Mesh generation requires INGRID, TRUEGRID or any other mesh generator that can provide an output file in DYNA3D format.



**Figure 4-4:** The software as supplied from LLNL consists of three significant components. GEN3D – grid and “restart” file generator, ALE3D – The main solver, VisIt – a post processor that can be used to visualize output.

#### 4.4.4. Sphere Implosion

##### 4.4.4.1 Previous studies

Previous work on imploding spheres has concentrated on better understanding the formation of shock waves by the imploding spheres through experimentation [Orr & Schoenberg, 1976]. The University of Hawaii performed some studies to evaluate the effect of these shock waves on cabling and mooring components for the DUMAND project [Gorham, Rosen, Boles, Learned, Reise, 1999]. Other efforts include numerical simulations evaluating the relative vulnerability of the MiniBoone detector as compared with the geometry in the Super K [Brookhaven National Laboratory].

#### 4.4.4.2 Base case

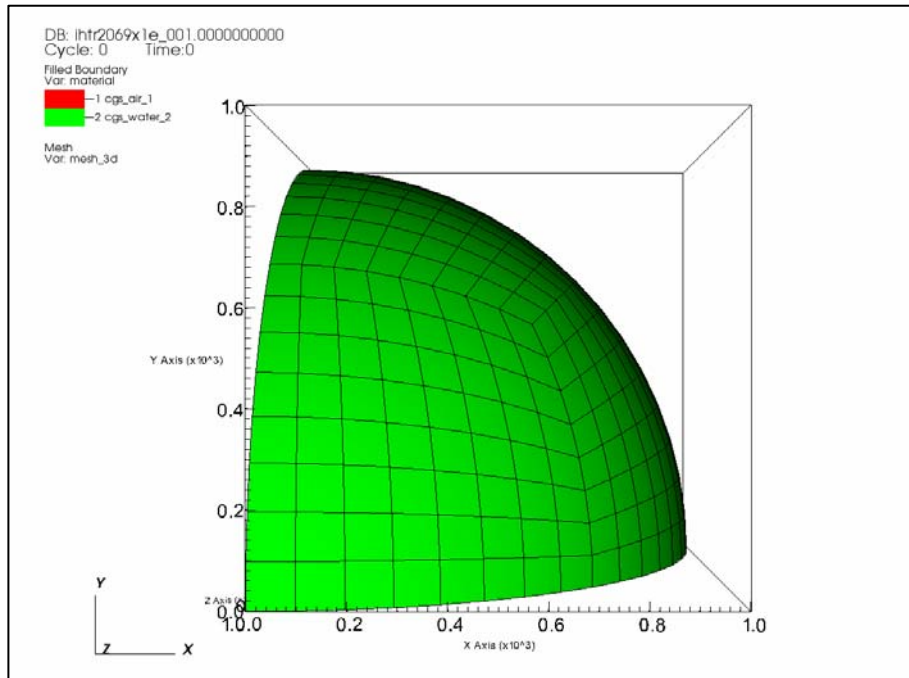
The objective of this computational modeling work has been to simulate the effects of various sympathetic implosion mitigation concepts. The first task was to establish a base case, simply modeling the implosion of a sphere at a depth of 4000 m. The challenge was in not allowing the model to become too complicated, and thus computationally intensive, whilst obtaining results that are as realistic and as accurate as possible. The model setup consisted of an unstructured grid of approximately 12,000 elements forming an eighth of a sphere (see Figure 4-5), thus we are assuming perfect problem symmetry. One of the principle advantages of this type of advective unstructured grid is that the computational effort is applied to the most active region. This is shown in Figure 4-6, below; the grid becomes coarser towards the center of the spherical domain where the implosion and shock wave will be formed.

It was assumed that the PMT pressure housing would consist of a sphere approximately 30 cm in diameter. In the model, the PMT housing was represented as a bubble of air at room temperature and pressure – an eighth sphere radius 15 cm. The bubble was initialized surrounded by seawater at a pressure of 40 MPa (~400 ATM).

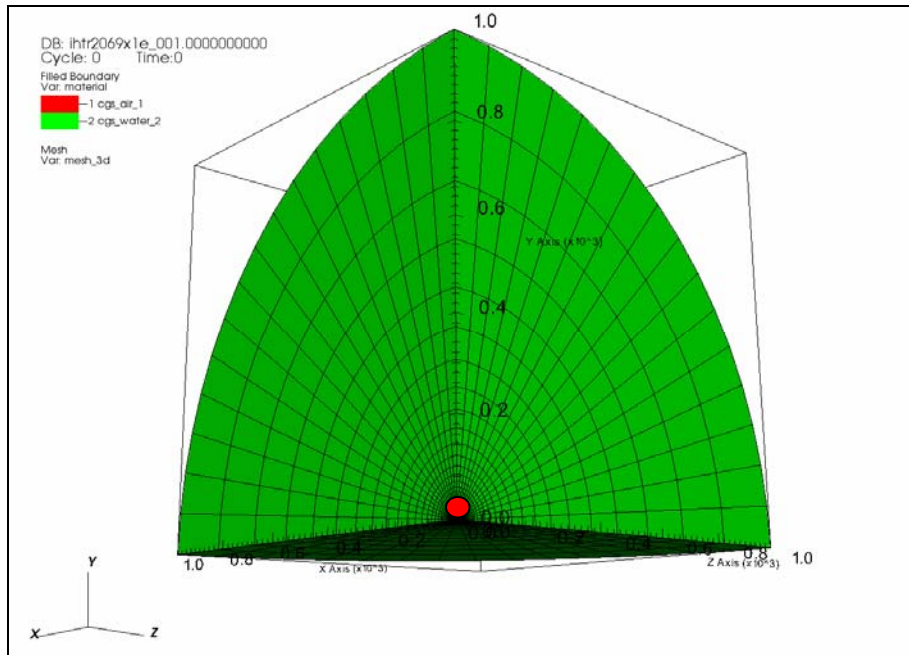
#### 4.4.4.3 Routine

Each simulation consisted of four main steps:

1. Define the physical problem by adjusting key parameters of the input file. The input file consists of a text file several pages in length with the file extension “.in” or “.ain”. Important key parameters are: mesh type, element distribution, time stepping, boundary conditions, initial conditions, output requirements, and material definitions.
2. The input file is directed to “GEN 3D” which performs pre-processing resulting in the creation of a “restart” file. This file contains more detailed run time information, library references, and the grid is built.
3. The input file and “restart” file are directed to the “ALE3D” executable. The model steps through time following the prescribed constraints until completion. Animation files and raw data files are produced according to the requirements set out in the input file.
4. The animation databases that are output from “ALE3D” are viewed using “VisIt”. Raw data can be viewed as a text file or imported to a spreadsheet or database program. An example of raw data is the monitoring of pressure at a particular location as a function of time.



**Figure 4-5:** A view of the eighth sphere domain boundary, radius = 15 cm.



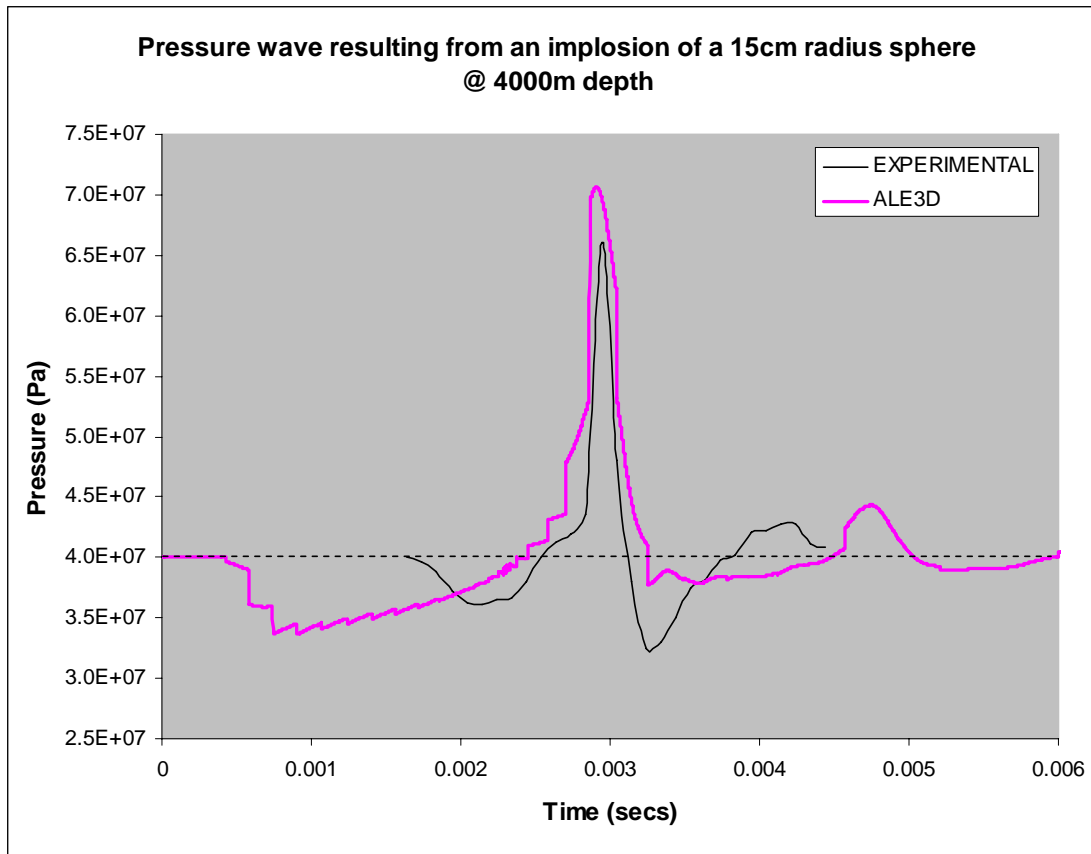
**Figure 4-6:** A radial view of the implosion simulation domain.

Figure 4-7 shows the pressure wave as experienced at 1m from the implosion of a 30 cm diameter sphere located in approximately 4000 m depth. The profiles of two waves are shown; the magenta (thicker) line is the pressure wave as predicted by the ALE3D computational model. This has a peak pressure of approximately 70 MPa (30 MPa above

ambient). The black line (thinner) is the pressure wave derived from implosion test experimental data. This profile shows a peak pressure of 66 MPa. The dotted line indicates the ambient conditions – 40 MPa.

In general, the prominent features of the two profiles are in agreement, although the time scales differ substantially. The pressure signature of the experimental data appears as though it has been compressed when compared with the ALE3D prediction. The following observations are made:

- An initial negative pressure of similar magnitude (-5MPa below ambient) is experienced as the spherical bubble begins to collapse.
- Following complete collapse, the momentum directed towards the center is converted to a sudden peak pressure (shock). The experimental data and the computational model are in close agreement (within 6%).
- After the peak, smaller oscillations about the ambient pressure are observed.
- The experimental data shows a larger and sharper negative pressure immediately following the shock.



**Figure 4-7:** A comparison between an experimentally derived implosion pressure wave (experienced at 1m from the center of the imploding sphere) and the prediction made by ALE3D. Note: for the purposes of comparison,

*the experimental data has been shifted through time such that the peak pressure is aligned with that shown by the ALE3D prediction.*

The computational model considers only a spherical air bubble of the hollow glass sphere's approximate size. The reasonable agreement between experimental and ALE3D predictions lead one to believe that the glass does not play a significant role in the development of the implosion shockwave.

The overall implosion signal is only a few milliseconds in duration. Over the first millisecond, the bubble begins to collapse and a significant negative pressure is felt over the first few meters. Between 2 and 2.5 milliseconds the bubble completely collapses and the shockwave emanates. Subsequently, the shockwave propagates further through the domain.

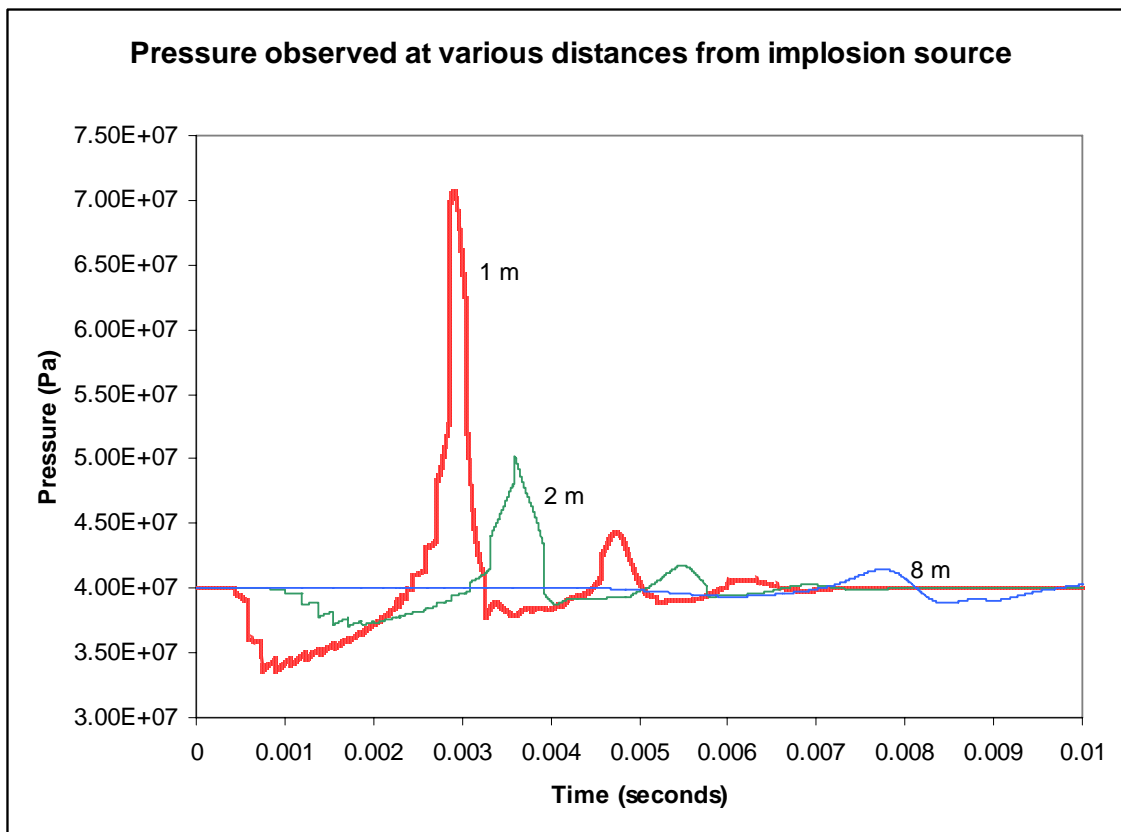


**Figure 4-8:** *It was possible to have the model output pressure as a function of time anywhere in the domain. This figure compares the progress of the spherical pressure wave as it moved past 1m, 2m and 8m radius monitoring positions. The 1/r attenuation of pressure can be seen.*

#### 4.4.5. Fill the void

The implosion of a glass sphere generates a sudden release of energy proportional to its volume times the pressure (>400 atmospheres). The energy released is in excess of 600 kJ. By incorporating energy absorption materials inside all available free space within the

sphere, the shock wave intensity will be reduced. For instance, deformable and crushable materials will slow the sudden collapse and absorb energy – reducing the total energy released and widening the release period (thus reducing the intensity).

The ALE3D computational model has been used to simulate the relative effects of inserting materials into the void space of the sphere. The available space has previously been calculated as 30%. For all cases, the void filling material was representatively placed at the center of the air bubble, forming a smaller inner sphere equal to 30% of the overall volume. Figure 4-9 compares steel and a stiff syntactic foam as a filler. As might be intuitive, the steel reduces the overall energy released, but creates a sharp shock front. The foam is also effective at lowering the energy released (mostly by occupying the void) but also spreads and softens the peak. Figure 4-10 shows the crush characteristics of the foams defined in the model. These characteristics are based upon commercially available syntactic foams designed specifically for the oil industry with precisely controlled crush strength. The application required that when conditions reached preset limits, the syntactic foam undergoes a sudden and dramatic collapse, preventing excessive overpressure.

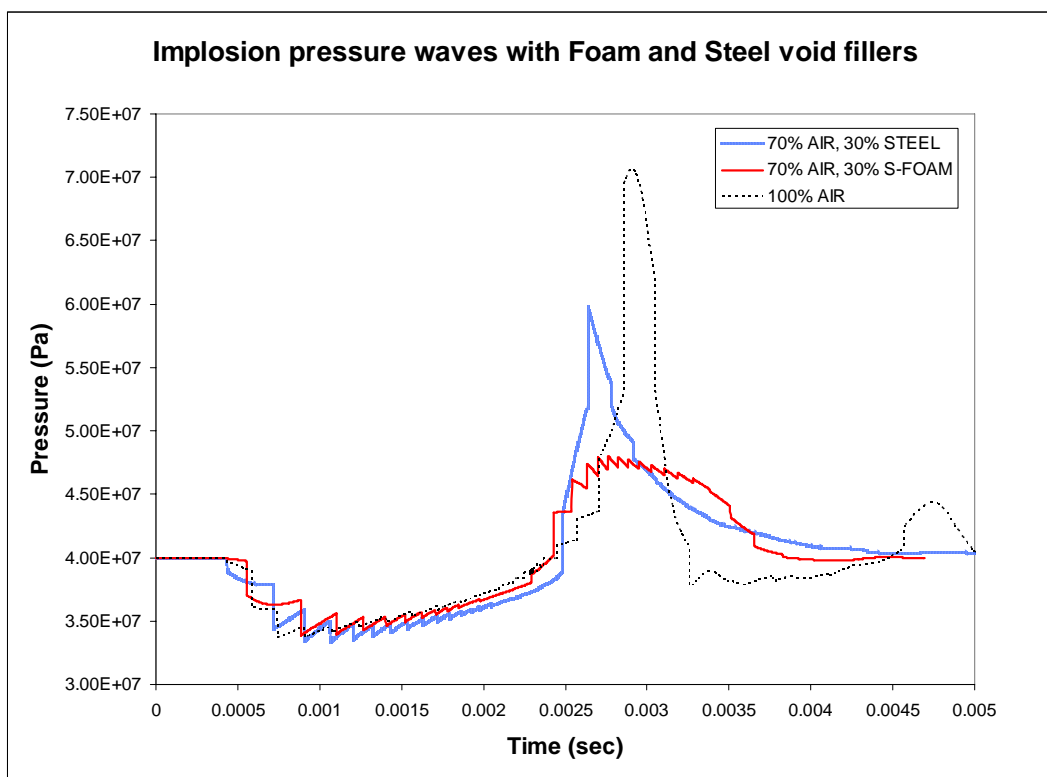


**Figure 4-9:** Comparison of the effect of filling 30% of the void with steel or foam.

The relative performance of three different foam fillers were compared (see Figure 4-11). The profiles of the foams were as follows:

- FOAM 20 – Major deformation begins at 20 psi (138 kPa) crush pressure, continuing until a volume change of approximately 45%
- FOAM 8000 – Major deformation begins at 8000 psi (55 MPa) crush pressure (see Figure 4-10).

- FOAM 12000 – Major deformation begins at 12000 psi (83 MPa) crush pressure (see Figure 4-10).

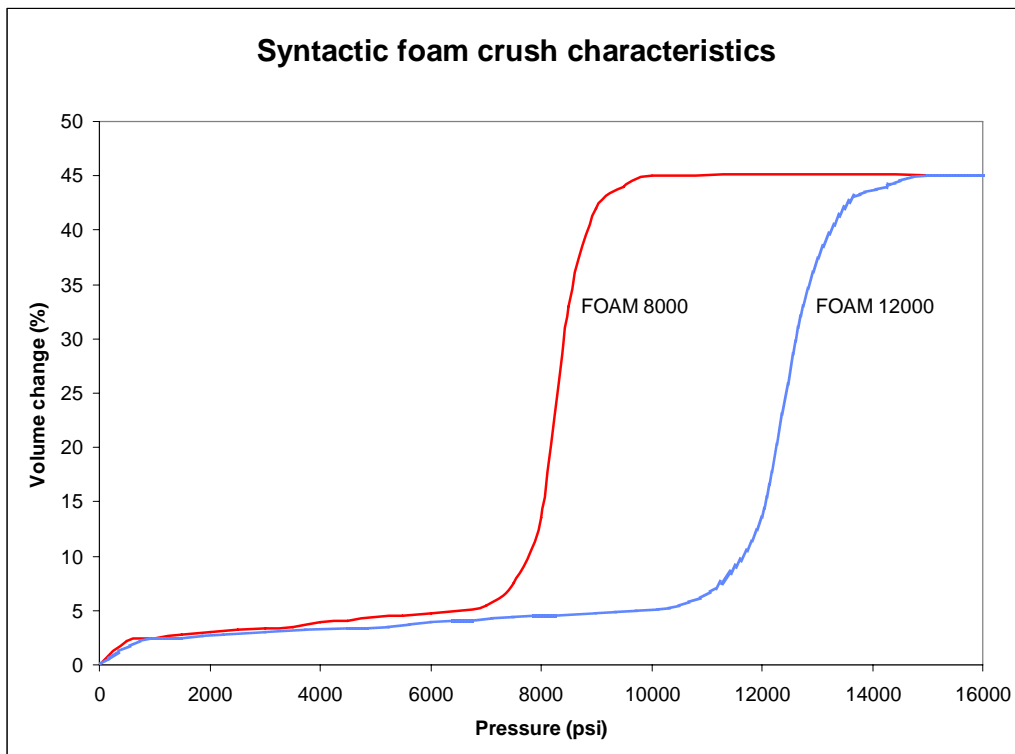


**Figure 4-10:** The basic characteristics of actual commercially available syntactic foams were used in the model. Three foams were considered, the crush properties of two are shown above.

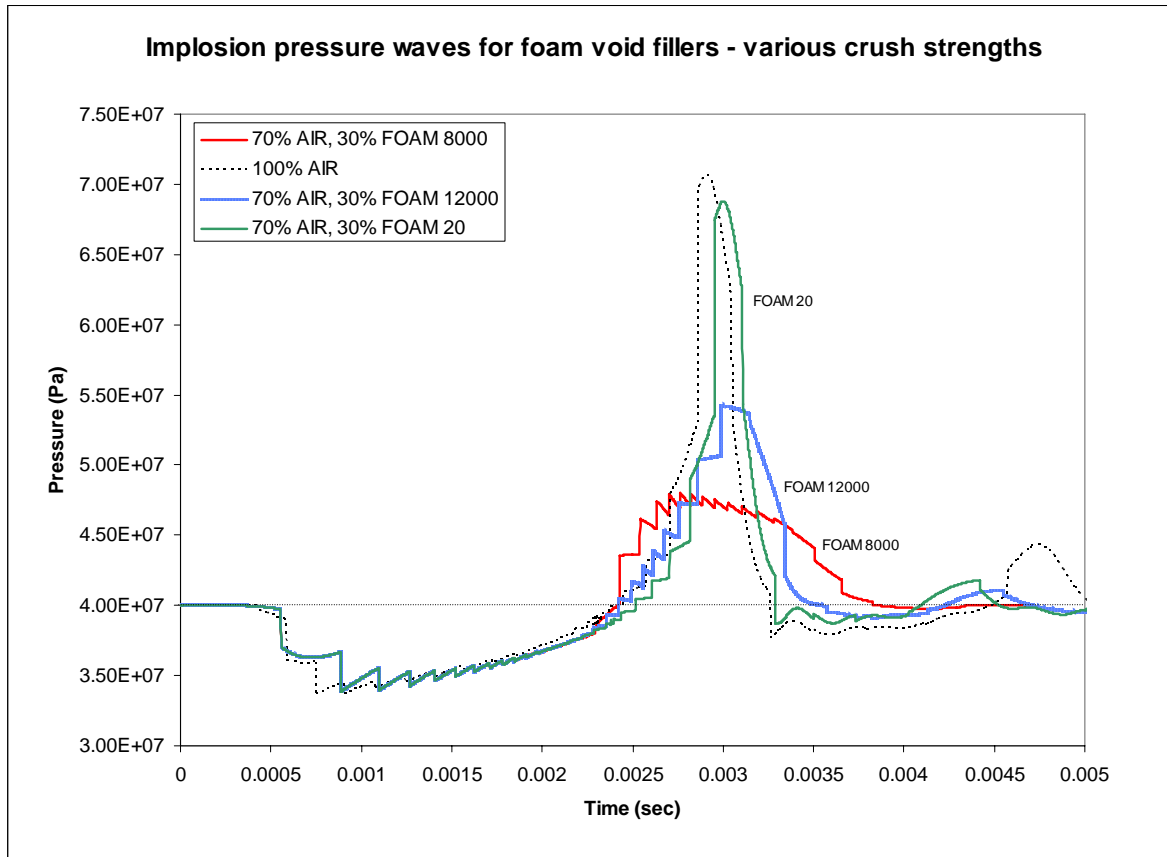


**Figure 4-11:** Simulations were run with various foams occupying 30% of the spherical bubble void. The foams each had unique crush strength characteristics. All pressures are measured at 1m from the implosion source center.

#### 4.4.6. Barriers

##### 4.4.6.1 Setup

The ALE3D model was used to consider the effectiveness of protective barriers between spheres. A sphere separation of 1 meter on center was accepted, and the barrier was placed midway between the spheres. Figure 4-12 shows conceptually the arrangement of implosion sphere and barrier. This screenshot shows deformation of the barrier.

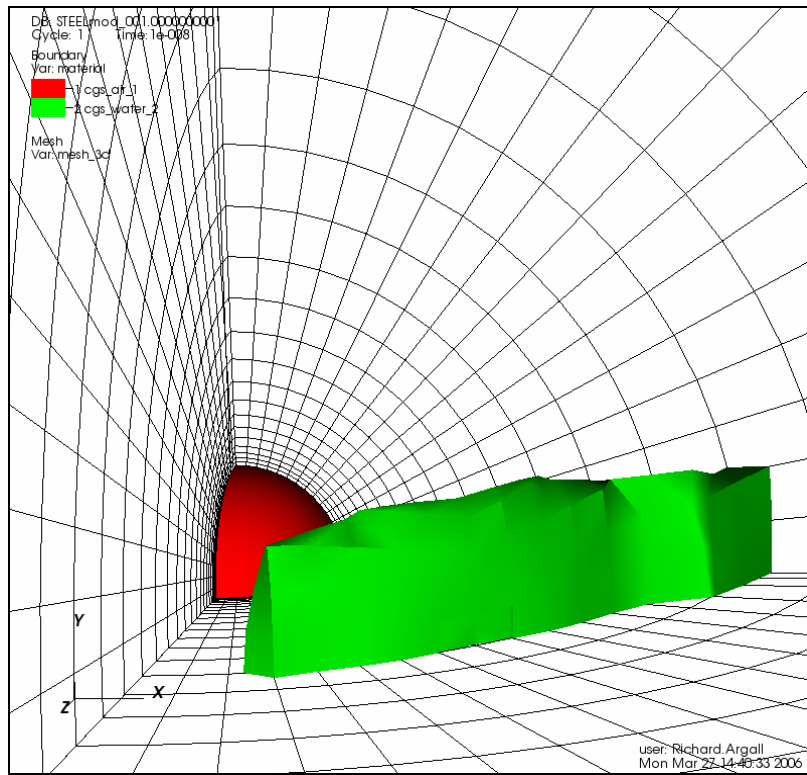


**Figure 4-12:** This figure shows conceptually the arrangement of a barrier at a stand off distance of 0.5 m from the implosion source.

#### 4.4.6.2 Over-pressure attenuation

Several barrier materials were postulated, but because of practical limitations inherent with the model, only acrylic and steel barriers were tested. Figure 4-13 shows the attenuation of the implosion pressure wave for two cases; i) 10cm steel barrier, ii) 3cm acrylic barrier. The initial negative pressure artifact of the signal is approximately 10% deeper when a barrier is present in the domain. To some extent, this may be expected because of the restraining effect.

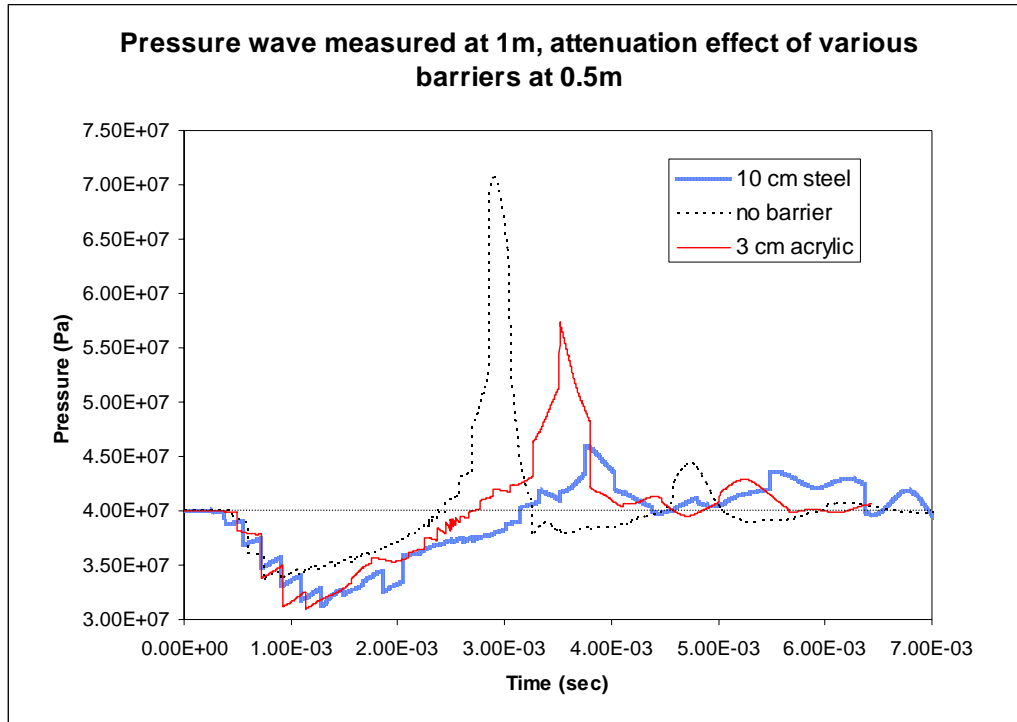


**Figure 4-13:** The attenuation effects of a thick steel barrier and an acrylic barrier. Pressure is measured at 1m from the imploding sphere center.

#### 4.4.6.3 Conclusions

The ALE 3D model produces a good representation of an implosion shockwave. The results compare well with experimental data, which gives us confidence that ALE 3D is able to satisfactorily simulate underwater shockwave phenomena. This computational model shows good potential for further development within subsequent phases of this project. It is envisioned that the entire detector structure could be represented by the model, and not only the physics and effects of implosions considered, but other scenarios such as deployment and recovery dynamics. The primary areas of development will be expansion to a bigger domain, a finer grid and improved profiling of materials used.

## 4.5 PHYSICAL MODELING

It was originally hoped that we could model implosions with weaker and lower-energy spheres. Light bulbs have previously been used as a weak acoustic source and this was a favored candidate to perform some tests in a shallower, more observable environment. Unfortunately, dimensional analysis revealed that the physics would not allow meaningful scale modeling. The most confining restriction: model tests would have to be conducted at the same depth as the intended real scenario to be a fair representation. In other words, a technique suitable for protecting a light bulb in shallow water would not necessarily be a suitable solution for our problem.

With the option of shallow scale model tests eliminated, we chose to do more analytical modeling and increase the level of planned at-sea tests. The level of at-sea testing using full depth and actual spheres was increased considerably over that proposed. This was also prompted by our lack of

funding from CEROS for the second year and the need for more progress on this topic for our Office of Naval Research (ONR) proposals.

#### 4.5.1. Location

Physical modeling consisted of two separate days onboard ship at a location where the Ocean depth is in excess of 4800 m. This constituted a position approximately 32 nautical miles southwest of Honolulu harbor (Oahu, Hawaii). At this location, packages of test spheres, including some that were weakened, were deployed into the deep ocean. Hydrophone and recording equipment were used on the surface vessel to listen to the implosion events. Some of the packages were designed be non-recoverable; others were designed to be retrieved after a descent/ascent cycle.

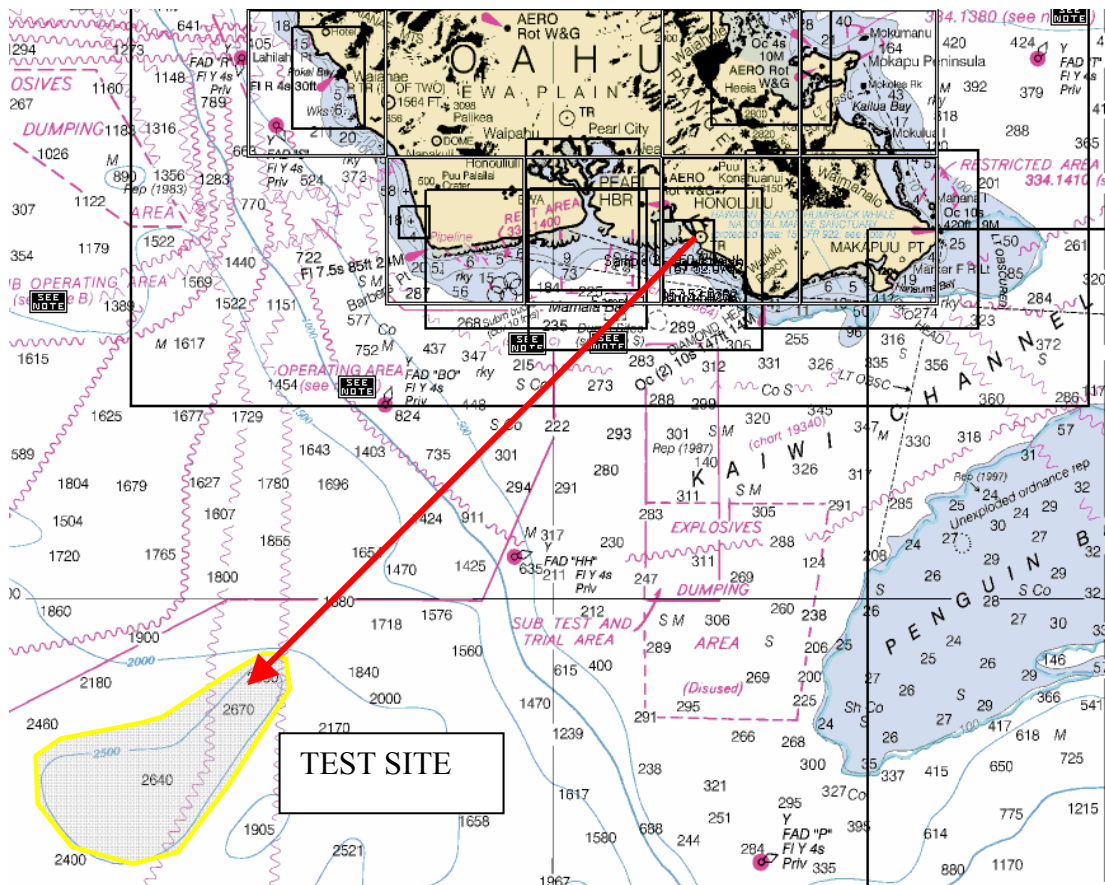


**Figure 4-14:** Implosion test site, approximately 32 nautical miles South West of Honolulu harbor.

#### 4.5.2. Vessel

To facilitate the at-sea tests a 43' workboat owned and operated by Sea Engineering was used. The M/V Huki Pono is currently set up to support marine survey and diving operations in the Hawaiian Islands, and provided a convenient working platform for test deployment. She has a 180 sq ft aft working deck with an articulating stern A-frame and winch of 2000 lb capacity. The vessel has a 10 knot cruising speed and 300 nautical mile

range. Loading and mobilization occurred at Honolulu harbor, where the vessel is normally berthed.



**Figure 4-15:** *The M/V Huki Pono.*

#### **4.5.3. Objectives**

The purpose of the at-sea implosion tests was to obtain physical data relevant to understanding the issue of sympathetic implosions. The specific objectives were:

- Confirm the occurrence of sympathetic implosion with 13" spheres at 4000 m depth.
- Obtain acoustic data to assist validation of analytical and computational modeling.
- Examine the effect of inserting filler materials into imploding spheres.
- Examine the effect of placing a concrete barrier between spheres.
- Investigate different weakening strategies and different thickness of grind.

#### **4.5.4. First at-sea tests**

The first day of testing took place on August 30<sup>th</sup>. The intended emphasis of day one testing was physical data recovery, with hydrophones used for secondary data collection. Two test series were planned,

- non-recoverable weakened spheres with various fillings
- recoverable ascent/descent strings

The DAY 1 two test series are summarized here:

#### 4.5.4.1 Filler study

Test series ONE was to consist the release in close succession of six non-recoverable packages. Each package would be made up of a pre-weakened 13" glass sphere attached to a heavy depressor weight (see Figure 4-16). Once released, each package would take approximately 30 minutes to descend to the target implosion depth of 4000 m.

Two of the packages were to have spheres with 30% of the internal volume filled with one of the following materials: a) precision strength syntactic foam, b) oil/water. A third package would have a completely empty sphere. The remaining three packages of test series ONE would have the same fillers (EG: none, oil/water, foam), but with differing grind thicknesses or grind locations.

Hydrophone equipment on the surface vessel would be used to record the profile of each implosion event. A relative comparison, and where possible, a quantitative analysis would be made using the acoustic wave profiles of each implosion.

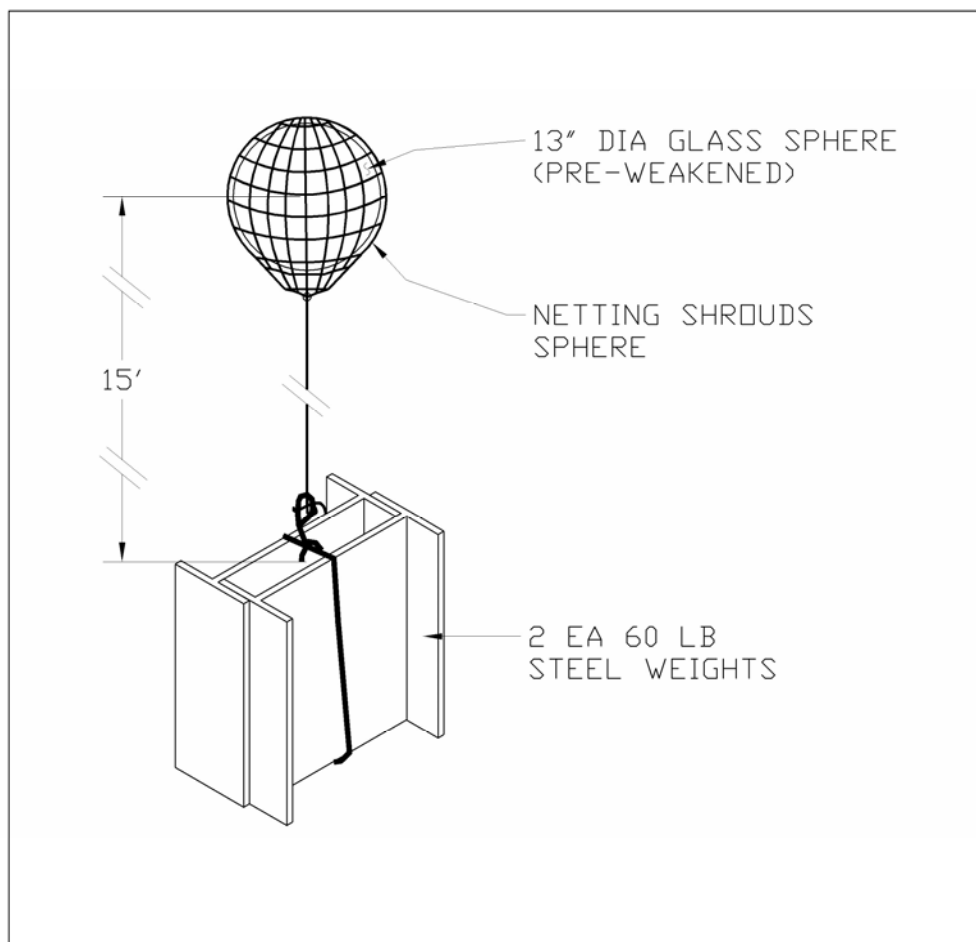


**Figure 4-16:** Non-recoverable single weakened spheres – filler study.

#### 4.5.4.2 Stand-off distance study

Test series TWO was to consist of a recoverable string of spheres, intended as a stand-off distance study. A large depressor weight would be attached to the lower end of the string, configured to release when the pre-weakened sphere above the weight implodes (~4000 m depth). Four standard 13" glass spheres would act as targets, placed on the string above the implosion shock wave source at successively greater spacing (see Figure 4-18).

A buoyancy package and locator equipment would be placed at the top of the string so that it could be recovered at the surface after a descent/ascent cycle. After physical inspection, the string could be loaded with new spheres and weight, and then re-deployed. The number of test cycles would be decided in the field, and would be a function of remaining boat time, experiment outcome and remaining materials.

Hydrophone equipment on the surface vessel would be used to record the profile of each implosion event. At a minimum, the hydrophone equipment would indicate the number of spheres, if any, that sympathetically implode.

#### 4.5.4.3 Estimated Ascent/Descent times of packages

A hydrodynamic drag analysis of the three test string configurations resulted in estimates of ascent/descent times shown in Table 4-2. Transit times are calculated for a depth of 4000 m, assuming an ocean of uniform density. The stated range is a reflection of the uncertainties in drag coefficients for each component. In the case of test series ONE, a significant range of times is shown, as each string deployed will have a slightly different payload (depending on the sphere void filler).

**Table 4-2:** *Estimated Ascent/Descent times for the two test series.*

Test series	DESCENT TIME (mins)	ASCENT TIME (mins)	<b>TOTAL (mins)</b>
1	22-31	-	<b>22-31</b>
2	49-55	41-64	<b>90-119</b>



**Figure 4-17:** From left to right: Steel weights, surface flags, hydrophone cables, sphere string wire rope, netted spheres (resting in concrete filled buckets – also weights) and buoyancy modules (yellow).

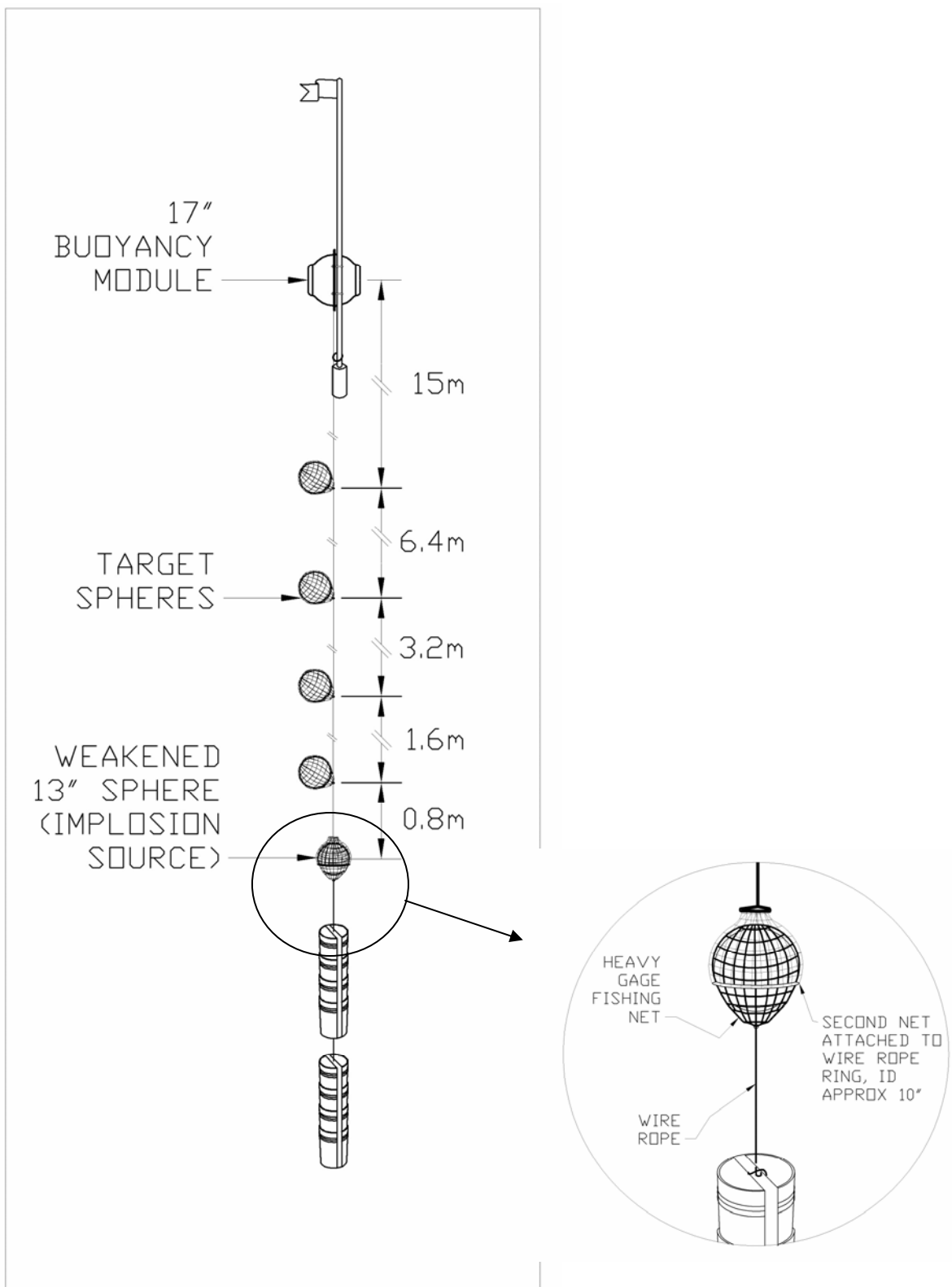


**Figure 4-18:** Recoverable string layout – stand-off distance study.

#### 4.5.4.4 Weakening strategy

As was shown by Orr and Schoenberg (1976) and later by Gorham et al. (1992), glass instrument housings can be prepared in such a way that they will implode at a predetermined depth. A standard technique for providing this weakening is to grind a flat on a section of the sphere exterior. The extent of the flat grinding stated as the Flat Thickness Ratio; this is defined as the ratio of minimum wall thickness at flat center to overall sphere radius. Some empirical data for 17" diameter Benthos spheres exists for the relationship between FTR and implosion depth. In general, this method of inducing a specific depth implosion is quite reliable.



**Figure 4-19:** A weakened sphere, netted up awaiting deployment.

Only one data point for 13" spheres was available, so under the guidance of the sphere manufacturer, spheres were ground with varying levels of grind thickness and type. Most of the grind thicknesses were centered around the one data point: a FTR = 0.024. This corresponded to an implosion depth of 4000m. The manufacturer Benthos supplied all the spheres for these tests, and was able to provide the grindings on 12 of the spheres. A total of 35 spheres were obtained from Benthos, 29 purchased and 6 kindly donated. It was determined that an additional 4 spheres needed to be weakened for the day 2 tests. This was done at a local glass shop in Hawaii. It was difficult to obtain the same precision as Benthos, and spheres were ground slightly deeper – resulting in FTR = 0.022.

#### 4.5.4.5 Filling spheres

All spheres supplied by Benthos are shipped assembled and held together by an internal vacuum and taped around the equatorial join. Makai devised a method to rapidly disassemble and reassemble the 13" spheres using a larger 17" sphere as a vacuum

chamber. To disassemble a sphere the tape was removed, and the sphere placed inside the larger sphere. The larger sphere was then assembled and a vacuum applied using a vacuum pump. Once an adequate vacuum was reached, the two halves of the smaller sphere would slide apart. The chamber was then disassembled and objects could be placed inside the open 13" sphere. To reassemble, the 13" sphere was loosely taped together and a vacuum applied. The vacuum was removed quickly from the 17" chamber and the inner 13" sphere would clam together. Now this sphere could be equatorially sealed and taped ready for deployment.

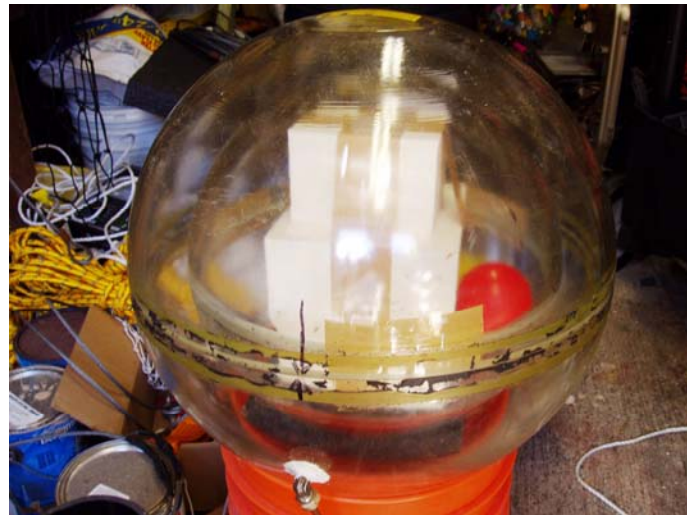


**Figure 4-20:** A 13" sphere contained inside the 17" vacuum chamber. Foam has been placed inside the previously disassembled 13" sphere. A balloon is used to verify that a vacuum has been achieved and maintained.

#### 4.5.4.6 Hydrophones

Two complete hydrophone and laptop computer recording systems were used for both at-sea tests. These hydrophones were generously loaned from University of Washington Department of Physics. These were spherical hydrophones with an integral preamp; previously used in the DUMAND neutrino project tests (c. 1991). These hydrophones had a 5 to 50 kHz bandwidth and a raw sensitivity of -200 dBV re 1 micro Pascal. The custom designed preamp gave 25 dB gain when supplied with 24V DC.

The hydrophones were lowered from the surface vessel to approximately 100' depth. For the second day of testing, one hydrophone was normally deployed (looking down, but omni directional) and the second hydrophone was placed inside a 10" metal cowling with thick foam lining. The intention was to shield the hydrophone from surface noise.



**Figure 4-21:** One of the hydrophones used in the at-sea tests. This hydrophone was mounted on a 6' steel rod with lead weights to maintain downward looking.



**Figure 4-22:** Two complete laptop/hydrophone systems were installed for recording acoustic events.

#### 4.5.4.7 Day 1 summary

Before commencing deployment of a test string, several light bulbs weighted with bricks were released over the side of the vessel. This was intended as a way to test the hydrophone recording system and gage typical signal to noise ratio. The implosion signal of the light bulbs was very difficult to discern because of significant background noise. The noise had three main sources: the ship's engines, the diesel ship power generator and overall movement and slamming of the vessel in waves. We were able to eliminate noise from the engines and generators by shutting them off and allowing the vessel to lay-to in the seas. Unfortunately, these measures had implications of their own: Shutting off the vessel's engines allowed the vessel to lay beam on to the short period seas. This made deck work challenging and greatly increased hydrophone noise. Shutting off the generators limited us to laptop battery power, forcing us to stagger use of our redundant hydrophone/laptop system (see Figure 4-22).



**Figure 4-23:** Weighted light bulbs were used to assist with hydrophone system setup.

The first ascent/descent string deployed consisted of one weakened sphere, four target spheres, a floatation package and 720 lb concrete weight (as shown in Figure 4-18). The initial package carried a GPS/VHF location system that could be polled from the boat when the string was at the surface. This was tested, and confirmed working immediately prior to deployment.

Although we had no means to directly monitor the depth of the test array (via acoustic transponder etc.), we were able to establish the depth of the assembly at the time of implosion by considering the elapsed time between the direct signal and bottom reflected signal. Implosion of the weakened sphere occurred approximately 65 minutes after

deployment at a depth of ~4400 m. This would indicate that the package descended at 1.13 m/s, close to the predicted speed from drag calculations.

With limited information relative to current-depth profiles it was considered prudent to return to the area of initial deployment to commence our search for the surfacing test package. Unfortunately, exhaustive visual searching and attempts to poll the GPS/VHF location system were unsuccessful. After 90 minutes it was decided that our efforts should focus on continuing the test schedule and completing the deployment of the non-recoverable assemblies. Search efforts for the recoverable string were continued during subsequent deployments; however efforts were hampered by deteriorating weather conditions. By the afternoon, we were experiencing 6-8 ft ground swells, with short, wind driven seas mixed in. The increase in wind strength to 15-20 knots produced white-caps - this reduced the efficiency of visual searches.

The actual outcome from the first string is still not clear. Two possible outcomes are envisaged: i) the weight release mechanisms failed and the test assembly sunk to the ocean floor, ii) the test assembly returned to the surface and location systems failed. Although there were enough additional spheres, cables and materials for an immediate second recoverable string deployment, given the weather conditions and outcome of string 1, it seemed more prudent to save the resources for a redesigned test during day 2 of testing.

During day 1 of testing it was discovered that one of the two hydrophones being used for the acoustic data collection operation had what was believed to be some mechanical fault. On receipt of higher energy signals the hydrophone exhibited a ringing or reverberation characteristic (see Figure 4-24).



**Figure 4-24:** Example of hydrophone ringing – the upper pane is an implosion event recorded with the suspected faulty hydrophone, the lower pane is the same implosion event recorded with an alternative hydrophone.

Despite several challenges and teething problems encountered during the day 1 test excursion, high quality acoustic recordings were made of: i) the implosion of an empty sphere at 4280 m depth and, ii) the implosion of a sphere with 30% volume filled with syntactic foam at 4100 m depth. Lower resolution recordings provided sufficient information to determine at what depth the various implosions occurred. No implosion was observed and hence no record exists for two events. In general, the depth of implosion was greater than anticipated, it is therefore postulated that the depth of water (~4800 m) was not sufficient to trigger implosion for two of the weakened spheres. Estimated depths of implosion are summarized in Table 4-3.

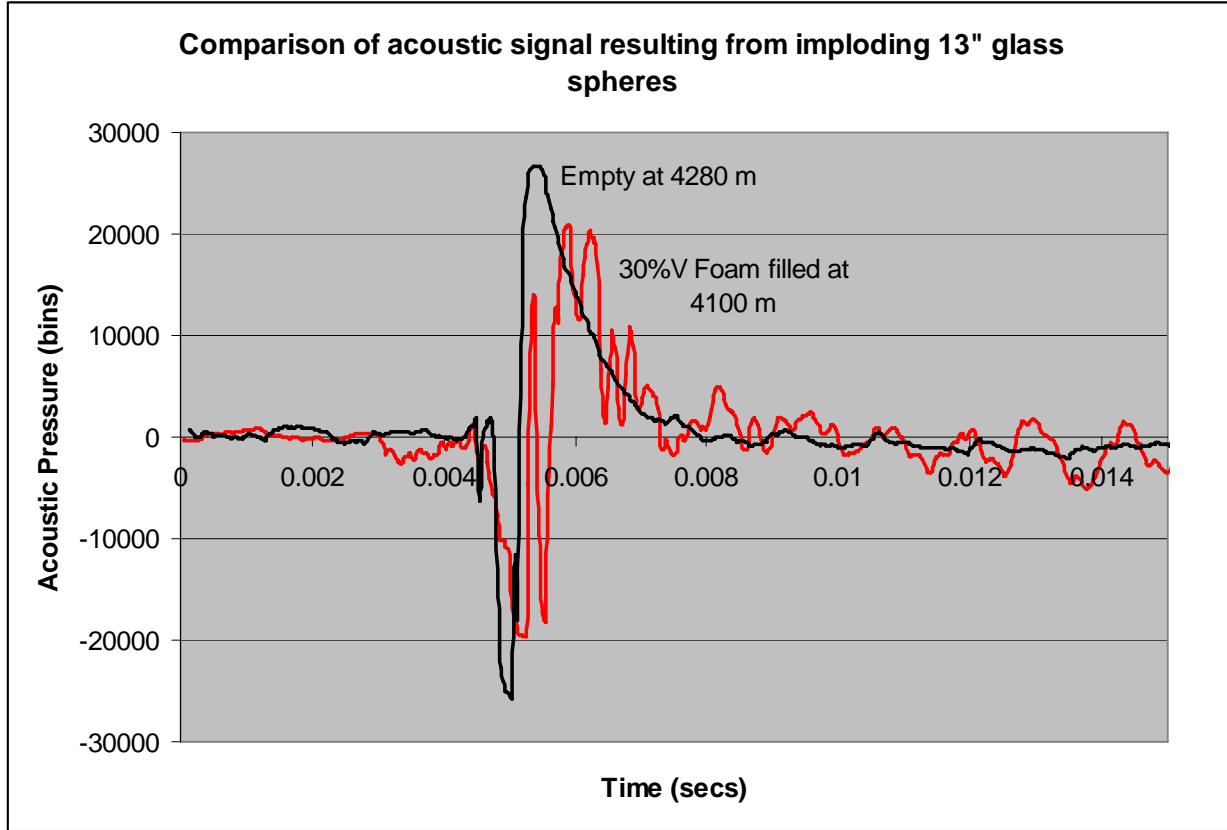


**Figure 4-25:** Acoustic signals as recorded by hydrophone.

Test name	Description	Time to implosion	Depth of implosion
Single 1	Sphere weakened FTR = 0.153 top grind, empty	0:25:30	4280m
Single 2	Sphere weakened FTR = 0.156 top grind, 30% foam filled	0:27:48	4425m
Single 3	Sphere weakened FTR = 0.159 top grind, 30% foam filled	NR	NR
Single 4	Sphere weakened FTR = 0.211 equator grind, empty	0:27:07	4315m
Single 5	Sphere weakened FTR = 0.210 equator grind, 30% foam filled	0:26:03	4105m
Single 6	Sphere weakened FTR = 0.156 top grind, 30% oil filled	NR	NR
String	Sphere weakened FTR = 0.155 top grind, empty + 4 target spheres, empty	1:05:05	4472m

**Table 4-3:** Summary of tests deployed and depths of implosion day1.



**Figure 4-26:** Deployment of 30% volume foam filled weakened sphere.

#### 4.5.5. Second at sea tests

The second day of testing occurred on October 20<sup>th</sup>. In response to the outcome of day 1 testing, all deployed tests were designed to be non-recoverable and specifically tailored to establishing what circumstances caused sympathetic implosion. Eight assemblies consisting of a weakened imploding sphere, a target sphere and a weight were readied for deployment (see Figure 4-27). Four of the weakened spheres were previously prepared (weakened) by the manufacturer Benthos. The additional four weakened spheres were ground locally in Hawaii at a Glass shop. These spheres were ground to a slightly greater depth, thus we expected them to implode closer to 4000 m. This was in response to the previous tests, where implosions were experienced as much as 10% deeper than 4000m.

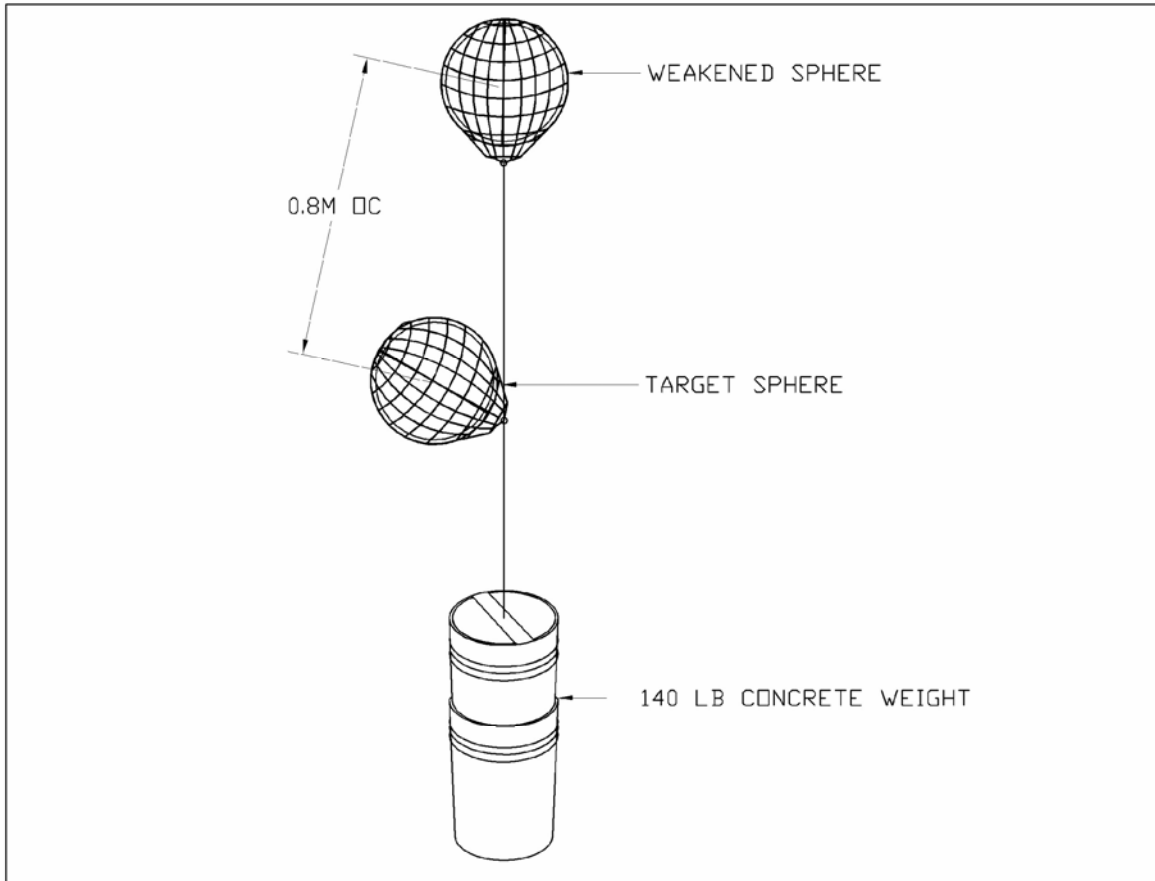


**Figure 4-27:** Simple double sphere sympathetic implosion assembly.



190

**Figure 4-28:** Two sets of weights and target spheres awaiting the addition of weakened implosion spheres at a stand off distance of 0.8m OC.



**Figure 4-29:** The arrangement of a source sphere, target sphere and concrete barrier between them.

#### 4.5.5.1 Day 2 summary

At 0900 we arrived on station approximately 32 nautical miles southwest of Honolulu harbor, the water depth was approximately 4900m. An empty weakened sphere and target sphere were immediately deployed and the hydrophone signals monitored. No implosion was observed so it was assumed this sphere did not fail before reaching the seafloor. A second empty weakened sphere and target sphere assembly was deployed, this time with a slightly greater degree of weakening. A clear implosion was heard and was calculated to be at a depth of 3200m. Closer analysis of the acoustic signal revealed that a second, sympathetic implosion had occurred.

Given the first result – that an empty sphere gives a sympathetic implosion – the next test deployed was a weakened sphere 30% oil filled. This sphere imploded at 3675m depth and also caused a sympathetic implosion in the target sphere. A further five tests were deployed. No implosion event was recorded for one of these additional tests. Out of the remaining tests it was found that a two inch concrete barrier did not prevent a sympathetic implosion, however, filling with precision strength syntactic foam (30% volume – 8000 psi collapse pressure) did save the adjacent sphere. A summary of times and depths to implosions is shown in Table 4-4.

Some significant discrepancy in elapsed times for descent is expected, not just because there were various depths of descent, but also on account of the different weighting systems used. For most of the tests, two concrete filled buckets were used – a combined weight of ~140 lb dry. In one of the first tests a 150' streamer was attached to the deployed assembly. This was used to calculate an approximation of descent time. The first 50' was discounted, but over the subsequent 100' of descent the assembly had a fall velocity of 4ft/s. This information helped us know when to expect an implosion.

Test name	Description	Time to implosion	Estimated depth of implosion	Sympathetic implosion?
Double 1	Empty FTR = 0.150	NR	NR	NR
Double 2	Empty FTR = 0.150 MOE	24:16	3200m	Yes
Double 3	Water filled FTR = 0.156	43:45	3675m	Yes
Double 4	Foam FTR = 0.156	39:19	3250m	No
Double 5	Concrete barrier FTR = 0.150 MOE	NR	NR	NR
Double 6	Concrete + Foam FTR = 0.150 MOE	43:35	3575m	No
Double 7	Foam FTR = 0.156	47:51	4300m	No
Double 8	Concrete barrier FTR = 0.150 MOE	42:00	?	Yes

**Table 4-4:** Summary of Day 2 testing

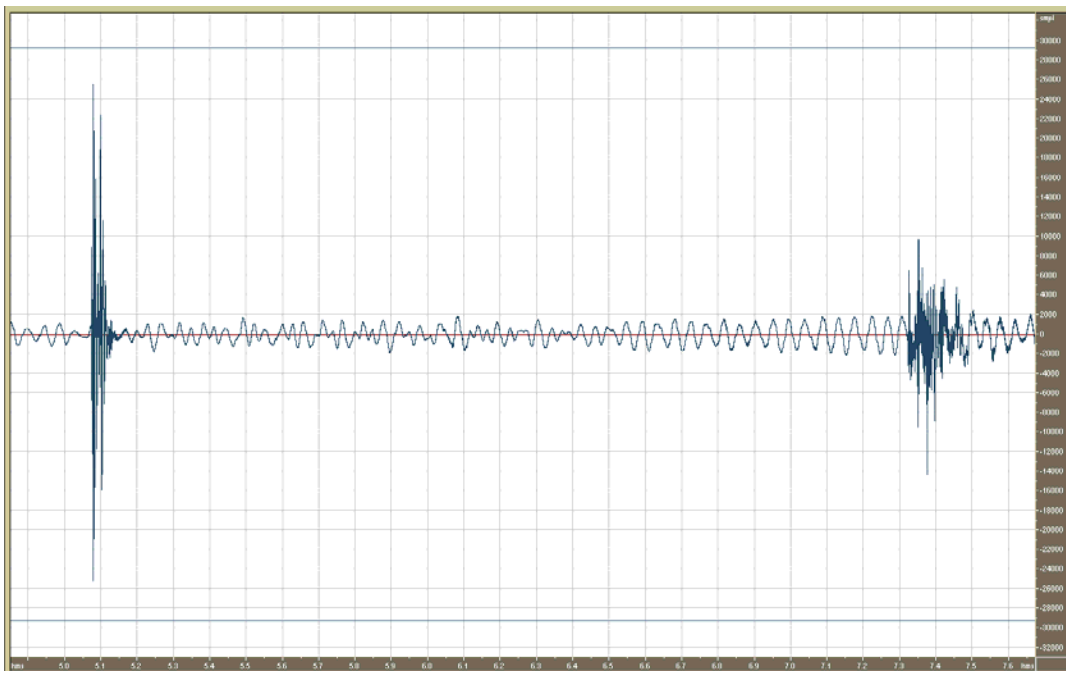


**Figure 4-30:** An example of an as-recorded implosion event and it's corresponding bottom reflection. The elapsed time between the primary acoustic signal and the reflected signal is approximately 2.2 seconds. This equates to a round trip distance of 3300m, indicated the implosion occurred in 3250m water depth.

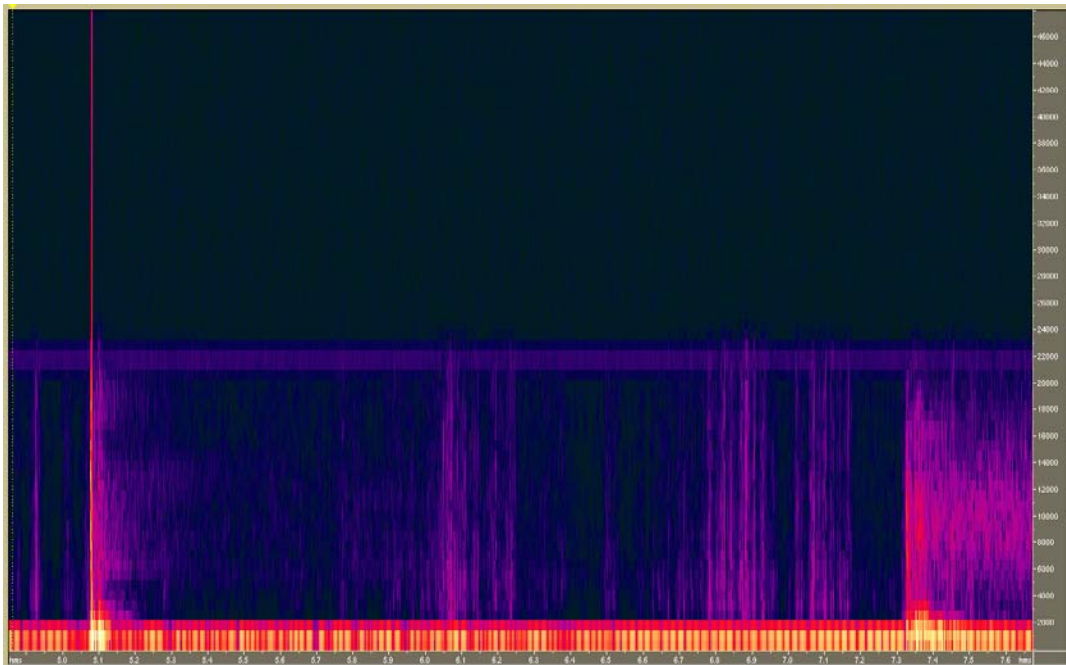


**Figure 4-31:** A spectral view of the as-recorded signals shown in Figure 4-30. Note the high intensity, broad spectrum implosion event.

**Implosion of a weakened empty sphere and the subsequent sympathetic implosion of the target sphere**

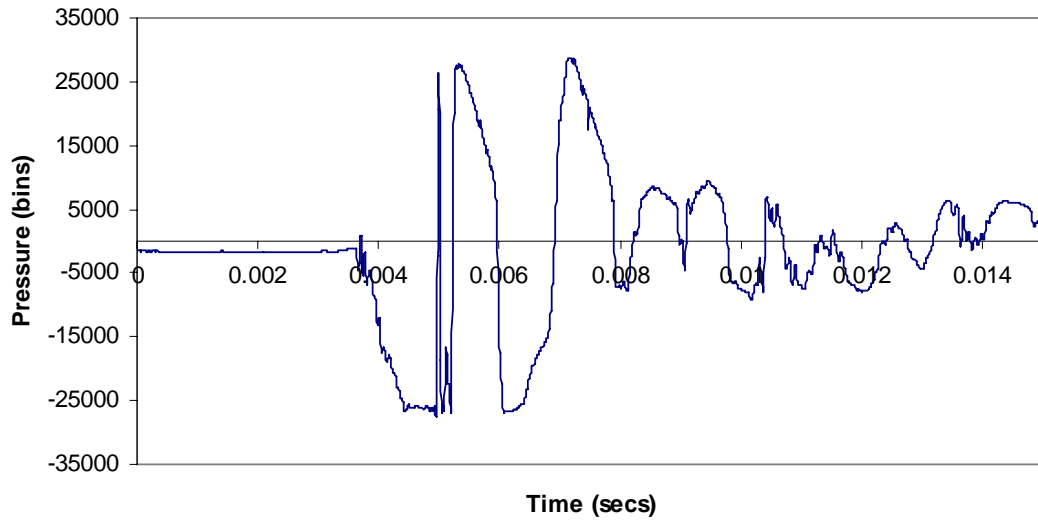


**Figure 4-32:** This as-recorded acoustic profile demonstrates two peaks, indicative of a double implosion event. The time difference between the two peaks corresponds to the expected signal delay due to the separation distance of the two spheres.

**Implosion of a weakened sphere 30% volume filled with oil**

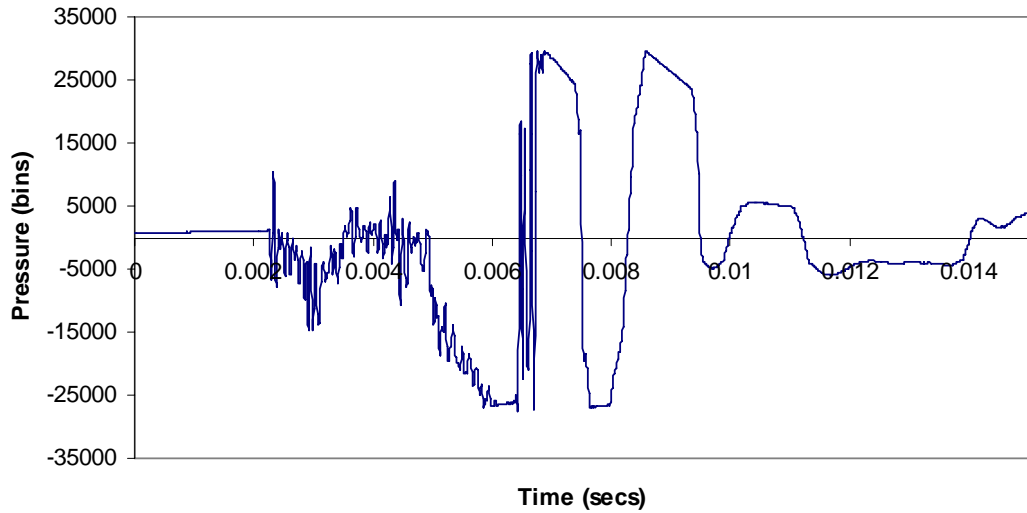


**Figure 4-33:** This as-recorded acoustic profile demonstrates a double implosion

event where the weakened sphere was 30% volume filled with oil. The profile of the implosion slightly differs from an empty sphere. The over-pressure wave is slightly spread in time and the lead-in negative part of the signal is of longer duration, with high frequency components. This may be attributable to a slower glass failure mechanism or the presence of the partial fill.

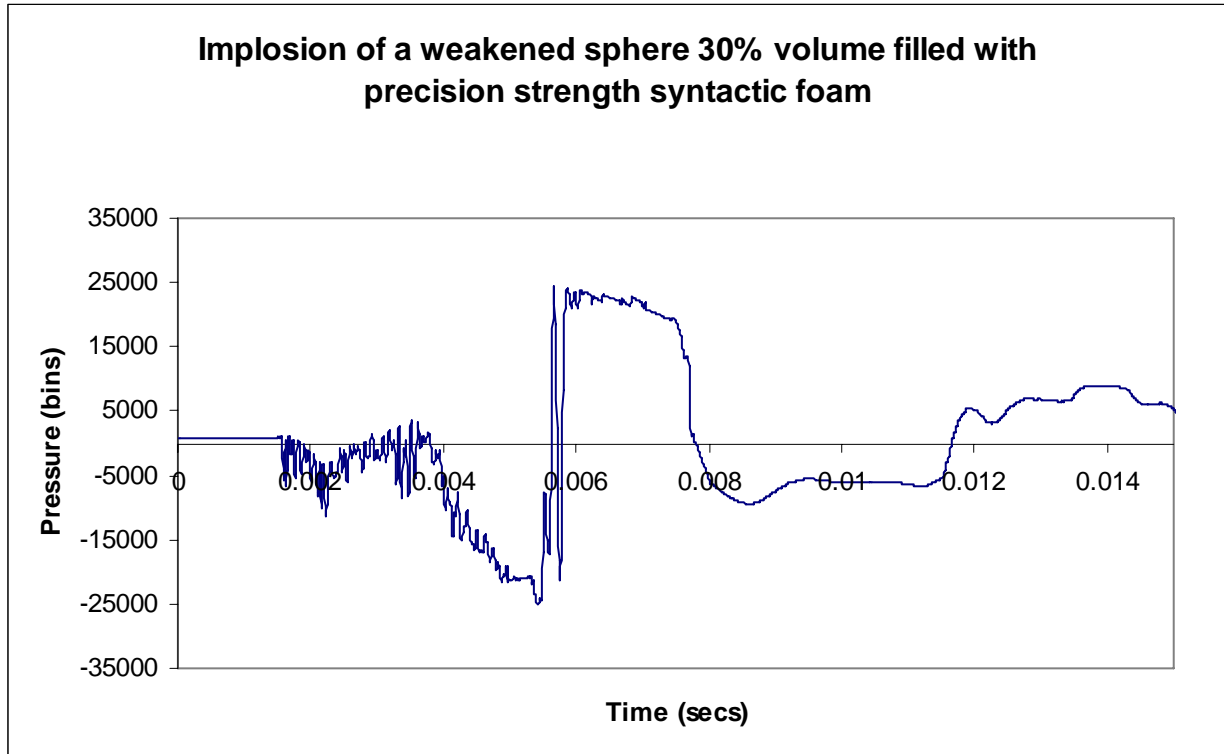


**Figure 4-34:** This as-recorded event shows the implosion of a sphere 30% filled with precision strength syntactic foam. The lead-in under-pressure portion of the signal is similar to the oil filled sphere. The over-pressure portion of the signal is significantly spread and of lower amplitude when compared with the empty sphere implosion.

#### 4.6 CONCLUSIONS

- *The energy released from an implosion is significant.* The theoretical energy stored scales proportionally with the Volume of the void and with the Pressure difference between the sphere's inner void and the exterior. For a 13" diameter glass sphere at a depth of 4000 m, the theoretical energy stored is approximately 600 kJ.
- *Only about a quarter of the potential energy is converted to acoustic energy.* When an implosion occurs, the potential energy stored is rapidly transferred into several other forms of energy that include heat and sound. Applying the estimation methods of Urick (1967) to our 13" sphere implosion analysis; the acoustic energy released in a 4000 m depth implosion event is 160 kJ (about 26% of the available potential energy). This proportion is in close agreement with previous implosion studies by Orr and Schoenberg (1976) who estimated conversion rates to acoustic energy of 21%. One can

expect some deviation on account of the slightly different depths and sphere configurations studied in each case.

- *The computational model (ALE3D) - a good representation of an implosion shockwave.* The results from computational modeling compared well with data from previous implosion shockwave studies and recent physical tests – this gave us confidence that ALE3D is able to satisfactorily cope with complex underwater shockwave phenomena. The ALE3D “full physics” model shows good potential for more in depth modeling that could be undertaken in subsequent phases of this project.
- *An adjacent sphere can sympathetically implode.* The at-sea tests confirmed the energetic shockwave released when a 13" glass sphere implodes at 4000 m depth is capable of triggering a secondary implosion of another sphere placed in close proximity (~0.8 m O.C.).
- *A two inch thick concrete barrier did not prevent sympathetic implosions.* Sympathetic implosion of a good sphere placed in proximity (~0.8m O.C.) to an imploding sphere was achievable, even with a 2 inch concrete slab placed equidistant between the two spheres. In the at-sea test, we are confident the concrete slab presented some form of obstruction for the shockwave; however, we cannot be sure of the absolute orientation of the slab at the time of the implosion event. Furthermore, the nature of the test was such that the concrete barrier was not firmly fixed relative to either sphere and the effects of shockwave interaction given this arrangement are unclear.
- *A 30% volume reduction by adding oil did not prevent sympathetic implosions.* Reducing the internal volume of an imploding sphere by filling 30% with a virtually incompressible material (oil) was not sufficient to prevent the sympathetic implosion of a good sphere in close proximity. Analysis of the acoustic signals recorded during at-sea testing suggest the implosion event signal for the oil filled sphere was of slightly lower energy level than the implosion signal generated by an empty sphere. Overall, it is hard to discern any huge differences in signal profile. This was somewhat counter-intuitive, and not what was expected. This may be explained by the fact that the water filled sphere imploded at a greater depth: perhaps offsetting some of the energy reduction achieved by reducing the interior volume.
- *A 30% volume reduction by adding foam did prevent sympathetic implosions.* Reducing the internal volume of an imploding sphere by filling 30% with precision strength syntactic foam did prevent the sympathetic implosion of a good sphere in close proximity. The patterns observed in recorded acoustic profiles from the second at-sea test were consistent with attributes noted from foam filled implosion signals recorded during the first at-sea test. The effect of the foam is to reduce the overall peak overpressure by as much as 30% and cause a stretching/scattering of the implosion signal. At least two smaller signal peaks can be observed. These are postulated to be 1) peak as a result of the initial glass shell collapse and in-falling until the internal foam is felt (and consequently loads up), ii) a peak resulting from the conclusion of the foam yield, collapse and hardening.
- *Good indication there is a solution, but it is expensive and not guaranteed.* Our analytical and physical investigations have shown that sympathetic implosion is an issue that must continue to be considered during subsequent design phases of this

project. In this phase, it has been shown in tests that filling all possible void space (about 30% of the original volume once the PMT and electronics are installed) with precision strength syntactic foam can reduce and spread the shockwave sufficiently to prevent sympathetic implosion. Filling the spheres with foam could indeed be one solution, but it is perhaps not optimal. This foam is highly specialized, and thus very expensive. Furthermore, the limited data points from these at-sea tests do not cover all the uncertainties or even changes to detector design.

- *Further modeling is required.* Overall, good progress has been made during this contract in characterizing the risks of sympathetic implosions and subsequent postulation of possible mitigation techniques. However, this work only constitutes a fundamental look at this technical challenge. A more in depth analysis including additional modeling is certainly required. To some extent, this must be undertaken in parallel with overall detector design development, such that not only cascading implosions are considered, but also the effects of an implosion shockwave on other detector components and structure. Indeed, the interaction of these elements could become part of a large scale sympathetic implosion strategy. For example, if further modeling revealed that the compartmentalized (current detector design has sealed and separated 3x3 sphere modules) nature of the detector limited a sympathetic implosion event to loss of only the other 8 spheres in that compartment, this may be an acceptable risk. After all, the detector would still be able to operate if a single module is lost - and the probability of a single sphere failing is very small.
- *Future work.* A combination of additional computational modeling and physical testing is anticipated. Ideally, the existing ALE3D model would be developed to consider an as-designed compartment of 9 spheres or even an entire detector. If the model was “built out” to consider the entire detector, there would be some additional advantages outside of just the sympathetic implosion issue. Owning to the full physics code nature of the computational model, it could easily be run to consider other design aspects such as deployment and recovery analysis. To compliment additional computational modeling, at-sea tests could be performed to investigate the interaction of structure and other components with a possible implosion shockwave.

## 5. PREPARATION OF LOW RADIOACTIVITY SCINTILLATION MATERIAL

### 5.1 SCINTILLATOR PURITY

The physics of the experiment requires that the scintillator be very pure and, most importantly, free of any radioactive contaminants. Therefore, all surfaces contacting scintillator must be very radioactively pure. This requirement results in strict rules for treatment of the scintillator and all surfaces that will come into contact with it. The plan outlined below is based upon the experience with the Boexino and KamLAND experiments, which provide a proof of principle that the desired radiopurity levels may be reached.

#### 5.1.1. Requirements during construction

During construction of the detector, storage tanks and plumbing, there are many substances which could contaminate the system and cause long-term radiation problems. Therefore, requirements for the construction of the inner cylinder of the detector, storage tanks and connecting plumbing are:

- Stainless steel with limited uranium content
- Welding electrodes must be free of thorium
- Welds will be checked by X-Ray, dye penetrant, and hydraulic tests
- Leak rate below  $10^{-5}$  atm cm<sup>3</sup>/s<sup>2</sup> for a mixture of 90% nitrogen and 10% helium
- Surfaces are to be electropolished
- Surface roughness less than 0.6 μm.

The above construction requirements will help limit radioactive contamination of any surfaces the scintillator comes in contact with, which in turn limits contamination of the scintillator. The requirements for the construction of the outer walls of the detector are less stringent since they only contact the water in the veto region, and not the scintillator itself.

#### 5.1.2. Cleaning the detector

The detector and scintillator storage tanks must meet the requirements of a class 100 clean room. The class designation sets a limit on the number and size of particles allowed inside the clean area, as seen in Table 5-1. A number of steps will be taken to meet these particle limits.

- Incoming air will be filtered
- Air inside the clean room will be continuously recirculated through more filters

- All people and equipment will pass through an airlock with an air shower
- Workers must wear clean suits, boots, and masks
- Objects brought into the clean room must first be cleaned and wiped with alcohol
- All materials, such as calibration devices, slated for long term placement will have to go through qualification testing, as has been developed for the KamLAND experiment.

Class	Particle/ft <sup>3</sup>					
	0.1 μm	0.2 μm	0.3 μm	0.5 μm	1 μm	5 μm
1	35	7	3	1		
10	350	75	30	10	1	
100	3500	750	300	100	10	1
1,000				1,000	100	10
10,000				10,000	1,000	100
100,000				100,000	10,000	1,000

**Table 5-1:** US FED STD 209E cleanroom standards

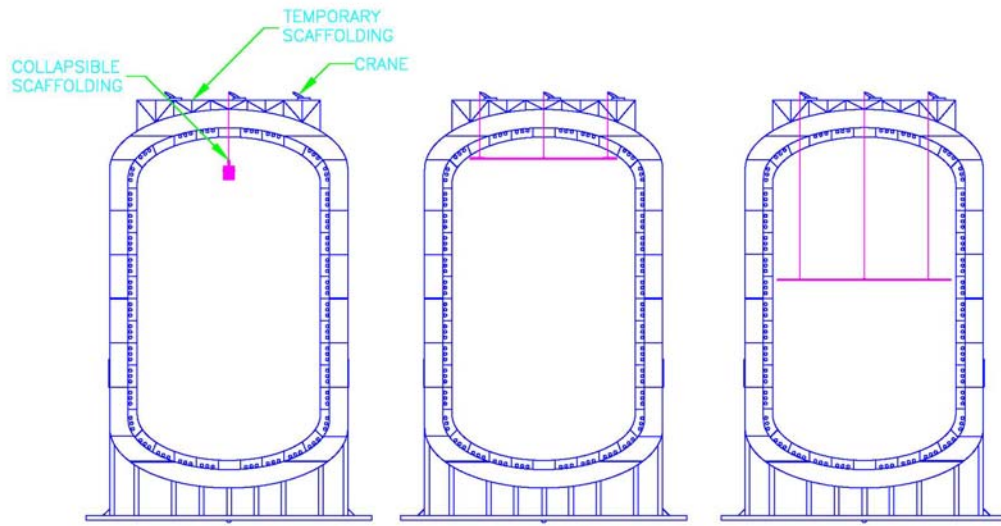
To prevent additional unnecessary contamination, all plumbing and electronics will be located in the veto region, where the purity requirements are less stringent. Therefore, while the inside of the plumbing must meet the strict requirements outlined above, the outside of the plumbing does not need to meet the same requirements. Limiting the amount of equipment located in the inner detector will limit contamination. Thus, any equipment that can be located in the veto region will be placed there.

After construction is completed, the clean room restrictions will be implemented. Despite the precautions, some dirt and dust will still get inside the detector and storage tanks. Following the clean room procedures, inner surfaces of the detector and storage tanks will be cleaned using:

1. C<sub>2</sub>HCl<sub>3</sub> before electropolishing
2. ECOCLEAN 200 after electropolishing
3. High pressure tap water
4. High pressure demineralized water

In order to reach all the inner surfaces of the detector, a large platform is necessary. However, it must fit through the two meter access panel in the center of the top of the detector. Therefore, a series of 1.5m segments will be used. The segments can be folded up to fit through the access panel, then unfolded and bolted in place once inside the detector. When unfolded, the platform will span the entire width of the detector. Since the

detector is narrower at the top and bottom, the two end sections of the platform can be folded in to make it small enough to fit in the narrower sections. A crane will support the platform on a cable through the central access hatch. In addition to the center cable, four additional lines will be necessary to keep the platform stable and level. Therefore, four PMT modules will be temporarily removed to create additional access points, and four more cables will be attached to the platform.



Once the cleaning process is finished, the inner surfaces must be dried using nitrogen, and all the air will be flushed out and replaced with nitrogen. From this point on, air is not allowed to contact the clean surfaces. Therefore, the detector and storage tanks will be stored full of nitrogen until they are filled with scintillator.

#### 5.1.3. Purifying the scintillator

Despite the precautionary measures taken during construction and cleaning, the scintillator will have some contaminants. Therefore, it is necessary to have a purification system onboard. Four methods of purification will be employed:

1. Water extraction will be used to remove polar and charged particles, such as ions and metal salts. The scintillator will be saturated with water, and any water soluble contaminants will dissolve in the water. When the water is removed, so are the contaminants.
2. Nitrogen stripping is the process of passing dry nitrogen over the scintillator. The nitrogen absorbs water, oxygen, and noble gases, including radon and krypton.
3. Vacuum distillation involves exposing the scintillator to a vacuum until compounds with lower vapor pressures evaporate. The remaining liquid will have a lower percent of contaminants. Typical distillation heats the solution, which would damage the scintillator. Vacuum distillation removes both radioactive and chemical impurities

- Filtration with a  $0.05 \mu\text{m}$  particulate filter eliminates dust that may contain radioactive uranium, thorium, and potassium

These four systems will be used to purify the scintillator. The detachable design will have space and plumbing for these systems on the barge. A possible arrangement of these four systems is shown in Figure 5-1. For the integrated design, the detector will have to be filled and the scintillator purified in port.

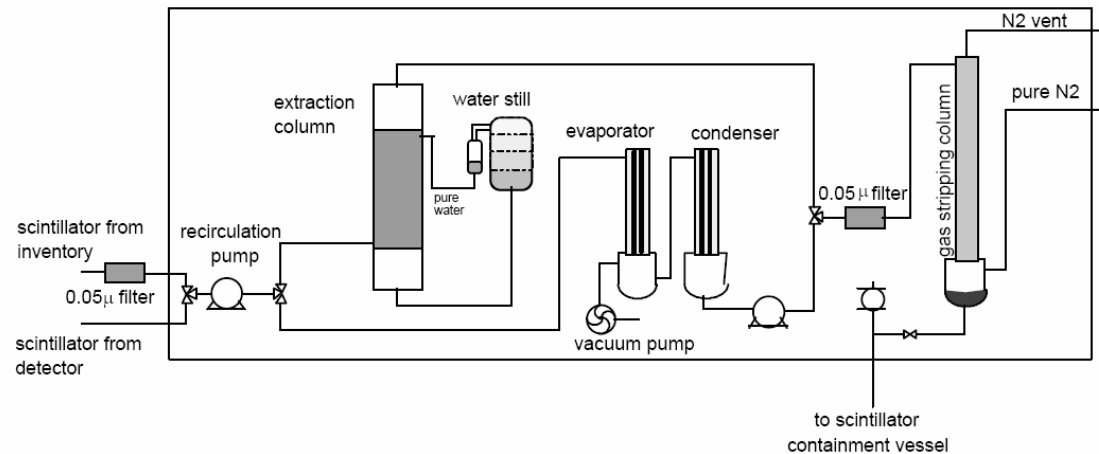


**Figure 5-1:** Four-step Purification System (*cite source*)

#### 5.1.4. Storage

For the detachable vessel, while the barge is underway, the scintillator will be stored in stainless steel compartments in the barge. The tanks will be constructed according to the specifications listed in section 1.3.6.1. They will be divided in order to limit the free surface. In addition, they will be distributed such that the weight distribution of the barge is not adversely affected at any time. For example, scintillator will be stored both fore and aft such that fluid can be taken from both ends and the vessel will remain level.

#### 5.1.5. Transporting the scintillator

The barge without the detector will pick up the scintillator at the refinery so that the scintillator only has to be handled once rather than being transferred several times. Each time the scintillator is transferred there is a risk of exposure to air. In addition, the more surfaces it touches, the more contaminants it will come into contact with. Therefore, minimizing the number of times the scintillator is moved greatly reduces the amount of contamination that occurs.

When the site of the experiment is reached, the scintillator must be transported from the storage tanks to the detector itself. During this process, the scintillator must only come into contact with radioactively pure materials, and may not come into contact with air. When underway, the storage tanks are filled with scintillator and the detector with nitrogen. Upon arrive at the location of the experiment, the scintillator is pumped into the detector, nitrogen will be routed back to the tank to replace the missing scintillator. Thus,

the scintillator and nitrogen will merely switch places. In this manner, all of the scintillator can be transferred to the detector without coming into contact with air.

## 6. OCEAN DEMONSTRATION

### 6.1 OBJECTIVE:

#### 6.1.1. PMT – Scintillator demonstration

The team believes that an ocean demonstration of the hardware (PMTs and electronics) and the detection medium (liquid scintillator) will be needed to move the Hanohano proposal ahead within the scientific and nuclear deterrence communities. All of the individual components may have been tested, but assembling a mini-detector and showing that it works in the real environment can be a convincing demonstration of feasibility. In thinking about the design of a small demonstration unit we have considered what we might accomplish. At such a small scale, we have not identified any standalone science, so this will be a pure technical demonstration.

- With several optical units, we can measure rates of single photoelectron emission in the scintillator mix and we can measure fake inverse beta events. (In this small size we cannot observe neutrino interactions due to too low a rate.) We can make a useful test of the shielding by embedding the inner scintillator volume in a larger "veto" volume.
- We have run computer programs calculating the attenuation for radiation from the ocean, and this measurement will test these calculations (which are not trivial because one is attempting to simulate very rare cases when gammas penetrate  $>10$  attenuation lengths into the inner volume)
- By having the electronics attached to the ship's cable we can demonstrate the operation of the optical modules with the real scintillator under the deep ocean pressure and temperature conditions. We can exercise the control, data transmission and simple trigger finding. These tests will demonstrate the suitability of the scintillator material.

#### 6.1.2. PMT implosion demonstration

A second major goal of the demonstration was further testing and demonstrating Hanohano's resistance to a PMT housing implosion. The original goal of this year of CEROS funding was to identify likely candidates for methods of preventing sympathetic implosions. A second round of implosion tests was envisioned in a second year of funding to perform more rigorous at-sea testing at 4000 m depth of implosions, methods of preventing sympathetic implosions, and the subsequent damage to other Hanohano structures.

### 6.2 LIMITED DESIGN:

The anticipated second year of funding from CEROS has not materialized so this planned demonstration will not be done. Without CEROS, the program badly needed to find other sources of funding. Our transition planning accelerated and funds were focused in areas where they would have the greatest impact upon successful transition. In particular, more emphasis was placed on:

- Additional at-sea implosion tests were conducted in order to achieve some immediate results (and not have to wait for the 2<sup>nd</sup> year component test). We felt that we had to demonstrate at least some success at preventing sympathetic implosions. See the discussion in Chapter 4. A second at-sea test was performed which showed success with inserted syntactic foam.
- Additional efforts were made, with CEROS assistance, at contacting other funding agencies.
- Additional engineering detail on the Hanohano conceptual design was performed in order to provide a complete description for subsequent proposals (this report).

The ocean demonstration module has been conceptually designed and budgeted, but it is not a complete design ready for fabrication and deployment.

## 6.3 PMT-SCINTILLATOR DESIGN

### 6.3.1. Requirements

The design requirements include:

- A minimum of 1 cubic meter (approximately one tonne) of scintillator fluid, LAB.
- Six active PMT's
- Three veto region PMT's
- Glass sphere enclosures for the PMT's, rigidly mounted, with optical cones.
- Clear LEXAN separation between the PMT's and the scintillator.
- No extraordinary purity processing of the scintillator.
- Oil surrounding the PMT's
- Pressure and temperature compensation of the oil, scintillator, water at a level approaching 5%.
- An outer veto region filled with fresh water.
- A frame and means of lowering.

### 6.3.2. Design Approach

**Deployment:** In practical terms, the smallest size is on the order of a cubic meter. Once surrounded by some shielding, this will amount to a few tonnes that would be lowered over the side from an oceanographic vessel. The typical handling gear (ship's cable and winches) will take up to 15 tonnes. Thus 1-10 tonnes is a manageable range. A vessel such as the UH Kilo Moana, has a cable with fiber optics on board, so there is minimal cost in outfitting the ship for such a test.

The conceptual design is shown in Figure 6-1. This design has the following features:

- The inner cylinder is a thin-walled HDPE polyethylene pipe section, DR 55. It is 55" OD. Overall length is 78 inches. The inside diameter is 53"; it has a one inch wall. The inside is machined from a DR 32 pipe section.
- The inner cylinder is divided into three sections: an inner volume of scintillator fluid that is 28" long, inside, and two end regions that are 24" long each on the inside volume.
- The two bulkheads between the inner chamber and the two end chambers is a 55" disk of  $\frac{1}{4}$ " lexan clear plastic. It is supported by a  $\frac{3}{4}$ " high inner flange that is left inside the HDPE pipe when it is machined from a DR 32 to a DR 55. This bulkhead is permanently installed and sealed with a silicone gasket.
- Each end of the inner HDPE cylinder is sealed with a flat plate of 1/4" HDPE sheet. It is also attached by stainless screws directly into the HDPE pipe and sealed with a silicone gasket. These end plates are removable in order to have access to the inner PMT's.
- Pressure compensation of these inner volumes during descent and ascent is achieved by distortion of the end plates and the lexan sheets.
- The PMT's are mounted in an aluminum frame that rests snugly inside the two end chambers. This frame does not obstruct the deflection of the end plates.
- Filling and draining the three inner chambers is accomplished through ports in the side of the HDPE pipe. Standard pipe fittings and valves are threaded directly into the HDPE.
- The above design is all plastic, aluminum, glass with stainless fasteners. There will be no contamination of the fluids and contact materials will be similar to the full design.

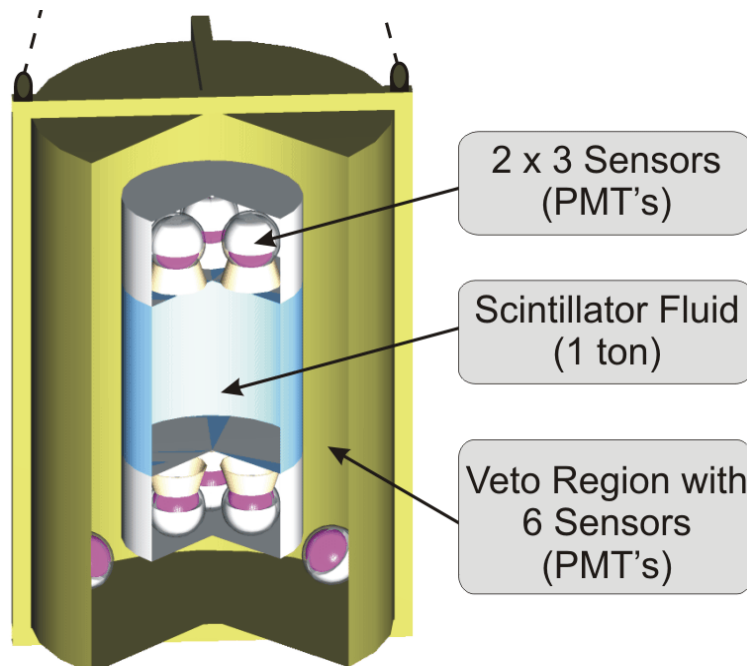


**Figure 6-1:** Arrangement for the Scintillator-PMT test module.

- The inner sphere constitutes the major experimental region.
- The displacement volume of the inner cylinder (3 compartments) is 3.0 cubic meters.
- A veto region of 15" can be used to keep the total displacement at 10 cubic meters.
- The outer cylinder is 85" OD and 108" long, it is 3/16" aluminum plate. An tubular frame of flooding aluminum is used for attachment points for lifting.
- Total air weight is close to 10 tonnes. An additional tonne of scrap steel is added to the bottom of the detector as a hanging anchor to assist in lowering the otherwise neutral-in-water detector.
- Electrical connectors and cables are oil filled. Connection is to the UH ship cable.

### 6.3.3. Cost Estimate

Inner cylinder, bulkheads, machining:	\$ 4,500
Outer cylinder, frame:	\$ 4,000
Fluids	\$ 1,000
PMT	\$ 45,000
Electronics	\$ 10,000
Labor, assembly, testing:	\$ 35,000
Ship Time:	Assumed by UH
	\$ 99,500

**Table 6-1:** Cost estimate for the PMT-scintillator demonstration module

## 6.4 PMT-IMPLOSION DESIGN – PHASE II

### 6.4.1. Requirements

The design requirements include:

- A representative structure for the 3x3 PMT housing module
- Nine PMT's
- Glass sphere enclosures for the PMT's, rigidly mounted, with optical cones.
- Clear LEXAN panel enclosing the housing module
- Use seawater to represent the oil filled region.
- Pressure balance between the module inner and the seawater outside.
- Typical stainless steel structural elements that shall be used in the Hanohano detector installation.
- A frame and means of lowering.
- Monitoring instrumentation.

#### 6.4.2. Design Approach

**Deployment:** The intention is to incorporate what we have learned during phase one implosion testing into the overall design and layout of the PMT's, and consequently test the modular 3x3 design. The 3x3 rectangular module is to be assembled with eight normal PMT's in spheres and one weakened sphere (also housing a PMT). The weakened sphere will be prepared such that it will implode at a depth of 4000m (see chapter 4). This sphere is to be placed at the center of the 3x3 matrix to maximize the number of target spheres and target structural elements. The assembled module would be lowered over the side or stern of an oceanographic vessel. Since the module will be assembled without oil, and instead allowed to flood with seawater, only modest handling gear will be required. Similar lifting requirements to the PMT scintillator test deployment are envisaged.

The conceptual design is shown in

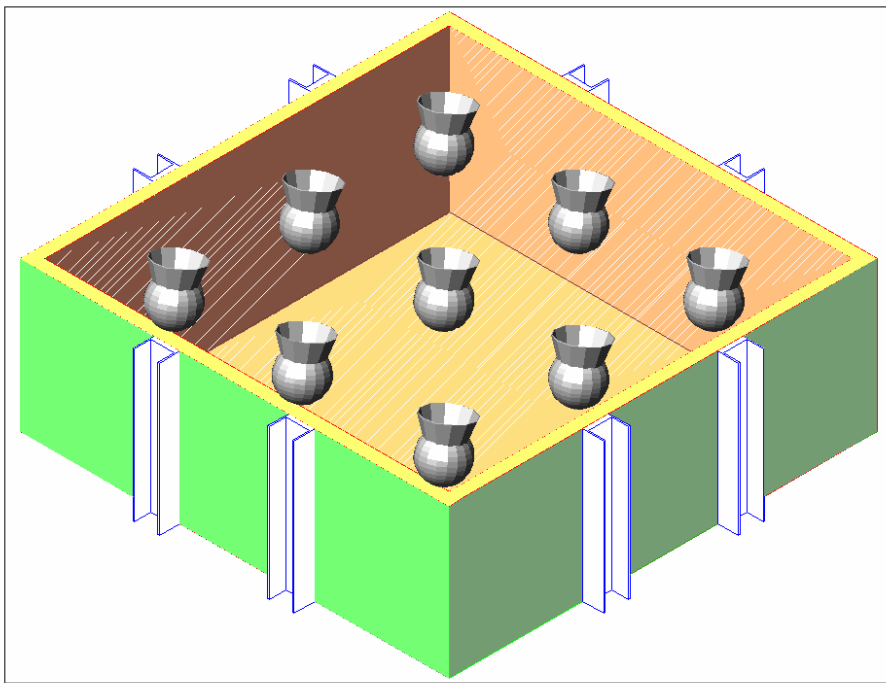
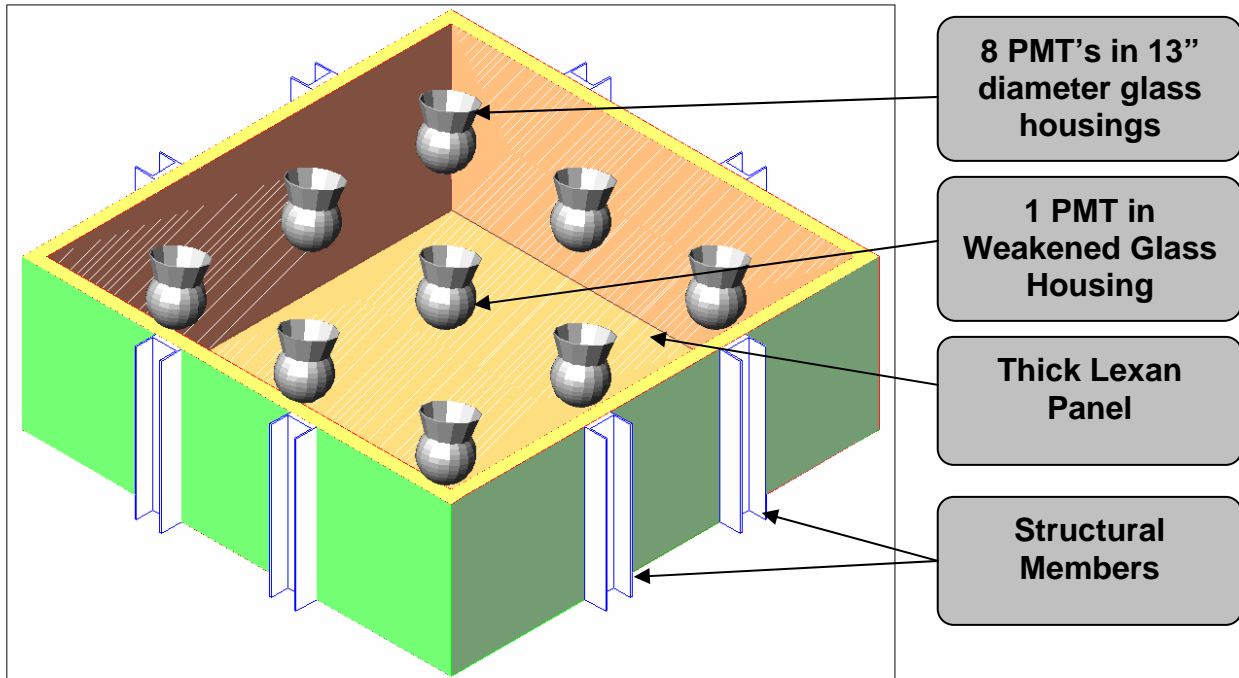


Figure 6-2. This design has the following features:

- The outer frame is stainless steel sheet. It is 2.8m x 2.8m. Depth is 1 m. The frame is slightly non-rectangular to match the draining and filling requirements of Hanohano.
- Total weight of the structure in air will be less than one tonne. It will flood with seawater (approximately 10 tonnes) when placed in seawater. Lifting and deployment will be easy, although the frame is large.
- The sheet covering is Lexan. It will be necessary to splice two 8'x8' sheets of lexan to form the total covering. (in the final design, these will be supplied as one special sheet).
- The nominal spacing between pmt spheres is 0.8m

- Sealing between the lexan and stainless is not critical. However, the flexibility of the Lexan should not be constrained.
- Instrumentation will be added inside the structure to log the pressure signal from the implosion.



**Figure 6-2:** Arrangement for the PMT sphere implosion test module.

#### 6.4.3. Cost Estimate

Stainless steel frame	\$ 19,000
Spheres, 18	\$ 5,400
Syntactic Foam inserts	\$ 4,000
Recycling, second test	\$ 12,000
Labor, assembly, testing:	\$ 23,000
Ship Time:	Assumed by UH
	\$ 63,400

**Table 6-2:** Cost estimate for the PMT-sphere implosion test module

## 7. CONCLUSIONS

### 7.1 ENGINEERING CONCLUSIONS

#### 7.1.1. Shape, Size

- An elevated cylindrical cylinder with rounded ends is the preferred shape; it can be built with less structural weight.
- A 10,000 m<sup>3</sup> detector meets the needs of the scientific community and is within our overall budget goal.
- A larger detector could be technically built, however costs would go up and a larger detector system would not fit through the existing Panama Canal.

#### 7.1.2. Configuration

- A detachable concept is structurally more feasible than an integrated concept.
- A detachable concept is more stable than an integrated concept.
- A detachable concept has a large safety factor on total weight than an integrated system.
- The detachable concept can be scaled up to use detectors of very large fiducial volumes.

#### 7.1.3. Design

- Pre-cooling the fluids in the detector is not cost effective.
- Reverse osmosis is a cost effective way to supply fresh water to the detector.
- Compensation can be accomplished by compensating the fresh water and scintillator only and allowing the structure to deflect for the oil compensation.

#### 7.1.4. Deployment

- The detector can be self-deployed without extraordinary buoyancy or lowering costs; it can perform as a large bathyscaphe.
- The detector must operate on a strict weight budget in order to return to the surface.
- The detector must follow specific operating procedures to maintain stability during deployment.
- Volume compensation will be needed to accommodate fluid contraction; this can be accomplished.

#### 7.1.5. Overall feasibility

- A 10,000 m<sup>3</sup> detachable, cylindrical anti-neutrino detector is technically feasible.

## **8. APPENDIX – BASIS OF DESIGN**

See attached document. For electronic copies, the Basis of Design is a separate document file.

## **Appendix**

**Task 3, 5, 7: Basis of Design Summary Document**

Appendix

**BASIS OF DESIGN SUMMARY DOCUMENT**

**HANOHANO NEUTRINO DETECTOR**

Prepared For  
**INTERNAL USE**  
**MAKAI OCEAN ENGINEERING, INC.**  
**ENGINEERING DIVISION**  
Makai Research Pier  
Waimanalo, Hawaii 96795

Prepared By  
**MAKAI OCEAN ENGINEERING (CEROS CONTRACT 7611 – DESIGN TEAM)**  
PO Box 1206, Kailua, Hawaii 96734  
September, 2006 – Revision 3.0.

# TABLE OF CONTENTS

A Summary of Makai's Report Format

<b>TABLE OF CONTENTS .....</b>	<b>I</b>
<b>1. INTRODUCTION .....</b>	<b>4</b>
1.1. INTENTION OF BOD DOCUMENT.....	4
<b>2. PURPOSE OF THE SYSTEM .....</b>	<b>5</b>
2.1. PHYSICS REQUIREMENTS .....	5
2.1.1. Scintillator liquid: fiducial volume.....	5
2.1.2. Oil buffer.....	5
2.1.3. Water veto region.....	5
2.1.4. Location of Neutrino Detector.....	6
2.1.5. Power and Communication requirements.....	6
2.2. DESIGN LIFE .....	6
<b>3. NEUTRINO DETECTOR CONCEPT .....</b>	<b>7</b>
3.1. OVERALL DESCRIPTION BASELINE CONCEPT .....	7
3.1.1. Scintillator tank.....	7
3.1.2. Oil buffer – Sensor region .....	7
3.1.3. Water buffer – veto region.....	7
3.1.4. External structure.....	7
3.2. OPERATIONAL REQUIREMENTS.....	7
3.2.1. Scintillator Fluid source.....	8
3.2.2. Hanohano Structural Assembly .....	8
3.2.3. Hanohano outfitting and instrumentation assembly .....	8
3.2.4. Testing .....	8
3.2.5. Transport to Location.....	9
3.2.6. On Site .....	9
3.2.7. Submergence, Bottom Placement .....	9
3.2.8. Comunication/power connections.....	9
3.2.9. Bottom time .....	10
3.2.10. Recovery .....	10
3.2.11. Tow back to port .....	10
3.2.12. Recycle for another site .....	10
3.3. VISION – THE STORY OF HANOHANO .....	10
3.3.1. The “story” of Hanohano .....	10
3.4. DESIGN AND CONSTRUCTION CRITERIA.....	12
3.4.1. Construction of support structure .....	13
3.4.2. Installation of detector components in support structure.....	13
3.4.3. Testing and final confirmation of performance .....	14
3.4.4. Flooding and ballast systems .....	14
3.4.5. Damage Limitations.....	14
3.4.6. Tow-to-field .....	15

3.4.7.	Installation to final position on seabed .....	15
3.4.8.	shore cable .....	15
3.4.9.	Long term seabed stability.....	16
3.4.10.	Recovery: .....	16
3.4.11.	Final recovery & disposal .....	16
3.5.	INDIVIDUAL DETECTOR COMPONENTS.....	17
3.5.1.	Fluid densities: .....	17
3.5.2.	Backup scintillators.....	17
3.5.3.	Photo Detectors & internal sphere electronics.....	18
3.5.4.	Instrument housings (Glass spheres) .....	18
3.5.5.	Acrylic boundary & material specs .....	19
3.5.6.	Cabling – electrical .....	19
3.5.7.	Cabling – optical .....	20
3.5.8.	Control units & multiplexers(?).....	20
3.5.9.	Total power requirements .....	20
<b>4.</b>	<b>SHORE CABLE.....</b>	<b>21</b>
4.1.	PURPOSE .....	21
4.1.1.	Communications requirements .....	21
4.1.2.	Power requirements .....	21
4.2.	MATERIALS.....	21
4.2.1.	Cable .....	21
4.2.2.	Terminations .....	23
4.3.	PLANNING AND INSTALLATION .....	23
4.3.1.	Bathymetry and cable selection .....	23
4.3.2.	Near shore protection .....	23
4.3.3.	Termination at Neutrino detector.....	23
<b>5.</b>	<b>ENVIRONMENTAL CONDITIONS .....</b>	<b>24</b>
5.1.	HARBORS.....	24
5.1.1.	Depth of harbors .....	24
5.1.2.	Harbor entrance (widths) .....	24
5.2.	CANALS – LONG TRANSITS .....	24
5.2.1.	Panama Canal .....	24
5.3.	BATHYMETRY .....	25
5.4.	OCEAN WAVES .....	25
5.5.	OCEAN CURRENTS .....	25
5.6.	SEISMIC EVENTS .....	25
5.7.	MARINE LIFE .....	25
<b>6.</b>	<b>COST.....</b>	<b>26</b>
6.1.	MATERIAL COST .....	26



## 1. INTRODUCTION

### 1.1. INTENTION OF BOD DOCUMENT

This document is intended to do the following:

- Define the design criteria, design issues, and construction issues associated with the Hanohano Neutrino detector
- Provide a common understanding of what is to be built. The budget for the preliminary design is limited. It is therefore important that UH and Makai both have the same understanding on what is to be built.
- This document will be updated as the project proceeds and as new information is provided. Later issues will be identified by the date in the footer. Makai will provide periodic updates to this document. Portions of the document that are updated will be clearly marked.
- In order to highlight critical items, Makai has marked action items as follows:
  - **Items in red:** need to be defined by UH
  - **Items in blue:** defined by Makai with agreement by UH

09/06 Updated based on considerable design work by both UH and Makai.

08/24/05 Updated document based on Task1-report from UH. Most important update: The overall scintillator volume was increased from 1000 to 4000 m<sup>3</sup>.

06/27/05 Updated due dates, Scintillator and Acrylic material spec. Also made many other smaller edits to the content.

05/16/05 This is the first edition of this document. The primary objective at this point is to provide an agreed upon set of design parameters suitable for completing task 1 of the CEROS proposal.

## 2. PURPOSE OF THE SYSTEM

The purpose of this deep ocean Anti-Neutrino detector is to measure natural earth background radioactivity for three purposes: (1) measure radioactive activity in the earth's crust (fundamental to understanding the formation and makeup of the earth), (2) determine whether the earth has a nuclear core reactor, and (3) provide background measurements critical to designing a much larger nuclear deterrence detector. The longer range purpose is to establish the ability to carry out deep ocean anti-neutrino monitoring for purposes of anti-proliferation monitoring.

### 2.1. PHYSICS REQUIREMENTS

The sizing of the detector should be such that a reasonable number (>25 or a better than 20% measurement) of the sought after particle-events will occur for the duration of the project (time in operation), that the backgrounds be sufficiently low (KamLAND levels or better), and that the sensitivity be adequate to the task (~10% resolution at 1 MeV). This section is a condensed summary and interpretation of the report from Task-1 of this project: "Detector Size and Sensitivity". The term "Task1 Report" will be used in this section when making references to this document.

#### 2.1.1. Scintillator liquid: fiducial volume

The detector will have a large fiducial mass of scintillator fluid held in an optically clear container with no internal partitions. This container can be in the form of a sphere, cube or cylinder. The nominal volume is 10,000 m<sup>3</sup>.

The scintillation response should be as good or better to that of KamLAND. The combined response of the LS and PMTs should exceed 100 photoelectrons/MeV of ionizing energy deposition. The purity of the LS should be better than or equal to that of KamLAND, except in Radon contamination where it should exceed KamLAND (initial installation).

#### 2.1.2. Oil buffer

Encapsulating the fiducial volume is a layer of oil on all sides. The thickness of this oil-buffer shall be: ~1 m. This region is where the Photo Multiplier Tube (PMT) instrument housings (glass spheres) are mounted. The outside wall of this layer is opaque and structural. It is also desirable that the structure not be visible to the inner volume, and be designed to be as far as possible from the boundary of the fiducial region (to minimize gamma rays from reaching same).

#### 2.1.3. Water veto region

Veto sensors (approximately 100-400 PMT's, of the same type as used for the inner volume) will need to be placed in the outer region to serve as veto for penetrating muons. This veto system tag muons which can produce neutrons and gammas which may penetrate the inner volume causing false signals, or which if penetrating the detector may cause long lived nuclear decays which also might mimic the rare signals of interest. The outer wall of this region is structural. Outside this wall is seawater.

#### 2.1.4. Location of Neutrino Detector.

A location close to the Hawaiian Islands, in water depth of 4000m will satisfy the criteria outlined in the Task1 Report. The detector can rest on or above (~100m) the seabed without significant loss in performance. A promising location would be west of Keahole Point, just north of Kailua Kona on the Big Island. A water depth in excess of 4000 m is available at a distance offshore of 20 km. This is close to the location of the original DUMAND project, an area that is well documented, and a shore facility already exists.

#### 2.1.5. Power and Communication requirements

The detector will require high-bandwidth communication with shore via standard E-O ocean cable. The anticipated data transmission rate is 1Gb, well within existing technology. Power requirements will be approximately 1 kW. It is strongly desirable to install a parallel redundant E-O cable for reliable operations, though this can be done at other than the time of initial detector deployment (earlier or later).

## 2.2. DESIGN LIFE

It is anticipated that the Neutrino detector and the associated communication cable will need to be operational for 1.1 to 2 years, yielding a 10 kt-y exposure or more (Ref. Task 1 report). Multiple deployments are anticipated for other locations and other experiments. For design purposes, we should assume a lifetime of 10 years.

### **3. NEUTRINO DETECTOR CONCEPT**

#### **3.1. OVERALL DESCRIPTION BASELINE CONCEPT**

The following section is a description of the baseline-concept for the detector. Various alternate concepts may be considered, but the baseline-concept outlined here is the most promising at this point in time.

##### **3.1.1. Scintillator tank**

The core of the baseline-concept consists of a cylindrical acrylic tank with scintillator fluid. This region is where the particle collisions are taking place. The working volume is 10,000 m<sup>3</sup>. There will need to be additional scintillator in a compensator system to account for volume change due to pressure and temperature. A key issue for the tank design is minimization of radioactivity in the tank wall.

##### **3.1.2. Oil buffer – Sensor region**

Outside the Scintillator tank is an oil-filled layer with a thickness of 1m. The sensors that detect particle events inside the Scintillator tank are mounted here. Each sensor consists of a Photo Multiplier Tube (PMT) mounted inside glass-sphere instrument housings. External light collectors (Winston cones) and magnetic shields are mounted to the glass spheres to improve the overall performance of the PMT. The sensors are focused towards the center of the Scintillator tank.

To prevent any light from entering the scintillator tank or the oil region surrounding the sensors, a light-impenetrable membrane is mounted behind the sensor housings.

A key issue for the housings is the risk associated with housing implosion. High reliability of housings and acceptance testing will make implosion unlikely, but design must allow for implosion of a single housing which will not proliferate.

##### **3.1.3. Water buffer – veto region**

The region outside this membrane is used for vetoing purposes. Multiple veto-sensors are mounted in this region to monitor for external events.

##### **3.1.4. External structure**

A strong external steel hull encapsulates the oil buffer layer. The purpose of this structure is to protect the inner volumes and provide a robust and rugged detector that can be handled at sea without risk of leakage.

Since the detector may need to be towed to field and lowered to the seabed, it needs to have hydrodynamic stability and also have a stable base suitable for resting on the seabed or anchoring close to the seafloor.

#### **3.2. OPERATIONAL REQUIREMENTS**

The following describes the basic requirements for operating the detector. These requirements may change, as the detector is designed, due to design constraints and opportunities. The design criteria are summarized in each section as bullets.

### 3.2.1. Scintillator Fluid source

The scintillator fluid is a particularly sensitive Hanohano component. It is a very large volume (approximately 10,000 m<sup>3</sup>) that needs to be loaded and maintained within Hanohano at an extraordinary purity. The Scintillator is likely to be LAB provided by Salsol in Baltimore. There is a second supplier in the Toronto area.

Transport of the LAB to Hawaii may be a cost and contamination issue. The project needs the material delivered to Hawaii with minimum contamination and at a reasonable cost. The quantity is small for a dedicated tanker, and yet very large for standard chemical containers.

If properly configured, Hanohano may be able to serve as the transport vessel for the scintillator. A configuration that could provide such clean transport economically would be desirable.

- Desirable: be able to provide clean transport for the scintillator fluid from the East Coast of the US to the Pacific.

### 3.2.2. Hanohano Structural Assembly

Hanohano is envisioned as one or two large steel structures. Construction is likely in a shipyard using traditional shipbuilding fabrication methods. Unique characteristics will be the inner hull of the detector (acrylic) and the middle hull (stainless steel). The outer hull of the detector can be carbon steel.

Fabrication is likely to be outside of Hawaii due to cost competition. The empty detector must be easily transported to Hawaii. Due to size, this detector must be easily towed.

- Can be built in a shipyard
- Carbon steel and stainless steel can be primary structural materials
- Transportable to Hawaii and elsewhere in the world via an ocean tow

### 3.2.3. Hanohano outfitting and instrumentation assembly

After delivery to Hawaii, Hanohano will be docked in a harbor (Snug Harbor) for final outfitting. That outfitting may include all delicate fabrication not completed in the shipyard (possibly mounting the acrylic plates for the inner cylinder), mounting all instrumentation, cleaning the detector and cleaning the scintillator fluid.

- Dockside outfitting of all instrumentation
- Dockside fabrication of interior of detector: acrylic plates, photo detector mounts, etc.
- Storage of scintillator for clean processing, prior to loading into detector.

### 3.2.4. Testing

It will be desirable to test the detector fully loaded with scintillator near the surface. An in-harbor location would be preferable.

- Dockside testing fully loaded preferable
- Back-up testing in shallow water may be acceptable

The Scintillator and oil will need to have extraordinary purity. See article J.B. Benziger. *A Scintillator Purification System for a Large Scale Solar Neutrino Experiment,*

[<http://theta13.phy.cuhk.edu.hk/aberdeen/useful\\_links/purification.pdf>](http://theta13.phy.cuhk.edu.hk/aberdeen/useful_links/purification.pdf)

1998

- Scintillator purification systems need to be available for processing and re-processing scintillator at the dock and whenever possible.
- Scintillator processing will involve transfer between tanks – extra storage tanks will be needed.
- SS scintillator tanks are preferable. Some plastic liners may be possible.

### 3.2.5. Transport to Location

Hanohano will then be moved to the final destination. The initial destination may be off the Big Island of Hawaii, but other locations are likely for subsequent measurements.

- Safely transportable, will all necessary components including scintillator and buffer oils

### 3.2.6. On Site

Once on site, Hanohano will be prepared for submergence. This preparation may involve the transfer of fluids, final filling of the detector, final testing, and re-configuring the detector from a towable form into a submersible form.

- Configured at sea for deep submergence

### 3.2.7. Submergence, Bottom Placement

Hanohano is then submerged, most likely in a free-fall, to a depth of 4000m. Temperatures and pressures will change considerably and the material densities will increase. Hanohano descent will halt as it hits the bottom.

- When released, it has sufficient weight to submerge
- Safe and reliable landing on the seabed at 4000m
- Provide compensation for compressing fluids
- Preferably the detector is just off the bottom

### 3.2.8. Communication/power connections

Once on the seabed, a communication and power cable is established between Hanohano and shore (The Big Island). These cables may be connected to Hanohano prior to submergence, and laid to shore prior to or after Hanohano submerges.

- Establish reliable power and communication connections to shore once on the seabed

### 3.2.9. Bottom time

Hanohano then sits on the seabed for one or more years. The fluids cool.

- Reliable operation at 4000m
- Provide compensation for cooling fluids

### 3.2.10. Recovery

After 1+ years on the seabed, Hanohano releases an anchor weight, disconnects its cables, and buoyantly rises to the surface.

- Have sufficient buoyancy for liftoff at the end of the experimental period
- Is stable upon ascent and on the surface

### 3.2.11. Tow back to port

### 3.2.12. Recycle for another site

- Access to all parts for maintenance, cleaning, replacement

## 3.3. VISION – THE STORY OF HANOHANO

This section presents the outcome of the Hanohano Anti-Neutrino detector project in the form of a future “news-story” about the project, after it’s successful completion. It is pure speculation and “virtual”. However, the process of updating this “story” as the project develops is a good forum for building a common understanding of what we are trying to design. It also may uncover new problems or requirements that we may never have anticipated.

### 3.3.1. The “story” of Hanohano

Construction of the Hanohano started in January 200\*. The two primary components: the barge and the Hanohano detector, were welded together at a mainland, East Coast, shipyard. After the hull was complete, all carbon steel surfaces were sand-blasted, cleaned and epoxy coated. All tanks were completed with transfer piping and pumps. The inner stainless steel hull was completed in the shipyard, but the assembly of the inner acrylic hull was delayed until the structure’s arrival in Honolulu.

The delivery of the barge and the Hanohano detector from the mainland coincided with the transport of the scintillator fluids and buffer oil. The oils were loaded into clean storage tanks within the barge. The barge has a capacity slightly greater than the full scintillator and oil requirement of the Hanohano detector. After picking up the liquid cargo, the barge with its liquid cargo and the empty detector was towed to Honolulu via the Panama Canal.

In parallel with the activity in the yard, the research team had leased a warehouse where the several thousand sensors could be assembled and tested. Each PMT was taken through a performance test before being mounted inside the pressure housings (glass spheres). The glass spheres were then sealed off and pressure tested to 6000 m. These spheres were then mounted on panels that could later be

mounted into the voids in the inner hull. These panels were manufactured with integrated light collectors and magnetic shields (grids).

As the sensors were being manufactured and tested, the first shipment of acrylic panels for the inner acrylic hull arrived from the Mainland. The geometry of the stainless steel structure was measured precisely before the first acrylic panel was glued to the adjustable elastic mounting pads. All panels had been precision-machined from the factory, so the process of building the inner hull was one of precise positioning and careful bonding. All support points could support small displacements, and could be individually adjusted to achieve desired stress levels. As the inner hull took form, the flexible pads were re-adjusted to counteract the increasing weight, and distribute the support-load evenly. All bonds were machined and polished to achieve a smooth finish.

After towing to pier-side at Snug Harbor, a temporary opening in the detector hull was employed to facilitate easy access at dock level. With installation of temporary access structures in the veto region, the detector was outfitted with internal instrumentation. Optical modules were installed and cabled to their local controllers in batches of 32 (64?). The cables and connectors were all inside oil filled Tygon hoses for maximum reliability against leaks. The local controllers were wired to twin redundant master controllers. At the same time, the pressure-housings controllers were installed and tested. Light sources were installed inside the acrylic tank to provide a source for the sensor tests. A light-protecting membrane was mounted outside each panel of sensors to prevent any light from entering the area inside the sensors. Section by section, the OMs were mounted, connected (during day shift) and tested (at night). This process took 8 weeks.

A purification facility had been setup at Snug Harbor for the operation of the sensor during its Hawaii experiments. The scintillator was moved from tank to tank within the barge as it was being cleaned by this facility.

With all equipment in place, a test "charging" of the detector took place. Hanohano was moved off of Honolulu Harbor and temporarily moored in 100m water depth. Scintillator fluid and mineral oil were pumped from the barge storage into the detector, evenly filling the detector compartments. Fresh water was manufactured by an RO plant on board and the outer buffer layer was flooded in stages to keep the entire detector stable at all times. As the detector was filled with fluids, it became lower and lower in the water, slipping through the moonpool of the barge. At all times, the detector was free floating. Once fully flooded, the detector continued to float with less than 1 meter of freeboard; the detector did not submerge because the bottom anchor was not in place for this test.

Continuous tests of the sensor equipment were conducted. A month-long performance test was then carried out with different calibration sources in the scintillator tank, measuring both the absolute response and the geometrical variations of the detector response. After the tests were complete, the oil and scintillator was pumped out of the detector and stored again in the barge. The fresh

water was pumped out and discarded. The detector rose inside the moonpool until it locked tightly against the bottom of the barge. Hanohano was then ready for towing to its final destination (which could have been anywhere in the world's oceans).

A large tug pulled the 100-m long barge loaded with the detector and all equipment a speed of 5 kts, and the entire tow lasted for 2 days. After arriving on site, the sea-state exceeded the maximum outlined in the deployment procedures. The tugboat maintained position for 3 days before conditions were acceptable for flooding and submergence. In the process, fresh water production was started with the onboard RO equipment.

The scintillator and oil were pumped into the detector, together with fresh water made on board, and the detector again slowly lowered itself into the ocean. Once fully flooded, the detector continued to float on the surface and final checks were made of the electronics.

A fiberoptic and power cable was attached to Hanohano and the cable ship pulled back from the barge position a distance of 1.5 km. A long suspended catenary of cable connected the ship to the detector; the shape was adjusted such that the cable would not be over-tensioned or grounded during the detector descent.

A 600-tonne wet weight anchor, stored tight against the barge bottom, was then lowered below the detector. The anchor was connected to the base of the detector by a 150m long synthetic tether. The winch lowering transferred the anchor load to the detector and then released the anchor. Hanohano sank quickly, gaining speed as it compressed and lost buoyancy. Total descent time was approximately 40 minutes. As the Hanohano anchor contacted the seafloor at 4200m, the tether line between Hanohano and the anchor went slack and Hanohano overshot its final destination depth by 40 meters. Hanohano continued to oscillate on the seafloor for several minutes, the anchor bouncing on the bottom for several cycles.

The detector was live and monitored from the cable ship. If problems had occurred with Hanohano, it could have been resurfaced. All equipment was functioning properly; The cable-laying vessel then proceeded with lay-operation for the 40 km long shore connection cable to Keahole Point

After 14 months of continuous operation, An acoustic release was used to sever the synthetic line between the buoyant Hanohano and the bottom anchor. Hanohano successfully surfaced and was at the surface in less than 40 minutes. The surface support barge and tug was waiting. With the assistance of a second tug, the barge's docking slot was aligned with the detector and finally the detector was centered in the moonpool. After engaging the fender restraints, the detector was unloaded of fresh water, oil and scintillator until it again raised high above the barge and was ready for towing back home.

### 3.4. DESIGN AND CONSTRUCTION CRITERIA

This section attempts to provide specific details and design criteria for use in the design process. These criteria exist in order to arrive at a detector that may fulfill the requirements & assumptions described above.

### 3.4.1. Construction of support structure

- (1) Welding & cleaning requirements
  - (a) Scintillator region most critical – super clean and cleanable surfaces. Minimal crevices. Polished surfaces.
  - (b) Acid etch of stainless containers required.
  - (c) Low radiation weld rod. Will require testing.
- (2) Corrosion protection and surface treatment?
  - (a) Carbon steel: all primary structure, outer hull. Anodes and epoxy coating.
  - (b) Inner structural hull: stainless, or stainless clad inner hull. Acid etch. Continuous and smooth. No corrosion protection (will be in contact with scintillator and oil only).

### 3.4.2. Installation of detector components in support structure

- (1) Scintillator tank (acrylic, glass, lexan)

Primary scintillator tank is lined with optically clear panels that are compatible with the scintillator and oil (one on each side). Optical properties and mechanical properties remain constant at pressure and temperature.

Acrylic is compatible with LAB and mineral oil (short term tests by SNO - Canadians). Long term tests are lacking. Lexan is a likely candidate, compatibility tests not done.

- (2) Sensors

- (a) PMT installation in pressure housing

PMT housed in 13" benthos glass sphere. PMT mounted to glass sphere with clear silicone sealant. Approximately 30% of the inner volume is unused (could be used by oil or syntactic foams).

- (b) Closing & testing of pressure housing

Housings are closed with a slight vacuum inside and sealed around the perimeter. Place gage in each one to show there is a vacuum for quality control

- (c) Winstone cone and magnetic shield

See UH report on the PMT design.

(d) Mounting mechanism

Mount simply with snap-in connectors. Holds PMT sphere securely even as volumes change slightly with increased pressure and drop in temperature.

(3) Wiring

Most if not all wiring through oil-filled hoses. Mostly twisted pairs. All wiring runs through veto region where accessible.

(4) Veto sensors

Mounted as needed to provide good coverage of the veto region. Final number and location determined once the final structural design is complete. The steel structure should keep veto region open as much as possible.

**3.4.3. Testing and final confirmation of performance**

(1) Replace / repair individual sensor housings.

All PMTs, wiring and plumbing are accessible from the veto region. The veto region is designed for human access with grate floors and internal stairways.

However, the fluids in the oil-filled chambers and scintillator will have to be lowered below the PMT elevation in order to open the hatch between the veto region and the PMT chamber.

**3.4.4. Flooding and ballast systems**

Structural pressure requirements:

- Structure can take free-standing oil + scintillator load without fresh water. Ie, structure could sit on the bottom somewhere and be filled inside. This filling would allow human access to empty veto region.
- Structure can be supported with internal pressure of the buoyant oil and scintillator.
- Structure can be flooded with oil and scintillator and submerged with the veto region partially empty (as required for stability and buoyancy).
- There shall be no floodable compartments that have an opportunity to trap any fluids or gases during flooding or draining. All horizontal surfaces shall be sloped for proper drainage and venting.
- Separate compensators will be required for the fresh water, oil, and scintillator fluids.
- Instruments will be needed to monitor the flooding progress.

**3.4.5. Damage Limitations**

Difference between bulk compressibility of the different materials must be taken in account when designing attachments etc.

### (1) Oil/Scintillator leakage

If there is a leak or damage to a PMT compartment, the oil/scintillator mixing should be limited to that compartment only. Each compartment is isolated from the other underwater.

Change in density due to accidental mixing due to rupture of shell between Scintillator fluid and Buffer region fluid. Need to verify density of mix between fluids to ensure that overall buoyancy is not affected. Since the true density of a mix ( $\rho_{\text{MixTrue}}$ ) of two fluids is not always the same as the density calculated from a simple mix-ratio formula ( $\rho_{\text{MixCalc}}$ ), we might get in trouble if the membrane between scintillator and the outer veto-compartment breaks:

$$\rho_{\text{MixCalc}} = (\text{VolSci} * \rho_{\text{Sci}} + \text{VolWtr} * \rho_{\text{Wtr}}) / (\text{VolSci} + \text{VolWtr})$$

$\rho_{\text{MixTrue}}$  = The actual density of mix between scintillator and pure water, should the membrane leak.

Potential buoyancy loss due to density increase ( $d\rho$ ):

$$d\rho = \rho_{\text{MixTrue}} - \rho_{\text{MixCalc}}$$

There shall be excess volume in the scintillator compensator to account for the above volume changes.

#### 3.4.6. Tow-to-field

- Easily towed to final location – distances may be many thousands of miles.
- Survive SS 7 conditions.

#### 3.4.7. Installation to final position on seabed

- (1) Lower to the seabed without use of cranes or winches. Use internal ballast control and buoyancy of the oil and scintillator.
- (2) Provide a means of confirming submerged weight prior to sinking – getting assurances that Hanohano will come back once the anchor is dropped.
- (3) Provide a safety factor on the submergence and ascent to allow for miscalculations on displacements on the seabed.

#### 3.4.8. shore cable

- (1) Shore cable to be laid attached to the detector prior to submergence, monitored during descent, and laid to shore once there is a touchdown.
- (2) A second, redundant cable can be laid, if necessary. An ROV would be used to make the connection to Hanohano on the seabed and the cable would be laid toward shore.

- (3) If there is a problem with the detector primary connector, the secondary can be utilized. If both connectors are damaged at the detector end, the instrument can be retrieved and these connectors can be diver replaced at the surface.

#### 3.4.9. Long term seabed stability

- (1) Bottom currents are 0.2 m/s max. Roll and pitch are not critical for Hanohano on the seafloor. Keep tilt angle below one degree.

#### 3.4.10. Recovery:

- (1) Hanohano will be a pendant buoy floating above the seabed. A concrete anchor will contact the seabed; a synthetic line will connect Hanohano to the anchor.
- (2) The length of the synthetic line will be determined by the dynamics of the descent. Once Hanohano contacts the seafloor, it will oscillate. The main structure should not come close to the seabed. (elevation 100m or more).
- (3) Recovery by use of acoustic release that cuts the synthetic line between hanohano and the concrete anchor. The anchor is abandoned on the seafloor.
- (4) The disconnection of the shore cable (and redundant backup, if installed) will take place automatically after the ballast is released. The cable(s) and (ocean mate/un-mate) connector mechanism(s) will remain on the ocean bottom.
- (5) Once surfaced, Hanohano can be prepared for rapid towing (for some locations, this may be many hundreds of miles to the nearest major port). The fresh water in the veto region can be dumped.
- (6) Hanohano can be recycled. By replacing the anchor and pendant, and refurbishing any damaged electronics, the detector would be ready for another deployment elsewhere.

#### 3.4.11. Final recovery & disposal

- 1) Liquid oil to be disposed of in local recycling/power plant by burning.
- 2) LAB is a commercial product and could be sold.
- 3) Detector internal parts to be recovered for use in further research.
- 4) Detector and tanks may be recycled.

### 3.5. INDIVIDUAL DETECTOR COMPONENTS

#### 3.5.1. Fluid densities:

Density of Hanohano fluids:

	Temp	Depth, m	Ambient Seawater Salinity	Ambient Seawater Density	Flooding Seawater Salinity	Flooding Seawater Density	Fresh Water Density	LAB Density	DD Dodecane Density	LAB 501 linear alkylbenzene	LAB 540 linear alkylbenzene
Surface:	C	m	ppt	kg/m^3	ppt	kg/m^3	kg/m^3	kg/m^3	kg/m^3	kg/m^3	kg/m^3
Pressure only	28	0	35	1022.397	35	1022.397	996.237	852.339	746.000	852.339	852.292
Temperature only	28	4000	35	1039.137 1.64%	35	1039.137 1.64%	1013.695 1.75%	881.474 3.42%	771.500 3.42%	-100.00%	-100.00%
Temperature only	1.5	0	35	1028.010 0.55%	35	1028.010 0.55%	999.924 0.37%	870.159 2.09%	765.396 2.60%	870.159 2.09%	869.782 2.05%
Temp and Pressure	1.5	4000	35	1046.391 2.35%	35	1046.391 2.35%	1019.476 2.33%	899.903 5.58%	790.896 6.02%	-100.00%	-100.00%
Temp and Press and Salinity	1.5	4000	34.6	1046.082 2.32%							

**Table 3-1:** Table of fluid densities for surface and at-depth conditions

#### 3.5.2. Backup scintillators.

- (1) Type: HPhenylxylylethane (PXE), an organic liquid Scintillator.  
[Ref. Borexino Collaboration, August 2004]

(a) Chemical description: C16-H18

(b) Material properties

Typical density: 988 kg/m3

Range in density: 980 – 1000 kg/m3

Viscosity (40 celsius) 5.2 cSt

...additional properties available in [Ref. above]

- (2) Type: Dodecane mix (80% Dodecane, 20% Trimethylbenzene) [Ref KamLand]

(a) Chemical description:

Dodecane: C12H26

1,2,4-Trimethylbenzene (pseudocumene)

+1.5 g/l 2,5-diphenyloxazole (PPO)

...Please confirm the above...

(b) Material properties

Typical density: 778 kg/m3 (Kamland – ref.UH) (...or: 820 kg/m3)

Range in density: 749 – 876 kg/m3. (for various mix ratios)

Dodecane density: 749 kg/m3

Pseudocumene density: 876 kg/m3

Viscosity (...Celsius) \_\_\_\_ cSt

### 3.5.3. Photo Detectors & internal sphere electronics

- (1) PMT Type: Photonis XP1804. 27.0 cm hemispherical 11-stage tube.
- (2) Quantities: ~4000 PMT's + 200 units in outer region
- (3) Physical properties
  - (a) Dry weight PMT: 1.744 kg.
  - (b) Estimated dry weight of other electronics inside the spheres: 1.744 kg (Same as PMT weight, or as low as half of this according to Gary Varner)

### 3.5.4. Instrument housings (Glass spheres)

- (1) Quantities: 2000 + 200 units for outer region
- (2) Manufacturer A: Benthos
  - (a) Type: "Deep Sea Glass Spheres"
  - (b) Glass quality: Borosilicate (low expansion)
  - (c) Physical properties
    - 13" OD (330mm)
    - 12" ID (305mm)
    - 9.07 kg dry weight
    - 10.4 kg buoyancy
    - Depth rating: 11034m
  - (d) Cost: \$305 per unit.
  - (e) Hard hat option: \$104 per unit

- (3) Manufacturer B: Nautilus / Schott

Type: Deep Sea Glass Spheres

Glass quality: Vitrovex (3.3 borosilicate glass)

Physical properties:

Refractive index (nd): 1.472

Dispersion (nf-nc): 72.6e-4

Standard models

13" OD (330mm)

306 mm ID  
8.5 kg dry weight  
107 Newton buoyancy  
Depth rating: 9000m

### 3.5.5. Acrylic boundary & material specs

- (1) Type: Polycast
- (2) Manufacturer: Spartech Polycast
- (3) Physical properties

Dry weight: 1190 kg/m<sup>3</sup>  
Thermal expansion: 0.000042 in/in/deg.F  
Water absorption: 0.26% after 26 days  
Refractive index: 1.49

- (4) Tensile strength

Yield: 11250 psi  
Elongation at rupture: 6.4%  
E modulus: 450000 psi

- (5) Flexural strength

Rupture: 15250 psi  
E modulus: 475000 psi

- (6) Compressive strength

Yield: 18000 psi  
E modulus: 440000 psi  
Sheer strength: 9000 psi

### 3.5.6. Cabling – electrical

- (1) Cable type: Coax - \_\_\_\_\_.
- (2) Estimated Quantity: \_\_\_\_\_ m
- (3) Manufacturer: \_\_\_\_\_
- (4) Physical properties

(a) Dry weight: \_\_\_\_ kg/m

(b) Submerged weight: \_\_\_\_ (in liquid: \_\_\_\_ at pressure \_\_\_\_)

3.5.7. Cabling – optical

(1) Cable type: \_\_\_\_\_

(2) Estimated Quantity: \_\_\_\_ m

(3) Manufacturer: \_\_\_\_\_ ---

(4) Physical properties

(a) Dry weigh: \_\_\_\_ kg/m

(b) Submerged weight: \_\_\_\_ (in liquid: \_\_\_\_ at pressure \_\_\_\_)

3.5.8. Control units & multiplexers(?)

(1) Dimensions: \_\_\_\_\_

(2) Dry weight: \_\_\_\_\_

(3) Pressure housing required: yes/no?

(4) Submerged weight: \_\_\_\_ (in liquid: \_\_\_\_ at pressure \_\_\_\_)

(5) Power consumption

3.5.9. Total power requirements

(1) \_\_\_\_\_

## 4. SHORE CABLE

### 4.1. PURPOSE

#### 4.1.1. Communications requirements

Single fiber adequate. Multiple fibers desirable for redundancy.

#### 4.1.2. Power requirements

Approximately 7,000 watts.

### 4.2. MATERIALS

#### 4.2.1. Cable

##### **OALC-5 (14mm) CABLE AND ASSOCIATED UNDERWATER PLANT**

CABLE TYPE	STOWAGE FACTOR Cubic metres / km	OUTSIDE DIAMETER (mm)
Light Weight LW	0.18	14 (PE sheath)
Light Weight Screened LWP	0.34	19.6 (PE sheath)
Single Armour SA	0.6	26 (PP rovings)
Double Armour DA	1.2	35 (PP rovings)

#### **Weights (Nominal)**

CABLE TYPE	WEIGHT IN AIR Tonnes / km	WEIGHT IN WATER Tonnes / km
LW	0.44	0.28
LWP	0.63	0.32
SA	1.6	1.0
DA	3.5	2.4

#### **A.4 Tensile Strength of Cable Types**

CABLE TYPE	NPTS (kN)	NOTS (kN)	NTTS (kN)	Min Cable Breaking Load (kN)
LW	20	30	50	60
LWP	20	30	50	60
SA	50	130	160	190
DA	50	150	200	270

These figures are for 1.8% fibre proof tests.

#### **A.5 Hydrodynamic Constants**

CABLE TYPE	(Rad.m/Sec) Lay / Recovery	(Degree.knots) Lay / Recovery
LW	0.416 / 0.488	46 / 54
LWP	0.376 / 0.441	42 / 49
SA	0.577 / 0.577	64 / 64
DA	0.770 / 0.770	86 / 86

*Typical mechanical characteristics of fiber optic cable suitable for supporting Hanohano*

21

**Typical / Maximum Deployment Depth for Cable Types**

Cable Type	Typical Depth		Maximum Depth	
	Surface Lay	Burial	Surface	Burial
LW	7000 m	-	8000 m	-
LWP	3500 m	-	7000 m	-
SA	1500 m	1500 m	2000 m*	2000 m*
DA	200 m	200 m	500 m	500 m

**Recovery Depths for cable with R3/4 6fp Repeater with 5kN margins from NTTS.**

Cable Type	Adverse Conditions (1knot,75degree,4m)	Standard Conditions (0.7 knot,80 degree,4m)
LW	5700	7100
LWP	4400	5800
SA	2000	2000
DA	500	500

**14 mm / 84 mm Joint Data**

14 mm / 84 mm Joint ID	LW/LWP	SA	DA
Length over bend limiters (m)	<b>1.480</b>	<b>1.710</b>	<b>1.710</b>
Rigid length (m)	<b>0.370</b>	<b>0.590</b>	<b>0.590</b>
Maximum diameter (m)	<b>0.170</b>	<b>0.140</b>	<b>0.140</b>
Diameter at mid point of joint (m)	<b>0.130</b>	<b>0.123</b>	<b>0.123</b>
Weight of joint in air (kg)*	<b>27</b>	<b>47</b>	<b>50</b>
Weight of joint in water (kg)*	<b>9</b>	<b>25</b>	<b>28</b>
Minimum bend radius of joint under tension (m)	<b>1.5</b>	<b>1.5</b>	<b>1.5</b>
Minimum bend radius of joint under no tension (m)	<b>1.5</b>	<b>1.5</b>	<b>1.5</b>

*Deployment and Recovery depths for fiber optic cables and joint characteristics – From Alcatel Submarine Networks*

### **14 mm Cable Electrical DC Characteristics**

The following are typical values for ASN 14 mm cable :

Capacitance	0.22 microfarad / km (typical)
Conductor resistance	< 1.6 ohms / km at 10 C
Insulation resistance	> 10 <sup>5</sup> MegaOhms.km

*Power transmission characteristics of the fiber optic cable*

#### **4.2.2. Terminations**

Hard connection preferable for cost and reliability.

### **4.3. PLANNING AND INSTALLATION**

#### **4.3.1. Bathymetry and cable selection**

For the purpose of this project, the shore-cable can be assumed laid on the seabed between the detector location and Keahole point. There is a tunneled shore connection at Keahole.

#### **4.3.2. Near shore protection**

For estimating purposes, the cable shall be assumed armored down to a water-depth of 500m.

#### **4.3.3. Termination at Neutrino detector**

Cable is attached to the detector prior to submergence. Cable is monitored during descent (through very large catenary, with cable ship 1 km offset). Cable is monitored during descent and controllably laid to shore after Hanohano is established on the seafloor and properly operating.

## 5. ENVIRONMENTAL CONDITIONS

### 5.1. HARBORS

#### 5.1.1. Depth of harbors

An initial operational site off the Big Island has been identified, but other global sites may be used. A survey of typical harbor depths worldwide shows that a design goal draft, fully loaded, of 10m would be acceptable for most harbors.

None of the harbors in State of Hawaii has sufficient depth for complete submergence of a Hanohano structure. Pearl Harbor is the deepest with it's ~15m draft. To completely flood the neutrino detector, the structure needs added buoyancy. For the purpose of design, we assume a design draft of 10m, keeping in mind that the detector should be maintainable on the Big Island too.

- (1) Honolulu: 40' (12.2m)
- (2) Pearl harbor: 49' (14.95m)
- (3) Barbers point: 38' (11.6m)
- (4) Hilo: 35' (10.7m)
- (5) Kawaihae: 35' (10.7m)

#### 5.1.2. Harbor entrance (widths)

- (1) Honolulu: 500' (Not a problem)
- (2) Pearl harbor: 1200' (Not a problem)
- (3) Barbers point: 450' (Not a problem)
- (4) Hilo: 800' (Not a problem)
- (5) Kawaihae: 525'

### 5.2. CANALS – LONG TRANSITS

#### 5.2.1. Panama Canal

- (1) The panama canal draft limit is: 12m, but PCC now restricts to 11m draft maximum to reduce water usage. This is fresh water draft
- (2) The beam limit is: 32.3m, but if under 30.5 m the passage takes less time since the vessels can then pass each other.
- (3) Panamax vessels are the largest specially constructed to cross the canal, and have a beam in excess of 30.5m.

### 5.3. BATHYMETRY

For the purpose of this project, no bathymetric survey will be required. For design purposes, the detector will be placed on the seabed in a water-depth of 4000m. The expected bottom conditions can be assumed ideal: Firm, stable, bottom sediments with moderate slopes of <2 degrees. The area can be assumed 20 km west of Keahole point.

### 5.4. OCEAN WAVES

The anticipated deep-water particle motion due to surface-wave action can be assumed negligible. However, the waves during launch, tow-to-field and final lowering will however affect the safety of the detector. The following conditions can be assumed:

- Assembly location: Sea-State 4-5 for severe weather, SS 3 for operational
- Tow-To-Field route: Sea-state 7 or less severe.
- Lowering of detector: Sea-state 3

### 5.5. OCEAN CURRENTS

Design currents should be based on “typical” deep-water Pacific currents in the region of Hawaii. For the purpose of deployment analysis, the following current profile can be assumed:

- Depth Current magnitude
- 0 m 1.0 m/s.
- 100 m .8 m/s.
- > 200m .3 m/s
- Bottom 0.1 m/s

### 5.6. SEISMIC EVENTS

The bottom-resting detector shall be designed to survive seismic events typical to Hawaii. Horizontal sea-bed accelerations of 0.5 g should be accounted for when designing the detector and all internal sub-systems. (on a pendant system, Hanohano will be relatively unaffected by earthquakes). Vertical accelerations can be assumed 50% of horizontal values.

### 5.7. MARINE LIFE

Under normal operation, the detector should be designed to have no adverse effect on the marine life. The Neutrino Detector contains a combination of pure water, mineral oil and scintillator fluids. The fluid containment system should be designed with double protection against spills. If applicable, all USCG regulations need to be followed. The exterior detector surface will be surface-treated similar to any marine vessel to prevent corrosion and limit marine growth. Standard treatment procedures, using approved materials needs to be used.

## 6. COST

### 6.1. MATERIAL COST

The average cost of steel (2003) was \$250-350 per ton, but has since January of 2004 has risen to \$650-\$750 per ton.

Stainless steel prices have tripled in the same period.

A standard LNG tanker (insulated) (130000m<sup>3</sup>) cost \$150 – 250 million (\$1923 per m<sup>3</sup> tank volume) (Ref. 185.pdf from eneken.ieej.or.jp/en/data/pdf/185.pdf)

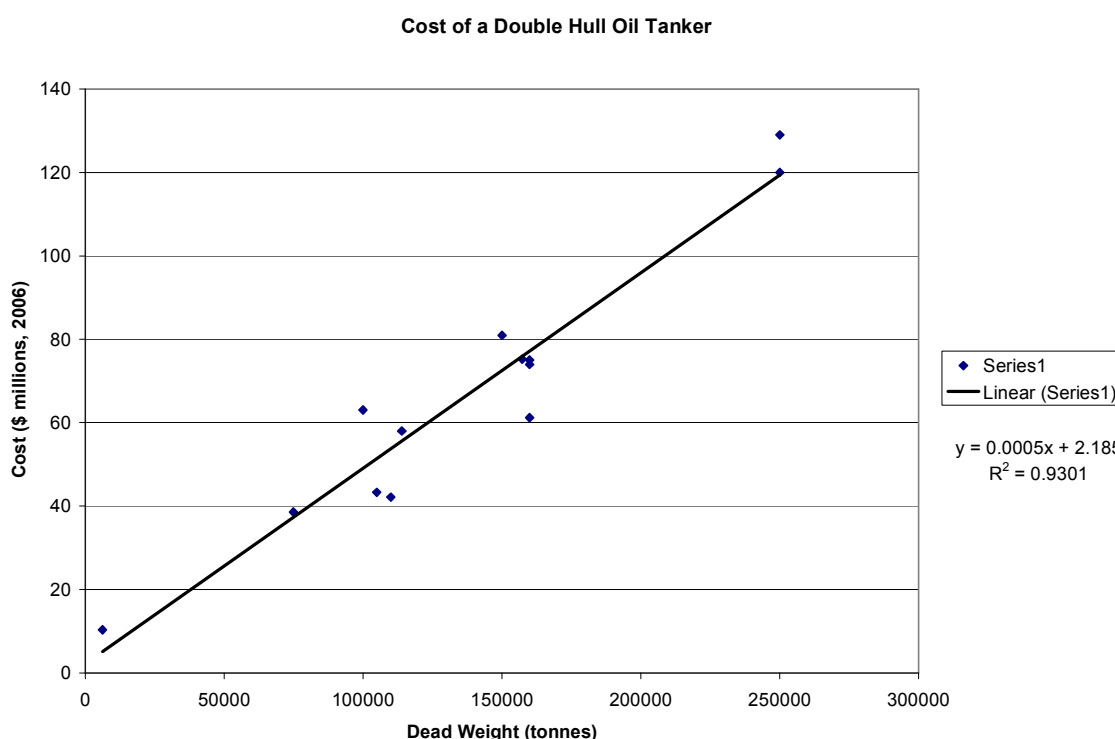
A standard LPG tanker (not insulated) cost \$60 million / 130000m<sup>3</sup> (\$461/m<sup>3</sup>)

Plastic sheet:

Lexan: sheet clear at 0.5" thick: \$143/m<sup>2</sup>.

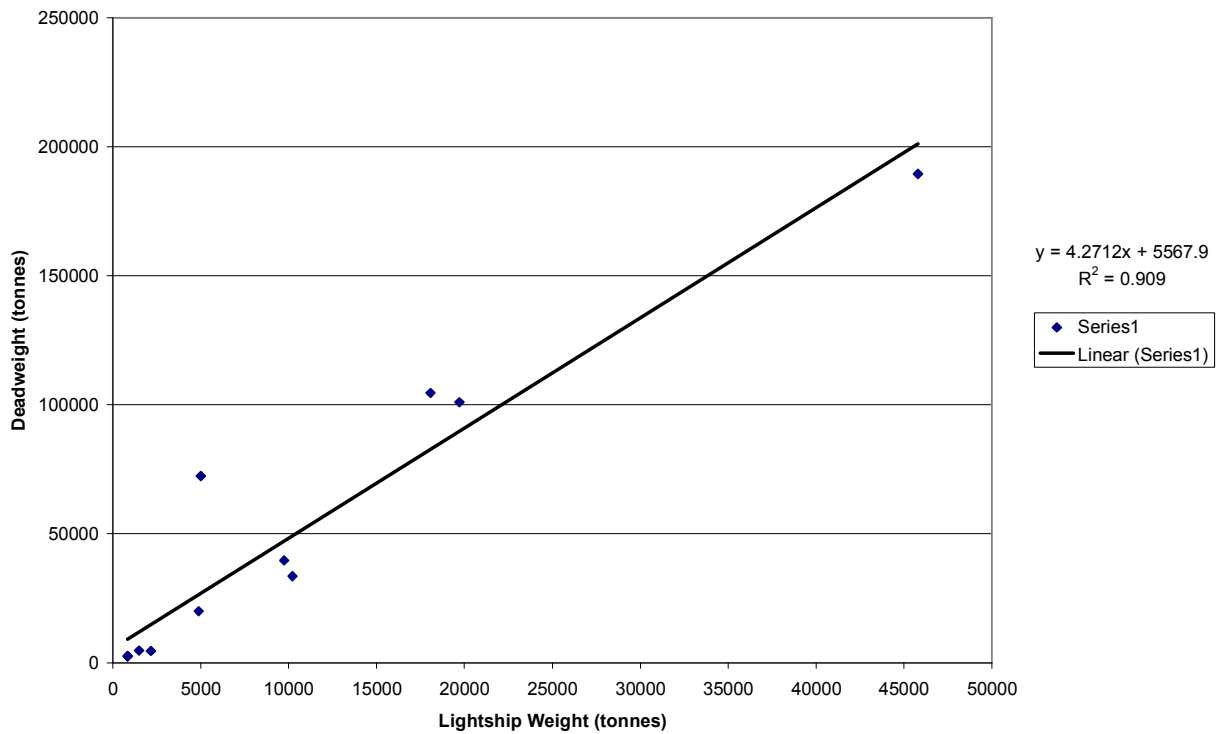
PMT: with glass sphere and electronics: \$5k.

Based on construction costs for recent tankers:



The above is \$480/DWTonnes or about \$430/m<sup>3</sup> for oil space (similar to the un-insulated standard LPG tanker above).

**Lightship Weight vs. Deadweight**



Final, all up, cost for the tankers is \$2400/tonne of steel.

The following is a probable cost summary for the Hanohano project.

<b>Total Cost</b>				<b>\$40,169,378</b>
<b>Barge Cost</b>				<b>\$8,970,720</b>
<b>Detector Cost</b>				<b>\$29,170,249</b>
<b>Deployment Cost</b>				<b>\$2,028,409</b>
Component Costs	Number	Units	Unit Cost	Item Cost Category Cost
<b>Construction</b>				<b>\$12,287,000</b>
Detector Structural Steel	1600	tonne	\$3,500.00	\$5,600,000
Barge Structural Steel	2477	tonne	\$2,500.00	\$6,192,500
Concrete Ballast	541	m^3	\$500.00	\$270,500
Concrete Releasable Anchor	448	m^3	\$500.00	\$224,000
<b>Fluids</b>				<b>\$1,813,209</b>
Scintillating Fluid Delivered to Barge	10558	m^3	\$100.00	\$1,055,800
Oil Delivered to Barge	3970	m^3	\$100.00	\$397,000
Fresh Water Made Via Reverse Osmosis	7796	m^3	46.23	\$360,409
<b>Compensation</b>				<b>\$91,949</b>
Compensator Bags	945	m^3 stored	\$97.30	\$91,949
<b>Reverse Osmosis Equipment - 182,000 gallons per day</b>				<b>\$520,000</b>
Equipment FOB Factory	1	ea	\$320,000.00	\$320,000
Delivery and Installation	1	ea	\$200,000.00	\$200,000
<b>Transportation</b>				<b>\$900,000</b>
Tug - 3400hp in Honolulu	30	day	\$20,000.00	\$600,000
Barge Operation	30	day	\$10,000.00	\$300,000
<b>Machinery</b>				<b>\$2,090,417</b>
Scintillator Pump - 4200 GPM	1	ea	\$46,866.00	\$46,866
Motor	1	ea	\$5,400.00	\$5,400
Oil Pump - 1850 GPM	1	ea	\$35,750.50	\$35,751
Motor	1	ea	\$2,400.00	\$2,400
Scintillator Purifying Equipment	1	ea	\$2,000,000.00	\$2,000,000
<b>Plumbing</b>				<b>\$167,804</b>
Scintillator Fill Pipes - 12" HDPE Pipe	200	m	\$29.50	\$5,900
Oil Fill Pipe - 8" HDPE Pipe	100	m	\$13.49	\$1,349
N2 Drain and Fill Lines - 1/2" Stainless Steel Pipe	1020	m	\$11.29	\$11,516
Installation	850	joints	\$3.74	\$3,179
Oil Drain and Fill Lines - 3" Stainless Steel Pipe	1020	m	\$100.00	\$102,000
Installation	850	joints	\$51.60	\$43,860
<b>Electronics</b>				<b>\$21,755,000</b>
Photomultiplier Tube Modules - similar to ICECUBE	4350	ea	\$4,500.00	\$19,575,000
64 Channel Digitizers and Connections	64	ea	\$20,000.00	\$1,280,000
Multiplexer Control Module	2	ea	\$100,000.00	\$200,000
Power Controller and Conditioner	1	ea	\$200,000.00	\$200,000
Calibration Gear	1	ea	\$500,000.00	\$500,000
<b>Personnel</b>				<b>\$544,000</b>
PMT Installation, Cleaning, and Calibration	120	man-month	\$3,200.00	\$384,000
Deployment Team	20	man-month	\$8,000.00	\$160,000

## Appendix

### Task 4: Optical Module Design

Appendix

# Optical Module Design

*A report submitted to Makai Ocean Engineering*

S.T. Dye and J.G. Learned  
*University of Hawaii at Manoa*

## Introduction

This report documents the design of an optical module for possible use in the deep ocean antineutrino observatory Hanohano. We have explored existing optical module designs and identified two available candidates from the high energy neutrino projects IceCube and NESTOR. Actual working modules of each design have been built and tested. For each module we have evaluated its suitability for our application, cataloged its characteristics, and summarized the results as presented below.

Both modules consist of large-area, hemispherical photomultiplier tubes (PMTs) housed in pressure-tolerant glass spheres. Each has printed circuit board electronics for controlling PMT voltage and collecting PMT signals. Candidate modules differ primarily in their size. The IceCube module employs the Hamamatsu (R7081-02) 25-cm diameter tube in the 13-inch Benthos (2040-13V) instrument housing. The NESTOR module employs the Hamamatsu (R8055) 33-cm diameter tube in the 17-inch Benthos (2040-17V) instrument housing.

Optical module evaluation for the present application includes many criteria. Important characteristics include photocathode area, timing resolution, multi-photoelectron discrimination, power requirement, dark noise rate, buoyancy, and implosion risk. The primary concern of this report is photocathode area. Remaining characteristics are addressed in other reports.

## Photocathode Area

Photocathode area is necessary for collecting photons produced in antineutrino interactions. A discussion of the optical budget for Hanohano is presented in Appendix A. Basically the goal is to subtend as much solid angle as possible. In this regard the larger the PMT diameter the better, although there are tradeoffs as discussed below. Photon collection can be augmented by coupling the optical module to an external light concentrator called a Winston cone. The design of Winston cones is covered in Appendix B.

## Glass Pressure Housing

The borosilicate glass instrument housings are manufactured by both Benthos and Nautilus. We note that the NESTOR project found damage to about 20% of the 70 Vitrovex (or Duran) spheres made by Nautilus after pressure tests. Benthos housings of 13-inch (17-inch) diameter have a buoyancy of 10.3 kg (25.4 kg) and a depth rating of 11,034 m (6700 m). Other properties of the Benthos 13-in spheres include:

- low expansion borosilicate glass
- potassium content in the glass: .027-.035%
- density of approximately 2.368 g/cc
- % transmission at 320 nm >14%,
- wavelength at 50% transmission 338 nm
- % transmission at 500 nm >90%

## Evaluation of Tradeoffs

Two working options for the optical module design are identified above. It is excellent to have options to evaluate. Some of the many tradeoffs to consider are listed below.

- 1) Pressure rating- 13-in spheres are rated to 11 km; 17-in spheres 6.7 km. Are the 13-in spheres less prone to failure at the nominal 4 km working depth of the deep ocean antineutrino detector and therefore safer than the 17-inch spheres? What triggers the failure mechanism and how does it depend on depth? These questions are investigated in a subsequent report on implosion studies.
- 2) Volume- 17-in spheres have more than twice the volume as 13-in spheres. Hence twice the stored energy (pressure times volume) to deal with should one implode. Can design modifications like syntactic foam-filling sufficiently mitigate damage to prevent sympathetic implosion of other spheres? Are these modifications workable with both 13-inch and 17-inch spheres? These questions are investigated in a subsequent report on implosion studies.
- 3) Pixels/number of spheres- The monolithic anti-neutrino detector images vertices of positron annihilations and neutron captures. Vertex resolution improves as the square root of the number of pixels, although many other factors contribute (PMT timing, scintillation decay time, etc.). The ability to localize positron annihilations directly impacts the uncertainty in a measurement of absolute antineutrino flux through uncertainty in the number of antineutrino targets. On the other hand more spheres increases the probability of an implosion failure and closer spacing may increase the probability of sympathetic implosions.
- 4) Photocathode area per pixel- Sufficient photocathode area is needed to achieve the required energy resolution. The cross-sectional area of the 25-cm PMT is about 43% less than that of the 33-cm PMT. Therefore achieving the same cross-sectional photocathode area requires 43% more 25-cm PMTs than 33-cm PMTs. Since optical module cost is a major expense of the project the relative cost of each module needs evaluation. Nonetheless, instrumentation cost scales roughly as the number of channels. In this regard fewer, larger area pixels would be more cost effective than more, smaller area pixels.
- 5) PMT timing- Smaller PMTs usually have better timing resolution than larger PMTs. Good timing leads to good vertex resolution. Many factors (distance to the first Compton

scatter, scintillation decay time, light scattering, etc.) other than PMT timing contribute to the ability to locate the true vertex. The timing resolution of each of the candidate optical modules needs to be compared with the timing uncertainties due to other factors to determine which dominates.

6) PMT noise- PMT dark noise introduces uncertainty to both position and energy measurements. Because dark noise is thermal in nature the low temperature of deep-ocean water is a benefit. Noise is typically reduced by a factor of two for every 10° C decrease in temperature. The dark noise rate of each of the candidate optical modules needs to be compared and evaluated for effect on detector performance.

7) PMT pulse height discrimination- The ability to evaluate the number of photoelectrons produced in a given optical module determines energy resolution. This is particularly important when PMTs are recording multiple photoelectron pulses. Thus, it is more of an issue for a detector design employing fewer, large area PMTs than for one using more, smaller area PMTs. The pulse height discrimination of each of the candidate optical modules needs to be compared and evaluated for effect on detector performance. We note, however, that for presently available PMTs this criterion is not so much of an issue, and mainly has to do with electronic choices.

An evaluation of the tradeoffs presented by the two design options are briefly discussed below. Pressure rating and volume considerations (1 & 2 above) seem to argue for using smaller 13-in spheres with 10-inch PMTs. This needs to be confirmed by results from the implosion studies. Photocathode area per pixel (4) argues for the larger 17-inch modules. Number of pixels (3), PMT timing (5), PMT noise (6), and PMT pulse height discrimination (7) require further evaluation.

The following sections present information on each of the candidate optical modules.

### **IceCube Module**

The IceCube optical module (Tarasova et al., 2005) considered here is shown in Figure 1. A module on loan from the IceCube experiment is presently in the University of Hawaii physics laboratory for testing. Additional information on the IceCube module including a rough cost breakdown by component can be found in Appendix C.

### **NESTOR Module**

The NESTOR optical module (Anassontzis et al., 2002) considered here is shown in Figure 2. Pulse height distributions for this module are shown in Figure 3.

### **Conclusion**

Two candidate optical modules are identified. Both are suitable for use in a deep ocean antineutrino detector. Further detailed evaluation is required to ascertain if one module is better suited than the other. This evaluation likely requires a detector Monte Carlo program. Although such program is under development at the time of this writing, its execution is beyond the scope of this task.

Figure 1: Photographs show the ICECUBE Optical Module in the physics laboratory at the University of Hawaii. Front (top) and rear (bottom).



Figure 2: NESTOR Optical Module: Drawing of the NESTOR optical module shows the Hamamatsu R8055 PMT inside a 17-inch Benthos sphere. A photograph of a NESTOR module is below.

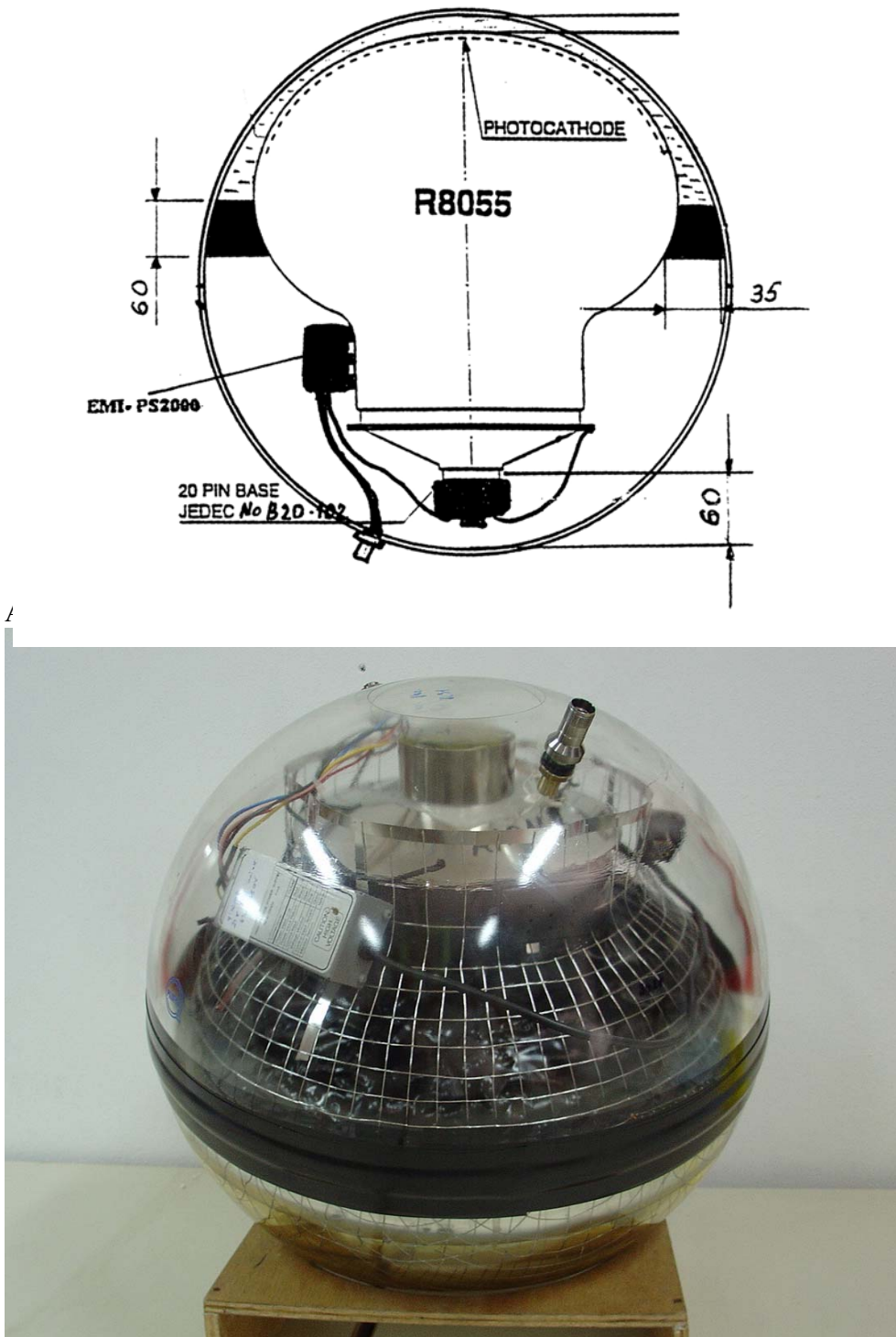
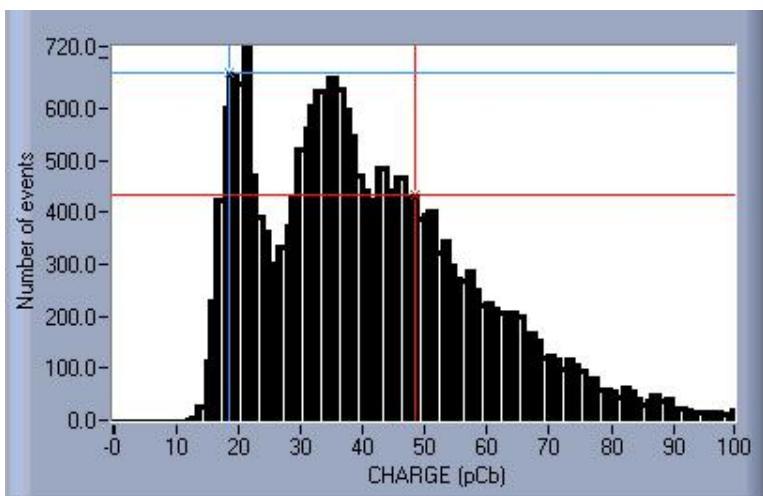
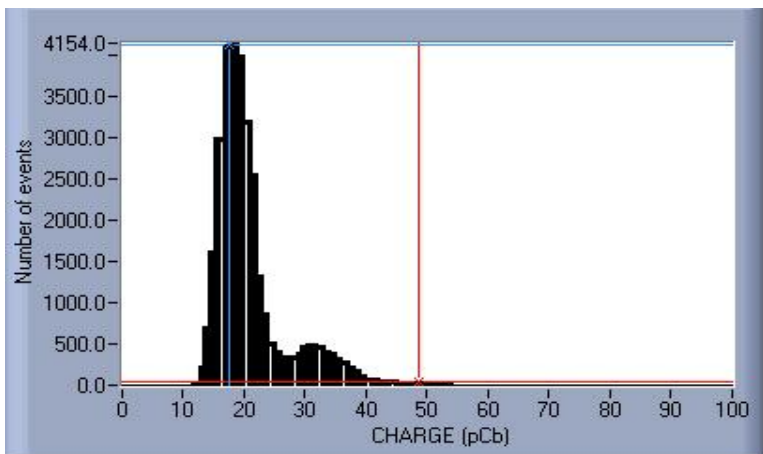


Figure 3: Pulse Height Discrimination: The following plots (provided by Leonides Resvanis of NESTOR) depict pulse height discrimination afforded by the Hamamatsu R8055 13-inch diameter hemispherical PMT. The first plot shows the one photoelectron shoulder emerging from the main dark noise peak for a weak light source. The second plot shows a distinct single photoelectron peak with a two photoelectron shoulder emerging for a strong light source.



## Appendix A

[E-log note (Message ID 43) by John Learned (6/20/05)]

We need a baseline optical budget. So far we have been using KamLAND, which provides a reliable starting point, which I will review below. After that I present a test optical budget for Hanohano, with an assumed spherical geometry. The quick summary is that with an assumed 2000 optical modules consisting of 10 inch PMTs placed on a 17-m diameter spherical surface, we should get a response of 238 pe/MeV. For this configuration, the 13 inch housings would be spaced on 20.5 inch centers.

### KamLAND

First let me give the numbers for KamLAND, from our paper (PRL94, 081801 (2005), hep-ex/0406035, and the earlier hep-ex/0212021). So here are some baseline numbers: 13m diameter balloon (roughly spherical), with 1 kiloton of scintillator (80% pseudocumene + 20% dodecane, doped with 1.5 gm/l PPO, H/C = 1.969, rho = 0.780 gm/cm<sup>3</sup>). The number which is most important to us here is the final event-by-event energy resolution. This is quoted as  $dE/E = 6.2\%/\sqrt{E/1\text{MeV}}$ , and corresponds to 34% photocathode coverage of the PMTs mounted on the inside of the 18m diameter SS Inner Detector sphere. If we take this resolution to be Poisson dominated (energy scale calibrations are much better), then the equivalent number of photoelectrons is  $N_{\text{pe}} = (1/0.062)^2 = 260 \text{ pe/MeV}$ .

Going back to the KamLAND US proposal (3/99), the quoted expected resolution there is only 10%/sqrt(E/1MeV), or 100 pe/MeV. When I try to get that number from scratch I get a larger predicted output: I have found on the web that pseudocumene + PPO is listed as having output as 50% Anthracene, the old standard for scintillator efficiency. This may be equivalent to 10,000 photons/MeV (the definition of "photons" is a bit slippery too as it depends upon spectral response, etc.) Nonetheless, if I take 1/3 as collection efficiency for KamLAND, 1/5 as quantum efficiency, and 80% as transmission from the center of the balloon (as indicated in the US proposal), I get 533 pe/MeV. Moreover this number is consistent with the number measured at the Borexino Counting Test Facility.

For the record, the buffer oil, which is outside the (0.135mm thick nylon/EVOH) balloon, is a mixture of dodecane and isoparaffin, adjusted to be 0.04% lower density than the LS in the balloon. Aside from the balloon there is a 3mm acrylic Radon barrier at 16.6 m diameter, just inside the PMTs. There are also a significant number of ropes making a net supporting the balloon. If I assume that the losses of balloon, ropes, and acrylic barrier amount to 10% (just a guess) then the sensitivity without these would be 286 pe/MeV. If I take the distance from the center to effective PMT surface as 8.5 m, and the true source effective output as 533 pe/MeV, this implies an attenuation length of 13.65 m. While this is not precisely correct, since the color and attenuation length change with distance, and I have assumed a homogeneous medium, it is not an implausible result. One can see that getting the absolute sensitivity of Hanohano correct, *ab initio*, will not be easy. On the other hand, the errors are in the square root, and we seem in any event to have a fair amount of reserve. The limitations of the experiment will be dominated by target volume (numbers of events) and radioactive backgrounds, not photon counting statistics.

## Hanohano

So, let us assume the KamLAND effective numbers as given above as our most reliable design estimate. Let us take the PMTs to be at the same radius in a spherical geometry, 8.5 m. Since we are thinking of having only an acrylic barrier and no balloon (or ropes) we can continue to discuss the radius at which this barrier is placed without changing the light collection fraction. Fortunately all the indices of refraction are close to 1.5 (oil, acrylic and glass), so we do not have to pay significant toll to reflections at the interfaces.

If we assume:

$$\text{Eta} = \text{quantum efficiency} = 20\% \text{ pe/photon}$$

$$N_o = \text{LS source intensity} = 10,000 \text{ photons/MeV}, \text{ same as KamLAND}$$

$$L = \text{effective scintillator light attenuation length from center to PMTs} = 13.6 \text{ m}$$

$$D_{\text{pmt}} = \text{phototube effective photocathode diameter} = 10 \text{ inches} = 0.254 \text{ m}$$

$$G_W = \text{Winston cone collection efficiency gain factor over PMT} = 2.0$$

$$N_{\text{PMT}} = \text{number of optical detectors} = 2000$$

$$R_d = \text{effective radius of photocathode surface} = 8.5 \text{ m}$$

Then the sensitivity of Hanohano from an event in the center will be

$$S = 238 \text{ Pe/MeV} \times (N_{\text{PMT}}/2000) \times (D_{\text{PMT}}/0.254\text{m})^2 \times (8.5\text{m}/R_d)^2 \times \\ (G_w/2.0) \times (\text{Eta}/0.2) \times \exp\{-(R_d/L - 8.5\text{m}/13.6\text{m})\}$$

This will give us an energy resolution of  $6.5\%/\sqrt{E/1\text{MeV}}$  for events in the detector center.

For packing calculations, the area per optical module OM will be  $A_{\text{cell}} = 4\pi \times R_d^2 / N_{\text{PMT}} = 907.9 \text{ m}^2 / 2000 = 0.454 \text{ m}^2/\text{cell}$

If the cells are hexagonal-closest-packed (I do not know how close we can come to this), then the distance across the flats, or the distance between OM centers, will be

$$D_{\text{cell}} = 2 \times \sqrt{A_{\text{cell}} / (\tan(30^\circ) * 6)} = 72 \text{ cm} = 28.5"$$

If the outer diameter of the glass pressure housing is 13 inches, this means there will be 15.5 inches between glass spheres. If square packed, the spacing would be 26". (Thanks to Tore for correction of numbers).

If this is found to be too tight from engineering considerations, then we can have modules further apart by either (or both of) reducing the number of modules (lose as  $\sqrt{N_{\text{PMT}}}$ ), and/or making the detector radius larger (and compensating with larger Winston cones). The gains in each are linear.

## Appendix B

[E-log note (Message ID 59) by John Learned (6/27/05)]

This is a note about the design of Winston cones for enhancing light collection in Hanohano. I assume that the 13 inch housings are being used, containing 10 inch PMTs (perhaps Hamamatsu 7081), and there are 2000 of these modules at a radius of 8.2 m from the inner detector center. This is the radius of the optical detector module entrance aperture... the front surface of the Winston cones.

If we take the standard Winston cone formulae, for a PMT radius of 5 inches, and a 6-m sphere with 2 m clearance, the collection angle is required to be out to 48.6 deg from the axis (97.2 deg total angle). The nominal Winston cone diameter would then be 13.34 inches, and the cone length 10.29 inches. This cone would give an optical gain of 1.78 under ideal conditions.

Scaling from the SNO design, our cone may be 13.1 inches aperture, 9.66 inches at the PMT, and length 5.27 inches and give us a 75% increase in effective collection area.

In this note we first review the Winston cone derivation, then discuss light collectors for non-flat detectors (as in our case), and finally review the excellent design used for the SNO detector.

### Winston Cones

The classic book on "The Optics of Nonimaging Concentrators" by Welford and Winston (1978) is well worth reading. Many optical designs are considered therein, but the classic concentrator known as the Winston Cone, is the centerpiece. Much development of this subject has taken place for solar collectors, and in particle physics for use with photomultipliers in various scintillation and Cherenkov counters. The basic derivation comes about by considering the extreme rays at the edge of the desired solid angle of acceptance. One ray must just clip the edge of the internally reflecting surface and pass through the smaller collection aperture. The parallel ray which strikes the other side of the cone and is reflected inside, also just passes through the aperture. The surface on the far side is taken to be a parabola, which focuses rays just at the edge of the exit aperture. This parabola has a tipped axis, NOT parallel to the axis of the cone.

It can be shown (see the textbook) that this formulation is optimal for the two dimensional case.... it optimally transforms the etendue (solid angle-area of the incoming light bundle) to that getting through the exit aperture over  $2\pi$  steradians. Without going through the derivation algebra here, we can summarize the important formulae:

$r$  = balloon radius

$d$  = clearance distance

$x = r/d$

$g = \text{capture area gain} = (1+x)^2$

$\sin(\theta_i) = 1/(1+x)$

$$\begin{aligned} a' &= \text{detector aperture radius (PMT photocathode projected area)} \\ a &= a'/\sin(\theta_i) = a'*(1+x) = \text{Winston Cone entrance radius} \\ L &= a'*(2+x)^{3/2} * \sqrt{x} = \text{Winston Cone length} \end{aligned}$$

Notice that there are only three choices to be made,  $r$ ,  $d$ , and  $a'$ . Further the net collection area does not depend upon  $d$ , but only upon  $r$ . Thus for optical reasons alone, we might consider large radii ( $r+d$ ), but we will only collect as much light as though the tubes were all at the surface of the balloon.

The assumptions in this concept are that one wants all rays to go through a flat exit aperture, but this is not exactly our situation (about which more below). Secondly, we are considering only uniform index of refraction (largely true for our case). And thirdly, more important, this situation only applies to 2D Winston cones. One can see that skew, off-axis rays (out of plane with the axis of the cone) may not spiral in for capture. One can think of this as an angular momentum problem. For the 2D case the capture area versus angle is just the aperture area times cosine of the angle off axis. For real 3D cones it is not so bad, typically going from ideal to cutoff in several degrees. (See Winston's book for examples). But this becomes worse for large apertures such as we need.

### Spherical Cap Collectors

The ray construction for flat collector apertures needs minor reconsideration for our case where the active area of the photocathode is a spherical cap, somewhat less than a hemisphere. The surface protruding above the plane at the exit to the Winston cone, will collect some rays directly, and it turns out that the ray construction of Winston just needs to be those rays which are tangent to the photocathode. Read the excellent paper by Moorhead and Tanner, (1996) for details.

### SNO Design

We are fortunate that our friends working on the SNO experiment did an excellent study and design of almost exactly what we need for Hanohano. In that situation, discussed in great detail in Doucas, et al. (1996), they consider a sphere and clearance radius just about the same dimensions of our nominal Hanohano design. The main differences in their situation are that they are using 8-inch phototubes (Hamamatsu R1408) and they have no need for a pressure housing for the PMTs. Their design results in a collector of 10.5 inches aperture, 4.25 inches depth and 7.73 inches PMT aperture. They also trimmed the length of the cone a bit (25% reduced length for only 2% loss in collection). If we scale this to our nominal 10 inch PMT, the numbers are 13.1" entrance aperture, 5.27" depth and 9.66" PMT aperture. Their gain starts to fall at 46 degrees and reaches zero at 60 degrees, about right for our case.

The SNO group considered many details, such as fabrication of the collector from sheets cut from a flat substrate. They have a particular concern due to the extreme corrosiveness of ultra-pure water, which will attack almost any reflective surface. This is not a problem for us, since the reflective surface will be in oil, and hence probably bare metal would suffice (though perhaps coated to prevent oxidation during assembly).

Another concern studied by the SNO group was the angular response of the photocathode to photons arriving at various angles to the local normal to the surface. We need not go into detail here, but it is somewhat fortuitous that the maximum in the response is out at larger angles (60 degrees), and this is a good match to the transform of phase space by the cone.

The net gain achieved by the SNO group seems to have been about 75%, with all of the approximations and compromises of real optical devices. So this is well worth doing, equivalent to having 1500 more photomultipliers in our case.

### **Hanohano**

For our situation, there is the added complication of the pressure housing, which is taken to be 13" for the 10" PMT. The PMT nestles rather close to the pressure housing, with the photocathode covering a cap region of about 120 degrees. Our collection cone will miss a region of the pressure housing thickness. Inside, we can have a small cone, which could be in or at the surface of the clear gel used to optically mate the PMT to the pressure housing. A calculation will have to be made to see how much we lose due to this gap, and if there is some way to mitigate that loss. But for now, I think we can use the dimensions as given above as a starting point.

## Appendix C

Information on the IceCube optical module is presented in the form of e-mail messages from K. Hanson to J. Learned on 7/6/05 and on 11/3/05. These messages are below.

----- Forwarded message -----

Date: Wed, 06 Jul 2005 16:27:16 -0500  
 From: Kael Hanson <kael.hanson@icecube.wisc.edu>  
 To: jgl@phys.hawaii.edu  
 Cc: 'Bob Morse' <morse@icecube.wisc.edu>  
 Subject: IceCube PMTs

Hi John,

Bob asked me to respond with some information that you asked for regarding IceCube experience /w/ PMTs and DOMs. The numbers follow your questions.

1. We chose Hamamatsu PMT primarily because of low-noise. We got samples from EMI and Photonis. Neither came close to Hamamatsu - probably because of activity in glass - we cool these tubes down to -40 C. Burle doesn't make large cathode PMTs as far as I know so you are limited to these three companies.
2. By the time I got on board we were set on 10" tubes - primarily - I think - because of drill hole size and compatibility with the 13" pressure spheres. There was some talk about using smaller spheres of quartz (increased UV sensitivity) - never went anywhere, however.
3. I once asked Hamamatsu about the outline - but, you know what, I forgot the response.
4. We tried 3 R7081 models -01, -02, and -10. There is also a -20. -01 and -02 are 10 stages, -10 was 12 stages. The -02 was an enhanced version with some special low EA material applied to the dynodes that gives it higher gain.
5. We originally paid about \$1350 per tube incl. shipping costs which are substantial - about \$100 per PMT. But since the price has gone up - we fixed it in yen about 1.5 years ago and you know the current deal with the US dollar.
6. We are happy with the noise performance of the tubes. They have a very low activity glass - 10 Bq.
7. We aim for total DOM background (including glass sphere) of 500 Hz. We average about 650 Hz right now. I have bigger fish to fry so haven't

paid much attention to the noise. The tube generates about 250 Hz of that 650 Hz.

8. Dark rates in lab at -40 with no optical coupling are 2.5 kHz.  
When we tape the DOMs up they drop to 1.3 kHz. In the ice the rates are 650 Hz.

9. Afterpulsing is about 2.5% per PE - so 10 pe signal gives 25%. A little bigger than I'd have liked. Hamamatsu says it's elastic scattering from 1st dy.

10. P/V for dark counting is 2-3 typically at our nominal 1E7 gain.

11. We are using an incredibly high Z base - current is 30 uA at 2000V.

12. Magnetic shield is supplied by ITEP Moscow. It's OK - 120 Euro per cage, easy to mount. It bucks the terrestrial field down by 50%. We estimate maybe 5-10% increase in collection efficiency. It gets mounted inside the sphere in the gel.

13. Long story on mechanical mounting. We use GE 6156 RTV but are not 100% happy with it. We are shopping around even now. We had some contamination issues this year and GE is hard to work with. The gel gets degassed, A/B components mixed, degassed again, poured and then allowed to set for 4-8 hours. It holds everything: the PMT, the circuit boards are mounted on a collar placed around the PMT neck. Nice solution.

14. Sealing is done by pumping down to 40 kPa. Somehow - I can't remember offhand - we get an atmosphere of dry N2 in there before pumping down. Then we monkey dung and tape. Not much trouble there.

15. The capture ring - or harness as we call it - is the same used in AMANDA. I can send you mechanical drawings if you like. The ring itself does not carry any load - that is transferred through the cables.

16. We use the Seacon (Brantner) connector - XSJJ - it's probably custom. Well, it's OK. It's glass-reinforced epoxy which has broken under mechanical stress here in the test labs but all survived in the ice. It is beefier than the AMANDA connectors. I wish someone had thought to not make them rotationally symmetric. There is a key but it is usually the thing that breaks. There is a double o-ring seal inside the connector.

Kael Hanson  
IceCube - In-Ice Devices  
(608) 890-0540 : 222 W. Washington  
(608) 262-3395 : Chamberlin (Physics Dept.)  
(608) 877-2221 : Physical Sciences Lab (PSL)

----- Original Message -----

Subject: RE: ICECUBE Module  
 Date: Thu, 03 Nov 2005 13:30:54 -0600  
 From: Kael Hanson <kael.hanson@icecube.wisc.edu>  
 Reply-To: kael.hanson@icecube.wisc.edu  
 Organization: IceCube Project  
 To: 'John Learned' <jgl@phys.hawaii.edu>

Hi John:

Thanks for the accolades - we spent a lot of time and dollars designing the module - so the industrial look is not cheap. The modules, however, are not that expensive. The (approximate) cost breakdown is

glass	\$500
HV	\$500
penetrator	\$500
PMT	\$1350
flashers	\$250
delay trace	\$100
mumetal	\$150
gel	\$60
mainboard	\$1500
labor	\$250 (this is production labor - not testing)

so it's about \$5k when you sum it up. The total cost we usually estimate per string:

60 DOMs / string	= \$300k
1 cable	= \$300k
surface readout channels for 1 string	= \$12k

But then there's the cost of drilling the holes, electricity, ...

Kael

---

Kael Hanson  
 IceCube Project - Data Acquisition  
 (608) 209-3994 : Cell phone  
 (608) 890-0540 : 222 W. Washington (Main Office)  
 (608) 877-2221 : PSL Office

## References

Anassontzis, E.G., et al., NIM A 479 (2002) 439.

Doucas, G., et al., NIM A 370, (1996) 579.

H. Miyamoto for the IceCube Collaboration: A. Achterberg et al., *Calibration and Characterization of Photomultiplier Tubes of the IceCube Neutrino Detector*, Presented by H. Miyamoto at the 29th International Cosmic Ray Conference, 3-10 August 2005, Pune, India, session OG2.5.

<http://icrc2005.tifr.res.in/htm/PAPERS/OG25/jap-miyamoto-H-abs1-og25-poster.pdf>

Moorhead, M.E. and Tanner, N.W., Applied Optics 35, (1996) 3478.

O. Tarasova for the IceCube Collaboration, *Design, Production, and First Results from the IceCube Digital Optical Module* Presented at the 9th ICATPP Conference on Astroparticle, Particle, Space Physics, Detectors and Medical Physics Applications, Villa Erba, Comom, Italy, 17-20 October 2005.

[http://www4.tsl.uu.se/~botner/Conferences/como2005\\_tarasova\\_icecube\\_paper.pdf](http://www4.tsl.uu.se/~botner/Conferences/como2005_tarasova_icecube_paper.pdf)

Welford, W.T. and Winston, R., "The Optics of Nonimaging Concentrators", (Academic Press, 1978)

## **Appendix**

**Task 6: Electronic Design for Reliability and Low Power**

Appendix

# Electronic Design for Reliability and Low Power

*A report submitted to Makai Ocean Engineering*

J.G. Learned, G.S. Varner, and M.K. Wilcox

*University of Hawaii at Manoa*

## Introduction

This task produces a preliminary design for detector electronics which focuses upon the vitally important issues of achieving maximum system reliability, and minimizing power consumption. The section on detector communications discusses the system design trades and concludes that maximum system reliability can be achieved with a tree structure network, in which all the data is fed forward without processing to the shore station. Achieving the required gigabit/second data rates was not practical until the last decade, and since has become standard practice for long distance, and in particular undersea, telephony.

In previous experiments the power levels per optical module have been in the neighborhood of 1 to 10 watts per channel (the higher for laboratory installations). Recent advancements in low power electronic components for particle detection applications (most dramatically perhaps for the ANITA balloon borne neutrino detection project) open the possibility of deploying an underwater detector with a self-contained power source. This is an attractive prospect given the likely remote location of the detector and the simplification of deployment.

A thorough literature search for components of potential use has been carried out, and the experience of other similar projects surveyed. The preliminary design utilizes reliable, low power components which meet the operating criteria of the photo-detectors. First generation prototypes of the electronic components have been constructed and tested. We see no problems on the horizon, and conclude that a battery powered detector may indeed be practical (though not necessary for most applications).

## Photo-detectors

The choice of photo-detectors for this experiment is highly limited. There are many new designs for optical detectors discussed at present, but as of yet none can approach the requirements of low cost, low noise and large area of vacuum photomultiplier tubes (PMTs). Solid state detectors simply do not yet rival PMTs, though they are the device of choice for small collection areas and high pixelization, as in astronomical telescope applications. Discussions of “photo-detector wallpaper” are a few years from realization.

A possible criterion for selecting the size of a photo-detector is that such should not be larger than the scale at which one wishes to resolve the location of the neutrino interaction. Present detectors achieve a vertex resolution on an event-by-event basis of only about 1 m, or slightly less. There is the possibility to bring this scale down to perhaps 10 cm, and hence one would not want detectors with sensitive areas to be very

large compared to that scale (of course with many detectors recording signals from the same event one gains by fitting the arrival time at many sensor locations). Another constraint is the scintillating liquid fast decay time, which for present materials is on the order of 1 nanosecond, so there is no point in having a detector much smaller than the distance traveled in such a time ( $\sim 20$  cm in the oil). All of this suggests that there is not much to be gained by pixelization at smaller than about 25 cm.

Another physics criterion for photo-detector selection would be that one would not want a sensor area larger than that which will have one photoelectron (1 PE) in the light of a typical (1 MeV) event. This would be a detector of order  $10 \text{ m}^2$  for the scale and sensitivity of this experiment. We are in no danger of approaching that limit, with the largest PMT on the market only  $0.4 \text{ m}^2$ .

Below this scale there are PMTs ranging down to about  $1 \text{ cm}^2$  in photocathode area. With the large scale production of smaller tubes for medical applications, the prices of PMTs in the 1-5 cm diameter are attractive (of order \$100/PMT, as compared to \$3K for the largest). In fact it has been noted widely that the cost per unit photocathode area has become roughly constant. This might make one consider employing many small tubes, which would have the advantage of less volume per unit and less trouble with isolation to prevent runaway implosion in the (unlikely) event of an optical detector housing collapsing. One difficulty with the extreme of this approach in employing many small PMTS is that while the PMT costs may be constant, the ancillary costs of housings, connectors and cables, and electronics will scale with the number of channels (though smaller housings are somewhat less expensive, but are not a major factor on the overall detector costs, ~10%)

Perhaps we should restate the obvious: it is necessary to place the PMTs in pressure housings for depths greater than about 10 atmospheres equivalent (100m). This is because the overall detector cannot possibly be inside a pressurized hull; the economics of such a hull would be prohibitive. And since the PMTs are not spherical they do not well resist compression. There has been talk of manufacture of spherical PMTs, but it has not been realized. Moreover there would be problems with the real size change (several mm) of PMTs going to ocean depths, and spallation from the inner surface, commonly seen in the instrument housings.

A practical constraint on detector size choice is the availability of deep ocean glass instrument housings (typically called “Benthos spheres”, after the company that brought them into common use). These are presently available in 10”(9.3” ID), 13”(12” ID) and 17”(15.9” ID) versions. The largest PMT on the market, the Hamamatsu 20” tube (12,000 of which are employed in Super-Kamiokande in direct immersion in water up to 40m deep) will only fit in a sphere at least 30 inches in diameter. Aside from the fact that no manufacturer offers such a huge housing, the handling and mounting of such would be extremely awkward, not to mention the roughly nine times stored energy compared to a ten inch housing. For this reason the underwater and under-ice high energy neutrino experiments have settled upon housings of either the 13” or 17” scale.

Photomultiplier tubes in the range of 10-16 inches are thus selected as the fundamental transducer for recording neutrino events. A photomultiplier requires a high voltage DC ( $\sim 2$  kV) divided across the 10-14 electron pulse multiplying dynodes. Gains in the range of  $10^7$  and higher will not require amplification at the photomultiplier.

After surveying available photomultiplier tubes and reviewing the choices made by the most relevant experiments (ICECUBE, NESTOR and ANTARES) we narrowed the list to several 10 inch PMTs, which fit in the standard 10 inch housings. This will be our baseline choice, but probably ought to be revisited in the near future since several PMTs in the 13 inch range may become available and might tip the choice to the slightly larger tubes.

### PMT Examination

Three photomultiplier tubes were purchased for evaluation: Two Hamamatsu 10-inch R7081-20 ([www.hamamatsu.com](http://www.hamamatsu.com)) at \$2200 each and one Photonis 10.6-inch XP1804 ([www.photonis.com](http://www.photonis.com)) for \$1586. Preliminary testing of the Hamamatsu photomultiplier tube (PMT) is presented. Hereafter PMT refers to the Hamamatsu R7081-20. The weight of each PMT is approximately 1200g. Each PMT has a 20-pin socket type JEDEC No. B20-102 attached as required for testing. Figure 1 below shows a schematic drawing of the PMT and its test socket.

Manufacturer specifications allow for operating temperatures of the PMT in the range of  $-55$  °C to  $+28$  °C. The rate of PMT pulses due to thermal emission of electrons from the photocathode, which is called dark noise, is given as a typical value and a maximum value. For a temperature of  $+25$  °C, the dark noise is 7,000 counts per second (cps) for the typical value and 15,000 cps for the maximum value. For a temperature of  $-40$  °C, the dark noise is 500 cps for the typical value and 1,000 cps for the maximum value. These values are plotted in Figure 2 allowing interpolation for intermediate temperatures. For a temperature of 4 °C, the approximate temperature on the ocean floor, the dark noise is approximately 5,000 cps for the typical value and approximately 11000 cps for the maximum value.

There is a pre-pulse (at 50 photoelectrons illumination) possibility from 10 ns to 100 ns before the main output pulse of the PMT. Pre-pulsing can introduce systematic errors in pulse arrival times. There is also a possibility of a late-pulse from 25 ns to 100 ns following the main output pulse. The PMT also has an after-pulse possibility from 100 ns to 16,000 ns following the main output pulse. This is typical of this class of tubes and proves to be no serious problem in data analysis.

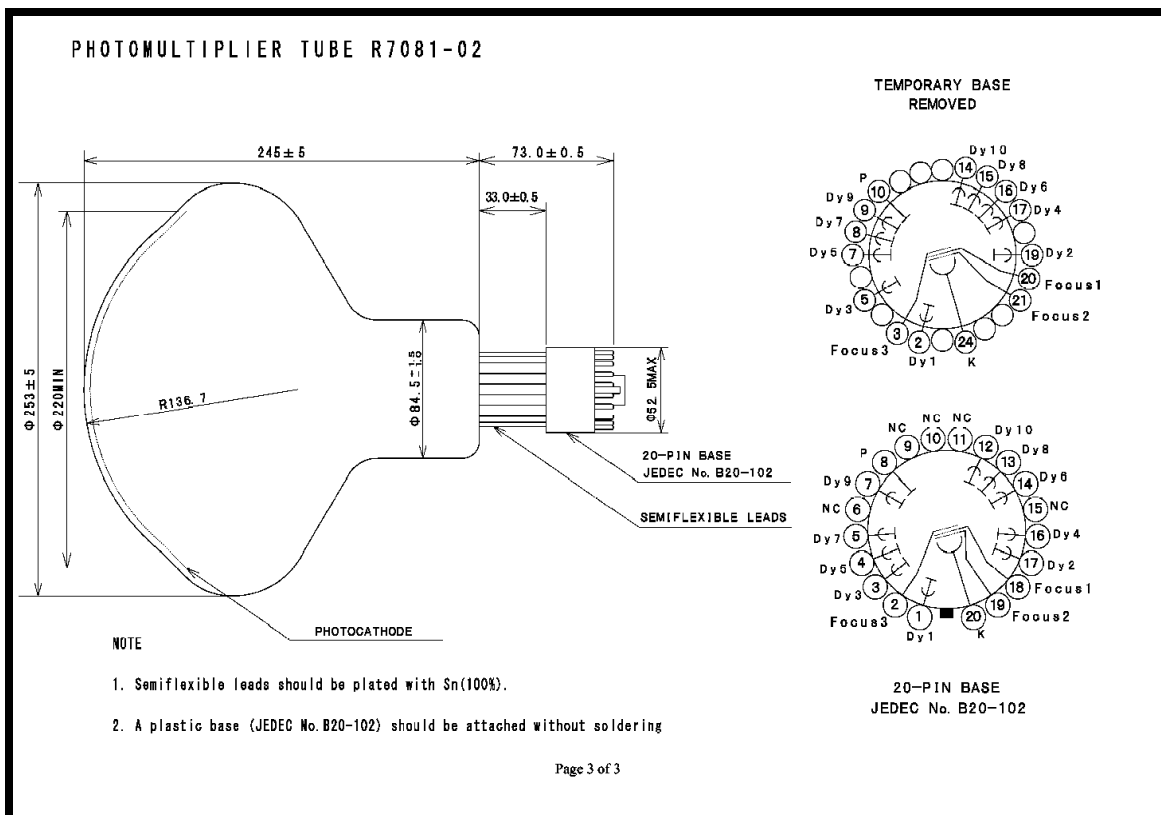


Figure 1: Schematic of the Hamamatsu R7801 PMT and its test socket.

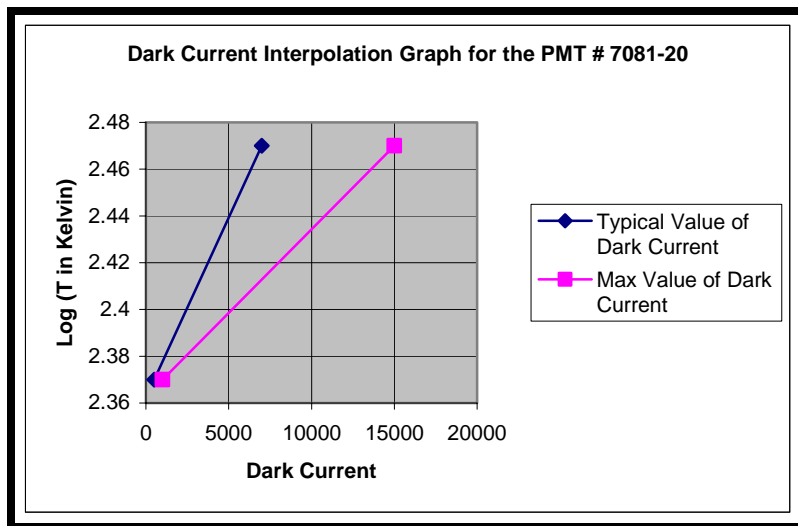


Figure 2: Dark noise versus temperature for the Hamamatsu 7081-20 PMT.

## PMT Base Electronics

The PMT base electronics is a modular printed circuit board which generates the high voltage needed to operate the photomultiplier tube. Two PMT base electronics boards were purchased for evaluation from ISEG (<http://www.iseg-hv.com>). Total cost with shipping for both was \$685.00.

One of the first tests conducted on the PMT base electronics board was to produce a transfer curve. A transfer curve maps out the relationship between the input DC voltage and the output voltage. Clearly established is a linear relationship between the input and output high voltage. The test was conducted by supplying a DC input directly to the PMT base and measuring the output of the anode pin. These results are shown in Figure 3.

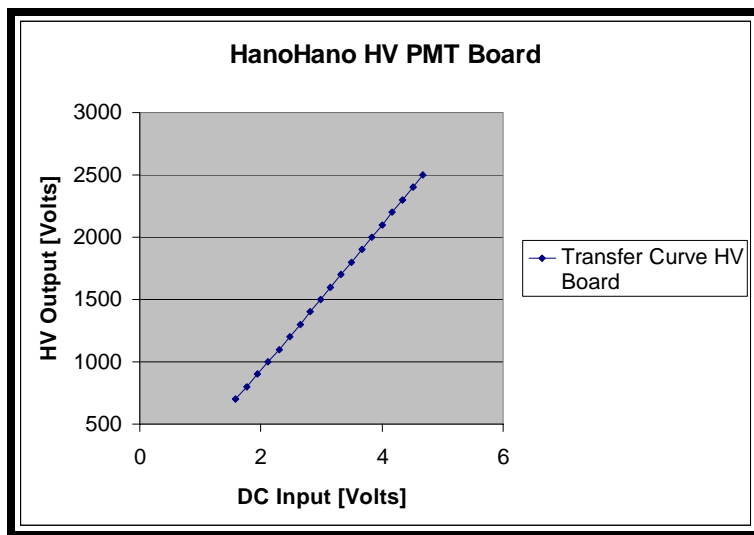


Figure 3: Transfer curve for the ISEG PMT base electronics.

## PMT Digitizer Electronics

The first phase was to make a prototype PMT high-voltage controller with low power digital readout electronics and a bi-directional fiber optic board (BiDFO). All electronics boards were designed by the Instrumentation Development Laboratory at the University of Hawaii Physics and Astronomy Department.

The prototype controller board supplies low voltage DC current to the PMT base electronics, acquires and digitizes the PMT analog pulses, provides a time stamp from a master clock, and forms local coincidence logic for event validation. A discriminator threshold range and resolution need to be determined. PMT pulses above threshold are encoded and transmitted to a workstation (shore station). The controller prototype board is implemented with a field programmable gate array (FPGA) from Xilinx ([www.xilinx.com](http://www.xilinx.com)). Data and power are transmitted via the same coaxial cable in a bi-directional fashion, sending down low-voltage DC power and transferring up the AC-coupled PMT signal. Figure 5 shows the prototype controller currently being used for testing. This evaluation card provided both a fiber-optic link for testing with the Bi-Direction Fiber-Optic (BiDFO), as well as a USB2 interface for stand-alone testing.

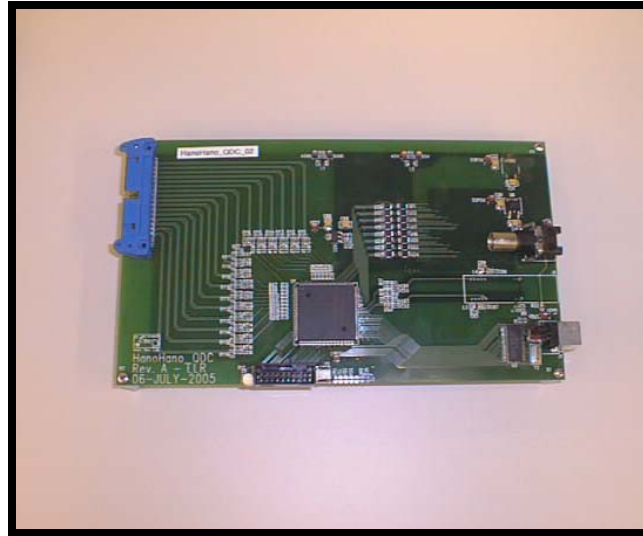


Figure 4: Image of the prototype controller board

The BiDFO board in Figure 5 provides the data collection interface which allows computer control of the readout chain via the fiber optic downlink and the return of data via the fiber optic uplink. This compact-PCI (cPCI) card interfaces to an embedded CPU, for control via a linux-based data acquisition program.

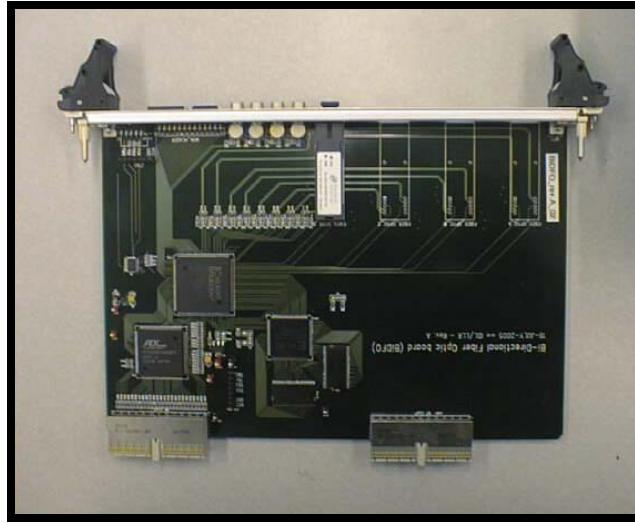


Figure 5: Image of Bi-Directional Fiber Optic board (BiDFO)

A schematic of the test setup using the prototype controller integrated with the BiDFO is shown in Figure 6 and images of the test setup are shown in Figure 7.

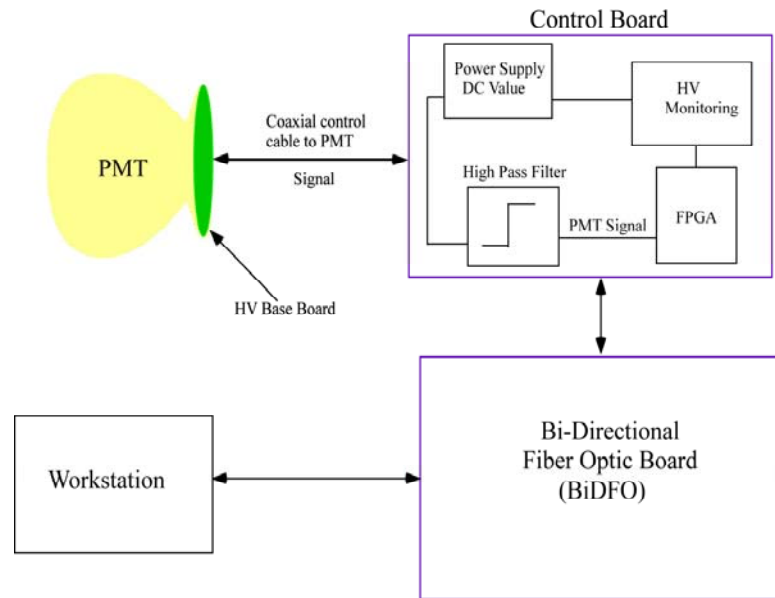


Figure 7: Diagram of PMT readout electronics testing

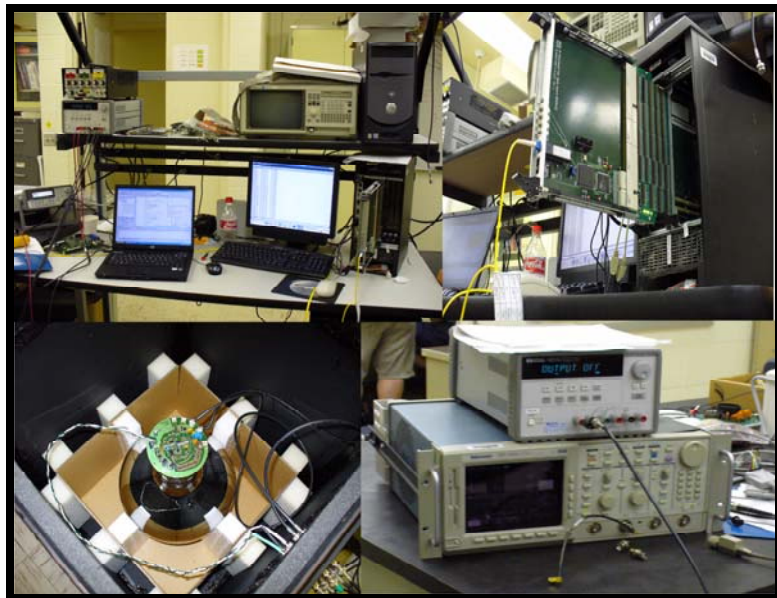


Figure 8: Testing apparatus- Lower left shows photomultiplier tube with base electronics attached in a dark box; Upper left shows workstation; Upper right shows control board and bi-directional fiber optic board in computer control crate; Lower right shows oscilloscope and DC power supply.

## Performance of the electronics

The circuitry was able to digitize phototube pulses at a rate greater than 100 kcps, while we expect in practice rates of <10 kcps. The information transmitted is in the form of a start time and time over threshold, along with tube ID. The breakdown is 12 bits for tube ID, 28 bits for start time, and 8 bits for charge. The device performed as expected from earlier tests with digital sample pulses. This is seen in Figure 9 and 10, which demonstrate performance of the timing and charge (TOT).

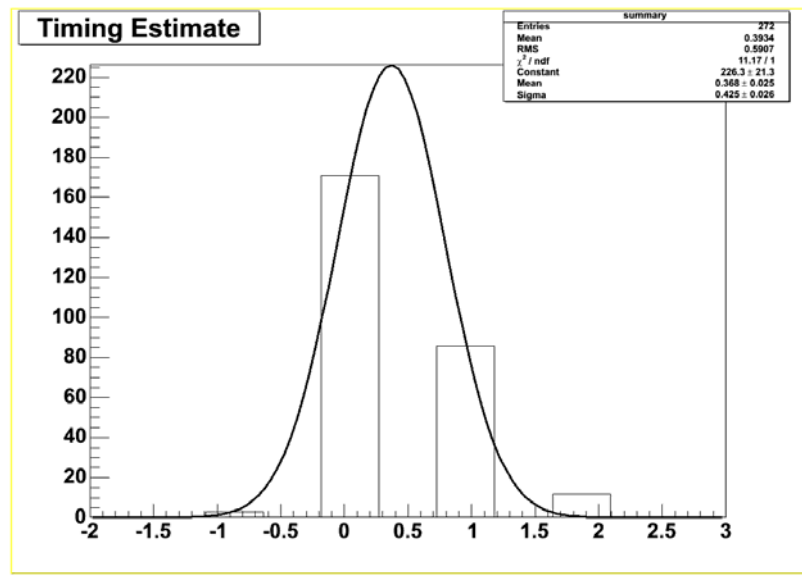
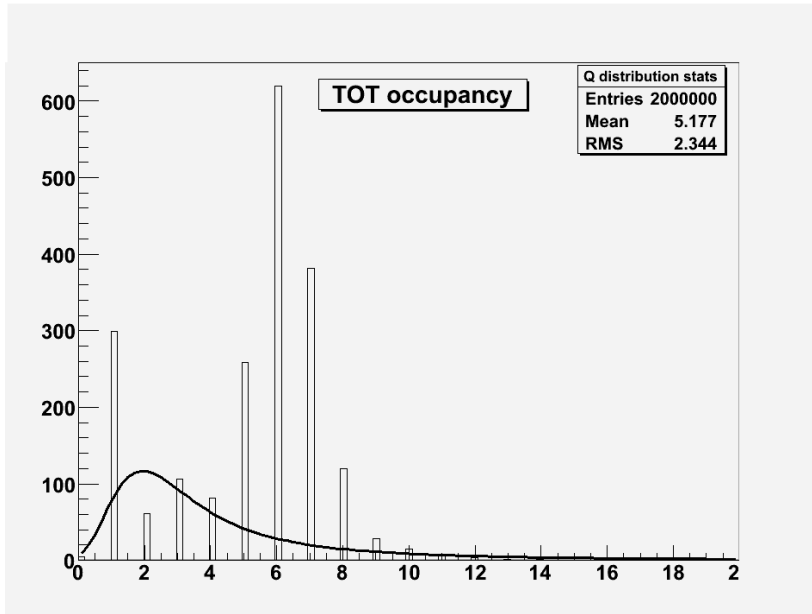


Figure 9: Timing resolution distribution as recorded with test set-up, with x-axis units in 2.5ns counts, indicating a time resolution of just over 1ns.

These measurements were taken with a single-photon threshold rate of about 15 kcps and logged over the fiber optic link into the BiDFO. Cuts are made to select cosmic muon events striking the PMT glass. In these tests the data transfer rate was limited not by the fiber optic link, but by the PCI bus interrupt latency. Caching of events and an interrupt-driven data acquisition software would push the limit back toward the fiber link intrinsic speed.



*Figure 10:* Charged distribution in Time-Over-Threshold for cosmic muon PMT glass events, where x-axis units are number of 5 ns intervals.

### Power Estimates

The following is an estimate of power requirements per channel of PMT electronics. As one sees in the following Table 1, the inherent power draw of the PMT through dark current is small. Normally one employs a resistor string supplied at the PMT high voltage (several kV) to divide the potentials for the various dynodes. Capacitors are placed in the voltage divider to hold up the potential during current drain when a pulse comes by. Normally this is only a factor in the last few dynodes, as the signal multiplies to an appreciable traveling charge. A typical rule-of-thumb for dividers is to have the tube base current 10 times the dark current at the PMT anode. In normal conditions this will be no more than 1  $\mu$ A of anode current. Thus a tube base string passing 10  $\mu$ A, and requiring a typical 20 mW, would suffice. High current bases are used in accelerator experiments which experience enormous short term rates, and these can be as high as 10 mA and dissipate a few watts of power. Fortunately we do not require such, and can probably make do with a base current of 10  $\mu$ A.

It is best to generate the high voltage at the PMT location, rather than risk connector failure. This is the route taken by all of the underwater and under-ice experiments, but contrary to large mine experiments, which send the HV to the PMTs by cable. It is perhaps noteworthy that the KamLAND experiment, with cables in oil has had little or perhaps no cases of HV breakdown near the PMTs, while the water submerged PMTs in the Super-Kamiokande and SNO experiments have had problems. Nonetheless we will take the conservative approach at this time and specify that the PMT HV should be generated in the PMT housing.

This leaves two possibilities. First is standard DC-DC converters, working from, say, 12 V to several kV, as regulated by an input low voltage signal. The typical commercially

available DC-DC supply has two disadvantages. First and foremost is power. Typically these devices require more than 1 W (at 12 V), even though the output power may be only several mW. The second problem is noise, since all of such devices use an internal oscillator (typically 10-100 kHz), and this makes electrical noise, particularly on the input leads. The second possibility is to employ a Cockcroft-Walton (CCW) style of HV supply, which generates the potentials for the dynodes without a resistor string. Designs for such are seen to dissipate on the order of 50 mW, yet the ANTARES team has chosen a commercial item (iSeg Technologies, Germany), which dissipates 300 mW. We purchased one of these for testing and it appears to function as advertised. Yet, the power dissipation is larger than we would like. In the end we may be forced to build our own devices.

Table 1: Estimate of PMT parameters:

PMT	Hamamatsu 10" R7081-20
Gain	6.2E+07
Dark Rate	<10,000 counts per second
Dark Current	$\sim 0.1 \mu\text{A}$
DC Voltage (maximum)	3kV Max, 2kV typical
Dark Power	<0.3 mW (tube only)
Quantum Efficiency	0.25 typical
PMT base current	1 $\mu\text{A}$ – 1 mA
PMT Base Power	3 mW – 3 W, 50-300 mW typical

### Total Detector Power:

Below we present our first estimates of the detector power, about 500. One sees that the total PMT power utilized is negligible, while most of the power required at the sensor is for the HV supply, which we take to be a Cockcroft-Walton drawing 50 mW. If we accept the unit employed by the ANTARES group at 300 mW, the total power required by the PMT units will go up to 600 W and dominate the detector totals. Final selection will thus focus strongly on the DC-DC supply selection, or barring finding one commercially, designing and making our own (for which designs employed in previous experiments are available).

Note that the second largest consumer of power is the local fiber optics links, running from digitizer to central (parallel redundant) modules. This is simply because there are 62 total links and available units consume several watts per link. We might want to consider utilizing lower-power fiber links, since the links are not long. The grand total is somewhat less than 500 W, a remarkably low value compared to previous experiments in the laboratory (10's of kW). The DUMAND project, for example, budgeted 10 W/OM. The present design comes to less than  $\frac{1}{4}$  W/OM including all electronics.

We have not tried very hard to reduce these values, so it is worth asking how far this may be pushed. We estimate that the total might be reduced by 200 W. On the other hand, with considerations of larger detectors than the initial 2000 optical module canonical design, rising as high as 10000 OM's the total might be as high as 2 kW.

Table 2: Estimated total detector power consumption for 2000 optical module array.

<i>Item</i>	<i>Quantity</i>	<i>Unit</i>	<i>Description</i>	<i>Total Power (Watts)</i>
PMTs	2000	<0.3 mW	Dark Current	6
PMT HV Supply	2000	50 mW	Cockcroft-Walton	100
Digitizer	62	0.5 W	32 Channel	31
LO Fiber Link	62	3.0 W	Dig <-> Riser	186
Shore Fiber Link	2	20 W	Riser -> Shore	40
Regulation Efficiency		0.8	Regulator losses	(91)
<b>Grand Total</b>				<b>453</b>

## Battery Power

If we have 500 W continuous power drain for operating the detector, which we think is conservative, then the total energy needed to operate for a year is about  $1.6 \times 10^{10}$  J. A typical (deep ocean capable) lead-acid battery will store a charge of about 80 A-Hr (DeepSea power and Light), with output which we take to be 10 V in the cold deep ocean. This is equivalent to  $7.2 \times 10^6$  J/battery. Hence for a year of operation we would require about 2200 such batteries. In large quantities these can be purchased for about \$100/battery, so the battery cost, even if sacrificed after one use, would be \$500K, which is only a few percent of the detector cost. So it would appear that battery power with an annual detector recovery cycle is indeed possible. Such batteries weigh about 42 pounds in water, so the entire battery pack would provide about 100 tons of anchoring mass, which may be useful given the significant net buoyancy of the scintillating oil.

Table 3: Estimate of detector power:

Charge/battery	80 A-hr
Voltage	10 V
Energy/battery	~3.0 MJ
Detector Draw	500 W continuous
Detector Energy/Year	15,778 MJ
Batteries/Year	~5000

## Summary

We have made a first iteration of a deisng for electronics for the proposed Hanohano detector. The electronics has been tested in the laboratory and operates as designed, providing time resolution to the nanosecond scale, and amplitude via time-over-threshold. Data rates are expected to be compatible with existing fiber optic links. There are multiple choices in photomultiplier available at present, and more reputed to be on the way for availability within several years. We are deigning to utilize a module which looks very much like that designed for the ICECUBE array, except we will have much less active electronics on board. Thus the remaining design challenges are those of optimizing reliability and cost.

We foresee a total array power requirement of less than 500W in the 2000 optical module design. It appears that battery powering may thus be economically viable. We might settle upon a system with batteries on board, but which batteries mainly function as backup, keeping them charged via cable to shore. In any case, minimizing the array power has benefits. For example, with a 500W load one can send 1kV down the shore cable with  $\frac{1}{2}$  A. With a typical resistive cable load of order 10 Ohm, the voltage drop across the cable is then only 5 V, completely negligible. This can be a problem when the cable consumes half the power, as is true in some other systems. Then one requires rather complex power regulation for startup loads to stabilize the load voltage during startup or shutdown. Minimal array power is thus beneficial in several ways.

We have made a first pass at the electronics system design for Hanohano and find the situation to be well under control, no stoppers and remaining tasks being design choices and optimization.

## **Appendix**

**Task 8: Scintillator testing**

Appendix

# **Testing and Preparation of Scintillation Materials**

*A Report submitted to Makai Ocean Engineering by University of Hawaii- 11/13/06*

## **Introduction**

A critical issue in the development of a 10-kt deep ocean antineutrino observatory is the effect on the scintillating liquid of the high pressure and low temperature of the benthic environment. Prominent concerns include optical clarity, light output, density change, viscosity change, and miscibility of components. This document reports excellent progress toward identification of a candidate scintillating liquid. It describes a unique instrument for testing optical clarity and a materials preparation system both developed under this task, introduces the chemicals acquired under this task, and presents test results for several potential scintillating liquid candidates.

Scintillating liquids are typically cocktails of organic molecules designed to absorb energy deposited by ionizing particles and to emit electromagnetic radiation at detectable wavelengths. These cocktails are blended for specific applications of radiation detection. They are commercially available in relatively small quantities compared with the 10 kt ultimately required for this application.

## **Methods**

The instrument required to measure optical clarity of uncontaminated liquids at extreme static pressure did not exist when this task began. It was necessary to design, fabricate, and calibrate a special purpose tool. The result was a one-of-a-kind apparatus capable of performing the optical measurements required to specify a suitable scintillating liquid for use in a deep ocean antineutrino observatory.

The completed instrument is constructed of electro-polished stainless steel with synthetic sapphire end windows. There is a high pressure pump, an isolation cylinder, a pressure gauge, a bleed valve, an optical rail, a photodiode, and various light sources including light emitting diodes and a laser. It has an initial length of 1 m and is adaptable to other lengths to accommodate various other measurements.

While the apparatus was being constructed and tested samples of known applicable scintillating liquid components were acquired. These included the ionization energy absorbing solutes 1,2,4- trimethyl-benzene (pseudocumene, PC), 1,2-dimethyl-4-(1-phenylethyl)-benzene (phenyl-o-xylylethane, PXE), 2-phenyldodecane (linear alkyl-benzene, LAB), the solvent dodecane, and the fluors 1,4-bis[2-methylstyryl]benzene (Bis-MSB) and 2,5-diphenyloxazole (PPO). These hygroscopic chemicals were carefully handled and prepared to prevent optical degradation.

Dissolved oxygen and water are known to readily degrade the optical clarity of scintillating liquids. Chemicals are prepared and then are sparged with dry nitrogen to remove dissolved oxygen and water before they are transferred to the instrument for

testing. The dry nitrogen sparging system is made of a N<sub>2</sub> tank, a pressure regulator, copper tubing, brass fittings and valves, and rubber stoppers.

The optical clarity of the prepared chemicals was measured using the apparatus described both at high pressure (~6000 p.s.i.) and at low temperature (4°C). Pressure had less effect on optical clarity than did temperature. Results indicated at least one promising candidate energy absorber in LAB.

## **Discussion**

Excellent progress towards identification of a suitable scintillating liquid for use in a deep ocean antineutrino observatory was made. Scientific literature was searched for information on materials considered for other similar applications. The physics community had recorded significant development in this area, which was of tremendous benefit to this task. A specialized optical clarity instrument was designed and constructed. Completion of this task was delayed by the unforeseen complexity of this project. A scintillating materials preparation system was designed and implemented. Chemicals were acquired and tested. Optical measurements of scintillating liquids under high pressure and low temperature were found to be complex and challenging. Details of this task and the excellent progress were documented in the attached graduate student thesis of Peter Grach.

The major hurdle, however seems to have been overcome: while we had been assured by expert expectations of no serious problems due to pressure or temperature (as long as one stays away from the freezing of the liquids), we now know that no serious change in optical properties does take place at high pressure and temperatures in the range of the deep ocean (few degrees C). Much remains to be done, however, in studying the degree of filtration that is needed, the exact optical properties, and the optical output under deep ocean conditions in order to optimize the choice of scintillation mixture.

## **Report**

The following is a master's thesis from a University of Hawaii student. The thesis details the testing and preparation methods, results, and conclusions outlined above.

PHYSICAL PROPERTIES OF LIQUID SCINTILLATORS

A THESIS SUBMITTED TO THE GRADUATE DIVISION OF THE  
UNIVERSITY OF HAWAI'I PER THE REQUIREMENTS FOR THE DEGREE OF

MASTER OF SCIENCE

IN

PHYSICS

DECEMBER 2006

By  
Peter D. Grach

Thesis Committee:

John Learned, Chairperson  
Stephen Dye  
Shigenobu Matsuno

We certify that we have read this thesis and that, in our opinion, it is satisfactory in scope and quality as a thesis for the degree of Master of Science in Physics.

THESIS COMMITTEE

---

Chairperson

---

---

## Acknowledgments

During the course of this project, I have benefited from the support of many individuals. I would like to express my appreciation to all, and in particular I would like to thank the following:

My advisor, John Learned provided me with an extraordinary opportunity; an opportunity to have ownership of a complete piece of a larger project. His decisive action, contacts, and “lets do the physics now” demeanor were significant in guiding my project forward. His patience and accommodation enabled me complete this research in spite of the “non-traditional” physics graduate student situation I am in.

Steve Dye’s questions were critical in the development of careful test system protocol and procedure. His questions further influenced the depth of analysis performed. Many extraneous variables were eliminated which may have otherwise adversely influenced the results I acquired.

Marc Rosen completed the finite element analysis on the stainless steel flange design, providing pertinent suggestions and direction for the final flange design moving it to production.

Ian Gordon saved me an inordinate amount of time rendering the stainless steel flange design in 3-D. His AutoCAD experience and work helped bring the flange from concept to integral test system component.

Troy Hix who measured the wavelength distribution for the LED’s.

Mark Olsson from DeepSea Power and Light provided excellent guidance in the development of the SS test assembly.

National Defense Center of Excellence for Research in Ocean Sciences (CEROS) whose financial support provided for this research under contract #53439. CEROS is a part of the Natural Energy Laboratory of Hawaii Authority (NELHA), an agency of the Department of Business, Economic Development and Tourism, State of Hawaii. CEROS is funded by the Defense Advanced Research Projects Agency (DARPA) through grants and agreements with NELHA. This work does not necessarily reflect the position or policy of the Government, and no official endorsement should be inferred.

Mahalo nui Loa.

# Table of Contents

<b>Acknowledgments .....</b>	<b>ii</b>
<b>List of Tables .....</b>	<b>v</b>
<b>List of Figures.....</b>	<b>vi</b>
<b>1 Research Impetus.....</b>	<b>1</b>
<b>2 Liquid Scintillator Background .....</b>	<b>3</b>
2.1 LS Candidate Selection .....	3
2.1.1 Safety .....	3
2.1.2 Feasibility.....	4
2.1.3 Physical Properties.....	4
2.1.4 Contamination.....	4
<b>3 Measurement Criteria .....</b>	<b>8</b>
3.1 Pressure Dependence .....	8
3.2 Temperature Dependence .....	10
3.3 Combined Pressure/Temperature Dependence .....	11
<b>4 Test System Design .....</b>	<b>13</b>
4.1 Design Criteria .....	13
4.2 System Architecture.....	13
4.2.1 High Pressure Test System .....	13
4.2.2 Optical Components.....	16
4.2.3 Control Systems .....	16
4.3 Systematics .....	16
4.3.1 Cleaning procedure .....	16
4.3.2 Fill System .....	17
4.3.3 Component Reliability .....	17
4.3.4 Baseline Tests .....	18
<b>5 Test System Protocol/Lab Procedure.....</b>	<b>19</b>
5.1 Alignment .....	19
5.1.1 LED.....	19
5.1.2 Laser.....	20
5.2 Temperature Control.....	21
5.2.1 Water Bath .....	21
5.2.2 End Caps .....	21
5.3 Test System Control.....	21
5.3.1 Pressure .....	21

5.3.2	Post-Test .....	22
<b>6</b>	<b>Pressure Test .....</b>	<b>23</b>
6.1	Sample Test Results .....	23
6.1.1	Dodecane.....	23
6.1.2	Pseudocumene.....	23
6.1.3	KamLAND Mix .....	24
6.1.4	LAB.....	25
6.1.5	PXE .....	25
6.2	Pressure Analysis.....	25
<b>7</b>	<b>Temperature Test.....</b>	<b>27</b>
7.1	Temperature Results .....	27
7.1.1	Dodecane.....	27
7.1.2	Pseudocumene.....	28
7.1.3	KamLAND Mix .....	28
7.1.4	LAB 540L .....	28
7.1.5	LAB N501.....	28
7.1.6	PXE .....	29
7.1.7	Dodecane/PXE (70/30) .....	29
7.2	Temperature Analysis .....	29
<b>8</b>	<b>Application of Findings .....</b>	<b>31</b>
8.1	Optical Properties Stability .....	31
8.2	LS Selection .....	31
8.3	Ocean Deployment Test.....	31
8.4	Recommended LS System Improvements .....	32
8.4.1	Test Tube Anodizing.....	32
8.4.2	LS Sample Purification .....	32
8.4.3	10-cm Spectra-Photometer LS Testing .....	32
8.4.4	Refrigeration System .....	32
<b>Appendix 1 (Scintillator Optical Tests).....</b>		<b>33</b>
<b>Appendix 2 (Bi-Ocular Scintillator Temperature Evaluation) .....</b>		<b>36</b>
<b>Appendix 3 (LS Physical Parameters) .....</b>		<b>37</b>
<b>Bibliography .....</b>		<b>38</b>

## List of Tables

<u>Table</u>		<u>Page</u>
1	LS Selection Matrix .....	7
2	Appendix 1 (LS Scintillator Test Data).....	33
3	Appendix 2 (Bi-Ocular Scintillator Temp. Test).....	36
4	Appendix 3 (LS Physical Parameters) .....	37

## List of Figures

<b>3.1</b>	<b>Dodecane Pressure Dependence .....</b>	<b>9</b>
<b>3.2</b>	<b>Density as a function of Pressure.....</b>	<b>9</b>
<b>3.3</b>	<b>Dodecane Temperature Dependence.....</b>	<b>10</b>
<b>3.4</b>	<b>N501 Alkylate .....</b>	<b>11</b>
<b>4.1</b>	<b>1-Meter SS Test System.....</b>	<b>14</b>
<b>4.2</b>	<b>SS Flange Assembly .....</b>	<b>15</b>
<b>4.3</b>	<b>Blue LED Wavelength Profile.....</b>	<b>16</b>
<b>4.4</b>	<b>Green LED Wavelength Profile.....</b>	<b>16</b>
<b>4.6</b>	<b>Synthetic Sapphire Transmission Curve .....</b>	<b>18</b>
<b>5.1</b>	<b>Optical Bench Test Setup .....</b>	<b>19</b>
<b>5.2</b>	<b>LED Alignment Light Rings .....</b>	<b>20</b>
<b>6.1</b>	<b>Pressure Test Divergence .....</b>	<b>23</b>
<b>7.1</b>	<b>Optical Transmission Thermal Dependence .....</b>	<b>27</b>
<b>7.2</b>	<b>LAB Purification Spectrophotometer Graph.....</b>	<b>30</b>

# Chapter 1

## Research Impetus

Neutrino oscillation studies at KamLAND in Japan using a liquid scintillator detector concluded the “Solar Neutrino Problem” by observing that the electron anti-neutrinos from the reactors around Japan were oscillating. The parameters of the oscillation matched those deduced from solar neutrinos, so additionally demonstrated that the electron anti-neutrinos are not behaving differently from electron neutrinos in any significant manner. The data fits also eliminate some models competing with the oscillatory hypothesis [1, 2].

The secondary signal observed and presented by the collaboration involves the signal coming from the Earth itself, the “Geo Nu’s” or geo-neutrinos [3, 4].

The next step in studying the geological neutrinos is to characterize radioactivity within the layers of the earth using anti-electron neutrinos emanating from the Earth’s mantle and core. This characterization requires the ability to discriminate radiation coming from the mantle and core separately from the crust. This characterization requires that the detector is far removed from significant background signal contribution due to the crust and man-made nuclear reactors [5, 6].

Modeling the parameters of this type of neutrino experiment demonstrated the need for a 10 kilotonne liquid scintillator detector, ten or more times the size of the KamLAND detector. In order to avoid the neutrino background from regional man-made reactors and escape the contribution from the continental crust, we plan to place a detector over the thin mid-ocean crust. Submerging the detector in the deep ocean ( $> 3000$  m) provides excellent shielding from the cosmic ray muons which otherwise induce background events. A key to the success of this detector is the liquid scintillator and its physical properties.

Any design for an underwater neutrino detector at a depth of a few thousand meters adds two new key parameters beyond land-based detectors such as KamLAND [2] and BOREXINO [14]. The first constraint on the scintillator to be employed is temperature; the temperature of seawater is approximately  $4^{\circ}\text{C}$  at depth. The second constraint is pressure; the pressure is approximately  $\sim 6000$  psi (400 atmos.) at 4 km depth.

The goal is to find a liquid scintillator candidate that does not exhibit significant deterioration of the scintillators optical properties due to change in pressure and temperature. The concerns are mechanical and optical properties, about which there is little or no available relevant literature. Viable candidates must demonstrate little if any pressure dependence over a temperature between  $0^{\circ}\text{C}$  and  $25^{\circ}\text{C}$ . They must also

maintain a stable attenuation length at 0°C comparable to their attenuation length at ambient near surface conditions, between 20°C and 25°C.

An ideal liquid scintillator candidate would meet the following criteria:

- A very high light output (~ 10,000 photons/ MeV)
- An attenuation length on the order of 20 m at pressure and temperature.
- A high flash point; > 60°C to satisfy safety and deployment criteria.
- No chemical phase transitions within the constraint ranges.
- Optically stable near 4°C.
- Low Toxicity.
- Compatibility with Acrylic plastics.
- Cost Effective & available in industrial quantities.
- High Hydrogen Fraction (per unit weight).
- Low radioactive contamination.

Several candidate liquids have been identified and tested as will be discussed hereafter.

## Chapter 2

# Liquid Scintillator Background

### 2.1 LS Candidate Selection

The following four major liquid scintillator (LS) projects are operating or in proposal: KamLAND, SNO+, BOREXINO, and LENA. These projects have overall done a great deal of development work in locating acceptable materials and understanding how to make them radioactively extremely pure. These provide a starting point for evaluating possible LS candidates for a deep ocean detector.

KamLAND uses an 80/20 mix of Dodecane and Pseudocumene [28]. The SNO+ collaboration has proposed using Linear Alkyl benzene (LAB) and has explored its properties [9]. BOREXINO is evaluating the feasibility of using Pseudocumene and Phenyl-o-xylylethane (PXE) for their detector [10]. The LENA collaboration has proposed using PXE, or an 80/20 Dodecane and PXE mix [29]. Each of these LS candidates is an excellent scintillator at ambient temperature and pressure. Little or nothing has been studied about the pressure dependence, and only a little about temperature response (mostly just freezing temperature).

The following criteria were considered for each:

- I. Safety: Flash Point, Toxicity
- II. Feasibility: Cost, Availability, Acrylic Compatibility
- III. Physical Properties: Density, Fluor Dissolution, Hydrogen Fraction
- IV. Optical Properties: Light Yield, Attenuation Length
- V. Contamination: Radioactive impurities, chemical impurities

See Table 1 which summarizes the properties of the materials considered.

#### 2.1.1 Safety

Federal safety regulations would prompt the use of LS with a “Flash Point” beyond the range of working temperatures, including a safety margin. Surface temperatures for an ocean deployment vessel may reach above 30°C. As a result, the use of Pseudocumene (PC) containing solutions may not meet stated safety standards. Both PXE and LAB with flash points well above 100°C pose no risk for explosion.

Based on the MSDS sheet information for the LS mixes considered, all candidates other than pure PC do not pose a significant health risk for exposure in small quantities, or significant contamination risk to the environment. There would not appear to be a problem in obtaining relevant permits and approvals from interested government agencies at the federal or the state level. The environmental risks are comparable for PXE, LAB, and the KamLAND mix. Moreover, the use of a double

hull design for the vessel should satisfy USCG requirements, according to Makai Ocean Engineering.

### **2.1.2 Feasibility**

Both PXE and LAB are industrial chemicals with high volume production and available from a multiplicity of sources. PXE is available from Dixie Chemical in Houston Texas in the quantities required, among a couple domestic producers. Of note, the VP for Research and Development at Dixie is very willing to work closely with us to meet the stringent criteria in quality, consistency, and process.

LAB is available from SASOL in Baltimore, Maryland in the quantities proposed, as well as from other companies in North America, Africa, and Europe. The total US capacity is some three times consumption, with most of it presently going to surfactant production [7]. LAB is the base for the familiar clear dish-soap with which almost everyone is familiar. Our contact at SASOL has been enthusiastic in working to develop the best LAB composition for use as a LS.

The structural framework for the proposed underwater detector utilizes a modular acrylic sphere. Any viable LS must be compatible with acrylic. The integrity of the structural and optical properties of the acrylic must not be degraded with time. Acrylic is incompatible with PC and its primary constituent Benzene according to acrylic vendor Ineos. The KamLAND mix (80/20) reduces the concentration of PC to an acceptable level, preventing polymer disassociation. PXE also needs to be diluted to at least (70/30), while (80/20) is recommended. Concentrated PC and PXE produce significant surface “crazing”, significantly reducing the optical properties of the acrylic [8].

LAB on the other hand has excellent compatibility with acrylic [9]. In summary; the KamLAND mix, an (80/20) mix of Dodecane and PXE, and LAB are sufficiently compatible with acrylic to be considered as LS candidates in the proposed underwater detector.

### **2.1.3 Physical properties**

Density is a critical concern when considering the structural design for a 10 kilotonne LS detector. A LS density that is too high (~1.0) would require a design which included supplemental buoyancy. A density that is too low (~0.70) would prompt the need for significant extra ballast as well as a secure method of anchoring the detector to its ocean floor mooring. Each of the LS candidates’ density is within the design parameters of the proposed detector.

### **2.1.4 Contamination**

Each LS candidate was initially selected meeting the minimum criterion for: Light Yield, Attenuation Length, Proton Target Ratio, and Fluor Dissolution. The production process produces highly pure material for each LS. Contamination is introduced during the transport and storage process as well as the introduction of

fluors. The primary contaminates are:  $^{238}\text{U}$ ,  $^{232}\text{Th}$ ,  $^{226}\text{Ra}$ ,  $^{222}\text{Rn}$ ,  $^{85}\text{Kr}$ ,  $^{39}\text{Ar}$ ,  $^{40}\text{K}$ , and  $^7\text{Be}$ .

Uranium, thorium, and radium are siliceous particulate contaminates. A solid column Silica gel filter has been shown to remove colloidal particles larger than 0.05 microns reducing  $^{238}\text{U}$  and  $^{232}\text{Th}$  from 10 ppm to  $10^{-16}$  g/g [10]. Phase separation techniques are required to remove particles from 2 - 500 nm [11]. Measurements taken at Brookhaven on LAB showed that they were able to improve the attenuation length from the accepted value  $\sim 25$  m to an attenuation that was too small to discriminate with a 10 cm cell, where the absorption at 430 nm is negligible [12].

Vacuum Distillation is used to remove low volatility components such as radioactive metals as well as chemical impurities that degrade the optical properties of the LS. It has been shown to reduce the  $^{40}\text{K}$  measured in the fluor PPO at  $\sim 10^{-6}$  g/g to  $10^{-11}$  g-K/g-PPO [13]. It also improved the attenuation length of PC by a factor of three, from  $\sim 7$  m to  $\sim 21$  m according to the Brookhaven tests.

Radon, krypton, and argon are most likely to be introduced due to air exposure. The inert gases may be mitigated by maintaining a closed system and selecting materials for the structural frame which have a low permeability (to noble gasses) and low radioactive content for the LS detector [14]. This may also require cooperation on the part of a vendor to upgrade their distillation and manufacturing plant to meet the stringent production requirements necessary to minimize radioactive contamination in the LS.

Tritium and carbon 14 are inherent contaminants and can not be removed (economically) with current technology and industrial processes [14]. The only suggestion found in the literature was to minimize cosmogenic exposure by minimizing the shipping time and maintaining tight control of logistics.  $^{14}\text{C}$  has a long half life and is unaffected by filtering, therefore the only viable option is to minimize the amount generated cosmogenically [15].

The preferred method to remove polar and charged ionizable metals and salts such as uranium, thorium, potassium, and beryllium is water extraction. It is the method of choice since it allows for processing at ambient temperature  $\sim 20^\circ\text{C}$  and avoids possible degradation of the LS [16]. It has the added safety benefit of avoiding temperatures near the flash point of the scintillator being filtered.

$^7\text{Be}$  is produced cosmogenically from  $^{12}\text{C}$ . Equilibrium exposure of the LS at the surface will produce a background of  $\sim 10^5$  events/day which requires 1.5 years to decay to  $\sim 10^0$  events/day [17]. Therefore it is advantageous to minimize the time from LS production to detector deployment to minimize the background from this decay chain.

Dry Nitrogen Stripping (Sparging) is employed after water extraction. This strips the water from the LS. Sparging also strips oxygen from the LS which if not removed quenches scintillation, which reduces the effective attenuation length. As an added benefit, nitrogen strips dissolved radioactive gasses such as  $^{222}\text{Rn}$  and  $^{85}\text{Kr}$  from the LS [18].



# Chapter 3

## Measurement Criteria

The key measurement criteria this study reports upon are the effects on the optical properties of liquid scintillator candidates due to an increase in pressure of 400 atmos, and a decrease in temperature of 20°C to approximately 4°C. There is industry consensus that there is no inter-dependence between temperature and pressure on LS materials. It is expected that there is a linear relationship between pressure and volume as well as between temperature and volume in the range of interest.

The Benedict-Webb-Rubin-Starling (BWRS) Equation of State provides a series expansion for the relationship of liquids, such as liquid scintillators, in terms of P = pressure, R = Ryberg Constant, T = temperature, and  $\rho$  = density, and a number of constants:

$$P = \rho RT + \left( B_0 RT - A_0 - \frac{C_0}{T^2} + \frac{D_0}{T^3} - \frac{E_0}{T^4} \right) \rho^2 + \left( bRT - a - \frac{d}{T} \right) \rho^6 + \frac{c\rho^3}{T^2} (1 + \gamma\rho^2) \exp(-\gamma\rho^2)$$

In “Fluid Properties for Light Petroleum Systems”, Starling provides mixing rules for compounds and procedures for calculating coefficients:  $A_o$ ,  $B_o$ ,  $C_o$ , etc. [18]. As may be inferred from this equation; density is linear with pressure and temperature to first order. Since T is in Kelvin, the terms in  $T^{-n}$  fall off speedily. To first order there is also no inter-dependence between pressure and temperature for a liquid while maintaining a constant phase.

### 3.1 Pressure Dependence

To first order at the 95% level, it is expected that density of LS candidates will demonstrate a linear dependence on density due to pressure. The physical result of pressure at depth on Dodecane will produce a volume compression on the order of 3%; this volume differential must be accommodated in the design of an ocean detector at a depth of ~4000 m, and a pressure of ~400 atmos. [19].

Dodecane is the one component common to nearly all LS mixes in use currently or being proposed. As a result, its physical properties and measurements will be used throughout this report as a benchmark reference.

As may be observed in the Figure 3.1, in the range of 1 and 1,500 Torr there is a linear relationship between pressure and the density of n-Dodecane as measured by Caudwell [20]. This graph shows that a 10% increase in density corresponds to a pressure increase of three orders of magnitude.

The physical properties of pseudocumene may be inferred from Benzene, its dominant constituent. Based on the properties of Benzene and the volume

composition of the KamLAND mix it is expected that there will be no significant differences due to pressure between the KamLAND mix and Dodecane [21].

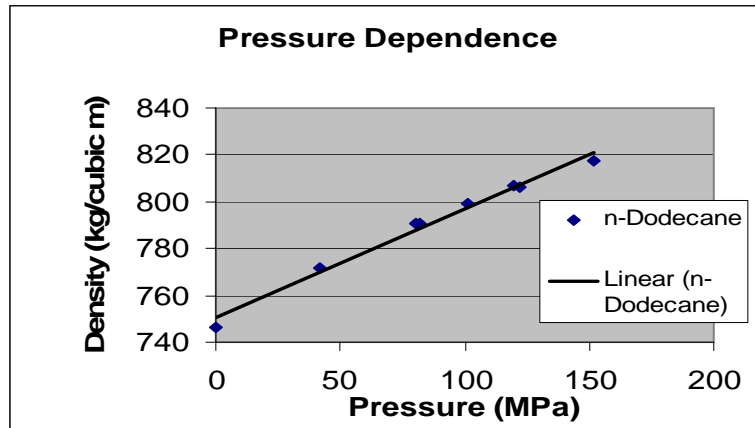


Figure 3.1: Dodecane density pressure dependence.

The physical properties of PXE and LAB have been insufficiently measured and reported to provide a reference baseline with which to confidently compare laboratory data measured in this experiment. In the case of PXE mixed with Dodecane at 1:4 with a resultant mix density of 0.82, it is reasonable to expect that there should be no significant differential effects scaled off of the Dodecane results.

LAB may be compared only loosely with the Dodecane but it can be expected to follow a similar scaling factor since the LAB estimate is based on only three data points over a range of 100 psi. (Figure 3.2) Extrapolating the LAB data reflects a change of only 0.41% in density over 1000 psi [22]. Using the more reliable data from the Dodecane analysis provides a solid upper bound on the requisite amount of make-up volume that needs to be engineered for in an underwater detector.

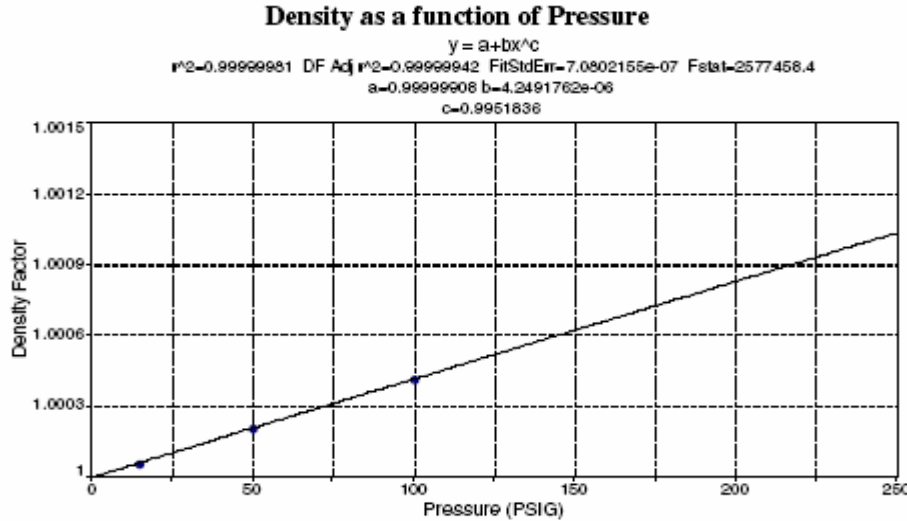


Figure 3.2 shows the extrapolation and the increase in density with pressure at 293K, for LAB.

Based on experience working with LS materials, industry experts expect that there is no measurable degradation in the optical properties of liquid scintillators due to pressure. To date there has been no published work on the effect of pressure on LS optical properties. This study then will attempt to isolate and measure changes in the optical transmission of LS candidates due to pressure.

### 3.2 Temperature Dependence

The BWRS equation gives the general formula for the dependence of fluid density on temperature. This assumes that temperature is changing along one isotherm and there are no phase changes over the range of interest. As may be inferred from the equation, to first order at the 95% level, there is linear dependence due to a change in temperature on fluid density.

An analysis of Caudwell's data on Dodecane in the graph below (Figure 3.3) shows that as temperature drops the trend lines for different pressures converge [23]. As may quickly be observed, the data reflects a linear dependence on density due to temperature as predicted.

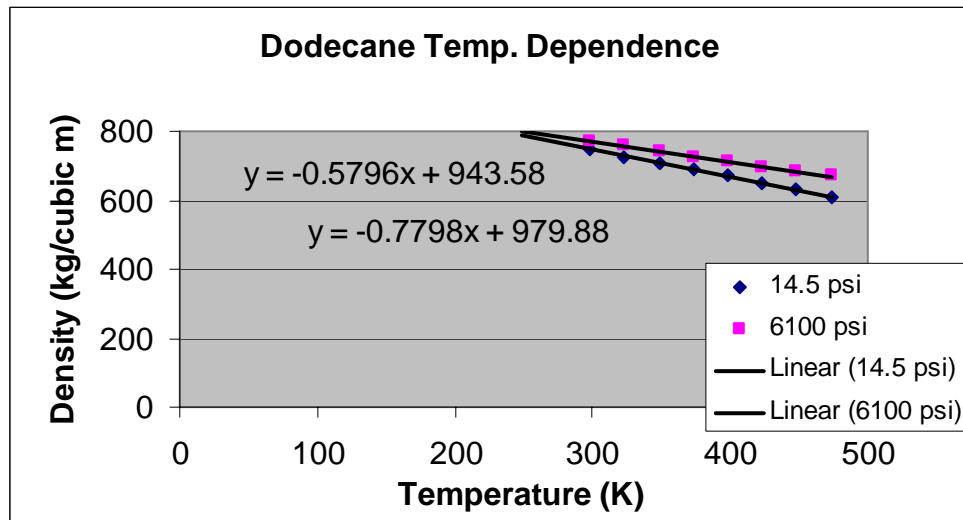


Figure 3.3: Dodecane density temperature dependence.

At ambient pressure, extrapolating on the graph to 0°C from 20°C represents a reduction of 2.8% due to the change in temperature. The extrapolated density of Dodecane is 767 kg/m<sup>3</sup>. Extrapolating along the 6100 psi fit line to 0°C from 20°C reflects a loss of 1.7% due to the change in temperature. Here the extrapolated density is 785 kg/m<sup>3</sup>.

Comparing the extrapolated Dodecane density reduction with data provided by SASOL for LAB 501 shown in Figure 3.4 below, the results due to temperature are comparable, reflecting a change in density of –2.1% [24]. This value, as with that for pressure, represents a smaller variation than for Dodecane, but one that would not significantly change the proposed design for the Hanohano detector. As for the effects

of temperature on LS candidates' optical properties; researchers familiar with liquid scintillators suggest that there should be no change in optical properties due to a change in temperature over the proposed range. The prediction is that there will be no degradation in attenuation length or light yield.

The only study found which attempted to measure the effect of temperature on LS optical properties measured a decrease in light output of 1% per degree Celsius [25]. This study then will attempt to isolate and measure changes in the optical transmission of LS candidates due to temperature.

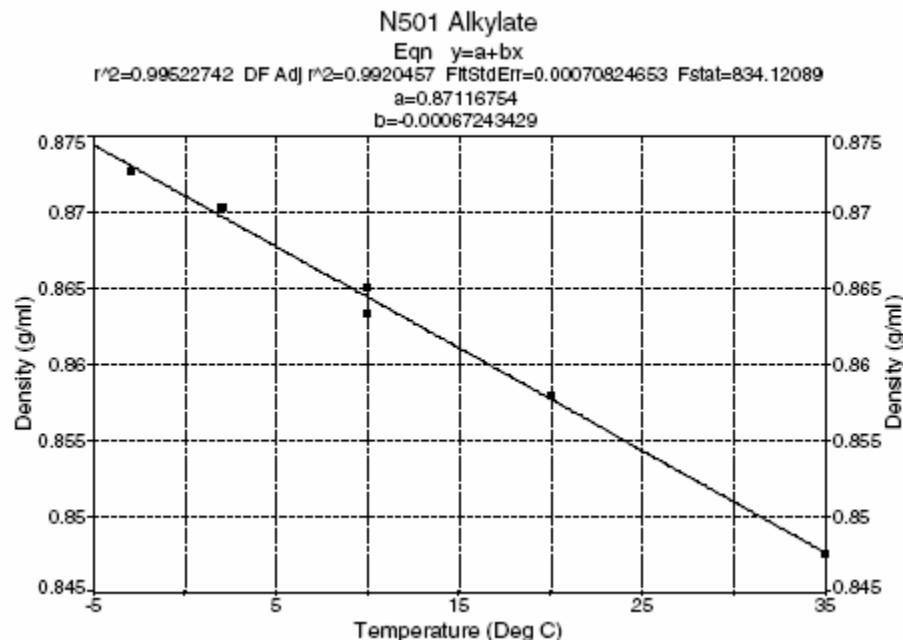


Figure 3.4 shows the correlation between the density of LAB 501 and temperature. The densities were measured using a digital density meter (Mettler-Paar) using water and n-Decane as calibration fluids. For lower temperatures, ethanol was used instead of water for calibration.

### 3.3 Combined Pressure/Temperature Dependence

Compared to Dodecane at STP, the combined effect of the conditions at depth on the Dodecane is a 5.2% volume reduction. The structural design for the LS detector must accommodate a 5% loss in volume. For a 10 kilotonne detector, this represents a makeup volume of 0.5 kt. The cost estimate on this makeup volume alone runs from approximately \$100K - \$1000K, depending on the scintillator mix chosen (but the material is not wasted, being employed in the detector when at depth, slightly increasing the target mass).

Interpolating between the data sets in Figure 3.3 reveals that increased pressure suppresses the effect due to temperature. As a result, it is expected from analyzing Figure 3.3 that there is a 2.0% change in volume due to a 25°C change in temperature, beyond the change due solely to increased pressure.

Reviewing the data on the melting points for all LS candidate constituents, it is expected that there are no phase transition points within a few degrees of the expected minimum ocean bottom temperature 4°C at any contemplated location. The above total estimate of 5% for Dodecane may be used as a benchmark then for the volumetric changes due to changes in pressure and temperature for each candidate.

The resulting estimates assume that pressure and temperature effects are linearly independent, consistent with standard industry practice. Using the data for Dodecane and LAB provide an educated prediction for the upper (5.2%) and lower (2.5%) bound for the volumetric change due to temperature and pressure.

## Chapter 4

### Test System Design

The need is to create a laboratory test setup in which samples of LS may be pressurized to deep ocean equivalent pressures and determine if any significant optical changes take place. A large volume is expensive and dangerous; moreover available materials without intolerable order times, necessitated designing a system with a small diameter, 1 m long assembly with windows.

#### 4.1 Design Criteria

##### Chemical

- Foreign Contaminant Free
- Non-Reactive with LS Constituents
- Cleanable

##### Mechanical

- Closed System
- Flow Through Rate (1 liter per second – minimum)
- Working Pressure ( $\leq$ 6100 psi)
- Good Thermal Conductivity
- Modular
- Quick Assembly/Breakdown
- Window Ports at ends

##### Process

- Materials Procurement (< 30 days)
- Common Fittings

#### 4.2 System Architecture

##### 4.2.1 High Pressure Test System

A Swagelok  $\frac{3}{4}$ " tube and connector components was employed in building the high pressure stainless steel test assembly. (Figure 4.1) This was mated to a custom 316 SS flange designed to hold the view ports at a working pressure up to 6100 psi. (Figure 4.2) 2.50" diameter, 0.250" thickness, clear Sapphire windows (Swiss Jewel model W63.25) were mounted in the flanges as view ports.

The design of the seat for the windows is a very sensitive matter, where the flexing of the flange under pressure must not distort the windows in such a way as to lead to failure. The design for the flange was greatly aided by advice from DeepSea Power and Light. Casually reviewing the design, one may think that the flange is

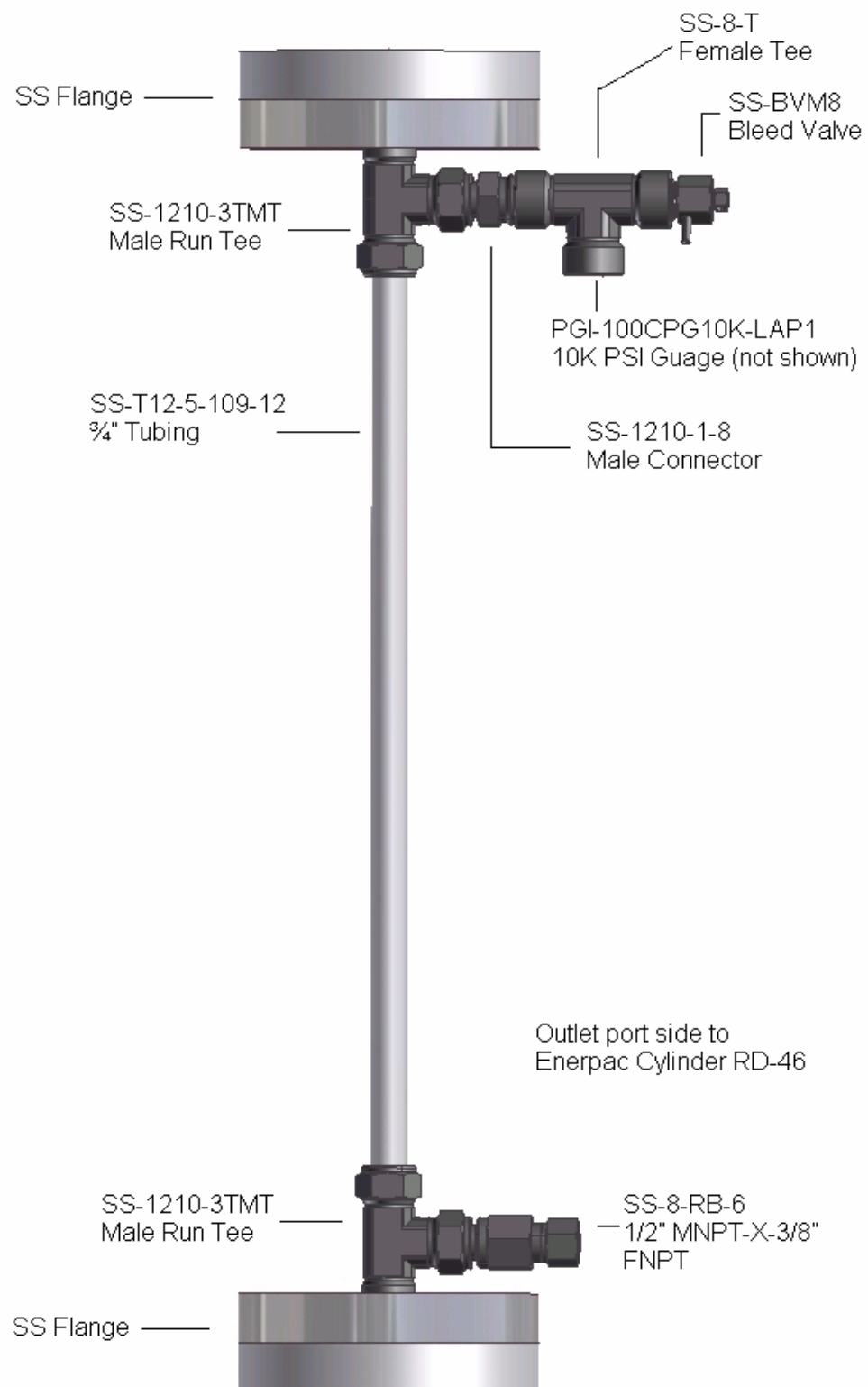


Figure 4.1: Stainless Steel Test Assembly

greatly over-designed looking at the substantial size, but that is not the case due to the requirement for not edge loading the Sapphire windows.

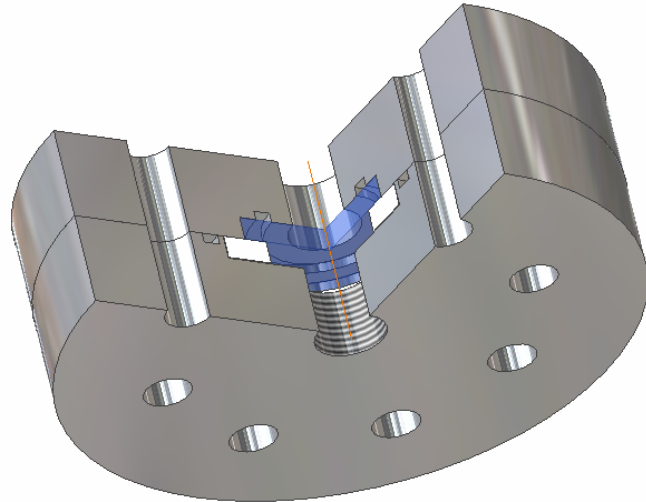


Figure 4.2 Stainless Steel Flange Assembly

The SS system has a working length of one meter. As one of the system requirements was a modular architecture, the system may be configured for a 3 m length simply by changing the tube used. The one meter system has a working volume of  $315 \text{ cm}^3$ . A larger diameter is to be preferred but the order time and minimum volume for larger SS pipe was prohibitive.

An Enerpak model 11-100 single speed hand pump is used. It is multi-fluid compatible; a requirement for pressurizing liquid scintillator components such as: Dodecane, pseudocumene, PXE, and LAB. With the installation of the (Enerpak) fluid isolation cylinder it became unnecessary, as well as undesirable, to use LS materials in the pump. In order to maintain the longevity of the pump and prevent failure, hydraulic fluid is preferred for use with the pump.

Testing demonstrated that Enerpak's standard high pressure hose connecting the pump with the isolation cylinder was incompatible with the polar molecules in the LS components. They were chemically reacting with the hose and degrading the physical integrity of the hose which would have led to catastrophic failure under high pressure, as well as contaminating the LS test samples. The hose was replaced with a thermo-plastic hose which solved the compatibility and safety issues.

An Enerpak model RD-46 double-acting cylinder is used to isolate the pump fluid from the test fluid contained in the SS system. The cylinder is attached to the system through the 3/8" NPTF ports. The inclusion of an isolation cylinder allowed for much greater sample quality control. No LS material is in contact with any pump parts, hydraulic fluid contaminants within the pump, nor with the hose.

#### 4.2.2 Optical Components

Polished flat blue and green LED's from Linrose Electronics were used for baseline measurements. The blue LED (B4304H6-1) wavelength peak was at 430 nm, with a full width-half max value of 60 nm. (Figure 4.3) The green LED (B43004H95) wavelength peak was at 520 nm, with a full width-half max value of 30 nm. (Figure 4.4)

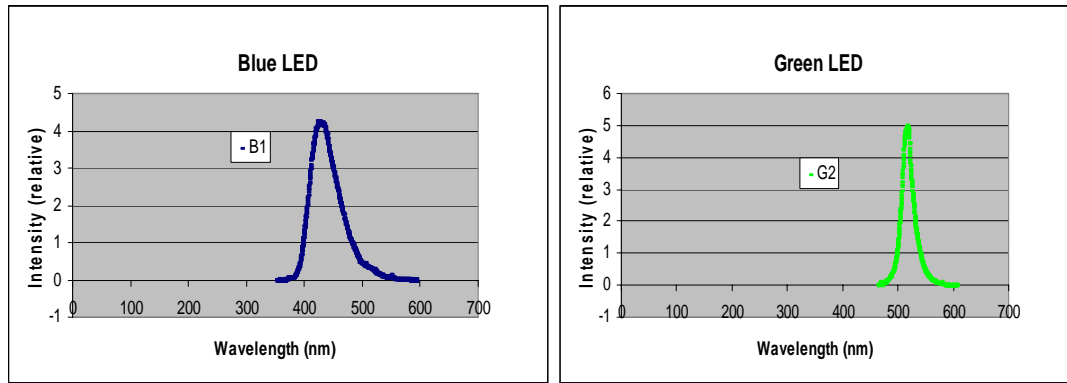


Figure 4.3: Blue LED Wave Length Profile

Figure 4.4: Green LED Wave Length Profile

A (CrystaLaser) 405 nm blue CW laser (BCL-025-405) was used as the primary source for evaluating the optical properties of each LS candidate and component. 405 nm is close to the emission peak and photomultiplier sensitivity maximum.

A United Detector Technology silicon photo-detector (J43053 053-1) connected to a Keethly pico-ammeter model #6517A provided the readout data.

#### 4.2.3 Control Systems

A decanting system was built to provide for dry nitrogen purging of the SS system in preparation for an LS optical test. It also was designed to decant each chemical being tested from its source container into the test system using pressurized dry nitrogen. The third use of this system was to “sparge” test chemicals with the dry nitrogen before decanting in order to strip them of moisture and oxygen (moisture is known to be detrimental to the optical properties of liquid scintillators, particularly at low temperatures).

Common refrigeration Copper tubing and Brass fittings were used for this decanting system, available at any hardware store. No special care was taken to control radiopurity at this stage of the measurements, the focus being on water and oxygen.

### 4.3 Systematics

#### 4.3.1 Cleaning Procedure

ASTM G-93 Level A requirement for cleaning methods and cleanliness levels for material and equipment was followed; in order to maintain the purity of each sample, and produce verifiable results free of contamination.

As part of this process, the SS system components were cleaned using an ultrasonic bath with an 80/20 bath of acetone and ethanol. Components were prepped using 100% ethanol. Cleaned components were promptly assembled and capped.

#### 4.3.2 Fill System Procedure

- The test system was dry nitrogen purged for 15 minutes prior to each test fill.
- An overpressure of 3 psi was maintained in the SS system while decanting to maintain a nitrogen atmosphere.
- Prior to decanting, each test sample was sparged for 30 minutes to strip water and oxygen.

#### 4.3.3 Component Reliability

##### 405 nm Laser

According to the vendor certification from CrystaLaser for the 405 nm laser:

- Beam diameter = 1 mm.
- Beam divergence at 0.5 mrad (full angle)
- Noise (rms) at less than 0.5%.

##### Keithley Ammeter

The Keithley Electrometer specification sheet lists the peak-to-peak noise at 0.75 fA. The resulting signal-to-noise ratio was some six orders of magnitude lower than the signal measured with the United Detector Technology's photo-diode (J43053 054-1).

##### Photodiode/ Output:

- *Photo-diode light sensitivity* is uniform over the photodiode surface (11 mm diameter) with an abrupt drop at the edge of the photodiode, consistent over two orthogonal axes using a surface pinhole test.
- Anticipated *photo-diode temperature dependence* was eliminated by removing the component from the system during cool-down. It was optimally positioned only when measurements were being performed and then set aside again.
- Dark current/noise was: 0.2 nA
- Drift was: +/- 1.5 nA; consistent over all power settings and both LED's.
- The zero point readout is: 0.04 nA

##### Power Source/ LED:

- *LED*: Input power was maintained by setting the power and either running the test with the system power/LED on or using the power button to turn off system and bring it back online. Any output voltage variation was below the sensitivity of the multi-meter (1 mV).
- *Laser*: Input power was set to 0.2 mW and consecutive tests were run using the key and switch to maintain a consistent output power.

#### 4.3.4 Baseline Tests

There is no signal/light loss due to the SS system (including windows) being cooled from ambient to 0°C. Over the same path length, the SS system reduces the direct beam signal by 25%.

The SS system optical path includes two 0.25 in. sapphire windows and the SS tubing. The transmission curve provided by the manufacturer Swiss Jewel shows 85% transmission for synthetic Sapphire. (Figure 4.5) For two windows, the expected loss on the order of 30%, so the result is consistent with the data provided by the manufacturer.

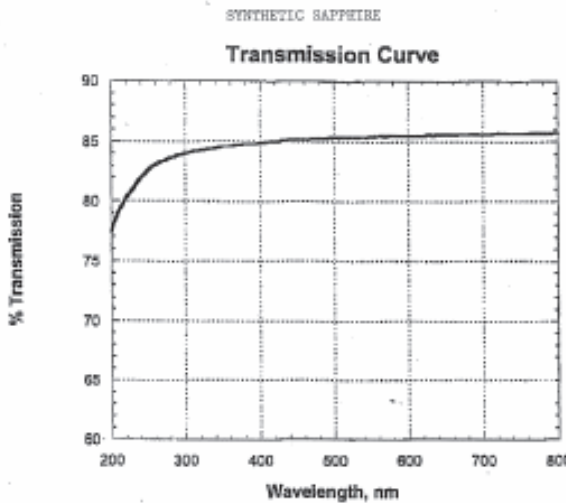


Figure 4.5: Sapphire Transmission Graph provided by Swiss Jewel.

Mechanical compression testing using the SS test system reflected a 2.2% volume reduction in the Dodecane at 6000 psi, and a 1.9% volume reduction for LAB 501. With a measured volume differential of 0.3%, there was no realizable difference in compressibility or increase in density. Comparing this data with that reported earlier for Dodecane at 3%, the compression test is in agreement within 1%.

Based on the mechanical compression test, it would be expected that LAB 501 has the same approximate density gradient as Dodecane at 6000 psi. Compared to the data presented in chapter two at 0.41% for the density change in LAB, there should have been a factor of five smaller change in volume compared to the Dodecane. As this was not the case; it may be inferred that using the SS test system for a mechanical compression test only provides an order of magnitude comparison, with an overall variance of +/- 1.5%.

# Chapter 5

## Test System Protocol/Lab Procedure

### 5.1 Alignment

An aluminum optical-bench rail was used to support and align all optical path components. The rail was leveled and checked for level while loaded (including water bath). The SS system tube was then checked for level to confirm alignment in the horizontal, parallel to the optical rail.

The silicon photodiode was centered along three orthogonal axes on the sapphire window and then locked down. The photodiode was the only component to be physically moved while an optical test was being conducted. In order to eliminate the effect on the signal due to the temperature dependence of the detector it was only placed in position to take readings at specified system temperatures, as developed in section 5.3.2.

A lens was employed to produce a collimated beam from the LED. A second detector-side converging lens ( $f_0=26$  cm) was at first employed to focus the light collected on the photo-detector. Experimentation showed though that once the light source was aligned, the detector side lens only degraded the signal received, making the signal more position sensitive. Changing the lens and the focal length did not eliminate the signal loss observed. Therefore the final optical arrangement used did not include the receiver side lens.

#### 5.1.1 LED

The LED optical setup includes the LED and a 10 cm focal length converging lens. The lens was positioned at a distance equal to the focal length from the LED, and centered on axis with the sapphire window in the SS system. (Figure 5.1) Measurement of the lens's focal length was 9.6 cm, at which distance the light output is maximized. There was a factor of three increases in signal strength with the lens included in the optical path compared to the bare LED.



Figure 5.1: Optical Bench Test Setup.

The following alignment procedure was applied; where all distances were measured from the source side sapphire window and observations were made from the detector side:

1. Center the LED face (polished) (5 cm).
2. Center the LED again at (15 cm).
3. (Check) center on lens (3 cm).
4. (Check)/center LED through lens (30 cm).
5. (Check)/center LED through lens (15 cm).
6. (Check)/center LED through lens at lens focus.

In steps four and five, alignment could be verified by the observation of a central bright spot surrounded by what looked like a set of concentric Newton's Rings when the LED was viewed from the detector side of the system on axis as illustrated here in Figure 5.2. Any asymmetry indicated that the LED was not in alignment.

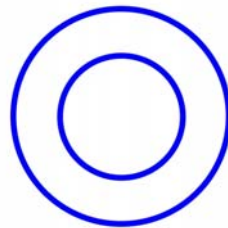


Figure 5.2: Correct alignment simulation for LED's.

Step six could be verified by the observation of an isotropic light as viewed from the detector side of the system. Secondly, the alignment could be checked by measuring the output signal from the detector at the end of the SS system and up to 8 cm away without a definitive drop in signal.

### 5.1.2 Laser

Experimentation demonstrated that the use of the source side converging lens with the laser reduced the output signal on center 5% when optimized (compatible with expectations from interface losses). Therefore the lens was removed from the optical arrangement for the 405 nm laser setup. The following alignment procedure was applied:

1. Center the laser on the sapphire window (5 cm). [horizontal, vertical]
2. Center the laser again at 30 cm on screen target through detector side window.
3. (Check)/center laser through detector side window (30 cm) on screen target along the three orthogonal axis.
4. Mark set positions, then verify position optimization with peak signal output in three dimensions with detector.

Alignment was performed after each test sample was prepared and the set up completed on the optical bench, including filling of the water bath and thermocouple placement.

## **5.2 Temperature control**

### **5.2.1 Water Bath**

It was determined by trial and error, that employing two bags (45 gallon plastic refuse bag) filled with water surrounding the SS tube and in contact with the inside face of each flange worked best in maintaining a constant temperature within the test assembly. Other water bath options considered were: using the 3 m tank, a single 45 gallon bag, and three or more 45 gallon bags.

The two bag system allowed for control of the temperature of each half of the test system. This arrangement produced the most consistent results, the smallest temperature gradients across the system, and resulted in the shortest time for thermal and optical stabilization.

Using an open bath (single bag) from end to end was shown to have greater variations in the temperature across the length of the tubing and end caps over time, even with systematic stirring. Subsequently, the system took longer to stabilize near 0°C.

Utilizing three or more bath bags made it increasingly difficult to produce the same temperature in each bag. The temperature variations were progressively worse for each bag added. As a result, the time for the test system to stabilize was the longest in the multiple bag arrangement.

### **5.2.2 End Caps**

The inside section of the each end cap provided the contact end for the water bath. The exposed surfaces were insulated to minimize the thermal gradient across the end cap. Insulating the caps reduced the thermal gradient by 40% on each cap. The temperature of the end caps were measured on each face and at the sapphire window. In general the end caps stabilized before the fluid in the system reached equilibrium, in the roughly eight hours each test setup took to stabilize.

## **5.3 Test System Control**

### **5.3.1 Pressure**

From initial system pressurization at 6100 psi, there was a system “relaxation” of ~300 psi to 5800 psi (compatible with adiabatic heating upon pressurization and subsequent cooling). This required a wait time of approximately one minute, at which point the pressure could be raised to 6100 psi again where it would remain stable over the duration of the test.

After the leak test for each system test was completed no further pressure drop should be observed over the duration of the test (~ 30 min.). In one case there was a leak at the face of one of the windows, this required a rebuild of the entire test system.

Were the system not used for a few days, it was necessary to cycle the Enerpak piston 5-10 times to lubricate the internal seal on the piston. The piston as may be recalled, maintains a sealed barrier between the LS candidate being tested in the SS test assembly and the hydraulic pump fluid. Failure to cycle the piston would result in drops of hydraulic fluid leaking out of the piston, producing a subsequent drop in pressure at 6000 psi.

In order to achieve repeatable pressure test data, the temperature of the SS system needed to be equal that of the water bath. Therefore after pressurization, approximately five minutes was required for the system and bath to come to equilibrium at the bath temperature. Another 25 minutes was required on average for the LS candidate in the system to reach optical equilibrium.

### **5.3.2 Post-Test**

In order to validate the results of each test, a benchmark of 5% was set for variation between the baseline signal measurement and the post-baseline measurement. Test runs with greater than 5% deviation were discarded, and the test rerun. Post tests results were taken after the system temperature and ambient room temperature were in agreement.

Movement of any of the optical path components in the horizontal or vertical quickly produced a significant change in the signal. Test runs where one or more of the optical path components were moved were invalidated. Notably, the detector diode once aligned allowed for removal from the optical bench and return without affecting the results. Test result variations were on the order of 0.1%.

Experimentation demonstrated that if the post test ambient temperature varied from the baseline by 3°C or more the post-baseline test signal diverged ~5%. The room temperature could be affected by having the adjoining door to the Anita Lab next door open. It could be (and was) radically affected by the occasional demise of the building air conditioning plant. Each test run that spanned a failure in the air conditioning system was scratched as the ambient temperature increased 5-8 degrees.

# Chapter 6

## Pressure Test

### 6.1 Sample Test Results

The data for each of the pressure and temperature tests may be found in appendix A. Sample tests that failed to produce a satisfactory post-baseline test for signal intensity were discarded and the sample retested. Recall that test designators in Figure 6.1 beginning with “B” reference the blue diode with the peak at 430 nm, and the full width-half max value of 60 nm, while those test designators beginning with “L” reference the 405 nm laser.

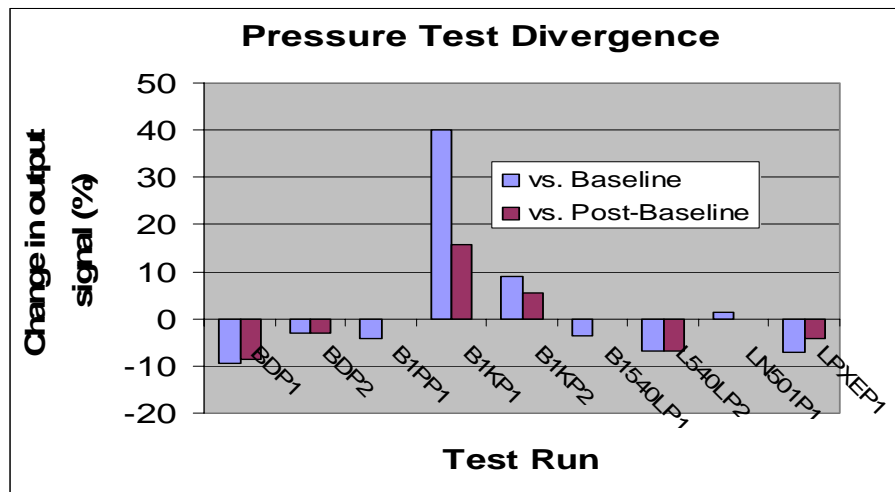


Figure 6.1: Pressure test results for LS candidates. The estimated instrumental and systematic error for the tests presented is +/- 2%.

#### 6.1.1 Dodecane

The pressure test on Dodecane (BDP2) produced a 3% loss in signal strength vs. both the baseline and the post-baseline measurements. The Dodecane test, being the first done did not have a water bath to maintain equilibrium, therefore the test temperature was 1.8°C above the ambient. There was an initial spike in temperature after pressurization of 4°C. In fact all of the test samples demonstrated an initial pressurization temperature increase of ~4°C before returning to equilibrium. It is of merit to note that although the post-baseline measurement was taken 15 hours later, it was equal to the baseline.

#### 6.1.2 Pseudocumene

Test B1PP1 showed a -4% change in signal strength vs. the baseline and no change vs. the post-baseline measurements. Beginning with the pseudocumene, all pressure tests had the added benefit of the water bath. Approximately 30 minutes was required

to reach thermal equilibrium. This includes the return of the sample temperature to that of the ambient bath and the output optical signal remaining stable.

The temperature increase for each sample when pressurized was matched with a similar decrease in temperature when the pressure was released. Significant optical distortion was observed in the tube shortly after the system was pressured. As a result, this and each subsequent post-baseline measurement was taken the following day to insure stability. I included the signal change vs. the post-baseline measurement in Figure 6.1, and it is this data that is the most accurate.

### 6.1.3 KamLAND Mix

Both test B1KP1 and B1KP2 produced an interesting and anomalous result. All of the other test samples demonstrated no change or a small degradation in signal due to pressure. The KamLAND mix had an increase in light signal under pressure. There was an astounding increase in light of 40% vs. the baseline and 16% vs. the post-baseline. These results differ significantly from the mix's constituents. It is expected that the KamLAND Mix follow closely with the results for Dodecane – its primary constituent. The optics were focused following the protocol developed, and the power reading for the LED remained constant.

Convinced that there was a mistake or tampering, test B1KP2 was set up from scratch and the pressure test run again on the same sample. Again there was a noticeable increase in light output under pressure, producing a 9% increase vs. the baseline and 5.5% vs. the post-baseline. Again there were no physical changes made to the system or optics.

There is no systematic explanation as to why the light transmission is greater for the pressurized test run than for the baseline measurements. Were there lensing or physical optical warping, one would expect that the results would be lower and not higher due to any change in the focal length from the optimized setup for the baseline test at ambient. In any event, if there was optical lensing due the flexing of the sapphire windows under pressure it would be identical for each material tested.

It is interesting to note and may merit further discussion pointing out that the post-baseline measurements for both tests are lower than the pressure test measurements. These were the only tests to show an increase in the post-baseline measurements over the baseline values.

Using a dental mirror to make observations showed a clear and isotropic sample under pressure. There was no evidence to suggest that there was any other optical process going on or that there was a change in the focal length. In fact moving the focal lens only reduced the signal during the pressure test as well as for the post baseline.

There were a number of suggestions as to what the possible cause of this anomaly is. They are as follows:

- Lensing (unaccounted for physically, but present none-the-less)
- A pressure hysteresis curve.
- A change in the index of refraction for the mix.
- A change in the chemical structure of the KamLAND mix.

Although interesting, no further study on the pressure dependence of the KamLAND mix is expected. The temperature test results effectively removed it from consideration for the proposed detector, ending further interest in it. Still, at a later time it would be interesting to explore this anomaly.

#### **6.1.4 LAB**

The pressure test on LAB 540L was consistent with other LS constituents. The test results produced a -3.7% change vs. the baseline and no change vs. the post-baseline measurements for the blue LED. The blue laser arrived in time for the test on the LAB samples. As a result, a pressure test was run with both the LED and the 405 nm laser for comparison. The laser test produced a ~ -7% change vs. the baseline and the post test. The laser setup, like the LED followed protocol developed for optimization of the focus along one axis parallel to the optical bench. In the subsequent LAB N501 pressure test there was an increase in signal output of 1.4% vs. the baseline and no difference with the post-baseline test.

#### **6.1.5 PXE**

The PXE pressure test produced results of -7.0% vs. baseline and -4.3% vs. the post-baseline value. Although these values are in line with the other samples, observation showed that the PXE has a longer relaxation time for reaching equilibrium. Each of the prior samples reached equilibrium with in 15-20 minutes – with the measurements taken at 30 minutes and one hour, the PXE on the other hand took nearly an hour and a half to stabilize. On the pressure down, the optical distortion effects took another 1.5 hours to dissipate.

The 70/30 Dodecane/PXE mix showed a change due to pressure of -2.3% vs. baseline and -1.6% vs. the post-baseline value. The time for this mix to come to equilibrium was in between that of Dodecane and the PXE, taking 40 minutes to stabilize. If PXE is chosen as a primary detector candidate, additional time must be built into the ocean test program for the scintillator to come to equilibrium. This issue of relaxation may become a significant factor in the reliability of the results for a detector with a PXE mix.

### **6.2 Pressure Analysis**

The estimate for systematic error is +/-2%, which includes the error for the light sources and the detector electronics. Looking at the test data, and using the post-baseline values for comparison there is negligible pressure dependence for the LS candidates evaluated. Only pure PXE and the anomalous KamLAND mix fell

noticeably outside the error range. Since the Dodecane/PXE mix is effectively within the error range, there is no concern of pressure dependence for using this LS candidate.

Each sample had a peak temperature increase of ~4°C when pressurized to 6100 psi, as noted earlier. During an ocean test, the LS candidate would be pressurizing over approximately one hour according to simulations run by Makai Ocean Engineering, rather than the five seconds in this test. The relaxation time; the time the sample takes to reach equilibrium and maintain an isotropic optical path, is of more importance in future measurements.

For purposes of validation of the proposed Hanohano detector conceptual design one may conclude that in the upper limit the absorption would increase by 3.7% over a 1 m path length. If the post-test were taken as a baseline, then this change would be less than 1%, and arguably the more accurate.

It is plausible that there was some coagulation of small chemical structures caused by the pressure. This would explain the hysteresis in the transmission measurement after return to ambient pressure. In future testing, this effect may be evaluated by heating the samples to redistribute the possibly coagulated material.

# Chapter 7

## Temperature Test

### 7.1 Temperature Results

Complete test results may be reviewed in appendix A. Below, figure 7.1 provides a snapshot of the optical transmission measured versus the ambient baseline. Samples' test values are reported at 4°C unless otherwise noted. The path length is 1 m.

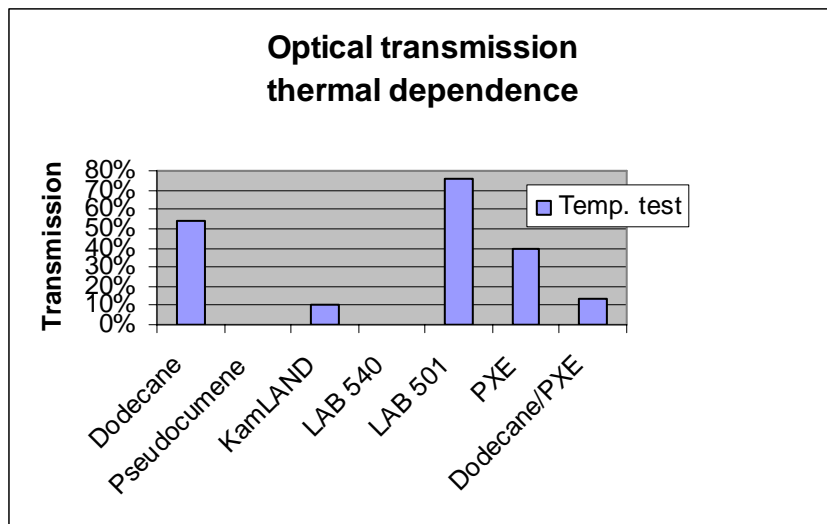


Figure 7.1: LS candidate light transmission at 4°C. The estimated instrumental and systematic error for the tests presented is +/-2%.

#### 7.1.1 Dodecane

There was a light signal loss of ~50% as a measure of the photo-diode output current due to a change in temperature of 20°C, from ambient to 0.3-4.5°C. Visual observation did not provide any clues to the loss in signal, which is not surprising considering visual response has a huge dynamic range and is sensitive on a log power scale.

Developing the test protocol determined that approximately 8 hours would be required from the initial cool down before the test samples would stabilize at a chosen temperature. Optical "Schlieren" (see section 8.1) layers were visible for ~4 hours. Test measurements indicated that no further improvement in output current could be achieved by using a test time of longer than ~8 hours.

The loss observed is consistent for both the blue (430 nm) and green (520 nm) LED's suggesting that there is no significant frequency dependence for Dodecane in the region the proposed study is interested in.

### **7.1.2 Pseudocumene**

Below 4.5°C, Pseudocumene is basically opaque to visible light. There was a transition observed between 3°C and 4°C from opaque to “clear”, but there was extreme distortion in observing the LED's through the one meter system. Repeated, carefully controlled testing produced similar results. Visual observations and optical test measurements demonstrated that below 12°C, Pseudocumene failed to produce non zero verifiable results.

### **7.1.3 KamLAND**

Considering the results for the pseudocumene, the measurements for the 80/20 mix of Dodecane and pseudocumene comes as no surprise. The light transmission was only 10% at 4°C. Like the pseudocumene, the mix was opaque below 3.5°C. Above 4°C the mix looked much like the pseudocumene did at the same temperature. Again, careful repeat tests confirmed the results found.

Since the KamLAND mix was the initial “primary candidate”, extra caution was used after the initial observations were made of the signal loss due to the decrease in temperature. Even doubling the time of measurement produced no measurable change in light transmission.

### **7.1.4 LAB 540L**

As in the case of the two prior test samples, the LAB 540L sample was opaque below 4°C. Above 4°C the sample looked “clear” with obvious schlieren effects creating distortion and lensing. Obvious gradient lines were visible.

In order to produce any transmission reference for this LAB sample; the temperature was slowly raised to 5.3°C, where the transmission was measured at 18%. This temperature was the first temperature where the signal remained stable for 5 minutes or more. As in the prior samples, the sample was cycled between 0°C and 7°C in order to confirm the optical quenching observed.

### **7.1.5 LAB N501**

The N501 LAB sample was the first to appear as a viable candidate. At 0°C this LAB sample remained “clear” without the accompanying thermal gradient lines visible in the other test samples. The initial visual test showed the sample to be free of distortion/ lensing. The image of the laser beam morphology appeared consistent on a screen, and appeared as strong as during the baseline test.

At 4°C, 76% of the baseline transmission value was recorded. At 6°C there was a further 6% increase in transmission. Using the result at 4°C, a preliminary

attenuation length calculation yielded  $\lambda = 4.5$  m. Although this value is smaller than that required for the proposed detector, this sample provides the first positive results for use as a liquid scintillator in the proposed detector.

An attenuation length of 4.5 m may conservatively be considered a lower limit for this LAB sample. In the LS purification study done at Brookhaven, electro-photometer results posted an order of magnitude improvement in transmission. The measured absorption was 0.011 at 410 nm for the unfiltered LAB sample and 0.001 for the silica column filtered sample. This result was accompanied by the claim that the resulting “attenuation length was too small to be measured by a 10 cm cell” [26].

#### 7.1.6 PXE

The PXE sample produced 39% of the baseline transmission at 2°C. The PXE remained “clear”, yet there was obvious optical distortion even after 8 hours of carefully controlled cooling. The (laser) beam morphology appeared consistent on a screen, just weaker in intensity as observed on the detector end of the system.

#### 7.1.7 Dodecane/PXE (70/30)

The Dodecane/PXE (70/30) mix appeared translucent at 4°C. Test LDPXET1 produced a transmission reading of 13%. This was a somewhat surprising result considering that the mix appeared “milky” visually. If there were compounds precipitating out of solution, this output value may be due significantly to scattering and reflection off the walls of the tube. No beam spot was observed during the screen test.

### 7.2 Temperature Analysis

Contrary to expert predictions, a change in temperature from ~22°C to 4°C did have a measurable and significant effect on the transmissivity of the LS candidates tested and the corresponding attenuation length. The dependence of the attenuation length on temperature would disqualify LS candidates using pseudocumene or PXE.

The only LS candidate that shows promise is LAB (N501). As noted above, the calculated attenuation length is 4.5 m at a temperature of 4°C. This is below the requirements of the proposed detector with a target of 20 m. This LAB mix deserves further investigation.

It is expected that with column filtering alone, among many purification options available it should be reasonable to achieve similar results to those demonstrated by Minfang Yeh at Brookhaven on LAB as shown in Figure 7.2 below.

The criterion of a 20 m attenuation length in the proposed detector would require a 4X-5X improvement over the present value. Were purification to improve the attenuation in our LAB samples at half of what Minfeng demonstrated, our

attenuation length goal would be reached. Were his results achieved, we would have an attenuation length of 45 m, well beyond that required.

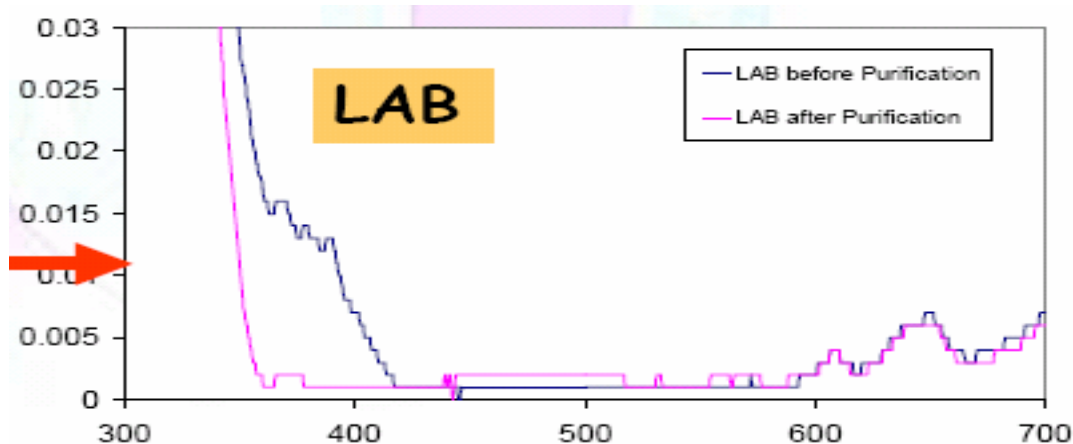


Figure 7.2: In this spectrophotometer plot of absorption vs. wavelength there is a marked improvement in the absorption after purification for wavelengths below 420 nm. As noted by the arrow; the absorption at 410 nm is 0.11 for the base sample – while that for the purified sample is ~ 0.001.

Experienced researchers familiar with filtering oil samples note that they are often somewhat of a mix of molecular types, and that some of these molecules may precipitate at low temperatures. In fact, string-like structures were observed in preliminary tests run on LS samples cooled in a freezer.

It is well understood in chemistry that precipitates form around particulate “seeds” at cloud point. By purification using silica or alumina gel columns these precipitate seeds can be removed.

The precipitation point for any compound is temperature dependent. Like moisture precipitating out of a cloud, long carbon chain molecules that may begin to change phase will remain in solution in liquid scintillators over a 20°C change in temperature with the “seeds” removed.

Filtering will produce a two fold benefit. First; removing particulate contamination will improve the attenuation length of the LS candidates at room temperature by as much as an order of magnitude. Secondly; by removing the “seeds” for precipitation, the temperature dependence of each LS may be mitigated and possibly eliminated.

## Chapter 8

### Application of findings

#### 8.1 Optical properties stability

Schlieren “the German term for striations or inhomogeneities”; was applied by Toeper in 1864 to the refractive index inhomogeneities in a transparent fluid region. These index of refraction gradients are usually produced by density gradients, temperature gradients, or concentration of one species into the others within the sample [27].

Schlieren effects were evident in each sample tested until the sample reached optical thermal equilibrium. As the tests done have shown, in the extreme, Schlieren effects may be responsible for the total loss of light within the test system. In each of the other cases, Schlieren was a limiting agent in determining the amount of time required for each test sample to reach equilibrium.

At 4°C, even waiting an extended time for candidates such as pseudocumene, the KamLAND mix, and the mixed PXE to reach thermal equilibrium did not improve results. This result suggests changes in the sample density beyond those due solely to temperature gradients. These changes may be a product of disassociation between the molecules in solution in the liquid scintillator candidates. This would be consistent with the other noted causes of Schlieren.

#### 8.2 LS selection

LAB N501 is the best candidate among those tested in meeting the all of the criterion given in the research impetus. The safety risks posed by a detector using LAB are nominal under the environmental conditions of deployment and during testing. LAB has excellent feasibility (see Table 1). The physical properties of LAB are adequate in meeting the required criteria. LAB N501 posted the only positive results for meeting the required optical properties. Finally, the contamination risk is among the lowest of all LS candidates tested. It is anticipated that the factory shipped N501 will be sufficient to produce positive test results in an ocean deployment test.

Purification will be a necessary next step in determining the true ability of LAB to perform as the LS in the proposed 20 m diameter detector. It is expected that purification of the LAB will improve the attenuation length of 405 nm light in the LAB from 4.5 m at 4°C to at least the detector criteria of 20 m.

#### 8.3 Ocean deployment test

In an ocean deployment test any LS candidate used must be pre-chilled to at least 4°C. Cooling the scintillator will mitigate the time it will take for a one kilotonne test volume to come to equilibrium. For a one meter diameter LS test volume, “days”

would be required for the sample to come to optical equilibrium from an ambient temperature ( $\sim 25^{\circ}\text{C}$ ) to  $4^{\circ}\text{C}$  at 4 km depth.

One kilotonne of LS cooled to  $4^{\circ}\text{C}$  would require a method for cooling it as well as an insulated container prior to deployment. The deployment process would require minimizing the time in filling the test detector vessel and deployment time. Also any process to transfer material must minimize the amount of contamination that may be introduced. Contamination would reduce the light yield as well as the effective attenuation length.

## 8.4 Recommended LS test system improvements

### 8.4.1 Test tube anodizing

Anodizing the inside of the SS test system tube black would reduce signal that may be reflecting off of the inside of the tube walls. Any light that is scattered inside of the test system may be reflected forward to the detector with the present surface. Reflected light would skew the received output signal higher. The size of the detector and the minimum required attenuation length predicate a definitive measurement for light absorption.

### 8.4.2 LS sample purification

Purification of the LS candidates is of critical importance. Further testing is incumbent on the outcome of any attenuation length measurements for LS's at  $4^{\circ}\text{C}$ . If attempts at improving the attenuation length of LAB 501 are unsuccessful at  $4^{\circ}\text{C}$  for example, the Hanohano project's feasibility becomes jeopardized. It is expected that column filtering would produce immediate positive results in naming a LS candidate for Hanohano.

### 8.4.3 10-cm Spectro-Photometer LS testing

Using a 10-cm spectro-photometer to test each sample would allow for verification of the tests using the SS system. It would also allow for comparing filtered and unfiltered samples for frequency dependence over the whole visible spectrum. Third, these measurements could be compared with the results of Minfang Yeh on LAB and pseudocumene, for example.

A 10-cm cell system is preferred over the 1-cm cell system due to the order of magnitude difference in the verifiable attenuation length measurement. Minfang Yeh noted that his recorded attenuation length was in fact limited by using a 10-cm cell.

### 8.4.4 Refrigeration System

Ideally, all test measurements could be performed in a test environment where there were no temperature variations in any part of the test system. This would require the use of a large temperature controlled room – a refrigerator large enough to contain the whole SS test system apparatus including the optical bench. This suggestion must be carefully considered for feasibility, benefit, and cost effectiveness.

## Appendix 2

### Bi-Ocular Scintillator Temperature Evaluation

All of the considered scintillator mixes passed the visual clarity test at zero degrees Celsius, and 1 atm. of pressure. Our working environment of 4°C thus will not eliminate any mix from consideration.

Proposed Mixes:

1. Dodecane, Pseudocumene (70/30)
2. Dodecane, Pseudocumene (80/20)
3. PXE
4. Dodecane, PXE (70/30)

*Evaluation:*

	<u>Temperature (C)</u>	<u>Observed</u>
<b>Dodecane:</b>	10	clear
	5	clear
	0	clear
	-10	clear, with a white/clear “fibrous weave” crystals along inside of beaker.
	-20	white/clear fibrous crystals throughout beaker.
<b>Dodecane, Pseudocumene (70/30)</b>	10	clear
	5	clear
	0	clear
	-3	clear
<b>PXE</b>	10	clear
	0	clear
	-5	clear
<b>Dodecane, PXE (70/30)</b>	10	clear
	5	clear
	0	clear

These tests were run in a freezer to eliminate water condensation from contaminating samples. When initial tests were run with an ice bath, each mix was observed to have temporary (~3 seconds) white strands in solution.

## Appendix 3

### Proposed LS Physical Parameters

Recipes of interest:

1. Dodecane, Pseudocumene (80, 20)
2. Dodecane, PXE (70, 30)

With these two primary recipes of interest the mechanical properties of Dodecane will dominate calculations for physical parameters and mechanical constraints.

#### Physical Properties:

	Pressure:	Temperature:	Density	Viscosity:
<b>Dodecane:</b> (C <sub>12</sub> H <sub>26</sub> )	14.5 psi 6091 psi	298.15 K 298.15 K	0.7460 0.7715	1.344 mPa 2.139 mPa
	14.5 psi 6120 psi	323.15 K 323.15 K	0.7274 0.7568	0.911 mPa 1.422 mPa

Where the Bulk Modulus is:  $B = 0.988 \text{ Gpa}$

Isothermal Compressibility:  $K = 9.9 \times 10^{11} (\text{sq.cms/dyne}) @ 310.95 \text{ K, 1 atm.}$

$K = 5.3 \times 10^{11} (\text{sq.cms/dyne}) @ 310.95 \text{ K, 1000 atm.}$

Or  $K = 9.88 \times 10^4 (\text{MPa}^{-1})^{-1}$

Cubic Thermal Expansion:  $T_c = 0.93 \times 10^3 \text{ K}^{-1} @ 298 \text{ K}$

<b>Pseudocumene:</b> (C <sub>9</sub> H <sub>12</sub> )	14.5 psi	298.15 K	0.876	----
---	----------	----------	-------	------

Undocumented Pseudocumene properties may be reasonably inferred from Benzene which is the primary molecular component.

#### Benzene: (C<sub>6</sub>H<sub>6</sub>)

Isothermal Compressibility:  $K = 8.09 \times 10^{11} (\text{sq.cms/dyne}) @ 273 \text{ K, 1 atm.}$

$K = 9.67 \times 10^{11} (\text{sq.cms/dyne}) @ 298 \text{ K, 1 atm.}$

$K = 5.07 \times 10^{11} (\text{sq.cms/dyne}) @ 298 \text{ K, 1000 atm.}$

Or  $K = 9.66 \times 10^4 (\text{MPa}^{-1})^{-1} @ 298 \text{ K}$

Cubic Thermal Expansion:  $T_c = 1.14 \times 10^3 \text{ K}^{-1} @ 298 \text{ K}$

#### Predicted Recipe Properties:

1. (80, 20)	14.5 psi	298 K	0.774
2. (70, 30)	14.5 psi	298 K	0.788

$K = 8.0 \times 10^{11} (\text{sq.cms/dyne}) @ 298 \text{ K, 6000 psi.}$

## Bibliography

- [1] K.Eguchi *et al.* *Phys.Rev.Lett.*, 90:021802, (2003)
- [2] T. Araki *et al.* (*KamLAND*), *Nature* 436 (2005), 499-503
- [3] Gianni Fiorentini *et al.* *Phys. Lett.* B629 (2005), 77
- [4] E.Sanshiro. Ph.D. Thesis, *Tohoku University*, (2005)
- [5] [Domogatsky, G.; Kopeikin, V.; Mikaelyan, L. et al oai:arXiv.org:hep-ph/0411163](#), (2004)
- [6] S.T. Dye et al., [hep-ex/0609041](#), (2006)
- [7] Modler, R.F., Gubler, R., Kishi, A., *CEH Marketing Report*. (2002)
- [8] F. Ardellier. *et al*, *Double Chooz: A Search for the Neutrino Mixing Angle  $\theta_{13}$* , arXiv:hep-ex/0606025 v2, (2006), 67
- [9] M. Chen, *PANIC Neutrino Satellite Meeting*,  
[<http://www.panic05/um/gov/neutrino/talks/chen\\_sno+>](#) (2005)
- [10] BOREXINO Coll. H.O. Back *et al.* *oia:arXiv:physics/0408032 v1*, (2004), 33
- [11] J.B. Benziger. *A Scintillator Purification System for a Large Scale Solar Neutrino Experiment*,  
[<http://theta13.phy.cuhk.edu.hk/aberdeen/useful\\_links/purification.pdf>](#) (1998), 2
- [12] M.Yeh, *Overview of Gd-loaded and Unloaded Liquid Scintillator for Reactor Anti-ve Experiments*. Brookhaven National Laboratory, Chemistry Department. [<http://bes.ihep.ac.cn/conference/PRC-US/file/0613/Overview%20of%20Gd-LS%20and%20LS%20for%20US-China%20Workshop%20Yeh%20BNL.pdf>](#), (2006)
- [13] J.B. Benziger. *A Scintillator Purification System for a Large Scale Solar Neutrino Experiment*,  
[<http://theta13.phy.cuhk.edu.hk/aberdeen/useful\\_links/purification.pdf>](#) (1998), 2
- [14] G.Alimonti, *et al.* *A Large Scale, Low Background Liquid Scintillator Detector: The Counting Test Facility at Gran Sasso*, Borexino-CTF Collaboration NIM A406, (1998)

- [15] R. Ford, SNO Collaboration; phone consultation, June 13, 2005
- [16] J.B. Benziger. *A Scintillator Purification System for a Large Scale Solar Neutrino Experiment*,  
 <[http://theta13.phy.cuhk.edu.hk/aberdeen/useful\\_links/purification.pdf](http://theta13.phy.cuhk.edu.hk/aberdeen/useful_links/purification.pdf)>  
 (1998), 2
- [17] J.B. Benziger. *A Scintillator Purification System for a Large Scale Solar Neutrino Experiment*,  
 <[http://theta13.phy.cuhk.edu.hk/aberdeen/useful\\_links/purification.pdf](http://theta13.phy.cuhk.edu.hk/aberdeen/useful_links/purification.pdf)>  
 (1998), 2
- [18] J.B. Benziger. *A Scintillator Purification System for a Large Scale Solar Neutrino Experiment*,  
 <[http://theta13.phy.cuhk.edu.hk/aberdeen/useful\\_links/purification.pdf](http://theta13.phy.cuhk.edu.hk/aberdeen/useful_links/purification.pdf)>  
 (1998), 3
- [19] K.E. Starling, *Fluid Properties for Light Petroleum Systems*. Huston, TX:  
 Gulf, (1973)
- [20] DR Caudwell et al, *The Viscosity and Density of n-Dodecane and n-Octadecane at Pressures up to 200 MPa and Temperatures up to 473K*,  
 Imperial College London, South Kensington Campus, (2003), 5
- [21] DR Caudwell. et al, *The Viscosity and Density of n-Dodecane and n-Octadecane at Pressures up to 200 MPa and Temperatures up to 473K*,  
 Imperial College London, South Kensington Campus, (2003), 6
- [22] CRC: *Handbook of Chemistry and Physics*, ed R.C. Weast, CRC Press, Boca Raton, FL. 86<sup>th</sup> edn., (1968), 6-141
- [23] Reid, Prausnitz, and Poling. *The Properties of Gases and Liquids*.  
 4th ed. mcgraw-Hill: New York. (1987)
- [24] DR Caudwell. et al, *The Viscosity and Density of n-Dodecane and n-Octadecane at Pressures up to 200 MPa and Temperatures up to 473K*,  
 Imperial College London, South Kensington Campus, (2003)
- [25] W.Sorensen, *Density of N501 and N540 Alkylates*, SASOL, (2006)
- [26] E. Chitamber, A. McGowan, M. Parker, *Measurement of the effect of temperature on some properties of liquid scintillators and PVC*, <<http://nova-docdb.fnal.gov/0003/000350/001/nova0050.doc>>

- [27] G. Tanda, *Application of schlieren technique to convective heat transfer measurements*, <<http://dau.ing.univaq.it/omhat/Papers/sch.pdf>>, (1999)
- [28] F. Suekane. *et al.* *An overview of the KamLAND 1-kiloton Liquid Scintillator*, <<http://arxiv.org/abs/physics/0404071>>, (2004)
- [29] *LENA Homepage*, <<http://www.e15.physik.tu-muenchen.de/research/lena>>

## **Appendix**

**Task 9: (not paid for by CEROS and not submitted for DARPA review)**

Appendix

## **Appendix**

### **Task 10: Internal Communications Networking**

Appendix

# Internal Communications Networking

*A report submitted to Makai Ocean Engineering*

J.G. Learned and G.S. Varner  
*University of Hawaii at Manoa*

## Introduction

This report presents a preliminary design for the communication network inside the detector vessel. On the order of 2000 photo-detectors require command and control signals from the central computer. These signals turn high voltage on and off, monitor noise rates, and run calibration procedures. The high rate data from optical modules being sent to shore dominates the design criteria, however. A networking structure to provide reliable communication without single point failure modes is required for a successful project. We have examined previous and related experimental designs (such as for DUMAND, KamLAND, NESTOR, ANTARES and ICECUBE). We conclude that a tree structure with one intermediate branching layer inside the detector, plus a redundant shore communication path, will satisfy our requirements. Other schemes are possible, but at this stage we have identified at least one plan which meets the needs of the experiment. We emphasize the benefits of making as much of the data communications in oil bath and with the minimum number of connectors and minimal pressure differentials.

## Detector Concept

The deep ocean antineutrino detector records scintillation light using a few thousand optical modules arrayed looking inward from the outer surface. An optical module comprising a photomultiplier tube (PMT) and high voltage base electronics is housed in a pressure-resistant glass sphere. Each module connects to a multi-channel controller in the Control Housing by a single coaxial (or possibly by twisted pair) cable.

The cable between a module and its controller carries electrical signals in both directions. In addition to low frequency command and control signals flowing back and forth between PMT and controller, the cable passes low voltage DC current to the PMT and high frequency PMT signals back to the controller. One issue requiring further study is the method for achieving continuity through the glass sphere housing the optical module (see discussion below). We have considered options without any glass penetration (eg. laser power or inductive coupling), but at present these are not realistic options. So for the baseline design we will stick with a traditional penetrator, of which many commercial versions are available, and being used in the experiments mentioned above.

We take PMT signals to mean analog pulses above a settable discriminator threshold, typically at the 0.1 PE level. The range and resolution of discriminator settings requires further study, but no problems are foreseen (again based upon the experience other experiments). A multi-channel controller harvests, digitizes, encodes, and transmits PMT signals to shore (surface). The control board key functions are to supply the low voltage DC current to the high voltage converter on the PMT base board as well as to acquire and process the PMT analog signals. Processing includes digitizing the analog signals,

encoding the data with channel number, local coincidence for event validation, and global time stamp from a master clock, and transmitting the digital data over fiber optic cable to a shore (surface) station. A master clock signal generated from the FPGA and broadcast through fiber optic cable synchronizes each PMT.

This basic detector concept is sketched in Figure 1.

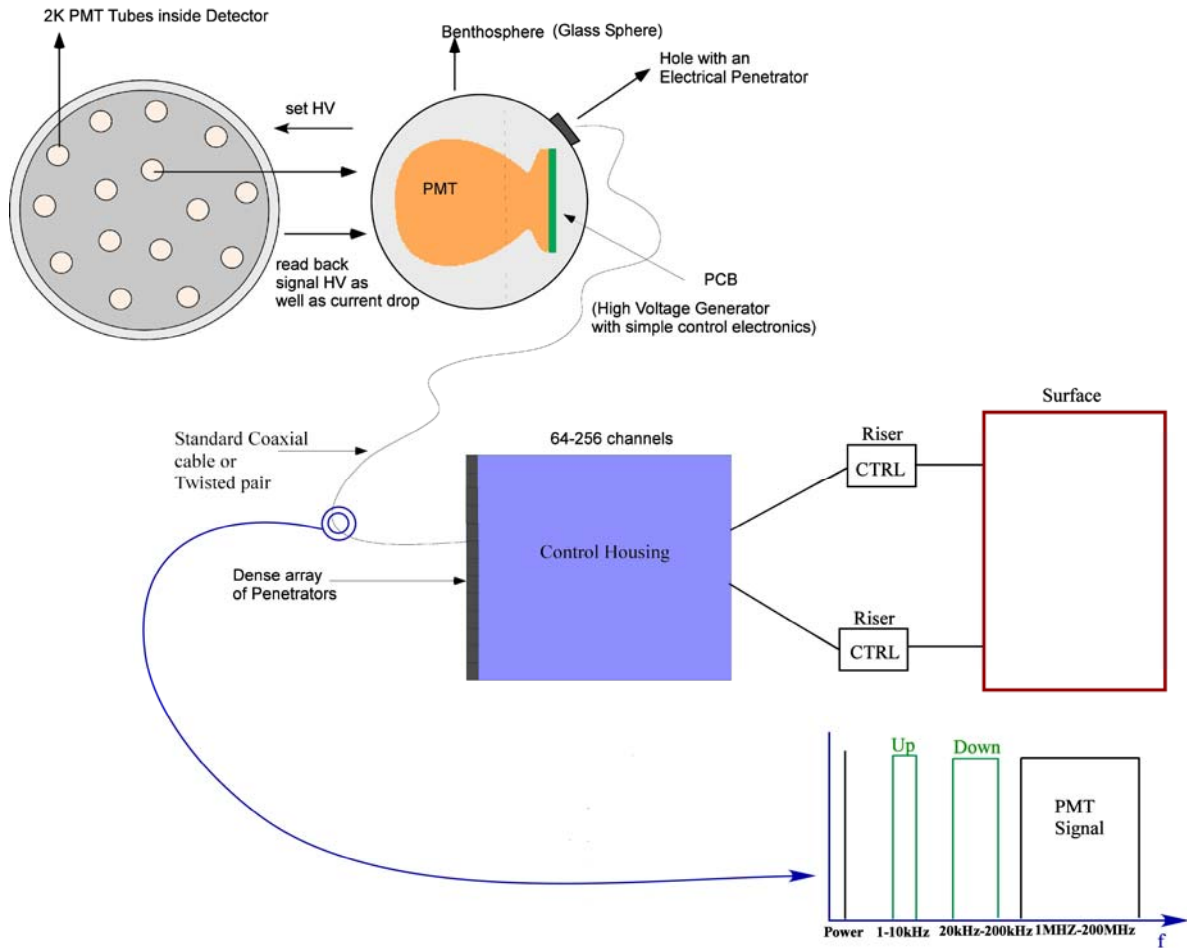
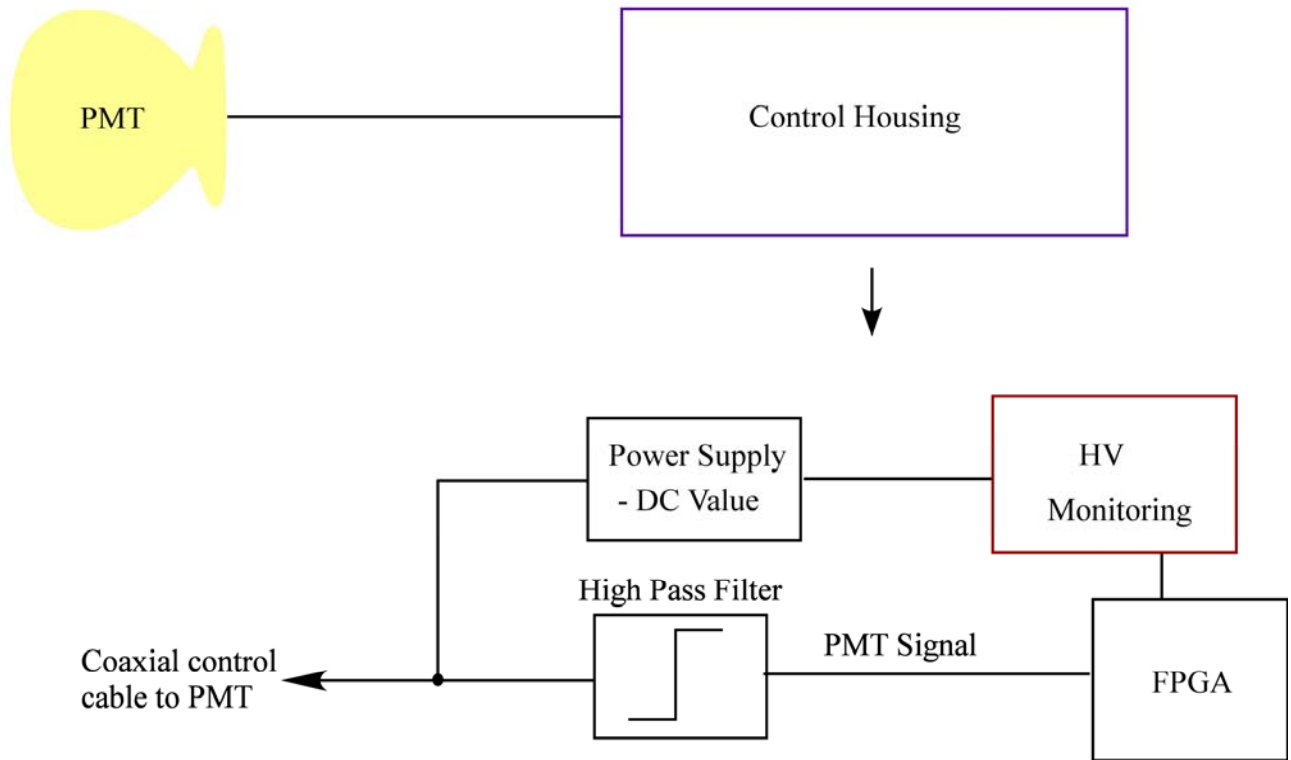


Figure 1: Schematic overview the detector concept

Shown below in Figure 2 is a schematic of the Controller Housing cabled to the PMT. The PMT has low-noise and a high maximum gain of  $10^8$  with a large hemispherical photocathode area, and a random count rate of order  $10^4$  counts per second or less. The PMT is capable of detecting single photoelectrons with an efficiency of order 25%. The photomultiplier tube detects photons, yielding an electronic signal proportional to the incident light, though for the physics considered here (at around 1 MeV of energy) the light signals will typically be only one photoelectron (PE). For resolution of higher energy events and for events near to PMTs, it is useful to have a good multi-PE resolution and substantial dynamic range (1000x, though not necessarily linearity).



*Figure 2: Schematic diagram of the Control Housing*

Each PMT will connect with a single channel directly to a Control Housing, or Node Control. Each Control Housing will communicate via a fiber optic cable to the two redundant Riser Controllers. The Spartan 3 field-programmable gate array (FPGA), which is located inside the Node Control, will have either 16 or 32 Channels depending on the best configuration for the cabling scheme (see Figure 3). We have not settled upon the optimal number of channels yet, but it should be of order of the square root of the total number of PMTs.

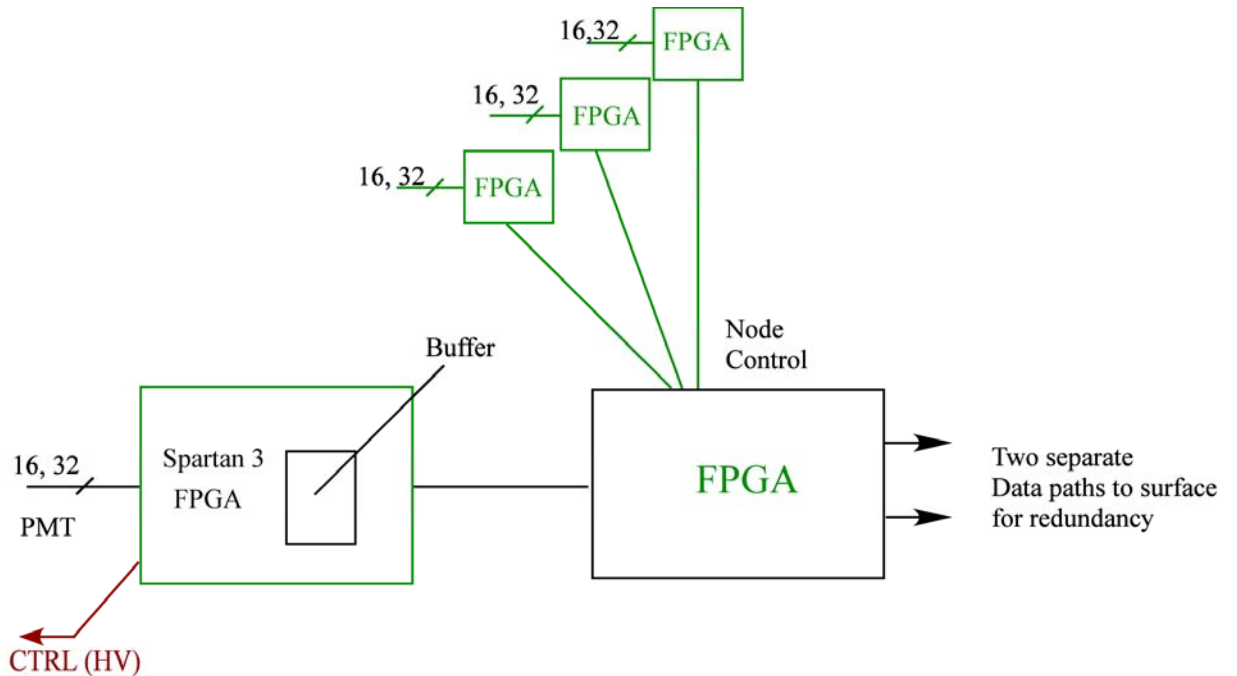


Figure 3: Schematic diagram of the field programmable gate array (FPGA)

Listed below in Table 1 are a few possible combinations of Node Control and Cabling schemes per Node Control.

Table 1: Various combinations of Node Control and Cabling Schemes

# of Channels	# of Node Controls	# of FPGAs per Node Control	# of Cables per Node Control
16	1	125	2000
16	5	25	400
16	25	5	80
16	50	3	40
32	1	63	2000
32	5	13	400
32	25	3	80

The shore data communications network shall support a network data rate of at least 8 Gb/s. The Riser Controller and The Riser TDL are the data concentrators/clocks and also function as the signal fan-out. Signals from each of the control nodes is collected together and sent to the Risers and then up a pair of single-mode fibers to shore. Signals from the surface are sent back to the Risers where they are fanned out to the control nodes. The overall system design is shown in Figure 4.

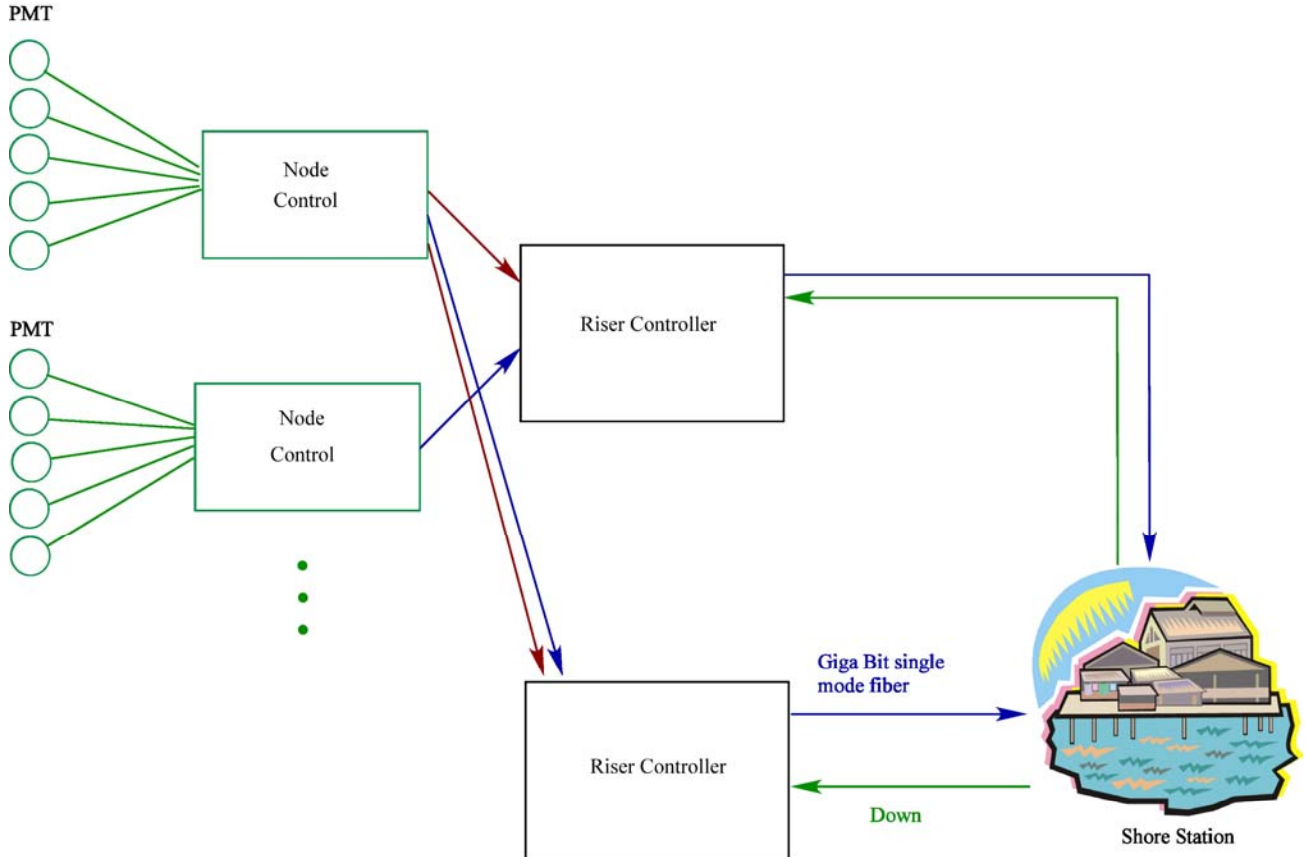


*Figure 4:* Overall system diagram

Two completely redundant riser controllers provide independent paths to the shore station, eliminating a possible single point failure that could take down the entire array. Likewise, each PMT has a pair of paths to the surface. We have some issues to resolve of how priority is assigned at startup and how alternative power can switch over without remote intervention. Again, we have identified engineering tasks here, but there is no stopper, just an optimization to be carried out.

A summary of the data flow is as follows:

- Data up: Time stamps, channel number, controller number, time, charge
- Data Down: Timing edge + control word
- Timing: Entire array running on a single clock

The data rate is entirely dominated by the individual PMT signals. If we take them to be 2000 modules with (upper bound) of  $10^4$  counts per second, and 6its(hit (with address information and both start and stop times), we have a data rate of 1.3 Gb/s. This being

well within current transoceanic fiber capacity (by a factor of more than ten), means that we can comfortably transmit all data, noise included, to shore for processing in a comfortable and adaptable location. Certainly a minimal amount of local triggering could be carried out at the detector to beat the data rate down by several orders of magnitude, but there seems to be no need to add the risk of failure of anything more complicated than is absolutely necessary at sea.

## **Discussion of Topology**

We have examined many variations on this simple scheme, as have others looking at this design question in similar arrays over many years. Generally everyone agrees that forwarding the raw data to laboratory conditions is preferable, though many designs have not had the luxury to do this.

We should say that an attractive alternative however, is a structure similar to that of ICECUBE, where all signals are digitized at the PMT location and then sent forward only after a trigger is recognized, and sent on a relatively slow link. One attraction of this topology is that failures of the digitizer probably only effect a single optical module. The disadvantage is that one must do local triggering, and this adds the complication of more local interconnection, and the possibility of a regional failure thereby. The ICECUBE group did not choose to forward all signals to the surface because they had experienced difficulties with fiber optic connectors under the stress of being frozen into the ice. 2km coaxial cables degraded the signals too much. So they opted for a local digitization scheme.

In the DUMAND, NESTOR and ANTARES cases, all would have preferred to send raw PMT signals to shore, but were limited in the ability to handle rate, and in the difficulty of multiplexing. An added problem in their cases is that the PMTs are distributed over a large region (hundreds of meters), and hence sending the signals to a nodal point for multiplexing becomes necessary. Due to the cost of fiber optics, cables are preferred for short runs from PMTs (<100m). However, one would expect that with the evolution of fiber optic technology, these experiments would evolve towards the scheme we are endorsing.

The underground experiments, such as KamLAND and SuperK, all follow the traditional topology of high energy physics experiments, and run cables from the PMTs to the digitization electronics directly on coaxial cables (with runs <200m). There are variations as to one or two cables/PMT, but all have only a high voltage divider at the PMT base. This is most convenient for these situations since the inner detector where the PMT is located is inaccessible, while the electronics can be in an electronics hut adjacent to the detection volume.

In the instance we are considering, given the advances in technology (the low power switched capacitor devices) we judge that the best strategy for Hanohano is a feed-forward topology, bringing all signals to shore. This does however require multiplexing of many signals onto one or a few fiber channels. Since the data rates available in

standard telephone communications systems now handle more than we require per fiber, we can have redundancy.

The judgment to employ two cables to shore can certainly be questioned. However, since the cost of the cable and cable laying is not large compared to the detector construction and operations, we think it justified. Indeed, though we have not worked out the details as yet, a viable plan may be to install the detector with a single cable to shore, and have the connector available for one (or more) alternate paths, which can be connected by robot after deployment of the detector.

## **Discussion of Detector Internal Connections**

The following is a discussion of the connector/feed-through problem and by implication the connection hierarchy inside the detector vessel. As those of us with DUMAND experience know, and from the experiences of the experiments in the Mediterranean, this is perhaps the most vulnerable area in terms of danger of failures, and can also be an area of heavy expense. Note, for example, that the ICECUBE group has paid about \$500 for each of their optical module (electrical) connector sets. The project has three regions to consider:

- The single coaxial or twisted pair connection to an optical module (OM)
- Cable feed-throughs from the oil region to the veto region (water or oil)
- Group connections to the area digitizer (32 or 64 per unit).

Discussion of each:

1) First one must bring power in to the OM and signals out, as well as carry low frequency control signals. In the past we have learned that we could live with the most inexpensive and tried-and-true type of Benthos feed-through which consists of simply two separate holes in the glass, about 1 inch apart, with pins entering through rubber plugs. We found that PMT signal into a 50 ohm cable was not terribly distorted by the impedance mismatch (as it is close to the source), but we will need to revisit this issue with faster tubes and more signal demands. Better would be a real coaxial cable feed-through, but these are not readily available, and only made by several manufacturers (DG O'Brien is one). More readily available are two pin connectors or feed-throughs, and one can use twisted pair instead of coax. Perhaps we can live with twisted pair for the entire connection between OM and digitizer. This needs study.

Connectors are expensive, and less reliable than (permanently connected) feed-throughs, so we want to minimize the number of these. Given that we have only a rather short cable run from the OM to digitizer, the best strategy may be to install the cable permanently with each module. This could make some problem, if have to exit the oil-filled inner region and travel some distance in the veto region to the digitizer. Moreover it may be worthwhile to cable the OM's so that failure of one digitizer would kill only a widely

distributed set of OMs, but this implies longer cable runs and a more complex cable harness.

Better would be to see if we can live with a dead region in case of digitizer failure, or perhaps half dead region, where we cable to digitizers nearer to their client OMs. This can be studied with a detailed detector Monte Carlo program, at a later stage in the design. In any event, direct cabling from PMTs to the digitizers seems to make for complexity in the cable harness and for difficulty in PMT replacement.

2) A better solution appears to be to have relatively short pigtails on each OM (3m or so), and a connector going to a bulkhead feed-through at the cell, in groups of nine. This feed-through is relatively simple, reliable and inexpensive, in that it will not see large differential pressure (probably an old standard BNC connector would suffice). This configuration would be convenient for installation and testing, since one puts in the OMs and closes up the cell hatch, and can then test a group prior to connection to the full DAQ electronics. The feed-through can be made to withstand the pressure of the detector oil when the detector is filled but veto region empty, as at pier-side while connecting and debugging the detector.

It seems further to be a good idea to have special cable channels from the individual feed-through panels all the way to the local controller/digitizer unit, and have the channels oil filled. This increases reliability, particularly if we have the connectors to the controller/digitizer in oil themselves.

3) Now at the next level we need to bring some rather large number of cables to each digitizer. We have not settled on the number of digitizers, but if we are working with 2048 modules total (plus veto region), then the natural number would be 32 OMs per digitizer and 64 digitizers, or 64 OMs into 32 digitizers, or somewhere in between. In any event, this requires a large number of holes if we were to run one cable per hole into the digitizer. There are many multi-pin (but no multi-coax that we have seen) connectors on the market, so probably we ought to think more about using twisted pair instead of coax. In this case we might want to put the connectors from each OM into a wall mounted box (between oil and veto region, as stated above), which box would then combine, say, nine OMs into one 18 wire cable which would travel in the veto region to the digitizer. If there are 36 OMs per digitizer, then we would have four of these multi-pin connections per digitizer. And this cable can be of the high reliability type which is inside a hose filled with oil (see the Ocean Design website for a description, for example). The digitizer in this example then would have four multi-pin connectors going to OMs, plus two connectors going to the two (redundant) main multiplexer/controllers, plus power connections.

If we have 64 digitizers, then perhaps the best strategy would be to have 8 cable harnesses each attaching to 8 digitizers, and going to one of eight connectors at the main controller. The main controller will also then attach to the shore cable. We may need a separate power conditioning unit as well, to be studied. Also we need to think more about how we would deal with alternate power sources if both controllers are simultaneously

active: Who supplies the OPM power and how do we switch between choices? One simple algorithm would be that the first controller powered up takes precedence in distributing power to the digitizers and OMs.

## Connectors on the Market

A list of some deep ocean connector manufacturers follows. One can Google any of them on the web. Almost all have lines of electrical and optical connectors and feed-throughs. The market has been much stimulated by the deep ocean (to 2km at least) oil industrial activity. This is just a short annotated list to get someone started on a serious survey of our options.

**Birns** (<http://www.birns.com/>): a USN favorite with good reputation

**Burton** ([http://www.burtonee.com/under\\_water\\_power.html](http://www.burtonee.com/under_water_power.html)): another older company with military experience, high reliability, but expensive.

**DG O'Brien** (<http://www.dgo.com/home.htm>): Another long term connector manufacturer with strong ties to submarine applications. But they do have a coax connector, though expensive.

**Euroceanique** (<http://www.euroceanique.com/>): We found reference to this company in an ANTARES optical detector design document, but are not sure it is really a connector company or a cable package company.

**Ocean Design** (<http://www.odi.com/>): Nautilus, Jim Cairns' company, noted for clever engineering and excellent quality. This is the choice of some of the European neutrino experiments.

**SeaCon (Brantner)** (<http://www.seacon-usa.com/>): old standard (ICECUBE choice), but we had some trouble with wrong O-ring sizes in DUMAND days. They are the major manufacturer in this field nowadays.

**SubConn** (<http://www.subconn.com/>): these were the nice flat simple connectors used for DUMAND OMs. Not so terribly robust, but maybe fine for our protected application, and they were reasonable in price.

## Summary

In summary then we propose, to zeroth order, the following configuration. It is not unique, but the proposed version seems simplest and most reliable. There are certainly no stoppers here, it is a matter of practical choices. We have selected a tree structure for data collection, with one intermediate layer within the detector, and the strategy of sending all PMT data to shore for trigger finding and processing in the laboratory

environment. Given present technology, no ocean bottom trigger finding and data selection will be needed. Such a system maximizes reliability and allows for evolution of the data filtering and trigger algorithms on shore. The shore connections should be designed to be redundant with at least two alternate paths, to evade the danger of single point failure. Slow communications and clock will be supplied from shore and generally all links will be full duplex though asymmetrical in rate.

- Build each OM with a short (3m) pigtail and two pin feed-through, with twisted pair cable leading to a simple in-oil low pressure connector. The alternative is to use coaxial cable.
- Each 9x9 OM cell will have an oil filled connector box which combines connections from nine (this could be some other number as well) modules into one fixed multi-wire (18) cable and thence to the nearby digitizer with connector on the digitizer end. Each PMT module is thus disconnectable from the bulkhead feed-through. The cable from bulkhead is a pre-made harness with connector only at digitizer/controller end, and everything is to be in oil, if manageable.
- Each digitizer receives signals via 4 multi-wire connectors (eg. 9x4 OMs), and passes data up the line on two cables (and perhaps separate power line) to the redundant main controller units. The digitizer connects to a cable harness which includes some number of regional units, say 8, and there are 8 connectors to the main controller. All these cables will be in oil-filled hoses.

We endorse the requirement to employ oil bath at every stage of the data collection and forwarding to the main controllers, to minimize the number of connectors, and to configure the system so that individual optical modules may be replaced without major disruption of the cable system.

In sum we envision a rather simple and robust communications design.

## **Appendix**

**Task 11: Power and Communication Cable to Shore**

Appendix

# **STUDY OF POWER AND COMMUNICATION LINKS TO SHORE**

*A report submitted to Makai Ocean Engineering*

J.G. Learned

*University of Hawaii at Manoa*

## **TASK 11**

### **1.1 OVERVIEW**

This task provides a recommendation for powering the detector and establishing communication links to shore. The results of previous tasks (1 and 6) provide estimates of the observing period, data rates and power consumption. Together these estimates determine the total energy which must be stored to run the detector prior to recovery. As discussed in Task 10, the power consumption of the detector is rated at 2-4 kW in the present preliminary design (about 1 W per optical module). The typical observation period we have settled upon is one year. Battery power is possible but not trivial at this level. Data rates required are about 1 Gb/s, well within present telecom (fiber optic link) practice. Power and data connections to shore, at levels which are well within present practice (as we discuss below) for submarine electro-optic cables, will be straight forward.

We are fortunate that several new projects have addressed precisely the issues that are unique to a high data rate, modest power consumption instrument at the end of an E-O cable. Indeed since some of their requirements are much more challenging than ours (as discussed below), the engineering of the shore link for Hanohano is reduced to common practice (very much not the case as recently as a decade ago). Given the experience of the high energy neutrino detectors being built in the Mediterranean, and the demands of the off-shore oil industry, the shore connection engineering task for Hanohano has become one of employing existing practice. We can predict total shore connection costs to be less than \$12/m including cable purchase, connections and deployment.

In a future round of component design we will aim for a power consumption level of 100 mW/optical module, and if this is achieved can consider battery power for annual renewal. In any event battery backup (and load stabilization) with an anchoring battery pack may be desirable at present power consumption levels.

### **1.2 INTRODUCTION**

Underwater communication via coaxial cable dates back more than 150 years, and thus has an extremely well developed technology for cable laying, recovery and repair. With the advent of fiber optic communication links came vastly increased data rates, going

from the MHz of coaxial links to Ghz in short order (1980-2000). Because the cost of submarine electro-optic cable runs at less than \$10/m, the cost of a transoceanic link is in the range of \$100M, to be compared with a communications satellite in the billion dollar range. Hence during the technology boom of the 1990's cables were laid at an unprecedented rate, with ever increasing capacity. In fact telecom organizations have been giving away early transoceanic fiber optic cables, and some science groups have availed themselves of the opportunity to place instruments in remote mid-ocean locations (cables can reliably be pulled up and new instruments spliced in, as in the Hawaii based H2O Project).

Communications cables have almost always carried power as well as information. Repeaters are needed on transoceanic links (on a scale of order 50 km, though now longer), and these get power from a single voltage drop across the entire cable of order a few thousand volts. Each repeater drops only a few volts, and has no necessary connection with the sea (not grounded). Thus submarine cables have been designed to handle up to around 10 kV, DC, which turns out to be fortunate for our application, but for different reasons (minimum current in our case).

The newer cables are smaller in diameter and lighter than the older coaxial cables, with dimensions of several centimeters instead of several inches, and weight (and cost) reduced by the diameter factor squared. Of course near shore cables require heavy armoring in some cases, and not much is gained there.

AC power has much to be said for the ease of voltage translation at the load end. However, due to an incident many years ago in which an unarmored AC cable was attacked by sharks in the Canary Islands, designers have shied away from alternating current. This tradition deserves re-examination, but for the present we will stick to the common practice of employing DC power, with a central conductor and high potential, and we will employ a sea-water return. The virtue of a high voltage is to minimize the current, which is desirable for an endpoint load, as we will discuss below.

Another facet of the 1990's boom in oceanic telecommunications was that many new cable laying ships were constructed, more suitable to the smaller cables (than earlier coax) and with the ability to do dynamic control. The station keeping and detailed course following ability, coupled with GPS position monitoring, meant that cable laying became far more precise than earlier. The over building of ships has lead to ready availability of such vessels. This is also an area of Makai Ocean Engineering expertise.

### 1.3 CABLE CONNECTION TO SHORE.

For the present work we take our first candidate site near the Big Island of Hawaii as the design study example. Figure 1.3-1 shows the bathymetric profile and Figure 1.3-2 a possible cable route to the closest site at 4,200 m depth to shore. The shore location is the Natural Energy Laboratory of Hawaii Authority. NELHA has laboratory space close to shore and can (and has) supported similar offshore experiments and operations. NELHA

has a drilled tunnel from the laboratory to an offshore location at 30m depth, thus providing a conduit for easily landing and protecting the cable to shore.

The distance offshore is 17.988 km; the cable length along the bottom (including required slack) is about 19 km. For practical considerations, about 22 km of cable would be needed. The location is 156.32 W, 19.725 N. This is a well surveyed cable and pipe route and has known bottom characteristics and has been visually surveyed by submersible.

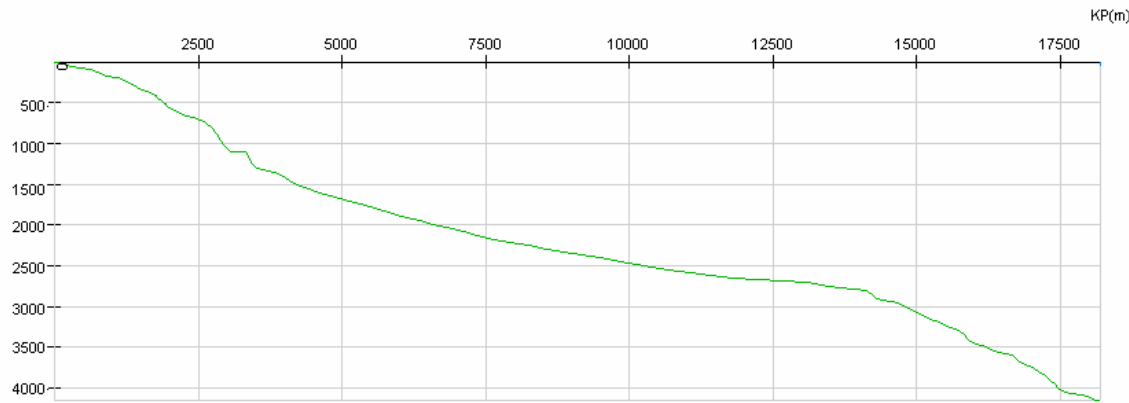


**Figure 1.3-1** Depth Profile (in meters) of a possible cable run from the Keahole Point Laboratory on the Big Island of Hawaii to > 4km deep ocean, in a distance of about 18 km. Note vertical scale exaggeration.

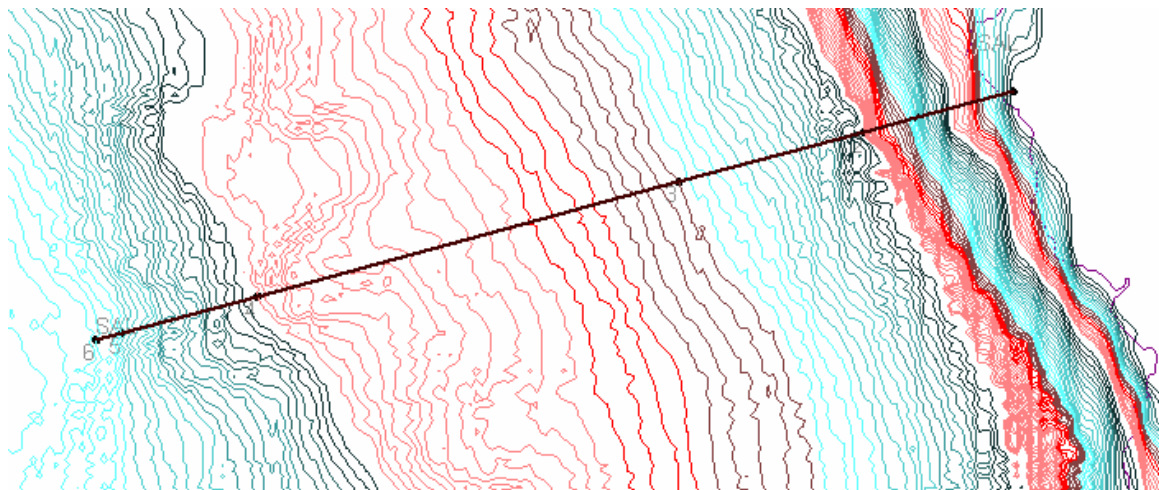


**Figure 1.3 -2:** Site location and profile, West Hawaii at Keahole, Point. Cable distance from shore laboratory to Hanohano is 18.7 km. Contours are at 20 m intervals.

## 1.4 CABLE CHARACTERISTICS

The cable supplying power and communications to Hanohano will be a standard fiber optic cable used for cross ocean communications. These cables typically have 4 or more pairs of fiber optic strands plus a power conductor that supplies typically 10 kW of power at high voltage (several thousand volts). The mechanical properties of typical Alcatel (major supplier on the world market) cables are shown in Table 1.4-1, below. Cables types that would be used in this installation would be Lightweight (LW) or Lightweight Protected (LWP) in deep water and Single Armor (SA) approaching shore and going through the shoreline crossing.

Cable such as this is readily available in the lengths we require (tens of km), which are mere mill ends for a transoceanic run (thousands of km). We know of several stored in Honolulu, available for the asking (cable companies happy to get rid of them as they are not allowed to be dumped). Even in the event that we must purchase the cable, the cost will be about less than \$10/m, or with 40km of cable it would be about \$400k. This is probably an overestimate, since the cost projected for the 3000 km of cable to be layed for the Neptune Project (in the Northwest near Seattle, Wash. and Vancouver, B.C.) is about \$36M, including purchase, junction boxes and deployment.

**OALC-5 (14mm) CABLE AND ASSOCIATED UNDERWATER PLANT**

CABLE TYPE	STOWAGE FACTOR Cubic metres / km	OUTSIDE DIAMETER (mm)
Light Weight LW	0.18	14 (PE sheath)
Light Weight Screened LWP	0.34	19.6 (PE sheath)
Single Armour SA	0.6	26 (PP rovings)
Double Armour DA	1.2	35 (PP rovings)

**Weights (Nominal)**

CABLE TYPE	WEIGHT IN AIR Tonnes / km	WEIGHT IN WATER Tonnes / km
LW	0.44	0.28
LWP	0.63	0.32
SA	1.6	1.0
DA	3.5	2.4

**A.4 Tensile Strength of Cable Types**

CABLE TYPE	NPTS (kN)	NOTS (kN)	NTTS (kN)	Min Cable Breaking Load (kN)
LW	20	30	50	60
LWP	20	30	50	60
SA	50	130	160	190
DA	50	150	200	270

These figures are for 1.8% fibre proof tests.

**A.5 Hydrodynamic Constants**

CABLE TYPE	(Rad.m/Sec) Lay / Recovery	(Degree.knots) Lay / Recovery
LW	0.416 / 0.488	46 / 54
LWP	0.376 / 0.441	42 / 49
SA	0.577 / 0.577	64 / 64
DA	0.770 / 0.770	86 / 86

**Table 1.4-1:** Typical mechanical characteristics of fiber optic cable suitable for supporting Hanohano

**Typical / Maximum Deployment Depth for Cable Types**

Cable Type	Typical Depth		Maximum Depth	
	Surface Lay	Burial	Surface	Burial
LW	7000 m	-	8000 m	-
LWP	3500 m	-	7000 m	-
SA	1500 m	1500 m	2000 m*	2000 m*
DA	200 m	200 m	500 m	500 m

**Recovery Depths for cable with R3/4 6fp Repeater with 5kN margins from NTTS.**

Cable Type	Adverse Conditions (1knot,75degree,4m)	Standard Conditions (0.7 knot,80 degree,4m)
LW	5700	7100
LWP	4400	5800
SA	2000	2000
DA	500	500

**14 mm / 84 mm Joint Data**

14 mm / 84 mm Joint ID	LW/LWP	SA	DA
Length over bend limiters (m)	<b>1.480</b>	<b>1.710</b>	<b>1.710</b>
Rigid length (m)	<b>0.370</b>	<b>0.590</b>	<b>0.590</b>
Maximum diameter (m)	<b>0.170</b>	<b>0.140</b>	<b>0.140</b>
Diameter at mid point of joint (m)	<b>0.130</b>	<b>0.123</b>	<b>0.123</b>
Weight of joint in air (kg)*	<b>27</b>	<b>47</b>	<b>50</b>
Weight of joint in water (kg)*	<b>9</b>	<b>25</b>	<b>28</b>
Minimum bend radius of joint under tension (m)	<b>1.5</b>	<b>1.5</b>	<b>1.5</b>
Minimum bend radius of joint under no tension (m)	<b>1.5</b>	<b>1.5</b>	<b>1.5</b>

**Table 1.4-2:** Deployment and Recovery depths and other characteristics for fiber optic cables and joint characteristics – From Alcatel Submarine Networks.

Capacitance	0.22 microfarad/km (typical)
Conductor Resistance	<1.6 ohms/km at 10C
Insulation Resistance	> 100 megohms-km

**Table 1.4-3:** Typical ASN 14 mm Cable DC Electrical characteristics

## 1.5 CABLE LAYING

Laying the cable to shore can be accomplished in the same operation as the deployment of the detector. The cable is loaded onto a separate cable lay ship (either a stand-by cable ship or a specially outfitted University vessel); the total

cable length for this run is short and cable can be laid on deck if the ship is not a specialty cable ship.

Just prior to the Detector being fully flooded and ready to submerge, the cable ship comes alongside and makes the connection to the Detector. A short length of cable can be passed to the cable shop from the detector support barge, and a splice is put into the cable.

The cable ship can either stay close or back off several km from the Detector. During submergence, the cable ship will be in tension control mode and will keep the surface cable tension at a constant level. This will pay out cable as needed. Makai has simulated several possible cable deployments with our cable control software, MakaiLay. The results of one analysis are shown in Figure 1.5-1. One sees successive snapshots of the cable profile at intervals of about 3 minutes during the descent of the detector. Note that the offset of the landing point from a vertical descent is about 65 m.

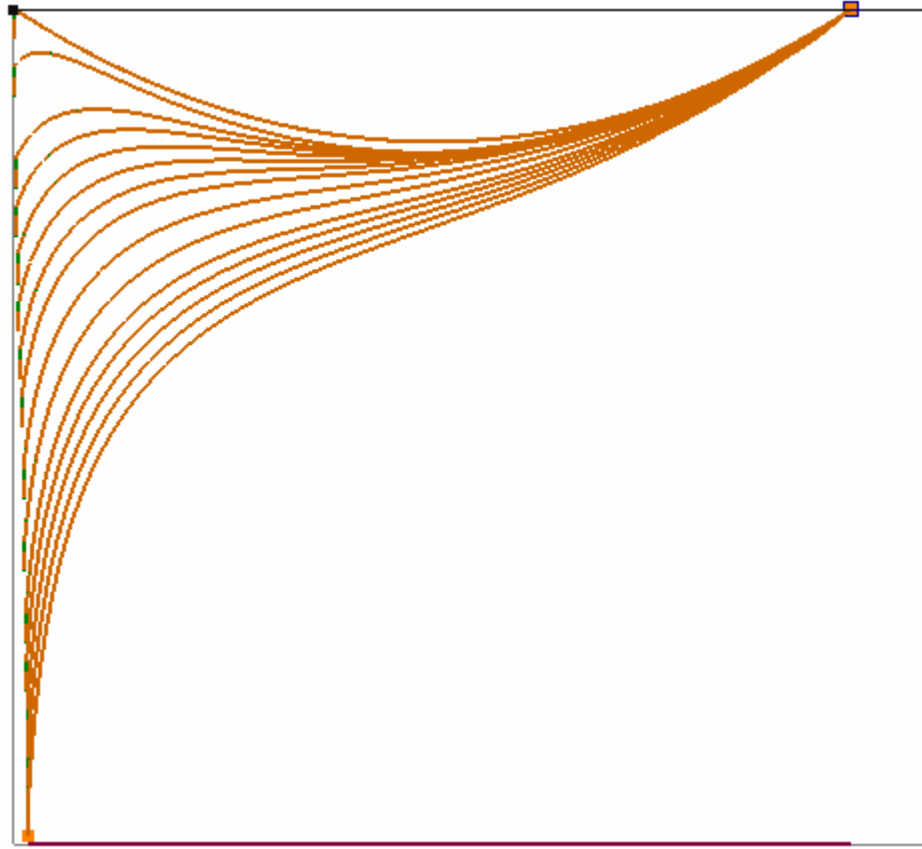


**Figure 1.5-1:** A safe deployment of the Hanohano shore cable during free fall detector descent. The scale is for a 4 km deep deployment, with cable ship standing off by 4 km from deployment barge. The time is about 48 minutes.

Once the detector has reached bottom and been checked out the cable laying can proceed along the predetermined path and with pre-calculated payout rates. The important issue here is maintaining some longitudinal tension on the shore cable, so it has no opportunity to hockle. It is well known that essentially any deep ocean cable will twist up if given an opportunity by becoming slack at the bottom (hanging tension produces torque). Laying the cable up-slope makes this problem easier than the converse. The cable payout rates are not a big issue for the relatively short run we are concerned with here, so we can be slow and cautious. At a typical payout speed of 30 m/min the lay would take about 10 hours. The whole operation should take about one day.

As mentioned, for the Keahole Point case, there are slant-drilled conduits, through which the cable can be pulled up to shore. The ship approaches shore, standing off some safe distance (order of 1 km), and the cable is put out on floats, and finally cut and the end passed to hauling line and pulled ashore, as floats are cut free. Divers may be used to guide the cable, and to tie it down to anchor points in the shallow water.

Other venues for Hanohano will require different techniques of bringing the cable to shore, but this is all involves mature technology and standard submarine cable industry practice.

Cable ship costs can be substantial depending upon which vessel is employed. The daily costs can run from \$25K/day (UH Class 1 oceanographic research vessel, Kilo Moana) to about \$100K/day for a typical large cable layer. Since the actual cable laying operation will require about one day, ship costs will be dominated by transit and preparation times. It may be possible to employ a standby ship (kept on watch by a cable company consortium), or a transiting ship at minimal cost, perhaps even free. This has been done before, considered as a practice run for the ship's crew. Transit from Honolulu adds one day on each end. If a cable must be picked up from the continental US however, and we must pay for transit, then the cost can be perhaps \$100K, so we are strongly motivated to use a local vessel or a ship of opportunity and employ available cable. In any event, a total cost for cable laying, even with commercial rates should not exceed \$250K

## 1.6 POWER DISTRIBUTION

The estimated power requirement for the detector at this time is less than 4 kW. A long standing problem has been the limited detector input voltage for DC-DC. The standard choice (Vicor, high reliability and efficiency) devices handle 375-420V input (with many choices of output). Let us take 400V in as the working example of the voltage to be supplied at the ocean bottom detector. In this instance the current required for a 4 kW load is 10 amperes. If we have a 40 km cable, and the resistance is 1.25 Ohms per kilometer the total cable DC resistance will be 50 Ohms (plus a few ohms for ocean return, which we can ignore for this example). Thus the IR drop across the cable will be 500 V. Hence the power supply on shore will be required to deliver 900V at 10

Amperes, 9kW. However the input voltage at 900 V is considerably greater than the DC-DC supply can survive, if it should “see” that full voltage. This could happen if somehow a large fraction of the load trips off at the detector end, and the voltage then soars at the DC-DC supply. Another type of problem can occur when the power is interrupted suddenly and the cable effective inductance can lead to a momentary voltage doubling. There are other troublesome scenarios. This is a well known and studied engineering problem. The traditional solution has involved the employment of a load regulation package at the detector end, along with voltage clamping and dummy load. While this has certainly been done for a number of ocean projects, it introduces complexity and single point modes of failure.

A far better solution is to employ higher voltage and lower current on the undersea cable. Since the standard telecom cables are manufactured to employ 7-10 kV, then one may reduce the current proportionately. Again to take the simple example with 4kW load, if we operate at a modest 4kV, the current is only 1 ampere, and the voltage drop across the cable is 50 V, and thus well within the range of normal DC-DC supply variable inputs. Hence one may simply bring the voltage up (rate control is important due to inrush current of the supply as well as some hang states if too slow) to operating range, and one does not have to worry as the system powers up at the detector, adding load as modules are turned on. Of course over-voltage protection is still desirable at the load, but regulation becomes trivial.

We are most fortunate that the Neptune Project in the Northwest (ultimately of order a \$300M project) has done a great deal of study and engineering upon this issue (also in predecessor projects Mars and Venus). They want to string a 3000 km network of cables in the vicinity of the Juan de Fuca fault zone, off Vancouver Island, which cables will have many nodes where instrument stations can permit a huge variety of instruments to be deployed. The power (10’s of kW) and data (many Gb/s) requirements dwarf our needs for Hanohano, so they are more than solving our engineering problems. Hence for our present engineering study we need only refer to the Neptune project, and we can utilize their cost estimates as upper limits for ours: \$12/m including cable, stations, and deployment.

Other projects, such as the high energy neutrino projects NESTOR, NEMO and ANTARES in the Mediterranean, have similar engineering requirements, and we have studied their solutions. The oil industry drilling off-shore has also pushed the technology a great deal, all to our benefit, and much within the last few years. As the technology has matured, telecom levels of reliability have been incorporated in system designs, where MTBFs of order 100 years or more are common.